Vol. 347: 121–126, 2007
doi: 10.3354/meps06972

MARINE ECOLOGY PROGRESS SERIES
Mar Ecol Prog Ser

Published October 11

OPEN ACCESS

THEME SECTION

Advances in modelling physical–biological interactions in fish early life history

Idea and coordination: **Alejandro Gallego*, Elizabeth W. North, Pierre Petitgas, Howard I. Browman**

CONTENTS

*Email: a.gallego@marlab.ac.uk

Introduction: status and future of modelling physical–biological interactions during the early life of fishes

Alejandro Gallego[1,*], Elizabeth W. North[2], Pierre Petitgas[3]

[1]FRS Marine Laboratory, PO Box 101, Victoria Road, Aberdeen AB11 9DB, UK
[2]University of Maryland, Center for Environmental Science, Horn Point Laboratory, Cambridge, Maryland 21613, USA
[3]IFREMER, Centre de Nantes, rue de l'Ile d'Yeu, BP 21105, 44311 Nantes Cedex 03, France

ABSTRACT: Modelling physical–biological interactions in the early life of fish is becoming an integral part of theoretical and applied marine ecology. A workshop on 'Advancements in modelling physical–biological interactions in fish early-life history' (WKAMF) was held in April 2006 to review recent developments and identify future research directions. Here we provide an overview of the information presented at WKAMF (some of which is published in this Theme Section), discussions that took place at the workshop, and the authors' perspectives as workshop co-Chairs. The major themes identified at the workshop were the need for enhanced model validation and sensitivity methods and improved understanding of physical and biological processes. Using the appropriate level of model complexity required for each model application is important; developing quantitative consistency of model results with good quality observational data is critical. In addition, improving our prediction of physical processes, such as circulation patterns and turbulence, will advance our knowledge of fish early life, as will a better understanding of biological processes like mortality, behaviour, and energetics. The latter stage-dependent, often species-specific, processes pose particular challenges, although technical advances in field and laboratory observations are likely to result in considerable progress in the near future. Finally, there is a clear requirement for interdisciplinary collaboration between modellers, field scientists and laboratory scientists. Studies receiving input from a wide range of disciplines will increase our understanding of fish early-life ecology and prediction of recruitment to fish populations.

KEY WORDS: Biophysical modelling · Fish · Eggs · Larvae · Individual-based methods · Workshop

Modelling physical–biological interactions in the early life history of fish has expanded considerably in the last decade (Miller 2007, this Theme Section [TS]). It is increasingly becoming an integral tool for understanding the processes that affect interannual variability in fish recruitment (Werner et al. 1997) and the degree of connectivity between fish sub-populations (Cowen et al. 2006). These themes are crucially important in the global context of anthropogenic and climatic pressure on marine ecosystems in general and on fished species in particular.

The International Council for the Exploration of the Sea (ICES) Working Group on Modelling Physical–Biological Interactions (WGPBI) called for a review of recent developments in the field of modelling fish early life history, in order to evaluate the current state-of-the art, compile a manual of 'best practices' and identify future research directions. In response, the workshop on 'Advancements in modelling physical–biological interactions in fish early-life history' (WKAMF), was held in Nantes, France, in April 2006 under the auspices of WGPBI and the ICES Working Group on Recruitment Processes (WGRP). Papers in this TS are based on research presented at WKAMF. This introduction to the TS provides an overview of work presented at WKAMF, a synthesis of open discussions that took place at the workshop, and the authors' perspectives as workshop co-Chairs. Products of the workshop can be found at http://northweb.hpl.umces.edu/wkamf/home.htm.

The WKAMF workshop was focused on the main aspects of biophysical models of fish early life history, and addressed numerical techniques, validation issues, and case studies. It was organized around 7 core information sessions, from eggs to juveniles and from smaller to larger scales, with discussion and consensus-building sessions. This introduction follows the thematic structure of the workshop core information sessions.

*Email: a.gallego@marlab.ac.uk

Initial conditions: egg production, spawning location/time. The level of detail required for initial conditions depends upon the objectives of the model. Models are often used in a heuristic way, i.e. to increase our understanding of complex processes, or in a predictive role. Even beyond this general classification, specific objectives (e.g. predicting recruitment vs. identifying population connectivity) will have a major influence on the required level of complexity in initial conditions. For example, particles can be distributed uniformly over wide spatial and temporal scales to investigate whether hydrographic conditions prevent transport between ecosystems (e.g. Lett et al. 2007, this TS). Alternatively, a model that predicts spatial and temporal patterns in the recruitment process (i.e. how the recruits are distributed in time and space) requires input in the form of spatially and temporally resolved egg production (e.g. Heath & Gallego 1998).

Numerical techniques are available that can help fill in gaps in understanding of spatial and temporal patterns in spawning. Sensitivity analyses can be used to estimate which characteristics of spawning (e.g. patchy vs. uniform, higher/lower frequency, spawning location/time, depth) are important for the model application. Pattern-oriented modelling is a useful strategy for identifying the patterns in observational data that can be used to determine model complexity and optimize model structure (Mullon et al. 2002, Grimm & Railsback 2005, Grimm et al. 2005). A promising technique to derive initial conditions is backtracking by individual-based modelling (Batchelder 2006, Christensen et al. 2007, this TS) which, by moving particles 'backwards' through a flowfield, can be applied to estimate the original distribution of fish eggs or early larvae from observations of the distribution of later stages. Although these techniques are useful, they supplement, not supplant, basic biological information on spawning processes that are required to predict recruitment. For many fish species, information is lacking on the factors that control the spatial and temporal patterns in spawning, including the potentially important effects of adult characteristics (e.g. maternal effects; Marteinsdottir & Steinarsson 1998).

Small-scale processes (turbulence, feeding success). The effect of turbulence on larval fish feeding and growth has been the object of considerable modelling and experimental effort since the pioneering work of Rothschild & Osborn (1988). However, *in situ* measurements of kinetic energy do not seem to fit turbulence theory in coastal environments (Osborn 2007, this TS), where many larval fish live. On the shelf, dissipation appears to be anisotropic, resulting in higher measured dissipation than predicted by isotropic theory. A better understanding of basic turbulent processes is required, as are measurements of turbulence relevant to larval fish at the scales of predator-prey interactions (i.e. from 1 mm to 1 m) instead of averaging turbulent dissipation over depths ≥1 m.

Observational data needed to parameterize predator escape and prey encounter, capture, and feeding processes at scales relevant to larval fish are scarce (e.g. Browman 1996, Skajaa et al. 2004, Skajaa & Browman in press). The influence of turbulence on feeding success is sensitive to the size and shape of the predator's perceptual field for prey (Galbraith et al. 2004, Mariani et al. 2007, this TS). Therefore, detailed species-specific observations (in the laboratory or *in situ*) of the feeding process are critical for improving and validating this component of biophysical models of larval fish. New observational techniques (e.g. Osborn 2007) show considerable promise in the laboratory and in the field; these are labour-intensive and rely on new technologies that are often expensive, but the information gained may be quite useful depending on the objectives of the model.

Mesoscale transport processes: physics and behaviour. Three-dimensional hydrodynamic models are increasingly being used as the basis for modelling fish early life history and, consequently, a well-validated hydrodynamic model is a fundamental requirement. The horizontal resolution of hydrodynamic models can influence predicted fish egg and larval trajectories. As a rule of thumb, the model grid size should be fine enough to capture the appropriate horizontal mixing processes (e.g. smaller than the internal Rossby radius; Hinrichsen et al. 2002).

Development of particle-tracking techniques and parameter optimization frameworks is improving the efficiency of individual based models (IBMs) and their integration into life cycle models. For example, although the majority of biophysical models are Lagrangian IBMs (Miller 2007), a computationally efficient compromise between Eulerian and Lagrangian models can be achieved by using a 'biased binned random walk', which does not track the exact vertical position of the particles but instead the layer in which they reside (Thygesen & Ådlandsvik 2007, this TS). In addition, a probability density function (PDF) can be used to condense the results of tens of thousands of particle trajectories and integrate tFhem into an optimization framework that estimates biological parameters, including larval mortality and growth (Brickman et al. 2007, this TS). Finally, the interaction between environmental variability and population change over decades can be simulated with Lagrangian trajectories coupled to evolutionary algorithms that include adaptive behaviour and fitness characteristics that can be passed on to subsequent generations (Huse 2005).

The need for parameterization of sub-grid scale mixing processes in particle tracking models (i.e. pro-

cesses that occur on scales smaller than the grid size of the hydrodynamic model) is now increasingly recognized (Hunter et al. 1993, Visser 1997, North et al. 2006, Christensen et al. 2007); however, important differences in parameterization remain, depending on the characteristics of different physical models and individual applications. Some models are implemented with only vertical sub-grid scale processes (e.g. Huret et al. 2007, this TS), some with only horizontal processes (e.g. Brickman et al. 2007), and others include both vertical and horizontal parameterizations (e.g. Paris et al. 2007, Sentchev & Korotenko 2007; both in this TS). A systematic assessment of the influence of these processes on model predictions, and guidelines for their appropriate use, is needed.

Larval vertical swimming behaviour can critically influence transport (e.g. Fiksen et al. 2007, Vikebø et al. 2007; both in this TS). Therefore, biophysical models should incorporate at least vertical movements instead of assuming that simulated larvae are passive (inanimate) particles. Horizontal orientation, and directed horizontal swimming, are greater unknowns as most models assume passive drift in the horizontal plane. Although *in situ* observations of tropical coral reef fish larvae demonstrate that they can be strong, directed (i.e. non-random) swimmers (Leis 2007, this TS), considerable differences in swimming ability exist between these and temperate fish larvae. Moreover, horizontal orientation of temperate fish larvae has not been sufficiently studied.

It is important to identify the internal (e.g. physiological) and external (environmental) drivers that control the behaviour of the early life stages of fish. Perspectives derived from behavioural ecology can enhance our understanding of fish early life and help identify processes that emerge from the interplay of physiological mechanisms and fitness. For example, realistic patterns can emerge from models that incorporate tradeoffs between growth and survival (Fiksen et al. 2007). Larval behaviour could influence growth as well as mortality by, for instance, influencing vertical position, which in turn affects light-dependent feeding success and predation risk (Fiksen et al. 2007, Vikebø et al. 2007). Given the potential for transport patterns to vary with depth when the flow is not vertically homogeneous, behaviour can also link the biological processes of growth and mortality to physical transport processes.

Biological processes: growth and mortality. Survival of fish throughout the early life stages is the outcome of a trade-off between growth and mortality. Some modelling studies have focused on growth processes, applying a simple size-dependent mortality function. Others have concentrated on mortality, especially that resulting from predation.

Knowledge of a hierarchy of factors is required to parameterize the growth and development of fish early-life stages. Although temperature and body size are often identified as primary factors (e.g. Heath & Gallego 1997, 1998), some models incorporate prey concentration (Bartsch & Coombs 2004) and increasingly complex mechanistic sub-models of feeding processes and bioenergetics (e.g. Werner et al. 1996, Hinckley et al. 2001). Many of these models are parameter-rich and/or empirically derived from specific environmental conditions, and there is often considerable uncertainty about the universal applicability of functional forms and specific parameter values. Care should be taken in understanding the model assumptions and the consequences of model formulation (e.g. Peck & Daewel 2007, this TS).

Our understanding of larval mortality in the field is incomplete and is challenged by the need to detect often subtle (Houde 1989) or sporadic variations in mortality rates over time. Predictions of predator feeding rates (and consequently mortality on young fish) from laboratory, field and simple models can differ by an order of magnitude (Paradis et al. 1996, Pepin 2004, 2006). Consequently, modelling predator feeding requires better observations and greater effort to validate model formulations (especially functional responses). Adequate knowledge of the degree of spatio–temporal overlap between (vertebrate and invertebrate) predators and larval fish prey is a critical pre-requisite for understanding predation mortality, which appears to follow a random encounter pattern on the local scale (Poisson distributed; Pepin 2004).

Biological processes: juvenile recruitment and settlement. Explicit modelling of post-larval stages through to recruitment is rare (Hinckley et al. 1996) and sometimes adding complexity (e.g. a simple settlement process) does not enhance the model fit to the observations (Brickman et al. 2007). The role of settlement and density dependence in nature needs to be further investigated and incorporated into models, where appropriate (e.g. see Gallego & Heath 2003). The study of older stages can also provide some insight into earlier life history, e.g. by backtracking (Christensen et al. 2007). Biophysical models can be used to generate indices (e.g. a coefficient of overlap between modelled larval and idealized prey distributions [Hinrichsen et al. 2005]) that can be correlated to juvenile recruitment and may complement traditional methods for recruitment prediction.

Future directions: integration with observing systems, operational models, monitoring programs, and management recommendations. Spatially-explicit coupled models have been useful for studying the transport of planktonic stages of marine fish. Further uses of these models to investigate more complex

mechanisms (see Miller 2007) such as recruitment, growth, predation, stock structure, effects of climate change, as well as optimal survey/marine protected area design, are becoming more commonplace in the scientific literature. These models have the potential to improve our predictions of population variability and ecosystem dynamics, and will advance our knowledge of important biophysical processes when used for hypothesis testing (Miller 2007).

The way forward entails overcoming many technical issues, including assessment of (1) model resolution in space (grid size and bathymetry) and time (time step), (2) particle tracking algorithms and interpolation schemes, (3) implementation of biological models within hydrodynamic models (on-line) or separate from them (off-line), (4) temporal resolution of physical forcing (e.g. hourly vs. daily wind data) and hydrodynamic model output (e.g. tidally explicit vs. averaged output), (5) sensitivity analysis, visualization and validation methods, (6) benchmark test cases for particle tracking models, and (7) data assimilation techniques. An important challenge is to integrate bio-physical models with monitoring programs to enhance model validation. We need to incorporate the data generated by monitoring programmes and even influence their design so that they generate the measurements that are useful to parameterize and validate biophysical models.

Consensus discussion. Workshop participants identified several major themes that would result in advances in the field of biophysical modelling of the early life stages of fish. The need for, and utility of, validation and sensitivity methods was addressed in every theme session and figured prominently in group discussions. Consistency between model predictions and observational data is crucial; quality of data is paramount. Methods of model-data comparison need to be applied and developed and the validity of quantitative metrics should be addressed. In addition, models should be as simple as possible but as complex as necessary. There are no fixed rules to determine the appropriate complexity of a model, although some useful tools (e.g. sensitivity analysis, pattern-oriented modelling) can provide guidance. The level of model complexity should also be adjusted to the model objectives and the observed biological patterns that it aims to reproduce.

Biophysical model results are critically influenced by hydrodynamic model predictions. Therefore, basic improvements in understanding of turbulence and in predicting mixing and circulation patterns will advance the field of larval fish modelling. Additionally, ensemble methods (combining a suite of simulations that have slightly different starting conditions or model assumptions [Gneiting & Raftery 2005]) and probabilistic approaches (e.g. Brickman et al. 2007) have been proposed as useful tools for integrating complex 3-dimensional predictions, environmental variability and uncertainty into biological life cycle models.

Fundamental information is needed on the biological processes of mortality, behaviour, and energetics to advance models of fish early life. These stage-dependent, and often species-specific, processes pose challenges for investigation; however, recent advances in field and laboratory techniques will likely revolutionize the field of larval fish modelling.

Finally, general recommendations were made at the WKAMF workshop: (1) models and model results should be made accessible to managers and other users, but mainly in close collaboration with scientists to ensure that model results are interpreted and applied appropriately; and (2) laboratory, field and modelling scientists must work together to advance the field. The groups that come to grips with both the rhomboidal approach to model complexity (with greatest complexity at the level of the target organism and decreasing towards higher and lower trophic levels; deYoung et al. 2004) and the laboratory/model/observation triad (Hannah 2007, this TS) will lead the advances in the field of fish early life ecology.

Acknowledgements. We thank WKAMF workshop participants and sponsors. WKAMF was hosted by the French Research Institute for Exploitation of the Sea (IFREMER) Centre de Nantes with support from IFREMER (France), the US National Science Foundation (OISE-0527221), Fisheries Research Services (Scotland, UK), the University of Maryland Center for Environmental Science (USA), and the US National Marine Fisheries Service. It was endorsed by GLOBEC and Eur-Oceans. Support for this publication was provided for E.W.N. by NSF (OCE-0424932, OCE-0453905). Partial support for P.P. was provided by Eur-Oceans (EC FP6 Network of Excellence). We also thank Howard Browman for his constructive comments on this manuscript.

LITERATURE CITED

Bartsch J, Coombs SH (2004) An individual-based model of the early life history of mackerel (*Scomber scombrus*) in the eastern North Atlantic, simulating transport, growth and mortality. Fish Oceanogr 13(6):365–379

Batchelder HP (2006) Forward-in-time-/backward-in-time-trajectory (FITT/BITT) modeling of particles and organisms in the coastal ocean. J Atmos Ocean Technol 23(5): 727–741

Brickman D, Marteinsdottir G, Taylor L (2007) Formulation and application of an efficient optimized biophysical model. Mar Ecol Prog Ser 347:275–284

Browman HI (ed) (1996) Predator–prey interactions in the sea: commentaries on the role of turbulence. Mar Ecol Prog Ser 139:301–312

Christensen A, Daewel U, Jensen H, Mosegaard H, St. John M, Schrum C (2007) Hydrodynamic backtracking of fish larvae by individual-based modelling. Mar Ecol Prog Ser 347:221–232

Cowen RK, Paris CB, Srinivasan A (2006) Scaling of connectivity in marine populations. Science 311(5760):522–527

deYoung B, Heath M, Werner F, Chai F, Megrey B, Monfray P (2004) Challenges of modelling decadal variability in ocean basin ecosystems. Science 304:1463–1466

Fiksen Ø, Jørgensen C, Kristiansen T, Vikebø F, Huse G (2007) Linking behavioural ecology and oceanography: larval behaviour determines growth, mortality and dispersal. Mar Ecol Prog Ser 347:195–205

Galbraith PS, Browman HI, Racca RG, Skiftesvik AB, Saint-Pierre JF (2004) Effect of turbulence on the energetics of foraging in Atlantic cod *Gadus morhua* larvae. Mar Ecol Prog Ser 281:241–257

Gallego A, Heath MR (2003) The potential role of settlement on the stock-recruitment relationship: numerical experiments using biophysical modelling simulations. ICES CM/P:11

Gneiting T, Raftery AE (2005) Weather forecasting with ensemble methods. Science 310:248–249

Grimm V, Railsback SF (2005) Individual-based modelling and ecology. Princeton University Press, Princeton, NJ

Grimm V, Revilla E, Berger U, Jeltsch F and 6 others (2005) Pattern-oriented modelling of agent-based complex systems: lessons from ecology. Science 310:987–991

Hannah CG (2007) Future directions in modeling physical–biological interactions. Mar Ecol Prog Ser 347:301–306

Heath MR, Gallego A (1997) From the biology of the individual to the dynamics of the population: bridging the gap in fish early life studies. J Fish Biol 51(suppl A):1–29

Heath MR, Gallego A (1998) Bio-physical modelling of the early life stages of cod and haddock in the North Sea. Fish Oceanogr 7(2):110–215

Hinckley S, Hermann AJ, Megrey BA (1996) Development of a spatially explicit, individual-based model of marine fish early life history. Mar Ecol Prog Ser 139:47–68

Hinckley S, Hermann AJ, Mier KL, Megrey BA (2001) Importance of spawning location and timing to successful transport to nursery areas: a simulation study of Gulf of Alaska walleye Pollock. ICES J Mar Sci 58(5):1042–1052

Hinrichsen HH, Möllmann C, Voss R, Köster FW, Kornilovs G (2002) Biophysical modeling of larval Baltic cod (*Gadus morhua*) growth and survival. Can J Fish Aquat Sci 59: 1858–1873

Hinrichsen HH, Schmidt JO, Petereit C, Möllmann C (2005) Survival probability of Baltic larval cod in relation to spatial overlap patterns with their prey obtained from drift model studies. ICES J Mar Sci 62:878–885

Houde ED (1989) Subtleties and episodes in the early life of fishes. J Fish Biol 35:29–38

Hunter J, Craig P, Phillips H (1993) On the use of random-walk models with spatially-variable diffusivity. J Comp Physiol 106:366–376

Huret M, Runge JA, Chen C, Cowles G, Xu O, Pringle JM (2007) Dispersal modeling of fish early life stages: sensitivity with application to Atlantic cod in the western Gulf of Maine. Mar Ecol Prog Ser 347:261–274

Huse G (2005) Artificial evolution of *Calanus*' life history strategies under different predation levels. GLOBEC Int Newsletter 11(1):19

Leis JM (2007) Behaviour as input for modelling dispersal of fish larvae: behaviour, biogeography, hydrodynamics, ontogeny, physiology and phylogeny meet hydrography. Mar Ecol Prog Ser 347:185–193

Lett C, Veitch J, van der Lingen CD, Hutchings L (2007) Assessment of an environmental barrier to transport of ichthyoplankton from the southern to the northern Benguela ecosystems. Mar Ecol Prog Ser 347:247–259

Mariani P, MacKenzie BR, Visser AW, Botte V (2007) Individual-based simulations of larval fish feeding in turbulent environments. Mar Ecol Prog Ser 347:155–169

Marteinsdottir G, Steinarsson A (1998) Maternal influence on the size and viability of Iceland cod *Gadus morhua* eggs and larvae. J Fish Biol 52(6):1241–1258

Miller TJ (2007) Contribution of individual-based coupled physical–biological models to understanding recruitment in marine fish populations. Mar Ecol Prog Ser 347:127–138

Mullon C, Cury P, Penven P (2002) Evolutionary individual-based model for the recruitment of anchovy (*Engraulis capensis*) in the southern Benguela. Can J Fish Aquat Sci 59:910–922

North EW, Hood RR, Chao SY, Sanford LP (2006) Using a random displacement model to simulate turbulent particle motion in a baroclinic frontal zone: a new implementation scheme and model performance tests. J Mar Syst 60: 365–380

Osborn T (2007) Applicability of turbulence measurement technology to small-scale plankton studies. Mar Ecol Prog Ser 347:139–143

Paradis AR, Pepin P, Brown JA (1996) Vulnerability of fish eggs and larvae to predation: review of the influence of the relative size of prey and predator. Can J Fish Aquat Sci 53: 1226–1235

Paris CB, Chérubin LM, Cowen RK (2007) Surfing, spinning, or diving from reef to reef: effects on population connectivity. Mar Ecol Prog Ser 347:285–300

Peck MA, Daewel U (2007) Physiologically based limits to food consumption, and individual based-modeling of foraging and growth of larval fishes. Mar Ecol Prog Ser 347:171–183

Pepin P (2004) Early life history studies of prey–predator interactions: quantifying the stochastic individual responses to environmental variability. Can J Fish Aquat Sci 61:659–671

Pepin P (2006) Estimating the encounter rate of Atlantic capelin (*Mallotus villosus*) with fish eggs, based on stomach content analysis. Fish Bull 104:204–214

Rothchild BJ, Osborn TR (1988) Small-scale turbulence and plankton contact rates. J Plankton Res 10:465–474

Sentchev A, Korotenko K (2007) Modelling distribution of flounder larvae in the eastern English Channel: sensitivity to physical forcing and biological behaviour. Mar Ecol Prog Ser 347:233–245

Skajaa K, Browman HI (in press) The escape response of food-deprived cod larvae (*Gadus morhua* L.). J Exp Mar Biol Ecol

Skajaa K, Fernf A, Folkvord A (2004) Ontogenetic- and condition-related effects of starvation on responsiveness in herring larvae (*Clupea harengus* L.) during repeated attacks by a model predator. J Exp Mar Biol Ecol 312:253– 269

Thygesen UH, Ådlandsvik B (2007) Simulating vertical turbulent dispersal with finite volumes and binned random walks. Mar Ecol Prog Ser 347:145–153

Vikebø F, Jørgensen C, Kristiansen T, Fiksen Ø (2007) Drift, growth and survival of larval Northeast Atlantic cod with simple rules of behaviour. Mar Ecol Prog Ser 347:207–219

Visser AW (1997) Using random walk models to simulate the vertical distribution of particles in a turbulent water column. Mar Ecol Prog Ser 158:275–281

Werner FE, Perry RI, Lough RG, Naimies CE (1996) Trophodynamic and advective influences on Georges Bank larval cod and haddock. Deep-Sea Res II 43:1793–1822

Werner FE, Quinlan JA, Blanton BO, Luettich RA Jr (1997) The role of hydrodynamics in explaining variability in fish populations. J Sea Res 37:195–212

Vol. 347: 127–138, 2007
doi: 10.3354/meps06973

MARINE ECOLOGY PROGRESS SERIES
Mar Ecol Prog Ser

Published October 11

OPEN ACCESS

Contribution of individual-based coupled physical–biological models to understanding recruitment in marine fish populations

Thomas J. Miller*

Chesapeake Biological Laboratory, University of Maryland Center for Environmental Science, PO Box 38, Solomons, Maryland 20688, USA

ABSTRACT: Annual publications involving the application of coupled physical–biological models for understanding fish recruitment processes have increased over the last decade. Sixty-nine papers were reviewed to assess the contribution these models have made to recruitment prediction and understanding. The majority of models reviewed were 2- and 3-dimensional numerical simulation models, although a limited number of 1-dimensional analytical models were included. Most models used a Lagrangian tracking algorithm to advect and diffuse particles within the model domain. The vertical and horizontal resolutions and temporal durations of the models varied widely. This review identified 3 categories of papers: explanatory, inferential and hypothesis generating. Reviewed papers were dominated by explanatory approaches. Assessment of the sensitivity of model predictions to the model parameters were rare, but not entirely absent in this group of papers. Inferential approaches were the next most common, and sought to infer the presence or role of a particular mechanism. Hypothesis-generating publications were the rarest, but perhaps have the most to contribute to a greater understanding of recruitment processes. An increase in the frequency of hypothesis-generating applications of coupled physical–biological models may be expected over time as the field matures and refinements to both the physical and biological processes included in the models are made.

KEY WORDS: Physical–biological models · Individual-based models · Recruitment · Fish populations · Feeding · Growth · Mortality · Behavior

INTRODUCTION

Since Hjort's (1914) seminal work, understanding the sources of variability in recruitment has been recognized as a central challenge of fisheries research. Understanding recruitment would benefit managers in establishing sustainable patterns of exploitation and provide fundamental insights into the regulation of fish populations generally (Hutchings 2000). Research conducted to date has documented the high and variable rates of mortality that characterize the early life histories of many fish (Houde 1989, Crowder et al. 1992). Changes in these rates are responsible for producing the wide variations in year classes observed in fish populations. Indeed, the principal challenge in predicting recruitment is that only subtle changes in these mortality rates are needed to cause dramatic alterations in year class strengths.

Many hypotheses have been developed that seek to explain and predict the variability in recruitment in fish populations. These hypotheses may be grouped into 3 broad themes: food and growth-related, transport-related and predation-related hypotheses. Cowan & Shaw (2002) and Govoni (2005) provide recent critical reviews of these ideas. Most of the hypotheses in these 3 categories invoke a physical context, thereby implying that understanding recruitment requires coupling physical and biological processes. However, as noted by Myers (1995), the relative coarseness of early biological and physical data prevented direct tests of

*Email: miller@cbl.umces.edu

hypotheses that invoked physical–biological interactions. Thus, initial efforts to understand the physical context in which biological processes occur were largely descriptive (Haury et al. 1978).

Developments over the last 25 yr in both physical oceanography and fish ecology have increased our ability to formulate testable hypotheses regarding the role of physical processes and recruitment. In their review of the contribution of physical processes to fluctuations in marine fish populations, Werner & Quinlan (2002) identified 3 important developments in physical oceanography that have advanced the coupling of physical and biological processes: the ability to collect synoptic data at appropriate spatial and temporal scales, improvements in the understanding of mesoscale ocean processes and the advent of powerful computational abilities. These advances allowed questions at scales appropriate to recruitment (i.e. on the order of 1 to 100 km and 1 to 90 d) to be posed for the first time. Similar substantial changes in ecological studies of recruitment paralleled the changes in physical oceanography. In this context, the most notable of these was the rise of individual-based thinking in fish ecology (DeAngelis & Gross 1992). This paradigm shift led researchers to ask not 'What is the mortality rate?' but rather 'What are the characteristics of the survivors?' (Crowder et al. 1992). Research findings led to the recognition that incorporation of individual variability into recruitment models is essential because survivors are not a random subset of the offspring. Differential offspring survival based on parental influences (Browman et al. 2006), spawning date (Rice et al. 1987), size and growth (Meekan & Fortier 1996), and location (Thorrold et al. 2001) has been documented. Under conditions where individual characteristics vary and are subject to selective sources of mortality, forecasts based on the average are likely to be unreliable (Lomnicki 1992).

The advances in physical oceanography and fish ecology allowed the development of the first individual-level, coupled physical–biological models (ICPBM) of fish early life history in the late 1980s (Bartsch 1988, Bartsch et al. 1989). Others followed quickly, so that by 2001 Werner et al. (2001b) suggested spatially explicit ICPBMs had become the de facto tool for studies of fish recruitment. ICPBMs now play a central role in the majority of large-scale fisheries oceanography programs around the world, e.g. FOCI in Alaska (Megrey et al. 2002), various national GLOBEC programs (Hinrichsen et al. 2002, Lough et al. 2005) and the IDYLE program off South Africa (Mullon et al. 2003). Therefore, it is an appropriate time to assess the contribution of ICPBMs to knowledge of recruitment in fish.

The focus of this review is on the contribution of ICPBMs to improving understanding of recruitment processes in marine fishes. Accordingly, this review does not focus heavily on the physical models, but rather on the integration of the biology with the physics. Those interested in the physical models are referred to Haidvogel & Beckman (1998). This review involved developing a simple classification of physical and biological processes and of scales used in each ICPBM. Based on this classification, I then identified commonalities among the reviewed papers with respect to the core processes of interest and the approach adopted. Finally, I assessed how these approaches affect the range of conclusions that can be drawn, and identified opportunities for future development.

METHODS

I reviewed the literature on the application of ICPBMs since 1989. The choice of 1989 was arbitrary, but was made to include the first broadly published example of the genre, that of Bartsch et al. (1989). The review was not an exhaustive list of contributions, but rather an unbiased sample of contributions selected to provide the foundation for a critical assessment of the different approaches that have been taken. Citations to be included in the review were selected in 2 phases. In the first phase, publications were identified using a keyword search of the ISI Web of Knowledge online database. Several search strings were used to identify likely publications. In the second phase of the literature search, I identified papers cited in or citing those publications identified in the first phase. In total, this process yielded 69 studies, published between 1989 and 2006. A full list of the citations is provided in Appendix 1 (available at: www.int-res.com/articles/suppl/m347p127_app.pdf) and the data extracted from each citation is provided in Appendix 2 (available at www.int-res.com/articles/suppl/m347p127_app.xls).

All publications were categorized according to objective, approach, biological processes physical forcing and scale (Appendix 2). The physical models were identified with respect to the model framework, domain, horizontal and vertical resolution, temporal resolution, environmental forcing and the particle-tracking algorithm. The biological components of the model were identified as to the focal species, how the processes of feeding, growth and mortality were represented, behavioral representation and the tracking duration. Once these fundamental properties had been identified, the objective of each paper was classified as either: distribution, transport/retention, spawning-site selection, growth and survival, or feeding. These are hierarchical categories because, for example, all models involved questions of distribution. Thus, models focusing on growth and survival are a subset of models

involving distribution. Similarly, most models of feeding were a subset of models of growth and survival. Finally, 3 categories of approach were recognized: explanatory, inferential and hypothesis generating. I characterized explanatory applications as those that sought to provide an explanation of an observed empirical pattern. Inferential approaches sought to quantify the relative contribution of different processes to producing the observed pattern, and had to include simulation with different levels of biological or physical factors. Hypothesis-generating approaches were those that led to hypotheses that could be tested either within the model itself or by independent empirical observations. A full listing of the data extracted from the review is provided in Appendix 2.

RESULTS

The literature review documented the increase in the use of ICPBMs in studies of fish recruitment since 1989 (Fig. 1). Not surprisingly, although ICPBMs have been developed for a range of different ecosystems, application of these models has been concentrated in areas that support industrialized fisheries: the Northeast Atlantic shelf, the Northwest Atlantic shelf and the Alaskan shelf (Table 1). Together, these 3 regions accounted for almost three-quarters of the reviewed papers. The majority of the remaining areas are mid- to high-latitude systems: only 3 studies involved tropical or subtropical systems.

Hydrodynamic modeling

Hydrodynamic processes have been represented in several different ways in ICPBMs (Appendix 2). The majority of the hydrodynamic models were 3-dimensional, numerical simulation models that represent the domain of interest as a series of discrete, small spatial elements. The numerical simulation models differed principally in the algorithm used to solve the hydrostatic primitive equations (finite difference vs. finite element) and in how the spatial elements were defined. Many of the early models were based on Geophysical Fluid Dynamics Laboratory modular ocean models (Bryan 1969, Cox 1984) that use the finite difference algorithm and fixed depth levels. A popular early implementation of this code was the Hamburg Shelf Ocean Model (HAMSOM), which has been parameterized for several different spatial domains (Bartsch & Coombs 1997, Gallego et al. 1999, Hislop et al. 2001, Hao et al. 2003). This modeling approach continues to see use, most recently in a series of papers by Hinrichsen and colleagues (Voss et al. 1999, Hinrichsen et al. 2001, 2002, 2003a,b, 2005, Koster et al. 2001). As a result of the use of fixed depth levels in these models, particular care has to be taken in matching the depth layers selected with the bathymetry. One approach to overcoming this challenge has been to use a terrain-following coordinate system in which depth is represented as a percentage of the total water column depth at any point. Such terrain-following, primitive equation models were also common in the review (Hinckley et al. 1996, 2001, Sætre et al. 2002, Adlandsvik et al. 2004). Most recently, this terrain-following scheme has been implemented in the Regional Ocean Model System (ROMS), for which applications have been increasing (Mullon et al. 2002, Huggett et al. 2003, Vikebo et al. 2005). Models that represent depth indirectly as isopycnals (constant density surfaces) have also been used (Paris et al. 2005, Cowen et al. 2006), although these were less common. The other principal 3-dimensional numerical simulation models were ones that used a finite element (FEM) algorithm rather than the finite difference scheme. These FEM models share a common heritage (Lynch et al. 1996), and have been implemented for the Northwest Atlantic shelf (Werner et al. 1994, Lough et al. 2005) and the mid-Atlantic Bight (Quinlan et al. 1999, Stegmann et al. 1999). A small number of ICPBMs that did not use numerical

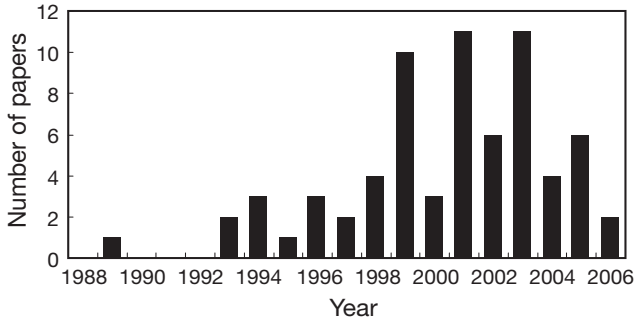

Fig. 1. Publication year of papers included in the review (listed in Appendix 1)

Table 1. Distribution of reviewed individual-level, coupled physical–biological models (ICPBM) by ocean region

Ocean region	Number of studies
NE Atlantic shelf (including North Sea, Baltic Sea and Bay of Biscay)	27
NW Atlantic shelf (including Georges Bank, Grand Banks and Scotian Shelf)	17
NE Pacific (including Alaskan shelf)	6
Western Atlantic shelf	6
SE Atlantic	5
NW Pacific	2
SW Pacific	2
W Pacific	1
Caribbean	2
Gulf of Mexico	1

simulation models as their foundation were identified in the review. These approaches include coarser scale box-models (Maes et al. 2005) or data-driven frameworks (Heath et al. 1998, Reiss et al. 2000, Helbig & Pepin 2002).

The spatial and temporal scales of the hydrographic models varied over several orders of magnitude (Appendix 2). The spatial scale of the model is critical to its ability to resolve features that may play important roles in the ecology of larval fish (Helbig & Pepin 2002). The finest horizontal resolution reported was 0.005 km (Brown et al. 2004), the coarsest 150 km (Suda & Kishida 2003). The distribution of horizontal resolutions was multimodal, likely reflecting the heritage of different hydrographic models rather than 'choices' by researchers of the resolution that was most appropriate for the question being studied. Surprisingly, there was no trend for models to become more highly resolved over time. The vertical resolution of models was much finer than their horizontal resolution, but also varied considerably. Determination of the finest vertical resolution used was problematical in S-coordinate models, which report the layers with regard to the fraction of the total water column. However, it is likely that the minimum vertical resolution was on the order of 1 m (North et al. 2005).

Several time scales can be identified to characterize hydrodynamic models. The numerical simulation models often used complex, time-stepping algorithms to ensure solution stability. However, for many models it was possible to determine a temporal resolution at which flow fields were estimated. Time steps varied widely from seconds (North et al. 2005) to on the order of an hour. In contrast to the numerical simulations, the simpler box model and matrix projection approaches (Suda & Kishida 2003, Maes et al. 2005) often had daily time steps. The other temporal scale of importance is the time scale at which environmental forcing was applied in the model. These time scales varied from hourly to daily (Appendix 2). Models were forced by a variety of environmental forcing functions (Appendix 2). The majority of models included forcing from M2 tides, wind stress and inflow. In many cases, models were driven by synoptic data from the model domain collected for the time period modeled; in other cases, climatological forcing was employed.

Coupling hydrodynamics and biology

Although described as coupled physical–biological models, the coupling of numerical simulation models was typically offline rather than in real time for computational reasons (see Hinckley et al. 1996 for a comparison of different coupling schemes). In this scheme, runs of the hydrodynamic model are completed and output is stored at set intervals. The stored flow fields are then used by the individual-based biological model to move and track individual eggs and larvae throughout the model domain. The adequacy of these particle-tracking algorithms is at the heart of the reliability of forecasts from ICPBMs. The principal challenge to these particle-tracking algorithms is to provide subgrid-scale resolution of fluid flows, as the horizontal and vertical spatial resolution of the hydrodynamic models (discussed above) are several orders of magnitude larger than the length scales of typical larvae (3 to 10 mm). This mismatch of scales challenges modelers in capturing small-scale features of the flow critical to larval behavior (Fiksen & MacKenzie 2002) or egg and larval distributions (Helbig & Pepin 2002). Because of stochasticity at subgrid scales, there is an ensemble of trajectories for each starting location. Early models used a simple scheme that updates the position of tracked particles based on spatially interpolated model velocities with small random components (Bartsch & Knust 1994). As the field has developed, the particle-tracking algorithms have become more sophisticated, with increasing attention being paid to the statistical aspects of subgrid-scale motion (Heath et al. 1998). Even when the model incorporates the correct statistical distribution of subgrid-scale motion, proper interpretation of the distribution of trajectories of individual larvae remains challenging (Brickman & Smith 2002).

As a result of uncertainties in the forecasted trajectories, the duration over which early life stages are tracked was an important feature of the models. Here, models diverged markedly owing to their differing objectives. For example, Fiksen & MacKenzie (2002) followed the fates of individual larvae for only 1 d in their work to explore the processes regulating feeding ecology of Atlantic cod *Gadus morhua* (hereafter 'cod') on Georges Bank. In contrast, several authors ran their hydrodynamic model over multiple years. In particular, Cowen et al. (2006) tracked the fates of larval reef fishes in the Caribbean produced by sequential monthly spawnings over a 5 yr period to estimate the connectivity among local populations on different island reef systems. However, the majority of tracking durations were for periods of <120 d, a time frame typical for early life-history stages of many species to carry out transition from plankton to nektonic or demersal habits.

Biological modeling

Taxonomically, the papers in the review were dominated by commercially important gadoid species (Fig. 2, Appendix 2). Studies of cod, haddock

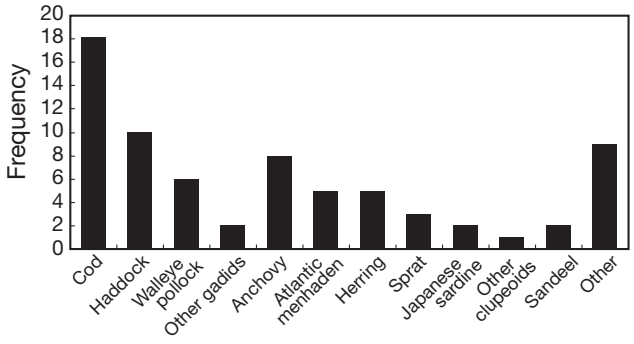

Fig. 2. Taxonomic distribution of species studied in reviewed models (listed in Appendix 2)

Melanogrammus aeglefinus and walleye pollack *Theragra chalcogramma* accounted for almost half (34) of the reviewed publications. The focus on these species reflects management interests rather than that these species are necessarily representative of ecological processes occurring in a broad class of species.

Biological representation within the model was characterized to assess the ability of the model to test the feeding-, transport- and predation-related recruitment hypotheses described above (Table 2). Not all models included feeding or growth processes. Approximately one-fifth (20.6%) of reviewed papers included feeding as a process within the individual-based model (IBM). All feeding routines included prey selection to some extent. Some models included a highly detailed and mechanistic description of feeding (Megrey & Hinckley 2001, Fiksen & MacKenzie 2002, Hinrichsen et al. 2003b, Lough et al. 2005). For example, Fiksen & MacKenzie (2002) developed a highly detailed model of the feeding process that modeled prey encounter and capture as explicit functions of light, turbulence, prey size and vagility, and of larval feeding behavior. Other representations of the feeding process were coarser. For example, Werner et al. (1996) used empirical relationships (Laurence 1978) to drive search and ingestion in their IBM. While almost a quarter of all reviewed papers included a process-level description of feeding, only approximately one-half of these papers included any dynamics in the prey community. As with the feeding process itself, how prey dynamics were modeled varied. For example, Bartsch & Combs (2004) used satellite-derived sea-surface temperature and chlorophyll fields to model the abundance of *Calanus* and *Acartia*, principal prey for larval mackerel *Scomber scrombrus.* Other researchers based the prey field on data interpolated from field collections (Lough et al. 2005).

Table 2. Distribution of representation of biological processes in ICPBMs. Note that proportions do not sum to 1 because multiple processes are represented in individual models

Process	Proportion
Feeding	0.206
Prey selection	0.188
Prey dynamics	0.101
Age	0.838
Growth	0.367
Mortality	0.308
Behavior	0.433

Growth is an emergent property of bioenergetic processes that is expressed in changes in size at age. Given the central role of size-dependent processes in fish early life history, it was anticipated that growth would be a common feature of ICPBMs. Yet only 36.7% of all reviewed studies included a growth component (Table 2). Two broad approaches to modeling growth were evident. In one approach growth was forecast based on the temperature field predicted by the hydrographic model (Heath & Gallego 1997, 1998, Brickman & Frank 2000). Alternatively, growth was modeled mechanistically with surplus energy from feeding (after meeting metabolic requirements) being allocated to growth (Werner et al. 1996, 2001a, Hinckley et al. 2001). Bartsch & Coombs (2004) employed an empirical growth model that was both temperature and food dependent.

All models reviewed were spatially specific, either implicitly or explicitly, and thus all dealt with the transport, retention, or distribution of eggs and larvae to some degree. Of the 69 reviewed papers, 10 were implicitly spatial and did not determine the precise location of early life stages in the model domain. These papers did not seek to explicitly test transport-related hypotheses. Rather, these papers dealt with issues of habitat selection (Lough & Manning 2001, Suda & Kishida 2003, Maes et al. 2005). In contrast the 59 other papers explicitly studied the consequences of transport of the early life-history stages of fish. These papers sought to explain or understand the role of transport and/or the retention of early life stages from spawning sites or to nursery grounds (Berntsen et al. 1994, Shackell et al. 1999, Reiss et al. 2000, Mullon et al. 2002, Hinrichsen et al. 2003b). Larval behavior can have a significant impact on their subsequent locations. Accordingly, 43.3% of the reviewed papers included some degree of larval behavior. The most common behavior included in models was age-dependent vertical migration (Heath et al. 1998, Hinckley et al. 2001, Adlandsvik et al. 2004). Light was also commonly used as a behavioral cue for vertical migration (Bartsch & Knust 1994, Pedersen et al. 2003, Hinrichsen et al. 2005).

The final class of hypotheses relating to fish recruitment invoke predation of eggs and larvae as a principal agent. Only 30.8% of the reviewed studies

included any egg or larval mortality in their formulations (Table 2). Of the 22 papers that included mortality, 8 considered only starvation mortality and not predation mortality directly (Werner et al. 1993, 2001a, Hinckley et al. 1996, 2001, Hinrichsen et al. 2002, 2003b). Of the others, the majority of models used general temperature-dependent (Mullon et al. 2002, 2003) or weight-dependent (Heath & Gallego 1998, Brickman & Frank 2000, Brickman et al. 2001) empirical relationships to represent mortality. Only Maes et al. (2005) included a dynamic predator–prey relationship; they were able to do so because they used a box-modeling approach rather than a detailed hydrodynamic model.

Model applications

In reviewing published papers for this review, 3 categories of application of ICPBMs could be recognized: explanatory, inferential and hypothesis generating (Table 3). In the section that follows, I identify the characteristics of each approach and review a limited number of examples of each.

Explanatory applications of ICPBMs were the first to appear in the literature. Fifty-eight percent of reviewed papers was deemed to be explanatory in nature. In explanatory applications, researchers sought to explain observed patterns in the spatial arrangement of the early life stages of fish. However, the comparison between observed patterns and those predicted by the models was at most qualitative in nature and rarely involved an assessment of the sensitivity of predictions to parameter values. Werner et al.'s (1993) groundbreaking work on the transport of cod and haddock 'eggs' on Georges Bank is a clear example of this approach. Werner et al. (1993) used a finite element model with an adaptive mesh to model springtime flows on Georges Bank. Coupling of physical and biological models occurred offline, with the calculated flow fields for the entire tracking period serving as inputs to an IBM. Within the IBM, passive particles representing cod and haddock eggs were released at known spawning times at depths of 1, 30, or 50 m and tracked using a Lagrangian stochastic particle-tracking model. Inclusion of vertical migration behavior decreased the probability of retention. The results from the ICPBM clearly indicated that only eggs released at 50 m were retained on the bank and completed a movement onto the northwest flank of the bank 90 d after release. In a second explanatory application, Voss et al. (1999) used an ICPBM to explain movement of cod larvae between ichthyoplankton surveys. They used a fixed-layer, finite-difference model with 28 depth levels and an approximately 5 km horizontal resolution to reproduce the hydrography of the Baltic Sea. Virtual cod larvae were released in a pattern that represented the distribution of cod larvae observed in the southern Baltic in August 1991, based on ichthyoplankton sampling. The particles in the model were tracked for 21 d, and then the distribution of cod predicted by the model was qualitatively compared to that observed during a second ichthyoplankton survey. Voss et al. concluded that drift simulations explained the change in distributions observed between the 2 survey dates. Explanatory ICPBMs have played an important role in furthering our understanding of retention and transport in the early life histories of fish. But it is important to note that the agreement between observed and predicted data does not imply that the mechanisms operating in the model are equivalent to those operating in the field.

Table 3. Proportion of approaches in the application of ICPBMs to studies of fish early life history

Approach	Proportion
Explanatory	0.579
Inferential	0.304
Hypothesis-generating	0.116

A second category of application employs ICPBM to infer the importance of particular processes or mechanisms. By this very definition, the approach compares alternative scenarios or parameter sets to determine which is more likely to occur in nature. This is a more powerful application of models and lends itself to hypothesis testing. Thirty percent of reviewed papers adopted an inferential approach. In one example, Brickman & Frank (2000) compared predictions of 2 alternative mortality models on the distribution, development and abundance of haddock cohorts in the Browns Bank–Bay of Fundy region off Nova Scotia, Canada. Hydrography in the model was predicted by a 3-dimensional, finite-element QUODDY model. Coupling the flow field produced by the hydrodynamic model and the individual-based biological model was achieved using a Lagrangian stochastic particle-tracking algorithm, Brickman & Frank (2000) compared the results of integrated and stage-specific mortality schemes in the IBM. By comparing modal characteristics of predicted and observed cohorts, they concluded that a stage-based mortality model was required to accurately represent cohort dynamics and recruitment. In a second example of an inferential application of an ICPBM, Fiksen & MacKenzie (2002) implemented a biological IBM with readily interpretable biological parameters within the flow fields calculated by the 3-dimensional FEM of Georges Bank used by Werner et al. (2001a). Fiksen & MacKenzie

(2002) contrasted the implications of different feeding models. They concluded that the different feeding models yielded different predictions regarding prey selectivity and the conditions under which larval cod experience prey limitation.

The final application category of ICPBMs was the rarest, but is perhaps the one that has the most to contribute to understanding recruitment. In these applications, ICPBMs were used to develop testable hypotheses that could be investigated either within an ICPBM framework or with independent, empirical data. Only 11% of reviewed papers adopted this approach. Two examples suffice to illustrate the power of the approach. Mullon et al. (2002) used an ICPBM to test hypotheses regarding the evolution of spawning sites and periods for anchovy *Engraulis capensis*. They implemented a 3-dimensional ROMS model of the Benguela ecosystem to generate climatological flow fields. The flow fields served as inputs to an IBM that tracked the trajectories of egg and larval anchovy. Lagrangian stochastic tracking generated differences among the trajectories followed by different cohorts of larvae. Mullon et al. (2002) postulated a simple evolutionary rule that larvae that successfully reached the known nursery area demonstrated natal fidelity, returning to their own spawning location to reproduce. To test hypotheses as to why observed spawning locations had become favored, Mullon et al. (2002) defined recruitment 'success' such that larvae could not be advected offshore, had to reach the nursery area within 30 to 60 d and could not have experienced temperatures <14°C. Larvae that successfully reached known nursery areas followed a simple rule of natal site fidelity in selecting where to spawn. Mullon et al. (2002) then quantified the 'evolution' of spawning sites over 60 generations. They found that only advection and temperature constraints were required to yield a strong convergence of observed and predicted spawning locations and dates. A second example of the hypothesis-generating application of ICPBMs demonstrates how such models could be used to generate hypotheses that could be tested external to the model. Quinlan et al. (1999) used an ICPBM to identify potential spawning sites of Atlantic menhaden *Brevoortia tyrannus* that recruit to estuarine nursery areas along the US mid-Atlantic Bight. They predicted that recruits to 3 potential nursery areas (Delaware Bay, Folly Inlet and Chesapeake Bay), but spawned in the same location, should differ in age at entry to the nursery by specific amounts. Alternatively, individuals that recruit to the 3 different nursery areas at the same age on the same day should be drawn from different spawning locations. These hypotheses are currently being tested using otolith microchemical and birthdate frequency analysis of recruits to 2 of the 3 nursery areas.

DISCUSSION

ICPBMs have contributed significantly to our understanding of recruitment processes in marine fish populations, particularly with regard to transport and retention. Their application has evolved rapidly over the past quarter of a century. Initially, development of a numerically stable, highly parameterized model that could reproduce patterns in the distribution and characteristics of the early life-history stages of fish was in itself a significant achievement. More recently, these models have become increasingly more spatially resolved and have included more biological detail. In parallel with increases in model sophistication there has been a change in the use of ICPBMs from a largely explanatory role to one of hypothesis generation. These developments of ICPBMs in fisheries have paralleled changes in the development and use of models in other ecological fields (Kingsland 1985). For example, Gentleman (2002) suggested that models of plankton dynamics evolved from descriptive to hypothesis-testing tools between the 1940s and the turn of the century. Not surprisingly, this field also experienced the development of coupled physical–biological models (Capella et al. 1992) and Lagrangian tracking algorithms (Ishizaka & Hofman 1988). The success of models in other ecological fields suggests cause for optimism for the future of ICPBMs in studies of fish recruitment.

ICPBMs show great potential benefit in understanding recruitment, because they inherently involve variation induced by local interactions between individuals and their resources, a key justification for individual-based approaches in ecology (Grimm & Railsback 2005). Transport-related recruitment hypotheses clearly meet this criterion. Individual eggs and larvae have different experiences and fates because they follow different spatial trajectories (Heath & Gallego 1997). Thus, addressing transport-related hypotheses requires individual-based approaches, whether in modeling or field studies. ICPBMs have allowed researchers to identify potential spawning locations (Quinlan et al. 1999, Bruce et al. 2001), quantify patterns of retention within spawning locations (Werner et al. 1993, Hermann et al. 1996, Brickman et al. 2001, Stenevik et al. 2003) and transport from spawning locations to potential nursery areas (Heath & Gallego 1998, Allain et al. 2001, Adlandsvik et al. 2004, Brown et al. 2004) for specific systems. Despite the success of ICPBMs in generating patterns similar to those observed in individual systems, these models have yet to be used to conduct strong tests of individual recruitment hypotheses, largely because of ongoing challenges related to the number of and duration over which individuals can be tracked and the need to close the life cycle. Few

of the 69 papers reviewed included spawning dynamics, and only 5 were multigenerational. Not surprisingly, all of these multigenerational models were either inferential or hypothesis generating. However, none specifically tested classical hypotheses related to the determination of year class strength. If ICPBMs are to be used to test such hypotheses, it is critical that they are developed as a part of whole life cycle models as has been accomplished by Rose and colleagues in the ecological literature using either solely IBMs (Rose et al. 1999b) or IBMs as a component in a nested modeling approach (Rose et al. 2003). Development of a nested modeling approach to addressing biological oceanographic questions generally would likely be most effective for recruitment questions (deYoung et al. 2004).

However, it is important to note that the reliability of findings from these models relies on the accuracy of the hydrographic model and the adequacy of the tracking algorithms. Recently, Friedrichs et al. (2006) have highlighted concerns regarding the impact of alternative hydrodynamic models on forecasts from coupled physical–biological models at the ecosystem scale. While impacts of alternative hydrodynamic models on the forecasts at this scale may be expected, because the models are often coupled in real time, rather than offline as is more common for early life history ICPBMs, there was no indication in the literature that such impacts have been considered.

Particle-tracking schemes have also received considerable attention. Brickman & Smith (2002) identify 2 concerns relating to particle tracking, which they term underseeding problems. Both concerns relate to the number of particles that must be tracked. The first concern is that sufficient particles must be tracked so that their ensemble average accurately (and hopefully precisely) reflects the true underlying distribution of the transport process. The second concern relates to the probability of detecting rare events in a stochastic process. Brickman & Smith (2002) discuss both problems in terms of the relative size of the spawning and nursery areas. If spawning and nursery areas are coincident and large, then only a small number of particles and a few simulations may be needed, because we are trying to estimate the average of a process. In contrast, if the spawning area is large and the nursery area is small, considerably more particles and a large number of simulations may be needed, because we are trying to estimate the rare event of reaching the nursery area. Brickman & Smith (2002) suggest tests that could be used to determine the adequacy of the number of particles and trials used. Few researchers appear to have considered this aspect of ICPBMs, and it deserves more attention.

To the extent that food-related and predation-related hypotheses rely on spatially generated differences, addressing these 2 questions may require individual-level approaches. ICPBMs induce variability in growth from spatially explicit differences induced by temperature (Heath & Gallego 1998, Brickman & Frank 2000) or the prey field exploited (Werner et al. 1995, Lough et al. 2005). However, the majority of ICPBMs have assumed that this is the only source of individual variability. Yet variation can arise from other processes. For example, there are likely inherent differences among larvae that will produce different growth patterns even under identical environmental conditions. In the presence of size-dependent sources of mortality, common in early life history (Miller et al. 1988), this inherent inter-individual variability can have important consequences (Rice et al. 1993). Although this is widely appreciated in IBMs developed in the field of fish ecology (DeAngelis et al. 1980, Cowan et al. 1993, Rice et al. 1993, Rose & Cowan 1993, Cowan et al. 1996, Letcher et al. 1996, Rose et al. 1999a), variation of this sort is much less frequently evident in ICPBMs (Hinckley et al. 1996). This omission may be particularly important as it is likely that recruitment is not regulated by a single mechanism, but rather results from the interaction of multiple mechanisms (Crowder et al. 1992, Cowan & Shaw 2002). Accordingly, not including inter-individual variability in vital rates may limit the utility of ICPBMs to address recruitment hypotheses other than transport-related ones. The consequences of this assumption must be assessed.

There have been 2 different approaches to exploring feeding and growth-related recruitment hypotheses in ICPBMs. One approach uses the temperature field predicted from the hydrographic model to predict growth. This approach is motivated by concerns over the accuracy of the representation of subgrid-scale processes in the hydrographic model. The conservative nature of temperature means that it is less sensitive to subgrid-scale concerns. The approach also has the advantage that there is no need to model prey populations. However, there are also potential pitfalls to this approach if the underlying temperature-dependent growth model is incorrectly parameterized, or applied to a population for which it was not developed (Folkvord 2005). The approach also implicitly assumes that there is no restriction on food-dependent growth variation. The alternative approach is to specifically model consumption and bioenergetic processes. This has the advantage of directly linking the prey field and environment to forecasted growth, a central feature of many feeding-related recruitment hypotheses (MacKenzie et al. 1994). This approach has been used to infer the importance of small-scale turbulence on larval feeding (Werner et al. 2001a) and the potential for prey limitation (Fiksen & MacKenzie 2002). However, the pro-

cess-level approach also faces significant challenges. The approach relies on extending hydrographic forecasts to subgrid scales that are perhaps 2 to 4 orders of magnitude smaller than the minimum horizontal resolution of the models. Even were this not a concern, encounter processes between planktonic predators and prey are generally not well understood, and are a focus of considerable research (Visser & Kiorboe 2006). However, inferential approaches can be used to select among alternative parameterizations (Megrey & Hinckley 2001, Fiksen & MacKenzie 2002, Lough et al. 2005). Thus, the application of process-specific ICBPMs may help inform our understanding of the importance of individual steps in the feeding cycle on recruitment.

Predation-related recruitment hypotheses have received little attention within an ICPBM framework (Maes et al. 2005). Two reasons likely account for the lack of attention. First, potential predators are highly vagile and their distribution and behavior is not driven by hydrography. In a hydrodynamic context, predators represent the crossing streamlines problem. However, this should not be a barrier to the inclusion of predators in ICPBMs. Predators have been included in spatially explicit IBMs in the ecological field (Rose et al. 1999b). Inclusion of predation will require consideration of whether and how potential predators respond to the distribution of the eggs and larvae modeled in the ICPBM and may require inclusion of alternative prey. Coupled NPZ-ICPBMs that include multiple trophic levels have already been developed (Hermann et al. 2001), suggesting that it is possible. Coupling of additional trophic levels to such models, while undoubtedly difficult, will be required if predation-related hypotheses are to be considered. The second barrier to inclusion of predation, or any mortality source, in ICPBMs has been concerns over the number of particles that must be tracked. Super-individual approaches (Scheffer et al. 1995) are one approach to overcoming this concern. Although widely used in ecological IBMs (Bunnell & Miller 2005), super-individuals have seen little use in ICPBMs (Hinckley et al. 1996, Bartsch & Coombs 2004, Bartsch et al. 2004). This approach allows individual particles in a model to represent a large number of individual organisms. While there are challenges to how variability is represented within the super-individual, this approach does permit a realistic population of potential recruits to be followed.

One reason that individual-based approaches have been successful in fish ecology has been the adoption of the 'characteristics of the survivors' approach, which relies on successive comparison of survivors with the distribution from which they were drawn (Meekan & Fortier 1996). Use of ICPBMs in hindcasting mode has been effective in determining potential spawning sites (Quinlan et al. 1999, Hislop et al. 2001). However, the hindcasting approach offers the potential to circumvent the challenge of incorporating mortality discussed above, because by definition those individuals that have reached a nursery ground are survivors. There are certainly limitations on when a hindcasting approach can be used in ICPBMs. For example, hindcasting trajectories of survivors will not result in a single-source location, but rather will generate a probability distribution of possible locations. This approach will lead to the development of a specific hypothesis that could then be tested in either other forward-projecting ICPBMs or with independent, empirical data.

Although not a focus of this review, the reliability of hydrodynamic models should not ignored. It is important that the model resolves the physical processes at a sufficient scale to allow pertinent physical and biological processes to be expressed. In particular, the biological processes of interest likely occur at scales many times smaller than the resolution of the physical model. Larval behaviors, which have been shown to have important ramifications on the distributions and fates of larvae in ICPBMs (Hare et al. 1999), all occur on subgrid scales. Indeed the behaviors and cues that elicit them are generally poorly understood for fish larvae (Weissburg & Browman 2005). Generally, the data that are available are from highly artificial laboratory experiments, which may not be relevant to field conditions. Even the extent to which physical processes are resolved may be problematical. For example Helbig & Pepin (2002) resampled high-frequency radar data at different scales to force an advection–diffusion model of Conception Bay, Newfoundland. Helbig and Pepin were interested in the effects of the temporal and spatial resolution of the hydrographic model on the prediction distribution of fish eggs. They found that significant deviations between observed and predicted distributions occurred at model resolutions as low as 3 km. Their results suggest that even sophisticated hydrographic models may not sufficiently resolve physical processes to permit accurate forecasts of ichthyoplanktonic distributions, yet the principal use to date of ICPBMs is in addressing transport-related hypotheses.

In summary, ICPBMs are maturing and will continue to be an important tool in furthering our understanding of recruitment. If they are to fulfill this potential, several trends should be encouraged. We should also encourage an expansion of focus from questions of distribution and transport toward strong tests of specific recruitment hypotheses. This can be helped by development of ICPBMs for different systems that use the same model structure. There should also be an evaluation of whether the failure to include sources of individual variation other than spatially induced ones

biases the forecasts of ICPBMs. This question can most easily be addressed by encouraging the adoption of inferential and hypothesis-generating approaches. The time for using ICPBMs to describe a single realization of a recruitment event is past. There should be increased attention on the impacts of uncertainty in parameter estimates on model predictions. This uncertainty can be addressed by using experimental design tools to structure ICPBM simulations (Hinckley et al. 2001) and to guide analysis of the rich and complex results these models produce. Only when ICPBMs are used as inferential or hypothesis-generating platforms and when parameter uncertainty is specified and accounted for fully will ICPBMs be able to provide the strong tests of hypotheses relating to recruitment mechanisms of which they are capable.

Acknowledgements. The author thanks the conveners for the invitation to participate in and support for attending the conference. The ideas expressed herein are my own, but they have benefited from discussions with many people. I thank in particular J. Dower, A. Folkvord, B. Leggett, B. MacKenzie, P. Pepin, J. Rice, K. Rose and C. Werner. This work was supported in part by a grant from the NOAA Chesapeake Bay Office (NA05NMF4571257). This is contribution number 4082 of the University of Maryland Center for Environmental Science Chesapeake Biological Laboratory.

LITERATURE CITED

Adlandsvik B, Gundersen AC, Nedreaas KH, Stene A, Albert OT (2004) Modelling the advection and diffusion of eggs and larvae of Greenland halibut (*Reinhardtius hippoglossoides*) in the north-east Arctic. Fish Oceanogr 13:403–415

Allain G, Petitgas P, Lazure P (2001) The influence of mesoscale ocean processes on anchovy (*Engraulis encrasicolus*) recruitment in the Bay of Biscay estimated with a three-dimensional hydrodynamic mode. Fish Oceanogr 10:151–163

Bartsch J (1988) Numerical simulation of the advection of vertically migrating herring larvae in the North Sea. Meeresforschung 32:30–45

Bartsch J, Coombs S (1997) A numerical model of the dispersion of blue whiting larvae, *Micromesistius poutassou* (Risso), in the eastern North Atlantic. Fish Oceanogr 6:141–154

Bartsch J, Coombs SH (2004) An individual-based model of the early life history of mackerel (*Scomber scombrus*) in the eastern North Atlantic, simulating transport, growth and mortality. Fish Oceanogr 13:365–379

Bartsch J, Knust R (1994) Simulating the dispersion of vertically migrating sprat larvae (*Sprattus sprattus* (L.)) in the German Bight with a circulation and transport model system. Fish Oceanogr 3:92–105

Bartsch J, Brander K, Heath M, Munk P, Richardson K, Svendsen E (1989) Modeling the advection of herring larvae in the North Sea. Nature 340:632–636

Bartsch J, Reid D, Coombs SH (2004) Simulation of mackerel (*Scomber scombrus*) recruitment with an individual-based model and comparison with field data. Fish Oceanogr 13:380–391

Berntsen J, Skagen DW, Svendsen E (1994) Modelling the transport of particles in the North Sea with reference to sandeel larvae. Fish Oceanogr 3:81–91

Brickman D, Frank KT (2000) Modelling the dispersal and mortality of Browns Bank egg and larval haddock (*Melanogrammus aeglefinus*). Can J Fish Aquat Sci 57:2519–2535

Brickman D, Smith PC (2002) Lagrangian stochastic modeling in coastal oceanography. J Atmos Ocean Technol 19:83–99

Brickman D, Shackell NL, Frank KT (2001) Modelling the retention and survival of Browns Bank haddock larvae using an early life stage model. Fish Oceanogr 10:284–296

Browman HI, St-Pierre JF, Skiftesvik AB, Racca RG (2006) Behaviour of Atlantic cod (*Gadus morhua*) larvae: an attempt to link maternal condition with larval quality. In: Browman HI, Skiftesvik AB (eds) The big fish bang: proceedings of the 26th annual larval fish conference. Institute of Marine Research, Bergen, p 71–95

Brown CA, Holt SA, Jackson GA, Brooks DA, Holt GJ (2004) Simulating larval supply to estuarine nursery areas: How important are physical processes to the supply of larvae to the Aransas Pass Inlet? Fish Oceanogr 13:181–196

Bruce BD, Condie SA, Sutton CA (2001) Larval distribution of blue grenadier (*Macruronus novaezelandiae* Hector) in south-eastern Australia: further evidence for a second spawning area. Mar Freshw Res 52:603–610

Bryan K (1969) A numerical model for the study of the circulation of the world ocean. J Phys Oceanogr 15:1312–1324

Bunnell DB, Miller TJ (2005) An individual-based modeling approach to per-recruit models: blue crab *Callinectes sapidus* in the Chesapeake Bay. Can J Fish Aquat Sci 62:2560–2572

Capella JE, Quetin LB, Hofman EE, Ross RM (1992) Models of the early life history of *Euphausia superba*—Part II. Lagrangian calculations. Deep-Sea Res 39:1201–1220

Cowan JH Jr, Shaw RF (2002) Recruitment. In: Fuiman LA, Werner RG (eds) Fishery science: the unique contribution of early life stages. Blackwell Science, Oxford, p 88–111

Cowan JH Jr, Rose KA, Rutherford ES, Houde ED (1993) Individual based model of young-of-the-year striped bass population dynamics. II. Factors affecting recruitment in the Potomac River, Maryland. Trans Am Fish Soc 122:439–458

Cowan JH Jr, Houde E, Rose K (1996) Size-dependent vulnerability of marine fish larvae to predation: an individual-based numerical experiment. ICES J Mar Sci 53:23–37

Cowen RK, Paris CB, Srinivasan A (2006) Scaling of connectivity in marine populations. Science 311:522–527

Cox MD (1984) A primitive equation 3-dimensional model of the ocean. Report No. 1, Princeton University Press, Princeton, NJ

Crowder L, Rice J, Miller T, Marschall E (1992) Empirical and theoretical approaches to size-based interactions and recruitment variability in fishes. In: Individual based models and approaches in ecology: populations, communities, and ecosystems. Chapman & Hall, London, p 237–255

DeAngelis D, Gross L (1992) Individual based models and approaches in ecology: populations, communities, and ecosystems. Chapman & Hall, London

DeAngelis D, Cox D, Coutant C (1980) Cannibalism and size dispersal in young-of-the-year largemouth bass: experiment and a model. Ecol Model 8:133–148

deYoung B, Heath M, Werner FE, Chai F, Megrey BA, Monfray P (2004) Challenges of modelling ocean basin ecosystems. Science 304:1463–1466

Fiksen Ø, MacKenzie BR (2002) Process-based models of feeding and prey selection in larval fish. Mar Ecol Prog Ser 243:151–164

Folkvord A (2005) Comparison of size-at-age of larval Atlantic cod (*Gadus morhua*) from different populations based on size- and temperature-dependent growth models. Can J Fish Aquat Sci 62:1037–1052

Friedrichs MAM, Hood RR, Wiggert JD (2006) Ecosystem

model complexity versus physical forcing: quantification of their relative impact with assimilated Arabian Sea data. Deep-Sea Res Part II 53:576–600
Gallego A, Heath MR, Basfrod DJ, MacKenzie BR (1999) Variability in growth rates of larval haddock in the northern North Sea. Fish Oceanogr 8:77–92
Gentleman W (2002) A chronology of plankton dynamics in silico: how computer models have been used to study marine ecosystems. Hydrobiologia 480:69–85
Govoni JJ (2005) Fisheries oceanography and the ecology of early life histories of fishes: a perspective over fifty years. Sci Mar 69:125–137
Grimm V, Railsback SF (2005) Individual-based modeling and ecology. Princeton University Press, Princeton, NJ
Haidvogel DB, Beckman A (1998) Numerical modeling of the coastal ocean. In: Brink KH, Robinson AR (eds) The sea, Vol 10. Harvard University Press, Cambridge, MA, p 457–482
Hao W, Jian S, Ruijing W, Lei W, Yi'an L (2003) Tidal front and the convergens of anchovy (*Engraulis japonicus*) eggs in the Yellow Sea. Fish Oceanogr 12:434–442
Hare JA, Quinlan JA, Werner FE, Blanton BO, Govoni JJ, Forward RB Jr, Settle LR, Hoss DE (1999) Larval transport during winter in the SABRE study area: results of a coupled vertical larval behaviour-three-dimensional circulation model. Fish Oceanogr 8:57–76
Haury LR, McGowan JA, Wiebe PH (1978) Patterns and processes in the time-space scales of plankton distributions. In: Steele JH (ed) Spatial patterns in plankton communities. Plenum Press, New York, p 277–327
Heath MR, Gallego A (1997) From the biology of the individual to the dynamics of the population: bridging the gap in fish early life studies. J Fish Biol 51:1–29
Heath MR, Gallego A (1998) Biophysical modelling of the early life stages of haddock, *Melanogrammus aeglefinus*, in the North Sea. Fish Oceanogr 7:110–125
Heath M, Zenitani H, Watanabe Y, Kimura R, Ishida M (1998) Modelling the dispersal of larval Japanese sardine, *Sardinops melanostictus*, by the Kuroshio Current in 1993 and 1994. Fish Oceanogr 7:335–346
Helbig JA, Pepin P (2002) The effects of short space and time scale current variability on the predictability of passive ichthyoplankton distributions: an analysis based on HF radar observations. Fish Oceanogr 11:175–188
Hermann AJ, Rugen WC, Stabeno PJ, Bond NA (1996) Physical transport of young pollock larvae (*Theragra chalcogramma*) near Shelikof Strait as inferred from a hydrodynamic model. Fish Oceanogr 5:58–70
Hermann AJ, Hinckley S, Megrey BA, Napp JM (2001) Applied and theoretical considerations for structuring spatially explicit individual-based models of marine larval fish that include multiple trophic levels. ICES J Mar Sci 58:1030–1041
Hinckley S, Hermann AJ, Megrey BA (1996) Development of a spatially explicit, individual-based model of marine fish early life history. Mar Ecol Prog Ser 139:47–68
Hinckley S, Hermann AJ, Mier KL, Megrey BA (2001) Importance of spawning location and timing to successful transport to nursery areas: a simulation study of Gulf of Alaska walleye pollock. ICES J Mar Sci 58:1042–1052
Hinrichsen HH, Bottcher U, Oeberst R, Voss R, Lehmann A (2001) The potential for advective exchange of the early life stages between western and eastern Baltic cod (*Gadus morhua*). Fish Oceanogr 10:249–258
Hinrichsen HH, Mollmann C, Voss R, Koster FW, Kornilovs G (2002) Biophysical modeling of larval Baltic cod (*Gadus morhua*) growth and survival. Can J Fish Aquat Sci 59: 1858–1873
Hinrichsen HH, Bottcher U, Koster FW, Lehmann A, St John MA (2003a) Modelling the influences of atmospheric forcing conditions on Baltic cod early life stages: distribution and drift. J Sea Res 49:187–201
Hinrichsen HH, Lehmann A, Mollmann C, Schmidt JO (2003b) Dependency of larval fish survival on retention/dispersion in food limited environments: the Baltic Sea as a case study. Fish Oceanogr 12:425–433
Hinrichsen HH, Kraus G, Voss R, Stepputtis D, Baumann M (2005) The general distribution pattern and mixing probability of Baltic sprat juvenile populations. J Mar Syst 58:52–66
Hislop JRG, Gallego A, Heath MR, Kennedy FM, Reeves SA, Wright PJ (2001) A synthesis of the early life history of the anglerfish, *Lophius piscatorius* (Linnaeus, 1758) in northern British waters. ICES J Mar Sci 58:70–86
Hjort J (1914) Fluctuations in the great fisheries of northern Europe viewed in light of biological research. Rapp P-V Reun Cons Int Explor Mer 19:1–228
Houde E (1989) Subtleties and episodes in the early life of fishes. J Fish Biol 35:29–38
Huggett J, Fréon P, Mullon C, Penven P (2003) Modelling the transport success of anchovy *Engraulis encrasicolus* eggs and larvae in the southern Benguela: the effect of spatio-temporal spawning patterns. Mar Ecol Prog Ser 250: 247–262
Hutchings J (2000) Collapse and recovery of marine fishes. Nature 406:882–885
Ishizaka J, Hofman EE (1988) Plankton dynamics on the outer southeastern US continental shelf. Part I. Lagrangian particle tracing experiments. J Mar Res 46:853–882
Kingsland SE (1985) Modeling nature: episodes in the history of population dynamics. University of Chicago Press, Chicago, IL
Koster F, Hinrichsen HH, St John MA, Schnack D, MacKenzie BR, Tomkiewicz J, Plikshs M (2001) Developing Baltic cod recruitment models. II. Incorporation of environmental variability and species interaction. Can J Fish Aquat Sci 58:1534–1556
Laurence G (1978) Comparative growth, respiration and delayed feeding abilities of larval cod (*Gadus morhua*) and haddock (*Melanogrammus aeglefinus*) as influenced by temperature during laboratory studies. Mar Biol 50:1–7
Letcher B, Rice J, Crowder L, Rose K (1996) Variability in survival of larval fish: disentangling components with generalized individual-based models. Can J Fish Aquat Sci 53:787–801
Lomnicki A (1992) Population ecology from the individual perspective. In: Individual based models and approaches in ecology: populations, communities, and ecosystems. Chapman & Hall, London, p 3–17
Lough RG, Manning JP (2001) Tidal-front entrainment and retention of fish larvae on the southern flank of Georges Bank. Deep-Sea Res 48:631–644
Lough RG, Buckley LJ, Werner FE, Quinlan JA, Edwards KP (2005) A general biophysical model of larval cod (*Gadus morhua*) growth applied to populations on Georges Bank. Fish Oceanogr 14:241–262
Lynch DR, Ip JTC, Naimie CE, Werner FE (1996) Comprehensive coastal circulation model with application to the Gulf of Maine. Cont Shelf Res 16:875–906
MacKenzie BR, Miller TJ, Cyr S, Leggett WC (1994) Evidence for a dome-shaped relationship between turbulence and larval fish ingestion rates. Limnol Oceanogr 39:1790–1799
Maes J, Limburg KE, Van de Putte A, Ollevier F (2005) A spatially explicit, individual-based model to assess the role of estuarine nurseries in the early life history of North Sea

herring, *Clupea harengus*. Fish Oceanogr 14:17–31
Meekan MG, Fortier L (1996) Selection for fast growth during the larval life of Atlantic cod *Gadus morhua* on the Scotian Shelf. Mar Ecol Prog Ser 137:25–37
Megrey BA, Hinckley S (2001) Effect of turbulence on feeding of larval fishes: a sensitivity analysis using an individual-based model. ICES J Mar Sci 58:1015–1029
Megrey BA, Hinckley S, Dobbins EL (2002) Using scientific visualization tools to facilitate analysis of multi-dimensional data from a spatially explicit, biophysical, individual-based model of marine fish early life history. ICES J Mar Sci 59:203–215
Miller TJ, Crowder LB, Rice JA, Marschall EA (1988) Larval size and recruitment mechanisms in fishes: toward a conceptual framework. Can J Fish Aquat Sci 45:1657–1670
Mullon C, Cury P, Penven P (2002) Evolutionary individual-based model for the recruitment of anchovy (*Engraulis capensis*) in the southern Benguela. Can J Fish Aquat Sci 59:910–922
Mullon C, Fréon P, Parada C, Van Der Lingen C, Huggett J (2003) From particles to individuals: modelling the early stages of anchovy (*Engraulis capensis/encrasicolus*) in the southern Benguela. Fish Oceanogr 12:396–406
Myers RA (1995) Recruitment of marine fish: the relative roles of density-dependent and density-independent mortality in the egg, larval, and juvenile stages. Mar Ecol Prog Ser 128:308–309
North EW, Hood RR, Chao SY, Sanford LP (2005) The influence of episodic events on transport of striped bass eggs to the estuarine turbidity maximum nursery area. Estuaries 28:108–123
Paris CB, Cowen RK, Claro R, Lindeman KC (2005) Larval transport pathways from Cuban snapper (Lutjanidae) spawning aggregations based on biophysical modeling. Mar Ecol Prog Ser 296:93–106
Pedersen OP, Slagstad D, Tande KS (2003) Hydrodynamic model forecasts as a guide for process studies on plankton and larval fish. Fish Oceanogr 12:369–380
Quinlan JA, Blanton BO, Miller TJ, Werner FE (1999) From spawning grounds to the estuary: using linked individual-based and hydrodynamic models to interpret patterns and processes in the oceanic phase of Atlantic menhaden *Brevoortia tyrannus* life history. Fish Oceanogr 8(Suppl 2): 224–246
Reiss CS, Panteleev G, Taggart CT, Sheng J, deYoung B (2000) Observations on larval fish transport and retention on the Scotian Shelf in relation to geostrophic circulation. Fish Oceanogr 9:195–213
Rice J, Crowder L, Holey M (1987) Exploration of mechanisms regulating larval survival in Lake Michigan bloater: a recruitment analysis based on characteristics of individual larvae. Trans Am Fish Soc 116:703–718
Rice JA, Miller TJ, Rose KA, Crowder LB, Marschall EA, Trebitz AS, DeAngelis DL (1993) Growth rate variation and larval survival: inferences from an individual-based size-dependent population model. Can J Fish Aquat Sci 50:133–142
Rose KA, Cowan JH Jr (1993) Individual-based model of young-of-the-year striped bass population dynamics. I. Model description and baseline simulations. Trans Am Fish Soc 122:415–438
Rose KA, Cowan JH Jr, Clark ME, Houde ED, Wang SB (1999a) An individual-based model of bay anchovy population dynamics in the mesohaline region of Chesapeake Bay. Mar Ecol Prog Ser 185:113–132
Rose KA, Rutherford ES, McDermot DS, Forney JL, Mills EL (1999b) Individual-based model of yellow perch and walleye populations in Oneida Lake. Ecol Monogr 69:127–154
Rose KA, Murphy CA, Diamond SL, Fuiman L, Thomas P (2003) Using nested models and laboratory data for predicting population effects of contaminants on fish: a step toward a bottom-up approach for establishing causality in field studies. Human Ecol Risk Assess 9:231–257
Sætre R, Toresen R, Soiland G, Fossum P (2002) The Norwegian spring-spawning herring — spawning, larval drift and larval retention. Sarsia 87:167–178
Scheffer M, Baveco JM, DeAngelis DL, Rose KA, van Nes EH (1995) Super-individuals: a simple solution for modelling large populations on an individual basis. Ecol Model 80: 161–170
Shackell N, Frank K, Petrie B, Brickman D, Shore J (1999) Dispersal of early life stage haddock (*Melanogrammus aeglefinus*) as inferred from the spatial distribution and variability in length-at-age of juveniles. Can J Fish Aquat Sci 56:2350–2361
Stegmann PM, Quinlan JA, Werner FE, Blanton BO, Berrien P (1999) Atlantic menhaden recruitment to a southern estuary: defining potential spawning regions. Fish Oceanogr 8:111–123
Stenevik EK, Skogen M, Sundby S, Boyer D (2003) The effect of vertical and horizontal distribution on retention of sardine (*Sardinops sagax*) larvae in the northern Benguela — observations and modelling. Fish Oceanogr 12:185–200
Suda M, Kishida T (2003) A spatial model of population dynamics of early life stages of Japanese sardine, *Sardinops melanostictus*, off the Pacific coast of Japan. Fish Oceanogr 12:85–99
Thorrold S, Latkoczy C, Swart P, Jones C (2001) Natal homing in a marine fish metapopulation. Science 291:297–299
Vikebø F, Sundby S, Adlandsvik B, Fiksen Ø (2005) The combined effect of transport and temperature on distribution and growth of larvae and pelagic juveniles of Arcto-Norwegian cod. ICES J Mar Sci 62:1375–1386
Visser AW, Kiørboe T (2006) Plankton motility patterns and encounter rates. Oecologia 148:538–546
Voss R, Hinrichsen HH, St. John M (1999) Variations in the drift of larval cod (*Gadus morhua* L.) in the Baltic Sea: combining field observations and modelling. Fish Oceanogr 8:199–211
Weissburg MJ, Browman HI (eds) (2005) Sensory biology: linking the internal and external ecologies of marine organisms. Mar Ecol Prog Ser 287:263–307
Werner FE, Quinlan JA (2002) Fluctuations in marine fish populations: physical processes and numerical modelling. ICES Mar Sci Symp 215:264–278
Werner F, Page F, Lynch D, Loder J, Lough R, Perry R, Greenberg D, Sinclair M (1993) Influences of mean advection and simple behavior on the distribution of cod and haddock early life stages on Georges Bank. Fish Oceanogr 2:43–46
Werner FE, Perry RI, Lough RG, Lynch DR (1994) A coupled individual-based trophodynamics and circulation model for studies of larval cod and haddock on Georges Bank. US Globec News 7:1–8
Werner FE, Perry RI, MacKenzie BR, Lough GR, Naimie CE (1995) Larval trophodynamics, turbulence, and drift on Georges Bank: a sensitivity analysis of cod and haddock. ICES CM 1995/Q:26
Werner FE, Perry RI, Lough RG, Naimie CE (1996) Trophodynamic and advective influences on Georges Bank larval cod and haddock. Deep-Sea Res Part II 43:1793–1822
Werner FE, MacKenzie BR, Perry RI, Lough RG, Naimie CE, Blanton BO, Quinlan JA (2001a) Larval trophodynamics, turbulence, and drift on Georges Bank: a sensitivity analysis of cod and haddock. Sci Mar 65:99–115
Werner FE, Quinlan JA, Lough RG, Lynch DR (2001b) Spatially-explicit individual based modeling of marine populations: a review of the advances in the 1990s. Sarsia 86:411–421

Editorial responsibility: Alejandro Gallego (Contributing Editor), Aberdeen, UK

Submitted: July 20, 2006; Accepted: March 27, 2007
Proofs received from author(s): September 5, 2007

Vol. 347: 139–143, 2007
doi: 10.3354/meps06974

MARINE ECOLOGY PROGRESS SERIES
Mar Ecol Prog Ser

Published October 11

Applicability of turbulence measurement technology to small-scale plankton studies

Thomas Osborn*

The Johns Hopkins University, 3400 N Charles Street, Baltimore, Maryland 21218, USA

ABSTRACT: This article contains the author's personal thoughts and prejudices about present techniques for turbulence measurements, and the limitations of these techniques for solving problems in physical–biological interactions.

KEY WORDS: Turbulence · Physical–biological interactions

Small-scale turbulence and mixing are fundamental in the early life stages of oceanic creatures. Mixing is accomplished by molecular diffusion that 'diffuses' away gradients. Turbulence is the stirring process that tends to increase gradients and increase the interfacial area over which these gradients occur (Eckart 1948). Turbulence also increases the contact rate between predator and prey (Rothschild & Osborn 1988). Furthermore, turbulence induces behavioral responses in some organisms. There is a rich body of literature concerning the effects of turbulence on predator–prey interactions and on survival of planktonic, early life stages.

Here, I briefly review some of what is known about turbulence in the ocean, consider what needs to be better delineated, and consider how to measure turbulence and planktonic response simultaneously.

What is turbulence?

It is more appropriate to say the flow is turbulent rather than the fluid itself is turbulent. A turbulent flow has certain characteristics: the motion is random, it is 3-dimensional, it contains vorticity (i.e. $\vec{\omega} = \nabla \times \vec{u} \neq 0$ where the vorticity, $\vec{\omega}$, is the curl of the velocity, $\vec{u}$, and is denoted as the vector cross product of the gradient operator, ∇, with the velocity vector), and kinetic energy is dissipated. The turbulent motion can transport heat, salt, and other properties. It tends to increase the transport (observable at large scales) above that due to molecular diffusion alone. Experience has shown that a useful parameter for scaling the intensity of small-scale turbulence is the dissipation rate, ε, which is the rate at which kinetic energy is dissipated by viscosity and converted to heat.

How do we observe turbulence in the ocean?

Hot films and shear probes

An excellent review on the measurement of small-scale, turbulent, velocity fluctuations in the ocean is given by Lueck et al. (2002). The modern era of small-scale turbulence measurements in the ocean began with the pioneering work of Grant et al. (1962). They used a towed body with a hot film anemometer to measure the turbulent velocity fluctuations to scales of millimeters. This sensor measures variations in the heat transfer between a hot film and the adjacent boundary layer. Variations in the flow modify the boundary layer and lead to variations in the heat flux. The probe is predominantly sensitive to fluctuations in axial velocity, i.e. in the direction of travel of the probe through the water. This system was moved from the towed body to the Pisces submersible (Gargett 1982), which is very difficult to operate, but produces data with the highest spatial resolution.

Vertical profiling of ocean turbulence is appealing because freely falling profilers are decoupled from the

*Email: osborn@jhu.edu

motion of the surface vessel. As well, they are moving across the horizontal layers in the ocean and should give a picture of the distribution of turbulence versus depth. Here, the velocity sensor of choice is the airfoil probe, developed by Siddon & Ribner (1965) and modified to work in the ocean by Osborn (1972). This sensor responds to the water motions that are transverse to its relative motion through the water. It is used on free-fall profilers, autonomous underwater vehicles, submersibles, expendable profilers, and gliders. Again, Lueck et al. (2002) have provided a review of the systems.

Hot films and airfoil probes have one great advantage—their output can be differentiated electronically. Since it is the spatial gradients of the velocity that are used to calculate the dissipation rate, the variance of the shear spectrum can be used to directly estimate the dissipation rate. While the airfoil probe is much easier to operate and more robust than the heated probes, it has limited spatial resolution due to its finite size. For many oceanic applications this effect can be removed spectrally (Macoun & Lueck 2004), but when we want to look in detail at the velocity variations with scales smaller than a centimeter or so, spatial averaging by the probe is a problem. Unfortunately, this is the size regime in which many interesting predator–prey interactions take place.

Acoustic techniques

There are a variety of acoustic velocity sensors that have been developed over the years (for a good introduction to the principles and the capabilities of small-scale measurements see Lhermitte [1981, 1983] and Lhermitte & Lemmin [1993]). All rely on the Doppler shift of the sound frequency as it is reflected by particles (and other sources of variations in the speed of sound). These probes are very useful because they can profile and can sample remotely, without intruding into the flow. There is a trade off between spatial resolution (which requires high frequency) and range (which decreases with increasing frequency). Since these sensors measure velocity, and cannot measure velocity gradients directly, the dissipation rate is generally estimated from fitting the velocity spectra to, so-called, 'universal shapes'.

Particle image velocimetry and particle tracking velocimetry

Particle image velocimetry (PIV) involves the illumination of a thin sheet of fluid with 2 flashes of a laser. The displacement of groups of particles in the flow, between the 2 exposures, is determined from the correlation of small subsets (e.g. 64 pixels by 64 pixels) of the image with the entire imager (2000 pixels by 2000 pixels). The displacement and time interval are used to infer the velocity of the fluid in the plane of the light (Bertuccioli et al. 1999, Doron et al. 2001, Nimmo Smith et al. 2002, 2005). The data consist of 2-dimensional maps of the velocity vectors (projected onto the plane of the light sheet), with each vector based on the average of several particles.

Particle tracking velocimetry (PTV) differs from PIV in that individual particles are tracked using continuous lighting and a continuously running video camera. Examples from the system of Nimmo Smith can be seen at www.coastalprocesses.org/. Like PIV this system depends upon the particles following the motion in order to infer the flow from the displacement of the particles.

Larger scale estimates of ε

There are 3 approaches to estimating the dissipation rate of kinetic energy that do not rely on small-scale velocity measurements. Dillon (1982) shows that the Thorpe scale, the root mean square displacement needed to reorder a measured density profile to produce a density profile that appears statically stable, is comparable to the Ozmidov scale $L_z = (\varepsilon/N^3)^{1/2}$, where ε is the kinematic energy dissipation rate in m^2 s^{-3}, and N is the Brunt–Vaisala frequency in radians per second. This enables estimation of the dissipation rate from well-resolved density profiles (or sometimes temperature profiles). This approach involves no measurement of velocity fluctuations, although it does involve small-scale measurements of the scalar field.

The second approach measures the turbulent eddies that contain kinetic energy (Gargett 1999). The idea is that almost all of the kinetic energy is at larger scales, characterized by a spatial scale L, and that this energy cascades to smaller scales where it is dissipated. The dissipation rate is the kinetic energy (estimated as U^2, where U is the speed associated with the turbulence at the larger spatial scales) divided by the eddy time scale (L/U) and hence $\varepsilon \approx U^3/L$. This approach requires measurements of velocity fluctuations, but not on dissipation scales.

Finally, there is a technique that involves measuring one component of the temperature gradient and using Batchelor's (1959) theoretical spectrum to infer the dissipation from the shape of the temperature gradient spectrum. This involves a measurement of the small-scale temperature fluctuations; here, the spatial resolution of the sensors is most problematic and often not

documented. Furthermore, the most definitive paper comparing predictions against measurements (Gargett 1985) strongly suggests the universal spectral shape is not found consistently in the ocean. For the problem of biological interactions, where we are really interested in the details of the small-scale velocity fluctuations, inferring averaged values (i.e. dissipation) from a scalar quantity like temperature is probably inappropriate.

What do we know about turbulence in the ocean?

During the last 50 yr there has been a dramatic augmentation of the literature on oceanic turbulence. A recent compilation, in book form, by Thorpe (2005) covers our present understanding of oceanic turbulence, over a wide range of spatial scales.

Vertical distribution

In the upper ocean (from the surface to the pycnocline) turbulence is forced by surface cooling, wind stress, and energy from breaking waves. The turbulence is redistributed by convection, Langmuir circulation, and large-scale vortical motions. Below the level of the wave troughs, the turbulence often scales with the 'law of the wall,' $\varepsilon = u_*^3/\kappa z$, where ε is the dissipation, u_* is a velocity-scaling parameter derived by taking the square root of the ratio of the wind stress to the water density, κ is the Von Karmen constant ~0.4, and z is the depth below the water surface. There is a surface layer of enhanced dissipation between the crest and troughs of the waves. The energy for this dissipation is derived from the surface waves (Agrawal et al. 1992). Cooling of the sea surface drives convection, and dissipation can be calculated from buoyancy flux (Shay & Gregg 1984).

There are large structures in the upper layer. Langmuir cells align (almost) with wind direction and redistribute the turbulence and bubbles vertically (Thorpe et al. 2003a,b). There are also large-scale vortices aligned perpendicular with wind direction that produce temperature ramps and redistribute turbulence throughout the upper layer (Thorpe et al. 2003a). In addition, recent measurements with a submersible in Lake Geneva (Ozen et al. 2006) have revealed organized structures forcing turbulence up from the bottom of the mixed layer/thermocline. The interactions between these 3 mechanisms are unknown.

The thermocline contains layers of turbulence with vertical scales of meters and horizontal scales of hundreds of meters or more. These patches seem to have time scales of many hours and are likely associated with shears from inertial motions and internal waves. Bulk averages of dissipation seem to increase rather than decrease with stratification, $\varepsilon \propto N$ or N^2. The most likely explanation is the increase in internal wave energy with increasing stratification. Below the thermocline, a patchy distribution continues, with a general decrease in intensity with depth (and decreasing stratification).

Universal spectral shape

The pioneering work by Grant et al. (1962) verified the hypothesis of a universal shape for the turbulent velocity spectrum in the case of high Reynolds number, isotropic, and homogeneous flow. The −5/3 spectral slope predicted from the work of Kolmogorov was observed to separate the energy containing low wave number portion of the spectrum from the high wave number dissipation portion. Nasmyth (1970) provides an improved measurement of the shape, and the numerical values are found in Oakey (1982). Gargett et al. (1984) report a slightly different shape. Their measurements of all 3 velocity components show isotropy throughout the dissipation range, with an effect of stratification at lower wave numbers. When affected by buoyancy, the low wave number portion of the velocity spectrum follows a universal shape that can be nondimensionalized with buoyancy parameters.

The peak of the dissipation spectrum is at $k \approx 0.2\ k_s$, where $k_s = (\varepsilon/\nu^3)^{1/4}$ is the Kolmogorov wave number in radians per meter and ν is the kinematic viscosity. The exact numerical value depends on whether a lateral or axial velocity component is being considered. The wavelength corresponding to the peak of the dissipation spectrum is $\lambda = 2\pi/k_s \approx 10\pi\eta$, where $\eta = (\nu^3/\varepsilon)^{1/4}$ is the Kolmogorov length scale. At separations associated with this portion of the spectrum, the relative motion between particles is a viscous-straining motion. The Reynolds number at these scales is ≤1.

For biological interactions, a paper by Yamazaki & Lueck (1990) has shown a lognormal distribution for dissipation rates when averaged over scales substantially smaller than patch size, but larger than 3η. Particles with separation smaller than 3η are essentially in the same strain field. Theirs is the only paper to my knowledge that considers the details of shear at small scales. The interesting point is that average dissipation, over distances from 0.5 m to several meters, does not represent the instantaneous strain associated with predator–prey interactions over the time scale of those interactions. The time scale is related to the Kolmogorov spatial scale, $\tau = \left(\frac{\nu}{\varepsilon}\right)^{1/2}$, which is an estimate of the lifetime of the eddies at that scale.

PIV measurements of spectra

Recent measurements with PIV in the bottom boundary layer of the coastal ocean have given us results completely different from those obtained via hot films and airfoil probes. The data are time series, at a fixed location, of 2-dimensional vector maps of flow, with resolution almost to the Kolmogorov scale (Bertuccioli et al. 1999, Doron et al. 2001, Nimmo Smith et al. 2002, 2005, L. Luznik et al. unpubl.).

The measurements have been done in the bottom boundary layer of the coastal ocean, which is not the same oceanographic environment usually sampled with hot films and airfoil probes. There are several results from the present work that have significant impact on understanding turbulence in the coastal ocean and the impact of turbulence on predator–prey interactions. The measurements (L. Luznik et al. unpubl.) reveal that turbulence (1) appears to be anisotropic at all scales, (2) shows a Reynolds number effect on spectra, (3) does not fit universal shape, and (4) in some components, has more high wave number energy than expected.

Some conclusions about turbulence at small scales

Measurements to date do not really provide the information needed to thoroughly understand the role of turbulence on predator–prey interactions because (1) measurements of turbulent motions on scales of centimeters and smaller are really quite limited and (2) the temporal and spatial variability of the intensity is not well known.

Since the spectrum is not always universal or isotropic at dissipation scales, we cannot reliably predict the small-scale distribution of shear based on larger scale estimates of the dissipation rate.

Way forward

To truly understand the role of turbulence in early life stages, we need to observe the interactions and reactions that occur in conjunction with turbulent motion. Perhaps this can be done in laboratory experiments with freely moving organisms and realistically generated turbulence. However, while many laboratory results to date have been quantitative and performed with well-documented procedures, they represent environments never encountered by man or beast. It is unclear whether these results can be applied to the oceanic regime. Hence, observations must be made *in situ*: in the ocean, under realistic conditions. The requirement for such studies is that the organisms, their motions and actions, as well as the water motion be sampled simultaneously. The combination of holography and PIV offers the technology to accomplish this task. By making repeated holographic images with a digital camera, it is possible to track predators, prey, and smaller particles that follow the motion of the water.

Malkiel et al. (2003, 2005, 2006a,b), Pfitsch et al. (2005), and Sheng et al. (2006) describe the development and use of such a system. Further details are available at www.me.jhu.edu/~lefd/shc/shc.htm.

Holography has the advantage of resolving particles over a wide range of sizes. The interference pattern of the coherent light that makes the hologram spreads out the information from particles that are smaller than individual pixels in the digital camera so that they can be registered and reconstructed in the later analysis. Thus, the system can record dinoflagellates and copepods and resolve both.

LITERATURE CITED

Agrawal YC, Terray EA, Donelan MA, Huang PA, Williams AJ III, Drennan WM, Kahma KK, Kitagorodski SA (1992) Enhanced dissipation of kinetic energy beneath surface waves. Nature 359:219–220

Batchelor GK (1959) Small-scale variation of convected quantities like temperature in turbulent fluid. Part I. General discussion and the case of small conductivity. J Fluid Mech 5(1):113–133

Bertuccioli L, Roth GI, Katz J, Osborn TR (1999) Turbulence measurements in the bottom boundary layer using particle image velocimetry. J Atmos Oceanogr Technol 16(11): 1635–1646

Dillon TM (1982) Vertical overturns: a comparison of Thorpe and Ozmidov length scales. J Geophys Res 87:9601–9613

Doron P, Bertuccioli L, Katz J, Osborn TR (2001) Turbulence characteristics and dissipation estimates in the coastal ocean bottom boundary layer from PIV data. J Phys Oceanogr 31:2108–2134

Eckart C (1948) An analysis of the stirring and mixing processes in incompressible fluids. J Mar Res 58:265–275

Gargett AE (1982) Turbulence measurements from a submersible. Deep-Sea Res A 29:1141–1158

Gargett AE (1985) Scalar spectra in decaying stratified turbulence. J Fluid Mech 159:379–407

Gargett AE (1999) Velcro measurements of turbulent kinetic energy dissipation rate ε. J Atmos Oceanogr Technol 16: 973–993

Gargett AE, Osborn TR, Nasmyth PW (1984) Local isotropy and the decay of turbulence in a stratified fluid. J Fluid Mech 144:231–280

Grant HL, Stewart RW, Moilliet A (1962) Turbulence spectra from a tidal channel. J Fluid Mech 12:241–263

Lhermitte R (1981) Observations of water flow with high resolution Doppler sonar. Geophys Res Lett 8(2):155–158

Lhermitte R (1983) Doppler sonar observation of tidal flow. J Geophys Res C 88(1):725–742

Lhermitte R, Lemmin U (1993) Turbulent flow microstructures observed by sonar. Geophys Res Lett 20(9):823–826

Lueck RG, Wolk F, Yamazaki H (2002) Oceanic velocity microstructure measurements in the 20th century.

J Oceanogr 58:153–174
Macoun P, Lueck RG (2004) Modeling the spatial response of the airfoil shear probe using different sized probes. J Atmos Oceanogr Technol 21(2):284–297
Malkiel E, Sheng J, Katz J, Strickler JR (2003) The three-dimensional flow field generated by a feeding calanoid copepod measured using digital holography. J Exp Biol 206:3657–3666
Malkiel E, Sheng J, Katz J (2005) Measurements of 3-D flows with a digital holographic microscope. Bull Am Phys Soc 50(9):121
Malkiel E, Abras JN, Widder E, Katz J (2006a) On the spatial distribution and nearest neighbor distance between particles in the water column determined from *in situ* holographic measurements. J Plankton Res 28:149–170. Available at: http://plankt.oxfordjournals.org/cgi/reprint/fbi107?ijkey=HgUwHjKuHuY72oN&keytype=ref
Malkiel E, Pfitsch DW, Katz J (2006b) *In situ* digital holographic cinematography of plankton in a coastal estuary. Ocean Sci. Meet. Suppl., Abstract OS36H-02. EOS Trans Am Geophys Union 87(36)
Nasmyth PW (1970) Oceanic turbulence. PhD thesis, University of British Columbia, Vancouver
Nimmo Smith WAM, Atsavapranee P, Katz J, Osborn TR (2002) PIV measurements in the bottom boundary layer of the coastal ocean. Exp Fluids 33:962–971
Nimmo Smith WAM, Katz J, Osborn TR (2005) On the structure of turbulence in the bottom boundary layer of the coastal ocean. J Phys Oceanogr 35:72–93
Oakey NS (1982) Determination of the rate of dissipation of turbulent kinetic energy from simultaneous temperature and velocity shear microstructure measurements. J Phys Oceanogr 12:256–271
Osborn TR (1972) Vertical profiling of velocity microstructure. J Phys Oceanogr 4:109–115
Ozen B, Thorpe SA, Lemmin U, Osborn TR (2006) Cold-water events and dissipation in the mixed layer of a lake. J Phys Oceanogr 36(10):1928–1939
Pfitsch DW, Malkiel E, Ronzhes Y, King SR, Sheng J, Katz J (2005) Development of a free-drifting submersible digital holographic imaging system. Oceans 1:690–696
Rothschild BJ, Osborn TR (1988) The effect of turbulence on planktonic contact rates. J Plankton Res 10(3):465–474
Shay TJ, Gregg MC (1984) Turbulence in an oceanic convective layer. Nature 310:282–285 (Corrigendum 311:84)
Sheng J, Malkiel E, Katz J (2006) A digital holographic microscope for measuring three-dimensional particle distributions and motions. Appl Optics 45(16):3893–3901
Siddon TE, Ribner HS (1965) An aerofoil probe for measuring the transverse component of turbulence. J Am Inst Aeronautics Astronautics 3:747–749
Thorpe SA (2005) The turbulent ocean. Cambridge University Press, Cambridge
Thorpe SA, Osborn TR, Jackson JFE, Hall AJ, Lueck RG (2003a) Measurements of turbulence in the upper ocean mixing layer using AUTOSUB. J Phys Oceanogr 33(1): 122–145
Thorpe SA, Osborn TR, Farmer DM, Vagle S (2003b) Bubble clouds and Langmuir circulation: observations and models. J Phys Oceanogr 33(9):2013–2031
Yamazaki H, Lueck RG (1990) Why oceanic dissipation rates are not lognormal. J Phys Oceanogr 20:1907–1918

Editorial responsibility: Alejandro Gallego (Contributing Editor), Aberdeen, UK

Submitted: March 20, 2006; Accepted: March 18, 2007
Proofs received from author(s): August 28, 2007

Vol. 347: 145–153, 2007
doi: 10.3354/meps06975

MARINE ECOLOGY PROGRESS SERIES
Mar Ecol Prog Ser

Published October 11

OPEN ACCESS

Simulating vertical turbulent dispersal with finite volumes and binned random walks

Uffe Høgsbro Thygesen[1,*], Bjørn Ådlandsvik[2]

[1]Danish Institute for Fisheries Research, Technical University of Denmark, Jægersborg Allé 1, 2920 Charlottenlund, Denmark
[2]Institute of Marine Research, PO Box 1870, Nordnes, 5817 Bergen, Norway

ABSTRACT: Early life stages in fish are often modeled by individual-based models. The transport of individuals with ocean currents is addressed through particle-tracking techniques, which typically simulate vertical turbulent dispersal with random walk schemes. These schemes, however, perform poorly when the eddy diffusivity displays steep gradients, as in stratified water columns, and near the surface and sea floor. In the present paper, we advocate the use of a binned random walk, which keeps track, not of the exact vertical position of a tracer particle, but only of the layer in which the particle resides. The binned random walk is derived by discretizing the Eulerian equations governing the vertical dispersal with the finite-volume method. The scheme is easily implemented, even when layers are non-uniform and turbulence statistics originate from a circulation model, and, by construction, always satisfies the well-mixed criterion. We demonstrate the scheme and discuss its applicability.

KEY WORDS: Individual-based models · Dispersal · Random walk

INTRODUCTION

Many model studies in both physical and biological oceanography concern the transport and dispersal of tracers in the ocean. Examples of important processes are the transport of fish eggs or larvae between spawning grounds and nursery grounds (e.g. Christensen et al. 2007, this Theme Section), and the vertical distribution of fish eggs (e.g. Ådlandsvik et al. 2001, Boyra et al. 2003). Such studies can be done in the Eulerian framework, which models the density of tracers as it evolves in time, or in the Lagrangian or individual-based framework, which adds single particles or individuals to a numeric model of the ocean and tracks their motion. One advantage of the individual-based framework, which is particularly relevant for early life stages of fish, is the ease of adding internal states such as condition or developmental stages. The present paper concerns individual-based models (see also Thygesen et al. [2006] for comparisons and connections between the Eulerian and the individual-based approach).

In many situations, it is important to include turbulent dispersal in the model. Dispersal is typically modeled with diffusion and simulated by means of random walk schemes (Visser 1997). This is a reasonable approach when the time scales of interest exceed the so-called Lagrangian time scale, which measures the persistency of the velocity of a passive tracer in turbulent flow (U. H. Thygesen & A. W. Visser unpubl.). For the vertical component, this time scale is on the order of minutes (Yamazakiet al. 2002), whereas the horizontal component is on the order of days (Garrett 2006). It is often sufficient to model the vertical coordinate with a random walk. This is because the horizontal dispersal may be dominated by longitudinal, or shear, diffusion (Taylor 1954), i.e. the combined effect of vertical mixing and the horizontal velocities varying over the water column, or because horizontal eddies are resolved by the circulation model. In this paper we, too, will focus on vertical mixing.

One practical problem with random walk schemes is that they perform poorly when the eddy diffusivity profile is not smooth; then small time steps are required. This is problematic in an oceanographic context, where stratification may impose large local gradients and curvatures. Moreover, when the eddy diffusivity

*Email: uht@difres.dk

profile is the output of a numerical model, the discrete data points must be interpolated sufficiently smoothly. Another issue concerns the boundaries at the surface and bottom. Here, the standard algorithms implement reflecting boundaries, but in this case the well-mixed criterion requires the diffusivity to be constant near the boundary (Ross & Sharples 2004), which does not agree with physics. A similar problem arises even with constant diffusivity when a vertical bias is present, whether due to buoyancy, sedimentation, or active vertical migration. Thus, the practical use of random walk schemes for turbulent dispersal in combination with circulation models is complicated by numerical considerations and statistical verifications that the well-mixed criterion (Thomson 1987) is met also in practice. See Brickman & Smith (2002) and references therein for a discussion of these difficulties.

On the other hand, in the literature of stochastic processes (Gardiner 1985, Grimmett & Stirzaker 1992; see also Csanady 1973, Okubo & Levin 2001), a common cartoon model of 1-dimensional diffusion is a random walk on a lattice in discrete time: at each time step, the particle moves 1 step 'up' or 'down' with equal probability. The standard construction goes on to demonstrate that if the spatial grid size k and the time step h go to zero such that $2D = k^2/h$ is constant, then the limiting process is diffusion with diffusivity D.

The aim of the present paper is to point out that this simple construction generalizes very easily to a situation in which the diffusivity is neither constant in space nor in time and the grid is not equidistant. In this situation, the transition probabilities may be obtained from a finite-volume discretization (Ferziger & Perić 2002) of the underlying diffusion equation. Thus, it is straightforward to implement the scheme using output from a circulation model that is discrete in space and time. It does not require this output to be smooth, so no vertical smoothing of diffusivity profiles is required. By construction, this scheme always satisfies the well-mixed criterion. This holds regardless of discontinuities and boundary behavior of the diffusivity profile, and does not require the time step to be infinitesimal, although the basic algorithm does have a maximum allowable time step.

We call the resulting algorithm a *binned random walk*, since it does not keep track of the exact position of the particle, but only models the bin (layer or cell) in which the particle resides. Thus, if one is willing to settle with this spatial resolution, then one may avoid the difficulties with verifying the well-mixed criterion. This allows the focus to shift towards the accuracy of the transients.

This binned random walk can also be used when a vertical bias is present, for example, when fish eggs are non-neutrally buoyant. The results will then be comparable to the Eulerian finite-volume approach used by Ådlandsvik et al. (2001) and Boyra et al. (2003), and has the advantage that it can be used as a component in a wider particle-tracking or individual-based framework.

The paper is organized as follows. In the section 'The diffusion equation and its finite-volume discretization', we consider the diffusion equation, which models unbiased dispersal and its discretization in space using finite volumes. In the section 'Lagrangian simulations', we discuss individual-based simulation of dispersal, using the discretized diffusion equation. The section 'An idealized example with stratification' uses a hypothetical example to illustrate dispersal when the rate of mixing changes abruptly; this serves as an extreme benchmark test for numerical schemes. The section 'Biased random walks in the vertical' includes vertical bias, e.g. due to the dispersing particles being non-neutrally buoyant. Finally, the 'Discussion' offers some conclusions and a discussion of the merits, limitations, and applicability of the scheme.

THE DIFFUSION EQUATION AND ITS FINITE-VOLUME DISCRETIZATION

The starting point for our analysis is the concentration field $C(z,t)$ giving the concentration C of a passive tracer substance, measured in mass or numbers per volume. Here, $t > 0$ is the time and $z \in [0, d]$ is the height over the ocean floor, so that $z = 0$ corresponds to the bottom and $z = d$ to the surface. It is governed by the diffusion equation:

$$\dot{C} = -J' = (DC')' \tag{1}$$

with no-flux boundary conditions, i.e. $J = -DC'$ vanishes at $z = 0$ and $z = d$. $\dot{C}$ indicates the time derivative $\partial C/\partial t$, whereas the prime in, e.g., C' denotes the spatial derivative $\partial/\partial z$. $J(z,t) = -D(z, t)C'(z,t)$ is the vertical diffusive flux. Note that the eddy diffusivity D may depend on position and time, i.e. we have $D = D(z,t)$.

To resolve this equation numerically, we pursue a finite-volume discretization (Ferziger & Perić 2002) of the vertical dimension, using a grid:

$$0 = z_0 < z_1 < \ldots < z_n = d \tag{2}$$

while we keep time a continuous variable. The discretized system uses n control volumes, with volume i containing the layer between $z = z_{i-1}$ and $z = z_i$. The system keeps track of the amount of material m_i in each control volume:

$$m_i(t) = \int_{z_{i-1}}^{z_i} C(z,t)\mathrm{d}z \tag{3}$$

with $i = 1,\ldots, n$, but not of how this material is distributed within the layer. (We will think of m_i as a biomass; it could equally well be measured in numbers of indi-

viduals). Note the difference between this approach and a pure finite-difference method, which will model the concentration of matter at grid points rather than the amount of matter within grid cells. To pose a dynamic equation for these amounts m_i, we first rewrite the diffusion equation (Eq. 1) in its integral form, which is the mass balance equation:

$$\dot{m}(t) = J(z_{i-1},t) - J(z_i,t) \quad (4)$$

To close the system, we must approximate the fluxes $J = -DC'$ in terms of the masses m_i. To this end, first note that the average concentration in control volume i is m_i/k_i, where $k_i = z_i - z_{i-1}$ is the width of layer i. Next, the distance from the center of layer i to that of the neighboring layer $i+1$ is $(k_i + k_{i+1})/2$. Combining these, we obtain a first-order, finite-difference approximation of the spatial derivative C', which leads to the approximation:

$$J_i = D_i \frac{2}{k_i + k_{i+1}} \left(\frac{m_i}{k_i} - \frac{m_{i+1}}{k_{i+1}} \right) \quad (5)$$

of $J(z_i, t)$. Here, D_i is the diffusivity at the interface between cells i and $i+1$, i.e. at z_i. Note that J_i, D_i and m_i will depend on time, but that we suppress this for notational convenience. Combining with the mass balance of control volume i, we obtain:

$$\dot{m}_i = p_{i-1}m_{i-1} - (p_i + q_i)m_i + q_{i+1}m_{i+1} \quad (6)$$

where the coefficients are:

$$p_i = D_i \frac{2}{(k_i + k_{i+1})k_i} \quad (7)$$

$$q_i = D_{i-1} \frac{2}{(k_{i-1} + k_i)k_i} \quad (8)$$

These equations apply to all inner boundaries between cells, but at the boundaries at the bottom and surface there is no flux. This is achieved by setting $p_0 = q_{n+1} = 0$.

Note that the scheme is guaranteed to conserve the total mass or number of tracers, since we are explicitly modeling the fluxes; this is the advantage of the finite-volume method. Also, the uniform concentration is necessarily stationary: if there are no concentration gradients, then there are no fluxes. These 2 desirable properties are independent of the grid and also of the diffusivities D_i applied to the interfaces; they may vary arbitrarily between adjacent cells, and they may be interpolated from the output of a numerical circulation model. So while interpolation requires some computational overhead and may give less accuracy, it does not jeopardize the well-mixed criterion.

So far we have discussed the numerics of an Eulerian model. For our development of the particle-following algorithm, the following interpretation of the balance equation (Eq. 6) is key: focusing on the term $-p_i m_i$ in the derivative, we see that in a short time interval h, there is an amount $p_i m_i h$ of matter that is initially in cell i and moves to cell $i+1$. Thus, a fraction $p_i h$ of the material that is initially in cell i moves into cell $i+1$. Taking a random tracer molecule that is initially in cell i, we see that the probability that this molecule moves to cell $i+1$ during the time interval is $p_i h$. Similarly, the term $-q_i m_i$ means that the same random tracer molecule has probability $q_i h$ of moving into cell $i-1$. These are exactly the probabilities that we need to know in order to simulate the random motion of a tracer molecule.

LAGRANGIAN SIMULATIONS

Lagrangian *random walk* simulations of vertical turbulent dispersal take as a mathematical starting point the *diffusion processes* Z_t (see Gardiner 1985 for background material). This is a stochastic process in continuous time that models the trajectory of a single particle; Z_t is the vertical position at time t. It is connected with the diffusion equation (Eq. 1), which governs the transition probabilities of Z_t. One characterization of this process Z_t is that it solves the stochastic differential equation:

$$\mathrm{d}Z_t = D'(Z_t,t)\mathrm{d}t + \sqrt{2D(Z_t,t)}\,\mathrm{d}B_t \quad (9)$$

This equation specifies the change dZ_t in the vertical position Z_t over an infinitesimal time interval dt. Here, B_t is Brownian motion, i.e. a stochastic process for which the increment $B_{t+h} - B_t$ is a Gaussian distributed random variable with mean 0 and variance h, for any positive t and h. Note that the physical unit of B_t is the square root of time, $s^{1/2}$. Equations such as Eq. (9) allow several different interpretations (Gardiner 1985), but to obtain pure diffusion and, in particular, a uniform steady-state concentration we must use what is known as the interpretation of Itô. That is to say that Z_t can be approximated in discrete time with the Euler scheme:

$$Z_{t+h} - Z_t = D'(Z_t,t)h + \sqrt{2D(Z_t,t)}(B_{t+h} - B_t) \quad (10)$$

This is a stochastic recursion: given Z_t, we may use a random number generator to simulate $B_{t+h} - B_t$ from a Gaussian distribution with mean 0 and variance h, and thus compute Z_{t+h}. Note the term $D'(Z_t,t)h$; with heterogeneous turbulence, this is a biased random walk. Visser (1997) found that a more careful evaluation of the square root improved accuracy. It is a result from the theory for numerical analysis of stochastic differential equations (Kloeden & Platen 1995) that, as the time step h goes to 0, the transition probabilities of the discrete-time recursion converge to the solution of the diffusion equation (Eq. 1). Fig. 1 gives a schematic of the first few time points in such a simulation.

For accuracy, the Euler scheme (Eq. 10) requires that the relative change in diffusivity over a single time step is small. To assess this change, we use Itô's lemma (Gardiner 1985); this is a stochastic version of the chain rule of differentiation. We find that the change in diffusivity $D(Z_t)$ experienced by the tracer over a small time step h has mean $(|D'|^2 + D''D)h$ and standard error $|D'|\sqrt{(2Dh)}$, to the lowest order in h. Thus, the time step h must be small relative to both $D/(D')^2$ and $1/|D''|$ (compare Thomson 1987, Wilson & Flesch 1993). More powerful numerical schemes are available (Kloeden & Platen 1995), but in practical applications, where the eddy diffusivity is not a theoretical profile but the output from a circulation model, high-order schemes are not well suited for increasing performance. This is because the diffusivity is only known at discrete grid points or as averages over discrete cells. This makes it difficult to determine the derivatives of the diffusivity that are needed in the typical higher-order scheme.

Due to these obstacles, we may choose to pursue the less ambitious goal of just keeping track of which cell (bin, layer) the particle is in. Recall the interpretation of the finite-volume scheme (Eq. 6), that in a short time interval of duration h a fraction $p_i h$ of the material initially in cell i moves into cell $i + 1$, and likewise for the other terms. For the Lagrangian simulation, this means that a particle in cell i should, with probability $p_i h$, move into cell $i + 1$ during the time interval. This leads to the following discrete-time algorithm:

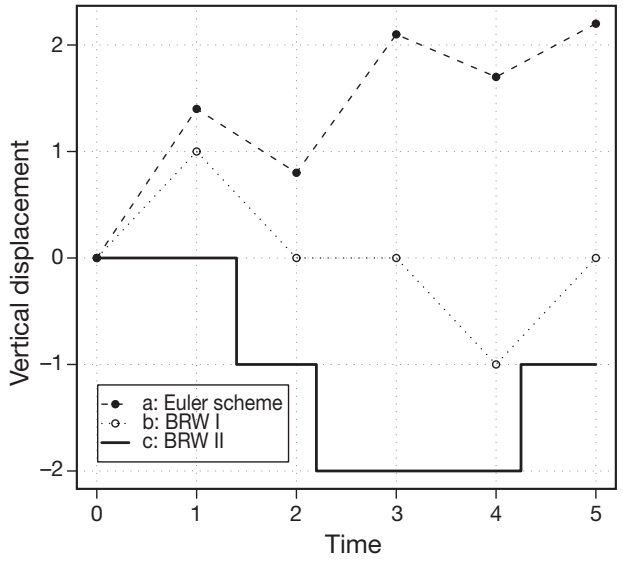

Fig. 1. The 3 schemes approximating diffusion, in the dimensionless case, with constant diffusivity $D = 0.3$. a, the discrete-time continuous-space Euler scheme (Eq. 10); b, BRW I: Binned Random Walk I, discrete in space and time, with a vertical grid size of 1 and a time step of 1; c, BRW II: continuous-time Binned Random Walk II, with a vertical grid size of 1. Note that these are 3 different realizations, so the actual sample paths are not expected to be identical

Binned Random Walk I:

(1) Let i be the number of the cell in which the particle resides at time t.
(2) Sample a random number U, uniformly distributed between 0 and 1.
(3) a. If $0 \le U < q_i h$, move the particle to cell $i - 1$.
    b. If $q_i h \le U < 1 - p_i h$, do not move the particle.
    c. If $1 - p_i h \le U < 1$, move the particle to cell $i + 1$.
(4) Advance time t to $t + h$ and go to Step 1.

This algorithm simulates a Markov chain, which approximates the diffusion process Z_t. The transition probabilities of this Markov chain converge to those of the diffusion process Z_t in the limit as the cell widths and the time step h go to zero. The scheme requires that the time step h is smaller than $\min_i 1/(p_i + q_i)$, because it should be impossible to remove more material from a cell than is available. As a note, this condition is also known in the context of numerical analysis of the Eulerian equation (Eq. 6), where it avoids negative concentrations and guarantees stability of the explicit time-marching scheme (see e.g. Ferziger & Perić 2002, p. 145).

The scheme has the advantage that it works robustly also when the jump rates p_i and q_i depend on time. Although we concentrate on the 1-dimensional case, this makes it possible to apply the scheme also in 3-dimensional situations; we comment briefly on this in the discussion section. Note that the uniform distribution, where the probability of the particle residing in each cell is proportional to the size of the cell, is necessarily stationary in time for any time step below this upper limit, by the construction of the finite-volume scheme. Thus, no extra effort is needed to assure or confirm that the well-mixed criterion is met.

With a uniform grid, constant diffusivity, and the appropriate time step, the algorithm reduces to a standard unbiased random walk on a lattice (Csanady 1973, Okubo & Levin 2001). Furthermore, with a uniform grid but varying diffusivity, the algorithm matches exactly the mean and the variance of the displacement of a particle over a short time interval (see Appendix 1).

When the jump rates p_i and q_i are constant in time, we can approximate the diffusion process Z_t with a continuous-time Markov chain, thus eliminating the fixed time steps and only sampling the process when it shifts from one cell to another. To this end, we exploit that the residence time in each cell is a random variable following the exponential distribution with mean $1/(p_i + q_i)$ (Grimmett & Stirzaker 1992). We arrive at the following continuous-time algorithm:

Binned Random Walk II:

(1) Let i be the number of the cell in which the particle resides at time t.

(2) Sample random numbers U and I, uniformly between 0 and 1.
(3) Compute the residence time H in cell i as $-(p_i + q_i)^{-1} \log U$.
(4) a. If $0 \le I < q_i/(p_i + q_i)$, move the particle to cell $i-1$.
b. If $q_i/(p_i + q_i) \le I < 1$, move the particle to cell $i+1$.
(5) Advance time t to $t + H$ and go to Step 1.

This algorithm avoids errors associated with discretization in time, which is appealing. However, when many particles are simulated at once, it will result in a different sequence of time steps for each particle, which leads to a slightly more complicated implementation. When studying idealized flows, one will often prefer to output the sequence of time steps as well as the cell number, for each particle. In other situations, one may choose to simply output the position of each particle at fixed, regularly-spaced time steps.

Finally, when the jump rates p_i and q_i are constant, we can compute the transition probabilities over long time intervals as $\exp(Ah)$. Here, A is a tridiagonal matrix with elements p_i on the first superdiagonal, q_i on the first subdiagonal, and $-p_i - q_i$ on the diagonal. In the theory of Markov chains, A is known as the 'generator'. Algorithms for computing this matrix exponential are well known (Moler & Van Loan 2003) and are available in standard software packages. This allows us to take arbitrarily long time steps without any error associated with the time step, and thus also to verify the effect of using finite time steps.

AN IDEALIZED EXAMPLE WITH STRATIFICATION

We consider vertical dispersion in a stratified water column, with a total water depth of 50 m, and with perfect stratification so that the diffusivity is 0.1 $m^2\ s^{-1}$ above the pycnocline at 25 m and 0.02 $m^2\ s^{-1}$ below it. This is not meant to accurately represent the physics near a pycnocline, where we would expect a much reduced diffusivity at the very interface. Rather, it serves as an extreme benchmark for numerical schemes. The reason for this is that the gradient of the diffusivity D' is effectively infinite at the interface and zero everywhere else. Since this gradient term appears in the Euler scheme (Eq. 10), the scheme cannot be implemented directly; also, the maximum time step as computed in the section 'Lagrangian simulations' is zero. We will see, however, that the binned random walk performs well even in this extreme case.

We chose a non-regular grid with smaller grid cells near the interface. This demonstrates that the spacing in the finite-volume method needs not be regular, but also increases resolution in the initial phase when particles are concentrated near the interface. Sufficient resolution for the plots was obtained with 75 layers; note that the well-mixed criterion will be met for any number of layers. The pycnocline itself is in the middle layer, Number 38.

We release an ensemble of 10 000 tracers at time $t = 0$ at the pycnocline, i.e. in the central layer. Fig. 2 shows the vertical distribution during the initial phase of the dispersion (Fig. 2b), when the effects of bottom and surface are not yet noticeable. In this phase the solution is analytically available (Appendix 2); note that more than half the material moves into the zone with high diffusivity, where the tail is also longer. Fig. 2b also shows histograms of the vertical position of tracers, which move according to Binned Random Walk I (see the section 'Lagrangian simulations'). Fig. 2b demonstrates the good agreement between the stochastic simulation and the analytical solution, also during transients.

Fig. 2 also shows the final phase (Fig. 2d–f), when the material is approaching the final uniform distribution over the water column. Note that the time scale of the final transition to uniformity is between 10 000 and 30 000 s; this may be confirmed by computing the half-time of the slowest mode of the transition rate matrix A, which is 5790 s.

The dots in Fig. 2d–f are histograms of stochastic simulations with the naive random walk model $Z_{t+h} = Z_t + \sqrt{2D(Z_t)}(B_{t+h} - B_t)$, obtained by omitting the bias term $D'(Z_t)h$ in the Euler scheme (Eq. 10) (cf. Visser 1997). (Recall that D' in our case is zero everywhere except at the pycnocline where it is infinite). It is well known (Visser & Thygesen 2003) that this scheme produces an incorrect steady-state concentration of $C(z) \sim 1/D(z)$, compare Fig. 2f. Fig. 2d,e demonstrates that also the transients are qualitatively wrong, in that initially the majority of particles move down rather than up.

Finally, Fig. 2 contains sample paths obtained using Binned Random Walk I (see the section 'Lagrangian simulations'; Fig. 2c).

BIASED RANDOM WALKS IN THE VERTICAL

While the previous derivation was for pure diffusion, many applications have a vertical bias due to buoyancy, sedimentation, or active vertical migration of individuals. For example, Ådlandsvik et al. (2001) derive the dynamics of the vertical distribution of fish eggs and larvae from their buoyancy. Another example of such a bias is diel vertical migrations. The starting point for a simulation of vertical motion is the advection–diffusion equation:

$$\dot{C} = -(uC - DC')' \tag{11}$$

Here, $u = u(z, t)$ is the bias, which mathematically appears as an advective term and which may again

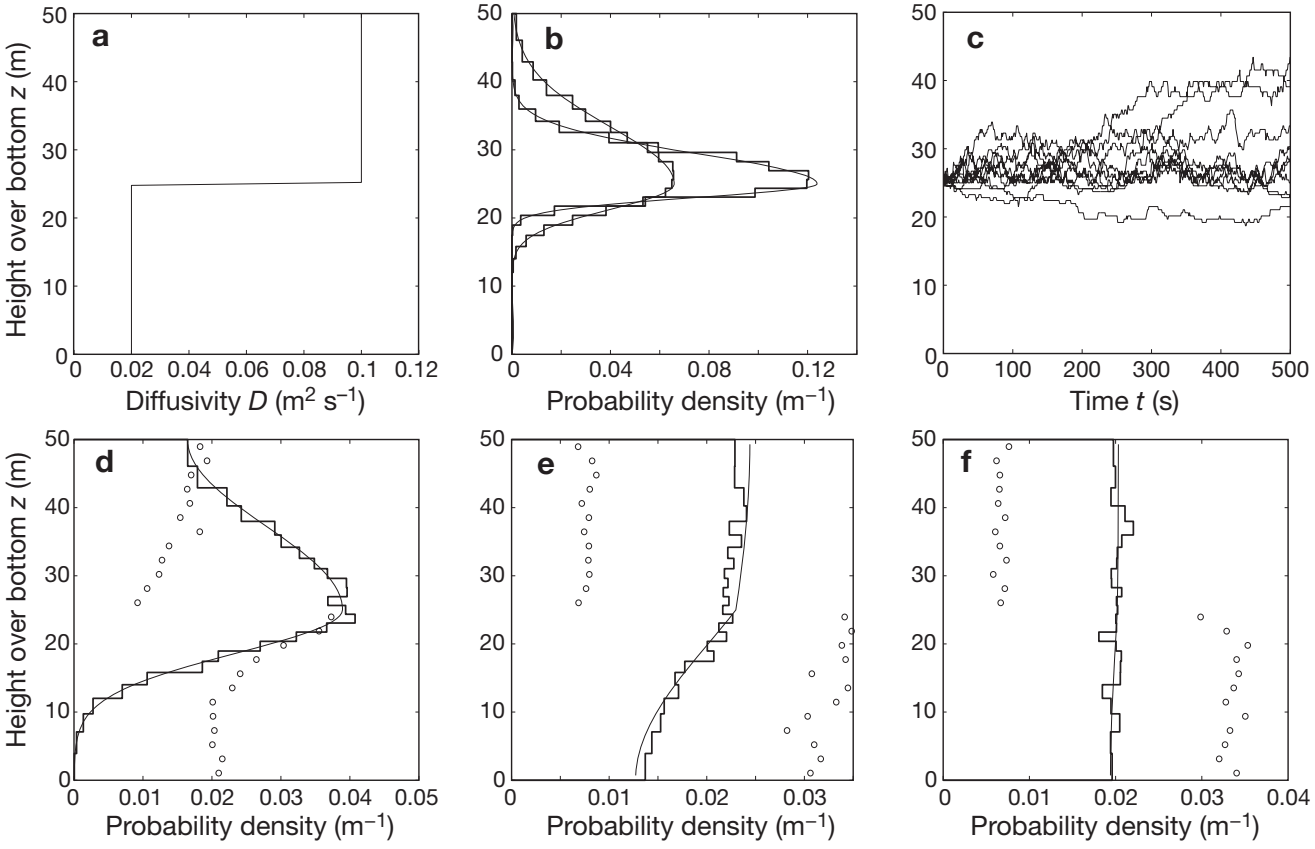

Fig. 2. Numerical solution of the diffusion equation with stratification. (a) The diffusivity profile. (b) The initial self-similar (scaling) phase; analytical solution (smooth curves) versus histograms (staircases) of the stochastic simulation of Binned Random Walk I. The more peaked distribution is for $t = 100$ s and the less peaked for $t = 350$ s. (c) Sample paths for Binned Random Walk I. (d) The final transition to a stationary state. Numerical solution using the final-volume method (smooth curve), histograms for Binned Random Walk I (staircase), and histogram for naive random walk (dots); time $t = 1000$ s. (e) As (d); time $t = 10\,000$ s. (f) As (d); time $t = 30\,000$ s

vary with space and time. The appropriate boundary conditions are *no flux*, i.e. that $J = uC - DC'$ vanishes at the boundaries $z = 0, d$. To simulate the motion of a particle, one may modify the Euler scheme (Eq. 10) to include the bias term, but, once again, the boundary behavior causes difficulties. In fact, a simple reflection scheme with constant diffusivity corresponds to a boundary condition $C' = 0$ rather than $uC - DC' = 0$. This provides another motivation for performing the simulation using a discrete-space Markov chain rather than the Euler scheme (Eq. 10).

For a finite-volume discretization of Eq. (11), it is always possible to use a first-order upwind scheme, where the net advective flux from cell i to $i + 1$ is approximated as:

$$\frac{m_i}{k_i}(u_i \vee 0) + \frac{m_{i+1}}{k_{i+1}}(u_i \wedge 0) \tag{12}$$

Here, we use the shorthand $u_i = u(z_i)$, i.e. the velocity is evaluated at the cell boundary. The notation $a \wedge b$ means $\min(a, b)$ and $a \vee b$ means $\max(a, b)$. From the Lagrangian point of view, it means that the rate of transition to cell $i + 1$ for a particle in cell i is now:

$$p_i = D_i \frac{2}{(k_{i+1} + k_i)k_i} + \frac{u_i \vee 0}{k_i} \tag{13}$$

and likewise the rate of transition to cell $i - 1$ for the same particle is:

$$q_i = D_{i-1} \frac{2}{(k_i + k_{i-1})k_i} - \frac{u_{i-1} \wedge 0}{k_i} \tag{14}$$

With these modified transition rates, the simulation proceeds according to the algorithms of the section 'Lagrangian simulations'.

Since this is only a first-order scheme, it introduces numerical diffusion, which leads to poor accuracy. It is therefore tempting to use a second-order central scheme, in which the net advective flux from cell i to cell $i + 1$ is approximated as:

$$u_i \frac{k_i^2 m_{i+1} + k_{i+1}^2 m_i}{k_i k_{i+1}(k_i + k_{i+1})} \tag{15}$$

This expression is derived by linear interpolation of the concentrations m_i/k_i and m_{i+1}/k_{i+1} from the cell centers to their interface. This leads to transition rates:

$$p_i = \frac{2D_i + u_i k_{i+1}}{k_i(k_i + k_{i+1})} \quad \text{and} \quad q_i = \frac{2D_{i-1} - u_{i-1} k_{i-1}}{(k_i + k_{i-1})k_i} \qquad (16)$$

This will improve the accuracy, so that fewer levels may be needed, although the requirement of positive transition rates leads, in the uniform case, to the constraint $P < 2$, where $P = |u|k/D$ is the cell Peclet number. This condition is also well known in the field of numerical analysis of partial differential equations; it avoids oscillations (Vreugdenhil & Koren 1993) and guarantees boundedness (Ferziger & Perić 2002, p. 145] in the corresponding second-order numerical scheme for the Eulerian advection–diffusion equation. As for the time step, whether we use the first-order upwind scheme or the second-order central scheme, the requirement $(p_i + q_i)h < 1$ in this case incorporates the Courant-Friedrichs-Levy stability condition for the advection part. In the uniform case this simplifies to:

$$\left(\frac{2D}{k^2} + \frac{|u|}{k}\right)h < 1 \qquad (17)$$

In summary, seen from a numerical perspective, it is easy to include vertical bias, whether this is due to non-neutral buoyancy or active vertical behavior: given an advection–diffusion equation (Eq. 11), which governs the concentration, we may use the technique of this section to simulate the motion of an individual. From a modeling perspective, however, it may not be trivial to establish the right bias and diffusivity in Eq. (11). Even for passive but non-neutrally buoyant particles like fish eggs, the dispersal will differ from that of a fluid element. When active vertical migration is present, as may be the case for fish larvae, dispersal is the result of both turbulence and unpredictable individual motion. Although statistics may be obtained from careful observations of individuals (Grünbaum 1999, Visser & Thygesen 2003), the variability in behavior is likely to limit the fidelity of the model. In this situation, there is a limit to the effort that should be invested in the accuracy of the numeric algorithms.

DISCUSSION

Although the theory of random walk models for turbulent dispersal is fairly complete, at least in the single-particle setting, the practical use remains impaired by difficulties concerning the choice of time step, the interpolation of eddy diffusivity profiles that are only available in discrete points, and reflection laws at the boundaries. These issues may lead to accumulation of particles in disagreement with the laws of physics, as may plain omission of the corrective bias term, and require statistical efforts to verify that the well-mixed criterion is not seriously violated. In this situation, we believe that the binned random walk discussed in this paper is a worthy alternative, because it satisfies the well-mixed criterion, by construction, and is substantially simpler to implement than any other scheme to our knowledge.

The binned random walk will not deliver vertical resolution beyond the width of the layers used. This in itself is no disaster, as it can be argued that the vertical resolution will, in any case, be bounded by the width of the layers in the underlying circulation model. Nevertheless, a practical question is how many layers to include in the binned random walk. One should at least use the same number as in the underlying circulation model, but one can easily use more, although the number of layers is naturally limited by computational resources. The computational burden per time step is largely independent of the number of layers, but the required time step to get accurate transients will decrease with the number of layers squared. Thus, the number of layers is a trade-off between computational resources and the need for vertical accuracy imposed by the variability of other fields, e.g. the horizontal flow velocity. These trade-offs are similar to the choice of time step for a standard random displacement model; although we have not done a detailed comparison of numerical performance, the 2 methods appear similar in terms of computing time.

With a fixed discretization of the vertical, the choice stands between the 2 algorithms described in the section 'Lagrangian simulations'. Binned Random Walk II is the more efficient in ideal case studies where the fields do not change with time, whereas Binned Random Walk I is able to handle the time-varying fields of typical realistic cases. With this algorithm, the choice of time step h still remains. The absolute requirement for the scheme to be well defined is that $h < 1/(p_i + q_i)$ for all i, so that all probabilities are between 0 and 1. For accuracy, the time step must be small enough so that >1 state transition in the continuous process is unlikely. This, it may be shown, requires that $h^2(p_i + q_i)^2/2$ is small. While this gives some guidance, the quantitative effect of discretizing time (and, for that matter, space) is easily analyzed using the Eulerian counterpart, under frozen conditions, or Binned Random Walk II. This should be contrasted with, for example, the random walk scheme (Eq. 10), where it is substantially more difficult to determine even how much the stationary distribution differs from the uniform one for a given time step, let alone errors in transients. Note, however, that the Euler scheme (Eq. 10) does not have absolute requirements for the time step, only requirements for accuracy.

One disadvantage of a binned random walk for vertical dispersal is that the vertical position is necessarily

discrete and, thus, cannot be a continuous function of underlying parameters. This makes it more difficult to base sensitivity analysis on individual trajectories rather than on ensemble statistics, as may be done with continuous-space, random walk schemes (U. H. Thygesen & A. W. Visser unpubl.).

We have focused on the vertical dimension. Binned random walk methods can easily be extended to 2- or 3-dimensional situations. However, for advection-dominated horizontal flow these methods will suffer from the same kind of numerical diffusion and dispersion problems as the finite-volume/differences methods from which they are derived. It is therefore recommended to use ordinary particle tracking in the horizontal, maintaining the continuous particle position. This can be combined with a binned random walk in the vertical for approximate treatment of mixing, buoyancy, and/or biological behavior. In this situation, the vertical jump rates (i.e. the probabilities p_i and q_i) will typically vary with both time and horizontal position.

The oceanographic community generally agrees that it is of primary importance that Lagrangian simulations of turbulent dispersal do not display aggregation of particles due to artifacts of models or implementations. In this regard, the formal statement of the well-mixed criterion (Thomson 1987) was seminal in that it gave a continuous-time, random-flight process governing the motion of a tracer, which displayed the correct steady-state statistics and the right inertial subrange. Unfortunately, the numerical issues regarding discretization of this process, including interpolation of gridded data and boundary behavior, mean that the well-mixed criterion remains a hurdle for practitioners, also when using random walks. In the present paper, we have directed attention to the fact that the well-mixed criterion can be satisfied in practice, also in discrete time, by using a binned random walk. Thus, we hope that the focus can shift towards the accuracy of the transients, which in many applications is of greater importance than the steady state.

Acknowledgements. The work of U.H.T. has been supported by the SLIP research school under the Danish Network for Fisheries and Aquaculture Research (www.fishnet.dk) as well as by the REX project, financed by the Danish Ministry for Food, Agriculture and Fisheries and the Danish Agricultural and Veterinary Research Council. The work of B.Å. has been supported by the project Effects of North Atlantic Climate Variability on the Barents Sea Ecosystem (ECOBE), financed by the Norwegian Research Council. We thank 3 anonymous referees for helpful and constructive comments.

LITERATURE CITED

Ådlandsvik B, Coombs S, Sundby S, Temple G (2001) Bouyancy and vertical distribution of eggs and larvae of blue whiting (*Micromesistius poutassou*): observations and modelling. Fish Res 50:59–72

Boyra G, Rueda L, Coombs SH, Sundby S, Ådlandsvik B, Uriarte A (2003) Modelling the vertical distribution of eggs of anchovy (*Engraulis encrasicolus*) and sardine (*Sardina pilchardus*). Fish Oceanogr 12:381–395

Brickman D, Smith PC (2002) Lagrangian stochastic modeling in coastal oceanography. J Atmos Ocean Technol 19: 83–99

Christensen A, Daewel U, Jensen H, Mosegaard H, St. John M, Schrum C (2007) Hydrodynamic backtracking of fish larvae by individual-based modelling. Mar Ecol Prog Ser 347:221–232

Csanady GT (1973) Turbulent diffusion in the environment. Springer, Heidelberg

Ferziger JH, Perić (2002) Computational methods for fluid dynamics, 3rd edn. Springer, Heidelberg

Gardiner CW (1985) Handbook of stochastic models, 2nd edn. Springer, Heidelberg

Garrett C (2006) Turbulent dispersion in the ocean. Prog Oceanogr 70:113–125

Grimmett GR, Stirzaker DR (1992) Probability and random processes, 2nd edn. Oxford University Press, Oxford

Grünbaum D (1999) Advection–diffusion equations for generalized tactic searching behaviors. J Math Biol 38:169–194

Kloeden PE, Platen E (1995) Numerical solution of stochastic differential equations. Springer, Heidelberg

Moler C, Van Loan C (2003) Nineteen dubious ways to compute the exponential of a matrix, twenty-five years later. SIAM (Soc Ind Appl Math) Rev 45(1):3–49

Okubo A, Levin S (2001) Diffusion and ecological problems: modern perspectives. Springer, Heidelberg

Ross ON, Sharples J (2004) Recipe for 1-D Lagrangian particle tracking models in space-varying diffusivity. Limnol Oceanogr Methods 2:289–302

Taylor GI (1954) The dispersion of matter in turbulent flow through a tube. Proc R Soc Lond A 223:446–468

Thomson DJ (1987) Criteria for the selection of stochastic models of particle trajectories in turbulent flows. J Fluid Mech 180:529–556

Thygesen UH, Nilsson AFN, Andersen KH (2006) Eulerian techniques for individual-based models based on additive processes. J Mar Syst doi 10.1016/j.marsys.2006.10.005

Visser AW (1997) Using random walk models to simulate the vertical distribution of particles in a turbulent water column. Mar Ecol Prog Ser 158:275–281

Visser AW, Thygesen UH (2003) Random motility of plankton: diffusive and aggregative contributions. J Plankton Res 25(9):1157–1168

Vreugdenhil CB, Koren B (eds) (1993) Numerical methods for advection–diffusion problems, Vol 45. Notes on numerical fluid mechanics. Vieweg, Wiesbaden

Wilson JD, Flesch TK (1993) Flow boundaries in random flight dispersion models: enforcing the well-mixed condition. J Appl Meteorol 32:1695–1707

Yamazaki H, Mackas DL, Denman KL (2002) Coupling small-scale physical process with biology. In: Robinson AR, McCarthy JJ, Rothschild BJ (eds) The sea, Vol 12, Chap 3. John Wiley & Sons, New York, p 51–112

Appendix 1. Incremental mean and variance in random walks on grids

Consider first the Euler scheme (Eq. 10) and assume Z_t is given. The mean displacement is $\mathbf{E}\{Z_{t+h}|Z_t\} = Z_t + D'(Z_t,t)h$, whereas the variance of the displacement is $\mathbf{V}\{Z_{t+h}|Z_t\} = 2D(Z_t,t)h$. For the continuous-time diffusion process given by the stochastic differential equation (Eq. 9), these expressions are correct to first order in the time increment h (Kloeden & Platen 1995). Note also that the mean-square of the increment coincides with the variance to first order in h, since the mean is of first order in h.

Next, consider Binned Random Walk I (see section 'Lagrangian simulations'), assume that the grid is uniform so that $z_i - z_{i-1} = k$ for all i, and assume that the particle at time t is in cell i. The mean displacement in the interval $(t, t + h)$ is:

$$-kq_ih + kp_ih = \frac{D_i - D_{i-1}}{k}h$$

Since the probability of a displacement of $-k$ is q_ih, just as th probability of a displacement of $+k$ is p_ih. Using the usual finite-difference approximation of D', this agrees with $D'h$ where D' is evaluated at the midpoint of cell i.

Next, the mean square displacement is:

$$k^2q_ih + k^2p_ih = (D_i + D_{i-1})h$$

Again, using $(D_i + D_{i-1})/2$ as an approximation for the diffusivity at the midpoint of cell i, this agrees with $2Dh$. In summary, the mean and variance of the increment in the Binned Random Walk I agree with the underlying diffusion process, to first order.

Appendix 2. Diffusion with piecewise constant diffusivity

We consider the concentration field $C(z,t)$ of a tracer in an infinite 1-dimensional space, subject to pure diffusion with diffusivity D_+ for $z > 0$ and diffusivity D_- for $z < 0$. If a unit quantity of a tracer substance is released at the interface at $t = 0$, then its density at time t is:

$$C(z,t) = \frac{1}{\sqrt{\pi t}}\frac{1}{\sqrt{D_+}+\sqrt{D_-}}\exp\left(-\frac{z^2}{4D(z)t}\right)$$

To see that this is the right solution in the presence of the discontinuity of D at the interface, note that this C satisfies the integral form of the conservation equation, from which the diffusion equation (Eq. 1) is derived:

$$\frac{\mathrm{d}}{\mathrm{d}t}\int_a^b C(z,t)\mathrm{d}z = J(a,t) - J(b,t)$$

where $a < b$ are arbitrary and $J = -DC'$ is the diffusive flux.

Notice that the tracer substance is not equally divided between the 2 regions; more material will be present in the region where the diffusivity is higher.

Editorial responsibility: Alejandro Gallego (Contributing Editor), Aberdeen, UK

Submitted: June 16, 2006; Accepted: March 18, 2007
Proofs received from author(s): September 25, 2007

Vol. 347: 155–169, 2007
doi: 10.3354/meps07092

MARINE ECOLOGY PROGRESS SERIES
Mar Ecol Prog Ser

Published October 11

OPEN ACCESS

Individual-based simulations of larval fish feeding in turbulent environments

Patrizio Mariani[1,*], Brian R. MacKenzie[1], Andre W. Visser[1], Vincenzo Botte[2]

[1]Danish Institute for Fisheries Research, Technical University of Denmark, Kavalergården 6, 2920 Charlottenlund, Denmark
[2]Laboratory of Biological Oceanography, Zoological Station 'A. Dohrn,' Villa Comunale 1, 80100 Napoli, Italy

ABSTRACT: We used an individual-based model coupled to a realistic turbulence flow field to assess the effects of a wide range of turbulence levels on encounter rate (E), pursuit success and ingestion rate in fish larvae. We parameterized the model for larvae of Atlantic cod *Gadus morhua* and evaluated how the geometry of their prey search volume (hemisphere, wedge) affected feeding rates. We then compared model outputs with feeding rates for cod larvae in previous laboratory and field studies. Search volume is smaller and E is lower for wedge searchers than hemisphere searchers. However, as turbulence increases, larvae encounter more prey but pursuit success decreases exponentially (relative to calm water), yielding a dome-shaped relationship between turbulence and ingestion rate. These results are robust to search volume geometry (wedge or hemisphere). The increase in ingestion rates at moderate turbulence for wedge searchers (relative to calm water rates) was higher than for hemisphere searchers. However, model results derived using hemisphere geometry are consistent with previous laboratory and field observations of cod larvae in turbulent environments. Cod larvae observed in a field study on Georges Bank in 1993–1994 could feed at rates which corresponded with observed growth rates if they behaved as hemispherical searchers and consumed a diet consisting of relatively large prey (e.g. copepodites and adults of *Pseudocalanus*); if they used wedge-shaped volumes, their ingestion and growth rates would have been ca. 80% lower, resulting in higher mortality. Models like those developed here will increase future understanding of factors affecting larval feeding rates and dietary composition.

KEY WORDS: Feeding · Ingestion · Encounter · Pursuit · Turbulence · Cod larvae · Growth · Predation

INTRODUCTION

The feeding of larval fish in the sea is influenced by ocean turbulence via several direct and indirect mechanisms. These effects include changes in (1) the production, concentration and distribution of prey (Kiørboe 1993, Bakun 1996), (2) vertical distributions of larvae (Heath et al. 1988, Franks 2001) and (3) the probabilities of encounter, pursuit and capture of prey by individual larvae (Dower et al. 1997, MacKenzie 2000). All of these processes vary with the intensity of turbulence in highly nonlinear ways and often in opposing directions. These responses of biological and physical processes to ocean turbulence complicate attempts to predict and understand how variations in turbulence affect larval fish ecology—in particular, the feeding success of larvae (Dower et al. 1997, MacKenzie 2000, Porter et al. 2005).

In the present study, we develop and apply new individual-based modelling approaches to investigate feeding processes of individual fish larvae in turbulent environments. These models are then combined with a realistic simulation of ocean turbulence at scales relevant to larval fish feeding. Previous modelling studies (Table 1) have used analytical modelling approaches forced by bulk-average turbulent dissipation rates and have demonstrated that encounter rates (E) increase with turbulence intensity, but that overall ingestions rates have a dome-shaped relationship to turbulence (Matsushita 1992, MacKenzie et al. 1994). These theoretical models have experimental support (Landry et al. 1995, MacKenzie & Kiørboe 1995, MacKenzie &

*Email: pat@difres.dk

Table 1. Meta-data of the development of modelling approaches for investigating predation by zooplankton and fish larvae in calm and turbulent environments. ε: dissipation rate; Re_λ: Reynolds number

Predation components modelled Encounter	Pursuit; capture	Modelling approach	Search volume geometry	Levels of turbulence investigated	Source
✓		Analytical	Spherical	None	Gerritsen & Strickler (1977)
✓		Analytical	Spherical	Many (wide range)	Rothschild & Osborn (1988)
✓	✓	Analytical	Spherical	Many (wide range)	Matsushita (1992)
✓		Analytical and direct numerical simulation	Spherical	Low level ($Re_\lambda = 38$)	Yamazaki et al. (1991)
✓	✓	Analytical	Spherical	Many (wide range)	MacKenzie et al. (1994)
✓	✓	Analytical	Spherical	Many (wide range)	Jenkinson (1995)
✓	✓	Analytical	Spherical	Many (wide range)	Caparroy et al. (2000)
✓		Analytical and numerical simulations	Spherical	Low level (estimated $\varepsilon = 5.53 \times 10^{-9}$ m^2 s^{-3})	Lewis & Pedley (2000)
✓		Analytical and numerical simulations	Spherical	Low level (estimated $\varepsilon = 5.53 \times 10^{-9}$ m^2 s^{-3})	Lewis (2003)
✓		Analytical	Spherical, hemi-spherical, wedge	Encounter: $\varepsilon = 1.8 \times 10^{-6}$ m^2 s^{-3}; no turbulence used for pursuit success	Galbraith et al. (2004)
✓	✓	Individual-based, object-oriented	Spherical	Many (wide range)	Mariani et al. (2005, in press)
✓	✓	Analytical and numerical simulations	Hemi-spherical, wedge	Low level (estimated $\varepsilon = 5.53 \times 10^{-9}$ m^2 s^{-3})	Lewis & Bala (2006)
✓	✓	Individual-based, object-oriented	Hemi-spherical, wedge	Many (wide range)	This study

Kiørboe 2000, Utne-Palm & Stiansen 2002). However, this type of modelling framework becomes impractical when analyses involve more complex aspects of organisms' feeding behaviour (Mariani et al. 2005), e.g. typical swimming and search behaviour (swim durations and frequencies, turn angles) of fish larvae, the swimming and escape behaviour of their prey, the intermittent nature of realistic turbulence.

We use our new models initially to investigate whether they yield comparable results to those seen in previous theoretical and experimental studies. We then explore the sensitivity of larval feeding to assumptions regarding the shape of the search volume of larval fishes. Early larval feeding behaviour studies (Rosenthal & Hempel 1970, Blaxter 1986) and clearance rate experiments in moderately turbulent water (Kiørboe & Munk 1986, MacKenzie & Kiørboe 1995) have suggested that larvae search a hemispherical volume of water in pursuit of prey. However, detailed video recordings of larval search behaviour in calm water suggest that the search volume is wedge shaped (Browman & OBrien 1992, von Herbing & Gallager 2000, Galbraith et al. 2004). Moreover, the difference in volume of the visual fields (e.g. 11.5-fold for 10 mm cod larvae, Galbraith et al. 2004) affects foraging strategy and costs; for larvae with wedge-shaped search volumes, successful predation strategies would require a combination of foraging in higher concentrations of prey, switching to larger prey, longer search periods and higher growth efficiency than if search volumes are 11.5-fold larger. The differences in search-volume geometry and size may also influence estimates of how turbulence affects larval feeding rates (Lewis & Bala 2006), although the functional relationship between turbulence intensity, E and pursuit success has not yet been investigated for wedge searching predators (Table 1). We therefore use our models to demonstrate their general applicability to larval fish ecology and in particular to explore how assumptions of larval search-volume geometry affect estimates of the role of turbulence on larval fish feeding.

METHODS

Our model framework consists of 2 integrated modules: (1) the flow field and its turbulence characteristics; and (2) the individual-based larval fish feeding component (which consists of feeding and swimming behaviours of a virtual larva based on experimentally

derived traits) and a prey field (which, for simplicity, is a field of uniform-sized non-swimming prey particles). Both the larva and prey positions are influenced by the turbulence in the flow field and their locations change over time relative to each other.

Flow field. In the hypothesis that the flow at individual scales is isotropic (Gargett 1989), a simplified but realistic representation of the turbulent flow field can be obtained by using a sum of unsteady random Fourier modes: a so-called kinematic simulation of the flow. This technique was proposed by Kraichnan (1970) and modified versions have been widely used to study physical phenomena. More recently, it has also been applied to analyze plankton interactions (Lewis & Pedley 2000, 2001, Lewis 2003, Visser & Jackson 2004, Yamazaki et al. 2004, Mariani et al. 2005, in press).

The turbulent velocity field at a point $\mathbf{x}$ at time t, $\mathbf{u}(\mathbf{x},t)$, is represented as a truncated Fourier series:

$$\mathbf{u}(\mathbf{x},t) = \sum_{n=1}^{N} \left(\mathbf{c}_n \times \hat{\mathbf{k}}_n\right) \exp[i(\mathbf{k}_n \cdot \mathbf{x} + \omega_n t)] \quad (1)$$

where N modes are selected independently, with randomly directed wave vectors $\mathbf{k}_n = \hat{\mathbf{k}}_n\, k_n$ and angular frequency ω_n. The Fourier coefficients in the form $(\mathbf{c}_n \times \hat{\mathbf{k}}_n)$ ensure that the velocity field is incompressible. The amplitude vectors $\mathbf{c}_n$ are chosen with amplitude given by:

$$|\mathbf{c}_n|^2 = 2\Pi(k_n)\delta k_n \quad (2)$$

and follow an inertial Kolmogorov energy spectrum:

$$\Pi(k) = \Pi_0 k^{-5/3} \quad (3)$$

although other spectral shapes can also be used (Fung & Vassilicos 1998, Malik & Vassilicos 1999, Lewis & Pedley 2001). Here $\delta k_n = (k_{n+1} - k_{n-1})/2$ for $n = 2,\ldots, N-1$, while on the boundaries, $\delta k_1 = (k_2 - k_1)/2$ and $\delta k_N = (k_N - k_{N-1})/2$. N discrete wave numbers are chosen to lie between the inverse of the integral scale, $k_1 = I^{-1}$, and the inverse Kolmogorov scale, $k_N = \eta^{-1}$. Hence, in physical space, this is equivalent to setting the inertial sub-range to lie between $2\pi I$ and $2\pi\eta$. Outside this range inertial kinetic energy is set to zero. This does not mean that turbulence-induced relative motion is zero at scales less than $2\pi\eta$; turbulent straining of the fluid continues all the way down to molecular scales. To avoid harmonic effects (Visser & Jackson 2004), discrete wave numbers are distributed in a geometric series within the inertial range:

$$k_n = \frac{1}{I}\left(\frac{I}{\eta}\right)^{\frac{n-1}{N-1}} \quad (4)$$

The angular frequency ω_n is:

$$\omega_n = 0.4\sqrt{k_n^3 \Pi(k_n)} \quad (5)$$

where the unsteadiness parameter is 0.4 (Malik & Vassilicos 1999, Visser & Jackson 2004). Finally, by choosing $\Pi_0 = 1.5\varepsilon^{2/3}[1 - (\eta/I)^{4/3}]^{-1}$ in Eq. (3), the appropriate relation between ε (dissipation rate) and $\Pi(k)$ is ensured (Tennekes & Lumley 1972).

By construction, the Eulerian 2-point spatial correlation function of velocities has the Kolmogorov form. However, the simulations do not represent the dynamical processes in turbulence, which affects higher order statistics such as intermittency. Consequently, the simulated turbulence will differ from hydrodynamic turbulence, since higher order Eulerian statistics will be Gaussian distributed (Fung et al. 1992, Reynolds 1995, Yamazaki et al. 2004). However the results of Fung et al. (1992) suggested that the detailed aspects of the flow are not so important when modelling many aspects of dispersion; these discrepancies are not likely to substantially influence the results presented here because we are mainly concerned with the small-scale 2-point velocity correlations.

Individual-based model. Neutrally buoyant point particles are used to simulate predators and prey. Each individual moves according to simple species-specific internal rules. The instantaneous swimming velocity of predator particles is the sum of the larval swimming and the local flow velocity, while the prey is assumed to passively drift in the turbulent flow field.

The predator's stochastic swimming motion is obtained by computing the cumulative distribution functions of observed larval behaviour (see below) and then randomly picking numerical values to determine the pause or move behavioural event with its duration, the horizontal turn angle and the swimming velocity.

Feeding processes in the model have been divided into 3 behavioural events: encounter, pursuit and capture (Fig. 1). The biological components for the model are based on laboratory studies conducted at 6 to 8°C (MacKenzie & Kiørboe 2000, Galbraith et al. 2004).

Encounter: We model cod larvae as a pause-travel searcher. This behaviour assumes that cod larvae only

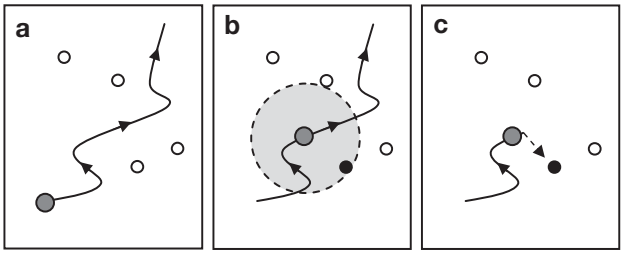

Fig. 1. Processes included in the individual-based model. (a) Each predator moves according to its individual behavior; (b) at each time step during the pause period, it evaluates the number of contacts; (c) if it finds a prey (●), the predator moves towards it until the prey is captured or the contact is lost

search for prey while pausing between swim events. Although this is likely an oversimplification of larval cod search behaviour (von Herbing & Gallager 2000, Lewis & Bala 2006), there is some experimental evidence which demonstrates that cod and other species of fish larvae do search for prey while pausing (MacKenzie & Kiørboe 1995, von Herbing & Gallager 2000, Galbraith et al. 2004). The duration and frequency of pause and move events were drawn from literature (Galbraith et al. 2004, and see details below). The distance moved during individual swim events is a combination of the swim speed and duration. If the distance moved is sufficiently large (and assuming no turbulence to advect prey into the search volume), the larva will search a volume of water which has not been searched in the previous pause. However, if the move distance is short, search volumes will partly overlap. The volume of the overlap between successive pauses will depend on search-volume geometry (Galbraith et al. 2004, Lewis & Bala 2006); we use our models to investigate how different levels of turbulence affect the volume of overlap, and subsequently *E*, for 2 search geometries.

An encounter is recorded by the model if prey are located in the predator's search volume during a pause event. Encounters can occur when larvae move to a location which has a prey in the new search volume, or when a prey is advected by turbulence into the search volume during a pause. Once an encounter occurs, the larva is programmed to begin pursuit; hence, additional prey that could be advected by turbulence into the larval search volume are ignored by the larva. This behaviour is reasonable, because the concentrations of those prey that dominate larval cod diets in the sea (nauplii and copepodites of *Pseudocalanus* sp. and *Calanus finmarchicus,* Heath & Lough 2007) are usually so low (e.g. 1 to 10 l^{-1}) that it is unlikely that 2 prey would co-occur in volumes of water comparable to a larval search volume (largest volume ~2 cm^3).

During pauses, the larva scans the surrounding water using the given search-volume geometry. We used 2 search-volume geometries to simulate prey encounter: hemispherical and wedge shaped. The former is defined using a perception radius (*R*) and horizontal and vertical half angle equal to 90°, while the latter is a function of *R*, the horizontal half-angle θ_h = 45° and a vertical half-angle θ_V = 10° (Galbraith et al. 2004; our Fig. 2). During pause events the predator's sight direction is kept constant and oriented according to the swimming direction of the last swimming event. Therefore the predator looks along its line of sight while pausing and scans the water in its perception field with no heading changes until the next swimming event.

In general, prey is encountered by the larva when the separation distance between larva and prey is lower than the perception radius and the prey is within the visual field of the predator (i.e. when the angle between the axis of the larva's search-volume geometry and the vector connecting predator and prey is lower than the corresponding angle given above).

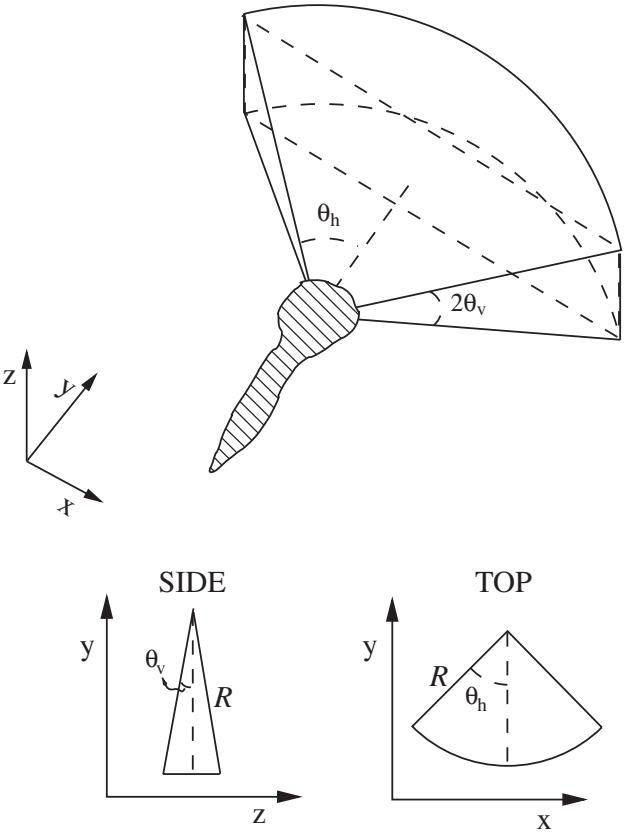

Fig. 2. Wedge-shape geometry of individual predator. *R*: perception radius; θ_h: horizontal half angle (45°); θ_v: vertical half angle (10°)

Pursuit: If the predator finds a prey, it starts to pursue the prey by moving toward it with a given pursuit velocity (V_P). This prey-tracking behaviour continues until an attack is executed or the prey is lost from view. If more than 1 prey is in the search volume, the predator chooses at random one of these prey as its target. During the pursuit, both predator and prey are affected by the flow field, which modifies the relative positions of the particles. If the predator loses visual contact with the prey it was hunting, the predator resumes its normal swimming behaviour and the pursuit is recorded as a failed pursuit event. Persuit success is derived as the ratio between the numbers of captures and pursuit events.

Capture: Predator pursuit behaviour continues until contact is lost or the prey is captured. Capture is assumed to occur after the predator has approached the prey close enough to enable final attack, i.e. forward thrusting and opening of the mouth. Modelled

attack success against pursued and fixated prey by cod larvae is high and independent of a wide range of turbulence levels; this is because direct observations (MacKenzie & Kiørboe 2000) and theory (Fiksen & MacKenzie 2002) indicate that cod larvae usually approach their prey slowly enough to avoid eliciting escape behaviour of their prey. We therefore assume that when prey-larval separation distance is smaller than a given capture distance (R_C), prey is successfully attacked and captured. Once the prey is captured, the prey particle is removed from the modelled prey population and the predator resumes its normal search behaviour. Then a new prey is created at a random location in the model domain outside the predator search volume to ensure a constant prey concentration.

Model setup. We analyzed 3 size classes of cod larvae with body dry weights equal to 40, 100 and 210 µg; these weights correspond to larval lengths (L) of 5, 6 and 10 mm based on weight–length relationships for larvae growing in large mesocosms at 8°C in non-limiting food concentrations (Otterlei et al. 1999). Swimming speed, contact radius, V_P and R_C vary according to these larval sizes (Table 2).

Predator swimming behaviour is introduced using the frequency distributions of lengths and durations of moves, swim speed, and turn angles (vertical and horizontal) of a 28 d old larvae reported in Galbraith et al. (2004), which corresponds to the largest L (10 mm) used in the present study (Otterlei et al. 1999). We assume that the same frequency distributions apply for the 2 other larval size classes, and that the swim speed changes according to a cod-specific functional relationship between swimming speed and body length for larvae and juveniles at 8°C (Peck et al. 2006). We used average swim speeds (u) of 1.1 and 0.8 mm s^{-1} for L = 6 and = 5 mm, respectively; the variability of swimming speed for each size group was based on u for L = 10 mm (u = 5.4 mm s^{-1}) and its frequency distribution (Galbraith et al. 2004), and scaled downward for the smaller sizes (Fig. 3). As a result of this scaling procedure, larvae with slower u have less variability in swim speed.

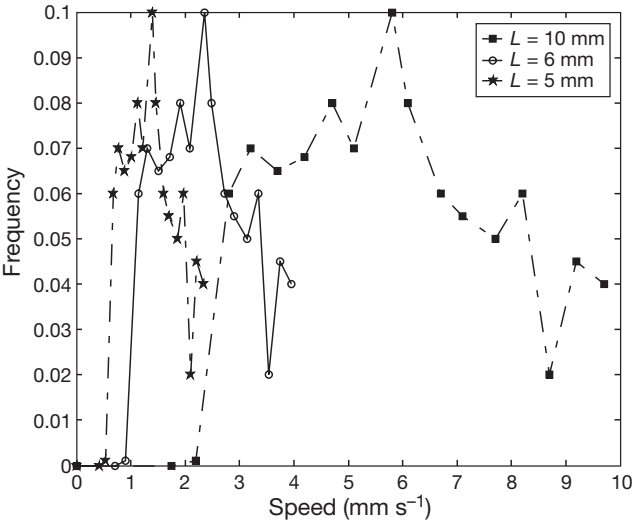

Fig. 3. Swimming speed frequency distributions of the 3 size classes considered in the model. For the largest class (L = 10 mm) we used data reported in Galbraith et al. (2004), while in the other 2 classes (L = 6 and 5 mm) we scaled the distribution to fit their average swimming speed

R is assumed to be equal to L and R_C is assumed to be 20% of this value (MacKenzie & Kiørboe 2000). V_P has been estimated by dividing R by the pursuit time (t_p). t_p for cod larvae of different sizes is assumed to be a function of body length, as determined empirically from laboratory observations of several species of larval fish (Werner et al. 2001):

$$t_P = 3.9(L/10)^{-0.6} \quad (6)$$

The larval body lengths, weight and age, together with the resulting u, R, R_C and V_P are reported in Table 2. We assumed 10% variation in mean values of R_C and V_P.

We used 10 000 passive moving prey particles and a single predator swimming in a numerical cubic box of 1 m^3 in volume. The prey concentration we used (10 l^{-1}) is comparable to concentrations of nauplii and copepodites that are found in many areas where fish larvae feed and grow (MacKenzie et al. 1990).

We analyzed larval feeding processes at 9 different turbulence levels ($\varepsilon = 10^{-9}$ to 10^{-4} m^2 s^{-3}) and in calm water. This range encompasses turbulence typical of natural systems, from the deep ocean interior up to strong tidal and wind-mixed regimes (Peters & Marrasé 2000, Thorpe 2004). Kinematic simulations have been used with 32 Fourier modes and I = 0.5 m (i.e. integral length scale is 3.6 m, Table 3).

The integration of the trajectories is performed with a time step of 0.1 s. Such a short time step is required to prevent a

Table 2. Fish larvae size classes used in the present study. V_P: pursuit velocity; R_C: capture distance. Data sources are also shown

Weight (µg)	Length (mm)	Age (d)	Mean speed (mm s^{-1})	Radius (mm)	V_P (mm s^{-1})	R_C (mm)
40[a]	5[a]	8[a]	1.3[c]	5[d]	0.8 ± 0.1[e]	1.0 ± 0.1[d]
100[a]	6[a]	19[a]	2.2[c]	6[d]	1.1 ± 0.1[e]	1.2 ± 0.1[d]
210[a]	10[a]	28[b]	5.4[b]	10[b]	2.6 ± 0.3[e]	2.0 ± 0.2[d]

[a]Otterlei et al. (1999); [b]Galbraith et al. (2004); [c]Peck et al. (2006); [d]MacKenzie & Kiørboe (2000); [e]Werner et al. (2001)

Table 3. Dissipation rate (ε), 2π Kolmogorov length scale (2πη), rms turbulence velocity scale (W) and Reynolds number (Re_λ) of the kinematic simulations for kinematic viscosity εν = 10^{-6} m^2 s^{-1}, integral length scale 3.6 m (I = 0.5 m) and 32 Fourier modes

ε ($\times 10^{-6}$ m^2 s^{-3})	2πη (mm)	W (mm s^{-1})	Re_λ
0.001	35.3	0.8	77.2
0.01	19.9	1.7	113.2
0.05	13.3	2.9	148.1
0.1	11.2	3.7	166.2
0.5	7.5	6.3	217.4
1	6.3	7.9	244.0
5	4.2	13.6	319.0
10	3.5	17.1	358.1
100	2.0	36.8	525.6

predator from missing any prey that might be passing through its contact area between time steps, and also because swim and pause events are short (MacKenzie & Kiørboe 1995, von Herbing & Gallager 2000, Galbraith et al. 2004). Numerical tests showed that when using this time step, there is no real difference between the results obtained integrating in time with a fourth-order Runge-Kutta method and those obtained with a first-order Euler scheme. Therefore, the much faster Euler integration scheme was used in all simulations to reduce computing time.

In order to maintain the initial concentration in the numerical box, when particles reach the boundary of the box they are reinserted in the domain using pseudo-periodic boundary conditions (Mariani et al. 2005). A particle that leaves one of the sides of the domain is repositioned at random on the opposite side, with the condition that the direction of the velocity at the point is directed towards the interior of the domain.

To test the ability of the kinematic simulations to realistically represent ocean turbulence at scales relevant to larval fish feeding, we ran the model at different turbulence levels using 100 equally spaced passive particles. We then derived the particle-particle velocity difference and separation distance. According to well known theories of turbulent energy dissipation (Tennekes & Lumley 1972, Rothschild & Osborn 1988), relative velocity scales with separation distance according to $w = 1.8(\varepsilon s)^{1/3}$, where the relative velocity (w) is a function of ε and the separation distance (s).

The distribution of relative velocities between particles showed a wide range of values. We calculated mean velocities for a uniform range of bins of logarithmically spaced s. This averaging procedure is similar to that used for binning small-scale velocity shear and ε data obtained in the sea with shear micro-structure profilers (Oakey & Elliott 1982, Simpson et al. 1996). The resulting average velocity as a function of s at 2 turbulence levels (ε = 10^{-8} and 10^{-6} m^2 s^{-3}) was then plotted and compared with the theoretical values (see Fig. 4a).

Model execution and outputs. Our model approach incorporates randomization and stochasticity in many of its parameterisations (e.g. swimming behaviour, turbulence flow fields). We executed the model 5 times per dissipation rate (9 levels + calm water) for each of 3 larval size groups for each of the 2 search-volume geometries (i.e. a total of 5 × 10 × 3 × 2 = 300 simulations); each simulation was executed by initiating the run using a different random number sequence. Feeding output data are shown as means of the 5 runs for each combination of larval size and search-volume geometry. Because we used realistic concentrations of prey (10 prey l^{-1}) in our model, each simulation was allowed to run 4 h (hemisphere) or 12 h (wedge) to enable sufficient encounters and captures for meaningful interpretation. We derive the following biological outputs from the model: E (prey h^{-1}), pursuit success and ingestion enhancement factor (ψ) defined as:

$$\psi = \frac{\beta_T - \beta_C}{\beta_C} \quad (7)$$

where β_C and β_T are the clearance rates derived from the number of captures under calm and turbulent conditions, respectively.

Encounter, pursuit and capture can be illustrated visually in virtual format by reconstructing the predator–prey interactions and the associated trajectories. The simulated feeding processes can be viewed in Video clips 1 to 4 (Video clips 1 & 2: calm water conditions; Video clips 3 & 4: turbulent water conditions), available as MEPS Supplementary Material online at www.int-res.com/articles/suppl/m347p155_videos/.

The model is developed in C++ with an entirely object-oriented programming approach. Each of the 300 simulations using the model setup as described here and with turbulence, typically required 1 h on a 64-bit Intel® Xeon 3.2Ghz processor and 2 Mb cache size.

Validation of model outputs with observations. We conducted 3 sets of comparisons of our modelling results with independently derived feeding and growth data. We first compared our model outputs with literature observations of cod larvae feeding behaviour in calm and turbulent water. As no direct observations of E or pursuit success are yet available for wild cod (or any other) larvae growing in the sea, we used 2 different sets of laboratory data (E, pursuit success) for this comparison. The laboratory observations of E (MacKenzie & Kiørboe 1995) and pursuit behaviour (MacKenzie & Kiørboe 2000) in different levels of quantified turbulence were compared with the model outputs derived using wedge and hemi-

spherical search volumes. The sizes of larvae used in the laboratory experiments were similar to those used in the present modelling study.

The third comparison involved ingestion rates derived from our model and ingestion rates estimated for cod larvae growing in nature. We extracted field estimates of larval cod growth rate data from a detailed literature case study and estimated ingestion rates and food requirements, given reasonable assumptions of growth efficiencies and prey sizes and concentrations. Further details of the comparison are given in 'Results.' This comparison enabled us to estimate which search-volume geometry could satisfy observed feeding rates in the wild, and how prey size and concentration could interact with search volume geometry to affect larval feeding and growth rates.

RESULTS

Turbulence

The relative velocities as derived from the kinematic simulation at 2 turbulence levels ($\varepsilon = 10^{-8}$ and 10^{-6} m^2 s^{-3}) reproduce the main features and patterns of the turbulence flow field (i.e. turbulence velocity and the overall structure of the flow field) at scales relevant to encounter and pursuit (Fig. 4a). As an illustration of those processes, we show in Fig. 4b a typical velocity field with the trajectories of a hundred drifting particles. The flow field is an instantaneous 2-dimensional snapshot extracted from a 3-dimensional kinematic simulation at $\varepsilon = 10^{-7}$ m^2 s^{-3}. Particles were initially released 1 cm apart and they show the streamlines of the turbulence field, where areas of convergence and divergence are both present along their paths. Also shown is the presence of a small eddy within the turbulence flow field with size comparable to the predator perception distance (Fig. 4b at $x \approx 0.8$, $y \approx 0.7$ cm).

Feeding processes

E increased as dissipation rates increased for both search geometries (Fig. 5a–c). E for larvae using the wedge-shaped search volumes are lower than for those using the hemisphere in all 3 size classes; 10, 6 and 5 mm larvae using hemisphere search volumes encountered, on average, 8-, 6- and 5-fold more prey, respectively, than larvae using wedge-shaped search volumes (Fig. 5a–c).

The different search-volume geometries show different sensitivities to the influence of turbulence. Maximum E for larvae using the hemisphere search-volume geometry increased ca. 10-, 7- and 5-fold for 5, 6 and 10 mm larvae, respectively (Fig. 5a–c). E for the wedge shape increased ca. 11-, 8.5- and 7-fold for the 3 size classes (Fig. 5a–c).

The average relationship between E and turbulence using all the geometries and size classes is $E \sim \varepsilon^{1/6}$. The

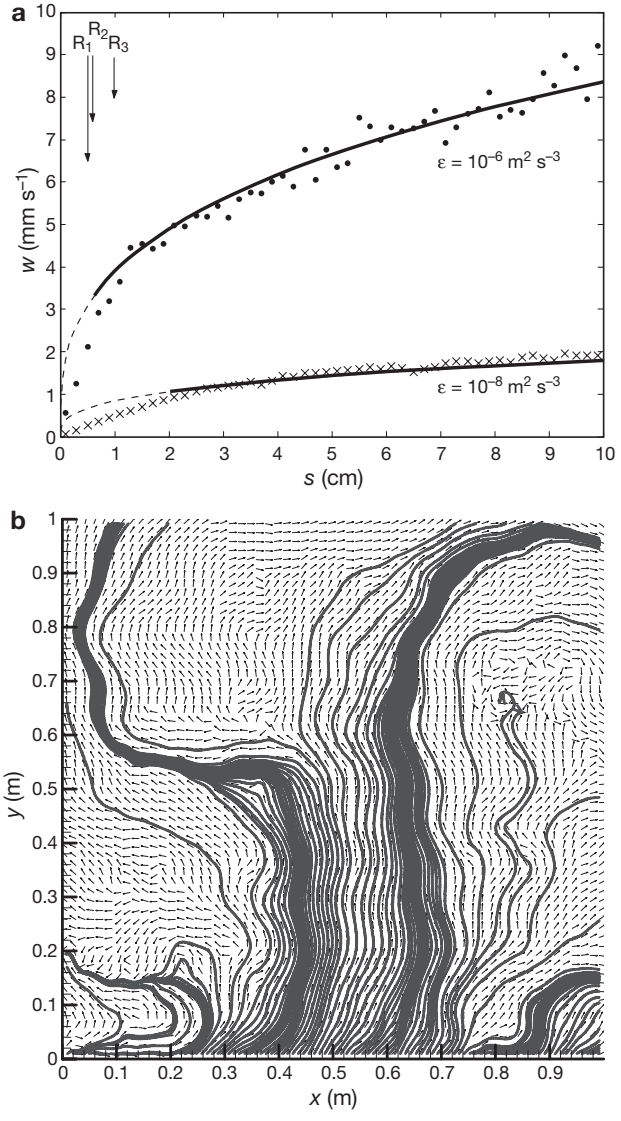

Fig. 4. (a) Structure function between particle-particle separation distance (s) and relative velocity between particles (w) for 2 different turbulent dissipation rates. Distances and velocities were derived by releasing 100 particles in the synthetic turbulent field (see 'Methods' for details). Average relative velocities at each separation distance were then compared with the theoretical structure function in the inertial range, i.e. solid lines, $w = 1.8(\varepsilon s)^{1/3}$. Note at small scales (top line: 6 mm; lower line: ~20 mm) the transition to a viscous dominated flow. ●: high turbulence ($\varepsilon = 10^{-6}$ m^2 s^{-3}), ×: low turbulence ($\varepsilon = 10^{-8}$ m^2 s^{-3}). Arrows indicate the values of the reactive distances used in this work ($R_1 = 5$ mm; $R_2 = 6$ mm; $R_3 = 10$ mm). (b) Representation on a grid of the simulated flow field and trajectories of passive particles as represented by the modelled turbulence. Particles have been released at $y = 1$ mm and at equally distant values of x using separation distance of 1 cm

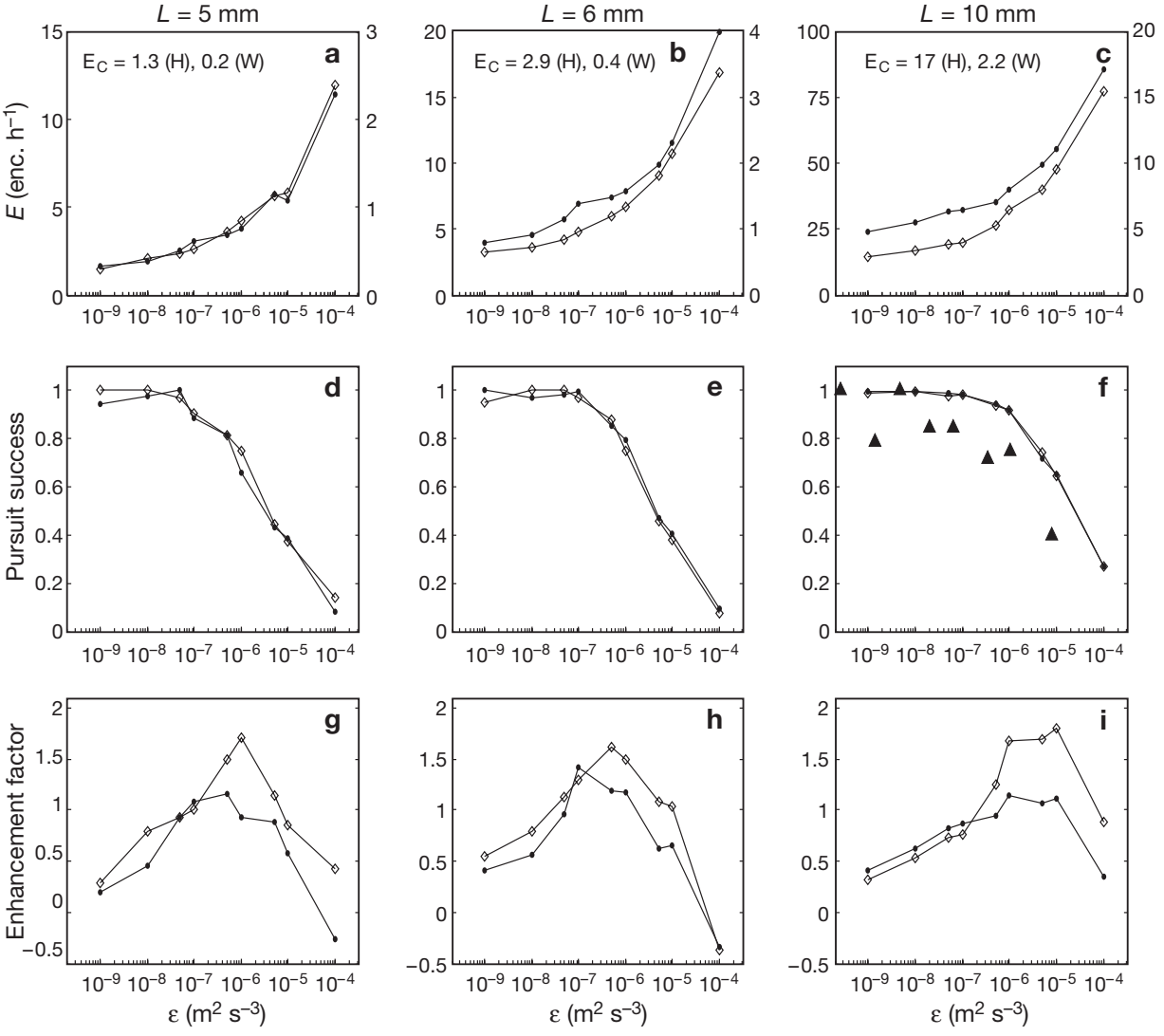

Fig. 5. (a–c) Modelled encounter rate (E), (d–f) pursuit success and (g–i) enhancement factor based on ingested prey, all as a function of dissipation rate (ε) and cod size (L = 5, 6, 10 mm). Two search geometries are considered: hemisphere (●) and wedge-shaped (◇). The number of encounters in calm water (E_C) for the hemisphere (H) and wedge (W) are reported in (a–c). Note E has 2 y-axes, left and right for the hemisphere and wedge cases, respectively. Observed values of pursuit success (▲, MacKenzie & Kiørboe 2000) for 10 mm cod larvae shown in (f) for comparison

resulting proportionality between dissipation and E is therefore lower than theoretical relationships which assume that all intersections of prey with predator search volumes are encounters, i.e. $\sim\varepsilon^{1/3}$. The smallest exponent represents the largest larval size class with hemisphere search geometry; the exponent increases among smaller size classes and larvae using the wedge-shaped search geometry. Exponents differ among search volumes and larval sizes because the predator cannot encounter other prey during the pursuit events. An increase in the turbulence level yields more encounters and therefore more pursuits; however, time allocated for pursuit reduces the time available for prey search and encounter.

Pursuit success decreases exponentially with turbulence for both the wedge and the hemisphere search volumes (Fig. 5d–f). The functional relationship to turbulence for the 2 search geometries is nearly identical. Pursuit success was 100% by larvae during relative low turbulence regimes (0 to 10^{-7} m^2 s^{-3}), but further increases in turbulence reduce the success.

The increase in the number of encounters in combination with the reduced pursuit success results in a dome-shaped distribution of the captures and overall ingestion rate (Fig. 5g–i). The enhancement of ingestion rate with turbulence peaks at between 10^{-6} to 10^{-5} m^2 s^{-3} for the largest size, but at lower turbulence levels for smaller sizes of larvae. The dome-shaped relation-

ship of ingestion to turbulence is evident for both the wedge-shaped and hemisphere search geometries. The magnitude of the enhancement is similar for wedge-shaped and hemisphere geometries at low turbulence levels; however, when turbulence was $>5 \times 10^{-7}$ m^2 s^{-3}, the enhancement was larger for the wedge-shaped. The relatively higher ingestion rate at intermediate levels of turbulence for the wedge-shaped geometry is due to its greater sensitivity of E to turbulence.

Comparison with observations

Many of the main results from the model outputs compare favorably with feeding behaviours directly observed and estimated with real cod larvae. We first consider E. The model indicates that 6 mm cod larvae, if assumed to have hemispherical search volumes, encounter 2.9 and 7.0 prey h^{-1} in calm and turbulent ($\varepsilon = 10^{-7}$ m^2 s^{-3}) water, respectively, at a prey concentration of 10 l^{-1}. These E values are similar to those observed directly by MacKenzie & Kiørboe (1995): 3 and 10 encounters h^{-1} for cod larvae (L = 5.2 mm) in calm and turbulent ($\varepsilon = 7.4 \times 10^{-8}$ m^2 s^{-3}) water, respectively, at the same prey concentration. If wedge-shaped search geometry is applied in the model, estimated E is around 6-fold smaller than that observed.

The model predicts that pursuit success declines nonlinearly as a function of ε, regardless of which of the 2 search volumes are assumed (Fig. 5d–f). The form of the modelled pursuit success is similar to the relationship between pursuit success and turbulence directly observed for cod larvae in several turbulence treatments in laboratory experiments described by MacKenzie & Kiørboe (2000). They found an inverse exponential relationship between the probability of a successful pursuit and the turbulent velocity consistent with the modelled relationships derived here (Fig. 5f). They also observed that pursuit success was higher at a given turbulence level among larger (12.3 mm) larvae than smaller (8.7 mm) larvae. This pattern is also evident in our new model calculations (Fig. 5d–f).

The third comparison uses field-estimated growth rates. Growth rates of cod larvae, for example on Georges Bank, can reach 14% body weight d^{-1} at a temperature of 7 to 8°C (Buckley et al. 2004, Lough et al. 2005, Buckley & Durbin 2007); growth rates at similar temperatures (provided that food supplies are non-limiting) can be higher in areas where longer photoperiod allows more search time per day (Otterlei et al. 1999, Helle 2000). Assuming 33% growth efficiency for converting ingested prey to body tissue (a typical value for many larval fish species; Houde 1989, MacKenzie et al. 1990), the number of ingested prey as a function of weight-specific growth rate can be derived if prey weights are known. Diets of early stages of larval cod in most areas of their distribution are dominated by nauplii of *Pseudocalanus* spp. and *Calanus finmarchicus* (Heath & Lough 2007). We used prey concentrations (2 l^{-1}) similar to those observed on Georges Bank and considered 2 prey sizes in our analyses: small, i.e. 0.26 µg (*Pseudocalanus* sp. nauplii, Monteleone & Peterson 1986) and big, i.e. 1.5 µg C (*Calanus finmarchicus* nauplii, Davis 1984).

The number of prey required to satisfy observed growth rates can therefore be compared with the ingestion estimated by the model for wedge and hemisphere, assuming a daily feeding period equal to 12 h and that all feeding occurred at the turbulence level which maximized ingestion rates.

The calculations and comparisons show that if larval diets only comprise small prey at 2 l^{-1}, they are not able to acquire the daily ration required for a low growth rate (6% d^{-1}), regardless of search volume geometry or larval size (Fig. 6a). The discrepancy between required and ingested prey amounts is higher for larvae growing at faster rates (up to 14%, as observed in the field) and decreases as prey concentration increases (Fig. 6b,c). Alternatively, if larvae are able to locate and capture large prey, and if they employ hemisphere search geometry, then all sizes of larvae are able to acquire enough prey to grow at moderate rates (6 to 10% d^{-1}) at low prey concentration. However, at the same prey concentration, if they have a wedge search geometry, none of the 3 size groups will be able to meet the observed food demand even when ingesting large prey; ingestion rates based on wedge search geometry are ca. 80% lower.

DISCUSSION

Our integrated object-oriented numerical modelling approach reproduced many aspects of the complicated process of larval feeding in turbulent environments. We first showed that the turbulence simulation scheme used produces realistic levels of turbulent velocity at scales important for larval fish feeding. Although the model is a simplified description of turbulence, our relationship between the relative velocity of simulated particle-pairs and the separation distances between them was consistent with well-known theories of turbulent motion at small scales (Tennekes & Lumley 1972) and with experimental evidence based on direct tracking of particles (neutrally buoyant beads, copepods) in turbulent water (Hill et al. 1992, MacKenzie & Kiørboe 2000). These results assure us that the equations used to estimate the turbulent velocities and dissipation rates in our framework were reliable and that the velocities themselves were reasonable.

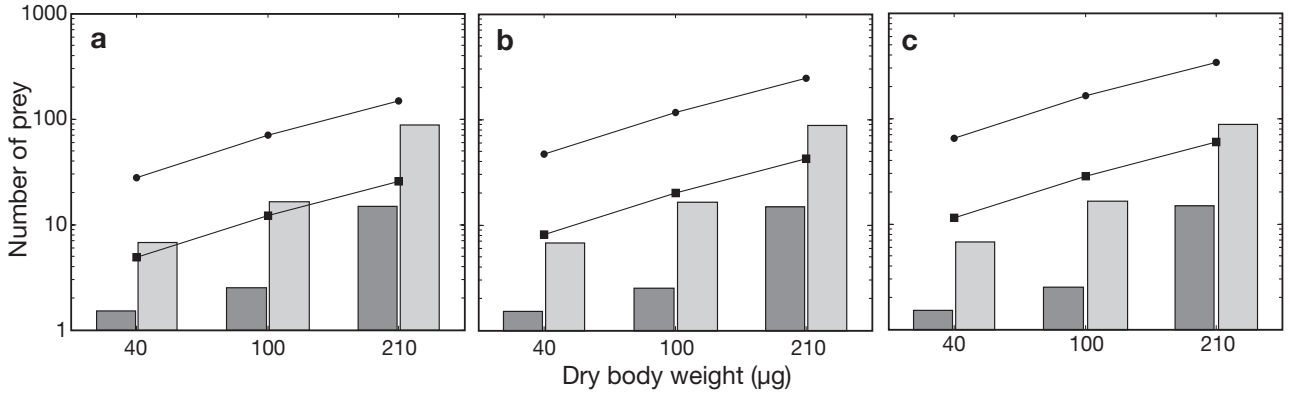

Fig. 6. Larval cod ingestion rates at prey concentration 2 l^{-1}. Vertical bars represent model predictions of maximum daily ingestion rate using wedge (dark gray) or hemisphere (light gray) search-volume geometry for 3 size classes (weights shown correspond to L = 5, 6, 10 mm; Otterlei et al. 1999). Modelled ingestion rates assume feeding occurred at a turbulence level which maximizes ingestion rate and during a 12 h daily feeding period. Also shown for comparison (lines) is the number of prey ingested by wild cod larvae on Georges Bank growing at 3 different rates (a: g = 6 % d^{-1}, b: g = 10 % d^{-1}; c: g = 14 % d^{-1}; Lough et al. 2005), 33 % growth efficiency and 2 prey sizes (circles: 0.26 µg dry weight; squares: 1.5 µg dry weight). Note that the y-axis is expressed in logarithmic units

The model also produced biological results which are consistent with key features of many previous analytical and experimental studies. In particular, our simulation using hemispherical search volume produced results similar to those in 3 prior analytical models (Matsushita 1992, MacKenzie et al. 1994, Jenkinson 1995): an increase in E with turbulence, a nonlinear decrease of pursuit success as turbulence increases, and the familiar dome-shaped response of capture or ingestion rate to increasing turbulence. Our results from modelling the role of wedge-shaped search geometry across turbulence levels also yielded an exponential decay of pursuit success and a dome-shaped response of ingestion rate to increasing turbulence intensity. Highest ingestion rates with both geometries are predicted to occur in moderately turbulent environments, such as tidally mixed frontal zones where dissipation rates are ca. 10^{-6} to 10^{-5} m^2 s^{-3}.

Since we excluded escape responses of prey and possible effects of turbulence on the orientation of predator, the model consistently estimated 100 % pursuit efficiency in low turbulent regimes. Therefore the mechanism associated with the decrease in pursuit success as turbulence increases is the decrease in time for which the encountered prey is within the larval fish search volume (MacKenzie et al. 1994, MacKenzie & Kiørboe 2000, Lewis & Bala 2006). These findings, and their consistency with experimental evidence, indicate that the biological component of our model also produced reliable results. The results differ, however, in some details (e.g. pursuit efficiency and level of enhancement of E at particular turbulence levels) because of specific differences in biological assumptions used in the models.

The high pursuit efficiencies at low turbulence levels, including calm water, are consistent with laboratory observations in calm and low turbulent water (MacKenzie & Kiørboe 2000) using larvae whose sizes were similar to those used in our modeling study. However, we would expect lower pursuit success in both calm and turbulent water for some other combinations of larvae and prey sizes; larval foraging success improves with size and age (Rosenthal & Hempel 1970, Blaxter 1986, von Herbing & Gallager 2000), and copepods can detect approaching predators and initiate escape manoeuvres (Visser 2001 Fiksen & MacKenzie 2002). These size-based interactions can result in lower pursuit and capture successes than those estimated here, and likely are important factors influencing the prey size spectra of larvae captured in the field (e.g. Munk 1992, 1995, Pepin & Penney 1997). See also 'Future prospects' section below.

Sensitivity to search volume geometry

Each of the 3 feeding processes we investigated (encounter, pursuit, ingestion) showed similar functional responses to increasing turbulence, regardless of whether a hemisphere or wedge-shaped volume was assumed; E increased exponentially, pursuit success declined nonlinearly and ingestion rate was related in a dome-shaped way to turbulence. Moreover, and as expected, employing a wedge-shaped search volume resulted in substantially lower encounter and ingestion rates than use of a hemispherical search volume. This has implications for estimates of larval feeding rates in nature, and the size composition of

prey that larvae must locate and consume in order to survive (see 'Influence of search volume geometry on larval feeding in nature' below).

The relative impact of turbulence on ingestion rate was higher when assuming a wedge-shaped search geometry than when assuming a hemispherical geometry. In both instances, the large decrease in pursuit success at increasing turbulence is partly offset by increases in prey encounter.

The difference in sensitivity to turbulence between the search geometries is due to 2 mechanisms, and can be summarized in a simplified model of the processes involved in prey encounter by a pause-travel predator (MacKenzie & Kiørboe 1995):

$$E = \frac{(SV - \text{overlap})\rho_p}{T_{tot}} + A\rho_p w \frac{T_p}{T_{tot}} \quad (8)$$

Here, E is a function of 2 basic processes: what is in the search volume when it pauses, and what enters while it is paused. SV is predator search volume, ρ_P is the prey concentration, A is area of the search space, w is the turbulent velocity, T_p is the time spent pausing (searching) and T_{tot} is duration of the pause + travel events.

First, it can be shown that the overlap between successive search volumes for a hemispherical searcher is much larger than for a wedge searcher, given experimentally observed movement distances and speeds, and pause durations and frequencies (Galbraith et al. 2004, Lewis & Bala 2006). Given these behaviours, the larvae do not move to completely unsearched volumes of water when moving to new locations. Consequently, successive search volumes partly overlap each other and the volume of the overlap itself is greater for hemisphere geometry than for wedge geometry. Volume of overlap decreases as turbulence intensity increases. This decrease is due to the turbulent velocity which (when combined with the larva's swim velocity and duration) effectively increases the distance moved by the larva during individual swim events, relative to the distance moved in calm water. Because the volume of a hemisphere is ca. 11-fold larger than the volume of a wedge, the decrease in overlap with increasing turbulence is greater for the hemisphere than for the wedge.

The second reason the search geometries have different sensitivities to turbulence is the difference in surface-area-to-volume ratios between the 2 shapes. Switching from a hemispherical to a wedge-shaped search space leads to a ca. 11-fold reduction of the volume of the search space, but only a ca. 5-fold reduction in the surface area exposed to the turbulent flux of prey into the search volume. Hence the greater surface area-volume ratio of wedges compared to hemispheres means that turbulence (relative to the calm situation) will have a greater influence on E of wedge-shaped search geometries. Qualitatively, these surface area-volume considerations are represented by the ratio of the 2 terms in Eq. (8), $(V - \text{overlap})/(AwT_p)$. Some earlier analyses have excluded the role of turbulence on advection of prey into the search volume (Galbraith et al. 2004); consequently, when using the wedge, the influence of turbulence on larva encounter and net energy gain was underestimated.

Development of modelling approaches

Our study extends the work of some earlier modelling investigations into the role of turbulence on feeding in larval fish (Table 1) to include several combinations of search-volume geometry (hemisphere, wedge), turbulence level (calm to storm/tidal front levels) and predatory components (encounter, pursuit). We believe that the numerical, individual-based approach has many benefits because the E and pursuit success of individual larvae can be followed and recorded over time, and because complex behaviours can be relatively easily incorporated into the modelling framework. This flexibility could be useful, for example, when simulating larvae of different sizes preying on a zooplankton community composed of prey having different sizes and escape behaviours.

The modelling approach we have used includes many assumptions about larval search behaviour and search geometry. In particular, we have assumed that cod larvae are pause-travel searchers. However, cod larvae also perceive prey while gliding and swimming (von Herbing & Gallager 2000, MacKenzie & Kiørboe 2000) and can encounter prey as they are being advected towards them (MacKenzie & Kiørboe 2000). For example, we have observed cod larvae in our laboratory studies which use their body posture and fin positions to hover so they remain oriented against small scale flow structures associated with turbulence (see Video clip 5 in MEPS Supplementary Material online at www.int-res.com/articles/suppl/m347p155_videos/). The flow carries prey towards the larva, and if sufficiently slow, enables capture of the advecting prey. Hovering behaviour has been observed in some other fish species occupying habitats with flow (McLaughlin et al. 2000).

In these situations, the larvae display search behaviour similar to a cruise predator, where E depends on relative velocities between prey and predator (Gerritsen & Strickler 1977, Rothschild & Osborn 1988). Adopting a strategy of reduced or no swimming in turbulent water has been suggested in the literature (Sundby & Fossum 1990, Dower et al. 1997, MacKenzie 2000), has been observed in the laboratory (Munk & Kiørboe 1985, Munk 1992, 1995, MacKenzie & Kiørboe

2000), and has theoretical bioenergetic benefits (Lewis & Bala 2006). This behaviour is common among juvenile and larger sizes of fish, particularly among those inhabiting streams (McLaughlin et al. 2000) and near coral reefs (Hamner et al. 1988), and may be a behaviour that develops rapidly during larval ontogeny. We hypothesise that it is also common among larvae in turbulent environments of open and coastal seas, and technologies and methodologies now exist for testing this and other feeding-related hypotheses (MacKenzie 2000). Larval search behaviour may at times therefore be pause-travel, while at others it may more closely resemble cruise or sit-wait behaviour, depending on factors such as prey concentration, larval hunger level and turbulence intensity (see also von Herbing & Gallager 2000).

Our modelling approach employs a turbulence routine which allows all prey to be advected by the small-scale motion of the turbulence. As a result, some prey can be advected into the search volumes of larval fish predators, and the separation distances and relative velocities of the prey to each other and to the larva are changing in a realistic way (see Fig. 4). This approach differs from an earlier analysis of turbulence on E and net energy gain (Galbraith et al. 2004), which assumed that turbulence advects the larvae, but not the prey. These authors simulated turbulence by adding at each time step a random velocity of 5 mm s^{-1} to the predator while keeping the prey fixed in space. The final result is therefore a translation of the prey field relative to the predator at each time step, and is analogous to a larva moving through a 'frozen field' of prey.

Influence of search volume geometry on larval feeding in nature

It is unknown which search-volume geometry larvae use in nature; there are still no direct observations of larval fish feeding behaviour (i.e., E, pursuit success, reaction distances) in the field (MacKenzie 2000), and only a few observations of larval fish feeding behaviour in turbulent environments in the laboratory (Munk & Kiørboe 1985, Munk 1995, MacKenzie & Kiørboe 1995, 2000, Utne-Palm & Stiansen 2002). In nature, where turbulence is a common feature of larval habitats, prey will approach larvae from a wide variety of angles due to the randomly directed nature of the velocity fluctuations associated with the turbulence. As a result, and especially in field situations where ingestion rates often are food-limited, there may be strong selection for larvae to be able to react to prey approaching them from a variety of directions. Such an ability may be one of several behavioural adjustments that allow fish larvae to increase search and clearance rates when they are hungry and when food is limiting (Munk 1995). We note that under some situations, a wedge-shaped search volume projected from each of the larval eyes could yield a shape approximating a hemisphere: detection angles measured for cod larvae nearly define a hemisphere volume (von Herbing & Gallager 2000).

Our comparisons of model- and field-derived ingestion rates for cod larvae on Georges Bank in 1993–1994 suggest that larvae could only grow at observed rates (given other controlling factors such as prey concentration, temperature and photoperiod) if they were hemispherical searchers and were able to encounter and capture relatively large prey. Given the concentrations of preferred prey in these years (primarily *Pseudocalanus* sp. nauplii and copepodites, Lough et al. 2005), wedge-shaped searchers would grow much slower and presumably suffer higher mortality rates, even if they were able to locate and capture large prey. Moreover, an estimate of gross growth efficiency for the wild cod larvae on Georges Bank during 1993–1994 (ca. 26%, L. Buckley pers. comm.) is lower than that assumed in our comparisons (33%). The lower growth efficiency and the (unlikely) assumption that larval feeding always occurred at a combination of turbulence and light which maximized ingestion rates, implies an even higher requirement for prey than we have estimated. These considerations suggest to us that the larvae observed during the Georges Bank field study most likely employed hemisphere search volumes. The larvae could also attain the observed growth rates using hemisphere search geometry and by switching to consumption of smaller prey and other species in addition to *Pseudocalanus*. However, the available gut content data for this study shows that diets were dominated by *Pseudocalanus*, so we consider this possible modification of feeding behaviour unlikely.

We do not exclude the possibility that larvae can employ wedge search geometries under some circumstances; for example, if larvae are able to detect prey at much larger distances (>1 larval length, as some of the cod larvae were able to do in experiments by von Herbing & Gallager 2000), and/or if prey concentrations are much higher than we have assumed, it could be possible for larvae to encounter and capture sufficient prey to meet the observed growth rates in the field.

Future prospects

There are relatively few studies of larval fish feeding behaviour in turbulent environments and even fewer where the turbulence has been quantified (Dower et al. 1997, MacKenzie 2000). The number of species

used in these studies is small (2: cod and herring), and from boreal-temperate habitats. Many aspects of larval feeding behaviour still require further investigation (e.g. direct visual observation in laboratory or natural environments, ontogenetic changes) and the number of species for which observations in quantified turbulence are available should be increased.

We have applied our model to simulate feeding behaviour in a simple food environment in order to understand the specific interaction of a larval fish predator with its prey. Larvae were exposed to a single prey species which was initially randomly distributed and in an environment where light was assumed to be optimal for larval feeding. Moreover, prey were not assigned any predator detection and escape behaviour, even though theoretical and experimental studies demonstrate that zooplankters exhibit such behaviours (Visser 2001, Fiksen & MacKenzie 2002). We are aware that in nature all of these factors complicate attempts to model and understand larval fish feeding rates. For example, prey concentrations are strongly affected by storms and other turbulence-generating processes and larvae do alter their vertical distributions depending on wind speed (Heath et al. 1988, Porter et al. 2005). Larval behaviour which leads to avoidance of strong surface turbulence could be a direct reaction to the high relative velocities associated with strong mixing, or could be a response to a change in the vertical distribution of prey (Franks 2001), whose vertical distributions themselves are sensitive to turbulence intensity (Visser et al. 2001, Incze et al. 2001). Moreover, recent statistical analyses of the interaction between larval feeding, vertical distribution, turbulence and light intensity in the sea shows that if a high turbulence event occurs during daylight hours under cloudy conditions, larval feeding rates will decrease (Porter et al. 2005). If, instead, the turbulence event occurs during well-lit conditions (e.g. under clear skies), then feeding rates will remain high or even increase, because light conditions, turbulence levels and prey concentrations at depth will be closer to values which optimize larval feeding success. These complex interactions are likely partly responsible for the contrasting results of many field studies investigating how turbulence affects larval feeding in nature (MacKenzie 2000).

In the future, we will apply our modelling approach to investigate some of the higher-order interactions described above. The individual-based, object-oriented methodology can easily incorporate, for example, prey detection and escape behaviour and assign different behaviours to different sizes and species of prey. These behaviours are important mechanisms which differ among larval fish species and which nonetheless lead to the dominance of larval diets by a relatively few species (Munk 1995, Hillgruber et al. 1997, Heath & Lough 2007). Our modelling approach can potentially enable us to investigate how larval diets in the field change depending on prey characteristics and turbulence conditions (Dower et al. 1998, Hillgruber & Kloppmann 2000, Fiksen & MacKenzie 2002). Future climate change will affect not only the spatial and temporal pattern of exposure of larvae to wind and tidally induced turbulence, but will also affect the relative timing of production of individual species of zooplankton (Edwards & Richardson 2004) and larval fish (Greve et al. 2005). Investigations of processes which affect larval fish-zooplankton interactions in environments with varying turbulence and light will increase our understanding of how larval fish locate and ingest their prey in nature, and how these processes will be influenced by expected climate changes.

Acknowledgements. This work is a contribution to a European Network of Excellence on Ocean Ecosystems Analysis (www.eur-oceans.org) and GLOBEC. P.M. was supported by a EUR-OCEANS postdoctoral fellow grant and by the Danish Institute for Fisheries Research (Departments of Marine Ecology and Aquaculture, and Sea Fisheries) and the Stazione Zoologica 'Anton Dohrn' (Napoli, Italy). We thank Dr. F. Köster for assistance and Drs. L. J. Buckley, R. G. Lough and M. Peck for discussions regarding larval cod growth and feeding on Georges Bank. An earlier version of this work was presented at the 'Workshop on advancements in modelling physical-biological interactions in fish early–life history: recommended practices and future directions,' Nantes, France, April 3-5, 2006 (co-chairs Alejandro Gallego, Elizabeth North and Pierre Petitgas).

LITERATURE CITED

Bakun A (1996) Patterns in the ocean: ocean processes and marine population dynamics. California Sea Grant System, NOAA and Centro de Investigaciones Biologicas del Noroeste, LaJolla, CA

Blaxter JHS (1986) Development of sense organs and behaviour of teleost larvae with special reference to feeding and predator avoidance. Trans Am Fish Soc 115:98–114

Browman HI, O'Brien WJ (1992) Foraging and prey search behaviour of golden shiner (*Notemigonus crysoleucas*) larvae. Can J Fish Aquat Sci 49(4):813–819

Buckley LJ, Durbin E (2006) Seasonal and inter-annual trends in the zooplankton prey and growth rate of Atlantic cod (*Gadus morhua*) and haddock (*Melanogrammus aeglefinus*) larvae on Georges Bank. Deep-Sea Res II 53: 2758–2770

Buckley LJ, Caldarone EM, Lough RG (2004) Optimum temperature and food-limited growth of larval Atlantic cod (*Gadus morhua*) and haddock (*Melanogrammus aeglefinus*) on Georges Bank. Fish Oceanogr 13:134–140

Caparroy P, Thygesen UH, Visser AW (2000) Modelling the attack success of planktonic predators: patterns and mechanisms of prey size selectivity. J Plankton Res 22(10): 1871–1900

Davis CS (1984) Predatory control of copepod seasonal cycles on Georges Bank. Mar Biol 82(1):31–40

Dower JF, Miller TJ, Leggett WC (1997) The role of microscale turbulence in the feeding ecology of larval fish. Adv Mar Biol 31:169–220

Dower JF, Pepin P, Leggett WC (1998) Enhanced gut fullness and an apparent shift in size selectivity by radiated shanny (*Ulvaria subbifurcata*) larvae in response to increased turbulence. Can J Fish Aquat Sci 55:128–142

Edwards M, Richardson AJ (2004) Impact of climate change on marine pelagic phenology and trophic mismatch. Nature 430:881–884

Fiksen Ø, MacKenzie BR (2002) Process-based models of feeding and prey selection in larval fish. Mar Ecol Prog Ser 243:151–164

Franks PJS (2001) Turbulence avoidance: an alternate explanation of turbulence-enhanced ingestion rates in the field. Limnol Oceanogr 46(4):959–963

Fung CH, Vassilicos JC (1998) Two-particle dispersion in turbulent like flows. Physiol Rev E 57:1677–1690

Fung CH, Hunt JCR, Malik NA, Perkins RJ (1992) Kinematic simulation of homogeneous turbulence by unsteady random Fourier modes. J Fluid Mech 236:281–318

Galbraith PS, Browman HI, Racca RG, Skiftesvik AB, Saint-Pierre JF (2004) Effect of turbulence on the energetics of foraging in Atlantic cod *Gadus morhua* larvae. Mar Ecol Prog Ser 281:241–257

Gargett AE (1989) Ocean turbulence. Annu Rev Fluid Mech 21:419–451

Gerritsen J, Strickler JR (1977) Encounter probabilities and community structure in zooplankton: a mathematical model. J Fish Res Board Can 34:73–82

Greve W, Prinage S, Zidowitz H, Nast J, Reiners F (2005) On the phenology of North Sea ichthyoplankton. ICES J Mar Sci 62:1216–1223

Hamner WM, Jones MS, Carleton JH, Hauri IR, Williams D (1988) Zooplankton, planktivorous fish, and water currents on a windward reef face: Great Barrier Reef, Australia. Bull Mar Sci 42(3):459–479

Heath MR, Lough RG (2007) A synthesis of large-scale patterns in the planktonic prey of Dietary dominance of larval and juvenile cod. Fish Oceanogr 16(2):169–185

Heath MR, Henderson EW, Baird DL (1988) Vertical distribution of herring larvae in relation to physical mixing and illumination. Mar Ecol Prog Ser 47:211–228

Helle K (2000) Does the midnight sun increase the feeding rate and hence the growth rate of early juvenile Arcto-Norwegian cod *Gadus morhua* in the Barents Sea? Mar Ecol Prog Ser 197:293–297

Hill PS, Nowell ARM, Jumars PA (1992) Encounter rate by turbulent shear of particles similar in diameter to the Kolmogorov scale. J Mar Res 50:643–668

Hillgruber N, Kloppmann M (2000) Vertical distribution and feeding of larval blue whiting in turbulent waters above Porcupine Bank. J Fish Biol 57(5):1290–1311

Hillgruber N, Kloppmann M, Wahl E, von Westernhagen H (1997) Feeding of larval blue whiting and Atlantic mackerel: a comparison of foraging strategies. J Fish Biol 51(Suppl A):230–249

Houde ED (1989) Comparative growth, mortality and energetics of marine fish larvae: temperature and implied latitudinal effects. Fish Bull 87:471–496

Incze LS, Hebert D, Wolff N, Oakey N, Dye D (2001) Changes in copepod distributions associated with increased turbulence from wind stress. Mar Ecol Prog Ser 213:229–240

Jenkinson IR (1995) A review of two recent predation-rate models: the dome-shaped relationship between feeding rate and shear rate appears universal. ICES J Mar Sci 52:605–610

Kiørboe T (1993) Turbulence, phytoplankton cell size, and the structure of pelagic food webs. Adv Mar Biol 29:1–72

Kiørboe T, Munk P (1986) Feeding and growth of larval herring, *Clupea harengus*, in relation to density of copepod nauplii. Environ Biol Fish 17(2):133–139

Kraichnan RH (1970) Diffusion by a random velocity field. Phys Fluids 13(1):22–31

Landry F, Miller TJ, Leggett WC (1995) The effects of small-scale turbulence on the ingestion rate of fathead minnow (*Pimephales promelas*) larvae. Can J Fish Aquat Sci 52: 1714–1719

Lewis DM (2003) Planktonic encounter rates in homogeneous isotropic turbulence: the case of predators with limited fields of sensory perception. J Theor Biol 222(1):73–97

Lewis DM, Bala SI (2006) Plankton predation rates in turbulence: a study of the limitations imposed on a predator with a non-spherical field of sensory perception. J Theor Biol 242(1):44–61

Lewis DM, Pedley TJ (2000) Planktonic contact rates in homogeneous isotropic turbulence: theoretical predictions and kinematic simulations. J Theor Biol 205(3):377–408

Lewis DM, Pedley TJ (2001) The influence of turbulence on plankton predation strategies. J Theor Biol 210(3): 347–365

Lough RG, Buckley LJ, Werner FE, Quinlan JA, Pehrson Edwards K (2005) A general biophysical model of larval cod (*Gadus morhua*) growth applied to populations on Georges Bank. Fish Oceanogr 14:241–262

MacKenzie BR (2000) Turbulence, larval fish ecology and fisheries recruitment: a review of field studies. Oceanol Acta 23:357–375

MacKenzie BR, Kiørboe T (1995) Encounter rates and swimming behavior of pause-travel and cruise larval fish predators in calm and turbulent laboratory environments. Limnol Oceanogr 40(7):1278–1289

MacKenzie BR, Kiørboe T (2000) Larval fish feeding and turbulence: a case for the downside. Limnol Oceanogr 45: 1–10

MacKenzie BR, Leggett WC, Peters RH (1990) Estimating larval fish ingestion rates: can laboratory derived values be reliably extrapolated to the wild? Mar Ecol Prog Ser 67:209–225

MacKenzie BR, Miller TJ, Cyr S, Leggett WC (1994) Evidence for a dome-shaped relationship between turbulence and larval fish ingestion rates. Limnol Oceanogr 39:1790–1799

Malik NA, Vassilicos JC (1999) A Lagrangian model for turbulent dispersion with turbulent-like flow structure: comparison with direct numerical simulation for two-particle statistics. Phys Fluids 11:1572–1580

Mariani P, Botte V, Ribera d'Alcalà M (2005) An object oriented model for the prediction of turbulence effects on planktonic contact rates. Deep-Sea Res II 52:1287–1307

Mariani P, Botte V, Ribera d'Alcalà M (in press) A numerical investigation of the impact of turbulence on the feeding rates of *Oithona davisae*. J Mar Syst

Matsushita K (1992) Possible importance of turbulence at the spatial scale of a larval fish visual field on feeding success. Arch Hydrobiol Beih (Ergebn Limnol) 36:109–121

McLaughlin RL, Grant JWA, Noakes DLG (2000) Living with failure: the prey capture success of young brook charr in streams. Ecol Freshw Fish 9(1-2):81–89

Monteleone DM, Peterson WT (1986) Feeding ecology of American sand lance *Ammodytes americanus* larvae from Long Island Sound. Mar Ecol Prog Ser 30:133–143

Munk P (1992) Foraging behaviour and prey size spectra of larval herring *Clupea harengus*. Mar Ecol Prog Ser 80: 149–158

Munk P (1995) Foraging behaviour of larval cod (*Gadus*

morhua) influenced by prey density and hunger. Mar Biol 122:205–212
Munk P, Kiørboe T (1985) Feeding behaviour and swimming activity of larval herring (*Clupea harengus*) larvae in relation to density of copepod nauplii. Mar Ecol Prog Ser 24:15–21
Oakey NS & Elliott JA (1982) Dissipation within the surface mixed layer. J Phys Oceanogr 12:171–185
Otterlei E, Nyhammer G, Folkvord A, Stefansson SO (1999) Temperature- and size-dependent growth of larval and early juvenile Atlantic cod (*Gadus morhua*): a comparative study of Norwegian coastal cod and Northeast Arctic cod. Can J Fish Aquat Sci 56:2099–2111
Peck MA, Buckley LJ, Bengtson DA (2006) Effects of temperature and body size on the swimming speed of larval and juvenile Atlantic cod (*Gadus morhua*): implications for individual-based modelling. Environ Biol Fish 75(4): 419–429
Pepin P, Penney RW (1997) Patterns of prey size and taxonomic composition in larval fish: are there general size-dependent models? J Fish Biol 51(Suppl A):84–100
Peters F, Marrasé C (2000) Effects of turbulence on plankton: an overview of experimental evidence and some theoretical considerations. Mar Ecol Prog Ser 205:291–306
Porter SM, Ciannelli L, Hillgruber N, Bailey KM, Chan KS, Canino MF, Haldorson LJ (2005) Environmental factors influencing larval walleye pollock *Theragra chalcogramma* feeding in Alaskan waters. Mar Ecol Prog Ser 302:207–217
Reynolds AM (1995) The relative dispersion of particles in isotropic homogeneous turbulence. Fluid Dyn Res 16:1–10
Rosenthal H, Hempel G (1970) Experimental studies in feeding and food requirements of herring larvae (*Clupea harengus* L.). In: Steele JH (ed) Marine food chains. Oliver & Boyd, Edinburgh, p 344–364
Rothschild BJ, Osborn TR (1988) Small–scale turbulence and plankton contact rates. J Plankton Res 10:465–474
Simpson JH, Crawford WR, Rippeth TP, Campbell AR, Cheok JVS (1996) The vertical structure of turbulent dissipation in shelf seas. J Phys Oceanogr 26(8):1579–1590
Sundby S, Fossum P (1990) Feeding conditions of Arctonorwegian cod larvae compared with the Rothschild-Osborn theory on small-scale turbulence and plankton contact rates. J Plankton Res 12:1153–1162
Tennekes HH, Lumley JL (1972) A first course in turbulence. MIT Press, Cambridge, MA
Thorpe SA (2004) Recent developments in the study of ocean turbulence. Annu Rev Earth Planet Sci 32:91–109
Utne-Palm AC, Stiansen JE (2002) Effect of larval ontogeny, turbulence and light on prey attack rate and swimming activity in herring larvae. J Exp Mar Biol Ecol 268(2): 147–170
Visser AW (2001) Hydromechanical signals in the plankton. Mar Ecol Prog Ser 222:1–24
Visser AW, Jackson GA (2004) Characteristics of the chemical plume behind a sinking particle in a turbulent water column. Mar Ecol Prog Ser 283:55–71
Visser AW, Saito H, Saiz E, Kiørboe T (2001) Observations of copepod feeding and vertical distribution under natural turbulent conditions in the North Sea. Mar Biol 138(5): 1011–1019
von Herbing IH, Gallager SM (2000) Foraging behavior in early Atlantic cod larvae (*Gadus morhua*) feeding on a protozoan (*Balanion* sp.) and a copepod nauplius (*Pseudodiaptomus* sp.). Mar Biol 136(3):591–602
Werner FE, MacKenzie BR, Perry RI, Lough RG, Naimie CE, Blanton BO, Quinlan JA (2001) Larval trophodynamics, turbulence, and drift on Georges Bank: a sensitivity analysis of cod and haddock. Sci Mar 65(Suppl. 1):99–115
Yamazaki H, Osborn TR, Squires KD (1991) Direct numerical simulation of planktonic contact in turbulent flow. J Plankton Res 13(3):629–643
Yamazaki H, Squires KD, Strickler JR (2004) Can turbulence reduce the energy costs of hovering for planktonic organisms? In: Seuront L, Strutton PG (eds) Handbook of scaling methods in aquatic ecology—measurement, analysis, simulation. CRC Press, Boca Raton, FL, p 493–505

Editorial responsibility: Matthias Seaman (Assistant Editor-in-Chief), Oldendorf/Luhe, Germany

Submitted: December 6, 2006; Accepted: June 5, 2007
Proofs received from author(s): September 12, 2007

Vol. 347: 171–183, 2007
doi: 10.3354/meps06976

MARINE ECOLOGY PROGRESS SERIES
Mar Ecol Prog Ser

Published October 11

Physiologically based limits to food consumption, and individual-based modeling of foraging and growth of larval fishes

Myron A. Peck*, Ute Daewel

Institute for Hydrobiology and Fisheries Science, University of Hamburg, Olbersweg 24, 22767 Hamburg, Germany

ABSTRACT: Larval fish individual-based models (IBMs) that include foraging subroutines to depict prey encounter, capture and ingestion often include static parameters (e.g. a maximum feeding rate, C_{MAX}) to prevent 'overfeeding' and unrealistically high growth rates. We formulated 2 physiologically based approaches to limit food consumption rate (C) based on gut capacity and evacuation rate (GER) and feeding rate-dependent changes in assimilation efficiency (AE). Parameterizations were based on data reported for a variety of marine and freshwater teleost larvae. The effects of the 3 approaches (C_{MAX}, GER and AE) on feeding and growth were compared in IBM simulations of 12 mm larval sprat *Sprattus sprattus* L. foraging within homogenous and patchy prey fields. Prey concentrations for maximum growth were between 5 and 10 copepodites l^{-1}, similar to thresholds determined for successful foraging by larvae of other marine fish species in laboratory studies. The AE limit allowed larvae to exploit prey patches (to consume prey at higher rates but at lower AEs). In simulations using prey concentrations observed in productive areas of the southern North Sea (e.g. 21.0 copepodites l^{-1}), larvae benefited little (benefited much) from adopting this patch feeding strategy when patch prey concentrations were ≤2-fold (≥5-fold) those outside of the patches. At ≤10 copepodites l^{-1}, foraging model predictions of C were close to limits imposed by C_{MAX}, GER and AE methods. In patches (20 to 40 copepodites l^{-1}), foraging model estimates of C were 2- to 4-fold greater than the highest (AE-based) limit. Physiological-based limits to C are recommended for larval fish IBMs and will be necessary to adequately assess the impacts of prey patchiness on survival and growth of marine fish larvae.

KEY WORDS: Larval fish · Foraging · Prey patches · Individual-based models · Gut evacuation · Assimilation efficiency · *Sprattus sprattus*

INTRODUCTION

Individual-based models (IBMs) utilizing functions to depict foraging, metabolism and growth have been used to explore the impacts of extrinsic factors such as turbulence, light and prey concentration on the vital rates of larval marine fish (e.g. Letcher et al. 1996, Werner et al. 1996, Fiksen & Folkvord 1999, Hinrichsen et al. 2002, Lough et al. 2005). However, simulating 'realistic' rates of food consumption (C) by a modeled larva is somewhat of a Herculean task, since it is not a trivial matter to define what is 'realistic' for field larvae. Field estimates of C for larval fish must often be based upon a number of assumptions regarding *in situ* prey fields (i.e. that the mean prey concentration calculated from net hauls adequately represents the prey field that individual larvae encounter) and/or aspects of larval physiology (i.e. that rates of digestion and gut evacuation are adequately known; Pepin & Penney 2000). Rates of food consumption have been quantified in laboratory studies for the larvae of a variety of marine teleosts (e.g. see Houde 1989, Houde & Zastrow 1993), but these rates do not always compare well with field estimates (MacKenzie et al. 1990).

Attempting to simulate the situation in the wild, larval fish C within IBMs is influenced by an amalgam of variables including prey concentration, one of the main factors modulating contact rates of predators and

*Email: myron.peck@uni-hamburg.de

prey. When prey concentrations are high, IBM estimates of C can be unrealistically high and 'overfeeding' can lead to unrealistically high growth rates. This problem has been solved by ignoring overestimates of C and defining growth limits (G_{MAX}) from age–length models (Hinrichsen et al. 2002, Bartsch & Coombs 2004) or laboratory growth rates during *ad libitum* feeding (Fiksen & Folkvord 1999). An upper limit to C (C_{MAX}) has also been employed (Werner et al. 1996, U. Daewel et al. unpubl. data). These approaches (G_{MAX} or C_{MAX}) supersede foraging model predictions and are not mechanistic. Moreover, growth models of larval, juvenile and adult fish are often most sensitive to such parameters (e.g. Bartell et al. 1986, Hinrichsen et al. 2002, Maes et al. 2005, U. Daewel et al. unpubl. data).

The requirement of simulating 'realistic' C in larval fish IBMs also makes it necessary to employ 'quasi-realistic' prey fields. Typically, this has been accomplished by utilizing average values of species- and/or stage-specific zooplankton concentration (no. m^{-3}) from *in situ* net sampling (e.g. Werner et al. 1996, Hinrichsen et al. 2002). These prey fields are likely adequate for projecting larval growth at relatively long time (several weeks) and large spatial scales (banks, shelves), but, at shorter time (days) and smaller spatial (frontal zones) scales, variability in prey fields may become an increasingly relevant factor affecting the vital rates of larval fish. Stochasticity in prey fields experienced, for example, by a larva foraging inside and outside of thin layers (e.g. Dekshenieks et al. 2001) or among prey patches at sub-meter scales (e.g. Owen 1989) was included in the seminal modeling work of Beyer & Laurence (1980) and Laurence (1985). However, in the following decades, modeling efforts have rarely included stochasticity in prey fields (see Letcher et al. 1996). This is interesting in light of the advances made in video sampling systems (e.g. video plankton recorder and other optical packages) that now provide estimates of fine-scale prey distributions over large areas, such as across frontal zones (e.g. Broughton & Lough 2006). Including prey field variability in models will undoubtedly become more relevant as researchers explore sources of variability in short-term larval growth rates (e.g. Lough et al. 2005, 2006). Furthermore, it has been argued that implementing stochasticity in foraging processes on both short and long time scales may be required to understand growth and recruitment variability (e.g. see Pitchford et al. 2005).

In the present modeling study, we (1) reviewed the available literature on larval feeding, gut evacuation and assimilation efficiency, (2) formulated interspecific, mechanistic limits to larval fish C and (3) conducted a series of 8 d IBM simulations within homogeneous and patchy prey fields. Model runs employed a variety of prey (copepod) concentrations that had an abundance-at-size spectrum that was characteristic of the southern North Sea. Model simulations investigated how mechanistic feeding limits, as opposed to the prevalent approach of using non-mechanistic limits (e.g. a C_{MAX} parameter), influenced short-term projections of larval feeding and growth.

MATERIALS AND METHODS

IBM foraging and growth. The IBM used in this study is thoroughly described elsewhere (U. Daewel et al. unpubl. data). Model formulations and parameterizations were based on laboratory studies on larval Atlantic herring *Clupea harengus* L. and field data collected for larval sprat *Sprattus sprattus* L., and only the main features of the subroutines are presented here. Larval growth (G, in µg dry mass per model time step) was calculated as the difference between net energy input and metabolic losses:

$$G = C \times AE \times (1 - R_{SDA}) - R \quad (1)$$

where consumed prey mass (C, µg dry mass per model time step) was reduced by an assimilation efficiency (AE) and metabolic losses (R) that were divided into several subcomponents to account for standard (R_S), feeding (specific dynamic action, R_{SDA}) and active (R_A) rates of energy loss. In Eq. (1), R represented R_S when light was below a threshold for feeding, otherwise it represented R_A. Effects of body mass (Kiørboe et al. 1987) and temperature (Almatar 1984) on R were taken from work on larval herring.

The mass of prey consumed was calculated as a function of encounter rate ($N_{SL,i}$), prey mass (m_i), capture success ($CS_{SL,i}$), handling time ($HT_{SL,i}$) and the time interval (Δt) (Letcher et al. 1996):

$$C = \frac{\sum_i m_i N_{SL,i} CS_{SL,i}}{1 + \sum_i N_{SL,i} HT_{SL,i}} \Delta t \quad (2)$$

where SL is larval fish standard length and i refers to a specific prey class. An optimal foraging approach was used in which different prey types were ranked according to their mass, capture success and handling time. Prey items were included in the diet sequentially on the basis of rank until profitability decreased (see Letcher et al. 1996 and references therein). The capture success was calculated as a function of prey length and larval length based on the attack success function of Munk (1992) for larval Atlantic herring parameterized using field data on larval sprat gut contents (Dickmann 2006). The handling time was calculated following an empirically derived equation from Walton et al. (1992). The model also incorporated light level and turbulence to modify prey capture success (see U. Daewel

et al. unpubl. data), but these factors were not examined in the present study.

Assimilation efficiency was given by:

$$AE_{std} = 0.7(1 - 0.3e^{-0.003(M_D - M_{DMIN})}) \quad (3)$$

where M_D was larval dry mass (µg) and M_{DMIN} was larval dry mass at first feeding (µg). The functional form of Eq. (3) was based upon measurements made on larvae of different marine fish species, including summer flounder *Paralichthys dentatus*, spot *Leiostomus xanthurus* and American sole *Achirus fasciatus* (Buckley & Dillman 1982, Govoni et al. 1982, Houde & Schekter 1983).

In the present study, the output from Eq. (2) is referred to as 'foraging model estimates of *C*'. In the next sections, we describe 3 different approaches to place limits on foraging model estimates of the food consumed and assimilated during each model time step.

Case 1—C_{MAX}: The first approach used to prevent overfeeding was to employ a C_{MAX} function:

$$C_{MAX} = 1.315 M_D^{0.83} 2.872^{\left[\frac{(T-15)}{10}\right]} \quad (4)$$

that yielded larval dry mass (M_D, µg)- and temperature (T)-specific limits to C that balanced *in situ* estimates of temperature-specific larval sprat growth in the North and Baltic Seas (Munk 1993, Ré & Gonçalves 1993, Huwer 2004, Baumann et al. 2006). Eq. (4) was employed when foraging model estimates of C were $>C_{MAX}$. In this case, the standard formulation of *AE* (Eq. 3) was used, and the product of Eqs. (3) and (4) provided the non-mechanistic limit to assimilated *C*.

Case 2—gut evacuation rates: A physiologically based approach to limit *C* was based upon gut evacuation rate (*GER*) and knowledge of the maximum gut fullness. This method has recently been used in an IBM for Georges Bank larval cod *Gadus morhua* (Lough et al. 2005). In that study, *GER* was assumed to be linear and to take approximately 4 h. A linear *GER* model was able to explain the rate of decrease in gut contents observed during repeated field samplings in darkness for larvae and young juveniles of 8 fish species (Bochdansky & Deibel 2001, Bochdansky et al. 2006). The rate of decrease in gut contents of larval sprat in the field also appeared to be linear, with a mean (±SE) slope (*GER*) of 0.46 (0.08) h^{-1} (M. A. Peck unpubl. data). This rate implies complete gut emptying within ~2 h and agrees well with that calculated for larval Atlantic herring by Pedersen (1984) and rates calculated for similar-sized larvae of other species at similar temperatures (Table 1).

The effect of body size and temperature (T) on *GER* was based upon an analysis of data presented within 27 studies on 22 fish species (Table 1). The effect of *T* on *GER* was described by a Q_{10} of ~2.4 for Atlantic herring larvae feeding upon *Balanus* nauplii (Blaxter 1962), and the same value was found for northern pipefish *Syngnathus fuscus* feeding upon wild zooplankton (Ryer & Boehlert 1983). Boehlert & Yoklavich (1983) measured *GER*s of 0.0190, 0.0293 and 0.0385 h^{-1} at 7, 12 and 18°C (Q_{10} = 1.88) in juvenile (69 to 82 mm *SL*) black rockfish *Sebastes melanops*. Temperature-normalized (12°C, Q_{10} = 2.0), log-transformed *GER*s of 16 species (studies for which both fish size and water temperature were provided) decreased with log body size in a linear fashion (Fig. 1A). Based upon the literature review, an equation relating *GER* to body size and temperature was formulated:

$$GER = 1.79 SL^{-0.83} Q_{10}^{\left[\frac{(T-12)}{10}\right]} \quad (5)$$

where the Q_{10} parameter was set to 2.0.

A review of the literature also suggested that a 2- to 5-fold increase in *GER* occurred when measurements made during feeding were compared to those made after the cessation of feeding (e.g. Chiba 1961, Pedersen 1984, Talbot et al. 1984, Shepherd & Mills 1996; see Table 1). In one study, prey passed through the guts of bay anchovy *Anchoa mitchilli* within minutes during continuous feeding (Chitty 1981). Correspondingly, *GER* calculated using Eq. (5) was employed when a larva was not feeding (e.g. at the onset of darkness), and the rate was tripled during periods when feeding was continuous.

During any time step, the ingested mass of prey was limited by the available empty space in the gut, which was based upon previous gut fullness and the rate of removal of food from the gut per time step. The maximum capacity of the gut was based upon the length-specific maximum dry mass of prey found within the guts of larvae of 10 different marine fish species (Pepin & Penney 2000, their Fig. 2). The pooled (digitized) data indicated that the mean (±SE) maximum gut prey biomass increased isometrically with larval size and was equal to 6.4 (0.7)% of larval dry mass (Fig. 1B). In this case, if foraging model estimates for *C* were greater than the maximum capacity of the gut, the product of Eq. (3) (*AE*) and the maximum capacity of the gut were used to limit assimilated *C*.

Case 3—digestive capacity: Case 3 was based upon the relationships among *C*, *GER* and *AE*, as affected by both larval body size and temperature. Results of laboratory studies on a variety of organisms (i.e. mollusks, insects, rotifers, copepods) including fish larvae indicated that *AE* tends to decline when foraging takes place within increasing prey concentrations (PC) (Doohan 1973, Dagg & Walker 1978, Boehlert & Yoklavich 1984, Broekhuizen et al. 2002). This is thought to be associated with the positive relationship between *GER* and PC. In copepods, the shapes of the *GER*–PC relationship and the *GER*–*AE* relationship

Table 1. Gut evacuation rates for marine and freshwater fish larvae and early juveniles of different species at different body sizes, temperatures (T) and prey concentrations. In all cases, prey were zooplankton (either calanoids, cyclopoids, or daphnids), except for rockfish (ground squid) and Atlantic salmon (pellet diet). dph: days post-hatch; n.p.: not provided

Species	Age (dph)	Length (mean, range) min.	max.	T (°C)	Prey concentration (no. l^{-1})	Evacuation rate Single meal (h^{-1})	Constant feeding (h^{-1})	Source
Marine species								
Clupea harengus	n.p.	10	12	7	n.p.	0.111		Blaxter (1962)
				11		0.200		
				15		0.222		
Clupea harengus	12	9	9	8	n.p.	0.125		Blaxter (1965)
				15		0.250		
Clupea harengus	8–22	10.5	12	6–9	$4–5 \times 10^3$	0.667		Fossum (1983)
Clupea harengus	26–40	12.5	18.1	9.5	0.011–0.198	0.400	0.706	Pedersen (1984)
Clupea harengus	21–63	n.p.	n.p.	9.2	3×10^1–10^2	0.143		Werner & Blaxter (1979)
					3×10^3	0.200–0.333		
					3×10^4	0.170–0.250		
Clupea harengus		35	74	n.p.	*in situ*	0.178		Arrhenius & Hansson (1994)
Cynoscion regalis	n.p.	60	70	24	n.p.	0.121–0.219		Lankford & Targett (1997)
Gadus morhua	7		(4–5)	5	n.p.	0.500–0.667		Tilseth & Ellertsen (1984)
Logadon rhomboids					*in situ*	0.380		Peters & Kjelson (1975)
Sardinops sagax		10.1	13.9	20	*in situ*	0.250–0.500		Herrera & Balbontin (1983)
Sebastes malanops	n.p.	35	93	7	*ad libitum*	0.019		Boehlert & Yoklavich (1983)
				12	*ad libitum*	0.029		
				18	*ad libitum*	0.038		
Sprattus sprattus	n.p.	13	16	8–15	*in situ*	0.460		M. A. Peck et al. (unpubl. data)
Syngnathus fuscus	n.p.	150	200	15	n.p.	0.038		Ryer & Boehlert (1983)
				23	n.p.	0.078		
				27	n.p.	0.107		
Theragra chalcogramma	<7		(5.92)	6.2	1200–1500	0.207–0.246		Canino & Bailey (1995)
Thunnus alalunga	n.p.	2.7	10	26	*in situ*	0.333–0.250		Young & Davis (1990)
Thunnus maccoyii	n.p.	2.7	10	26	*in situ*	0.250–0.333		Young & Davis (1990)
Trachurus declivis.	n.p.	2.4	14.3	15–18	*in situ*	0.167–0.250		Young & Davis (1992)
Ulvaria subbifurvata	n.p.	4	13	14	*in situ*	0.165–0.290		Bochdansky et al. (2006)
Freshwater species								
Cyprinus carpio	n.p.	8	12	18–29		0.050	0.125–1.000	Chiba (1961)
Coregonus albula	14		8.7	18	n.p.	0.280		Karjalainen et al. (1991)
Dorosoma cepedianum	n.p.	25	89	21	n.p.	0.130–0.250	0.550–1.250	Shepherd & Mills (1996)
Micropterus salmoides	n.p.	20	60[a]	18	n.p.	0.192	0.357	Laurence (1971)
				23		0.263	0.500	
Perca flavescens	n.p.		(17–19.5)	21	n.p.	n.p.	1.667	Noble (1973)
			30–40	22	n.p.	0.154	0.667	
			(60)	15	n.p.	0.083	0.167	
Perca flavescens	n.p.	20	69	14–21	n.p.	n.p.	0.417–3.333	Mills et al. (1984)
Perca fluviatilis	n.p.		(13.1)	n.p.	field	0.400		Worischka & Mehner (1998)
Salmo salar	n.p.	43	99	9–13	n.p.	0.017	0.068	Talbot et al. (1984)
Stizostedion lucioperca	n.p.		10.6	n.p.	field	0.430		Worischka & Mehner (1998)
Stizostedion vitreum	n.p.	10.4	16.2	15	n.p.	0.109		Johnston & Mathias (1996)
				20	n.p.	0.245		
				25	n.p.	0.106		
Stizostedion vitreum	21		(29.4)	22	n.p.	0.167	0.500	Corazza & Nickum (1983)

[a]Estimate based upon range in dry weights (196 to 721 mg)

were described using both power and exponential models (e.g. Dagg & Walker 1978, Xu & Wang 2001, Besiktepe & Dam 2002). In fish, a negative correlation between *GER* and *AE* was reported by Johnston & Mathias (1996) for zooplanktivorous walleye *Stizostedion vitreum* larvae and by Elliott (1976) working on juvenile brown trout *Salmo trutta*, but the functional form of the relationship was not quantified.

Working with Pacific herring *Clupea pallasi* larvae, Boehlert & Yoklavich (1984) observed that carbon retained in the guts of fish feeding on rotifers *Brachionus* sp. and brine shrimp *Artemia* sp. nauplii decreased with increasing PC, indicating reduced *AE*. This suggested that the digestive capacity decreased with increasing feeding rates. Although *GER* increases with temperature, so does the activity of digestive enzymes (e.g. Alarcón et al. 1995, Gelman et al. 2003), suggesting that digestive capacity increases with increasing temperature, although few laboratory data exist on this topic for marine fish larvae.

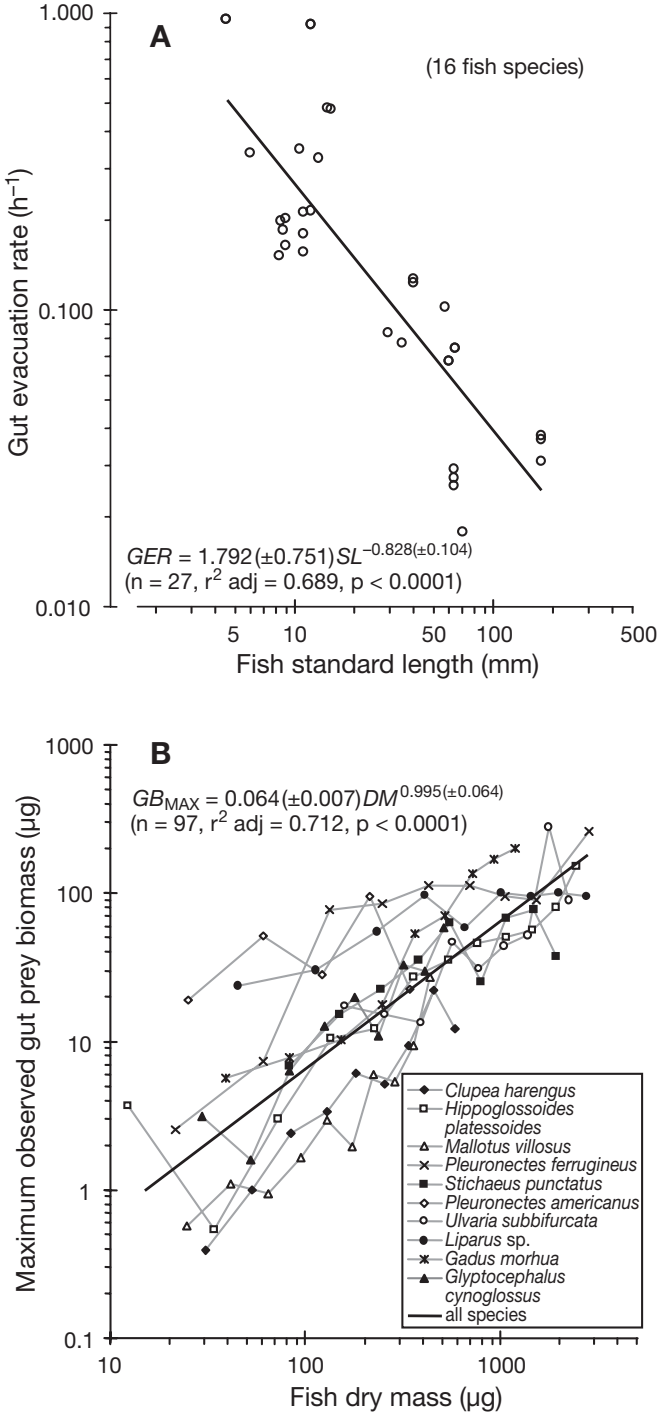

Fig. 1. Literature data on gut capacity and gut evacuation rate (*GER*) for marine and freshwater teleost larvae. (A) Temperature-adjusted *GER* (h^{-1}) versus body length (standard length, *SL*, mm) for 16 teleost species. Data are those reported in Table 1. All rates were expressed relative to 12°C using a Q_{10} of 2.0. (B) Maximum prey biomass (GB_{MAX}, µg) measured in the guts of larvae of each of 10 marine fish species versus larval dry mass (*DM*, µg). Data were digitized from Pepin & Penney (2000, their Fig. 2). The regression line is the best fit for the pooled data. In both panels, mean (±SE) regression parameter estimates are shown

In summary, the literature on fish physiology support the method explored in Case 3, in which *AE* and *GER* both change with body size and are negatively correlated with one another. In this case, a temperature-dependent *GER* and knowledge of the maximum biomass of prey in guts was used to define a body size–specific maximum gut capacity (Gut_{CAP}) (similar to the 'plug-flow reactor' model, e.g. see Canino & Bailey 1995). After Gut_{CAP} was exceeded, an exponential decrease in *AE* with increasing food consumption rate was assumed (Fig. 2), based upon the work of Boehlert & Yoklavich (1984):

$$AE = \begin{cases} AE_{std} & \forall C \le Gut_{CAP} \\ AE_{std} e^{-9.441\left(\frac{C - Gut_{CAP}}{M_D}\right)} & \forall C > Gut_{CAP} \end{cases} \quad (6)$$

Due to a lack of information, the decrease in *AE* after the Gut_{CAP} threshold was considered to be temperature independent in one case (Case 3A) and temperature dependent in another (Case 3B) (see Fig. 2 insert). Furthermore, to be ecologically and/or biologically reasonable, *C* increased with increasing prey concentration until the point where the product of *C* and *AE* declined (i.e. where the gross energy obtained by the larvae was maximal). In this study, no attempt was made to assess the potential impact of prey composition, another factor that affects both *GER* and *AE* in fishes (Karjalainen et al. 1991, Lankford & Targett 1997).

Model simulations and prey fields. Three different 8 d simulations (1-dimensional model, 1 h time step) were run using 12 mm *SL* (~275 µg dry mass) sprat larvae that foraged during a 14 h photoperiod. In each simulation, we used C_{MAX} (Case 1), *GER* (Case 2), or *AE* (Case 3) feeding limits. In Simulation 1, growth rates (mm d^{-1}) were quantified for larvae foraging at each of 8 prey concentrations and 3 temperatures (Table 2). In Simulation 2, the effect of different magnitudes of prey patchiness on modeled growth rates was investigated by allowing larvae to forage for different amounts of time within prey patches of 2-, 5-, or 10-fold increased prey concentrations. In Simulation 3, larvae experienced random fluctuations in the prey field and food consumption; assimilated food and growth rates within each hourly time step were compared among the 3 cases (1, 2 and 3).

Copepods form the vast majority of prey consumed by the larvae of marine fishes, including sprat (Dickmann 2006). The range of copepod concentrations and the relative abundance of different size classes used in this study were based upon zooplankton measurements at German GLOBEC Station 32 in the southern North Sea (54.66° N, 7.66° E). At Station 32, the total abundance of the 200 to 600 µm size classes of the 3 dominant copepods in larval sprat guts (*Acartia* spp.,

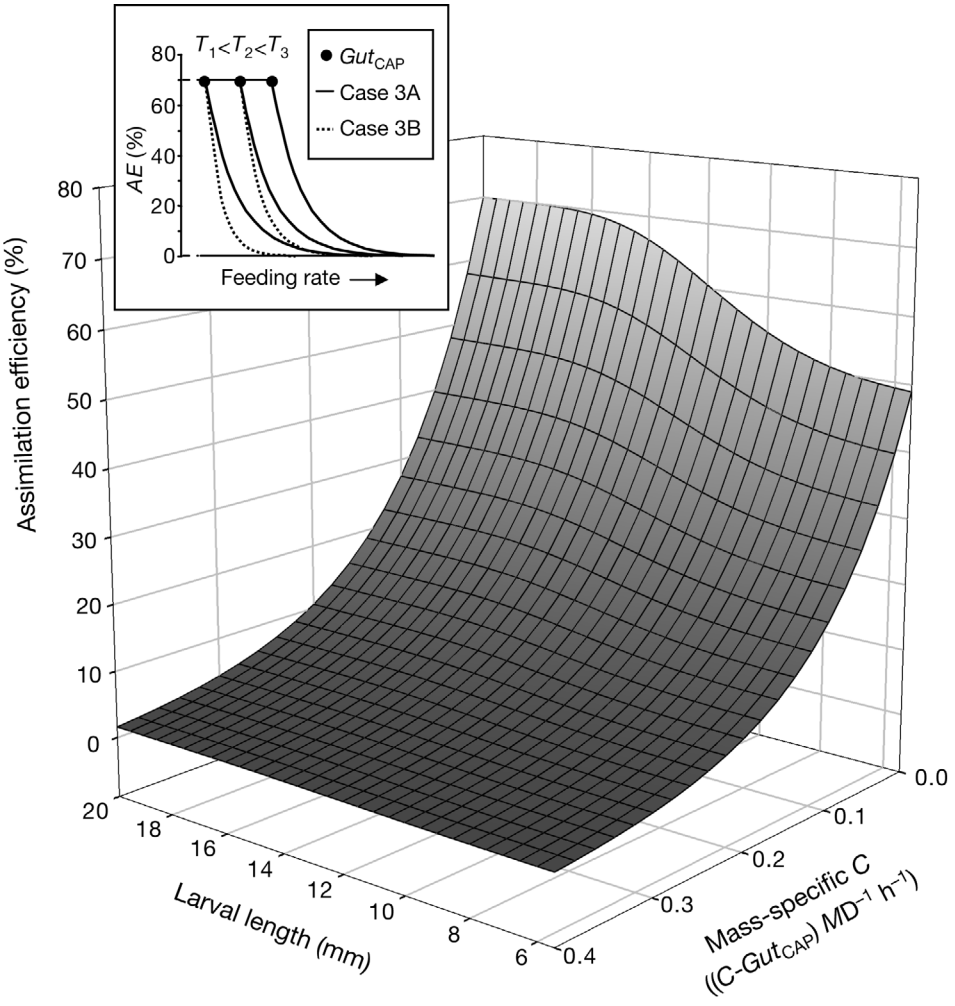

Fig. 2. Case 3 assimilation efficiency (*AE*,%) versus fish size (mm length) and food consumption rate in relative units of gut capacity (Gut_{CAP}). A relative consumption rate value of 0.0 indicates that the rate of food consumption within a model time step was equal to Gut_{CAP}. Insert: Diagram depicting the decrease in *AE* at each of 3 different temperatures (*T*). In Case 3A, the same decrease was used at each temperature. In Case 3B, the decrease was more rapid with decreasing temperature, a response that was based upon considerations of larval growth rates and threshold prey concentrations at different temperatures

Table 2. Summary information for 8 d individual-based model simulations comparing C_{MAX}, *GER*- and *AE*-based limits to larval fish food consumption rate. Copepod concentration is given as the relative abundance in 50 µm size classes 200:250: ... 550 µm = 1.00: 0.80: 0.64: 0.51: 0.41: 0.32: 0.26: 0.21. n.a.: not applicable

Simulation	Temp. (°C)	Prey patches	Copepod concentration (no. l^{-1}) Mean	Outside patch	Inside patch
1	5, 12, 18	No	1.5, 1.7, 2.0, 2.6, 3.4, 5.1, 10.2, 51.0	n.a.	n.a.
2a	12	Yes (2×)	21.0	14.8	29.7
2b	12	Yes (5×)	21.0	9.4	47.0
2c	12	Yes (10×)	21.0	6.6	66.4
3	12	Yes (random)	4.9	(0.3 to 30.0)[a]	

[a]Mean values for lower and upper 10% of cumulative frequency of prey concentrations encountered

Temora longicornis and *Pseudocalanus elongatus*) was ~21.0 l^{-1}. Starting at 200 µm, copepod abundance (*AB*, no. l^{-1}) decreased exponentially with increasing 50 µm size class (*SC*) as: $AB = 12.5 \times e^{-0.0045 \times SC}$ ($r^2 = 0.96$, $p < 0.001$). The range in prey sizes eaten by sprat increases with increasing larval length; 12 mm *SL* larvae eat prey of 200 to ~500 µm, while 18 mm *SL* sprat can eat 800 µm prey (Dickmann 2006). Although information on copepod patchiness in the southern North Sea is lacking, Owen (1989) reported that small-scale (dm to m) plankton patches in the Pacific most commonly contained 2-fold

higher concentrations of organisms, but that patch concentrations exceeded mean concentrations by >10-fold in some cases. We used (at most) a 10-fold range in prey concentrations within and outside patches in Simulation 2 and a 10-fold increase above the mean concentration in Simulation 3 (Table 2).

RESULTS

Temperature, prey and growth

Simulation 1 results indicated that (1) growth rate (G) was positively correlated to temperature (T) at higher prey concentrations, (2) G was negatively correlated to T at low prey concentrations and (3) the threshold prey concentration at which G was food-limited increased with increasing T (Fig. 3). The relationship between G and prey concentration had the same functional form in all 3 cases, but threshold prey concentrations were slightly higher in the *GER* and *AE* cases. The effect of T on G and on prey threshold concentration was similar in the first 2 cases, but was relatively small in Case 3A (*AE*). However, the influence of T on G was similar in all 3 cases when the decrease in *AE* with increasing C (above gut capacity) was temperature dependent (this is Case 3B, see Figs. 2 & 3). Relative to C_{MAX}, maximal growth rates resulting from *GER* and *AE* limits were higher at the same temperatures and prey concentrations, but were in closer agreement with G at C_{MAX} when Case 3B was employed.

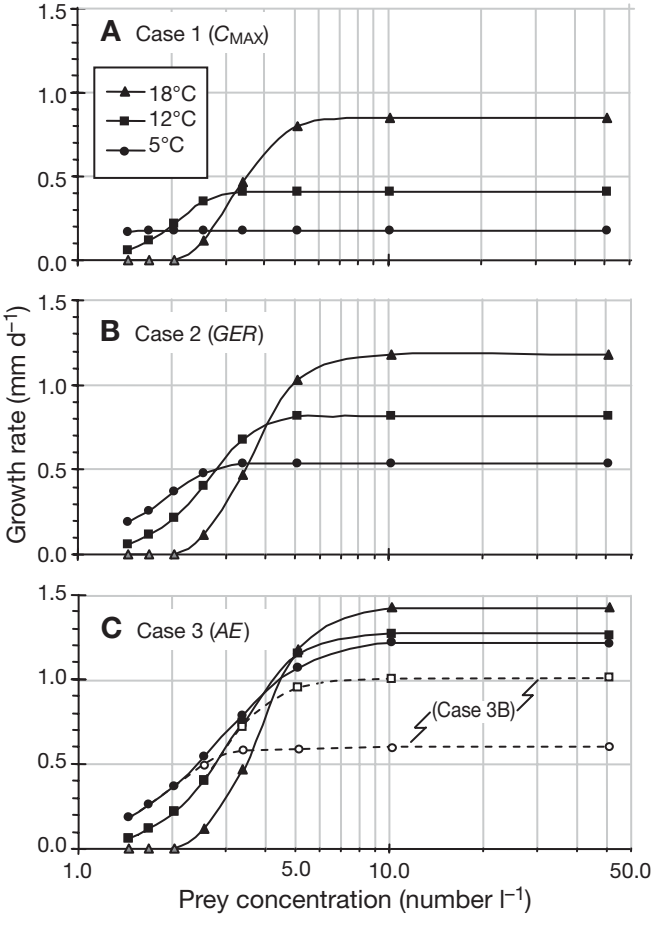

Fig. 3. Simulated growth rates (mm d^{-1}) of larvae after foraging for 8 d at 8 different prey concentrations at each of 3 temperatures (5, 12, or 18°C). Each panel depicts a different method of limiting modeled food consumption. Unfilled symbols in Panel C denote growth rates for larvae limited using the Case 3B approach (see Fig. 2). Gray-filled triangles denote mortality. All larvae were 12 mm *SL* at the start of simulations

Prey patches

When *GER* or *AE* feeding limits were used in Simulation 2, relative larval growth rates were increased by ≥10% when larvae spent only 12% of the 8 d foraging period within patches having 10-fold higher prey concentrations than outside patches (Fig. 4). Using the *GER*- and *AE*-based limits, when prey patches had

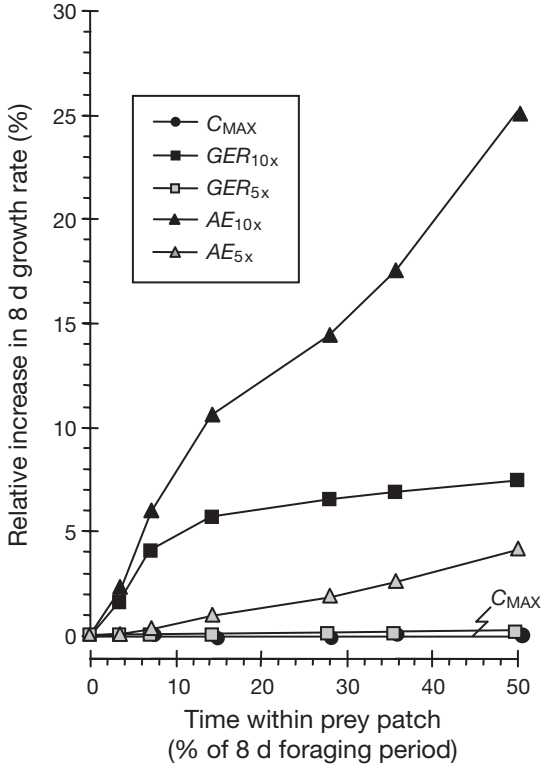

Fig. 4. Percentage increase in 8 d growth rate versus the duration of time within a patch (% foraging time). All values are case specific and relative to the no-patch condition (0). Growth responses to 5- and 10-fold patch prey concentrations are shown (see Table 2, Simulation 2a to c)

5-fold higher prey concentrations, the relative changes in growth were smaller. At 2-fold differences in prey concentration, no growth differences were detected because prey concentrations were above growth thresholds both outside and inside prey patches. Due to the lower prey threshold for maximum growth, relative growth of larvae was unchanged by the presence of prey patches when the C_{MAX} limit was employed.

Fluctuating prey fields

The differences among the 3 approaches to limit *C* were clearly evident when larvae were exposed to random fluctuations in the prey field in Simulation 3. For example, no differences in assimilated *C* were noted within and outside of prey patches using C_{MAX}, whereas 2- to 3-fold higher assimilated *C* was noted within patches using *GER* and *AE* approaches (Fig. 5). Within this random encounter simulation, larval *C* was saturated at concentrations of ≥15 copepodites l^{-1}, which were randomly encountered 11 times over the 8 d period. At these high concentrations, mean (±SD) *C* was equivalent to 41.3 (1.0), 56.3 (3.1) and 173.8 (1.1)% larval dry mass d^{-1} (hourly rates × 14 h foraging period) when feeding was limited by C_{MAX}, *GER* and *AE*, respectively. The mean (±SE) assimilated ration during the same periods was equivalent to 25.4 (0.2), 36.4 (1.0) and 49.7 (8.8)% larval dry mass d^{-1} in the same 3 cases. Estimates of assimilated *C* were more similar among the 3 cases, since *AE* within Case 3 decreased from a median value of 64% at concentrations <4 copepods l^{-1} to ~28% when larvae fed intensively within patches containing 15 to 40 copepods l^{-1}.

Foraging estimates of *C* (Eq. 2) and the limits to *C* imposed by each of the 3 approaches (C_{MAX}, *GER* and *AE*) were generally in close agreement at relatively low prey concentrations (Fig. 6A). However, at relatively high prey concentrations, foraging model estimates of *C* based on Eq. (2) were 2- to 4-fold higher than the highest *C* limit, the limit imposed by *AE* in Case 3 (Fig. 6B).

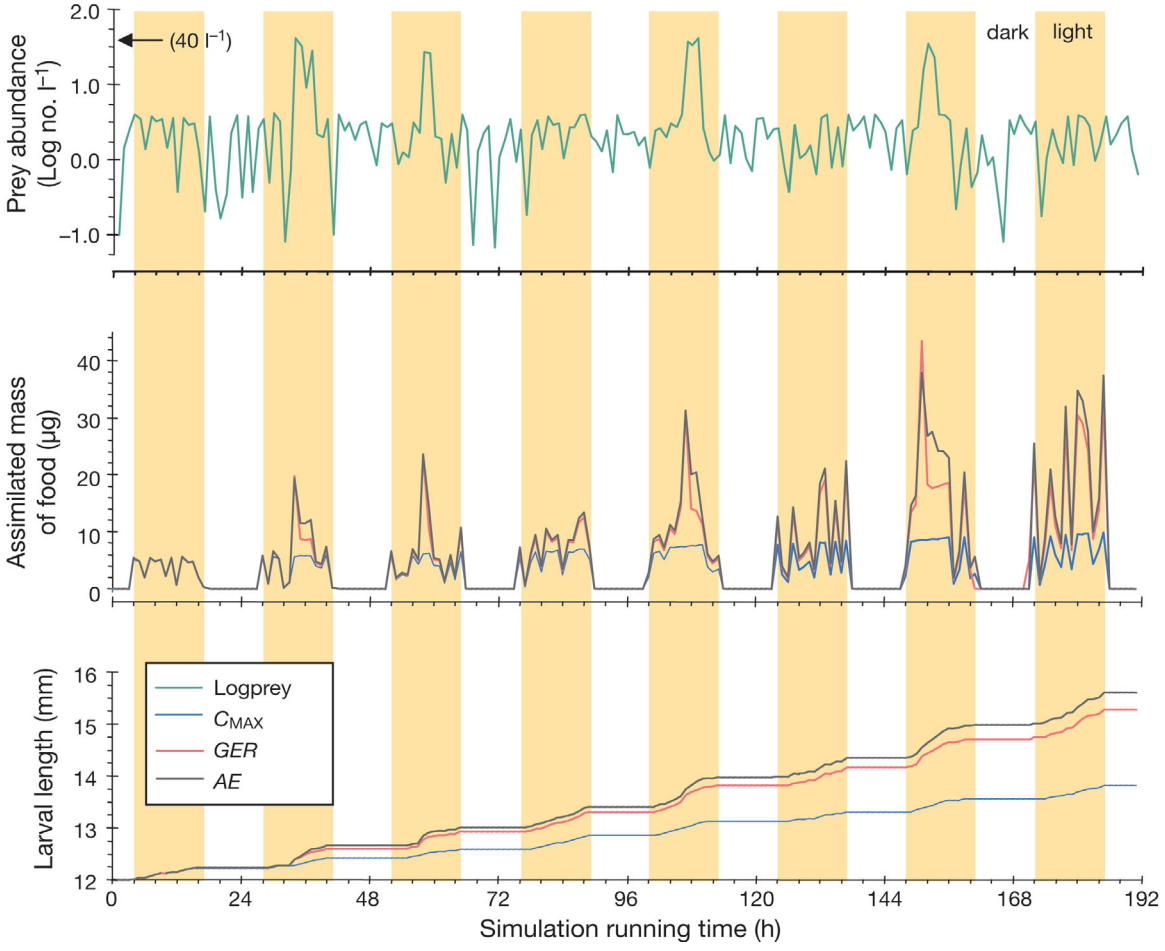

Fig. 5. Individual-based method simulation of random fluctuations in prey concentration and corresponding effect on changes in assimilated food and larval size (mm) per 1 h time step over the course of 8 d. The light regime and the value for peak prey abundance within a patch (upper panel) are indicated

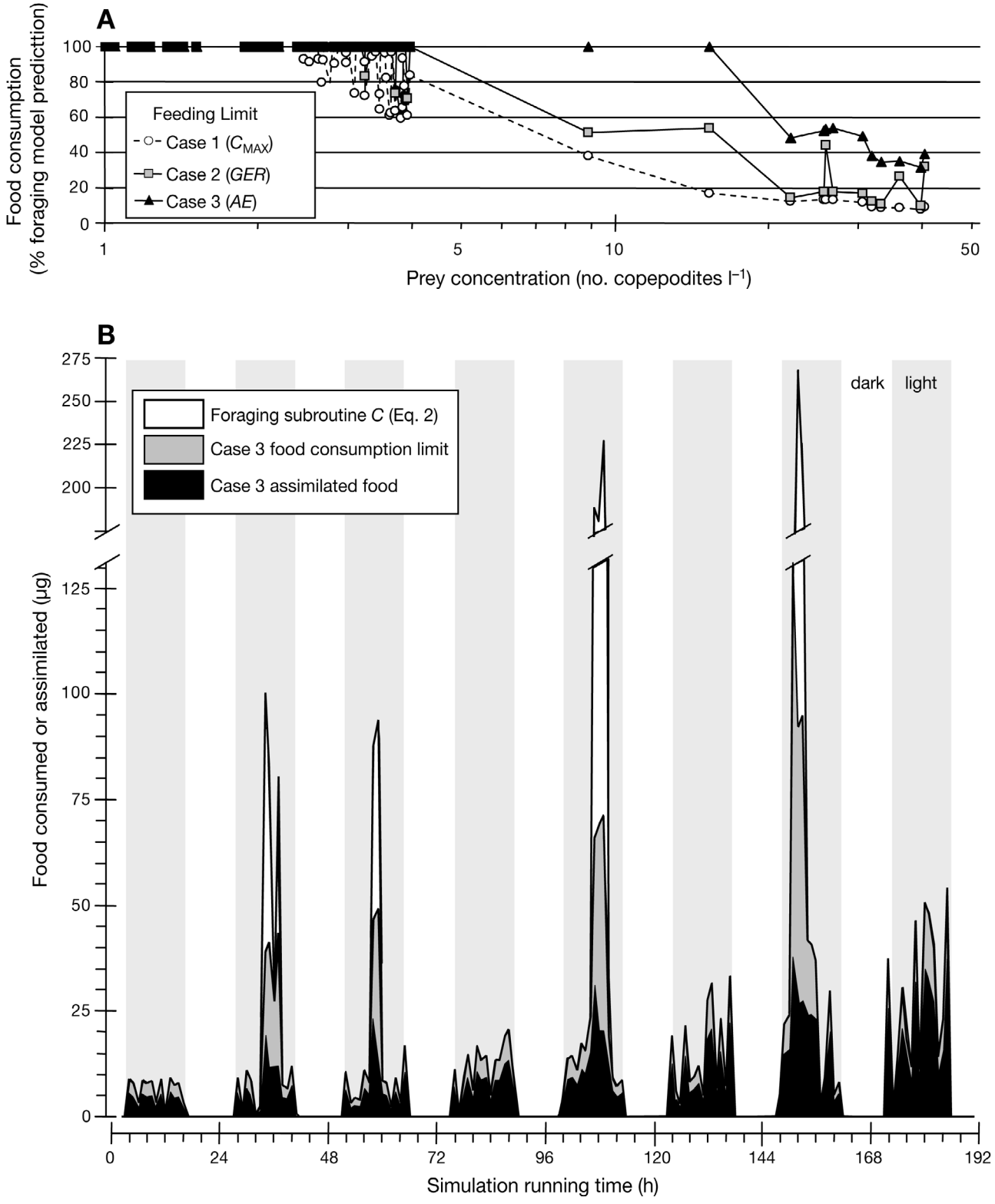

Fig. 6. (A) Food consumption rate (C) as limited by Case 1 (C_{MAX}), Case 2 (*GER*) and Case 3A (*AE*) relative to the individual-based method foraging subroutine estimate of C (based on Eq. 2 in the text) at different prey concentrations. Prey concentrations were those that were randomly encountered within model Simulation 3. (B) Comparison of foraging subroutine C, Case 3A-limited C and Case 3A-limited assimilated food ($C \times AE$) in each 1 h time step during the course of model Simulation 3. The randomly fluctuating prey field is shown in Fig. 5

DISCUSSION

Temperature, prey and growth

The results of our simulations performed at different, homogenous prey concentrations were consistent with expectations concerning larval fish physiology and interactions among temperature (T), feeding rate (C) and growth rate (G). Interestingly, for the effect of temperature on growth in Case 3 (*AE*) to be similar to that in the other 2 cases, the decrease in *AE* with increasing C (above gut capacity) had to be temperature dependent (this is Case 3B, see Figs. 2 & 3). We are unaware of any studies comparing the decline in *AE* with increasing C at different temperatures. However, the formulation appears to be biologically reasonable and laboratory studies should be conducted to test the validity of this model result. In the following discussion, we avoid further discussion of temperature and focus on comparing the 3 cases at the same temperature.

Clearly, growth rates of larval fish should be food limited in environments with low prey concentrations. However, the threshold prey concentrations reported in different studies to limit larval marine fish foraging and growth rates are equivocal. Based upon a review of laboratory functional response experiments conducted on 8 species of marine fish larvae, MacKenzie et al. (1990) calculated a threshold prey concentration of 179 µg l^{-1} below which larval fish C was food limited. Given the conversions used in their study, this corresponds to a concentration of ~660 nauplii l^{-1} or ~80 copepodites l^{-1}. In the present study, simulated growth rates declined (C was not maximal) at concentrations of 3 to 5 copepodites l^{-1} and were highest (feeding was maximal) at ~10 copepodites l^{-1} (Fig. 3). Our simulation predictions agreed well with the results of laboratory studies evaluating the effects of prey concentration on food searching and capture success of prey by larval marine fish (Munk & Kiørboe 1985, Munk 1995). In one study, 5.7 to 6.9 mm *SL* larval Atlantic cod foraged effectively at prey concentrations as low as 2 prey l^{-1} (Munk 1995).

Our estimates of C based upon the C_{MAX} limit (41.3%) and *GER* limit (56.3%) were similar to those obtained in a meta-analysis of 9 laboratory studies quantifying feeding rates by marine fish larvae (MacKenzie et al. 1990). In that study, ingestion by a 132.4 µg dry mass larva was equal to 75.8 µg d^{-1} (57% M_D) at 18.7°C, and estimates of relative ingestion varied by a factor of about 2 for the 12 species examined. Such interspecific differences underscore the problems that can arise whenever a 'generic' approach is taken to parameterize a model for a specific species. We illustrated this via the discrepancies between growth estimates using a C_{MAX} parameter (based upon data collected on sprat) and the other 2 limits (inter-specific parameterization). However, without parameter 'tuning', 2-fold differences in growth estimates were apparent among the 3 approaches, which were well within the range of inter-specific differences reported for most vital rates in teleost larvae (e.g. Houde 1989, Govoni et al. 1986, MacKenzie et al. 1990, Houde & Zastrow 1993).

When considered in light of values determined for the gross growth efficiency ($GGE = 100 \times G/C$) of larval fish, our value for *GGE* (64%) in Simulation 3 Case 3 (*AE* limit) was similar to that found in some species (*Blennius pavo* = 60%, *Clupea harengus* = 62%), but higher than the average calculated for larvae of a number of species (MacKenzie et al. 1990, Houde & Zastrow 1993). That our *GGE* value resulting from the *AE* limit agreed with published accounts was somewhat unexpected, since (1) our IBM was parameterized based on data for clupeids (sprat and Atlantic herring), (2) *GER*, gut capacity (Gut_{CAP}) and feeding-induced limits to *AE* were based upon data collected on a variety of non-clupeid species, and (3) no model tuning was used to adjust parameter values. A justifiable example of the latter would be adjustments made to active metabolism (R_A). Clearly, intensive feeding within patches would be expected to increase R_A, leading to lower energy available for growth (and lower values of *GGE*).

Prey patches and foraging

Our simulation results suggested that static limits to C such as C_{MAX} may not be adequate when modeled larvae forage in habitats with marked spatial and/or temporal variability in prey resources. In Case 3 (*AE*-based limit), larvae could exploit prey patches by consuming more food (at lower *AE*) per model time step. However, it should be noted that exploitation of prey patches in this manner could only benefit larvae (lead to higher growth rates) if prey concentrations outside the patch were lower than the growth-threshold prey concentration (~10 copepodites l^{-1}, see Fig. 3). The present simulation depicted a southern North Sea habitat having a mean copepodite concentration of 21.0 l^{-1}, with 2-, 5-, or 10-fold differences in concentrations within and outside patches (see Table 2). Foraging in this habitat, larvae benefited little (benefited much) from adopting a patch feeding strategy when prey concentrations in patches were ≤2-fold (≥5-fold) those outside patches.

An important finding of the present study was that, at high prey concentrations, a large discrepancy existed between foraging model estimates of C and the limits to C imposed by C_{MAX}, *GER*, or *AE* approaches. At concentrations >40 copepodites l^{-1}, the foraging

model predicted 2- to 4-fold higher C than the limit imposed by Case 3 (where C was highest among the 3 limits; see Fig. 6A). Differences between foraging model C and the limits imposed by C_{MAX} were not unexpected. A C_{MAX} parameter is derived from mass-based parameter rates of a balanced bioenergetics budget (e.g. metabolic losses and growth), while the foraging subroutine contains functions utilizing larval length (e.g. visual distance, capture success, swimming velocity). Since sprat larvae have relatively low mass-at-length compared to larvae of other teleosts (Peck et al. 2005), the foraging model prediction of C (based on length) exceeds the estimates of C required to obtain *in situ* growth rates (based on mass). However, the discrepancy of the foraging model estimates of C and the limit imposed by both of the other approaches (Cases 2 & 3) (e.g. see Fig. 6B) suggests that the current (commonly used) formulation of larval fish foraging yields unrealistically high C when larval fish encounter high prey concentrations.

Working knowledge

The physiologically based approaches to limit food consumption explored in this study relied upon knowledge of *GER* and *AE* and how these parameters were affected by changes in larval fish size, temperature and prey concentration. How robust are the estimates of *GER*? There appear to be many studies evaluating *GER* in fish, and the rates reported were similar after temperature and fish body size differences were taken into account. *GER* was generally between 0.2 and 0.5 h^{-1} for young larvae of a variety of marine and freshwater fish species, including 0.165 to 0.290 for larval radiated shanny *Ulvaria subbifurvata* (Bochdansky et al. 2006), 0.207 to 0.246 for walleye pollock *Theragra chalcogramma* (Canino & Bailey 1995), 0.38 for pinfish *Logadon rhomboids* (Peters & Kjelson 1975), 0.40 for perch *Perca fluviatilis* and 0.43 for zander *Stizostedion lucioperca* (Worischka & Mehner 1998). *GER* for post-larval stages tended to be lower, and was between 0.13 and 0.29 for young-of-the-year Atlantic herring (Arrhenius & Hansson 1994) and from 0.032 to 0.052 for larger, juvenile Atlantic salmon *Salmo salar* (Talbot et al. 1984). A 2- to 5-fold increase in *GER* during continuous feeding is also well documented. It appears as though laboratory studies indicating no effect of prey density on *GER* of larval and young juvenile fishes (e.g. Bochdansky & Dielbel 2001, Bochdansky et al. 2006) measured *GER* in fish that were no longer feeding.

How robust are estimates of *AE*? Compared to *GER*, far fewer studies have been conducted on *AE* using fish larvae. 'Inasmuch as it has bearing on models of larval growth and survival, the question of changing digestive and assimilative abilities with larval development… warrants the most immediate attention' (Govoni et al. 1986, p. 73). This statement is still true today. The values of *AE* differ depending upon the species. For example, *AE* was about 90% (based on carbon contents of copepod prey) in 13 to 34 dph (days post-hatch) Atlantic herring larvae (Pedersen & Hjelmeland 1988), but a range of lower values (i.e. from 30 to 90%) have also been reported (for reviews see Govoni et al. 1986, Houde & Zastrow 1993). In the present study, the effect of body size (developmental state) was incorporated into *AE* by evaluating literature data on a variety of species. It is reasonable to assume an improvement of *AE* with increasing body size (developmental stage), and this has been shown in several studies (Govoni et al. 1986). However, the largest species-specific differences in *AE* will undoubtedly be manifested in the effect of body size via differences among species in developmental characteristics. For this reason, more work is needed on *AE* in larval fish. Our simulation results (Case 3B) suggested that growth rates at different temperatures were only reasonable when the reduction of *AE* with increasing feeding rate was temperature dependent, and this should be tested.

CONCLUSIONS

Feedbacks between a marine fish larva and its environment have recently been explored using an IBM approach (e.g. behavioral modifications necessary to optimally forage within prey patches; Pitchford et al. 2003). In the present study, we included an interaction between the feeding physiology of a larva (consumption, digestion and assimilation of food) and characteristics of its prey field (different concentrations having patchy or homogenous distributions). Two physiologically based alternatives to C_{MAX} were parameterized, based upon the available literature on *GER* and *AE* for the larvae of a variety of freshwater and marine fish species. We recommend that larval fish IBMs utilizing foraging and growth subroutines also employ physiologically based limits to food consumption rate and that non-mechanistic parameters (C_{MAX} and/or G_{MAX}) be avoided. Employing mechanistic limits to feeding may be critical if models attempt to explore (and hope to understand) the consequences of both short- and long-term prey field variability on the growth and survival of marine fish larvae.

Acknowledgements. We are grateful to Susanne Tamm for the *in situ* prey abundance data and also thank Wilfried Kühn, Corinna Schrum and Mike St. John for thoughtful discussions relating to the IBM formulation. This research was presented

at the 'Workshop on advancements in modeling physical–biological interactions in fish early-life history: recommended practices and future directions' that took place in Nantes, France, from 3 to 5 April 2006. The present study was funded by the 'GLOBEC-Germany' program (FKZ No. 03F0320E), by the German 'AQUASHIFT' program (DFG No. JO556/1-1) and by 'UNCOVER' (EU, STREP No. 022717).

LITERATURE CITED

Alarcón FJ, Moyano FJ, Díaz M (1995) Digestión proteica en peces marinos: una visión general. In: Castello F, Calderer A (eds) Actas V Congreso Nacional de Acuicultura. Universitat de Barcelona, Barcelona, p 455–460

Almatar SM (1984) Effects of acute changes in temperature and salinity on the oxygen uptake of larvae of herring (*Clupea harengus*) and plaice (*Pleuronectes platessa*). Mar Biol 80:117–124

Arrhenius F, Hansson S (1994) *In situ* food consumption by young-of-the-year Baltic Sea herring *Clupea harengus*: a test of predictions from a bioenergetics model. Mar Ecol Prog Ser 110:145–149

Bartell SM, Breck JE, Gardner RH, Brenkert AL (1986) Individual parameter perturbation and error analysis of fish bioenergetics models. Can J Fish Aquat Sci 43:160–168

Bartsch J, Coombs SH (2004) An individual-based model of the early life history of mackerel (*Scomber scombrus*) in the eastern North Atlantic, simulating transport, growth and mortality. Fish Oceanogr 13:365–379

Baumann H, Gröhsler T, Kornilovs G, Makarchouk A, Feldmann V, Temming A (2006) Temperature-induced regional and temporal growth differences in Baltic young-of-the-year sprat *Sprattus sprattus*. Mar Ecol Prog Ser 317: 225–236

Besiktepe S, Dam HG (2002) Coupling of ingestion and defecation as a function of diet in the calanoid copepod *Acartia tonsa*. Mar Ecol Prog Ser 229:151–164

Beyer JE, Laurence GC (1980) A stochastic model of larval growth. Ecol Model 8:109–132

Blaxter JHS (1962) Herring rearing. IV. Rearing beyond the yolk-sac stage. Mar Res 1:1–18

Blaxter JHS (1965) The feeding of herring larvae and their ecology in relation to feeding. CALCOFI (Calif Coop Ocean Fish Investig) Rep 10:79–88

Bochdansky AB, Deibel D (2001) Consequences of model specification for the determination of gut evacuation rates: redefining the linear model. Can J Fish Aquat Sci 58: 1032–1042

Bochdansky AB, Brunemeyer ND, Leggett WC (2006) Model evaluation of linear gut evacuation in the larval radiated shanny using a combination of laboratory and field data. Trans Am Fish Soc 135:390–398

Boehlert GW, Yoklavich MM (1983) Effects of temperature, ration, and fish size on growth of juvenile black rockfish, *Sebastes melanops*. Environ Biol Fish 8:17–28

Boehlert GW, Yoklavich MM (1984) Carbon assimilation as a function of ingestion rate in larval Pacific herring, *Clupea harengus pallasi* Valenciennes. J Exp Mar Biol Ecol 79: 251–262

Broekhuizen N, Parkyn S, Miller D, Rose R (2002) The relationship between food density and short term assimilation rates in *Potamopyrgus antipodarum* and *Deleatidium* sp. Hydrobiologia 477:181–188

Broughton EA, Lough RG (2006) A direct comparison of MOCNESS and Video Plankton Recorder zooplankton abundance estimates: possible applications for augmenting net sampling with video systems. Deep-Sea Res II 53:2789–2807

Buckley LJ, Dillman DW (1982) Nitrogen utilization by larval summer flounder, *Paralichthys dentatus* (Linnaeus). J Exp Mar Biol Ecol 59:243–256

Canino MF, Bailey KM (1995) Gut evacuation of walleye pollock larvae in response to feeding conditions. J Fish Biol 46:389–403

Chiba K (1961) The basic study on the production of fish seedling under possible control. I. The effect of food in quality and quantity on the survival and growth of common carp fry. Tansuiku Suisan Kenkyusho Kenkyu Hokoku 11:105–132

Chitty N (1981) Behavioral observations of feeding larvae of bay anchovy, *Anchoa mitchilli*, and bigeye anchovy, *Anchoa lamprotaenia*. Rapp P-V Reun Cons Int Explor Mer 178:320–321

Corazza L, Nickum JG (1983) Rates of food passage through the intestinal tract of fingerling walleyes. Prog Fish Cult 45:183–184

Dagg MJ, Waker EW Jr (1978) Ingestion, gut passage, and egestion by the copepod *Neocalanus plumchrus* in the laboratory and in the subarctic Pacific Ocean. Limnol Oceanogr 32:178–188

Dekshenieks MM, Donaghay PL, Sullivan JM, Rines JEB, Osborn TR, Twardowski MS (2001) Temporal and spatial occurrence of thin phytoplankton layers in relation to physical processes. Mar Ecol Prog Ser 223:61–71

Dickmann M (2006) Feeding ecology of sprat (*Sprattus sprattus* L.) and sardine (*Sardine pilchardus* W.) larvae in the Baltic Sea and in the North Sea. PhD thesis, Institute für Ostseeforschung, University of Rostock

Doohan M (1973) An energy budget for adult *Brachionus plicatilis* Muller (Rotatoria). Oecologia 13:351–362

Elliott JM (1976) Energy losses in the waste products of brown trout (*Salmo trutta* L.). J Anim Ecol 45:561–580

Fiksen Ø, Folkvord A (1999) Modelling growth and ingestion processes in herring *Clupea harengus* larvae. Mar Ecol Prog Ser 184:273–289

Fossum P (1983) Digestion rate of food particles in the gut of larval herring (*Clupea harengus* L.). Fiskdir Skr Serie Havundersokelser 17:347–357

Gelman A, Kuz'mina V, Drabkin V, Glatman L (2003) Temperature dependent characteristics of intestinal glycyl-L-leucine dipeptidase in boreal zone fish. Comp Biochem Physiol B 136:323–329

Govoni JJ, Peters DS, Merriner JV (1982) Carbon assimilation during the larval development of the marine teleost *Leiostomus xanthurus* Lacepede. J Exp Mar Biol Ecol 64:287–299

Govoni JJ, Boehlert GH, Watanabe T (1986) The physiology of digestion in fish larvae. Environ Biol Fish 16:59–77

Herrera G, Balbontín F (1983) Tasa de evacuacion intestinal e incidencia de alimentacion en larvas de Sardinops sagax musica (Pisces, Clupeiformes). Rev Biol Mar Valparaíso 19:113–132

Hinrichsen HH, Möllmann C, Voss R, Köster FW, Kornilovs G (2002) Biophysical modeling of larval Baltic cod (*Gadus morhua*) growth and survival. Can J Fish Aquat Sci 59: 1858–1873

Houde ED (1989) Comparative growth, mortality, and energetics of marine fish larvae: temperature and implied latitudinal effects. Fish Bull 87:471–475

Houde ED, Schekter RC (1983) Oxygen uptake and comparative energetics among eggs and larvae of three subtropical marine fishes. Mar Biol 72:283–293

Houde ED, Zastrow CE (1993) Ecosystem and taxon-specific

dynamic and energetics properties of larval fish assemblages. Bull Mar Sci 53:290–335
Huwer B (2004) Larval growth of *Sardina pilchardus* and *Sprattus sprattus* in relation to frontal systems in the German Bight. Diplomarbeit, Christian-Albrechts-Universität, Kiel
Johnston TA, Mathias JA (1996) Gut evacuation and absorption efficiency of walleye larvae. J Fish Biol 49:375–389
Karjalainen J, Koho J, Viljanen M (1991) The gastric evacuation rate of vendace (*Coregonus albula* L.) larvae predating on zooplankters in the laboratory. Aquaculture 96: 343–351
Kiørboe T, Munk P, Richardson K (1987) Respiration and growth of larval herring *Clupea harengus*: relation between specific dynamic action and growth efficiency. Mar Ecol Prog Ser 40:1–10
Lankford Jr TE, Targett TE (1997) Selective predation by juvenile weakfish: post-consumptive constraints on energy maximization and growth. Ecology 78:1049–1061
Laurence GC (1971) Digestion rate of larval largemouth bass. NY Fish Game J 18:52–56
Laurence GC (1985) A report on the development of stochastic models of food limited growth and survival of cod and haddock larvae. In: Laurence GC, Lough RG (eds) Growth and survival of larval fishes in relation to the trophodynamics of Georges Bank cod and haddock. NOAA Tech Memo NMFS 36:83–150
Letcher BH, Rice JA, Crowder LB, Rose KA (1996) Variability in survival of larval fish: disentangling components with a generalized individual-based model. Can J Fish Aquat Sci 53:787–801
Lough RG, Buckley LJ, Werner FE, Quinlan JA, Edwards KP (2005) A general biophysical model of larval cod (*Gadus morhua*) growth applied to populations on Georges Bank. Fish Oceanogr 14:241–262
Lough RG, Broughton EA, Buckley LJ, Incze LS, Pehrson Edwards K, Converse R, Aretxabaleta A, Werner FE (2006) Modeling growth of Atlantic cod larvae on the southern flank of Georges Bank in the tidal-front circulation during May 1999. Deep-Sea Res II 2771–2788
MacKenzie BR, Leggett WC, Peters RH (1990) Estimating larval fish ingestion rates: can laboratory derived values be reliably extrapolated to the wild? Mar Ecol Prog Ser 67:209–225
Maes J, Limburg KE, van de Putte A, Ollevier F (2005) A spatially explicit, individual-based model to assess the role of estuarine nurseries in the early life history of North Sea herring, *Clupea harengus*. Fish Oceanogr 14:17–31
Mills EL, Ready RC, Jahncke M, Hanger CR, Trowbridge C (1984) A gastric evacuation model for young yellow perch, *Perca flavescens*. Can J Fish Aquat Sci 41:513–518
Munk P (1992) Foraging behaviour and prey size spectra of larval herring *Clupea harengus*. Mar Ecol Prog Ser 80: 149–158
Munk P (1993) Differential growth of larval sprat *Sprattus sprattus* across a tidal front in the eastern North Sea. Mar Ecol Prog Ser 99:17–27
Munk P (1995) Foraging behaviour of larval cod (*Gadus morhua*) influenced by prey density and hunger. Mar Biol 122:205–212
Munk R, Kiørboe T (1985) Feeding behaviour and swimming activity of larval herring (*Clupea harengus* L.) in relation to density of copepod nauplii. Mar Ecol Prog Ser 24:15–21
Noble RL (1973) Evacuation rates of young yellow perch, *Perca flavescens* (Mitchill). Trans Am Fish Soc 102: 759–763
Owen RW (1989) Microscale and finescale variations of small plankton in coastal and pelagic environments. J Mar Res 47:197–240
Peck MA, Clemmesen C, Herrmann JP (2005) Ontogenic changes in the allometric scaling of the mass and length relationship in *Sprattus sprattus*. J Fish Biol 66:882–887
Pedersen BH (1984) The intestinal evacuation rates of larval herring (*Clupea harengus* L.) predating on wild plankton. Dana 3:21–30
Pedersen BH, Hjelmeland K (1988) Fate of trypsin and assimilation efficiency in larval herring (*Clupea harengus*) following digestion of copepods. Mar Biol 97:467–476
Pepin P, Penney R (2000) Feeding by a larval fish community: impact on zooplankton. Mar Ecol Prog Ser 204:199–212
Peters DS, Kjelson MA (1975) Consumption and utilization of food by various postlarval and juvenile fishes of North Carolina estuaries. Estuar Res 1:448–472
Pitchford JW, James A, Brindley JA (2003) Optimal foraging in patchy turbulent environments. Mar Ecol Prog Ser 256: 99–110
Pitchford JW, James A, Brindley JA (2005) Quantifying the effects of individual and environmental variability in fish recruitment. Fish Oceanogr 14:156–160
Ré P, Gonçalves E (1993) Growth of sprat *Sprattus sprattus* larvae in the German Bight (North Sea) as inferred from otolith microstructure. Mar Ecol Prog Ser 96:139–145
Ryer CH, Boehlert GW (1983) Feeding chronology, daily ration, and the effects of temperature upon gastric evacuation in the pipefish (*Syngnathus fuscus*). Environ Biol Fish 9: 301–306
Shepherd WC, Mills EL (1996) Diel feeding, daily food intake, and *Daphnia* consumption by age-0 gizzard shad in Oneida Lake, New York. Trans Am Fish Soc 125:411–421
Talbot C, Higgins PJ, Shanks AM (1984) Effects of pre- and post-prandial starvation on meal size and evacuation rate of juvenile Atlantic salmon, *Salmo salar* L. J Fish Biol 25: 551–560
Tilseth S, Ellertsen B (1984) Food consumption rate and gut evacuation processes of first feeding cod larvae (*Gadus morhua* L.). Flödevigen Rapp 1:167–182
Walton WE, Hairston NG, Wetterer JK (1992) Growth-related constraints on diet selection by sunfish. Ecology 73: 429–437
Werner F, Perry RI, Lough RG, Naimie CE (1996) Trophodynamic and advective influences on Georges Bank larval cod and haddock. Deep-Sea Res II 43:1793–1822
Werner RG, Blaxter JHS (1980) Growth and survival of larval herring (*Clupea harengus*) in relation to prey density. Can J Fish Aquat Sci 37:1063–1069
Worischka S, Mehner T (1998) Comparison of field-based and direct estimates of daily food consumption in larval perch and zander. J Fish Biol 53:1050–1059
Xu Y, Wang WX (2001) Individual responses of trace-element assimilation and physiological turnover by the marine copepod *Calanus sinicus* to changes in food quantity. Mar Ecol Prog Ser 218:227–238
Young JW, Davis TLO (1990) Feeding ecology of larvae of southern bluefin, albacore and skipjack tunas (Pisces: Scombridae) in the eastern Indian Ocean. Mar Ecol Prog Ser 61:17–29
Young JW, Davis TLO (1992) Feeding ecology and interannual variations in diet of larval jack mackerel, *Trachurus declivis* (Pisces: Carangidae), from coastal waters of eastern Tasmania. Mar Biol 113:11–20

Editorial responsibility: Alejandro Gallego (Contributing Editor), Aberdeen, UK

Submitted: August 2, 2006; Accepted: March 1, 2007
Proofs received from author(s): September 17, 2007

Vol. 347: 185–193, 2007
doi: 10.3354/meps06977

MARINE ECOLOGY PROGRESS SERIES
Mar Ecol Prog Ser

Published October 11

OPEN ACCESS

Behaviour as input for modelling dispersal of fish larvae: behaviour, biogeography, hydrodynamics, ontogeny, physiology and phylogeny meet hydrography

Jeffrey M. Leis*

Ichthyology, Australian Museum, 6 College Street, Sydney, New South Wales 2010, Australia

ABSTRACT: Both morphology and behaviour develop during the pelagic larval stage of demersal teleost fishes. Demersal perciform fishes from warm-water habitats begin their pelagic larval stage as plankton but end it as nekton, with behavioural capabilities (including swimming, orientation and sensory abilities) that can influence, if not control, dispersal trajectories. The ontogeny of these behaviours, and the gradual transition from plankton to nekton, are central to understanding how larval fishes can influence dispersal and how behaviour can be integrated into dispersal models. Recent behavioural research shows that, from about 5 to 8 mm standard length, larvae of warm-water perciform fishes can directly influence dispersal, because they swim in an efficient inertial hydrodynamic environment, can swim for kilometres at speeds that heuristic models show will alter dispersal trajectories, can swim faster than ambient currents before settlement, can orientate in the pelagic environment and can detect sensory cues (light, sound, odour) that allow orientation. Fish larvae also control their vertical position (which may change temporally, spatially and ontogenetically), allowing indirect influence on dispersal. Most research on larval behaviour relevant to dispersal (i.e. swimming, orientation and sensory abilities) has been done with warm-water perciform species. This invites the question: Will the same be found in cool water or in species of other orders? The hydrodynamic and physiological effects of temperature indicate that larvae in warm water should swim more efficiently and initially at smaller sizes than larvae in cool water. Limited evidence suggests that larvae of perciform fishes are more behaviourally competent and attain morphological and behavioural milestones when smaller (and probably younger) than do larvae of clupeiform, gadiform and pleuronectiform (CGP) fishes. Perciform fishes dominate demersal fish communities in warm water, whereas CGP fishes dominate in cooler waters. These hydrodynamic, physiological, ontogenetic, phylogenetic and biogeographic factors imply that larval fish behaviour may have more influence on dispersal in warm seas than in cool seas. This hypothesis requires testing. Additional factors that should be taken into account when using behaviour of larvae to produce biophysical models of dispersal are discussed.

KEY WORDS: Fish larvae · Dispersal · Connectivity · Behaviour · Biophysical model · Swimming · Orientation · Sensory cues · Marine protected areas

INTRODUCTION

The fact that the large majority of marine, demersal, teleost fishes have a pelagic larval stage (Moser et al. 1984, Leis 1991, Fuiman & Werner 2002) has important implications for the dynamics of fish populations and for human management of them. Marine fish populations are thought to be open, with young potentially derived from sources perhaps many kilometres away (Sale 1991, 2004, Caley et al. 1996). Connectivity is the process that links these populations by dispersal (Palumbi 2003), and, for demersal teleost fishes, this takes place primarily during the pelagic larval stage, as it does for most marine invertebrates (Leis 1991,

*Email: jeff.leis@austmus.gov.au

Morgan 2001). Therefore, for most species, it is the pelagic larval stage, rather than the demersal adult stage, that sets the spatial scale for population connectivity and for the geographic size of fish populations (Cowen 2002, Sale 2004). Further, most mortality in marine fishes takes place during the pelagic stage (e.g. Cushing 1990), which limits the distances over which meaningful dispersal takes place (Cowen et al. 2000, 2006).

Understanding the scale of connectivity by dispersal during the pelagic larval stage is a major challenge in marine ecology (Cowen 2002, Sale 2004), and it is clear that management of marine fishes must incorporate the scales over which their populations are connected (Palumbi 2001, Cowen et al. 2003). For example, marine protected areas (MPAs) are expected to fulfil both biodiversity conservation and fishery replenishment roles, and their effectiveness in both depends on the scale of connectivity (Palumbi 2003). A major question of scale is whether MPAs can replenish themselves; however, regardless of their ability to do this, MPAs will not fulfil the fishery role for all exploited areas in between them if spaced too far apart. The MPA biodiversity role requires maintenance of genetic connections between MPAs, and, although this demands a lower and less regular exchange of propagules than does fishery replenishment, for optimal MPA design, it is important to understand the spatial scales involved.

Dispersal in marine systems has usually been assumed to operate over very large distances (100s of kilometres), with management scaled accordingly. We now know that marine fish populations can be demographically structured at more modest spatial scales; in some cases as little as 10s to 100s of metres (Iles & Sinclair 1982, Sinclair 1988, Swearer et al. 2002, Jones et al. 2005, Cowen et al. 2006). Predictive, individually based dispersal models provide a productive way to address the challenge of quantifying both the spatial and temporal scales of connectivity and the factors that contribute to them.

The importance of understanding where larvae are going and where they are coming from has led to dozens of models of dispersal as a purely physical process. These attempts make the 'simplifying assumption' (e.g. Frank et al. 1993, Roberts 1997, Leis 2006) that pelagic larvae of demersal fishes have swimming and orientation abilities so limited as to be irrelevant to dispersal: they treat larvae as passive particles. From this perspective, the only biological variable relevant to dispersal outcomes is the pelagic larval duration (PLD). No one contests the relevance of hydrography to dispersal, but, in contrast, until recently, larval behaviour other than vertical distribution has effectively been ignored in most dispersal models. This is changing rapidly. For example, James et al. (2002) state that 'further work is needed with more computationally intensive 3D circulation models to investigate the possible effects of known or proposed larval behaviours'. This is exactly what is required, but, increasingly, this can be based on known, rather than proposed, behaviour.

My goal here is not to review the literature on behavioural capabilities of fish larvae—this has been done elsewhere (see references below). Rather, I will attempt to briefly summarise the kinds of documented behaviours of fish larvae that are relevant to dispersal (dispersal-relevant behaviour). Reviews will be cited to point the reader who is interested in more detail in the right direction. I will argue that we now know enough about the behavioural capabilities of fish larvae that we should expect them to influence dispersal outcomes, and must, therefore, include them in our dispersal models. Then, I will provide a 'shopping list' and brief discussion of factors that I argue should be taken into account when incorporating the behaviour of fish larvae into hydrodynamic models if the goal is to produce realistic biophysical models of dispersal.

The present paper focuses on the pelagic, dispersive stage of demersal, teleost fishes. For the purposes of this paper, an ecological rather than morphological definition is adopted—this stage begins when the propagule leaves the adult, demersal habitat (at spawning for pelagic eggs and at hatching for non-pelagic eggs) and ends at settlement from the pelagic habitat. This focuses attention on the pelagic, potentially dispersive stage, regardless of what it is called, and has the advantage of avoiding sterile nomenclatural debates over when a larva becomes a juvenile. Behaviour has long been recognised as an important input to dispersal of adult, pelagic fishes, and adults of these species are, in general, more mobile than are demersal fish species. Much of what is said here about larvae of demersal fishes might also apply to larvae of pelagic species, but there has been relatively little study of dispersal-relevant behaviour in larvae of pelagic fishes. It is nearly certain that some differences will exist between larvae of demersal and pelagic species, and until we have data on behavioural capabilities of larvae of the latter, it is unwise to assume the two are equivalent.

DISCUSSION

Why behaviour of fish larvae can influence dispersal outcomes

Integration of biological and physical inputs has been impeded by poor knowledge of the behaviour of

fish larvae during their pelagic sojourn away from the demersal adult habitat and during the extraordinary ecological and morphological transition from the pelagic to benthic phase, which is termed settlement. Recent research on warm-water, larval marine, perciform fishes has revealed remarkable behavioural abilities that make the simplifying assumption untenable. We now know that, for most of the pelagic stage, these larvae are capable of exerting considerable direct and indirect behavioural control over their dispersal trajectories (reviewed by Kingsford et al. 2002, Leis & McCormick 2002, Sponaugle et al. 2002, Leis 2006, Montgomery et al. 2006). Larvae of warm-water, perciform demersal fishes have impressive behavioural capabilities (less is known about species in other orders), and heuristic models indicate that speeds and behaviours that are able to strongly influence dispersal trajectories both directly and indirectly are well within their capabilities (see review by Leis 2006). These behaviours are not reviewed in detail here. Rather, a brief summary is provided about what is known of the behavioural capabilities of larvae of warm-water perciform fishes, and relevant review papers are cited. Other than vertical distribution, research on behaviour of larvae from cool-water and non-perciform species has focused on feeding and predator avoidance, and dispersal-relevant behaviour has received little attention. Because so little is known about dispersal-relevant behaviour in larvae of cool-water species and in larvae of non-perciform species, this paper focuses on demersal, perciform species of warm-water fishes. I will then build upon Hunt von Herbing's (2002) hypothesis that in warm marine waters, swimming abilities of fish larvae are more likely to be able to directly influence dispersal outcomes than in cool waters, and the reasons for thinking this might be so.

Behavioural abilities of relevance to dispersal

It should be understood that the following refers to larvae of warm-water, demersal, perciform fish species. In no case do we have complete knowledge of all dispersal-relevant behaviours for any one species, and, for some types of behaviour, only a few species have been studied.

Vertical distribution can indirectly influence dispersal of fish larvae, and it is clearly under control of the larvae (see reviews by Pearre 1979, Sponaugle et al. 2002, Leis 2006). It is well established that vertical distribution of fish larvae is under precise behavioural control from very early in the PLD, often changes ontogenetically (and over other time scales), and may vary spatially. It has long been recognised that behaviour affecting non-random, vertical distribution can strongly influence dispersal outcomes where current velocity is not uniform vertically; this has been demonstrated in both warm and cold waters and with larvae from a variety of orders.

Horizontal swimming by fish larvae can directly influence dispersal if it is of sufficient speed, can be maintained for sufficient periods of time, and is orientated. Swimming speeds of fish larvae can be considerable (see review by Leis 2006). Over most of the PLD, larvae can swim at speeds that remove the larvae from the inefficient viscous hydrodynamic environment, and heuristic models indicate that this behaviour can influence dispersal outcomes. Over much of the pelagic period larvae can swim at speeds that are similar to or greater than mean current speeds in many marine environments. These swimming speeds are 3 to 10 body lengths s^{-1} (BL s^{-1}) in the ocean, increase by 0.5 to 4.0 cm s^{-1} for each millimetre increase in size, and can exceed 50 cm s^{-1} at settlement.

Swimming speed must be combined with swimming endurance to influence dispersal outcomes, and fish larvae do have considerable swimming endurance (see review by Leis 2006). Over a major portion of the post-flexion stage, larvae can swim for kilometres to 10s of kilometres, and this distance increases greatly with growth. Endurance may be nearly open-ended if larvae can feed, and larvae seem to be very energetically efficient when swimming (Nilsson et al. 2007).

Swimming in the absence of orientation is unlikely to influence dispersal outcomes, but fish larvae have good orientation abilities (see reviews by Kingsford et al. 2002, Leis 2006, Montgomery et al. 2006). The orientation abilities of individual larvae form early, reach a high precision by 5 to 8 mm, and do not improve further with growth. On a population basis, orientation abilities form in larvae by 7 to 8 mm. Direction of the orientation of larvae may change ontogenetically or between day and night. In short, larvae do not swim randomly on either an individual basis or a population basis, but the question of how this orientation is maintained remains.

Although other sensory cues may also be involved in orientation by fish larvae in the pelagic environment, there is clear evidence for the involvement of audition, olfaction and vision. Underwater sound can provide cues for orientation by larval fishes (see reviews by Montgomery et al. 2001, 2006, Kingsford et al. 2002, Myrberg & Fuiman 2002). Fish larvae can hear when very small (8 to 9 mm, which are the smallest larvae in which hearing abilities can currently be assessed; K. J. Wright pers. comm.) and perhaps throughout the pelagic phase. By settlement, and possibly earlier, larvae can distinguish among sounds and can locate underwater sound sources (i.e. use sound to navigate).

The distances over which underwater sound can be utilised by fish larvae for orientation are unclear, but sound travels well with little attenuation in water, and its spread is independent of current, so it has the potential to provide orientation cues over many square kilometres.

Fish larvae can use olfactory cues for orientation (see reviews by Leis & McCormick 2002, Kingsford et al. 2002, Atema et al. 2002, Wright et al. 2005). Very small larvae can detect dissolved materials (9 mm, which are the smallest larvae in which olfaction can currently be assessed; K. J. Wright pers. comm.). Using olfactory cues, settlement-stage larvae can distinguish among species, and among water types with different characteristics, and can locate odour sources. At present, this has been shown only over small spatial scales (10s of metres), usually in connection with settlement. Because the spread of odours is not independent of currents, odours may be less useful than sound for orientation.

Fish larvae can use vision for orientation (see reviews by Kingsford et al. 2002, Myrberg & Fuiman 2002, Leis 2006). By the time of settlement, larvae can apparently see as well as human divers, although earlier in development, visual abilities are more limited. This visual ability is used in avoiding predators and selecting settlement sites, but this is limited by water clarity to 10s of metres. There are indications, however, that settlement-stage larvae of some species may be able to use a solar compass, and, presumably, this is vision based.

There is little, if any, evidence that fish larvae can detect the speed and direction of currents in the pelagic environment, and thereby orientate their swimming into the current (see reviews by Leis 2006, Montgomery et al. 2006). A fish larva embedded in a moving water column may be able to detect turbulence (using its lateral line or otolith-based sensory system), and this might indicate it is within a current, but, without an external frame of reference, it cannot detect the direction or speed of the current. External reference points in the form of the ability to see the bottom, or, more speculatively, the ability to perceive, while drifting, the relative motion of a distant, fixed, sound source might be available and might enable a larva to determine the direction of the current, but this has not been demonstrated.

Species-specific patterns are an overriding theme in behavioural studies (see reviews by Leis & McCormick 2002, Leis 2006). Because of this, we should expect different species to have differing behavioural influences on dispersal trajectories.

How a combination of such behaviours might influence dispersal can be demonstrated with larvae of the sparid *Acanthopagrus australis* off the Australian east coast. On average, larvae of this species swam toward the coast (NW) when 7 to 10 mm in length and then parallel to the coast (NE) when 10 to 13 mm in length (Leis et al. 2006). At the same size at which the change in swimming direction took place, this species moved upward into the neuston from a relatively uniform vertical distribution over the upper 10 m (Leis et al. 2006). Over this range of sizes, the *in situ* swimming speed of this species increased from 5 to 10 cm s^{-1}, remaining at about 8 BL s^{-1} (Leis 2006), although the larvae can swim considerably faster (Clark et al. 2005). In contrast, over the same size range, there was no change in the precision of swimming directionality by individuals (Leis et al. 2006). This sparid settles into estuarine sea grasses, entering estuaries at 10 to 13 mm, while swimming at or near the surface (Trnski 2002). This combination of behaviours would help keep the smaller larvae relatively near the coast until they were ready to settle, whereupon they would swim parallel to the coast at the surface. This would be an effective way to intersect estuarine plumes extending over the shelf that the larvae might be able to follow into the estuary (albeit, nothing is known of the sensory abilities of larval *A. australis*). Clearly, dispersal outcomes for larvae of *A. australis* would be different from the oft-assumed passive drift, and the portion of the PLD for which passive drift is a reasonable assumption will be small.

Given these capabilities, larvae of warm-water, perciform fishes have the behavioural potential to greatly influence dispersal trajectories. Now that these abilities are documented in a range of taxa, we can begin to incorporate them into dispersal models. Existing attempts to include behaviour of larvae into dispersal models have focused on vertical distribution, but have, more often than not, ignored ontogenetic changes or variance in vertical distribution behaviour (there are some honourable exceptions: e.g. Bartsch & Knust 1994, Hare et al. 1999, Cowen et al. 2006). Attempts to include other behaviours (e.g. horizontal swimming, orientation abilities) have encountered difficulties because of a lack of appropriate data on relevant species, and modellers have sometimes resorted to the use of hypothesised abilities or arbitrary 'sensory zones' around settlement habitats (James et al. 2002, Cowen et al. 2006). Emerging data on the ontogeny of behaviour in the larvae of demersal fishes, and direct measurements of its variation will enable modellers to overcome this limitation and to fill the biological gap in contemporary dispersal models. This will allow the development of true biophysical dispersal models with realistic behavioural input and, therefore, realistic estimates of connectivity.

Could behaviour of larvae be more important in warm than in cool waters?

The work summarised above on dispersal-relevant larval behaviour has concentrated on warm-water, perciform species. It is not clear that these results will apply to larvae from cold water or of other orders. In fact, we should expect differences in dispersal of larvae between cold- and warm-water environments (Hunt von Herbing 2002). In particular, in warmer waters, larval behaviour may have more influence on dispersal outcomes. The reasons for this expectation come from several sources.

First, both physics (water viscosity) and physiology (muscle efficiency) predict that swimming by fish larvae—particularly smaller ones—will be more efficient in warmer water. Water is more viscous when it is cold, and this makes swimming more difficult and energetically inefficient (Fuiman & Batty 1997, Hunt von Herbing 2002, Leis 2006), and this effect is most pronounced for small larvae and larvae that swim slowly (e.g. 1 to 2 BL s^{-1}). Further, larvae swimming in colder water operate over an inefficient range of muscle-fibre-shortening velocities, and this will have an impact on swimming efficiency and limit swimming performance (Hunt von Herbing 2002). In larval herring and plaice, muscle-contraction speed increases by about one-third when temperature increases from 5 to 12–15°C (Blaxter 1992), for example, and, in herring larvae, this leads to a doubling of the swimming speed (Batty et al. 1991).

Secondly, in warmer water, larvae may grow faster, thus reaching a given size sooner than in cooler water (Houde 1987, 1989), which means that ontogenetic milestones, both morphological and behavioural, will be reached sooner. All else being equal, this should mean that larvae will be able to behaviourally influence dispersal outcomes sooner in warm water.

Third, perciform fishes dominate demersal fish communities and catches in tropical waters, whereas, in cooler waters, other orders (e.g. Gadiformes) dominate. For example, in the warm waters of the eastern Pacific between Mexico and Peru, the 696 perciform species constitute 62% of the coastal teleost species (Robertson & Allen 2002), whereas, in the much cooler waters of the Canadian Pacific, the 75 perciform species constitute only 30% of the coastal teleosts (Hart 1973). This is relevant to possible regional differences in dispersal, because perciform fishes seemingly reach developmental milestones at smaller sizes than do larvae of other orders (Moser et al. 1984, Moser 1996, Leis & McCormick 2002, Leis & Carson-Ewart 2004, Leis 2006), and the same presumably applies to behavioural milestones. Very limited information also suggests that larvae of perciform fishes may be more behaviourally capable at any given size than are larvae of other orders. In the clearest example of this, maximum routine swimming speeds (a measure of swimming speed in still water in the laboratory) of perciform larvae are of 2.5 to 11 BL s^{-1}, whereas larvae of clupeiform, gadiform and pleuronectiform fishes can achieve only 1 to 1.5 BL s^{-1} (Leis 2006).

These physical, physiological, biogeographic, ontogenetic and phylogenetic factors lead to the expectation that, in tropical waters, fish larvae will have more behavioural influence over dispersal than occurs in cool temperate waters. Some aspects of the above reasoning remain to be properly verified (e.g. the assertion that perciform larvae have greater relative swimming speeds [i.e. BL s^{-1}] than do larvae of other orders is based on limited data), and the overall hypothesis remains to be tested. Testing the hypothesis will require care to avoid confounded comparisons given the number of potentially interacting physical, physiological, biogeographic, ontogenetic and phylogenetic factors involved. Finally, if temperature is an important factor in determining the ability of fish larvae to behaviourally influence dispersal, then seasonal variation in this ability should be expected.

Factors to consider when integrating behaviour of larvae of demersal fishes into numerical models of dispersal

This listing should be considered a step toward 'best practice' in dispersal models, rather than an assertion that dispersal models have always failed to consider these things in the past. Most dispersal models have incorporated some or many of these factors, but numerous models, including contemporary ones, have not.

(1) The numerical physical model must be 3-dimensional so vertical distribution behaviour can be taken into account. Although 3-dimensional dispersal models have been available for some time, 2-dimensional models are still being produced today.

(2) Behavioural capabilities of larval fishes are best incorporated into dispersal models if the models are individually based.

(3) Many behaviours may operate at dimensions that would be sub-scale given the grid size of most contemporary dispersal models, and it is possible that behavioural interactions with sub-scale hydrodynamic features, particularly in areas of topographic complexity, are important in determining dispersal outcomes. Therefore, at least in areas of topographic complexity, it may be necessary to use a finer scale model grid than has usually been the case in order to take behaviour into account.

(4) When larvae are initially released into the ocean, their behavioural capabilities are poorly developed and may have little influence on their dispersal. So, it is particularly important to model the flow of water at a fine scale in the vicinity of the spawning location—which will frequently be an area of topographic complexity—to determine whether larvae can be passively retained near their natal area by fine-scale physical processes until they become behaviourally capable.

(5) Testing of both the physical portion of the models and of the integrated biophysical models is essential if they are to be credible. The former can utilise direct physical oceanographic measurements. The latter can use otolith data and physical markers (Thorrold et al. 2002) and some genetic measures (Hellberg et al. 2002).

(6) We need to be clear about whether a given model is to be used to examine demographic connectivity or genetic connectivity, as the spatial and temporal scales of the two are undoubtedly different (see 'Introduction'). For example, Cowen et al. (2006) recognised this and specified that they were concerned with demographic connectivity, which they defined as recruitment necessary to replace mortality.

(7) Understanding of adult fish behaviour with respect to the time and place of spawning needs to be improved to enable precise starting conditions to be incorporated into dispersal models. Some species spawn in a wide variety of locations, providing a diffuse source of propagules, whereas others spawn at particular, very limited, aggregation points, and thus provide a point source of propagules. In the same way, the timing of spawning can be either diffuse or concentrated. These starting conditions can have important implications for dispersal outcomes, yet, they are not always well understood, particularly in the tropics.

(8) Fish larvae (at least of perciform, warm-water demersal species) start their pelagic period as plankton but end it as nekton. This behavioural transition must be integrated into dispersal models. If the transition is considered at all, most models to date have arbitrarily divided the PLD into passive and active segments, ignoring the plankton to nekton transition. Tests with such models indicate that the duration of the passive segment has a very large effect on dispersal outcomes (e.g. James et al. 2002, Cowen et al. 2006). New behavioural data document more realistic gradual behavioural transitions, which can be incorporated into dispersal models.

(9) Larval fish behaviour varies both with ontogeny and among individuals. Not all individual larvae have equal abilities, and this among-individual behavioural variation—not just mean values—must be incorporated into dispersal models. Similarly, a 2 mm larva will behave differently than a 10 mm larva. Therefore, a key issue to be addressed is the best way to integrate this variation into hydrodynamic numerical models: the behavioural data must be size specific and the variation included in a form that can readily be incorporated into the model.

(10) A special kind of variation is best performance, and we need to investigate the dispersal implications of using data for the best performing individuals in dispersal models. Mortality rates of fish larvae are huge, and best performers (e.g. fastest growers; Jenkins & King 2006) may preferentially survive. This concept may also apply to performance of dispersal-relevant behaviour, and, if so, average performance may not be the appropriate metric to include in dispersal models. Thus, model individuals can be assigned the best behavioural performance for swimming, orientation, sensory abilities, etc. Similarly, some individuals can also be assigned the fastest growth or shortest PLD. If behaviour is important to dispersal, a large difference in dispersal outcomes between average and best performers might be expected.

(11) Laboratory observations and experiments on behaviour must be ground-truthed with direct *in situ* observations and experiments. Dispersal takes place in the ocean, and it is extremely difficult to duplicate a pelagic environment in the laboratory. *In situ* swimming behaviour of larvae is different from that in the laboratory, for example (Leis 2006). Perhaps research using mesocosms can help bridge the gap between laboratory and field studies. If there are good relationships between laboratory and field measures of performance, predictions of field behaviour from laboratory behaviour or from larval morphology may be possible (Fisher et al. 2005, Leis 2006).

(12) In conjunction with the physical model, sensitivity analysis can be used to determine which real behaviours of larvae make a difference to dispersal outcomes. Swimming speed, orientation and vertical distribution will probably be influential in most cases. It is likely that some behaviours may have relatively little influence on dispersal outcomes (at least until a certain stage in development), so including in models all behaviours over the full PLD may not be practical or even desirable.

(13) Incorporation of mortality into dispersal models is necessary to make clear over what spatial scales connectivity of demographic significance can take place. The ability to relate growth and mortality

rates to oceanographic conditions, both physical and biological, would be a valuable component of dispersal models, but may not be a realistic goal in the near future.

(14) A one-size-fits-all approach to incorporation of larval behaviour into models will be misleading at best, as it is clear that behaviour differs greatly among species. Extreme caution is necessary in applying data on behavioural information across taxonomic boundaries, particularly at the ordinal level. Therefore, modellers should seek to use behavioural data on the particular species of interest, or a close relative.

Biophysical, individually based models of dispersal are increasingly attempting to incorporate the behaviour of fish larvae and to apply the factors listed above. This was evident in many of the presentations at the WKAMF Workshop and in the papers included in this theme section resulting from it. In the broader literature, the most commonly included behaviour remains vertical distribution (e.g. Hare et al. 2002), with much less emphasis on horizontal swimming (e.g. Fox et al. 2006). Other contemporary models attempt to include swimming and sensory abilities of larvae indirectly in the form of 'active larval movement' and retention within a specified radius of settlement habitat once this radius is entered (e.g. Cowen et al. 2006). There is broad recognition of the importance of spawning location and time (e.g. Hinckley et al. 2001). Pushing other behavioural boundaries are attempts to incorporate mortality and growth as emergent properties of the model, and this involves behavioural interaction of larvae with prey and predators (e.g. Bartsch 2005). Clearly, many modellers are moving away from the concept of the passive larva, but this is not universal, and not enough of the behaviour input, other than vertical distribution, is empirically derived or based on the species being modelled.

Research needs in larval behaviour

Our empirical understanding of dispersal-relevant behaviour in fish larvae is still limited, particularly in the number of species studied. It is clear, however, that there are several areas where understanding is especially poor and where research is required to provide the empirical base from which to integrate behaviour into dispersal models. Aside from consideration of vertical distribution, observations of larval fish behaviour with conventional tools like plankton nets will seldom be informative. Lateral thinking is needed in this area.

We need a better understanding of the spatial scales over which sensory cues can be influential in orientation by fish larvae. We know, for example, that larval reef fishes can locate sources of sound or odours, but not from what distance. Nor do we know how they determine the direction to the sound or odour source.

Behaviour of larvae at night is particularly poorly understood, and this is an important gap to fill. Aside from vertical distribution studies using nets, we have very little field-based information on behaviour of larvae at night. Limited laboratory and field experiments indicate that behaviour can differ on a diel basis: swimming speed and direction can differ between day and night, for example (reviewed in Leis 2006). As night makes up an average of half the PLD, we need to know more about behaviour of larvae during that half. Similar arguments apply to behaviour at crepuscular periods and in poor weather conditions. There are indications that orientation of larvae can be less precise in cloudy conditions, for example (Leis & Carson-Ewart 2003).

Behavioural performance is strongly size related, so we need to have a better understanding of growth trajectories of larvae in the wild to allow performance to be related clearly to age, as well as to size. We need to know when to turn on or off particular model behaviours, and, because behaviour is more related to size than to age, both size and age of larvae are important inputs for dispersal models.

Given the strong influence that mortality rates can have on the scale of connectivity (Cowen et al. 2000), obtaining better estimates of mortality rates in the sea is a priority. It will be important to investigate to what extent mortality rates are species specific. There are no field data on larval mortality for many species, and obtaining these will be a challenge. Many of the mortality estimates used in dispersal models (e.g. 0.1 to 0.5 d^{-1}; James et al. 2002, Cowen et al. 2006) are from species that are, at best, not closely related to the species of interest, and many mortality estimates contain questionable assumptions.

Most available data on dispersal-relevant behaviour of larvae are from warm-temperate and -tropical species from a limited number of families. We need more data on cool- and cold-water taxa, and on a wider variety of families, because it seems that there are large among-species differences in behavioural capabilities and in the ontogeny of them.

Conclusions

I have summarised recent reviews that show the behavioural capabilities of larvae of warm-water, demersal, perciform fishes to be well developed from relatively early in the pelagic larval stage, and have argued that, because these capabilities have the potential to influence dispersal trajectories, they should be incorporated into biophysical dispersal models. Recent research makes it clear that larvae of at least

warm-water perciform fishes have behavioural capabilities that can influence their dispersal trajectories. The present challenge is to determine if they use them for this purpose. In effect, this requires testing the simplifying assumption. Dispersal models can be used in this way where field data exist for comparison. The model can be run without larval behaviour (the simplifying assumption applied) and again with behaviour included, and these 2 predictions can be compared to the observed result. Other more direct attempts to test the simplifying assumption are few, and have had mixed results (Leis 2006).

I have developed the hypothesis of Hunt von Herbing—that behaviour should play a larger role in dispersal in warm seas than in cold ones—by presenting additional factors that support it and by extending it by implication to differences between warm seasons and cold ones. The historical factors of phylogeny and biogeography also make such regional differences likely. Testing this hypothesis requires care given the many, potentially confounding elements involved. If sustained, this hypothesis will have important implications both for dispersal in different regions and for attempts to model dispersal. At the very least, the elements presented in my development of the hypothesis provide a sound basis to treat with great caution any assumption that one size fits all with respect to dispersal of demersal fish larvae, not only with respect to regions, but also with respect to taxa.

Realistic biophysical models of dispersal are needed for a variety of important purposes, but, before realism can be achieved, we must gain an understanding of the behavioural capabilities of the larvae whose dispersal we seek to model and not just ignore these capabilities. Once the knowledge is gained, incorporation of behaviour into hydrodynamic models must take into account the issues raised above. All of these represent challenges, and many also confront the comfortable simplifying assumptions of the past, but, due to recent advances, none are completely out of reach. If realistic biophysical dispersal models of use to both researchers and managers are the goal, then we must deal with all these issues, perhaps not all at once, but certainly in the end.

Acknowledgements. I thank the organisers of the WKAMF Workshop—Alejandro Gallego, Elizabeth North and Pierre Petitgas—for inviting me to participate, and Kelly Wright for sharing some results of her PhD work on sensory physiology of fish larvae and for editorial assistance. This work was supported by an ARC Discovery Grant (DP0345876) and a DST International Science Linkages Grant (IAP-IST-CG03-0043) to me, and by the Australian Museum. Portions of the above text were based on a joint grant proposal with Luciano Mason, Heather Patterson and Lynne van Herwerden, and benefited from their comments. Thanks to Sue Bullock and Matt Lockett for editorial and other comments on the manuscript.

LITERATURE CITED

Atema J, Kingsford MJ, Gerlach G (2002) Larval fish could use odour for detection, retention and orientation to reefs. Mar Ecol Prog Ser 241:151–160

Bartsch J (2005) The influence of spatio-temporal egg production variability on the modelled survival of the early life history stages of mackerel (*Scomer scombrus*) in the eastern North Atlantic. ICES J Mar Sci 62:1049–1060

Bartsch J, Knust R (1994) Simulating the dispersion of vertically migrating sprat larvae (*Sprattus sprattus* (L.)) in the German Bight with a circulation and transport model system. Fish Oceanogr 3:92–105

Batty RS, Blaxter JHS, Bone Q (1991) The effect of temperature on the swimming of a teleost (*Clupea harengus*) and an ascidian larva (*Dendrodoa grossularia*). Comp Biochem Physiol A 100:297–300

Blaxter JHS (1992) The effect of temperature on larval fishes. Neth J Zool 42:336–357

Caley MJ, Carr MH, Hixon MA, Hughes TP, Jones GP, Menge BA (1996) Recruitment and the local dynamics of open marine populations. Annu Rev Ecol Syst 27:477–500

Clark DL, Leis JM, Hay AC, Trnski T (2005) Swimming ontogeny of larvae of four temperate marine fishes. Mar Ecol Prog Ser 292:287–300

Cowen RK (2002) Larval dispersal and retention and consequences for population connectivity. In: Sale PF (ed) Coral reef fishes: dynamics and diversity in a complex ecosystem. Academic Press, San Diego, CA, p 149–170

Cowen RK, Lwiza KMM, Sponaugle S, Paris CB, Olson DB (2000) Connectivity of marine populations: open or closed? Science 287:857–859

Cowen RK, Paris CB, Olson DB, Fortuna JL (2003) The role of long distance dispersal versus local retention in replenishing marine populations. Gulf Caribb Res 14:129–138

Cowen RK, Paris CB, Sirnivasan A (2006) Scaling of connectivity in marine populations. Science 311:522–527

Cushing DH (1990) Plankton production and year class strength in fish populations: an update of the match/mismatch hypothesis. Adv Mar Biol 26:249–293

Fisher R, Leis JM, Clark DL, Wilson SK (2005) Critical swimming speeds of late-stage coral reef fish larvae: variation within species, among species and between locations. Mar Biol 147:1201–1212

Fox CJ, McCloughrie P, Young EF, Nash RDM (2006) The importance of individual behaviour for successful settlement of juvenile plaice (*Pleuronectes platessa* L.): a modelling and field study in the eastern Irish Sea. Fish Oceanogr 15:301–313

Frank KT, Carscadden JE, Leggett WC (1993) Causes of spatio-temporal variation in the patchiness of larval fish distributions: differential mortality or behaviour? Fish Oceanogr 2:114–123

Fuiman LA, Batty RS (1997) What a drag it is getting cold: partitioning the physical and physiological effects of temperature on fish swimming. J Exp Biol 200:1745–1755

Fuiman LA, Werner RG (2002) Fishery science: the unique contributions of early life stages. Blackwell, Oxford

Hare JA, Quinlan JA, Werner FE, Blanton BO, Govoni JJ, Forward RB, Settle LR, Hoss DE (1999) Larval transport during winter in the SABRE study area: results of a coupled vertical larval behaviour—three-dimensional circulation model. Fish Oceanogr 8(Suppl 2):57–76

Hare JA, Churchill JH, Cowen RK, Berger TJ and 5 others (2002) Routes and rates of larval fish transport from the southeast to the northeast United States continental shelf. Limnol Oceanogr 47:1774–1789

Hart JL (1973) Pacific fishes of Canada. Bull Fish Res Board Can 180:1–740

Hellberg ME, Burton RS, Neigel JE, Palumbi SR (2002) Genetic assessment of connectivity among marine populations. Bull Mar Sci 70:273–290

Hinckley S, Hermann AJ, Mier KL, Megrey BA (2001) Importance of spawning location and timing to successful transport to nursery areas: a simulation study of Gulf of Alaska walleye pollock. ICES J Mar Sci 58:1042–1052

Houde ED (1987) Fish early life dynamics and recruitment variability. Am Fish Soc Symp 2:17–29

Houde ED (1989) Comparative growth, mortality, and energetics of marine fish larvae: temperature and implied latitudinal effects. Fish Bull (Wash DC) 87:471–495

Hunt von Herbing I (2002) Effects of temperature on larval fish swimming performance: the importance of physics to physiology. J Fish Biol 61:865–876

Iles TD, Sinclair M (1982) Atlantic herring: stock discreetness and abundance. Science 215:627–633

James MK, Armsworth PR, Mason LB, Bode L (2002) The structure of reef fish metapopulations: modelling larval dispersal and retention patterns. Proc R Soc Lond B 269: 2079–2086

Jenkins GP, King D (2006) Variation in larval growth can predict the recruitment of a temperate, seagrass-associated fish. Oecologia 147:641–649

Jones GP, Planes S, Thorrold SR (2005) Coral reef fish larvae settle close to home. Curr Biol 15:1314–1318

Kingsford MJ, Leis JM, Shanks A, Lindeman K, Morgan S, Pineda J (2002) Sensory environments, larval abilities and local self-recruitment. Bull Mar Sci 70:309–340

Leis JM (1991) The pelagic phase of coral reef fishes: larval biology of coral reef fishes. In: Sale PF (ed) The ecology of fishes on coral reefs. Academic Press, San Diego, CA, p 183–230

Leis JM (2006) Are larvae of demersal fishes plankton or nekton? Adv Mar Biol 51:59–141

Leis JM, Carson-Ewart BM (2003) Orientation of pelagic larvae of coral-reef fishes in the ocean. Mar Ecol Prog Ser 252:239–253

Leis JM, Carson-Ewart BM (2004) The larvae of Indo-Pacific coastal fishes: a guide to identification. Brill, Leiden

Leis JM, McCormick MI (2002) The biology, behaviour and ecology of the pelagic, larval stage of coral-reef fishes. In: Sale PF (ed) Coral reef fishes: new insights into their ecology. Academic Press, San Diego, CA, p 171–199

Leis JM, Hay AC, Trnski T (2006) *In situ* behavioural ontogeny in larvae of three temperate, marine fishes. Mar Biol 148:655–669

Montgomery JC, Tolimieri N, Haine OS (2001) Active habitat selection by pre-settlement reef fishes. Fish Fish 2: 261–277

Montgomery JC, Jeffs A, Simpson SD, Meekan M, Tindle C (2006) Sound as an orientation cue for the pelagic larvae of reef fishes and decapod crustaceans. Adv Mar Biol 51: 143–196

Morgan SG (2001) The larval ecology of marine communities. In: Bertness MD, Gaines SD, Hay ME (eds) Marine community ecology. Sinauer Press, Sunderland, MA, p 159–181

Moser HG (1996) The early stages of fishes in the California Current region. Calif Coop Ocean Fish Invest Atlas 33: 1–1505

Moser HG, Richards WJ, Cohen DM, Fahay MP, Kendall AW, Richardson SL (1984) Ontogeny and systematics of fishes. Special Publication No. 1, American Society of Ichthyologists and Herpetologists, Lawrence, KS

Myrberg AA, Fuiman LA (2002) The sensory world of coral reef fishes. In: Sale PF (ed) Coral reef fishes: dynamics and diversity in a complex ecosystem. Academic Press, San Diego, CA, p 123–148

Nilsson GE, Östlund-Nilsson S, Penfold R, Grutter AS (2007) From record performance to hypoxia tolerance—respiratory transition in damselfish larvae settling on a coral reef. Proc R Soc Lond B 274:79–84

Palumbi SR (2001) The ecology of marine protected areas. In: Bertness MD, Gaines SD, Hay ME (eds) Marine community ecology. Sinauer Press, Sunderland, MD, p 509–530

Palumbi SR (2003) Population genetics, demographic connectivity, and the design of marine reserves. Ecol Appl 13: 146–158

Pearre S (1979) Problems of detection and interpretation of vertical migration. J Plankton Res 1:29–44

Roberts CM (1997) Connectivity and management of Caribbean coral reefs. Science 278:1454–1456

Robertson DR, Allen GR (2002) Shorefishes of the tropical eastern Pacific: an information system (CD-ROM, Version 1.0). Smithsonian Tropical Research Institute, Balboa

Sale PF (1991) Reef fish communities: open nonequilibrial systems. In: Sale PF (ed) The ecology of fishes on coral reefs. Academic Press, San Diego, CA, p 564–598

Sale PF (2004) Connectivity, recruitment variation, and the structure of reef fish communities. Integr Comp Biol 44: 390–399

Sinclair M (1988) Marine populations: an essay on population regulation and speciation. University of Washington Press, Seattle, WA

Sponaugle S, Cowen RK, Shanks A, Morgan SG and 7 others (2002) Predicting self-recruitment in marine populations: biophysical correlates. Bull Mar Sci 70:341–376

Swearer SE, Shima JS, Hellberg ME, Thorrold SR and 6 others (2002) Evidence of self-recruitment in demersal marine populations. Bull Mar Sci 70:251–272

Thorrold SR, Jones GP, Hellberg ME, Burton RS, Swearer SE, Neigel JE, Morgan SG, Warner RR (2002) Quantifying larval retention and connectivity in marine populations with artificial and natural markers. Bull Mar Sci 70:291–308

Trnski T (2002) Behaviour of settlement-stage larvae of fishes with an estuarine juvenile phase: *in situ* observations in a warm-temperate estuary. Mar Ecol Prog Ser 242:205–214

Wright KJ, Higgs DM, Belanger AJ, Leis JM (2005) Auditory and olfactory abilities of pre-settlement larvae and post-settlement juveniles of a coral reef damselfish (Pisces: Pomacentridae). Mar Biol 147:1425–1434

Editorial responsibility: Alejandro Gallego (Contributing Editor), Aberdeen, UK

Submitted: June 7, 2006; Accepted: April 30, 2007
Proofs received from author(s): August 28, 2007

Vol. 347: 195–205, 2007
doi: 10.3354/meps06978

MARINE ECOLOGY PROGRESS SERIES
Mar Ecol Prog Ser

Published October 11

OPEN ACCESS

Linking behavioural ecology and oceanography: larval behaviour determines growth, mortality and dispersal

Øyvind Fiksen[1,*], Christian Jørgensen[1], Trond Kristiansen[1,3], Frode Vikebø[1,2,], Geir Huse[2]**

[1]University of Bergen, Department of Biology, PO Box 7800, 5020 Bergen, Norway
[2]Institute of Marine Research, PO Box 1870 Nordnes, 5817 Bergen, Norway
[3]*Present address:* University of North Carolina, Department of Marine Sciences, Campus Box 3300, Chapel Hill, North Carolina 27599-3300, USA

ABSTRACT: Highly resolved general circulation models (GCMs) now generate realistic flow fields, and have revealed how sensitive larval drift routes are to vertical positioning in the water column. Sensible representation of behavioural processes then becomes essential to generate reliable patterns of environmental exposure (growth and survival), larval drift trajectories and dispersal. Existing individual-based models involving larval fish allow individuals to vary only in their attributes such as spatial coordinates, and not in their inherited behavioural strategies or phenotypes. We illustrate the interaction between short-term behaviour and longer-term dispersal consequences applying a model of larval cod *Gadus morhua* drifting in a GCM, and show how variations in swimming behaviour influence growth and dispersal. We recommend a deep integration of oceanography and behavioural ecology. First, we need to understand the causes and survival value of behaviours of larval fish, framed in terms of behavioural ecology. Second, we need practices to address how drift and dispersal of offspring are generating spawning strategies (timing and location) of adults, using life history theory. Third, the relative importance of local growth and mortality versus the need to drift to particular areas depend strongly on the mobility of organisms at the time of settling, or the spatial fitness-landscape. The field of 'individual-based ecology' provides sound methods to approach this interface between evolutionary theory and physical oceanography.

KEY WORDS: Behavioural rules · Larval ecology · Individual-based models · General circulation models · Predation · Habitat selection

INTRODUCTION

The sea is a constantly moving habitat, structured by physical processes. For fish and other marine organisms, this constrains dispersal and habitat choice, but it also harbours opportunities. Organisms can exploit eddies and circular current systems for retention within an area (e.g. Sinclair 1988), or hitch-hike with tidal or vertically sheared currents flowing in desirable directions (Harden Jones et al. 1979). Mature adults of many species swim long distances to release their fertilised eggs, and let currents transport the developing early life stages to favourable nursery areas (Harden Jones 1968).

We do not intend here to review or synthesise the vast field of individual-based modelling in larval fish ecology. Nor are we reviewing the linkages between recruitment and dispersal in marine populations. Instead, we argue that the integration of larval behaviour with general circulation models is a key step forward to improve our understanding of larval survival, growth and dispersal. Behaviour is the central mechanism that links these 3 elements together, despite how restricted the behavioural repertoire of larvae may seem. There are primarily 2 lines of argument leading to this conclusion. First, compared to adult fish, the outcome of larval behaviour is more tightly connected to physical oceanography. Lar-

*Email: oyvind.fiksen@bio.uib.no
**Present address: IMR, Bergen

vae distributed only a few metres apart in the vertical can end up in totally different geographical areas (Hinckley et al. 1996, Hare et al. 2005, Vikebø et al. 2005), which leaves a large scope for behaviour to influence dispersal as well as the environment for growth and mortality along the drift trajectory. Second, feeding opportunities and predation risks are spatially correlated for plankton. This is driven by the exponentially decreasing vertical profile of light—the key determinant for encounter rates with both predators and prey (Aksnes & Giske 1993). Larvae can control their exposure to light through vertical positioning, and thus effectively influence their own survival and growth (e.g. Olla et al. 1996). Besides these 2 main arguments, larval ecology has far-reaching implications for the life-history strategies of adults. The best spawning sites regarding larval drift patterns, growth and survival may require extensive spawning migrations at the adult stage, potentially conflicting with alternative ways to use energy and time.

An unfolding of larval fish ecology therefore requires an approach integrating physical oceanography and behavioural ecology, interpreted in the perspective of life-history theory. Using individual-based models (IBMs) rich in mechanistic detail, one can focus at the individual and let ecology emerge from individual processes; an approach recently termed 'individual-based ecology' (Grimm & Railsback 2005). For larvae, this would include processes such as temperature-dependent growth and starvation, encounter rates with prey and predators that depend on e.g. light and turbulence, and various adaptive behavioural strategies such as habitat selection, activity pattern and schooling. When scaling up to populations, this perspective views ecology as emerging from individuals and their processes. New patterns that can be compared with data then arise at the population level (Grimm et al. 2005), for example temporal and spatial distributions, growth variation between years and areas, and what can be considered good spawning sites and times.

Present use of IBMs in oceanography is hampered by the lack of individual variability in behaviour (genotypes), and by the absence of fitness as the criterion to model natural selection processes among alternative behavioural strategies. It is often tempting to simply impose behaviour on individuals, or to implement caricatures of observed behaviours in models, making them more descriptive and less explanatory. The assumption of fixed individual behaviour in, for instance, habitat selection (they follow prescribed trajectories) has some drawbacks: (1) the modeller determines to a large extent how growth and mortality rates should be traded against each other; (2) the larvae cannot respond behaviourally to changes in the environment; (3) the potentially conflicting objectives of short-term optimisation of growth and mortality versus long-term drifting in particular directions cannot be studied; and (4) it is impossible to predict how environmental change may alter behaviour through natural selection unless individual variability and heritability are included. The aim of the present paper is to clarify some methodological concepts and promote the use of evolutionary IBMs in conjunction with general circulation models to address the ecology of early marine life stages.

Larval ecology has a strong tradition in dealing with mechanisms: from miniature biomechanics and behaviour, via influence from physical environmental variables and oceanography, to the capabilities and constraints of sensory systems. Mechanistically rich representations, including behaviour and life histories, are essential to capture interactions between environmental variability and recruitment success, or to understand the ability of fish in general to adapt to environmental change and human activities such as harvesting (Jørgensen et al. 2006). A largely unutilised potential is, however, that existing IBMs of larval fish and zooplankton do not include larval behavioural strategies as adaptive traits, nor do the models analyse evolutionary implications. This paper has 3 sections. First, we present the role of behaviour for marine larvae in a drift phase, and how this constrains adult life-history strategies. In the second part, we focus on concepts that can promote an evolutionary interpretation of active movements by drifting marine larvae. In the third part, we discuss candidate modelling frameworks and some recommendations for future research.

IMPORTANCE OF BEHAVIOUR FOR GROWTH, MORTALITY AND DISPERSAL

Larval behaviour does not imply cognition or rationally made decisions. Larvae simply execute genetically pre-programmed responses to internal states or external stimuli. Since there are always small variations in genetic predispositions between individuals and since behavioural traits are heritable (Plomin et al. 2000, Fitzpatrick et al. 2005), individuals encoded to perform behaviour that benefits their growth or survival will simply increase in numbers over the generations (Fisher 1930, Dawkins 1976). In this way, evolution leads to behavioural adaptations to the prevailing conditions. Consequently, the answer to the first question is yes: we would indeed expect that larvae have behaviour and that it is of a type that appears rational to a human observer.

We first identify 2 important effects of behaviour. Vertical positioning influences (1) immediate growth and mortality rates and (2) large-scale and long-term

drift and dispersal. These 2 effects are not independent — priorities for one will influence the other.

Mortality and growth emerge from larval behaviour

The pelagic realm is characterised by strong environmental gradients in the vertical. Light may be the most influential physical variable structuring both productivity and predation in the pelagic (Aksnes et al. 2004). Because light decreases exponentially with depth, vertical behaviour can have tremendous effects on encounter rates with prey (spot prey in the light) and predators (hide in the dark). Habitat selection of larvae influences both growth and predation risk with a trade-off between the two: higher growth can normally be achieved only by accepting also a higher mortality. These rates must therefore be emergent properties of models, resulting from behavioural trade-offs, rather than imposed or parameterised values determined by the modeller (Grimm & Railsback 2005).

While growth is often modelled in great detail (Lough et al. 2005), mortality is rarely modelled explicitly. Cohort survival is sensitive to small variations in mortality rates, and we need to include both the basic mechanisms and the environmental forcing of predation processes in models of larval fish. This is a pre-requisite to understanding the trade-offs between growth and survival and to appreciate the role of behaviour in determining these rates.

Increased body size decreases predation risk from small and abundant predators (Bailey & Houde 1989). Growth is therefore important to fish larvae since it reduces the time spent in the most vulnerable phase (Houde 1997). In evolutionary terms, this would act as a motivation to maintain high growth rates even if this involves more exposure to predators. At the same time, increasing body size makes larvae more visible, thereby increasing their vulnerability to visual predation in the euphotic zone (Aksnes & Giske 1993). That fish larvae show ontogenetic development in depth distribution (Leis et al. 2006) and diel vertical migration (Lough & Potter 1993) is likely a response to changing mortality patterns as body size increases.

When foraging is traded against risk of predation, more prey may not lead to higher growth rates, but instead to lower predation rates (McNamara & Houston 1987, Lima & Dill 1990). Such behavioural mechanisms could confound studies on the link between prey availability and larval growth rates, with implications for observation programmes trying to establish the relationship between growth and prey abundance in larval fish. As an example, larval cod *Gadus morhua* tend to grow at temperature-limited rates over a range of environmental conditions in field observations (Folkvord 2005). Apparently, this contradicts the study of Beaugrand et al. (2003), which suggested a connection between zooplankton availability and recruitment success of North Sea cod. However, if feeding or growth is traded against predation risk, food abundance may not influence growth directly, but instead modify the strength of a recruiting cohort through behaviourally mediated exposure to predation (Fiksen et al. 2005). At low food availability, larval cod can maintain high growth rates either by increasing their activity level at the cost of running into ambush invertebrate predators more frequently, or by spending more time at higher light intensities where they are more likely to be detected by visually searching raptorial fish. Thus, although there is no observation of food-limited growth, low prey abundance may act through behavioural compensations and influence mortality and thereby recruitment variability.

However, a recurrent observation in larval fish ecology is that faster-growing larvae tend to survive better (e.g. Takasuka et al. 2003, Nielsen & Munk 2004). In a constant environment this would contradict the classical growth–mortality trade-off, but in a variable environment and with state-dependent behaviour, this is exactly what we would expect. Then, individuals accidentally in a low food environment would have reduced internal states (stomach fullness, condition) and higher motivation for growth. They would act more boldly, be less fearful (less diel vertical migration or schooling and higher activity) and be more exposed to predation. The strength of such behavioural effects relative to starvation or reduced escape abilities is, however, difficult to disentangle.

Larval drift and dispersal

Minor vertical displacements may expose larvae to different flow schemes due to vertical shear. For example, particles dropped at the Northeast Arctic cod spawning grounds at 10 and 20 m depth and traced for 100 d end up 100s of kilometres apart (Vikebø et al. 2005). Using a general circulation model (GCM) over the Gulf of Maine, Huret et al. (2007, this Theme Section) showed how even small differences in initial vertical position of cod eggs and larvae influenced the chance of drifting to suitable settlement, at least in stratified situations. This demonstrates the potential of habitat selection in the vertical in affecting large-scale dispersal. In addition, horizontal swimming does not necessarily have to compensate for displacement by currents: current strengths and directions vary in space and time, and even limited horizontal movements can associate the larvae more closely with certain current regimes. Leis et al. (2006) showed that larvae of several coral reef fish observed in the field were

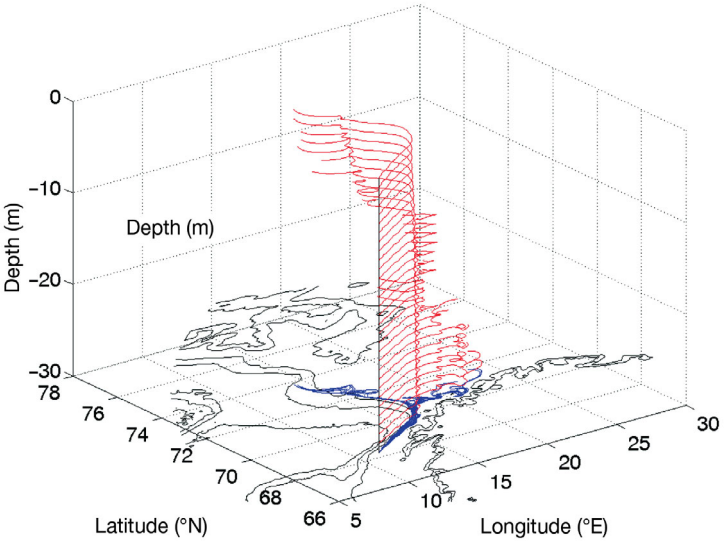

Fig. 1. Drift trajectories of larvae at fixed depths (0 to 30 m) on 1 April and 1 mo forward in time. The larvae were released simultaneously from a fixed point at Moskenesgrunnen. Red lines show the drift trajectories in 3-dimensional space, while blue lines are the geographical projections of the trajectories. These can be grouped in 2 bundles, the deep ones drifting along the coast, and the shallow trajectories drifting offshore, northwards. See Vikebø et al. (2005) for details

swimming in directions significantly different from random. It is not known what cues these larvae were using for orientation, but fish larvae have also been shown to detect reef sounds and the smell of conspecifics already at presettling stages (Wright et al. 2005).

An example of effects from vertical and horizontal swimming is illustrated in Fig. 1, which shows the trajectories of larvae drifting for 1 mo at fixed depths (1 to 30 m) when released from Moskenesgrunnen, a typical spawning site for Atlantic cod in northern Norway. The physical model and the larval growth as a function of temperature are described in Vikebø et al. (2005). The simulations show a surprising potential for larvae to affect their likelihood of ending up in the Coastal Current or the Atlantic Current by swimming horizontally or vertically. Vertical positioning has a strong effect (Fig. 1), but even directional horizontal swimming at the reasonable velocity of 1 body length (BL) s^{-1} will significantly impact the trajectory of the larvae, at all depths (Fig. 2a). If the swimming speed were 3 BL s^{-1}, then horizontal movements would

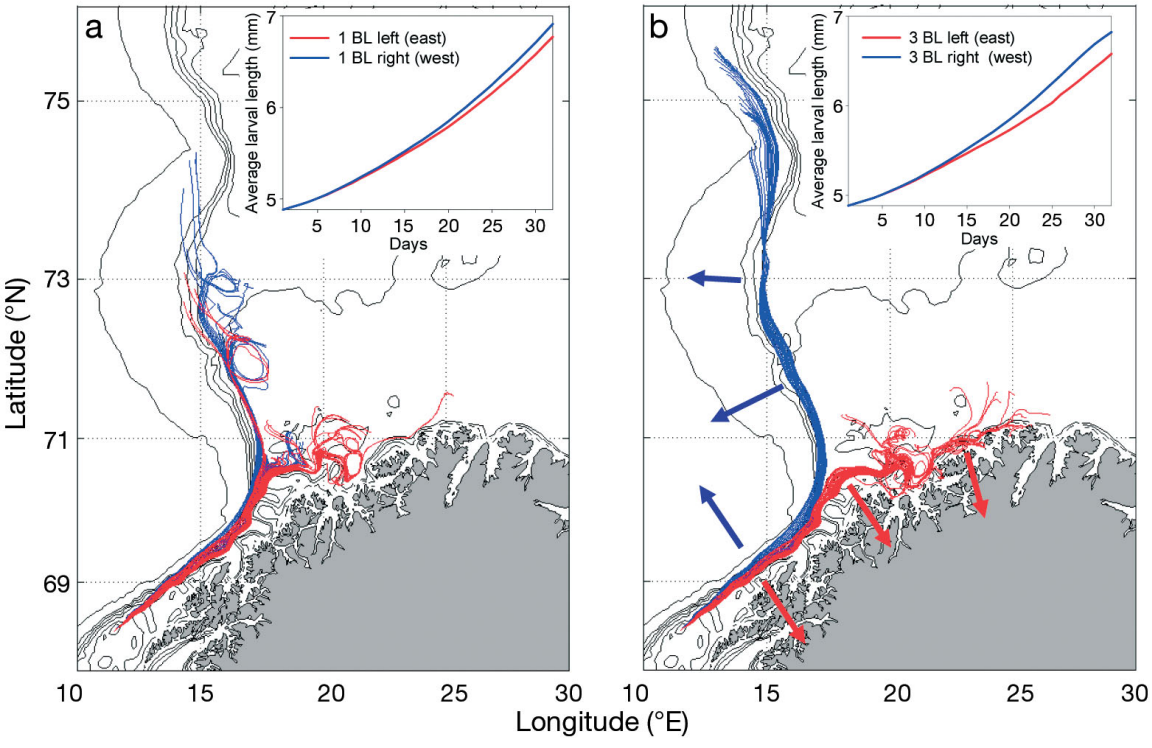

Fig. 2. Drift trajectories of larvae released at Moskenesgrunnen, northern Norway, on 1 April and 1 mo forward in time. Each line represents 1 larva inhabiting a fixed depth between 1 and 30 m (1 larva at each depth). Blue lines are larvae swimming constantly 90° to the right of their upstream orientation (blue arrows), while red lines are larvae swimming constantly 90° to the left (red arrows). They swim with a velocity of either (a) 1 or (b) 3 body lengths (BL) per second. Insets: average growth histories of the individuals. See Vikebø et al. (2005) for details

override the effects of depth position completely in this particular region (Fig. 2b). Growth histories averaged over depths diverge for the 2 behaviours: swimming to the right, facing the currents (north-west direction), results in the largest size (insets in Fig. 2). However, this also leads larvae northwards, out of the Barents Sea.

Routine swimming speeds are in the range from 0.3 to 0.5 BL s^{-1} for a cod larvae (Skiftesvik 1992, Peck et al. 2006). Although this is much lower than the 3 BL s^{-1} used in the numerical example above, both field and laboratory observations suggest that other species have higher capabilities (Leis 2007, this Theme Section). In a study of 89 species of coral reef fish larvae in their later stages, 90% of the species could swim faster than the local currents at 13.5 cm s^{-1} (Fisher et al. 2005). The most common critical swimming speeds were 2 to 3 times as fast, meaning that swimming could significantly affect dispersal and settlement. Coral reef fish larvae have been measured to have critical swimming speeds of 4 to 29 BL s^{-1} (Fisher et al. 2005), and some species can swim >20 km at a body length of 10 mm (Clark et al. 2005). Critical swimming speeds decrease with temperature, because viscosity is higher in colder water (Fuiman & Batty 1997), which could lead to warm-water species having higher larval swimming capabilities than species inhabiting colder waters (Leis 2007). Observations of swimming speeds in the laboratory and in the field correspond well (Leis et al. 2006), and critical swimming speeds normally develop in early ontogeny, while endurance develops somewhat later (Clark et al. 2005).

Direct evidence for the influence of larval behaviour comes from an impressively well-sampled study on the damselfish, a coral reef fish that stays within the proximity of a home coral all its life. Surface currents transported the pelagic larvae away from the reef, but at some stage they sought depths (60 m) at which directional currents would bring them back to their native reef (Paris & Cowen 2004). Studies such as this one exemplify how organisms can exploit ocean currents as a mechanism to influence dispersal. Other coral reef fish larvae also show ontogenetic shifts in depth, with some moving to shallower and some to deeper water as they grow larger (Leis et al. 2006). It would be interesting to know whether these depth shifts are due to changes in mortality rates or due to vertical shear and implications for drift trajectories or both.

Parental trade-offs in spawning strategies

The spatial and seasonal variability in growth and predation risk of fish eggs and larvae are important factors affecting the spawning strategies of adults. Spawning will, however, not necessarily take place at the optimal spawning locations. Rather, the benefits eggs and larvae will have at any particular spawning location is part of a trade-off in the parental life-history strategy: How much time and energy should they invest in the spawning migration to obtain benefits for their offspring? For example, how should fish store energy over the year to produce offspring at particular times and places (Schwalme & Chouinard 1999, Varpe et al. 2005), or how much energy, predation risk and lost feeding opportunities should they invest in the spawning migration (e.g. Slotte & Fiksen 2000). The ecology of early life stages therefore provides keys to understanding fish life histories on the whole, as the spawning strategy indicates both how important location and timing are to larvae and how much adults invest in offspring quality.

INTERPRETING FITNESS: THE EVOLUTIONARY ANALYSIS

The pioneering work by Mullon et al. (2002) demonstrated how evolutionary reasoning could be combined with GCMs to understand why fish spawn in particular regions. They tested the implications of various assumptions about larval survival on the adaptive spawning location of anchovies *Engraulis capensis* in southern Benguela and related their results to environmental exposure (temperature) and geographical position (the risk of drifting offshore). Larvae that survived their drift phase spawned again at their natal spawning location and at the time they were spawned themselves. By repeating this procedure for some generations, successful parental spawning strategies emerged from assumptions made in the model.

In this section, we discuss methodological extensions that may extend this approach, which was focused towards the strategy of the adults. Having established that the inconspicuous behaviour of marine larvae can affect growth, mortality and dispersal dramatically, the obvious question is: How can we study its fitness consequences? In this section, we suggest a composite fitness measure that incorporates survival until settlement, the value of settlement in a given area and the value of body size at settlement. In addition, we recommend using IBMs with rule-based behaviour. A further discussion of alternative methodologies for implementation of these concepts is postponed until the section 'Modelling toolbox and recommendations'.

Behavioural rules

A behavioural strategy can be interpreted as a set of rules determining how organisms respond to their

internal and external environment (e.g. directly as fixed strategies, as part of plastic strategies, behavioural rules, or as stimulus-driven neural networks), and how they are constrained by sensory input and physiological restrictions (Giske et al. 2003, Grimm & Railsback 2005, Hutchinson & Gigerenzer 2005). For drifting larvae, a key behavioural trait is vertical positioning, since growth, predation risk and horizontal advection are all functions of depth (Fig. 2).

The 'fixed-depth' rule applied in our example (Fig. 1) is obviously too simplistic. Larval fish change depth preference with ontogeny and size, with internal condition, such as hunger (stomach fullness), and also with the daily light cycle (Lough & Potter 1993, Leis et al. 2006). This choice does not need to be conscious, but may be a genetically hard-wired response to sensory cues (instinctive behaviour).

Assuming that individuals have sensory information about growth g_z and predation rate m_z in a range of depths z, they may use this information to decide which depth to choose. We have developed a more detailed version of the rule-based larval behaviour described in Vikebø et al. (2007, this Theme Section). One option is a rule that maximises the instantaneous rate of mass increase (i.e. maximise $g_z - m_z$; Persson & De Roos 2003). This rule avoids the problems associated with the classical rule by Gilliam (minimise the ratio m_z/g_z) when growth rates approach zero or become negative, as discussed in detail by Railsback et al. (1999). However, it may be profitable to take higher or lower risk than specified by this rule; therefore, risk sensitivity should emerge in models rather than be defined in advance. We can formulate a rule where the selected depth z_i, specific to individual i, optimises the trade-off, modulated by risk sensitivity π_i, between habitat-specific growth and mortality rates:

$$z_i = \max_z[(1 - \pi_i)g_z - \pi_i m_z] \quad (1)$$

A risk-averse (fearful) individual would carry π_i values close to 1, whereas a bold growth maximiser would have π_i near 0. The strategy $0 \leq \pi_i \leq 1$ thus has a straightforward interpretation as the risk sensitivity of an individual, while the risk sensitivity itself may be a mathematical function affected by a number of parameters translating local information into a value of π_i. The simplest version of the rule is $\pi_i = \beta_i$, then risk sensitivity is constant and influenced directly by a single gene. Such rules have been explored in more detail by Vikebø et al. (2007). The trade-off between growth and mortality may, however, be modulated by a number of stimuli, and the rule can easily be developed further by making π_i a function of internal states, such as stomach fullness or body size.

Rules act as simple heuristics translating local information into different behaviours when environmental conditions change (Hutchinson & Gigerenzer 2005). The ideal behavioural schedule should be evolutionarily robust, meaning it should work well across environmental variability, and be difficult to invade by alternative strategies in a long-term perspective. The rules should also conform to observed patterns of, e.g., distributions in depth or space from field studies (Grimm et al. 2005). The ultimate test is to set up gradients in the laboratory to experimentally challenge rules found by models and to see if larvae respond as predicted. Such experiments have generated much insight in limnology (e.g. Loose & Dawidowicz 1994).

Geographical fitness landscapes

Some organisms, for instance barnacles, are sedentary after the larval drift phase and for the rest of their life. Then larval behaviour must be fine-tuned to utilise currents in finding settlement habitat. A first requirement is that the settling area provides suitable habitat for further growth and survival (Larsson & Jonsson 2006). The settlement area has strong bearing on future reproductive success depending on circulation-driven connectivity.

Cowen et al. (2006) tracked dispersing larvae in a basin-wide study of the Caribbean using an ocean circulation model. Some reefs were highly connected, and larvae spawned there dispersed to multiple and sometimes distant reefs. Other spawning locations were reproductive dead-ends because ocean currents did not bring larvae close to any suitable settlement habitat. For species with limited mobility in their juvenile or adult stages, such a geographical picture of dispersal and settlement can be viewed as a fitness landscape: all that matters is to end up at a location where your offspring can survive and disperse to other suitable habitats. More-mobile species should be less concerned with their spatial location, and more focused on growth and mortality in their local environment along the drift trajectory. If juveniles and adults were mobile enough to compensate for a poor location, the fitness landscape would show smoother geographical variation.

What Mullon et al. (2002) did was actually to use a genetic algorithm to map the geographical fitness landscape based on a few assumptions about the early life stages in anchovies. This coupling of general circulation models and habitat connectivity with evolutionary reasoning make trade-offs in larval life and in adult spawning strategies explicit. Geographical position is not everything, however, and to strengthen the link with life-history evolution we need a broader perspective on what constitutes fitness.

Evaluating behavioural strategies

What criteria should be used to assess fitness of different rules or strategies? If the full life cycle including reproduction is modelled, one can use emergent fitness rather than an explicitly formulated fitness criterion (Menczer & Belew 1996, Giske et al. 1998, Strand et al. 2002). However, for models focusing on the larval phase it is often convenient to assess the success of individuals at a particular time or age, for example at settlement. There are different components that contribute to fitness, and below we have tried to split fitness consequences into functional categories. Let V_i denote fitness evaluated at the end of the drift phase when an individual i following strategy S_i (a rule or a set of rules) has reached a given size or developmental stage, then:

$$V_i(S_i) = l_i f(w_i) G(x_i, y_i) \quad (2)$$

The first component here is the survival until settlement l_i. The second component is a function $f(w_i)$ that describes the fitness value of size w_i at settlement. A larger body size may lead to increased competitive ability for food or shelter, or may influence starvation or predation rates after settlement. The last component includes the fitness consequences $G(x_i, y_i)$ of settling at the geographical position (x_i, y_i). This can be found by making assumptions about habitat suitability, and should ideally include connectivity and the potential for future reproduction found through an iterative schedule such as in Mullon et al. (2002). In such cases, the value of a given settlement area should include also a time dimension, i.e. $G(x_i, y_i, t_i)$.

The second and third components are in essence all assumptions of expected future reproductive value given individual state and position at the end of the drift phase. It resembles the terminal fitness function known from dynamic programming methods in behavioural ecology (e.g. Houston & McNamara 1999), which is typically a reward function of being in a particular state at a given time. The first component of fitness is accrued survival probability l_i of a larva throughout the drift phase. Survival depends on the environment along the drift trajectory (predation and starvation) and individual risk sensitivity or behaviour. Fitness V_i is then in units of expected lifetime reproductive success for a single individual following strategy S_i.

Eq. (2) is the simplest version of a fitness function. It summarises fitness elements from the water column, the drift trajectory and the settlement area (Fig. 3), i.e. tactic and strategic fitness components. One could envisage interaction effects between size and space for example, where a large body size gives advantages in some geographical areas compared to others. In that case the effect of size has to be accounted for together with the geographical fitness consequences, and the equation would become $V_i(S_i) = l_i G(w_i, x_i, y_i)$. For example, size-dependent swimming abilities may reduce the importance of position at settlement for larger larvae. In our larval drift example, fitness may be assessed as proportional to larval length after 1 mo (Fig. 2). However, the fitness of high temperature in

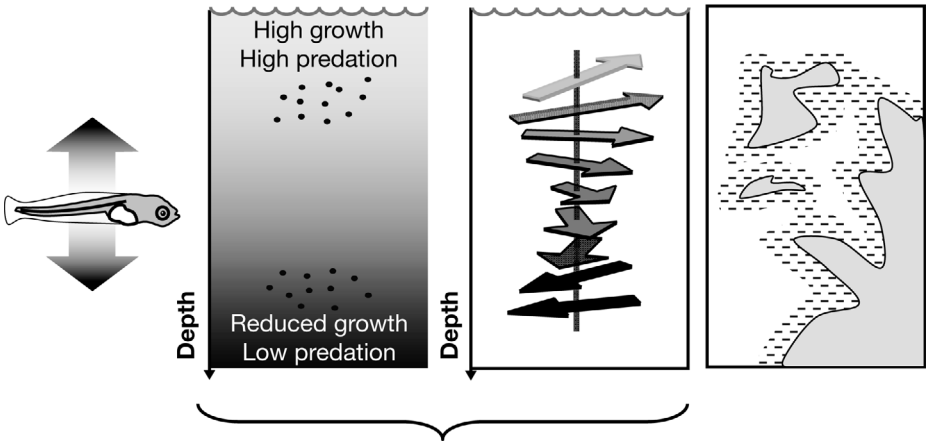

Fig. 3. This figure illustrates the local and strategic trade-offs in larval habitat selection. To the left are the classical behavioural elements of the pelagic environment, setting up a local trade-off between growth and survival. In the middle the large-scale drift consequences of local depth selection. The picture to the right illustrates the terminal settlement area when the drift phase is over. This area may also influence fitness and should be included in the evaluation of the success of the behavioural strategy. The table refers to the symbols introduced in the text

the 'Atlantic' drift trajectory must be weighted against the potential disadvantage of ending up in unfavourable areas, in our case in the deep off-shelf areas to the west or north of Spitsbergen. Larvae following short-term hedonic cues, such as high temperature, may end up as losers in the long term. A more realistic fitness measure would include the function $G(w_i,x_i,y_i)$, potentially derived from field data (Ciannelli et al. 2007), but this function is not easy to determine.

MODELLING TOOLBOX AND RECOMMENDATIONS

A blend of 4 different types of models is thus recommended to analyse the fitness consequences of larval behaviour: (1) models of the environment relevant to growth and survival; (2) mechanistic representations of how ecological processes are forced by the environment (growth, predation risk, drift patterns); (3) behavioural rules to derive adaptive responses or 'adaptive traits' in the terminology of Chambers (1993) and Grimm & Railsback (2005); and (4) models evaluating the success of rules in terms of fitness or components of fitness (as in Eq. 2). While models of marine larvae traditionally have focused on the first 2 categories, we argue that the third and fourth elements are crucial to understanding the coupling between the environment and the success of organisms. Understanding both how and why marine organisms have adapted so intricately to their moving environment is a necessary prerequisite if we are to predict how fish populations will respond to changes in their environment and to harvesting. In the following, we will discuss requirements for such an integrated modelling effort.

Physical and ecological environment

General circulation models can generate 'offline' matrices of flow and environmental variables. As oceanographers develop libraries of such matrixes, including the representations of tidal variability, IBMs can track a large number of individuals or particles through high-resolution, 3-dimensional space. With current technology such offline particle models can be executed on desktop computers on time scales of hours.

A major challenge is how to capture spatio-temporal variability in prey and predator fields. One method is to assimilate available data on prey (e.g. Hinrichsen et al. 2005) or predators (Garrison et al. 2000) into models of larval fish, but such fields are scarce and may need to be supplemented by modelling.

Individual properties

When implementing an IBM, it is instructive to keep a distinct separation between the strategy that contains the rules that specify behaviour and the bookkeeping of the phenotype. It has been common to describe the phenotype of an individual using an attribute vector $A_{i,t}$ (Chambers 1993), which contains all the states ($\alpha 1_i$..., αj_i) used to characterise the individual i at time t, such as age, weight, stomach fullness, length and spatial co-ordinates (x_i,y_i,z_i):

$$A_{i,t} = (\alpha 1_i,\alpha 2_i,\alpha 3_i, \ldots, \alpha j_i,x_i,y_i,z_i) \quad (3)$$

High mortality quickly reduces population size and deteriorates variation between individuals, which leaves the composition of the model population vulnerable to chance events (analogous to genetic drift in small populations). This can be solved using super-individuals (Scheffer et al. 1995). A super-individual represents many identical individuals, and the number of identical siblings (n_s) becomes an additional attribute:

$$A_{s,t} = (\alpha 1_s,\alpha 2_s,\alpha 3_s, \ldots, \alpha j_s,x_s,y_s,z_s,n_s) \quad (4)$$

Here, shown for super-individual s, the number of identical siblings n_s is reduced in proportion to the mortality rate (Scheffer et al. 1995). The number of different super-individuals in the model population and, therefore, the variation between them remain the same. An alternative interpretation is that n_s may represent the cumulative survival probability of individuals following strategy s. Super-individuals also link IBMs to population models and allow the simulation of 'true' abundances of fish populations (Huse et al. 2004).

The phenotype results from the individual's strategy in interaction with the environment. In IBMs this can be formalised by introducing a strategy vector S_i (Huse 2001):

$$S_i = (\beta 1_i,\beta 2_i,\beta 3_i, \ldots,\beta j_i) \quad (5)$$

where βj_i is the adaptive trait j of individual i. The traits specified by the strategy vector can for example be life-history traits or behavioural strategies that specify how individuals should live their lives or use information from their local environment. In the context of larval ecology, typical traits could be the level of risk acceptance, the onset or degree of vertical migration, or built-in responses to light or temperature to mention a few. For the simplistic example presented in Figs. 1 & 2, the strategy vector would be the depth-selected, swimming direction and swimming velocity. A strategy vector also makes it possible to include a multitude of stimuli in the decision rule, where sensory inputs are weighted differently (analogous to motivations) within individuals (Giske et al. 2003). Locally available information can also be processed by a neural network,

where the strategy vector prescribes weights for each of the connections (Huse et al. 1999, Strand et al. 2002).

The combination of attribute and strategy vectors enables most relevant characteristics of individuals to be implemented in IBMs, and the approach also specifies how fixed parameters for a strategy translate into behavioural and phenotypical differences between individuals. The classification based on attribute and strategy vectors can be used to describe IBMs even though the actual programming implementation is not vector based, as, for example, in object-oriented programming (Maley & Caswell 1993).

Evolutionary algorithms

The strategy vector may be considered as a genotype analogous to a biological chromosome, and we are therefore interested in how evolution would shape it over time. We can also interpret the strategy vector as a phenotype, and use the same type of algorithm to find optimal or adaptive types of behaviour. There are several alternative algorithms that search for solutions that evolution would favour. The broadest distinction is between optimisation models (e.g. Houston & McNamara 1999, Clark & Mangel 2000), which find the optimal solution to a given problem, and 'search heuristics' that use different types of search algorithms to find good and robust solutions, but not necessarily the optimal one (e.g. Holland 1992).

Because of the complexity of models that combine physical oceanography, drift patterns and behaviour, exhaustive search and optimality models rarely provide a viable route. Optimisation tools for finding the best possible behaviour are not available for the problem sketched in the previous sections. The reason is that a change in behaviour at any point in time will influence the future drift trajectory, and therefore one has no method for predicting the fitness consequences for the alternative behavioural options. Instead, one has to use heuristics, such as genetic algorithms, that simulate fast-forward evolution, or simply shower the models with solutions more like exhaustive search. These heuristic methods can be powerful search algorithms when one simulates populations that behave according to mathematically simple rules, and where individual variation in the rule parameters exists.

One suitable and widely used option is represented by genetic algorithms (Holland 1992, Huse et al. 1999). A genetic algorithm simulates evolution of the strategy vector by modelling a population consisting of individuals with different strategy vectors. Each generation, the individuals with highest fitness pass their strategy vector on to the next generation. The trait value is tested and improved iteratively over generations, and new variation can be introduced by processes analogous to mutation and recombination. This methodology searches for evolutionarily robust strategy vectors, for instance behavioural strategies that prevent larvae from drifting into harsh settlement regions.

SUMMARY

Selection of vertical habitat for larvae drifting in currents influences both the local short-term trade-off between growth and mortality and the more strategic and long-term consequences related to the large-scale circulation regime. The importance of ending up in particular habitats depends on the mobility of juveniles at settling. If organisms have strong swimming abilities at settlement, we expect them to prioritise growth and survival along the drift trajectory above settlement location. The procedure we have suggested here frames larval-behaviour and fish-spawning strategies in the tradition of evolutionary ecology, both conceptually and formally. We recommend IBM practices (Grimm & Railsback 2005) that emphasise (1) numerous emergent properties from basic, transparent and mechanistic assumptions on growth, mortality, behavioural abilities and drift processes; (2) behavioural strategies or rules that show variability between individuals; and (3) selection processes that incorporate fitness consequences along the trajectory and at the settlement location. One efficient tool for such investigations is represented by models that simulate evolution based on genetic algorithms. Such models tackle sufficient complexity and are capable of evaluating consequences of larval behaviour in flow fields and integrating effects across several time scales. Modelling should be done in close collaboration with laboratory and field studies on larval behaviour, their abilities, constraints, and temporal and spatial distributions. We recommend modelling practices that use transparent and mechanistic processes in growth, mortality, behavioural abilities and drift; apply behavioural strategies or rules that allow true variability between individuals; and include an evolutionary selection procedure to assess fitness consequences along drift trajectories and at the settlement location. This procedure enables studies on how organisms can adapt to environmental change through natural selection.

Acknowledgements. We are most grateful to D. L. Aksnes and J. Giske for their original views on mechanics and evolution in the sea, an important source of inspiration for this work. We acknowledge the Research Council of Norway for support, and reviewers for constructive suggestions. Thanks to Elizabeth North, Alejandro Gallego and Pierre Petitgas for organising the WKAMF Workshop, and to T. Torgersen and S. Eliassen for discussions and comments.

LITERATURE CITED

Aksnes DL, Giske J (1993) A theoretical model of aquatic visual feeding. Ecol Model 67:233–250

Aksnes DL, Nejstgaard J, Sædberg E, Sørnes T (2004) Optical control of fish and zooplankton populations. Limnol Oceanogr 49:233–238

Bailey KM, Houde ED (1989) Predation on eggs and larvae of marine fishes and the recruitment problem. Adv Mar Biol 25:1–83

Beaugrand G, Brander KM, Lindley JA, Souissi S, Reid PC (2003) Plankton effect on cod recruitment in the North Sea. Nature 426:661–664

Chambers RC (1993) Phenotypic variability in fish populations and its representation in individual-based models. Trans Am Fish Soc 122:404–414

Ciannelli L, Dingsør GE, Bogstad B, Ottersen G, Chan KS, Gjøsæter H, Stiansen JE, Stenseth NC (2007) Spatial anatomy of species survival: effects of predation and climate-driven environmental variability. Ecology 88:635–645

Clark CW, Mangel M (2000) Dynamic state variable models in ecology: methods and applications. Oxford University Press, New York

Clark DL, Leis JM, Hay AC, Trnski T (2005) Swimming ontogeny of larvae of four temperate marine fishes. Mar Ecol Prog Ser 292:287–300

Cowen RK, Paris CB, Srinivasan A (2006) Scaling of connectivity in marine populations. Science 311:522–527

Dawkins R (1976) The selfish gene. Oxford University Press, Oxford

Fiksen Ø, Eliassen S, Titelman J (2005) Multiple predators in the pelagic: modelling behavioural cascades. J Anim Ecol 74:423–429

Fisher R, Leis JM, Clark DL, Wilson SK (2005) Critical swimming speeds of late-stage coral reef fish larvae: variation within species, among species and between locations. Mar Biol 147:1201–1212

Fisher RA (1930) Genetical theory of natural selection. Oxford University Press, Oxford

Fitzpatrick MJ, Ben-Shahar Y, Smid HM, Vet LEM, Robinson GE, Sokolowski MB (2005) Candidate genes for behavioural ecology. Trends Ecol Evol 20:96–104

Folkvord A (2005) Comparison of size-at-age of larval Atlantic cod (*Gadus morhua*) from different populations based on size- and temperature-dependent growth models. Can J Fish Aquat Sci 62:1037–1052

Fuiman LA, Batty RS (1997) What a drag it is getting cold: partitioning the physical and physiological effects of temperature on fish swimming. J Exp Biol 200:1745–1755

Garrison LP, Michaels W, Link JS, Fogarty MJ (2000) Predation risk on larval gadids by pelagic fish in the Georges Bank ecosystem. I. Spatial overlap associated with hydrographic features. Can J Fish Aquat Sci 57:2455–2469

Giske J, Huse G, Fiksen Ø (1998) Modelling spatial dynamics of fish. Rev Fish Biol Fish 8:57–91

Giske J, Mangel M, Jakobsen P, Huse G, Wilcox C, Strand E (2003) Explicit trade-off rules in proximate adaptive agents. Evol Ecol Res 5:835–865

Grimm V, Railsback S (2005) Individual based modeling and ecology. Princeton University Press, Princeton, NJ

Grimm V, Revilla E, Berger U, Jeltsch F and 6 others (2005) Pattern-oriented modeling of agent-based complex systems: lessons from ecology. Science 310:987–991

Harden Jones FR (1968) Fish migration. Edward Arnold, London

Harden Jones FR, Arnold GP, Greer Walker M, Scholes P (1979) Selective tidal stream transport and the migration of plaice (*Pleuronectes platessa* L) in the southern North Sea. J Cons Int Explor Mer 38:331–337

Hare JA, Thorrold S, Walsh H, Reiss C, Valle-Levinson A, Jones C (2005) Biophysical mechanisms of larval fish ingress into Chesapeake Bay. Mar Ecol Prog Ser 303: 295–310

Hinckley S, Hermann AJ, Megrey BA (1996) Development of a spatially explicit, individual-based model of marine fish early life history. Mar Ecol Prog Ser 139:47–68

Hinrichsen HH, Schmidt JO, Petereit C, Mollmann C (2005) Survival probability of Baltic larval cod in relation to spatial overlap patterns with their prey obtained from drift model studies. ICES J Mar Sci 62:878–885

Holland JN (1992) Adaptation in natural and artificial systems. MIT Press, Cambridge, MA

Houde E (1997) Patterns and consequences of selective processes in teleost early life histories. In: Chambers RC, Trippel EA (eds) Early life history and recruitment in fish populations. Chapman & Hall, London, p 173–196

Houston A, McNamara J (1999) Models of adaptive behaviour. Cambridge University Press, Cambridge

Huret M, Runge JA, Chen C, Cowles G, Xu Q, Pringle JM (2007) Dispersal modeling of fish early life stages: sensitivity with application to Atlantic cod in the western Gulf of Maine. Mar Ecol Prog Ser 347:261–274

Huse G (2001) Modelling habitat choice in fish using adapted random walk. Sarsia 86:477–483

Huse G, Strand E, Giske J (1999) Implementing behaviour in individual-based models using neural networks and genetic algorithms. Evol Ecol 13:469–483

Huse G, Johansen GO, Bogstad L, Gjøsæter H (2004) Studying spatial and trophic interactions between capelin and cod using individual-based modelling. ICES J Mar Sci 61: 1201–1213

Hutchinson JMC, Gigerenzer G (2005) Simple heuristics and rules of thumb: where psychologists and behavioural biologists might meet. Behav Process 69:97–124

Jørgensen C, Ernande B, Fiksen Ø, Dieckmann U (2006) The logic of skipped spawning in cod. Can J Fish Aquat Sci 63:200–211

Larsson AI, Jonsson PR (2006) Barnacle larvae actively select flow environments supporting post-settlement growth and survival. Ecology 87:1960–1966

Leis JM (2007) Behaviour as input for modelling dispersal of fish larvae: behaviour, biogeography, hydrodynamics, ontogeny, physiology and phylogeny meet hydrography. Mar Ecol Prog Ser 347:185–193

Leis JM, Hay AC, Trnski T (2006) *In situ* ontogeny of behaviour in pelagic larvae of three temperate, marine, demersal fishes. Mar Biol 148:655–669

Lima SL, Dill LM (1990) Behavioral decisions made under the risk of predation — a review and prospectus. Can J Zool 68:619–640

Loose CJ, Dawidowicz P (1994) Trade-offs in diel vertical migration by zooplankton — the costs of predator avoidance. Ecology 75:2255–2263

Lough RG, Potter DC (1993) Vertical distribution patterns and diel migrations of larval and juvenile haddock *Melanogrammus aeglefinus* and Atlantic cod *Gadus morhua* on Georges Bank. Fish Bull (Wash DC) 91:281–303

Lough RG, Buckley LJ, Werner FE, Quinlan JA, Edwards KP (2005) A general biophysical model of larval cod (*Gadus morhua*) growth applied to populations on Georges Bank. Fish Oceanogr 14:241–262

Maley CC, Caswell H (1993) Implementing i-state configuration models for population dynamics — an object-oriented programming approach. Ecol Model 68:75–89

McNamara JM, Houston AI (1987) Starvation and predation as factors limiting population size. Ecology 68:1515–1519
Menczer F, Belew RK (1996) From complex environments to complex behaviors. Adapt Behav 4:317–363
Mullon C, Cury P, Penven P (2002) Evolutionary individual-based model for the recruitment of anchovy (*Engraulis capensis*) in the southern Benguela. Can J Fish Aquat Sci 59:910–922
Nielsen R, Munk P (2004) Growth pattern and growth dependent mortality of larval and pelagic juvenile North Sea cod *Gadus morhua*. Mar Ecol Prog Ser 278:261–270
Olla BL, Davis MW, Ryer CH, Sogard SM (1996) Behavioural determinants of distribution and survival in early stages of walleye pollock, *Theragra chalcogramma*: a synthesis of experimental studies. Fish Oceanogr 5:167–178
Paris CB, Cowen RK (2004) Direct evidence of a biophysical retention mechanism for coral reef fish larvae. Limnol Oceanogr 49:1964–1979
Peck MA, Buckley LJ, Bengtson DA (2006) Effects of temperature and body size on the swimming speed of larval and juvenile Atlantic cod (*Gadus morhua*): implications for individual-based modelling. Environ Biol Fish 75:419–429
Persson L, De Roos AM (2003) Adaptive habitat use in size-structured populations: linking individual behavior to population processes. Ecology 84:1129–1139
Plomin R, DeFries JC, McClearn GE, McGuffin P (2000) Behavioural genetics. Worth Publishers, New York
Railsback SF, Lamberson RH, Harvey BC, Duffy WE (1999) Movement rules for individual-based models of stream fish. Ecol Model 123:73–89
Scheffer M, Baveco JM, Deangelis DL, Rose KA, Vannes EH (1995) Super-individuals a simple solution for modeling large populations on an individual basis. Ecol Model 80:161–170
Schwalme K, Chouinard GA (1999) Seasonal dynamics in feeding, organ weights, and reproductive maturation of Atlantic cod (*Gadus morhua*) in the southern Gulf of St Lawrence. ICES J Mar Sci 56:303–319
Sinclair M (1988) Marine populations. University of Washington Press, Seattle, WA
Skiftesvik AB (1992) Changes in behavior at onset of exogenous feeding in marine fish larvae. Can J Fish Aquat Sci 49:1570–1572
Slotte A, Fiksen Ø (2000) State-dependent spawning migration in Norwegian spring-spawning herring. J Fish Biol 56:138–162
Strand E, Huse G, Giske J (2002) Artificial evolution of life history and behavior. Am Nat 159:624–644
Takasuka A, Aoki I, Mitani I (2003) Evidence of growth-selective predation on larval Japanese anchovy *Engraulis japonicus* in Sagami Bay. Mar Ecol Prog Ser 252:223–238
Varpe Ø, Fiksen Ø, Slotte A (2005) Meta-ecosystems and biological energy transport from ocean to coast: the ecological importance of herring migration. Oecologia 146: 443–451
Vikebø F, Sundby S, Adlandsvik B, Fiksen Ø (2005) The combined effect of transport and temperature on distribution and growth of larvae and pelagic juveniles of Arcto-Norwegian cod. ICES J Mar Sci 62:1375–1386
Vikebø F, Jørgensen C, Kristiansen T, Fiksen Ø (2007) Drift, growth, and survival of larval Northeast Arctic cod with simple rules of behaviour. Mar Ecol Prog Ser 347: 207–219
Wright KJ, Higgs DM, Belanger AJ, Leis JM (2005) Auditory and olfactory abilities of pre-settlement larvae and post-settlement juveniles of a coral reef damselfish (Pisces: Pomacentridae). Mar Biol 147:1425–1434

Editorial responsibility: Alejandro Gallego (Contributing Editor), Aberdeen, UK

Submitted: June 29, 2006; Accepted: April 30, 2007
Proofs received from author(s): August 24, 2007

Vol. 347: 207–219, 2007
doi: 10.3354/meps06979

MARINE ECOLOGY PROGRESS SERIES
Mar Ecol Prog Ser

Published October 11

OPEN ACCESS

Drift, growth, and survival of larval Northeast Arctic cod with simple rules of behaviour

Frode Vikebø*, Christian Jørgensen, Trond Kristiansen, Øyvind Fiksen

Department of Biology, University of Bergen, PO Box 7800, 5020 Bergen, Norway

ABSTRACT: Due to vertical variations in ocean circulation, larval Northeast Arctic cod *Gadus morhua* may influence their own drift routes by migrating vertically. By coupling a larval individual-based model and a general circulation model, we simulated larval vertical positioning according to simple rules based on individual risk sensitivity. This enabled us to investigate how larval growth, survival and horizontal distribution vary between individuals following different rules. Immediate depth selection follows from the rules, with implications for environmental exposure and instantaneous growth rates. The behavioural rules had long-term and large-scale consequences, since vertical positioning influences the drift trajectory of the larva, and thereby the physical environment the larva experiences along its way. Two alternative rule formulations were explored, each containing the full range of strategies, from maximising immediate growth to maximising immediate survival. Fitness was defined as accumulated survival probability up to 18 mm for larvae released at 2 important spawning grounds in the Lofoten area. Both rules gave better fitness than for individuals drifting at fixed depths. The most successful individuals performed active vertical migration and had an intermediate risk sensitivity. When risk sensitivity was allowed to change with ontogeny, larvae that first emphasised growth and then changed to intermediate risk sensitivity were the most successful ones, although improvements were minor compared to fixed sensitivities. The 2 spawning grounds led to slight differences in fitness, but success as a result of risk sensitivity was similar at both, suggesting that optimal larval strategies may be robust across different spawning grounds.

KEY WORDS: Individual-based model · Rule-based behaviour · Larval fish · Vertical migration · General circulation model · Adaptive behaviour

INTRODUCTION

Marine larvae of many species have pelagic phases during which they drift apparently haphazardly and arbitrarily through immense water masses. The swimming abilities of millimetre- to centimetre-sized larvae are often limited compared to the force of ocean currents. However, swimming ability normally increases throughout ontogeny (Clark et al. 2005), and may prove significant compared to drift if it is exerted in a non-random direction (Leis et al. 2006). In the present paper, we investigate the effects of vertical migrations, which can dramatically change the life of larvae in 2 important ways (e.g. Santos et al. 2006, Fiksen et al. 2007, this Theme Section [TS]). First, layered currents may carry vertically separated larvae in different directions and at different speeds. Ocean circulation models have shown that drifting particles fixed at depths only 10 m apart may end up in different oceans when spawned at times and sites typical for Northeast Arctic cod *Gadus morhua* (Vikebø et al. 2005). Second, light extinction down through the water column results in vertical gradients, in which the top layers have sufficient light for feeding, but also enough to be detected by predators. Only a few tens of metres deeper, the darkness provides a safer refuge from visual predators, but potentially too little light to feed. Additionally, a number of other important environmental variables such as prey density, turbulence and temperature may also vary strongly in the water column, contributing to distinct vertical habitats.

Field observations suggest that larvae perform diurnal vertical migrations (Ellertsen et al. 1984, Neilson & Perry

*Email: frode.vikeboe@imr.no

1990, Lough & Potter 1993). Several models of zooplankton and fish have interpreted such behaviour in relation to predator–prey interactions and the reduction of mortality (Fiksen 1997, Strand et al. 2002, Fiksen et al. 2005). Here, we couple vertical migrations with an ocean circulation model, and evaluate the effects of vertical migration on the ocean transport of larvae. The drift trajectories of eggs and larval fish depend on (1) the time and place of spawning (Hinckley et al. 2001, Mullon et al. 2002, Huggett et al. 2003) and (2) the complex interaction between ocean circulation and individual behaviour throughout ontogeny (Hinckley et al. 1996, Werner et al. 1996, 2001, Hinrichsen et al. 2002, Fox et al. 2006). In turn, this sets premises for individual growth and survival and, ultimately, for recruitment to the stock and contribution to the future gene pool.

Recent developments of ocean circulation models have provided new tools for investigating how organisms are influenced by circulation patterns. However, existing individual-based models (IBM) typically use fixed ad hoc formulations of larval depth positioning. Such imposed behaviours (sensu Grimm & Railsback 2005) are commonly justified from a set of observations of larval vertical distributions, and may also include observed responses to particular environmental cues such as light. The problems with this procedure are (1) that the ad hoc formulations are based on a limited number of observations and are therefore only valid for the environmental states during these observational periods; at other times there may be environmental cues that could modify or override the imposed behaviour (Neilson & Perry 1990, Giske et al. 2003), and (2) that the internal physiological condition of an individual typically feeds back on behavioural motivation, hunger and satiation may for example trigger different behaviours under similar environmental conditions (Houston & McNamara 1999, Clark & Mangel 2000). Using observations to parameterise important flexible behaviours thus, limits the prognostic value of the model when tested under new environmental conditions.

In addition, contemporary models of larval fish dispersal have only included individuals that vary in spatial position or physiological states. Individual differences or variability in behavioural strategies have so far been ignored (as noted by Huse 2001, Strand et al. 2002). Behaviours such as habitat selection are adaptive traits, evolved under the constraints imposed by the physical and biological environment. A successful larva must grow, survive and end up in favourable nursery areas, and, since their parents have succeeded, offspring that inherit their parents' behavioural strategies may also stand a fair chance of success (Fiksen et al. 2007).

Vikebø et al. (2005) demonstrated that the vertical distribution of larval cod influenced their drift trajectory and temperature exposure, which, in turn, has significant implications for growth and survival. However, the model did not take active larval migration, feeding, or predation risks into consideration. In the present paper, we include these factors and allow larvae to choose depth according to a rule-based risk sensitivity specific for each individual. In the simplest version, a single parameter determines how risk sensitive the larvae are. Larvae with a low risk sensitivity select a vertical habitat where growth is favourable and, consequently, mortality is high. Since currents change with depth, the vertical position has consequences for the drift trajectory the larvae follow. In this way, the behavioural strategy has both local effects on growth and mortality, as well as long-term and large-scale effects on dispersal and temperature along the drift route. We also explore a 3-parameter version of this strategy, whereby the first 2 parameters represent risk sensitivity in early and late ontogeny, while the third parameter determines when to switch between the 2 behavioural strategies. Finally, we compare the 2 rules with non-responsive individuals that stay at fixed depths.

This paper investigated the combined effects of vertical migration and ocean circulation on growth, mortality and dispersal of larval Northeast Arctic cod. More specifically, we asked the following questions: Does vertical migration increase survival throughout the larval period? How risk sensitive should the larvae be in order to maximise their probability of survival? How does risk sensitivity in the local water column affect long-term dispersal, growth and survival? Should risk sensitivity change as the larvae grow larger? And, should behaviour be different for larvae spawned in an embayment compared with larvae spawned at a more exposed location on the shelf?

METHODS AND MODELS

To assess the success of the rules, we used the accumulated mortality rate up to a given length. The rationale for this measure is that all individuals have to grow through the larval sizes to reach juvenile and adult life stages. From a life-history perspective, the only reason to stop growth would be to start reproduction. We only modelled larval cod far below the earliest observed maturation size for this species. The success of a behavioural strategy in these early life stages can therefore be summarised as the probability with which it survives until a given size—for us limited to 18 mm, as this is the maximum size to which the physiological submodels remain valid.

The ocean model. The numerical ocean model used in this study was the ROMS Version 2.0 (Ezer et al. 2002, Shchepetkin & McWilliams 2003, Shchepetkin & McWilliams 2005, available at www.myroms.org). The

model setup was similar to that described by Vikebø et al. (2005). Lateral boundary conditions were taken from a monthly mean climatology (Engedahl et al. 1998), while the mean daily vertical boundary conditions (air pressure, wind stress and heat flux) were taken from the NCEP/NCAR database (Kalnay et al. 1996) for the year 1985.

In Vikebø et al. (2005), the particle dispersion was run simultaneously ('online'), as a subroutine within the ocean model. However, the present exploration of behavioural strategies required much more CPU time, and particle dispersion was therefore detached ('offline'). The Lagrangian particle-tracking model (LADIM; Ådlandsvik & Sundby 1994) has a time step of 1 h, while the current and hydrography fields from the ocean model are daily averages. Multilinear interpolation provides necessary input for the dispersal of particles by use of a fourth order Runge Kutta advection scheme (Ramsden & Holloway 1991).

The range of resolved eddies and velocity shear is proportional to the spatial resolution of the ocean model. Hence, with increasing spatial resolution, the need for additional parameterised diffusion, e.g. random walk, is reduced. Ådlandsvik & Sundby (1994) used a spatial resolution of 20 km and included a random component for parameterising a Fickian diffusion of 100 $m^2 s^{-1}$. In the current model setup the horizontal resolution ranged from 3.5 to 8 km, moving from the upstream to the downstream boundary. We therefore did not include any random walk, although this omission will cause an underestimation of dispersal.

The individual-based model. ***Model organism:*** The larvae were characterised by standard length L (mm), body mass w (dry weight, mg), spatial coordinates (x, y, z) and accrued probability of survival Ps since hatching. The attribute vector of individual i at time t was thus:

$$A_{i,t} = (L_i, w_i, x_i, y_i, z_i, Ps_i) \quad (1)$$

The attributes were updated by local growth, mortality and velocity field at each time increment t (1 h) of the model. Growth and mortality were driven by light, the modelled temperature field and body size. Only horizontal velocities were considered for the advection of individuals, though the larva itself was allowed to migrate vertically at a velocity of $\frac{1}{3}$ L s^{-1}. Hence, the swimming capabilities of newly hatched larvae and of the largest larvae (18 mm) were about 4 and 22 m h^{-1}, respectively. With a daily vertical migration distance of up to 40 m and a time step in the IBM of 1 h, newly hatched larvae were therefore constrained by their ability to choose habitat based on potential growth and survival, while the large larvae were not.

It was essential for the model that growth and mortality rates emerge from habitat selection, which was specified by the behavioural rule. We used survival up to 18 mm length as a measure of fitness, since all individuals have to grow through this size to reach juvenile and adult life stages. We assumed that larvae can sense or assess growth opportunity and mortality risk in the upper 100 m of the water column, but that they are not able to make predictions for the future. How behaviour will change under limited information is a topic for future studies, for example, if larvae can only assess growth and mortality within their potential swimming range or in water bodies they have passed through. All larvae were initialised at the same size (0.03 mg, 3.53 mm: the same initial weight as in Otterlei et al. 1999) and at a fixed depth (1 m). We released larvae at Moskenesgrunnen and in the Vestfjorden, 2 important spawning grounds in the Lofoten region, at times near the peak spawning period, covering 4 × 3 grid cells or about 20 × 15 km (Fig. 1). Initiating larvae with spatial

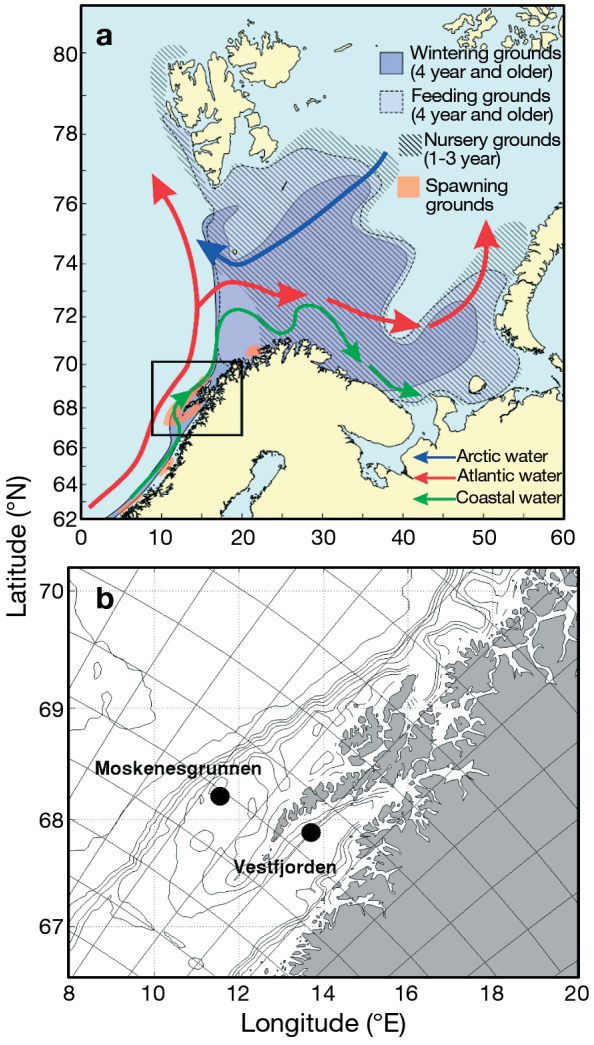

Fig. 1. (a) Spawning and nursery grounds of Northeast Arctic cod *Gadus morhua* in relation to different water masses. (b) The 2 spawning grounds included in this study. Curved grid delineates 10 × 10 grid cells

variation within these cells introduced divergence in larval trajectories due to horizontal velocity shear.

Submodels: *Growth:* The maximum specific growth rate $G(w,T_z)$ is an empirical function of larval body mass w and ambient temperature T_z for larvae fed ad libitum and reared under laboratory conditions (Folkvord 2005). Larval cod have high growth rates, and substantial food intake is required to sustain these rates. Their visual foraging mode makes feeding highly dependent on ambient light I_z (Fiksen et al. 1998, Fiksen & MacKenzie 2002), and this may constrain growth. To include food-limited growth and additional energetic costs, we added standard metabolic rate $SMR(w,T_z)$ to the estimated growth potential, limited this by food availability (we have not included prey explicitly here, food availability is dependent on light) and then subtracted the SMR (see Fiksen & Folkvord 1999). The standard metabolic rate of larval cod was estimated by Finn et al. (2002), and we applied their estimate here. Additional energetic costs, such as swimming costs $SC(w,\Delta z)$ depending on body size w and migration distance per time Δz, were subtracted from the potential growth rate. The realised growth rate g_z (s^{-1}) of a larva was thus a function of body mass w, temperature T_z, light I_z and swimming activity Δz, such that:

$$g_z(w,\Delta z) = [G(w,T_z)+SMR(w,T_z)] \cdot (1-e^{-10\frac{I_z}{K_e+I_z}}) - SMR(w,T_z) - SC(w,\Delta z) \quad (2)$$

The parameter K_e (determining food limitation with light) was set to 1 µmol photons m^{-2} s^{-1} as in Fiksen & MacKenzie (2002), and the coefficient 10 was chosen arbitrarily to limit growth rates at depths below ~50 m, where zooplankton availability (prey densities and light) is normally low. Swimming costs $SC(w,\Delta z)$ were included as a maximum of 10% of SMR at a fixed temperature (7°C) if the larvae swim up or down at a velocity of $\frac{1}{3}$ L s^{-1}, linearly decreasing with swimming speed or migration range (Δz). This meant that specific swimming costs decreased slightly with body mass. Growth was represented more simplistically here than by Kristiansen et al. (2007), to reduce the CPU time required for the high number of particles.

Predation: Larval fish are subject to predation from both invertebrates and fish (Bailey & Houde 1989). Typically, vulnerability to invertebrate predators decreases with larval size as they outgrow abundant, smaller ambush and cruising zooplankton predators. On the other hand, the efficiency of piscivores is very sensitive to detection distance, which increases with light and larval size (Aksnes & Giske 1993, Aksnes & Utne 1997). Larvae may therefore become more vulnerable to fish predators with size, unless behavioural strategies such as vertical migration offset increases in encounter rates.

We modelled predation from fish and invertebrates separately, similar to procedures described by Fiksen et al. (2002). Predation rate from invertebrates μ_n (h^{-1}) decreases with larval body length L (mm) as $\mu_n = 0.01L^{-1.3}$. Predation rate from fish is $\mu_f = 0.05R^2$, where R is the piscivore's sighting distance of a larva depending on light and larval size and the coefficient summarises all factors such as fish density and escape probability (see Fiksen et al. 2002 for details). The total instantaneous mortality rate $M_z = \mu_n + \mu_f$ is then a function of depth, surface irradiance and larval size. Little knowledge exists on how mortality risks are divided between invertebrates and fish for larvae, but this simple model captures some essential factors such as body size and light.

Light: Light is a crucial factor for both growth and mortality rates. We modelled surface light as a function of latitude, day of year and time of day (Skartveit & Olseth 1988), and assumed vertical light attenuation according to the Lambert-Beer law, with a diffuse attenuation coefficient of 0.18 m^{-1} and a maximum (midday) surface irradiance of 500 µmol photons m^{-2} s^{-1}.

Behavioural rules: Individuals follow a simple rule to select vertical position (Fiksen et al. 2007). We assumed that larvae have complete information about depth-dependent growth g_z and mortality m_z within the upper 100 m. The larva then decides on the next depth $z_i^*(t)$ from:

$$z_i^*(t) = \max_z[(1-\pi_i)g_z - \pi_i m_z] \quad (3)$$

where $0 \le \pi_i \le 1$ is the behavioural strategy of individual i and π can be interpreted as the individual's risk sensitivity. A low π_i characterises an individual always maximising instantaneous growth, and a high π_i characterises an individual maximising instantaneous survival. Individuals with high π_i thus can be interpreted as being fearful, and those with low π_i as being bold. The risk sensitivity of the individual thus colours its vertical migration behaviour, with major consequences for growth, mortality and drift trajectory. The rule makes larval habitat selection sensitive to local environmental variability in growth and mortality rates, while the simple formulation of the strategy mimics the genetic predispositions of individuals and can be subject to natural selection over generations.

We tested 2 alternative ways of coding risk sensitivity π_i. The first (Rule 1) was simply a fixed genetic value π_i, as described above. We tested the following values for π_i: 0, 0.01, 0.1, 0.25, 0.5, 0.75, 0.9, 0.98, 0.995, 0.997, 0.998, 0.999 and 1. The second (Rule 2) included 2 risk-sensitivity parameters, $\pi 1_i$ and $\pi 2_i$, one for early and one for the late part of ontogeny. A third parameter determined the size at which the individual switched between the 2 risk sensitivities. This rule allowed risk sensitivity to change ontogenetically. We

tested combinations of parameter values with the same resolution of $\pi 1_i$ and $\pi 2_i$ as for Rule 1, and with the following values for the size λ_i at which risk sensitivity switches (in mm): 4, 6, 8, 10, 12, 14, 16 and 18.

Fitness was then evaluated as the total survival probability from early larval phase to 18 mm. Within this range, all our empirical submodels remained valid, and most larvae with positive growth reached this size within the simulation time of 100 d.

RESULTS

First, we present some of the individual trajectories and dispersal patterns of single individuals released at the same time and from the same position, but with differing behavioural strategies. Then, we investigate emergent patterns by releasing a large number of larvae with various strategies that differ in their risk sensitivities. Finally, we look at the fitness consequences that emerge from behavioural rules over the full range of possible values and with drift stochasticity resulting in variability among individuals.

Individual trajectories and dispersal patterns

The first numerical experiment tracked a few larvae with different risk sensitivities (Rule 1) released in Vestfjorden and at Moskenesgrunnen (see Fig. 1). The geographical dispersal trajectories of individual larvae (Fig. 2a,b) were determined by interactions between the risk sensitivity of their behaviour and ocean circulation. Larvae with low risk sensitivity (π_i = 0.01) emphasised immediate growth and tended to remain near the surface throughout the simulation period (Fig. 2c,d). A consequence of this behaviour was that they were captured by the warmer Atlantic currents (Fig. 1b), drifted towards the more central parts of the Barents Sea and reached high growth rates. Larvae with high risk sensitivity (π_i = 0.99) sought out deep waters, grew slowly and remained in the colder coastal current. Larvae with intermediate risk sensitivity (π_i = 0.5) tended to move deeper with time, and, maybe surprisingly, decreased their range of diel migration (Fig. 2c,d). This was mainly driven by increasing day length, which influences predation risk during the night. Together with the absence of food below 50 m, this created a narrow vertical window (30 to 40 m) in which growth and mortality were acceptable. Larvae with intermediate risk sensitivity drifted in warm Atlantic water (Fig. 2f) into the Barents Sea from Moskenesgrunnen, but they drifted in cold coastal water (Fig. 2e) when released in Vestfjorden. These different trajectories significantly affected their respective growth histories (Fig. 2g,h). The purely size-dependent mortality rate decreased rapidly as the larvae grew, while mortality from visual predators increased due to larger size and longer days (Fig. 2i,j). This exemplifies the interaction between spawning strategy (parental decisions on timing and location of spawning) and larval behaviour. A robust larval strategy should therefore be one that functions well across the range of parental spawning strategies.

Emergent dispersal patterns from various risk sensitivities

To further explore the effects of risk sensitivity (Rule 1) and spawning location, we released 50 individuals at each of 13 levels of risk sensitivity, simultaneously at the 2 locations. The individuals were released twice, 3 d before and 3 d after the time of peak spawning in Northeast Arctic cod, with minor spatial perturbations around the spawning grounds. The strategies covered a range of possible vertical habitats, illustrated for single individuals released at the 2 spawning grounds for each of the 13 levels of risk sensitivity (Fig. 3). Although the general trend was to move deeper with time, this depended considerably on the growth potential in the water column. The transition to deeper habitats was quite abrupt for risk-averse strategies, leading larvae below 50 m where there is no food and growth was negative. Remaining constantly at these depths led to starvation, and larvae using such strategies consequently had low fitness. Some individuals encountered stratified water masses, which made growth sufficiently profitable near the surface to offset the increased risk associated with these habitats.

The consequences of individual trajectories on large-scale dispersal became apparent when 50 individuals were released with the same risk sensitivity and at the same spawning ground (Fig. 4). First, even minor perturbations around any given release point led to substantial spatial spread in larvae after 100 d, despite the deterministic scheme of particle tracking. Second, individuals originating from Moskenesgrunnen seemed to disperse more than those from Vestfjorden and tended to be more easterly distributed, independent of risk sensitivity. Third, bolder, growth-maximising individuals (low π_i) tended to disperse into the central parts of the Barents Sea from both spawning sites.

Fitness consequences of rules and spawning area

At each level of risk sensitivity, we tracked 50 individuals to 18 mm length and assessed accrued probability of survival (fitness). These values are presented,

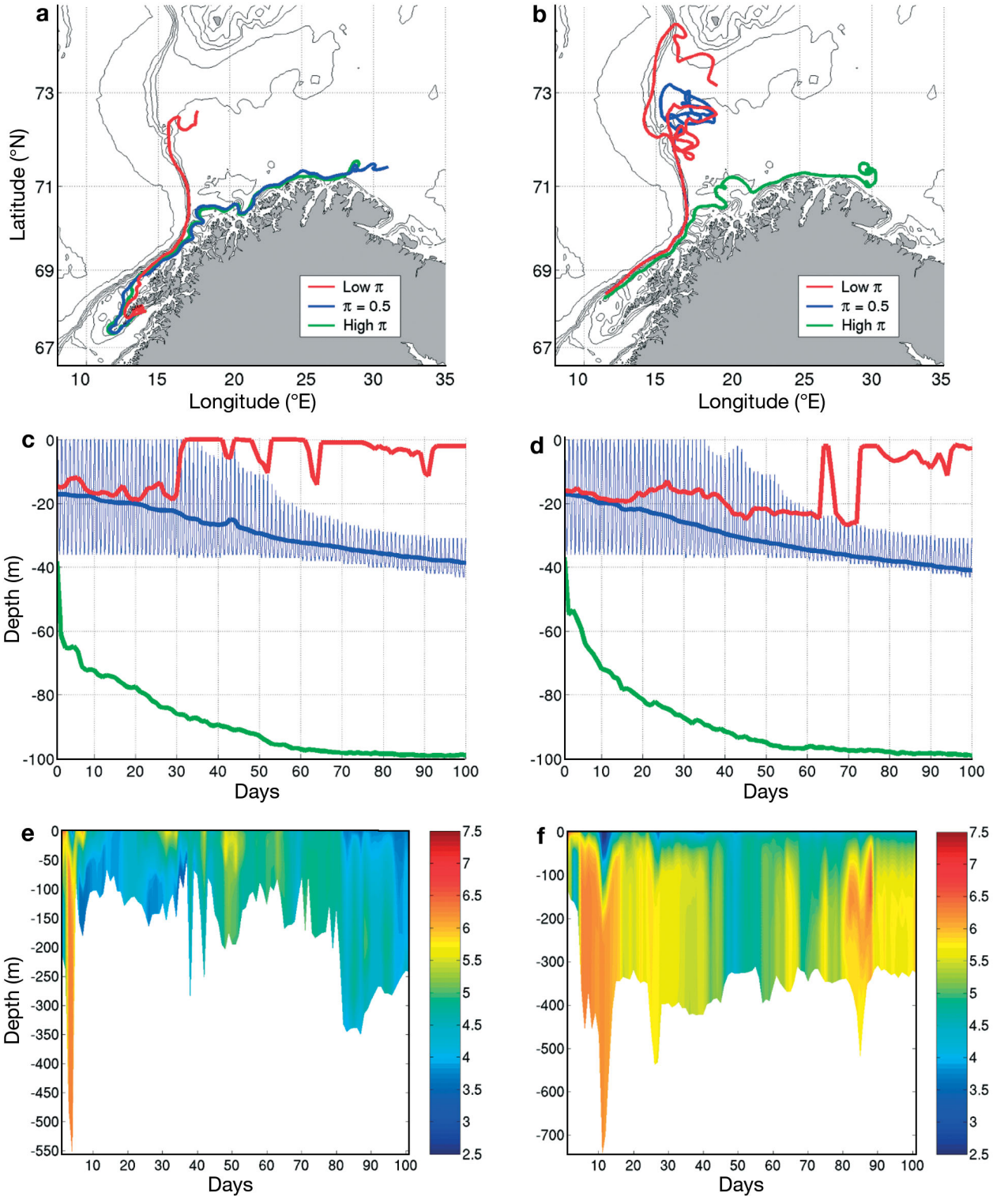

Fig. 2. *Gadus morhua.* An illustration of (a,b) dispersal, (c,d) daily mean depth and (e,f) temperature profiles along the drift-trajectories of larvae released in Vestfjorden (sheltered spawning ground; left panels) and at Moskenesgrunnen (offshore spawning ground; right panels). Dispersal and mean daily vertical depth for single individuals using Rule 1 for 3 strategies of risk sensitivity are included (π_i = 0.01, 0.5 or 0.99). Depth is shown with hourly resolution for π_i = 0.5 (to illustrate diel migration patterns), but only mean daily depth is shown for π_i = 0.01 and 0.99. Temperature profiles are shown for individuals with π_i = 0.5. 'Fearful' larvae (high π_i) give immediate survival high priority, migrate deeper, and drift closer to the coast. Also included are hourly (g,h) ambient temperature and growth history and (i,j) mortality rates from fish (μ_f) and invertebrates (μ_n)

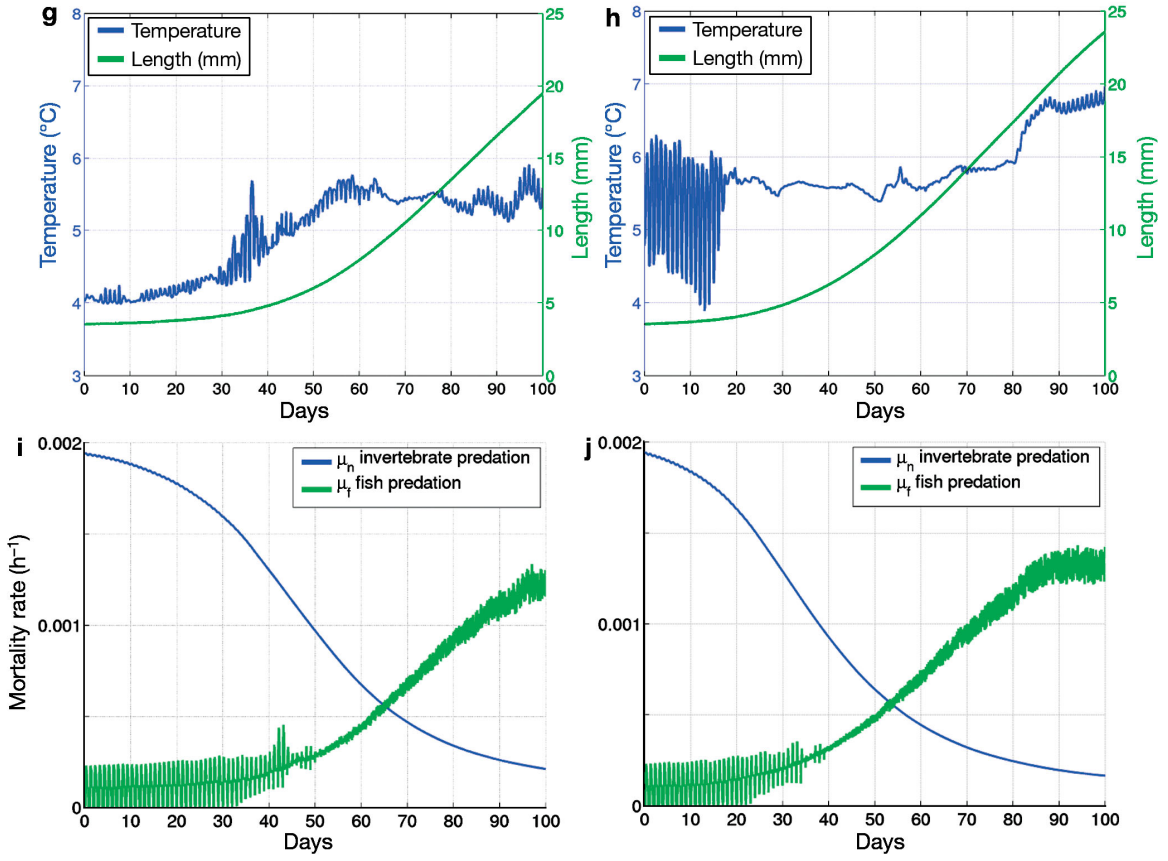

Fig. 2 (continued)

for each of the spawning sites, for the larvae with maximum fitness at each level of risk sensitivity, the average of the most successful 10 and 25%, and the total average (Fig. 5a). This will indicate how robust the different behaviours are in a fitness perspective. Finally, this is compared with survival up to 18 mm of larvae remaining at fixed depths (Fig. 5b).

Larvae with intermediate risk sensitivity (0.5 to 0.75) had the highest survival. They performed vertical, diurnal migrations, increasing towards an average depth of between 30 and 50 m in late ontogeny (Fig. 2c,d). Larvae with rule-based behaviour generally did better than larvae staying at fixed depths. Also, larvae from Moskenesgrunnen tended to do better than larvae from Vestfjorden in all these realisations, although less so for larvae staying at fixed depths. Note that larvae drifting at a fixed depth of 30 m achieved higher survival than larvae further up in the water column. Clearly, higher temperatures and enhanced feeding near the surface, which reduces the time needed to reach a length of 18 mm, did not compensate for the increased mortality. Larvae with a high level of risk sensitivity (>0.75) had low (or negative) growth and were unable to reach 18 mm.

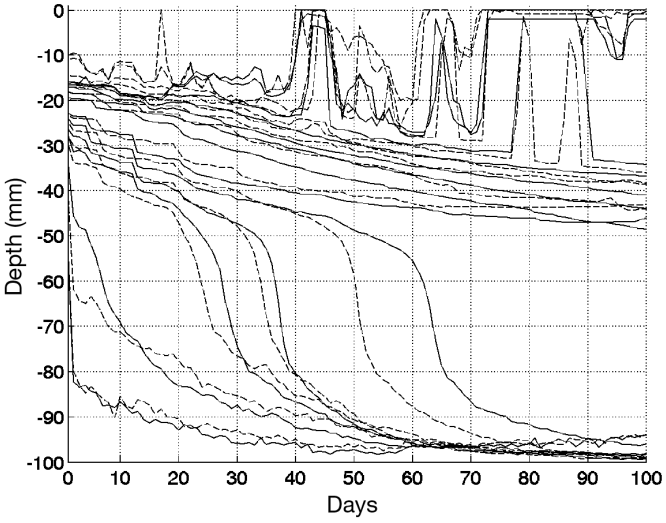

Fig. 3. *Gadus morhua.* Mean daily vertical positioning for single larvae released at the same time and place in Vestfjorden (broken lines) and Moskenesgrunnen (solid lines) for 13 values of π_i (0, 0.01, 0.1, 0.25, 0.5, 0.75, 0.9, 0.98, 0.995, 0.997, 0.998, 0.999, 1). Increasing risk sensitivity (π_i-value) takes larvae deeper. In addition, they move deeper with time due to increasing size (increased susceptibility to visual predation) and longer days

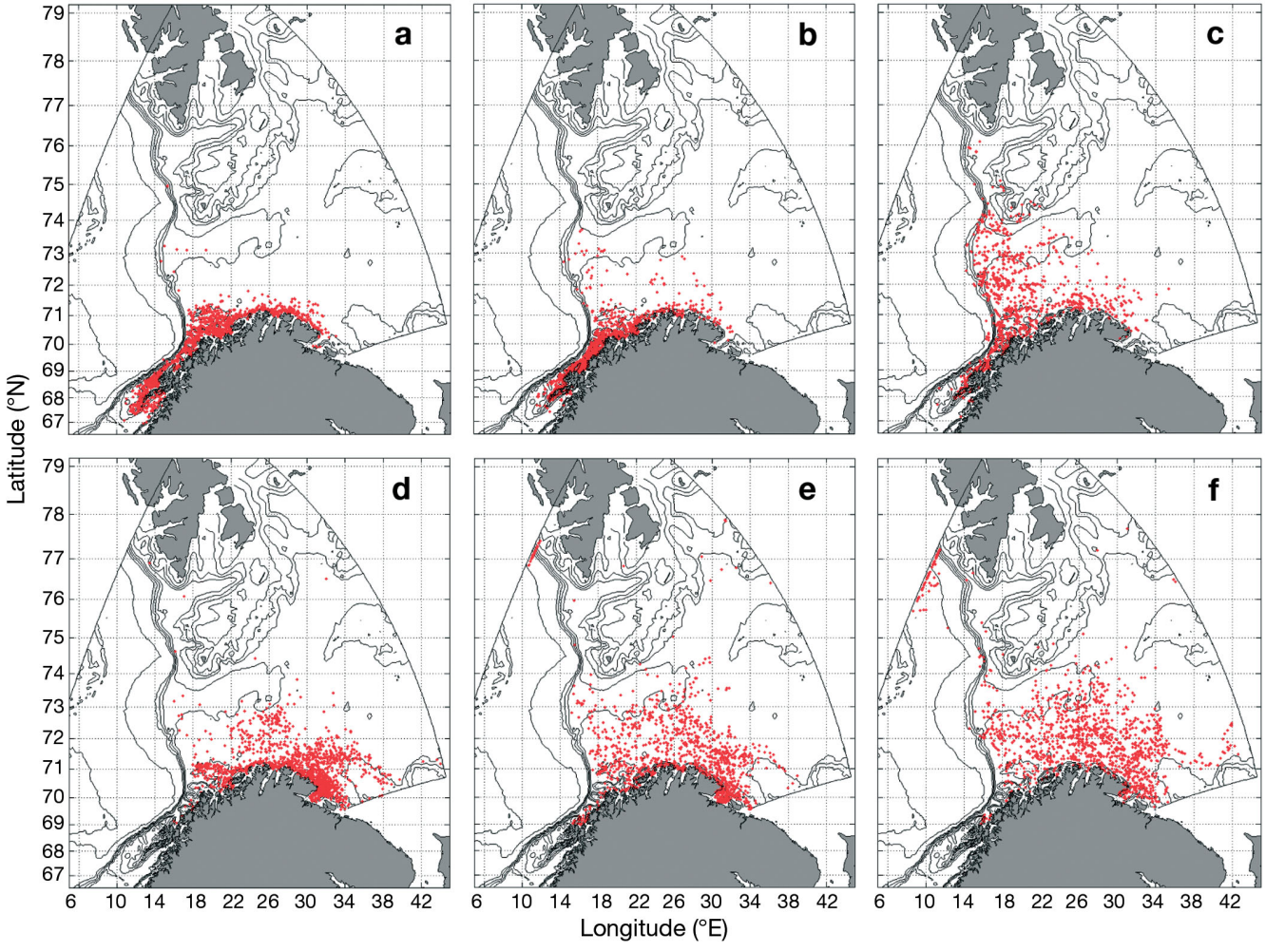

Fig. 4. *Gadus morhua.* The effect of risk sensitivity of vertical migration on larval dispersal. Each point represents the position of 1 larva after 100 d of drift from Vestfjorden (a–c) and Moskenesgrunnen (d–f) for π_i equals 1 (fearful larvae) (a,d), 0.5 (median risk sensitivity) (b,e) and 0 (bold larvae) (c,f). For each level of risk sensitivity, 50 individuals were released at the same time and place, with variability in drift paths introduced by minor spatial and temporal perturbations at the release point

Finally, we estimated the fitness for larvae switching between 2 risk sensitivities at 8 possible sizes (Rule 2; Fig. 6), by releasing 50 larvae at each level of risk sensitivity ($13 \times 13 \times 8$). To assess fitness, we extracted the 50 individuals with the highest fitness, ensuring that they had an optimal late (or early) behavioural strategy. Larvae changing their strategy ontogenetically did slightly better than those following the same rule throughout the larval stage, for any size of switch (compare Figs. 5 & 6). Larvae that changed their behaviour at an early ontogenetic stage emphasised growth ($\pi 1_i = 0.25$) before they shifted to a more risk-sensitive (fearful) behaviour ($\pi 2_i = 0.75$), in order to maximise their fitness (Fig. 6a,b). However, fitness was relatively flat across early risk sensitivity for larvae that switched early. A later switch favoured more fearful strategies also during the early stage (Fig. 6c,d). The similarity between the shape of the fitness curves for the 2 release sites is encouraging, as it suggests that strategies may be quite robust across different spawning grounds.

DISCUSSION

An important topic for general population and community ecology is to model organisms with flexible individual behaviour, motivated through individual states and environmental cues (Giske et al. 2003, Persson & De Roos 2003, Grimm & Railsback 2005). Here, we have explored 2 simple individual decision rules and their consequences for growth, mortality and drift trajectories of pelagic larval fish. The model experiments demonstrated that rules for larval vertical positioning have consequences on several scales. Locally, depth selection affects instantaneous mortality and

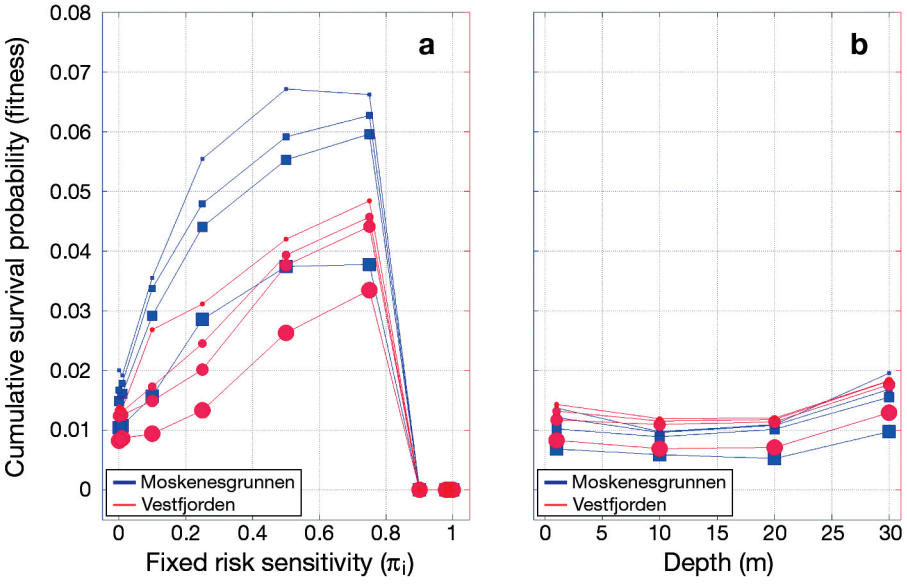

Fig. 5. *Gadus morhua*. Comparison of fitness consequences for larvae drifting from 2 spawning locations (a) with various fixed attitudes to risk using Rule 1 and (b) staying at fixed depths. Larvae from Moskenesgrunnen are indicated by blue squares and Vestfjorden by red circles. There are 4 curves for each of the spawning grounds, indicating the single most successful larvae, the top 10 and 25%, and the average overall larvae (indicated by increasing size in circles and squares). Fitness is measured as accumulated survival probability of larvae when they reach a length of 18 mm

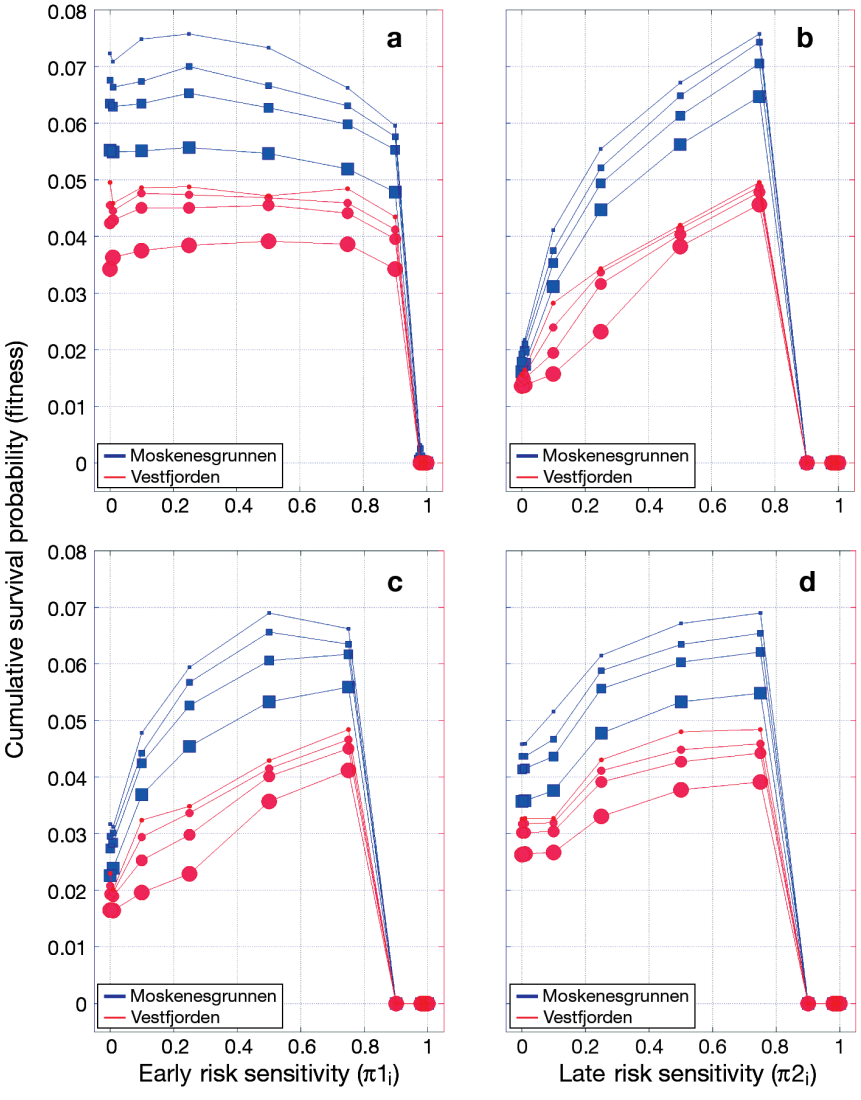

Fig. 6. *Gadus morhua*. Comparison of fitness consequences of strategies that vary in risk sensitivity using Rule 2. Results are shown for 2 spawning locations (Moskenesgrunnen by blue squares and Vestfjorden by red circles). The panels show fitness consequences of changing strategy at (a,b) 6 mm and (c,d) 16 mm; left panels are early risk sensitivity (given optimal risk sensitivity in the second period) and right panels show the effect of late risk sensitivity (given that early risk sensitivity is optimal). There are 4 curves for each of the spawning grounds, indicating the single most successful larvae, the top 10 and 25%, and the average over all larvae (indicated by increasing size in circles and squares). Fitness is measured as accumulated survival probability of larvae up to a length of 18 mm

growth rates, leading to higher survival through the larval period compared to larvae that were forced to stay at fixed depths. However, the strategy for depth selection also has long-term and large-scale consequences. First, since vertical migration interacts with ocean circulation, the strategy influences which drift trajectory a larva will follow and thereby the physical environment the larva experiences along its way. This means that the behavioural strategy, leading to a certain drift trajectory, has delayed effects on growth and survival, since temperature and light conditions vary according to the particular route. Temperature will affect growth rates directly, as physiological processes are faster in warmer water for the range observed in the model area. In turn, this will have indirect consequences for mortality, since fast-growing larvae spend less time in the size window where they are vulnerable to predation and since their ability to move vertically and thereby manipulate predation rates by fish increases with size. On the other hand, at higher temperatures, the predators of larvae will have higher metabolic rates and require more food. However, predation on larvae is not temperature dependant in our model at this stage. Other factors, for example the spatial and vertical distribution of predators and prey, will influence growth and survival in similar ways, but were not included in this model. Second, the area or region where the larvae end up after the drift phase can have important consequences for later life stages (Cowen et al. 2006). Not only does habitat type and climate vary geographically, but currents and distance can preclude the use of essential feeding and spawning sites later in life.

While the importance of vertical positioning has been realised in many coupled bio-physical models (e.g. Hinckley et al. 1996, Werner et al. 1996, Fox et al. 2006), this is the first attempt to model larvae that select depths based on an inherent trade-off rule between growth and mortality in a general circulation model. This involves giving larvae an individual opportunity to respond to the processes affecting immediate growth and mortality, rather than imposing vertical distribution as an assumption of the model. We tested 2 simple rule formulations, each with the full range of strategies from maximising immediate growth to maximising immediate survival. Both rules gave better fitness than for non-responsive individuals drifting at fixed depths. Both spawning grounds favoured active vertical migration, and an intermediate risk sensitivity seemed to be optimal under the assumptions given here. When risk sensitivity was allowed to change with ontogeny, larvae that emphasised growth first and then changed to an intermediate risk sensitivity at an early ontogenetic stage were the most successful ones. However, it appears that Rule 2 only slightly improved fitness compared to the simpler Rule 1, where larvae used the same risk sensitivity throughout.

Both growth and mortality depend on complex processes that link the physical environment and the distribution of predators and prey with behaviour and internal physiology. These processes must necessarily be simplified in models, and our results are likely to be sensitive to a number of parameters used in the different submodels. Especially, the benefit of behaviour is tightly linked to how mortality is modelled. Behaviour influences light exposure and therefore encounter rates with visual predators, but does not affect predation from invertebrates, which we have modelled as a purely size-dependent mortality that is high for small larvae and declining with size (McGurk 1986). Predation rates from invertebrates and fish are comparable at a larval length of about 9 mm, but above this length fish predation dominates. That fish predation plays a major role is supported by the strong indications that pelagic fish regulate the recruitment success of cod (Köster & Möllmann 2000, Swain & Sinclair 2000). In addition to cannibalism, both herring and capelin are abundant in the drift routes of Northeast Arctic cod *Gadus morhua* and are known to forage on cod larvae.

The purely size-determined mortality rate in our model is lower than the mortality rate in the empirical model compiled by McGurk (1986) for larvae <13 mm and slightly higher for larger larvae. Sundby et al. (1989) estimated the average daily mortality rate to be about 0.2, which is about 4 times higher than the mortality rate applied here (and thus also 4 times higher than the mortality rate used by McGurk [1986] for 13 mm larvae). However, survival probabilities (from hatching to 15 mm) on the order of 10^{-2} are probably too high, given that the mean annual egg production is around 1 to 2 million eggs per female (Kjesbu et al. 1996). The motivation for vertical migration is largely determined by the strength of predation from invertebrates relative to predation from fish. Increasing the invertebrate predation rate (μ_n) would make fish predation, the only depth-dependent component of mortality, less important. Larvae that grow faster would have higher survival probabilities, increasing the reward on rapid growth. Simulations (not shown here) indicate that the optimal π_i is then shifted to the left (from π_i = 0.5–0.75 to 0.25–0.5), favouring larvae with a shallower vertical distribution and with average depths of between 20 and 40 m in late ontogeny. Drifting at a fixed shallow depth will then result in a comparable fitness to individuals with active vertical migration, because exposure to higher mortality rates during early ontogeny in order to shorten this vulnerable stage becomes a good strategy. However, very little is known about the distribution of risk among

visual and non-visual predators, and only additional process-oriented field studies can improve our knowledge on this.

We have assumed that growth is a function of temperature and light, ignoring both spatial and temporal variability in prey distribution. The main prey items for larval cod are nauplii and copepodite stages of *Calanus finmarchicus*, and the production and abundance of these, in turn, depend on factors such as female abundance and primary productivity. These prey are also known to perform diel vertical migration; differences in vertical distribution between day and night of up to 20 m have been observed (Tilseth & Ellertsen 1984). Future refinements of the present analysis will be to include zooplankton models or assimilate data on prey abundance and distribution.

In the present study, we initialised larvae at hatching although Northeast Arctic cod has an egg stage lasting up to 3 wk. The transport of eggs is purely a function of egg density and ocean physics (Sundby 1997). The actual density of the eggs, including the chorion membrane and the amount of yolk and buoyant fat, may have evolved as a trade-off between predation risk and advection consequences of vertical positioning due to density gradients. Incorporating drifting eggs explicitly would perhaps change the initial dispersal of eggs and could therefore precondition initial larval distribution differently than what is presented here.

The modelled larvae swim to their preferred depth and are not affected by vertical mixing. Clearly this is a simplification, as vertical mixing may make it more difficult to remain at the preferred depth. However, a dynamical vertical positioning of individual cod larvae depends on the density equivalent of each larva relative to the stratification of the water column and the vertical mixing coefficient, which vary both in time and space. This could be implemented by following the numerical recipe by Thygesen & Ådlandsvik (2007, this TS). Under strong mixing, larvae with similar state and risk sensitivity would then have a broader vertical distribution.

Another complicating factor we have ignored is the consequence to fitness of drifting off to unfavourable settlement habitats (Fiksen et al. 2007). Although little is known about what determines the quality of settlement areas, it might be possible to combine spatial data from 0-group surveys (Dingsør 2005) with data on later stages from winter cruises to derive information about how fitness depends on geographical position at settlement (Dingsør 2006).

Observations on vertical migration by cod larvae and the corresponding distribution patterns are limited, but those described in literature indicate that diel migration occurs, depending on larval size and oceanographic conditions (Ellertsen et al. 1984, Neilson & Perry 1990, Lough & Potter 1993). Lough & Potter (1993) reported that Atlantic cod larvae on Georges Bank of >6 mm length were capable of regulating their depth when vertical mixing was low. The ability to control their depth and the extent of diel migration increased with larval size, while the mean daily depth increased throughout ontogeny until they settled close to the seabed. Similarly, Ellertsen et al. (1984) observed diel migrations in first-feeding Northeast Artic cod larvae. The larvae concentrated between 5 and 10 m during the night and spread out between 5 and 35 m during the day. The strong interaction between vertical positioning and horizontal ocean transport documented in this study suggests that further field observations of vertical distribution and its change with ontogeny should be a priority of future surveys. If possible, parallel recordings of other individual characteristics in the field, such as stomach fullness, swimming direction and speed, and activity level, could also guide both the further development of models coupling behaviour with oceanography, as well as our understanding of the ecology of early life stages.

The current analysis must be viewed as an initial exploration and an example of how simple behavioural rules can be used in combination with ocean models to study the interaction between local and strategic trade-offs in larval fish behaviour. We have only looked at 2 potential spawning grounds, and strategies may be very different when drift trajectories from further spawning grounds are included. A complete analysis of behavioural strategies would therefore need to take the whole geographical spawning range into account. To evaluate the success of a strategy, one should also assess parental spawning strategies, including migration costs, and repeat the analysis with physical forcing for several years to investigate environmental effects.

This study illustrates how adaptive habitat selection under realistic assumptions of local vertical gradients of growth and predation risk interacts with horizontal advection of larval fish. It serves as an example of how behavioural ecology can provide methods to improve the predictive and explanatory power of individual-based models for larval fish and to develop a generic approach for other marine species with pelagic larval stages. The coupled larval IBM and ocean circulation model represents a virtual laboratory that can prime our intuition and develop our understanding of processes and their relative importance throughout ontogeny. We are confident that this undertaking will provide hypotheses and direct future field and experimental studies. More specifically, the model also suggests a set of robust behavioural rules for vertical migration of Northeast Arctic cod that can be implemented in coupled IBM and ocean models and explored in laboratory experiments.

Acknowledgements. This research was supported by the projects 'ECOBE' and 'Sustainable harvesting of marine resources', financed by the Research Council of Norway. Computer time for the hydrodynamical model was partly granted by NOTUR: the super-computing programme of the Research Council of Norway. NOAA-CIRES Climate Diagnostics Center, Boulder, Colorado, USA, provided data through the NCEP/NCAR reanalysis project (www.cdc.noaa.gov/). Thanks to S. Eliassen and T. Torgersen for discussions and comments.

LITERATURE CITED

Ådlandsvik B, Sundby S (1994) Modelling the transport of cod larvae from the Lofoten area. ICES Mar Sci Symp 198: 379–392

Aksnes DL, Giske J (1993) A theoretical model of aquatic visual feeding. Ecol Model 67:233–250

Aksnes DL, Utne ACW (1997) A revised model of visual range in fish. Sarsia 82:137–147

Bailey KM, Houde ED (1989) Predation on eggs and larvae of marine fishes and the recruitment problem. Adv Mar Biol 25:1–83

Clark CW, Mangel M (2000) Dynamic state variable models in ecology: methods and applications. Oxford University Press, New York

Clark DL, Leis JM, Hay AC, Trnski T (2005) Swimming ontogeny of larvae of four temperate marine fishes. Mar Ecol Prog Ser 292:287–300

Cowen RK, Paris CB, Srinivasan A (2006) Scaling connectivity in marine populations. Science 311:522–527

Dingsør GE (2005) Estimating abundance indices from the international 0-group fish survey in the Barents Sea. Fish Res 72:205–218

Dingsør GE (2006) Influence of spawning stock size and environment on abundance and survival of juveniles in commercially important fish stocks in the Barents Sea. PhD thesis, University of Bergen

Ellertsen B, Fossum P, Solemdal P, Sundby S, Tilseth S (1984) A case study on the distribution of cod larvae and availability of prey organisms in relation to physical processes in Lofoten. In: Dahl E, Danielssen D, Moksness E, Solemdal P (eds) The propagation of cod. Flødevigen Rapp 1:453–478

Engedahl H, Ådlandsvik B, Martinsen EA (1998) Production of monthly mean climatological archives of salinity, temperature, current and sea level for the Nordic Seas. J Mar Syst 14:1–26

Ezer T, Arango HG, Shchepetkin AF (2002) Developments in terrain-following ocean models: intercomparisons of numerical aspects. Ocean Model 4:249–267

Fiksen Ø (1997) Allocation patterns and diel vertical migration: modeling the optimal *Daphnia*. Ecology 78:1446–1456

Fiksen Ø, Folkvord A (1999) Modelling growth and ingestion processes in herring *Clupea harengus* larvae. Mar Ecol Prog Ser 184:273–289

Fiksen Ø, MacKenzie BR (2002) Process-based models of feeding and prey selection in larval fish. Mar Ecol Prog Ser 243:151–164

Fiksen Ø, Utne ACW, Aksnes DL, Eiane K, Helvik JV, Sundby S (1998) Modelling the influence of light, turbulence and ontogeny on ingestion rates in larval cod and herring. Fish Oceanogr 7:355–363

Fiksen Ø, Aksnes DL, Flyum MH, Giske J (2002) The influence of turbidity on growth and survival of fish larvae: a numerical analysis. Hydrobiologia 484:49–59

Fiksen Ø, Eliassen S, Titelman J (2005) Multiple predators in the pelagic: modelling behavioural cascades. J Anim Ecol 74:423–429

Fiksen Ø, Jørgensen C, Kristiansen T, Vikebø F, Huse G (2007) Linking behavioural ecology and oceanography: larval behaviour determines growth, mortality and dispersal. Mar Ecol Prog Ser 347:195–205

Finn RN, Rønnestad I, van der Meeren T, Fyhn HJ (2002) Fuel and metabolic scaling during the early life stages of Atlantic cod *Gadus morhua*. Mar Ecol Prog Ser 243:217–234

Folkvord A (2005) Comparison of size-at-age of larval Atlantic cod (*Gadus morhua*) from different populations based on size- and temperature-dependent growth models. Can J Fish Aquat Sci 62:1037–1052

Fox CJ, McCloghrie P, Young EF, Nash RDM (2006) The importance of individual behaviour for successful settlement of juvenile plaice (*Pleuronectes platessa* L.): a modelling and field study in the eastern Irish Sea. Fish Oceanogr 15:301–313

Giske J, Mangel M, Jakobsen P, Huse G, Wilcox C, Strand E (2003) Explicit trade-off rules in proximate adaptive agents. Evol Ecol Res 5:835–865

Grimm V, Railsback S (2005) Individual based modeling and ecology. Princeton University Press, Princeton, NJ

Hinckley S, Hermann AJ, Megrey BA (1996) Development of a spatially explicit, individual-based model of marine fish early life history. Mar Ecol Prog Ser 139:47–68

Hinckley S, Hermann AJ, Mier KL, Megrey BA (2001) Importance of spawning location and timing to successful transport to nursery areas: a simulation study of Gulf of Alaska walleye pollock. ICES J Mar Sci 58:1042–1052

Hinrichsen HH, Möllmann C, Voss R, Köster FW, Kornilovs G (2002) Biophysical modeling of larval Baltic cod (*Gadus morhua*) growth and survival. Can J Fish Aquat Sci 59: 1858–1873

Houston A, McNamara J (1999) Models of adaptive behaviour. Cambridge University Press, Cambridge

Huggett J, Fréon P, Mullon C, Penven P (2003) Modelling the transport success of anchovy *Engraulis encrasicolus* eggs and larvae in the southern Benguela: the effect of spatio-temporal spawning patterns. Mar Ecol Prog Ser 250: 247–262

Huse G (2001) Modelling habitat choice in fish using adapted random walk. Sarsia 86:477–483

Kalnay E, Kanamitsu M, Kistler R, Collins W and 18 others (1996) The NCEP/NCAR 40-year reanalysis project. Bull Am Meteorol Soc 77:437–471

Kjesbu OS, Solemdal P, Bratland P, Fonn M (1996) Variation in annual egg production in individual captive Atlantic cod (*Gadus morhua*). Can J Fish Aquat Sci 53:610–620

Köster FW, Möllmann C (2000) Trophodynamic control by clupeid predators on recruitment success in Baltic cod? ICES J Mar Sci 57:310–323

Kristiansen T, Fiksen Ø, Folkvord A (2007) Modelling feeding, growth and habitat selection in larval cod: observations and model predictions in a macrocosm environment. Can J Fish Aquat Sci 64:136–151

Leis JM, Hay AC, Trnski T (2006) *In situ* ontogeny of behaviour in pelagic larvae of three temperate, marine, demersal fishes. Mar Biol 148:655–669

Lough RG, Potter DC (1993) Vertical distribution patterns and diel migrations of larval and juvenile haddock *Melanogrammus aeglefinus* and Atlantic cod *Gadus morhua* on Georges Bank. Fish Bull 911:281–303

McGurk MD (1986) Natural mortality of marine pelagic fish eggs and larvae: role of spatial patchiness. Mar Ecol Prog Ser 34:227–242

Mullon C, Cury P, Penven P (2002) Evolutionary individual-based model for the recruitment of anchovy (*Engraulis capensis*) in the southern Benguela. Can J Fish Aquat Sci 59:910–922

Neilson JD, Perry RI (1990) Diel vertical migrations of marine fishes—an obligate or facultative process. Adv Mar Biol 26:115–168

Otterlei E, Nyhammer G, Folkvord A, Stefansson SO (1999) Temperature- and size-dependent growth of larval and early juvenile Atlantic cod (*Gadus morhua*): a comparative study of Norwegian coastal cod and northeast Arctic cod. Can J Fish Aquat Sci 56:2099–2111

Persson L, De Roos AM (2003) Adaptive habitat use in size-structured populations: linking individual behavior to population processes. Ecology 84:1129–1139

Ramsden D, Holloway G (1991) Timestepping Lagrangian particles in two dimensional Eulerian flow fields. J Comput Phys 95:101–116

Santos AMP, Re P, Dos Santos A, Peliz A (2006) Vertical distribution of the European sardine (*Sardina pilchardus*) larvae and its implications for their survival. J Plankton Res 28:523–532

Shchepetkin AF, McWilliams JC (2003) A method for computing horizontal pressure-gradient force in an oceanic model with a non-aligned vertical. J Geophys Res 108: 1–34

Shchepetkin AF, McWilliams JC (2005) The regional oceanic modeling system (ROMS): a split-explicit, free-surface, topography-following-coordinate oceanic model. Ocean Model 9:347–404

Skartveit A, Olseth JA (1988) Varighetstabeller for timevis belysning mot 5 flater på 16 norske stasjoner. University of Bergen

Strand E, Huse G, Giske J (2002) Artificial evolution of life history and behavior. Am Nat 159:624–644

Sundby S (1997) Turbulence and ichthyoplankton: influence on vertical distributions and encounter rates. Sci Mar 61: 159–176

Sundby S, Bjørke H, Soldal AV, Olsen S (1989) Mortality rates during the early life stages and year class strength of the North-East Arctic cod (*Gadus morhua* L.). Rapp P-V Reun Cons Int Explor Mer 191:351–358

Swain DP, Sinclair AF (2000) Pelagic fishes and the cod recruitment dilemma in the Northwest Atlantic. Can J Fish Aquat Sci 57:1321–1325

Tilseth S, Ellertsen B (1984) The detection and distribution of larval Arcto-Norwegian cod, *Gadus morhua*, food organisms by an *in situ* particle counter. Fish Bull 82:141–156

Thygesen UH, Ådlandsvik B (2007) Simulating vertical turbulent dispersal with finite volumes and binned random walks. Mar Ecol Prog Ser 347:145–153

Vikebø F, Sundby S, Ådlandsvik B, Fiksen Ø (2005) The combined effect of transport and temperature on distribution and growth of larvae and pelagic juveniles of Arcto-Norwegian cod. ICES J Mar Sci 62:1375–1386

Werner FE, Perry RI, Lough RG, Naimie CE (1996) Trophodynamic and advective influences on Georges Bank larval cod and haddock. Deep-Sea Res II 43:1793–1822

Werner FE, Quinlan JA, Lough RG, Lynch DR (2001) Spatially-explicit individual based modeling of marine populations: a review of the advances in the 1990s. Sarsia 86:411–421

Editorial responsibility: Alejandro Gallego (Contributing Editor), Aberdeen, UK

Submitted: July 20, 2006; Accepted: April 30, 2007
Proofs received from author(s): September 5, 2007

Vol. 347: 221–232, 2007
doi: 10.3354/meps06980

MARINE ECOLOGY PROGRESS SERIES
Mar Ecol Prog Ser

Published October 11

OPEN ACCESS

Hydrodynamic backtracking of fish larvae by individual-based modelling

Asbjørn Christensen[1,*], Ute Daewel[2], Henrik Jensen[1], Henrik Mosegaard[1], Mike St. John[2], Corinna Schrum[1,3]

[1]Danish Institute of Fisheries Research (DIFRES), Charlottenlund Slot, 2920 Charlottenlund, Denmark
[2]Institute for Hydrobiology und Fisheries Science, Hamburg University, Olbersweg 24, 22767 Hamburg, Germany
[3]Geophysical Institute, University of Bergen, Allégaten 70, 5007 Bergen, Norway

ABSTRACT: We discuss methodological and implementation issues of spatial, temporal and combined spatio-temporal backtracking and illustrate larval backtracking for North Sea lesser sandeel *Ammodytes marinus* larvae, using a combined hydrodynamical and individual-based model. It was found that dispersal effects are important for larval backtracking predictions. Our results show large differences in average transport distance, as well as in shape and extent of predicted hatch areas, when backtracking advected larval cohorts in different regions of the North Sea, thus emphasizing the importance of using realistic, spatially and temporally resolved diffusivity fields in simulations of larval transport. In all cases, biologically likely hatching areas have been predicted. We discuss issues of methodological consistency and present a new scheme for including life-history stochasticity effects on growth in backtracking in a consistent way, as well as procedures for assessing the effects of larval mortality. Finally, fundamental limitations of larval backtracking are clarified, most importantly the time horizon and spatial resolution limit for backward prediction.

KEY WORDS: Individual-based modelling · Backtracking · Larval transport · Inverse stochastic methods · Hatch area identification

INTRODUCTION

Backtracking fish larvae is a potentially powerful tool for understanding early life-history aspects quantitatively. Backtracking may be performed either explicitly in space and time or just in time—in the latter case with implicit spatial assumptions about the environmental parameters affecting larval growth and behaviour. The goal of spatial backtracking is mapping hatching areas with high resolution, to understand conditions for survival (or larval excess mortality) and thereby develop minimal conceptual models of recruitment, based on key processes. Also, optimizing the design of closed marine habitats with respect to habitat definition and closure time is a potential application of backtracking.

Backtracking can also be used as an efficient biological parameter estimation tool, which may supplement forward tracking of larvae; the biological parameters of a larval tracking model should be fitted so that a simulation develops larvae into juveniles at the right area and time. If our knowledge on juveniles is more precise than on newly hatched larvae, it may require less trajectory simulations to backtrack from juveniles (because more trajectories will be successful). Additionally, biological parameter sensitivity may be different in backtracking, compared to forward tracking.

While backtracking is frequently used in other fields like pure computer sciences (Dechter & Frost 2002), atmospheric sciences (Uliasz & Pielke 1991) and pollution tracing (Spivakovskaya et al. 2005), larval/zooplankton backtracking is still at a premature stage, seen from a methodological point of view. However, recently Batchelder (2006) applied a backtracking scheme to planktonic organisms in a coastal geometry and advocated backtracking as a tool for identifying

*Email: asc@difres.dk

hatching sites. We go one step further and consider growth backtracking as well in a fully realistic hydrodynamic setup. Compared to passive particles, larvae have ontogenetic development as well as active behaviour, which complicates backtracking, due to the stochastic and nonlinear nature of these processes.

At first sight, the issue of tracing backwards the state of a larval sample in time appears simple: just advect larvae in a direction opposite the currents and shrink their size by the same amount as their growth, if time is running forward (Pedersen et al. 2000, Allain 2004); however, dispersion processes are present in the ocean and must be considered, as we will show later, because otherwise we have no information on the error margin in results and further simple backtracking opposite current lines may contain an error bias, since dispersion processes in the ocean are not spatially uniform. Batchelder (2006) similarly found that diffusion cannot be ignored in backtracking. Alternatively, larval origin might be estimated by a forward approach by releasing a vast number of particles in a forward simulation at potential spawning grounds and focussing on the small number that arrives in the area of interest (Allain et al. 2003). While it is straightforward and circumvents some of the methodological issues of backtracking, forward tracking remains inefficient for spawning-ground identification because the majority of particle trajectories are useless (they end up at a position different from the area of interest). This is especially true if arrival in the area of interest is a rare event (e.g. if the final area is small or the drift time is long); this point was also emphasized by Batchelder (2006). Further, backtracking may potentially point to unexpected spawning sites, whereas forward tracking has less room for surprises because potential spawning grounds are input to the simulation.

The aim of the present paper is to advocate larval backtracking as part of a testing suite of hydrodynamical individual-based models (IBM) for larvae, both as a submodel screening and validation device, as well as a result-generating method, and to clarify the formal basis of backtracking with focus on providing tools for consistent backtracking and identifying limitations of backtracking. The latter aspect is very important, because inverse problems often have no unique solution.

BIOLOGICAL AND PHYSICAL MODEL

In Lagrangian transport simulations, the positions ($s_i[t]$) of an ensemble of tracers $i = 1 \ldots N$ are monitored as a function of time t, along with the state variables ($L_i[t]$) of the tracers. This ensemble represents the fish larvae, with their length L_i as state variable, in our case. Each larva in the ensemble is propagated from time t to $t + dt$ by the dynamical equations:

$$\mathrm{d}L_i = G(L_i, s_i, t)\mathrm{d}t \quad (1)$$

$$\mathrm{d}s_i = [u(s_i,t) + a(s_i, L_i, t)]\mathrm{d}t + \mathrm{d}\Omega(s_i, t, \mathrm{d}t) \quad (2)$$

$$\mathrm{d}\Omega(s_i, t, \mathrm{d}t) = \nabla K(s_i, t)\mathrm{d}t + \sqrt{2K[s_i + \tfrac{1}{2}\nabla K(s_i,t)\mathrm{d}t, t]}\,W(\mathrm{d}t) \quad (3)$$

where $\mathrm{d}t$ is a small positive time increment. Eq. (1) describes the larval growth $L_i \rightarrow L_i + \mathrm{d}L_i$, which depends on larval size, position and time in season through a deterministic relation G. It is also possible to model G as a stochastic relation; we will return to this in section 'Growth stochasticity'. Eq. (2) describes the larval transport $s_i \rightarrow s_i + ds_i$, where $u(s_i,t)$ is the smooth advective field derived by linear interpolation in grid-resolved currents, obtained from the hydrodynamical model described below, and $\mathrm{d}\Omega$ is a random walk process modelling the effect of local turbulent fluctuations (Visser 1997). The active larval motion velocity is $a(s_i, L_i, t)$, including possibly buoyant velocity. In Eq. (3) $\mathrm{d}\Omega$ is controlled by the local diffusivity field $K(s_i,t)$, and $W(\mathrm{d}t)$ is a stochastic process with $\langle W(\mathrm{d}t)\rangle = 0$ and $\langle W(\mathrm{d}t)^2\rangle = \mathrm{d}t$, where $\langle\,\rangle$ indicates time average. Because of this, the limit $\mathrm{d}\Omega / dt$ does not exist, and Eqs. (1) to (3) cannot be stated as ordinary partial differential equations, but are kept in Itô form (Rogers & Williams 1987) as above. In Cartesian coordinates, the local diffusivity field is a vector $K = (K_x, K_y, K_z)$, and the gradient diagonal is $\nabla K = (\mathrm{d}K_x/\mathrm{d}x, \mathrm{d}K_y/\mathrm{d}y, \mathrm{d}K_z/\mathrm{d}z)$. The spatial distribution of an ensemble of larvae moving by Eq. (2) can also be described by the physics diffusion equation with local diffusivity K (Taylor 1921, Visser 1997), and equivalent results are obtained generally if consistent dynamical equations are used and the Lagrangian ensemble size is sufficiently large. The local diffusivity field K describes subgrid advective processes, like turbulence, in a statistical sense. Eqs. (1 to 3) describe virtual larval trajectories, i.e. without mortality. We return to mortality aspects in the section 'Discussion'.

Forward time model. A flexible, spatially explicit lesser sandeel *Ammodytes marinus* IBM has been developed on the basis of the ECOSMO (ECOSystem MOdel) framework (Schrum & Backhaus 1999, Hochbaum 2004, Schrum et al. 2006). The ECOSMO hydrodynamic model setup has been validated in detail against available observations (Janssen et al. 2001, Janssen 2002). In the present work, a biological model of the early larval life-stages of the lesser sandeel has been added, based on the underlying biophysical processes. The setup is shown in Fig. 1.

The hydrodynamic part of the ECOSMO model is based on a staggered Arakawa C-grid with a 5 nm horizontal resolution, free surface and 5 m layers down to a depth of 40 m (and 8 m layers below 40 m depth).

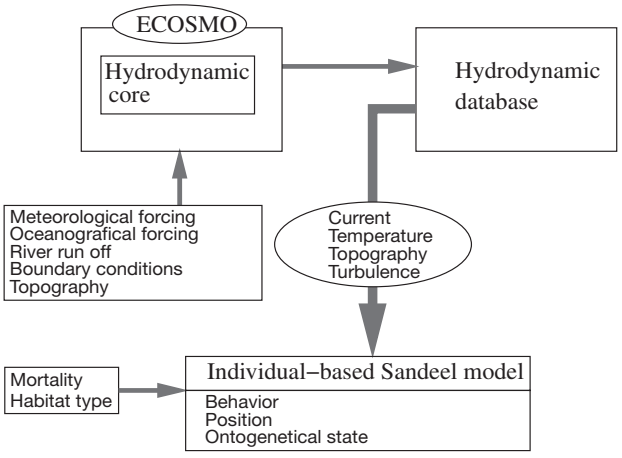

Fig. 1. Coupled 3-dimensional biophysical model. ECOSMO: ECOSystem MOdel

A database (Schrum et al. 2003) of 3-dimensional physical fields from the ECOSMO model—currents $u(s,t)$, temperature $T(s,t)$ and vertical local diffusivity $K_z(s,t)$—has been stored as daily averaged fields (for data compression purposes), and these fields are used for the IBM simulations. $K_z(s,t)$ is parameterized using an analytical k-ϵ approach, considering counteracting effects of local shear and stratification (Schrum 1997).

In the present work, we include no explicit active vertical/horizontal migratory behaviour, i.e. $a = 0$ in Eq. (2). This is a good approximation during night time, but during light hours there is a predominance of larvae in the water layers with high zooplankton abundance (Jensen et al. 2003). However, until the vertical behaviour has been accurately quantified for lesser sandeel, we will use $a = 0$.

Horizontally, the larvae are described as passive floaters. Only vertical turbulent dispersal is taken into account, i.e. $K = (0, 0, K_z)$, and $d\Omega$ is a vertical vector, since the dominant horizontal dispersal mechanism in the North Sea is vertical turbulent diffusion, coupled to current layer shear (Zimmerman 1986, Van Dam et al. 1999). As larvae hatch and are advected, they disperse relative to each other. Within the dispersed patch—which is on a scale of kilometres—there may be small-scale patchiness, due to larval schooling behaviour and subscale environmental patchiness. We will not consider these additional small-scale variations in the larval spatial distribution in this work, but rather concentrate on the kilometre-scale features in transport and dispersal of larval patches from the same area.

The larval population is mathematically sampled by a set of representative tracers (a virtual population), each of which represents a constant number of individuals (the ratio of real physical larvae per tracer needs not be stipulated, since density effects are not addressed explicitly in the present study, only relative numbers matter). The boundary condition $dK_z(s,t)/dz = 0$ along with tracer reflection is imposed vertically at the surface and bottom to avoid artificial aggregation of tracers at the surface or bottom of the water column. The vertical random walk of Eq. (3) is implemented as $W(dt) = \omega\sqrt{3dt}$, where ω is a uniform random distribution on [–1, 1], corresponding to $\langle W(dt)^2\rangle = dt$, so that local jump amplitudes reproduce local Eulerian field dispersal rates correctly, i.e. proportional to the square root of the local diffusivity $K(s,t)$ (Taylor 1921, Maier-Reimer 1973, Hunter et al. 1993).

The Lagrangian simulations were performed with a time step $dt = 30$ min, using Euler forward integration. In the section 'Spatial and temporal backtracking' we will show that higher order horizontal integration schemes change tracer trajectories negligibly for $dt = 30$ min, i.e. trajectories are appropriately integrated numerically with $dt = 30$ min, when using current fields averaged over tidal periods. Longer time steps in conjunction with higher order horizontal trajectory integration were not attempted, since this would imply large vertical jumps in the stochastic modelling of turbulent dispersal (Eq. 3).

The larval growth model in Eq. (1) is parameterized to the functional form:

$$G(L,T) = \lambda(T)\left(\frac{L}{L_0}\right)^{\gamma}\left(1-\frac{L}{L_\infty}\right) \quad (4)$$

where $T = T(s,t)$ is the local temperature experienced by each larva. The data set used for parameterization is North Sea length-at-age samples for *Ammodytes marinus* obtained by MIK trawl data from the years 1995 and 1996 (pooled together) (Jensen 2001). Larval ages were obtained by otolith analysis (Jensen 2001). The temperature modulation $\lambda(T)$ is approximated by a quadratic polynomial:

$$\lambda(T) = a_0 + a_1 T + a_2 T^2 \quad (5)$$

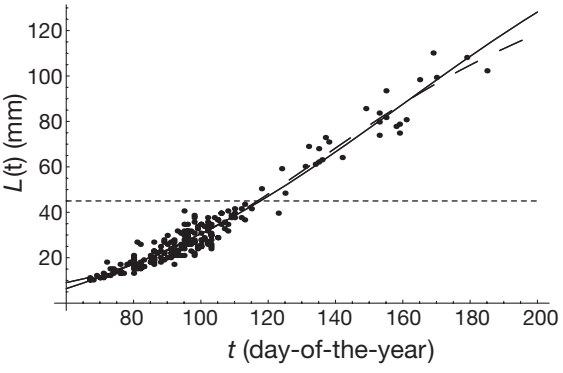

Fig. 2. Pooled length-age data (points) used for parameterizing the lesser sandeel *Ammodytes marinus* growth model. The horizontal line at $L_m = 45$ mm corresponds to the approximate length at metamorphosis. Continuous line: Model v1; dashed line: Model b1, see Table 1

In Fig. 2, we show the data and model fits, based on analytical integration of Eqs. (1) and (4), including the North Sea average seasonal temperature variation. It is important to include the average seasonal temperature variation in the parameter estimation process, since the average temperature rises from around 5°C at hatching time to around 12 to 14°C at the time when metamorphosis is complete ($L_m \approx 45$ mm) (Wright & Bailey 1996, Jensen 2001); otherwise, model forward simulation will not reproduce the growth pattern in Fig. 2. It appeared difficult to simultaneously resolve $\lambda(T)$ and the length scaling exponent γ, because the seasonal temperature variation and larval length are strongly correlated in the data set. There is a shallow residual minimum in the fit at $\gamma \approx 0.96$, but fits constrained to $\gamma = 0$ (Model v) or $\gamma = 1$ (Model b) produce essentially equally good fits for 0-group sandeels, as shown in Fig. 2. The parameters of the respective fits are given in Table 1, along with the estimated hatch lengths L_0, all of which are consistent with observations (Winslade 1971, Smigielskiet al. 1984) of $L_0 \approx 5$ to 7 mm. We use $L_\infty = 218$ mm (Macer 1966), which is not included as a free parameter when fitting data in Fig. 2, since it is of minor importance for larval growth (since $L_m \ll L_\infty$) and because the data set only has observations for $L \ll L_\infty$ (but L_∞ adds a little concavity to the growth curve).

Table 1. Parameters for the alternative sandeel *Ammodytes marinus* growth models. The fitting residual is normalized as $\rho = \sqrt{(1/M)\,\Sigma_{i=1}^{M}[L^{\mu}(t_i) - L_i]^2}$, where $(L_i, t_i)_{i=1\ldots M}$ is the length-age data set and $L^{\mu}(t)$ is the growth curve for Model μ

Model μ	γ	L_0 (mm)	a_0 (mm d^{-1})	a_1 (mm d^{-1} °C^{-1})	a_2 (mm d^{-1} °C^{-2})	ρ (mm)
v1	0	6.40	−0.354	0.167	0	10.8
v2	0	8.91	−1.81	0.515	−0.0196	11.9
b1	1	9.05	0.422	−0.0205	0	12.0
b2	1	9.15	0.401	−0.0153	−0.000272	12.1

From Fig. 2, it is seen that seasonal temperature variation is a surprisingly good proxy for the complex bioenergetic effects (spectrum, abundance and distribution of food, as well as complex food-switching patterns) (Letcher et al. 1996, Baron 2004). The quantitative growth predicted by Eq. (4), as parameterized here, is in good quantitative agreement with that presented recently by Gallego et al. (2004). Since the model parameterizes *in situ* data, it also integrates prey dependence on temperature variations, at a crude level. Currently, the model does not address density effects (e.g. food competition and cannibalism) explicitly, although they are believed to affect recruitment (Daan et al. 1990, Kishi et al. 1991, Kimura et al. 1992, Arnott & Ruxton 2002). There are also indications that population density effects may affect individual sandeel growth, currently reported for sandeel populations in the North Sea (Bergstad et al. 2002) and Ise Bay (Nagoshi & Sano 1979), but the influence has not yet been sufficiently quantified for larval stages.

Reversed time model. Let us start at the heart of the problem, which is shown in Fig. 3. Fig. 3a illustrates the familiar forward time modelling situation, where a larval patch (grey area) is traced from the hatching area to Patch J at a later time (which could symbolize the distribution of juvenile larvae). The larval patch increases in spatial extent, as the patch is advected along current lines, due to spatial dispersive processes. If we now catch a portion of the larvae in Patch J and consult the model as to where they came from, many people anticipate the situation in Fig. 3b: the model, when 'run backwards', should converge to the hatch area, where the forward simulation started from. We call this *inverse time* simulation. Since the Fourier spectrum of inverse time dispersion diverges for small spatial scales, the inverse time simulation is not numerically stable (Hadamard 1923). The physical meaning of this is that forward time diffusion quickly dissipates fine-scale features, while inverse time simulations enhances them. We want to calculate the initial distribution leading to a given final distribution

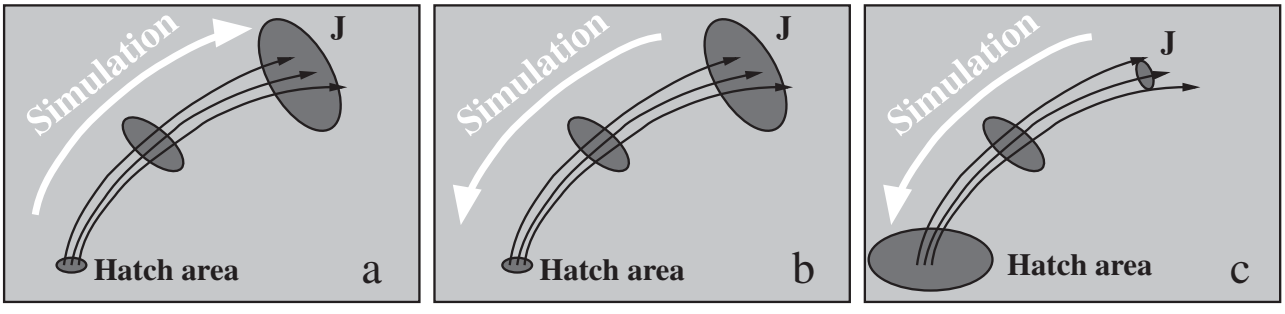

Fig. 3. Different types of hydrodynamical simulations. Black arrows: current steam lines. (a) Normal forward time simulation of a larval patch (grey area), starting from the hatch area with larvae and ending with a juvenile distribution at J. (b) Inverse time - simulation of a larval patch (grey area), starting from a juvenile sample at J. (c) Reversed time simulation of a larval patch (grey area), starting from a juvenile sample at J

of larvae in a statistical sense; this is called *reverse time* simulation (Fig. 3c). The major difference, compared to inverse time simulation in Fig. 3b, is that the larval patch will disperse in space when traced backwards in time. The point is that dispersive (and generally stochastic) processes delete knowledge on initial state when time progresses, and therefore the uncertainty of the larval origin also increases when they are traced back in time. In other words, given a larva in a specific place and state, we can only give a spatial probability distribution of places where it is likely to have hatched because it can end up in a specific place and state along many different life-history paths, when dispersive (and generally stochastic) effects are present in the model. This limitation is fundamental and insurmountable, and has important consequences. First, if we neglect spatial dispersive processes (if this is possible) and just backtrack along current lines, we will end up at a point somewhere in the hatch area distribution in Fig. 3c, but we have no guarantee that the point is at the centre of the hatch area distribution (and it will not be at the centre, when the dispersive processes have spatial gradients, which is usually the case), and we have no idea about the characteristic size of the hatch area distribution. Secondly, it implies a characteristic past time horizon, beyond which we will not be able to backtrack because the possible starting places cover all possible spawning areas. We will return to this issue in the section 'Discussion'.

Having now established that reversed time simulation is the appropriate methodology to identify hatch areas/hatch schedule probability distributions from a given larval catch, we will focus on reversed time simulation in the rest of this paper. We also note that probability distributions are obtained from larval ensemble trajectories by any standard smoothing technique. The spatial extent of larval distributions are obtained either from form parameters of the smooth distributions fitting larval ensemble positions, or by identifying areas where probabilities are larger than a given tolerance level. All qualitative conclusions below are unaffected by these technical steps and choices. Formally, Eqs. (1) to (3) cover 2 process classes: deterministic advection processes (by fields G, u, a) and local dispersal $d\Omega$. Both these process classes are unambiguously reversible: deterministic advection terms change sign, whereas local dispersal $d\Omega$ keeps its sign. This is due to the fact that random walk processes are fundamentally time reversible: it is impossible to judge whether the clock runs forward or backward from a random walk trajectory $s(t)$ in a stationary (or slowly varying) diffusivity field; more directly, $s(t)$ and $s(-t)$ are equally likely. Further, since the stationary state of a dispersive process is spatially uniform, the backward dynamics dispersion amplitude corresponds to the forward dispersion amplitude K. In other words, $d\Omega$ is formally invariant under time reversal. Hence, each larva in the ensemble is propagated from time t to $t - dt$ by the dynamical equations:

$$dL_i = -G(L_i, s_i, t)dt \quad (6)$$

$$ds_i = -[u(s_i,t) + a(s_i, L_i, t)]dt + d\Omega(s_i, t, dt) \quad (7)$$

$$d\Omega(s_i, t, dt) = \nabla K(s_i,t)dt + \sqrt{2K[s_i + \tfrac{1}{2}\nabla K(s_i,t)dt, t]}W(dt) \quad (8)$$

where $dt > 0$ is a small time step backward. We note that Eqs. (6) to (8) are the consistent way of running the forward model, Eqs. (1) to (3), backwards. When any aspect of the forward model is changed, the corresponding change must be performed in the reversed time model. In the section 'Growth stochasticity' we will discuss the impact and complications on backtracking, arising when G in Eq. (6) is generalized to a stochastic function reflecting life-history stochasticity.

As an implementation remark, we note that reverse time particle tracking is most simply performed offline, i.e. current fields, temperature, turbulent diffusivity, salinity, etc., are taken from a precalculated database, generated by running a hydrodynamical setup forward in time covering the period of interest. It is possible to run a hydrodynamical model backward in time as well, using adjoined primitive equations (Griffin & Thompson 1996). This avoids large amounts of storage data transfer, but may be more CPU intensive, depending on the hydrodynamical resolution. However, many realistic, operational hydrodynamic setups do not offer this advanced feature.

Apart from this, implementation of Eqs. (6) to (8) is a straightforward modification of the implementation of Eqs. (1) to (3): they are solved by trajectory integration backward in time, exactly like Eqs. (1) to (3) are used forward in time.

SPATIAL AND TEMPORAL BACKTRACKING

To illustrate the approach, we perform backtracking of 3 representative samples of larvae caught at different locations in the North Sea in 2001 (LIFECO 2004). The catch samples are summarized in Table 2.

Table 2. Catch data for 3 representative larval samples used for spatial backtracking examples. ⟨⟩ indicates spatial average; σ indicates root mean square

Sample	Catch date (2001)	Catch position	Catch statistics ⟨L⟩ (mm)	σ(L) (mm)	⟨age⟩ (d)
1	22 April	56.66° N, 6.66° E	18.2	1.6	23
2	27 April	55.68° N, 7.00° E	19.9	1.1	33
3	25 May	57.15° N, 8.01° E	22.0	1.0	32

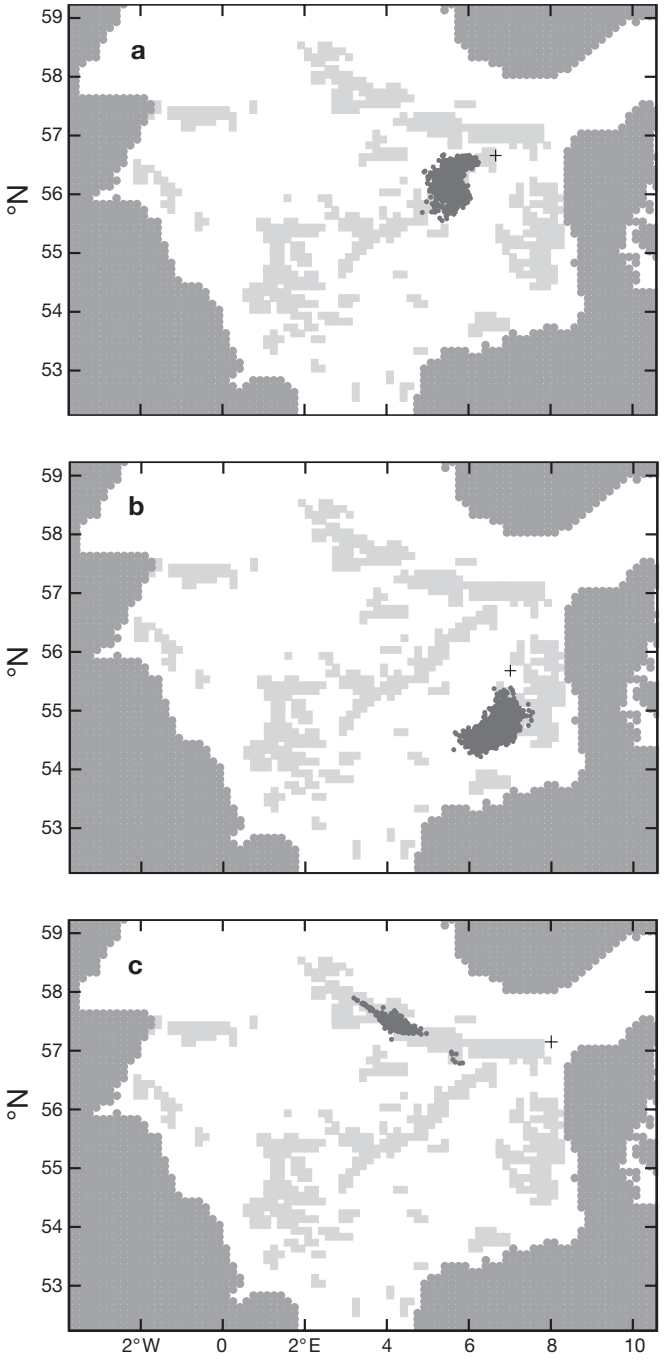

Fig. 4. Backtracking of larval samples in Table 2—(a), (b) and (c) are Samples 1, 2 and 3 respectively—using biological Model v1. Grey: land; light grey: sand banks suitable for sandeel *Ammodytes marinus* habitats; +: larval catch position; small, dark grey circles: backtracked larval ensemble positions that indicate potential hatch positions

In Fig. 4, we show the results of backtracking the larval samples in Table 2. Fig. 4 shows larval catch position, along with the spatial hatch probability distribution. The ensembles have been initialized at the catch position at catch time with normal length distribution, with form parameters from Table 2, and traced backward, until they have a hatch length of $L = L_0$, using growth Model v1. The figures are overlaid with identified sandeel *Ammodytes marinus* fishing banks, as obtained from detailed fishery loggings (Jensen & Rolev 2004). Habitat data have been projected onto the hydrodynamic grid, so that length-scale features below approximately 10 km are not resolved. It is assumed that larvae must originate from some of these sand banks, as sandeel spawn demersal eggs within their habitats (Reay 1970). Each ensemble size in Fig. 4 contains 2000 individuals, in order to roughly map the spatial hatch probability distribution.

Sample 1 was caught at the eastern tip of the central bank system and was under influence of the cyclonic North Sea circulation system, which, in this area, normally results in northeasterly transport. The sample was traced back to the eastern central bank system around the 'tail end' fishing area (approximately 56° N, 5.5° E), i.e. retained in the same major bank system. Sample 2 was advected along the northward Jutland coastal current, and was traced back to the south-western part of the Jutland sand bank system (approximately 54.5° N, 7° E). Sample 3 was under the influence of Norwegian trench inflow and could be traced back to the middle of the northern major sandeel bank system, around the 'Klondyke' fishing area, approximately 200 km west of catch position.

Comparing the 3 examples, we see prominent differences in the shape and extent of the predicted spatial hatch probability distributions, and also a clear difference in the advection distance, i.e. distance between the most likely hatch position and catch location. This puts clear emphasis on the necessity of explicitly including realistic advection, $u(s,t)$, and dispersal fields, $K(s,t)$, when backtracking larval ensembles. In all considered cases, the hatch probability distribution has a significant overlap with a sand bank system suitable for sandeel habitat (Jensen & Rolev 2004).

We illustrate the sensitivity of backtracked distributions by varying the backtracking model parameters for Sample 2 in Table 2. The central parameters are the horizontal integration time step dt and the growth model coefficients displayed in Table 1. The influence on backtracked larval positions is shown in Fig. 5. Comparing Fig. 5a and b, we see that the effect of changing the horizontal trajectory integration algorithm from Euler to Runge-Kutta 2nd order (Press et al. 1992) (with the same time step) is negligible. If tidal current fluctuation were not averaged out, Euler trajectory integration would display much larger errors for the same time step, due to the rotating nature and high amplitudes of tidal current fluctuation in the North Sea. Comparing Fig. 5a and c, we note the effect of using a quadratic temperature modulation $\lambda(T)$

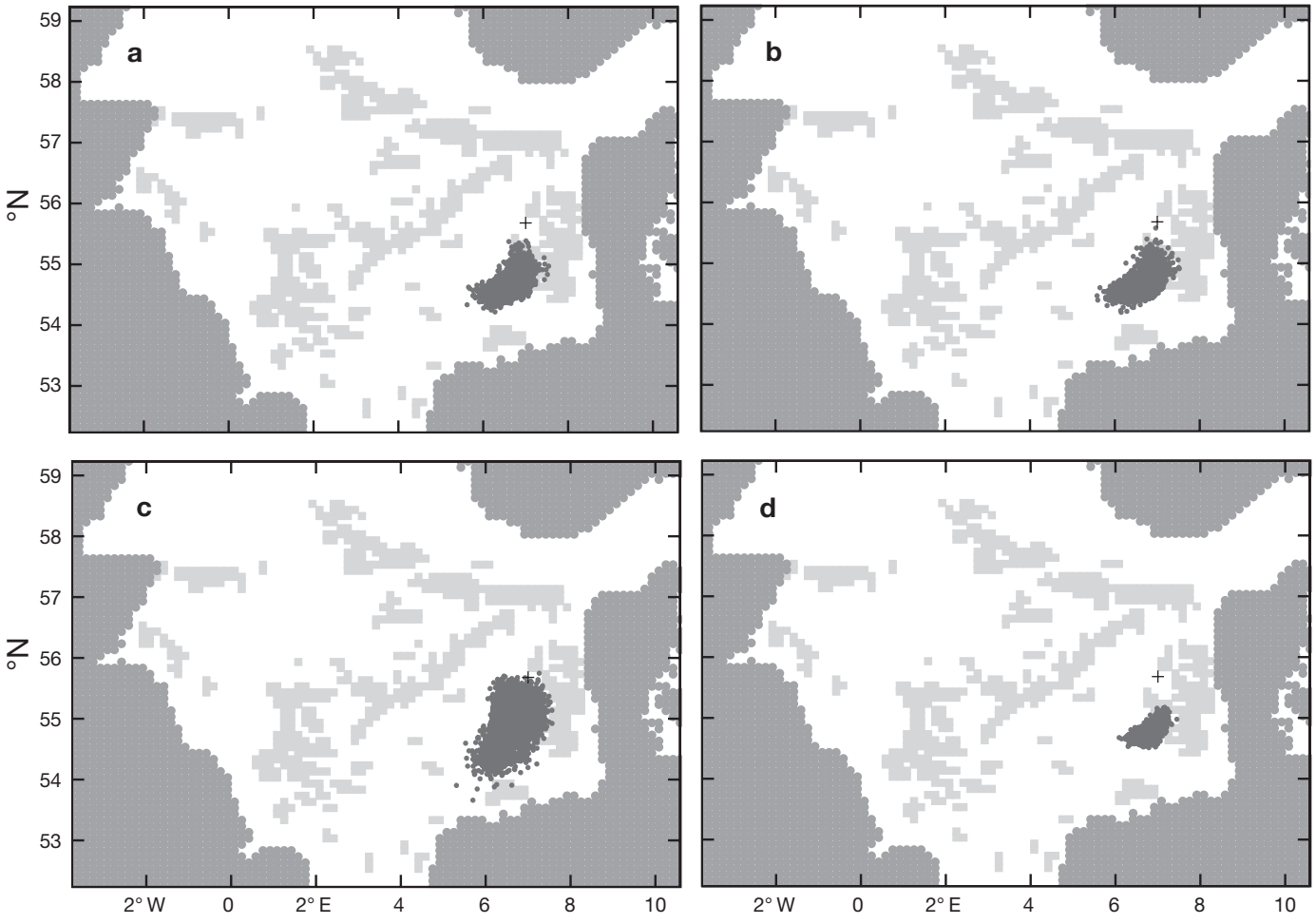

Fig. 5. Sensitivity test on model parameters, shown for backtracking of larval Sample 2 in Table 2. Grey: land; light grey: sand banks suitable for sandeel *Ammodytes marinus* habitats; +: larval catch position; small, dark grey circles: backtracked larval ensemble positions. Biological models/tracing algorithms are (a) v1/Euler, (b) v1/Runge-Kutta 2nd order, (c) v2/Euler and (d) b1/Euler

(Model v2) instead of a linear temperature modulation (Model v1): the predicted hatch areas are similarly centred, but the dispersal is significantly larger. Finally, comparing Fig. 5a and d, we see the effect of using a length-scaling exponent $\gamma = 1$ (Model b1) instead of $\gamma = 0$ (Model v1). Again, the predicted hatch centres are the same, but the dispersal is somewhat smaller. Generally, we predict approximately the same hatch centres for all models, but with some fluctuation in dispersal. There is no systematic bias in dispersal patterns, when comparing models over a larger test set (data not shown). Generally, we find that the effect of changing the horizontal trajectory integration algorithm from Euler to Runge-Kutta 2nd order is negligible.

The representative parameter sensitivity was displayed in Fig. 5; however, under certain hydrographic conditions a larger sensitivity is encountered. The most extreme case in our study is shown in Fig. 6, Sample 3 using Model v1 versus Model b1. In this case, there is an exceptionally large offset between predicted hatch areas, of the order of 100 km, but both are within the same major bank system. This is the largest variation found, and we stress that this case is isolated; the normal variability picture is as illustrated in Fig. 5. However, these isolated cases can also be very useful because they provide a clear prediction for validating specific models, when additional data are present for comparison. Unfortunately, we do not have data to ground truth larvae in Samples 1 to 3 by secondary means.

Until now we have focused on the spatial performance of backtracking. It is also interesting to assess the aptness in the temporal domain. Fig. 7 shows the hatch time distributions from backtracking the larval samples described in Table 2, where the spatial and temporal variability of the local physical environment has been included, i.e. the hatch time distributions for Model v1 correspond to the spatial distributions in

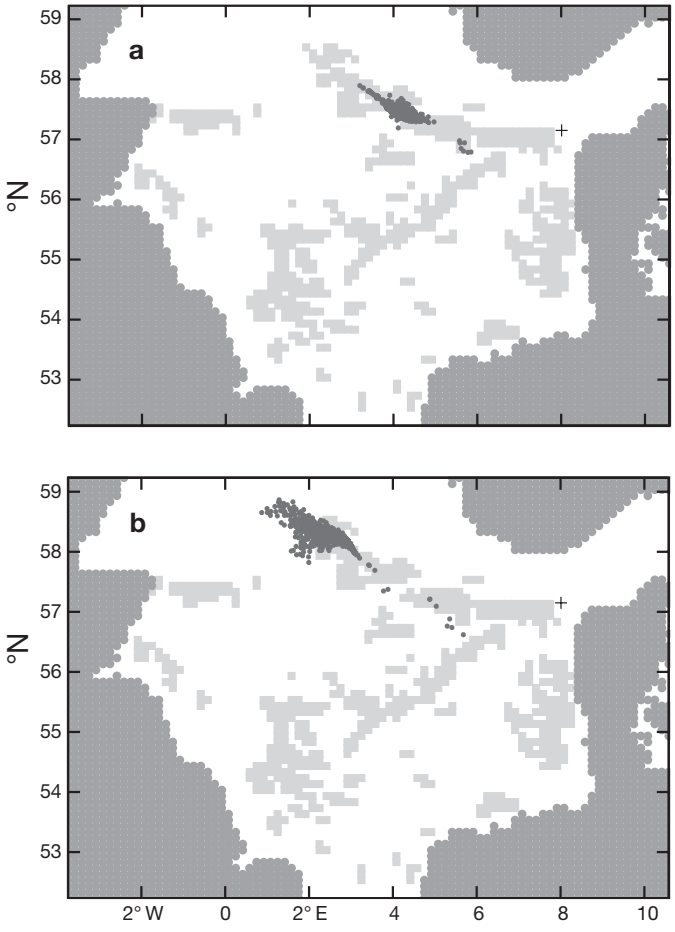

Fig. 6. Anomalous large parameter sensitivity: Sample 3, using (a) Model v1 and (b) Model b1. Grey: land; light grey: sand banks suitable for sandeel *Ammodytes marinus* habitats; +: larval catch position; small, dark grey circles: backtracked larval ensemble positions that indicate potential hatch positions

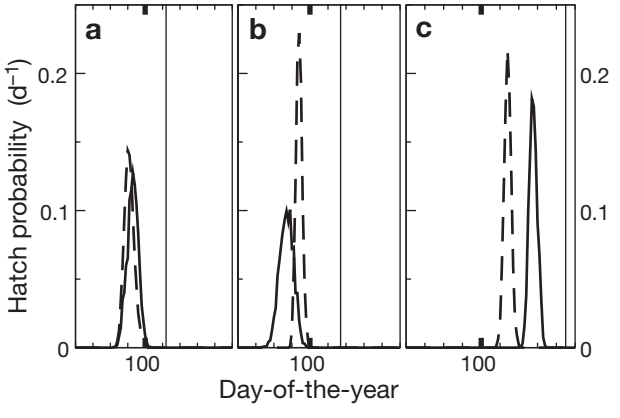

Fig. 7. Hatch time distributions from backtracking of larval samples in Table 2: (a), (b) and (c) are Samples 1, 2 and 3 respectively. Continuous line: Model v1; dashed line: Model b1; thin vertical lines: catch time of sample; tick marks on *x*-axes: 10 d intervals

Figs. 4 & 5d. Although Models v1 and b1 overlap in the spatial prediction of hatch area, somewhat larger relative differences appear in the prediction of drift period, with Sample 3 again being an outlier, but the overall predicted hatch periods are in reasonable agreement with age assessment from otolith readings (Table 2). Both growth models result in almost the same prediction of hatch peak for Sample 1, Model v1 performs a little better for Sample 2, whereas Model b1 is a little better for Sample 3, so there is no apparent bias toward length of drift period between Models v1 and b1, but both models indicate that there was large spatial heterogeneity in hatch periods over the North Sea in 2001, consistent with survey observations (LIFECO 2004).

GROWTH STOCHASTICITY

Growth variability within an ensemble of larvae arises from many sources, e.g. genetic variability, food patchiness and other environmental fluctuations on a subgrid scale. Growth variability over larger spatial scales will also appear indirectly, if spatial effects are not explicitly represented. From Fig. 2 we can roughly estimate the relative growth variability, i.e. $\sigma(G)/\langle G\rangle$, to be of the order of 20% for sandeel *Ammodytes marinus* larvae in the North Sea (this estimate is an upper limit, because it aliases some spatial and temporal variability as fundamental growth variability, because data in Fig. 2 are pooled). However, it is reasonable to expect different levels of variability for other fish species and other areas.

At this point, it is convenient to shift to a discrete representation in time and larval size, so the larval ensemble is characterized by a distribution vector p_t giving the size distribution of larvae in a suitable set of length classes at time t. If Eq. (1) is integrated forward by a fixed, small time step $\mathrm{d}t = h$, the larval length distribution development is characterized by the matrix Γ^h:

$$p_{t+h} = \Gamma^h p_t \tag{9}$$

which can be considered a Markov process, when the time scale of average temperature changes is large compared to h. Uniform mortality can be handled by multiplying a pre-factor to Eq. (9)—this does not alter the qualitative discussion. Put in another way, we focus on the relative length characteristics of a larval ensemble. The matrix Γ^h_{ij} gives the transition probability between length classes j to i during the time step h. Bayes' theorem provides the time-reversed process characterized by the matrix Q^h

$$p_t = Q^h p_{t+h} \tag{10}$$

$$\mathrm{Q}^h = (\kappa * \Gamma^h)^T \tag{11}$$

where the matrix κ_{ij} is the ratio of prior probabilities in states j, i and $\star$ means element-by-element matrix product. For regular Markov processes (as spatial dispersion), κ is straightforward, but for oriented stochastic processes, like growth, the larval/juvenile length classes have zero probability in the stationary state (all larvae have become adults) and therefore the prior ratio κ is ill defined.

To illustrate the effect of growth stochasticity on larval backtracking, we add a stochastic width of $\sigma(G) = 0.2G$ to the average growth G in Eq. (4), consistent with Fig. 2 (this means absolute growth fluctuations are smaller for early larvae than for juveniles) and again apply the North Sea average temperature variation in the backtracking period. In Fig. 8 we have backtracked growth of larval ensembles for 40 d under different premises. The Markov growth matrix Γ^h in Eq. (11) in this example is obtained by integrating Eq. (4) corresponding to h = 2 d and projecting onto size class bins of ⅓ mm. The backward Markov growth matrix Q^h has then been generated with Eq. (11), using a recently proposed alternative direct scheme (A. Christensen unpubl. data) to compute κ, which resolves the problems with the indefiniteness of κ by the usual definition. Fig. 8a,b shows that growth stochasticity adds width (continuous line) to the sharp length distribution obtained by deterministic backtracking (dashed line) of a narrow length distribution; the length distribution of growth Model b1 (Fig. 8b) is more narrow than that of growth Model v1 (Fig. 8a)

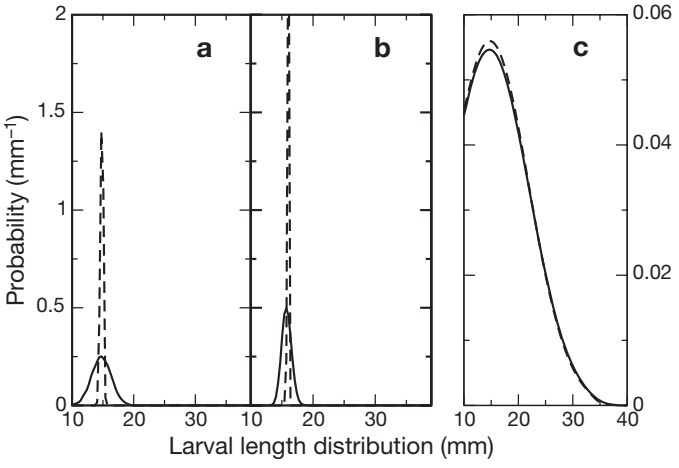

Fig. 8. Larval ensembles backtracked for 40 d, starting on the 120th day of the year, with initial average length $\langle L \rangle$ = 50 mm: (a) initial length root mean square (RMS) $\sigma(L)$ = 0 mm and growth Model v1, (b) initial length RMS $\sigma(L)$ = 0 mm and growth Model b1 and (c) initial length RMS $\sigma(L)$ = 10 mm and growth Model v1. Growth models are discretized in size classes of ⅓ mm, according to Eq. (9). Continuous lines: ensemble backtracking, using Eq. (11), with relative growth stochasticity $\sigma(G) = 0.2\overline{G}$; dashed lines: deterministic ensemble backtracking, using Eq. (6), i.e. $\sigma(G) = 0$

and also biased off centre. We see that Model v1 displays greater sensitivity than Model b1, which can be traced to the fact that Model b has less temperature sensitivity, because length scaling of growth explains the growth variation of very small larvae. Fig. 8c shows that effects of typical growth variability are dominated by typical variability in length distribution. This conclusion, however, need not be true for other species and other areas, especially if backtracking is performed for a longer part of their life history. We also emphasize the importance of a realistic prior κ, if the objective is to recover time scales, e.g. hatch schedules. Finally, we note that a peculiarity of Eq. (11) is that a process which is deterministic in forward time direction may become stochastic in reversed time (or vice versa) due to the transposition of the forward Markov matrix Γ^h.

DISCUSSION

In horizontal dispersal processes, transport distance R and transport time t scales (Taylor 1921) are linked by:

$$R = \sqrt{4\overline{D}t} \tag{12}$$

on a coarse scale, where $\overline{D}$ is a characteristic average effective horizontal dispersal rate. For the North Sea in the larval drift period, Fig. 4 indicates roughly that $\overline{D}$ is ~20 km^2 d^{-1} or ~230 m^2 s^{-1}, which is within the normal range, $\overline{D} \approx$ 100 to 1000 m^2 s^{-1}, of encountered dispersal rates in tidally dominated waters (Zimmerman 1986). This supports the earlier assertion (Zimmerman 1986) that the dominant horizontal dispersion pathway was vertical diffusivity coupled to vertical current shear. Explicit inclusion of other horizontal dispersion pathways can be expected to increase the average effective horizontal dispersal rate $\overline{D}$ somewhat, so our diffusivity fields are lower bounds on the total diffusivity. However, we believe that it will not change our conclusions, nor the qualitative picture we draw in our paper, because they hold also for increased spatial diffusivity fields. In the future, we plan to include other horizontal dispersion pathways for the sake of completeness.

In our context, this relation has 2 important implications

- A time horizon t_c: if we want to backtrack larvae and localize them with a spatial accuracy R (or better), we can only simulate backwards for $t < t_c = R^2 / 4\overline{D}$, before dispersion exceeds the desired spatial accuracy R. It should also be observed that R exceeds 2-fold the spatial grid resolution, which in our case is 2×10 km (this is the resolution limit of current structures)—otherwise the spatial grid resolution should be increased correspondingly. This lower grid resolu-

tion limit corresponds to roughly 5 d backtracking in the North Sea

- Spatial resolution limit R_c: if we want to simulate backwards for a specific time period t the spatial accuracy of the answer is $R_c = \sqrt{4\bar{D}t}$. For lesser sandeels in the North Sea, the drift period is on the order of 2 mo, so that the fundamental backtracking resolution for settled juveniles is roughly $R_c \approx 70$ km. This is somewhat larger than the typical area resolution in Fig. 4, which concerns presettled larvae but includes cohort length variation (see Table 2). On the other hand, including cohort length distribution directly gives the time distribution of a probable hatch.

Spatial backtracking provides an initial probability distribution. However, care must be taken in the interpretation of these probability fields. Batchelder (2006) suggested that the fraction of a planktonic sample originating from a specific area can be determined by considering overlap with the backtracked probability distribution; this can only be accomplished if all sites of origin have a uniform prior distribution of the planktonic organisms in question. Further, the mortality must be spatially uniform. Batchelder (2006) also suggested time round-trip experiments as an appealing and intuitive validation step of backtracking schemes. Here, a given situation is first run forward in time for a selected interval. Then, the resulting spatial distribution is run backward in time for the same time interval, and the final spatial distribution is overlaid with the initial state. In the light of our comments above, we want to emphasize that the final spatial distribution (i.e. after the time round trip) should not generally be expected to be strongly overlapping with the initial state. The overlap can be made arbitrarily small or large, depending on the choice of the round-trip time interval. It is not a question of good or bad performance, but of the speed of information loss, which is determined by the local diffusivity. Only a negative validation is possible, if strictly no overlap exists between final spatial distribution and initial state. We also want to note that the centre of gravity in the final spatial distribution should not be expected to coincide with the centre of gravity in the initial state, when the diffusivity is spatially heterogeneous.

Another interesting mechanism for particle dispersal is the potential presence of Lagrangian chaos (Zimmerman 1986). The presence of Lagrangian chaos is determined completely by the structure of the advective flow field transporting the particles. If it is due to spatial current structures above grid scale, it is automatically picked up by trajectory integration. However, if it is due to subgrid scale spatial current structures, it must appear as a contribution to the spatial turbulent density $K(s,t)$. An interesting aspect in this context is that diffusive trajectories starting close to each other diverge as the square root of time, whereas chaotic trajectories diverge exponentially with time. Since we have demonstrated the importance of using realistic dispersal fields $K(s,t)$, future studies should address the nature and parameterization of subgrid scale Lagrangian chaos contributions to particle dispersal, as well as disentangling the overlap with standard turbulent dispersal parameterizations, to avoid double accounting.

Even though the hydrodynamic database underlying our study has been validated in detail by available observations (Janssen et al. 2001, Janssen 2002), as pointed out in the section 'Biological and physical model', some level of circulation field uncertainty must be expected to be present. At the most crude level, this can be modelled as an additional, homogeneous diffusivity. In this case, it will not affect the qualitative conclusions of this paper. At a more sophisticated level, this can be modelled as a spatially and temporally dependent autocorrelated random walk process, overlain on the particle tracking described above. However, it is beyond the scope of the present paper to parameterize such an error model process.

We have not yet discussed the choice of larval ensemble size N, because we have focused on qualitative results rather than quantitative results. Two guiding figures apply here. If we want to observe a biological event in our simulations (e.g. a larva crossing a critical point in its life cycle), which has an approximate probability p, then $1/p < N$ should be satisfied. Conversely, if we are limited by computer resources to an ensemble size of N_c, we can only expect to observe events more likely than $1/N_c < p$. If we want to estimate p numerically in our particle tracking (with dispersal), we are bounded by the counting noise, which gives the relative variance of our estimate $\sigma(p)/p \approx 1/\sqrt{pN}$. This criterion is harsh to meet in reality, if p is small, and acceleration techniques, like Brownian Bridges (Rogers & Williams 1987) may become necessary.

Finally, we want to discuss the influence of mortality on our results. We have focused on virtual larval trajectories. If particles are passive and without internal states (e.g. size and condition, or mortality is independent of internal states), these trajectories can be corrected *a posteriori* by any mortality schedule. If mortality is spatially homogeneous, mortality effects will not affect many relative properties (like relative survival of ensemble sub-groups) or survival chance will trivially depend on drift time. In the case of a spawning-site distribution backtracked from a catch location, like in Fig. 4, spatially homogeneous mortality will not change the predicted spawning-site distribution. Thus, one could say that all our examples in the present paper are also valid for a constant mortality level. If the

mortality level is spatially and/or temporally varying, changes in the predicted spawning-site distribution must be expected.

An interesting example to study would be the impact of spatial predator distribution; in this case, survival chances along virtual larval trajectories (both forward and backward in time) can be assessed as path integrals along virtual particle trajectories of the spatial predator distribution. Virtual particle trajectories have another advantage, when comparing different mortality scenarios: the same set of particle trajectories can be computed once, stored, and used for all mortality scenarios. Re-using trajectories has the added advantage that the $1/\sqrt{N}$ sampling noise level is suppressed. If particles with internal states in forward tracking die, they are removed from the ensemble. What happens in backtracking? Then, they must be added to the ensemble at a rate corresponding to the local mortality. The less trivial question is what internal state (i.e. age, condition, etc.) should be assigned to these added particles. Clearly more research is needed to address this open question.

CONCLUSIONS

Forward simulation has often been used as a device to discriminate different potential underlying biological mechanisms. We have demonstrated larval backtracking as a versatile tool, complementary to normal forward simulations for model validation. Backward processes may exhibit a sensitivity not present in the forward processes. Model sensitivity is traditionally considered a weakness, because it makes assumptions important. Conversely, strong model sensitivity can be considered a powerful model validation asset, in the presence of auxiliary data—we advocate the latter point of view, used carefully, as a constructive attitude.

We have illustrated larval backtracking for North Sea lesser sandeel *Ammodytes marinus* larvae and tested several alternative biological growth models. We have found that dispersal effects are important for larval backtracking predictions, with large differences in shapes and extent of predicted hatching areas for larval patches originating from different regions of the North Sea, as well as large differences in the average advection distance. This emphasizes the need for future studies on the quality of sub-grid-scale turbulence parameterization, including possibly the effect of sub-grid-scale Lagrangian chaos. We have found backward prediction of hatch area more robust to model parameters than backward prediction of temporal hatch schedule. In all considered cases, a biologically reasonable hatching area has been predicted, without nudging the model in this direction. We have generally found reasonable agreement between backward predicted temporal hatch distribution and otolith reading data.

We have clarified fundamental limitations of larval backtracking due to information loss in stochastic processes, most importantly the time horizon and spatial resolution limit for backward hatch area prediction. For juvenile sandeel larvae in the North Sea, the lower backtracking resolution limit is 70 km, increasing if growth stochasticity and/or cohort length variance is included. The accuracy of backtracking is bounded by turbulence processes on long (monthly) time scales and by spatial hydrodynamic resolution on short (weekly) time scales.

Finally, we have found that growth stochasticity adds an uncertainty to the backtracked hatch estimate, similar to that in hatch area prediction. For North Sea lesser sandeel, we estimate the relative growth rate variability to be of the order of 20%. If the larval ensemble has a broad length distribution, it may be sufficient to use deterministic backtracking (i.e. use average growth instead of stochastic growth), provided growth stochasticity is small or moderate, which has been found to be the case for North Sea sandeels.

In a backtracking perspective, the most rewarding development on the biological side will be linking growth variability to the local biophysical environment, in order to capture the effects of regional, seasonal and interannual differences in environmental conditions with respect to growth variability. Also, more work is needed in elaborating unresolved processes and uncertainties on both the biological side, with emphasis on active behaviour and physical cue responses, and on the hydrodynamic side, with emphasis on improving the parameterization of hydrodynamic dispersal fields.

Acknowledgements. This work has, in part, been supported by EU FP6/SSP projects BECAUSE (Contract No. 502482) and PROTECT (Contract No. 513670).

LITERATURE CITED

Allain G (2004) Biophysical modelling for recruitment prediction. PhD thesis, Ecole Nationale Superieure Agronomique de Rennes (in French)

Allain G, Petitgas P, Grellier P, Lazure P (2003) The selection process from larval to juvenile stages of anchovy (*Engraulis encrasicolus*) in the Bay of Biscay investigated by Lagrangian simulations and comparative otolith growth. Fish Oceanogr 12(4–5):407–418

Arnott SA, Ruxton GD (2002) Sandeel recruitment in the North Sea: demographic, climatic and trophic effects. Mar Ecol Prog Ser 238:199–210

Baron PR (2004) The life history strategy of sprat (*Spratus sprattus*) in the Baltic ecosystem. PhD thesis, Universidad de Cadiz

Batchelder HP (2006) Forward-in-time/backward-in-time-trajectory (fitt/bitt) modeling of particles and organisms in the coastal ocean. J Atmos Ocean Technol 23:727–741
Bergstad OA, Høines AS, Jørgensen T (2002) Growth of sandeel, *Ammodytes marinus*, in the northern North Sea and Norwegian coastal waters. Fish Res 56(1):9–23
Daan N, Bromley PJ, Hislop JRG, Nielsen NA (1990) Ecology of North Sea fish. Neth J Sea Res 26(2–4):343–386
Dechter R, Frost D (2002) Backjump-based backtracking for constraint satisfaction problems. Art Intellig 136(2): 147–188
Gallego A, Heath MR, Cook B (2004) The origin and destination of sandeel larvae sampled in the northern North Sea: bio-physical modelling simulation result. ICES CM/P:9
Griffin DA, Thompson KR (1996) The adjoint method of data assimilation used operationally for shelf circulation. J Geophys Res 101:3457–3478
Hadamard J (1923) Lectures on Cauchy's problem in linear partial differential equations. Yale University Press, New Haven, CT
Hochbaum U (2004) Modellierung hydrodynamischer Einflüsse auf den Lebenszyklus von *Crangon crangon* in der Nordsee. Master's thesis, University of Hamburg
Hunter JR, Craig PD, Phillips HE (1993) On the use of random-walk models with spatially-variable diffusivity. J Comput Phys 106(2):366–376
Janssen F (2002) Statistical analysis of multi-year hydrographic variability in the North Sea and Baltic Sea. Validation and correction of systematic errors in a regional ocean model. PhD thesis, Fachbereich Geowissenschaften, Universität Hamburg (in German)
Janssen F, Schrum C, Huebner U, Backhaus JO (2001) Validation of a decadal simulation with a regional ocean model for North Sea and Baltic Sea. Clim Res 18:55–62
Jensen H (2001) Settlement dynamics in the lesser sandeel *Ammodytes marinus* in the North Sea. PhD thesis, University of Aberdeen
Jensen H, Rolev AM (2004) The sandeel fishing grounds in the North Sea. Information about the foraging areas of the lesser sandeel *Ammodytes marinus* in the North Sea. Working document prepared for the BECAUSE project. Technical report, Danish Institute of Fisheries Research, Copenhagen
Jensen H, Wright PJ, Munk P (2003) Vertical distribution of pre-settled sandeel (*Ammodytes marinus*) in the North Sea in relation to size and environmental variables. J Mar Sci 60(6):1342–1351
Kimura S, Kishi MJ, Nakata H, Yamashita Y (1992) A numerical analysis of population dynamics of the sand lance (*Ammodytes personatus*) in the eastern Seto Inland Sea. Fish Oceanogr 1:321–332
Kishi MJ, Kimura S, Nakata H, Yamashita Y (1991) A biomass-based model for the sand lance (*Ammodytes personatus*) in Seto Inland Sea. Jpn Ecol Model 54:247–263
Letcher BH, Rice JA, Crowder LB, Rose KA (1996) Variability in survival of larval fish: disentangling components with a generalized individual-based model. Can J Fish Aquat Sci 53(4):787–801
LIFECO (LInking hydrographic Frontal activity to ECOsystem activity) (2004) EU Fifth Framework Programme research project LIFECO (Q5RS-2000-30183), final report. LIFECO, Danish Institute of Fisheries Research, Copenhagen
Macer CT (1966) Sand eels (Ammodytidae) in the south-western North Sea; their biology and fishery. Fish Invest 24(6):1–55
Maier-Reimer E (1973) Hydrodynamisch-numerische Untersuchungen zu horizontalen Ausbreitungs- und Transportvorgängen. Mitt IFM Univ Hamb 21:56
Nagoshi M, Sano M (1979) Population studies of sand eel, *Ammodytes personatus*, in Ise Bay. I. Growth and its relation to population density. Jpn J Ecol 29:1–10
Pedersen OP, Tande KS, Slagstad D (2000) A synoptic sampling method applied to *Calanus finmarchicus* population on the Norwegian mid-shelf in 1997. Mar Ecol Prog Ser 204:143–157
Press WH, Flannery BP, Teukolsky SA, Vetterling WT (1992) Numerical recipes in C: the art of scientific computing. Cambridge University Press, New York
Reay PJ (1970) Synopsis of biological data on North Atlantic sandeels of the genus *Ammodytes*. FAO Fish Synop 82, FAO, Rome
Rogers LCG, Williams D (1987) Diffusions, Markov processes and martingales, Vol II. Ito calculus. Wiley, New York
Schrum C (1997) Thermohaline stratification and instabilities at tidal mixing fronts. Results of an eddy resolving model for the German bight. Cont Shelf Res 17(6):689–716
Schrum C, Backhaus JO (1999) Sensitivity of atmosphere–ocean heat exchange and heat content in North Sea and Baltic Sea. A comparitive assessment. Tellus 51A:526–549
Schrum C, Siegismund F, St John M (2003) Decadal variations in the stratification and circulation patterns of the North Sea. Are the 90's unusual? In: ICES symposium of hydrobiological variability in the ICES area 1990–1999. J Mar Sci 219:121–131
Schrum C, Alekseeva I, St John M (2006) Development of a coupled physical–biological ecosystem model ECOSMO, Part I: model description and validation for the North Sea. J Mar Syst 61(1–2):79–99, doi:10.1016/j.jmarsys.2006.01.005
Smigielski AS, Halavik TA, Buckley LJ, Drew SM, Laurence GC (1984) Spawning, embryo development and growth of the American sand lance *Ammodytes americanus* in the laboratory. Mar Ecol Prog Ser 14:287–292
Spivakovskaya D, Heemink AW, Milstein GN, Schoenmakers JGN (2005) Simulation of the transport of particles in coastal waters using forward and reverse time diffusion. Adv Wat Res 28(9):927–938
Taylor GI (1921) Diffusion by continuous movements. Proc Lond Math Soc 20:196–211
Uliasz M, Pielke RA (1991) Application of the receptor oriented approach in mesoscale dispersion modeling. In: van Dop H, Steyn DG (eds) Air pollution modeling and its application. VIII. Plenum Press, New York, p 399–408
Van Dam GC, Ozmidov RV, Korotenko KA, Suijlen JM (1999) Spectral structure of horizontal water movement in shallow seas with special reference to the North Sea, as related to the dispersion of dissolved matter. J Mar Syst 21(1–4):207–228
Visser AW (1997) Using random walk models to simulate the vertical distribution of particles in a turbulent water column. Mar Ecol Prog Ser 158:275–281
Winslade P (1971) Behavioral and embryological studies on the lesser sandeel *Ammodytes marinus* (Raitt). PhD thesis, University of East Anglia, Norwich
Wright PJ, Bailey MC (1996) Timing of hatching in *Ammodytes marinus* from Shetland waters and its significance to early growth and survivorship. Mar Biol 126(1):143–152
Zimmerman JTF (1986) The tidal whirlpool—a review of horizontal dispersion by tidal and residual currents. Neth J Sea Res 20(2–3):133–154

Editorial responsibility: Alejandro Gallego (Contributing Editor), Aberdeen, UK

Submitted: April 7, 2006; Accepted: June 20, 2007
Proofs received from author(s): October 4, 2007

Vol. 347: 233–245, 2007
doi: 10.3354/meps06981

MARINE ECOLOGY PROGRESS SERIES
Mar Ecol Prog Ser

Published October 11

OPEN ACCESS

Modelling distribution of flounder larvae in the eastern English Channel: sensitivity to physical forcing and biological behaviour

Alexei Sentchev[1,*], Konstantin Korotenko[2]

[1]Ecosystèmes Littoraux et Côtiers—FRE 2816, Université du Littoral—Côte d'Opale, 32 Avenue Foch, 62930 Wimereux, France
[2]Marine Turbulence Laboratory, P.P. Shirshov Institute of Oceanology, 36, Nakhimovsky Prospect, Moscow 117851, Russia

ABSTRACT: The Princeton Ocean Model coupled with a particle-tracking module is used to assess the effects of physical forcing and vertical migratory behaviour on the transport and dispersion of larvae in the region of freshwater influence (ROFI) of the eastern English Channel (EEC). Results of numerical modelling are compared with the observed concentrations of flounder *Pleuronectes flesus* larvae. The simulations show that accumulation of neutrally buoyant particles occurs on the ROFI margin, 20 km off the French coast. Tides and freshwater input induce the net along-shore northward transport. Tidal currents modulate the magnitude of horizontal transport, whereas the freshwater input controls the location of accumulation zones. The vertical migration of particles causes a significant departure from the passive transport pattern and modifies the intensity of dispersion. The diurnal (light dependent) migration tends to decrease the magnitude of the cross-shore dispersion of particles. When the vertical migration is controlled by the tidal (sea level variation) cycle, particles move northward faster, and exhibit less dispersion. The migratory behaviour synchronised with the tidal currents (ebb/flood cycle) produces a relatively slow northward migration and a low dispersion in both along- and cross-shore directions. This suggests that vertical migratory behaviour could control the intensity of dispersion and the relative dominance of either retention or downstream advection of the larvae in the EEC.

KEY WORDS: Larval transport · Vertical migration · Particle tracking · Tides · English Channel

INTRODUCTION

The role played by various physical processes in fish early life history is currently an area of active research. Among a variety of physical (abiotic) conditions, we considered 2 closely linked aspects that can have a large effect on recruitment. The first involves larval transport by non-stationary flow field and the second involves the response of larval behaviour to changes in environmental conditions. During the early life stages, pelagic larvae of many commercially valuable fishes execute horizontal migrations from spawning areas to estuarine nursery grounds. The influence of physical forcing on larval development has been studied by many authors. Larval growth and abundance may vary in response to wind and tidal circulation on different time scales (Nielsen et al. 1998, Van der Veer et al. 1998). The role that physical variability plays in observed abundance and recruitment of flatfish populations was examined by Werner et al. (1997). The effect of tides on larval transport and recruitment was documented by Brown et al. (2000) and Jenkins et al. (2000). Xie & Eggleston (1999) discussed the potential role of wind forcing on larval transport, while Boeuf & Payanb (2001) reported an influence of water salinity on fish development.

Measurements of the behavioural response of the larvae to changes in their habitat are demanding because of the difficulties in estimating *in situ* larval abundances, especially when simultaneous monitoring

*Email: alexei.sentchev@univ-littoral.fr

of the physical factors affecting the abundances is required. Factors which may influence the vertical migration include light, temperature, variation in hydrostatic pressure, speed and direction of the flow, availability of food, predation, turbidity and turbulence. To assess the influence of different environmental factors on larvae, laboratory experiments have been conducted in which larvae were observed under controlled conditions. Their response to changes in physical parameters was then extrapolated to behaviour in natural habitats (Burke et al. 1995, 1998).

A particle-tracking model coupled with a hydrodynamic model is a particularly efficient tool for examining the role played by various physical processes in combination with individual behaviour of sea organisms. Using the particle-tracking approach one can account for different migration cues, and study changes in the description of the larval transport in comparison with the transport of passive larvae. In this way, Franks (1992) has found that a horizontal or vertical patchiness of organisms may arise at fronts through retention and accumulation zones in accordance with the swimming behaviour of the organisms. This result has been obtained in the framework of a 2-dimensional model of a steady cross-frontal flow. Hill (1994) has considered a transport-inducing interaction between diurnal vertical migration of marine organisms and the S_2 tidal currents. Simulations of Jenkins et al. (1999), involving several vertical migratory behaviours of particles, revealed that the vertical migration does not influence the larval transport in Port Philip Bay (southern Australia). Bartsch (1988) has obtained different results in numerical simulations of the drift routes of herring larvae across the North Sea. His model, although 3-dimensional, included only residual advective fields and was thus unable to account for the migration–tide interaction. However, the transport pathways of larvae were found to be significantly affected by the interaction of the vertical migration with the mean current shear. A sensitivity of larval transport to vertical migratory behaviour of the larvae has been investigated by Bartsch & Coombs (2001) in the North Atlantic and by Graaf et al. (2004) in the North Sea, both by means of numerical modelling.

The freshwater inflow from a number of rivers on the northern coast of France gives rise to a haline front separating offshore waters of Atlantic origin from the region of freshwater influence (ROFI). Within the ROFI, the buoyancy input is responsible for producing a physical regime, which is different from that of the offshore waters. A variety of ROFI systems and their distinctive dynamical features were described in some detail by Simpson (1997). In a recent study, Sentchev & Korotenko (2004) developed an accurate numerical representation of the geometry, hydrology and circulation in the eastern English Channel (EEC). They have shown that, within the ROFI of the EEC, a certain combination of tides and buoyancy input produces patchiness in spatial distribution of particles. An along-coast northward particle migration was detected in the numerical experiments and confirmed by the field observations of larval abundance. According to field measurements, the main spawning areas of flounder *Pleuronectes flesus* in the English Channel are located within the central part of the domain, while the larvae are found most often in the coastal nursery grounds (Van der Land 1991, Grioche et al. 1997). Mechanisms of larval transport from source to nursery grounds are poorly understood.

The present study can be viewed as an extension of the above-mentioned work of Sentchev & Korotenko (2004), with emphasis on the interaction between the vertical migration of particles, representing the larvae, and tidal currents. We investigate horizontal larval transport and dispersal driven by a combination of tides and freshwater input and influenced by the vertical migratory behaviour of pelagic organisms. The behaviour is restricted to vertical migration driven by day-light variability and tidal motions (sea surface height and currents) observed in the English Channel.

MATERIALS AND METHODS

Hydrodynamic model. In this study we use the sigma-coordinate Princeton Ocean Model (POM) to simulate tidal circulation in combination with realistic freshwater runoff within the model domain shown in Fig. 1a. The detailed description of the model is given by Blumberg & Mellor (1987). POM solves finite-difference analogues of the primitive equations in 3 spatial dimensions with fully prognostic temperature and salinity fields, thus allowing time-dependent baroclinic motion. A free surface, essential for modelling tides, is also included. The entire region of the EEC, including the Strait of Dover and the southern part of the North Sea, is represented on a horizontal grid with homogeneous spacing of 2 km. The bottom topography has a complicated geometry, with numerous shallow banks separated by a series of 50 m deep basins, both oriented in the along-shore direction (Fig. 1a). The model uses the 'Arakawa C' differencing scheme for the momentum equations in the horizontal plane, a set of 21 vertical sigma levels, distributed so as to provide enhanced resolution in proximity to the surface and seabed, and the level 2.5 turbulence model of Mellor & Yamada (1982). A quadratic bottom-friction approximation is used with a uniform drag coefficient of 0.0025, usually adopted for the English Channel (Werner 1995).

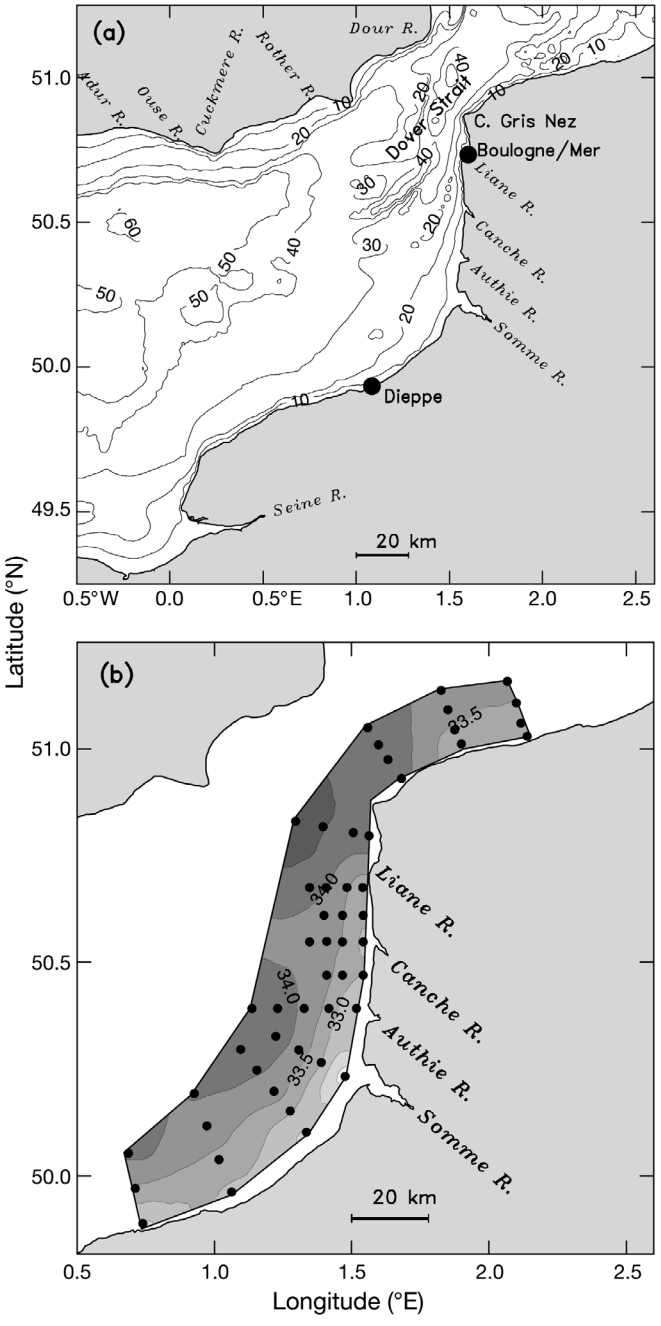

Fig. 1. (a) Bathymetry of the model domain (eastern English Channel). Contour interval is 10 m. Major rivers (R.) contributing to the buoyancy input to the domain are shown. (b) Surface layer (1 m thick) salinity (psu) distribution from the field experiments conducted from 2 to 5 May 1995. Locations of sampling stations are shown (solid circles)

Water flow through the EEC is a combined result of the interaction of astronomical tides, freshwater discharge, meteorological forcing and non-tidal sea-level changes. A haline front, separating offshore waters of Atlantic origin from near-shore, low-salinity waters, is one of the most significant features of the EEC (Fig. 1b). The model reproduces the front's position and its spatial extension reasonably well. Most of the freshwater inflow into the eastern channel comes from the Seine, Somme, Authie and some other rivers on the north-eastern coast of France and occurs in winter to early spring (Fig. 2a). During the period of numerical experiments, the cumulative inflow rate is of the order of 1500 $m^3 s^{-1}$ (Fig. 2b). Freshwater input from rivers on the English coast is much less important (about 4 %). Its effect on the transport and dispersion in the channel was considered by Sentchev & Korotenko (2005). Fig. 2c shows winds measured in April and May 1995 at Boulogne light tower during the same period.

The sea level variation inside the model domain is predominantly semi-diurnal (Fig. 2d). To simulate tidal motions, tidal forcing with 3 primary semi-diurnal astronomical constituents, M_2, S_2, N_2, and 1 non-linear constituent, M_4, was introduced along the open boundaries. A gravity-wave radiation condition was used to specify the normal component of the depth-averaged current at the model open boundaries, according to Flather's (1976) method. Elevations and normal velocities at the open boundaries for the individual constituents were determined from a 2-dimensional finite-element spectral tidal model. Tidal forcing for this model, in turn, was extracted from the global Finite Element Solution, Version 2.1, of 1995 (FES95.2.1) tidal database (Le Provost et al. 1995).

Modelling results were validated against the tides observed in 11 ports located in the eastern channel, surface current velocities measured by the OSCR HF radar in the Strait of Dover, and, finally, against the observed salinity distribution derived from the extensive field experiments conducted in the spring of 1995 (Sentchev & Korotenko 2004).

Particle-tracking model. A Lagrangian particle-tracking technique includes the random-walk approach that is significantly more effective than the finite-difference method in describing qualitatively the spatial distribution of tracers. Schematically, the algorithm for updating particle coordinates is the following: every time step, a total of N^p particles are moved in the 3-dimensional Cartesian reference frame by an advective translation $\boldsymbol{a}$ added to a diffusive jump $\boldsymbol{\eta}$. The advective movement within a grid cell is determined by linear interpolation of the velocity values from the 8 vertices of the grid cell, and computation of the displacement vector as a product of the interpolated velocity vector and the time step Δt. A diffusive jump of particles (random displacement due to sub-grid fluctuations of velocity) along each axis is determined in different ways. Along the horizontal axis i (i = 1, 2), the 'naïve random walk' (NRW) expression was used to generate diffusive jumps, $\boldsymbol{\eta} = \boldsymbol{\gamma}\,(2K\Delta t)^{1/2}$, where $\boldsymbol{\gamma}$ is a vector of size N^p whose components are computed by

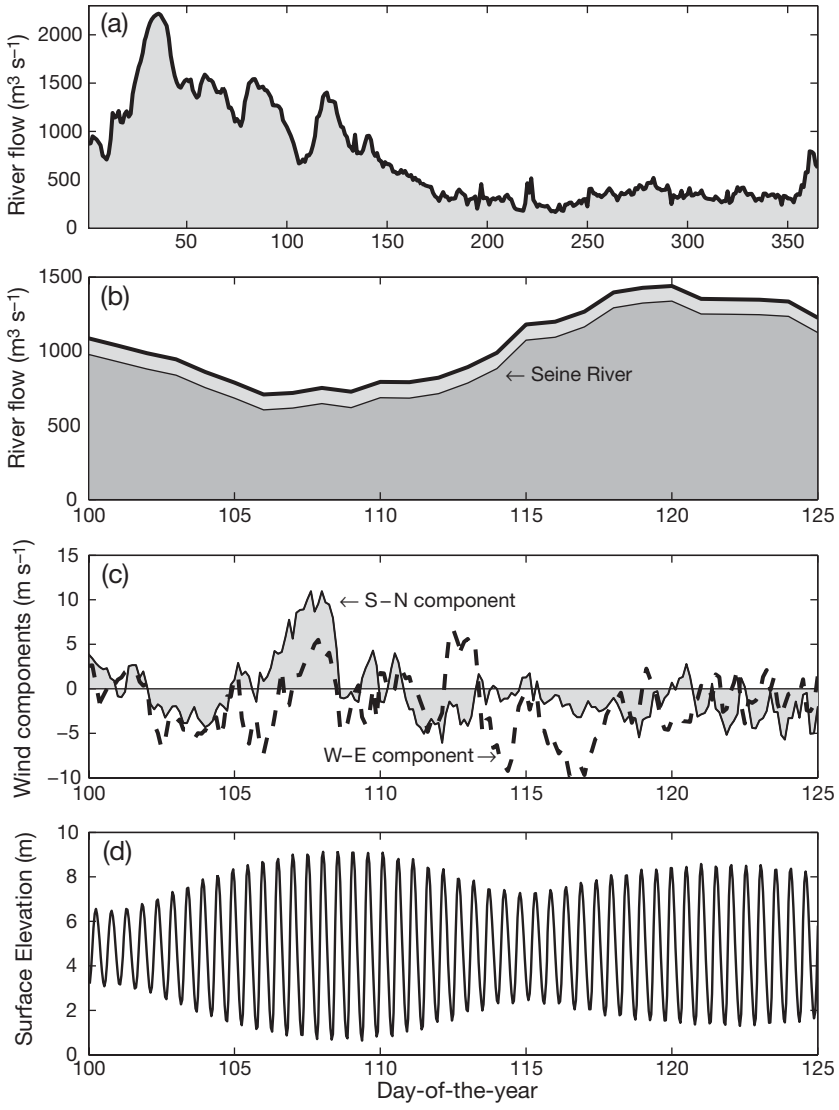

Fig. 2. Environmental data: (a) daily averaged values of the freshwater runoff in 1995 from the rivers located on the French coast between the mouth of the Seine and Cape Gris Nez and (b) the same values, but for the period of numerical experiments (thin line: Seine River; thick line: all rivers). The data are available on the website of the 'Seine-aval' national scientific project (http://seine-aval.crihan.fr) and the National Water Resources Society (www.eau-artois-picardie.fr). (c) Wind measurements were made at Boulogne light tower (Met-office data). Positive velocities are from the south to north (S to N) and from the west to east (W to E). (d) Sea surface tidal variation in Boulogne is based on historical observations

a random-number generator (RNG), then converted to yield the Gaussian distribution with zero mean and unit standard deviation, and K stands for the time-dependent horizontal diffusivity along each axis.

The water flow in the EEC is a combination of tidal motions, freshwater input and wind-driven circulation. This forcing contributes to generation of a non uniform vertical diffusivity profile, and therefore requires the use of the 'consistent random walk' (CRW) model (Hunter et al. 1993, Visser 1997) in the vertical direction. The following expression, adopted from Visser (1997), is used to simulate vertical displacements of particles: $\eta = K'(z)\Delta t + \gamma[2K(z^*)\Delta t]^{1/2}$. The CRW model includes a deterministic component and a diffusive, or random, component. The deterministic component causes a net displacement of the centre of mass of the neutrally buoyant particles toward increasing diffusivity at a rate K' (local gradient of K in the vertical direction), thus allowing avoidance of the artificial particle accumulation within layers of low vertical diffusivity. The diffusion coefficient K in the CRW model is estimated from the diffusivity profile at a vertical coordinate z^* shifted from the particle coordinate z by a small distance $\frac{1}{2}K'\Delta t$. We recognise that the CRW model could be used for simulating horizontal displacements. However, as we have assessed, within the ROFI, the largest horizontal and vertical diffusivity gradients are of the order of 10^{-3} and 10^{-1} m s^{-1}, respectively, suggesting that the effect of K'_H on horizontal distribution of particles is negligible, given the model grid spacing and time step.

The horizontal and vertical diffusion coefficients, K_H and K_V, as well as the mean current velocity components (u, v, w) are provided by the hydrodynamic model described in the previous section. The model computes the horizontal diffusion coefficients from the Smagorinsky (1963) formulae, while the vertical diffusivity is obtained from the level 2.5 turbulence closure scheme of Mellor & Yamada (1982). Thus, 3-dimensional dynamic fields are used as forcing in the particle-tracking model, which produces particle coordinates at every time step. The time step Δt for particle tracking is 360 s. This value satisfies the numerical integration criterion (Visser 1997), prevents particle jumping >1 grid cell, and thus guarantees an accurate estimate of particle displacement in each of 3 directions. A particle reflection condition is implemented at the model rigid boundaries in all simulations. Particles leaving the model domain through the open boundaries are assumed to be lost.

Larva sampling. To improve the knowledge of the spatial distribution of spawning and nursery grounds

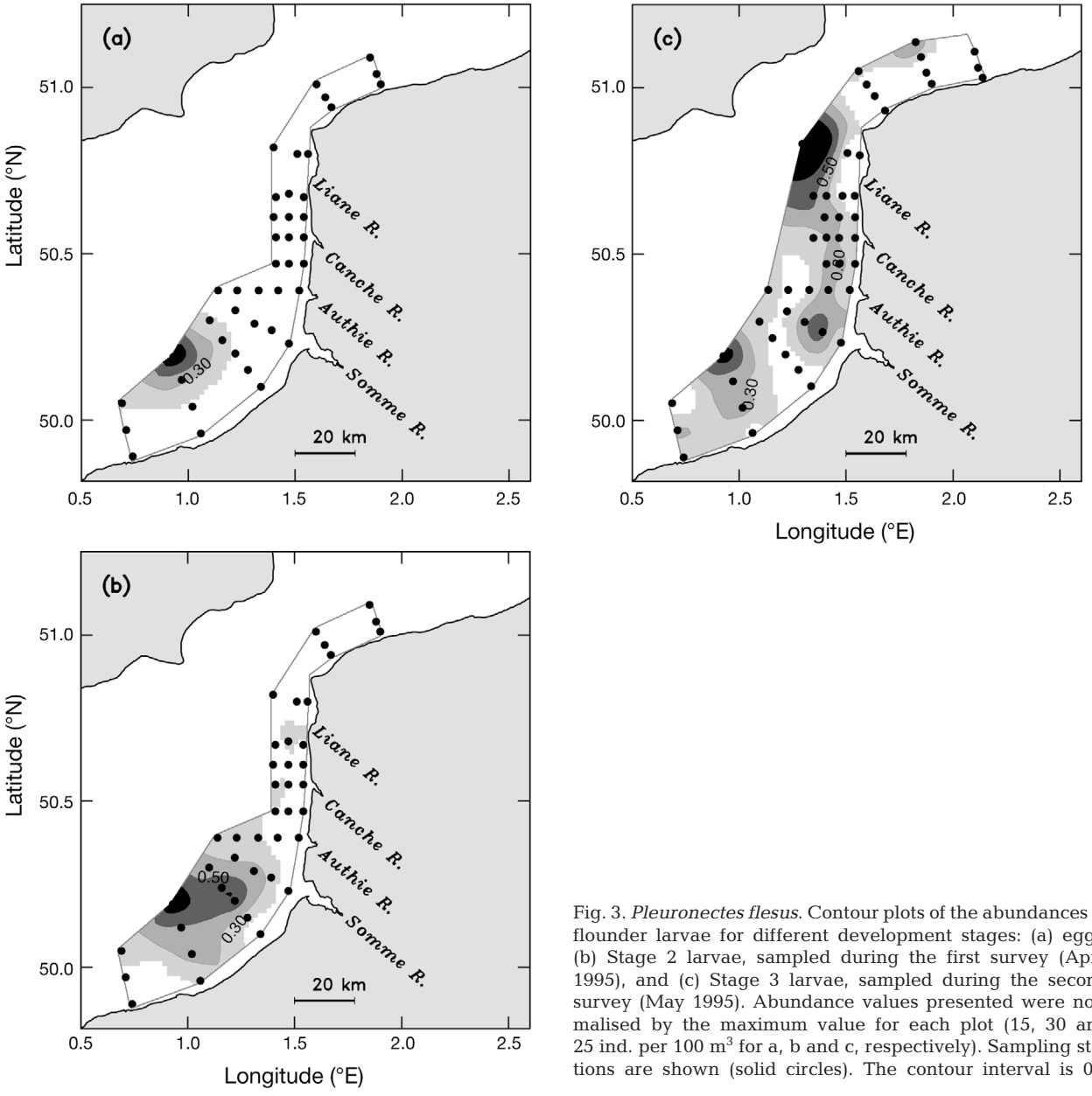

Fig. 3. *Pleuronectes flesus*. Contour plots of the abundances of flounder larvae for different development stages: (a) eggs, (b) Stage 2 larvae, sampled during the first survey (April 1995), and (c) Stage 3 larvae, sampled during the second survey (May 1995). Abundance values presented were normalised by the maximum value for each plot (15, 30 and 25 ind. per 100 m^3 for a, b and c, respectively). Sampling stations are shown (solid circles). The contour interval is 0.2

of flounder *Pleuronectes flesus* in the EEC, and to clarify mechanisms that might control the larval transport from source to nursery grounds, an extensive larval transport field experiment was organised in spring 1995. Two surveys, including cross-shore sections in the vicinity of the French coast (Fig. 1b), were conducted from 11 to 13 April and 2 to 5 May 1995. The description of the field experiment can be found in some detail in Grioche et al. (1997).

We present in Fig. 3 the flounder larval abundances obtained by interpolation of the raw data of Grioche et al. (1997), without introducing any hypothesis of patchiness in spatial distribution. Abundances, expressed in numbers per 100 m^3, were normalised by the maximum value in each plot. Fig. 3a shows that flounder eggs formed a patch, 40 km westward of the Somme estuary (spawning area), with a maximum abundance of 15 eggs per 100 m^3. Eggs were absent elsewhere in French coastal waters. The larvae of Stage 2 (1 wk old) were also found in a single patch extending in a northeast direction (Fig. 3b). The maximum abundance of the larvae, up to 30 larvae per 100 m^3, and fish eggs were detected at the same location. The spatial distribution of Stage 3 larvae, sampled in May 1995 (Fig. 3c), allows us to speculate that a northward larval advection along the French coast occurred. We can also deduce an ability of the larvae to exert shoreward migration. In May, high abundances were found within the ROFI, in

the low-salinity water, rich in chlorophyll *a*. The dominant wind was north-east during the field experiments (Fig. 2c) and could not explain larval drift toward the north. On the contrary, survivorship–mortality patterns can affect the observed distribution of abundances, but our knowledge about such spatial patterns in the EEC is poor to date. We must also recognise that the sampled region covers only a part of the spawning grounds presented in Fig. 3a. That is why a hypothesis of larval advection, derived from the observations (Fig. 3), might be adopted with a high degree of uncertainty.

Vertical migration of the larvae. The variability of migration pathways for some species (*Limanda limanda* and *Pleuronectes flesus*) has been observed in the North Sea, and a hypothesis showing the influence of larval behaviour on the vertical distribution has been proposed by Campos et al. (1994). Burke et al. (1995) and Boss et al. (1995) have documented that flounder larvae are found within the water column on flood and in the bottom layer on ebb. This behaviour facilitates shoreward displacement of larvae and even their upstream propagation within the estuary (Boss et al. 1995). A preliminary study of Grioche et al. (2000) indicated a possible light-dependent diurnal cycle in vertical displacement, with motions toward the bottom at daybreak and back up the following nightfall. Such migration might help to avoid visual predation.

As no comprehensive theoretical model of vertical migration pattern exists, we have adopted 2 simple models of vertical migration that are consistent with distributions of flounder larvae observed by different authors in different regions. The first model describes diurnal migration that is locked on the day–night cycle. It is assumed that the deepest part of the migration cycle is centred upon local nightfall (19 h UT in April) and that particles are rising towards the surface after nightfall and falling toward the bottom during daytime (Fig. 4a). Since the day in April is slightly longer than the night, the duration of upward motion is shorter and the corresponding velocity (2 m h^{-1}) is slightly higher than the downward velocity (1.7 m h^{-1}). Both, the upward and downward migratory velocities are kept constant during the total period of simulations, allowing the larvae to exert regular vertical oscillations within the 25 m thick water layer (Fig. 4a).

The second migration model is linked to semidiurnal tidal cycle. Three different situations are considered. In the first situation, the sign of vertical velocity depends upon the hydrostatic pressure tendency: particles sink at a constant speed during falling tide and move up during rising tide (Fig. 4b). In the second situation, the vertical migration is related to the tidal current cycle, which advances the sea surface height by approximately 2 h (Fig. 4c). In the third situation, we reverse the sign of vertical migratory velocity, thus allowing particles to sink during flood and to rise during ebb (Fig. 4d).

Numerical simulations. Several particle model runs are conducted under different tidal conditions, including a primary and a secondary neap to spring cycle (Fig. 2d), with or without freshwater inflow and wind

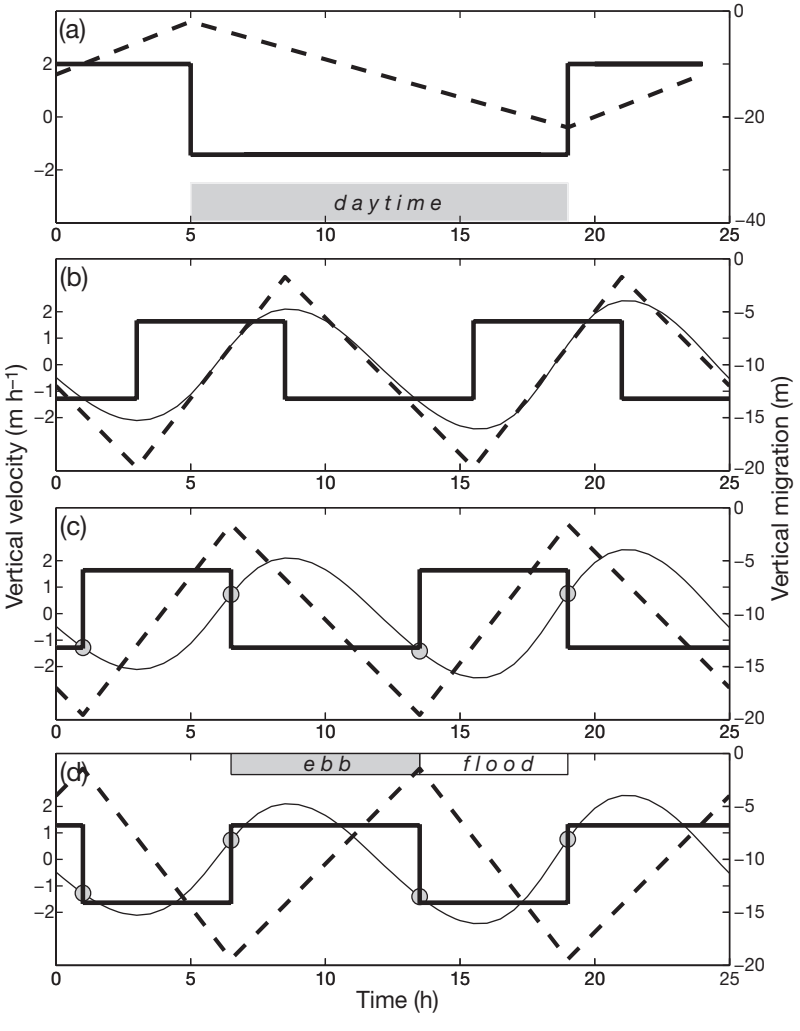

Fig. 4. Time-dependent vertical swimming velocity (thick solid line) assigned to particles in numerical experiments, and vertical displacement of particles (dashed line) relative to the sea surface. (a) Diurnal (light dependent) vertical migration, (b) tidally cued (sea level-locked) migration, (c,d) migration synchronised with tidal currents. The signs of vertical migratory velocities are reversed in c and d. Positive velocity is toward the surface; negative is toward the bottom. The thin line shows sea level variation in Boulogne on 11 April 1995; circles show the instant of current reversal

forcing. We also consider 3 scenarios accounting for larval behavioural response to light conditions, hydrostatic pressure and current variations. To assess the role that physical forcing terms play in particle dynamics, simulations are performed first with neutrally buoyant particles. A set of 960 (8 per grid box) particles was released over a small region (24×20 km^2) in front of the Somme estuary (see Fig. 5a) and tracked during a 25 d period. To examine the sensitivity of transport pathways and dispersion to a number of particles used in simulations, a set of 9600 particles was released within the same region. At release, particles are homogeneously distributed within a 2 m thick layer, with the upper limit at 1 m below the surface. Tidal motions and freshwater input, used in all the simulations, match the conditions corresponding to the period of the field experiments (Fig. 2b,d). Observed (Fig. 2c) and synthesised wind forcing were introduced in some model runs. The resultant distributions of particles are presented quantitatively in terms of the number of particles within a horizontal model grid cell by integrating the abundances vertically from surface to bottom. Additional simulations are performed with 960 particles; these enable vertical motions relative to the flow, with vertical velocity equating to the swimming behaviour of larvae. Appropriate tidal and freshwater forcing were used in these simulations.

To quantify the dispersion of particles and to discern the influence of vertical behaviour on the dispersion, we apply a principal component analysis (PCA) technique (Emery & Thomson 1997) to the horizontal distribution of particles at the end of the 18 d tracking period. This allows us to identify the main axes along which the dispersion of material is extreme. The distortion of a particle group is quantified by a horizontal covariance matrix, the components of which account for the covariances between particle displacements relative to their centre of mass. The dispersion is extreme in the direction of the semi-major axis, whereas its length gives the root-mean square (rms) displacement.

RESULTS

Transport of neutrally buoyant particles

Fig. 5 shows the spatial distribution of particles at the end of an 18 d tracking period. The model results indicate that under the appropriate forcing, including the neap to spring tidal cycle and buoyancy input, particles are transported northward. The trajectory of displacement of the centre of mass of the ensemble of particles reveals that, in the near-shore sector associated with the ROFI, the dominant direction of drift is northward. The highest concentrations of particles (up to 6 per grid box) are found 20 km offshore, on the margin of the ROFI, defined according to surface salinity, ranging between 34.0 and 34.5 psu. Particles start leaving the domain through the northern model open boundary after 16 d. We limited the analysis to the 18 d period. This allowed us to limit the bias of statistics due to the loss of particles.

When a set of 9600 particles is released within the previous zone at the same phase of the tidal cycle, the transport patterns look similar. Most particles are transported northward, slightly toward the French coast, then northward along the coast, with the highest concentrations detected again on the ROFI margin (Fig. 5b). Trajectories of the centre of mass of 2 particle ensembles (960 and 9600 particles) and the shape of the particle distribution look rather similar in both simulations.

To assess the role of buoyancy forcing in particle dynamics, tidally forced simulations were performed without freshwater input. In this case, model results do not reveal any accumulation of particles 20 km offshore. On the contrary, particles move shoreward and tend to be concentrated in the vicinity of the French coast, thus providing a very different distribution (Fig. 5c). The N to S (along shore) and E to W (cross shore) extensions of this patch are of the order of 120 and 45 km, respectively, and are comparable with those shown in Fig. 5a,b.

The wind forcing, corresponding to observations available in Boulogne, in conjunction with buoyant and tidal forcing, produces small perturbations of the trajectory of displacement of the centre of mass of particles and modulation of spatial distribution of particles relative to the coast (results not shown). The upwelling-favourable (N to E) wind tends to decrease the rate of northward migration, inducing a weak offshore component. Wind in the opposite direction (SW) generates coastal downwelling and enforces the northward and shoreward migration of particles.

Transport of vertically migrating particles

The computations were repeated with vertically migrating particles. This 'active' behaviour of particles simulates the ability of organisms to float, sink, or swim relative to the water motion. Particles were released within the area that was used in the previous experiments (Fig. 5a). Modelling results indicate that the vertical migration may cause a significant departure from the passive particle transport pattern. The essential differences are illustrated in Fig. 6a–d.

When the diurnal (light dependent) vertical migration is introduced, the rate of transport and the shape

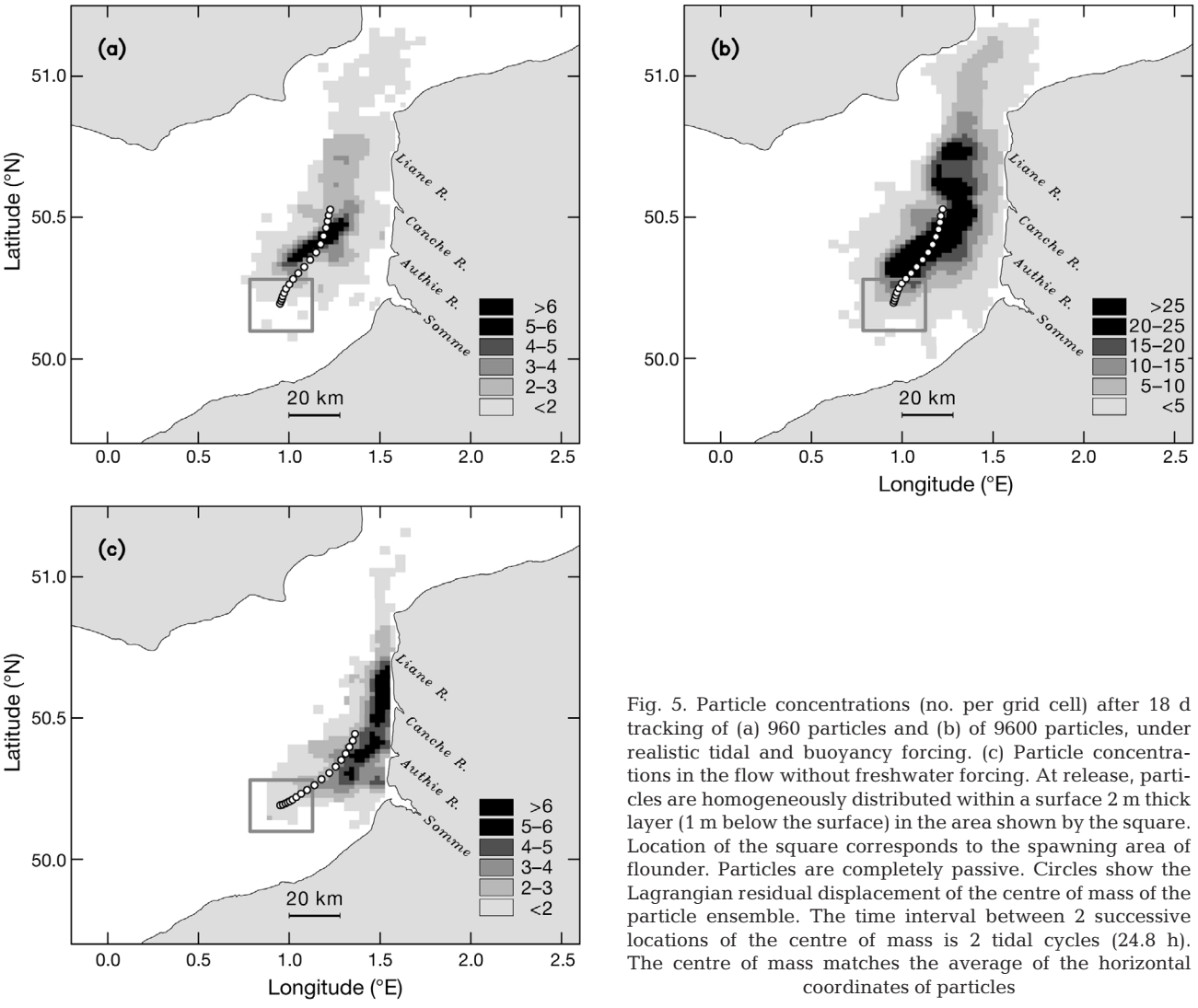

Fig. 5. Particle concentrations (no. per grid cell) after 18 d tracking of (a) 960 particles and (b) of 9600 particles, under realistic tidal and buoyancy forcing. (c) Particle concentrations in the flow without freshwater forcing. At release, particles are homogeneously distributed within a surface 2 m thick layer (1 m below the surface) in the area shown by the square. Location of the square corresponds to the spawning area of flounder. Particles are completely passive. Circles show the Lagrangian residual displacement of the centre of mass of the particle ensemble. The time interval between 2 successive locations of the centre of mass is 2 tidal cycles (24.8 h). The centre of mass matches the average of the horizontal coordinates of particles

of spatial distribution of particles change (Fig. 6a). The majority of particles are confined to the margin of the ROFI zone, with maximum concentrations (>6 per grid cell) found at a distance of 20 km offshore. Only a small amount of particles is found in the vicinity of the coast. The trajectories of displacement of the centre of mass of 'active' and 'passive' particles appear to be similar, but reveal a noticeable difference in the rate of migration. 'Active' particles tend to move faster and need 2 d less to attain the location of the centre of mass of 'passive' particles at the end of the 18 d period. Globally, the horizontal distribution of vertically migrating particles shows higher concentrations along an axis parallel to the shoreline, distant from the coast by 20 to 25 km, and higher speed of northward migration.

Fig. 6b shows the behavioural response of modelled particles to tidally cued vertical migration, i.e. the migration synchronised with the tidal cycle of sea surface elevation. After 18 d of tracking, the spatial distribution of particles reveals spreading in the along-coast direction and the northward advection, with a local maximum of particle concentration (up to 6 per grid box) found at a distance of 20 km offshore. The rate of northward advection of the centre of mass is the highest in comparison with all previously discussed situations. The centre of mass is located 80 km northeastward of the release point, and the trajectory of its displacement shows that particles spend 7 d less to reach the location occupied by neutrally buoyant particles at the end of the tracking period. Moreover, the trajectory of the centre of mass is only 13 km away from the coast after 12 d of tracking (Fig. 6b), indicating that some portion of the particles can reach the coast by the middle of the tracking period.

In the third scenario, the vertical migration is synchronised with the tidal current cycle, which advances the

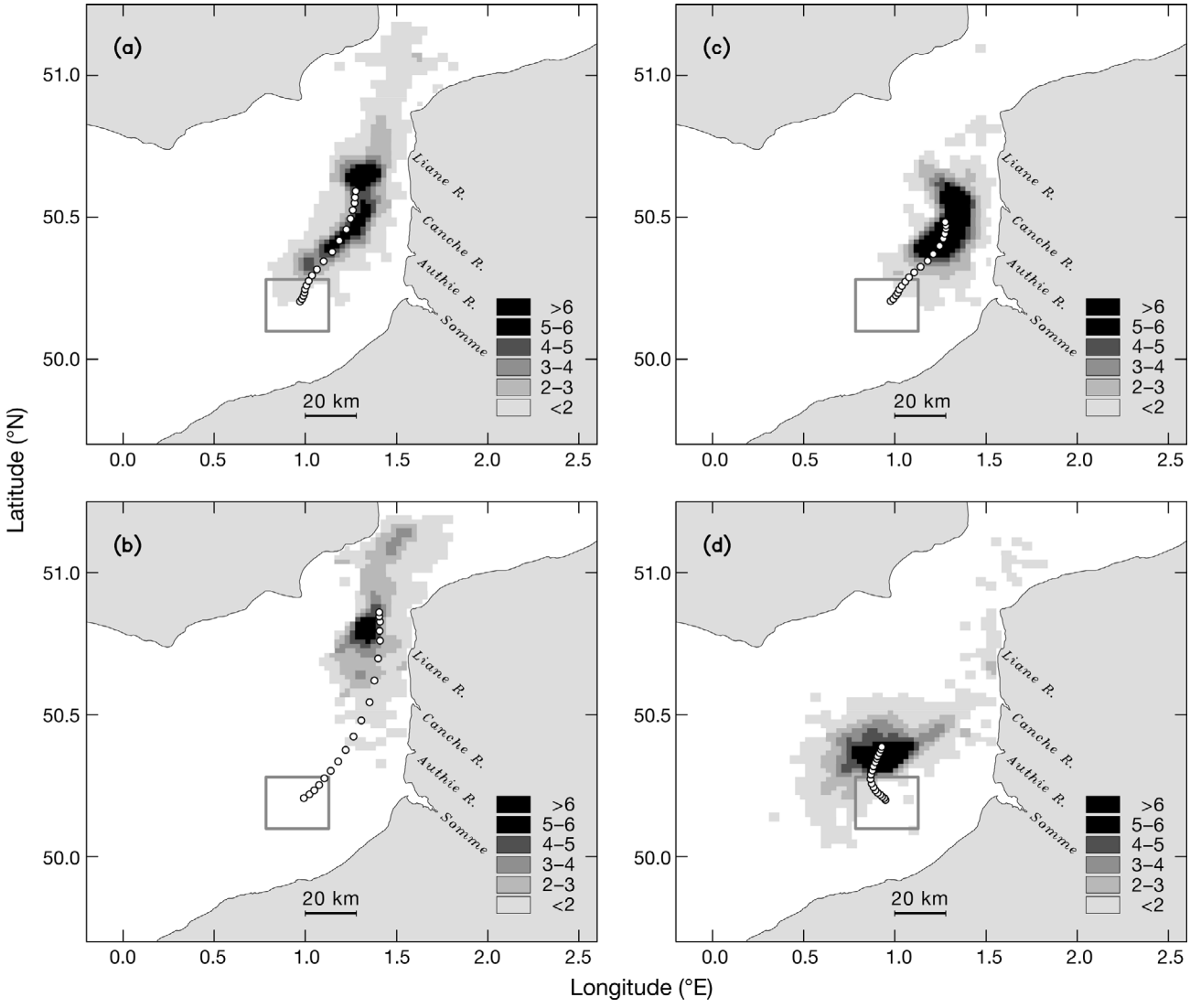

Fig. 6. Particle concentrations (no. per grid cell) after 18 d tracking with various behavioural models of vertical migration: (a) diurnal (light-locked) model, (b) tidal sea level-locked model, (c) tidal current-locked model, and (d) tidal current-locked model with the opposite sign of vertical swimming velocity. Particles were released in the area shown by the square. Circles show the Lagrangian residual displacement of the centre of mass of particles. The time interval between 2 successive locations of the centre of mass is 2 tidal cycles (24.8 h)

sea surface elevation by approximately 2 h (Fig. 4c). Particles executing such migration remain close together and retain their initial concentration (8 per grid box) for a long time during the tracking period. The spatial distribution reveals a low-spreading, along-coast orientation of particles in the group, with high concentrations found again 20 km offshore. Few of the particles can be seen in the vicinity of the coast. The speed of northward migration in this group of particles is 2 times smaller than in the case of tidally cued migration.

Fig. 6d shows the distribution of particles with the vertical velocity opposite in sign to the previous vertical migratory pattern, i.e. the negative velocity is attributed to particles during flood, and positive, to particles during ebb, as shown in Fig. 4d. The resultant distribution looks very different and reveals 2 tendencies in particle displacement. The majority of particles execute first northwestward, then northeastward drift in the middle of the channel, with a portion of the particles moving even to the southwest, in the opposite direction to the residual flow. The second group of particles, with low concentrations (3 per grid box) and separated from the main patch, executes shoreward, then along-coast drift. Particles of this group are found in the vicinity of the coast and also at the exit from the Dover Strait. A kind of stretching of particles in the cross-shore direction is induced by this vertical behavioural pattern.

Table 1. Synthetic properties of dispersion for different groups of particles. rms: root-mean square

Vertical migration pattern	Major axis orientation (°)	Along-axis rms displacement (km)	Cross-axis rms displacement (km)
No migration (960 particles)	69	23.7	8.3
No migration (9600 particles)	69	24.0	8.3
Light-dependent	67	23.8	6.2
Tidally cued	76	20.0	6.8
Locked to tidal currents	73	12.6	6.3

Dispersion processes

The PCA technique allows us to quantify the dispersion of particles and to discern the influence of vertical migration on horizontal spreading. We present in Table 1 the synthetic properties of dispersion: the orientation of the major axis of dispersion and the rms spreading of particles (relative to the centre of mass) along and across this axis. We analysed the horizontal distribution of 5 groups of particles, with and without vertical migration, at the end of the 18 d tracking period.

Both groups of 960 and 9600 neutrally buoyant particles reveal equivalent properties of dispersion, the direction and intensity of spreading, which confirm the observed similarity in the spatial distribution of particles and displacement of their centres of mass (Fig. 5a,b). Most striking is the difference in dispersion between the particle groups executing vertical motions. Particles with light-dependent vertical migration remain relatively close to the major axis of distortion (Fig. 6a). The rms magnitude of spreading along the minor axis (approximately in the cross-shore direction) is 6 km, while the neutrally buoyant particles show higher cross-shore dispersion (rms = 8 km) and a similar magnitude of dispersion in the along-shore direction. For all particle ensembles, the major axis tends to align with the direction of the dominant drift, and deviates clockwise from the north and from the coast line orientation by about 20°. Dispersion is weakest for particles executing vertical migration that is synchronised with tidal currents. The rms of spreading along the major axis is 2 times smaller than in the case of neutrally buoyant particles or particles executing light-dependent migration. Moreover, the dispersion of particles is more isotropic for this migratory pattern.

DISCUSSION AND CONCLUSIONS

The present study considers the coupled effect of barotropic (tidal) and baroclinic (forced by the freshwater input) circulation and the biological behaviour on larval transport in the EEC. It benefits from the increased spatial coverage of oceanographic and ichthyoplankton data available from the larval drift experiment (Grioche et al. 1997). These data and earlier results of Land (1991) indicated flounder larval transport from the spawning area (central part of the EEC, offshore the Somme estuary) to nursery grounds located along the French coasts and extending from the Somme mouth to the southern part of the North Sea. In their later study, Grioche et al. (2000) admitted a hypothesis of diurnal (light dependent) vertical migration of flounder larvae and a possible effect of migration on the rate and direction of the horizontal larval transport.

To verify these hypotheses and to analyse the sensitivity of larval transport to various forcing components, we performed a number of particle-tracking model simulations. In contrast to previous studies (Graaf et al. 2004), we consider particle displacement in a 3-dimensional flow field driven by a combination of tides and buoyancy input. The results of simulations reveal that the interaction between the turbulence, freshwater and tidal forcing leads to particle trapping and produces spreading along the coast, with the maximum concentration of particles observed at a distance of approximately 20 km offshore. The accumulation of particles along the French coast is found to be associated with the ROFI dynamics under a hypertidal regime. The modelling study of Sentchev & Korortenko (2005) shed light on the mechanisms of particle accumulation. The authors explored tidal circulation and transport in the ECC and have shown that, at the end of ebb, downward motions develop at the margin of the ROFI as a result of the surface current convergence, while near the coast and outside the ROFI the dominant vertical velocity is upward. At the end of flood, the situation is opposite: upward motions are detected along the coast, 15 to 20 km offshore. The downward motions are confined to a coastal area of 10 to 15 km width. It appears that particles are trapped and spread in the vertical direction within the water column by downward motions inside this convergence zone. The horizontal distribution of an ensemble of particles looks like the accumulation of particles. This feature of particle dynamics can be realistically represented only by means of a 3-dimensional hydrodynamic model.

Numerical Lagrangian tracking demonstrates that neutrally buoyant particles are not only concentrated on the margin of the ROFI, but move northward along the coast. This along-coast drift of particles is also related to ROFI dynamics combined with tidal motions. As shown by Simpson (1997), interaction between the density-driven flow and tidal stirring gives rise to a low-frequency residual flow along the coast. Sentchev & Korotenko (2005) have analysed the spatial extension of the coastal current in the EEC and provided an estimate of the residual velocity, the magnitude of which varies within the range of 5 to 30 cm s^{-1}. Field observations of surface currents along the northern coast of France (Sentchev & Yaremchuk 2007) have also indicated an along-shore residual current with typical velocity of the order of 20 cm s^{-1}. Thus, vertical motions, related to the surface current convergence within the ROFI system, in combination with the northward residual transport, strongly affect the vertical distribution of neutrally buoyant particles over multiple tidal cycles and can provide patchiness in the horizontal distribution of biological material. Without freshwater forcing, particles tend to be distributed in the vicinity of the shoreline and move northward with the residual tidal current at a lower speed. The analysis of our results suggests that the freshwater input controls the location of particle accumulation zones, whereas tidal currents determine the magnitude of the horizontal transport. The transport is strongly affected by the neap to spring variability of tidal current strength. Higher rates of displacement of the centre of mass of particles in Figs. 5 & 6 correspond to the period of primary spring tide, which occurred during the tracking period (Fig. 2d).

Numerical tracking experiments revealed that vertical migratory behaviour attributed to particles might cause relatively significant departure from the passive particle transport pattern. The essential differences concern the speed of northward drift of particles and the direction and intensity of dispersion. The drift and dispersion in the along-shore direction seem to be related. Low spreading and low speed of northward transport of particles are found together in the case of vertical migration synchronised with currents. Particles executing tidally cued and light-dependent migration move northward faster and exhibit stronger dispersion.

Regarding the dispersive part of transport, our simulations reveal that the intensity of spreading and the shape of particle distribution are strongly affected by vertical migratory behaviour, and also depend on the region (near-shore or offshore) where the drift occurs. Sentchev & Korotenko (2005) diagnosed 2 current regimes in the EEC: the offshore regime with low effective dispersion and the near-shore regime of high dispersion and stretching. In the near-shore waters, a relatively large horizontal dispersion in the along-shore direction is due to the interaction of tidally driven turbulence and the vertical shear generated by freshwater runoff. In turn, this mechanism interacts with the horizontal shear of residual currents, giving further increase of the effective dispersion in the direction of the residual current. The mechanisms of horizontal dispersion by oscillatory tidal and residual currents are also discussed in detail by Zimmerman (1986). The studies of Sentchev & Korotenko (2005) and Zimmerman (1986) suggest that shear dispersion is the basic mechanism responsible for strong deformation of a group of particles along the French coast in the ROFI system of the EEC. Our modelling results are in close agreement with these studies.

Experiments with vertically migrating particles show that the cross-shore dispersion is low for all of the considered migratory patterns. Particles, migrating at a diurnal or semidiurnal period, spend a part of the time in the middle and near-bottom layers, where the horizontal gradient of velocity is weaker than in the upper layer. Thus, the resultant horizontal cross-shore dispersion (Table 1) is weaker than that in neutrally buoyant particles travelling in the upper layer. We quantify the difference as 30%.

In the case of tidally cued vertical migration, vertical velocity depends upon hydrostatic pressure tendencies. In the EEC, the variation of sea surface height and currents over a tidal period is characterised by a strong asymmetry: the rising tide is 2 h shorter than the falling tide (Fig. 3b). This implies that after the current reversal at low water (LW), particles tend to reside in deeper layers and travel southward with lower velocity during a shorter period of time. Whereas particles travelling northward, after the current reversal at high water (HW), are found in the upper layer with a stronger current. The period of northward excursion of particles in this case is longer. In the EEC, tidal currents advance the sea surface height variation by approximately 2 h. If we assign this phase lag to migrating particles, the rate of northward drift of the ensemble of particles drops (Fig. 6c). We relate this effect to the vertical distribution of particles in different periods of the tidal cycle. Particles are found near the surface before and after the current reversal at HW, and at depths during the current reversal at LW (Fig. 2c). When the tidal current is strong, both upward- and downward-migrating particles are found at mid-depths. In this case, the difference between southward and northward excursion length appears to be smaller. These results suggest that the phase lag between the sea level and tidal current evolution, basically variable in space, might affect the intensity of larval drift differently in different parts of the basin, or might create conditions allowing

marine organisms to move in the opposite direction to the dominant flow (Hill 1994).

In summary, our computations have revealed the accumulation of neutrally buoyant and vertically migrating particles along the French coast, 20 km offshore. This happens because the interaction between the freshwater input and tidal currents produces particle trapping and spreading in a vertical direction within a convergence zone located on the ROFI seaward margin. Tides and buoyancy input induce the net along-shore northward transport, the intensity of which depends on the phase of 14 d tidal cycle and the vertical migratory pattern. Results of numerical modelling have been compared with the observed larval distributions and have shown consistency with the data. We have demonstrated that the vertical migratory behaviour of larvae can be an effective mechanism causing a significant departure from the transport pattern of passive tracers. It might also control the relative dominance of either retention or downstream advection of the larvae in the EEC. The vertical migration synchronised with tidal currents provides the lowest along-shore dispersion and a small rate of the northward drift of particles. Diurnal (light dependent) migration tends to decrease the magnitude of the cross-shore dispersion, whereas tidally (sea level) cued vertical migration induces a fast northward drift. Simulations with migrating particles revealed a strong sensitivity of the model to vertical migratory behaviour. Comparison with the field data led us to speculate that tidally (sea level) cued migration is most likely to occur. This behaviour, assigned to model particles, shows reasonable agreement with the observed distribution of abundances and a reasonable rate of northward migration. Though knowledge of the behavioural properties of larvae might help to explain horizontal transport, comparison of modelling results with observed abundances is important but far from being trivial. First, the sampled region covers only a part of the spawning grounds of flounder. Secondly, the spatial distribution of the larvae is affected, not only by the dynamic properties of flow and the biological behaviour of species, but also by the spatial patterns in survivorship, which are poorly known. Both accurate numerical simulations and large-scale sampling strategies, with precise observations of larval migratory behaviour and survival, are necessary for improving the efficiency of larval transport prediction.

Acknowledgements. This study was conducted as part of the project supported by CNRS Grant 12217. We thank A. Grioche and P. Koubbi for providing the biological data, and M. Yaremchuk for useful ideas and valuable comments on our manuscript. Constructive remarks and critical comments by anonymous referees and the scientific editors were very helpful in improving the paper.

LITERATURE CITED

Bartsch J (1988) Numerical simulation of the advection of vertically migrating herring larvae in the North Sea. Meeresforschung 32:30–45

Bartsch J, Coombs SH (2001) An individual-based growth and transport model of the early life-history stages of mackerel (*Scomber scombrus*) in the eastern North Atlantic. Ecol Model 138:127–141

Blumberg AF, Mellor GL (1987) A description of a three-dimensional hydrodynamic model of New York harbour region. J Hydraul Eng 125(8):799–816

Boeuf G, Payanb P (2001) How should salinity influence fish growth? Comp Biochem Physiol C 130:411–423

Boss A, Thiel R, Nellen W (1995) Distribution and transport mechanisms of the upstream migrating flounder larvae, *Pleuronectes flesus* Linnaeus, 1758, in the tidal Elbe River, Germany. ICES CM M41:1–10

Brown CA, Jackson GA, Brooks DA (2000) Particle transport through a narrow tidal inlet due to tidal forcing and implications for larval transport. J Geophys Res 105(C10): 24141–24156

Burke JS, Tanakab M, Seikai S (1995) Influence of light and salinity on behaviour of larval Japanese flounder (*Paralichthys olivaceus*) and implications for inshore migration. Neth J Sea Res 34:59–69

Burke JS, Ueno M, Tanaka Y, Walsh H 5 others (1998) The influence of environmental factors on early life history patterns of flounders. J Sea Res 40:19–32

Campos WL, Kloppmann M, von Westernhagen H (1994) Inferences from the horizontal distribution of dab *Limanda limanda* and flounder *Platichthys flesus* larvae in the south-eastern North Sea. Neth J Sea Res 32:277–286

Emery WJ, Thomson RE (1997) Data analysis methods in physical oceanography. Pergamon, New York

Flather RA (1976) A tidal model of the north-west European continental shelf. Mem Soc R Sci Liege Ser 6 X:141–164

Franks PJS (1992) Sink or swim: accumulation of biomass at fronts. Mar Ecol Prog Ser 82:1–12

Graaf M, Jager Z, Vreugdenhil CB, Elorche M (2004) Numerical simulations of tidally cued vertical migrations of flatfish larvae in the North Sea. Estuar Coast Shelf Sci 59:295–305

Grioche A, Koubbi P, Sautour B (1997) Ontogenic migration of *Pleuronectes flesus* larvae in the eastern English Channel. J Fish Biol 51(Suppl A):385–396

Grioche A, Harlay X, Koubbi P, Fraga Lago L (2000) Vertical migration of fish larvae: Eulerian and Lagrangian observations in the eastern English Channel. J Plankton Res 22: 1813–1828

Hill AE (1994) Horizontal zooplankton dispersal by diel vertical migration in S2 tidal currents on the northwest European continental shelf. Cont Shelf Res 14:491–506

Hunter J, Craig P, Phillips H (1993) On the use of random-walk models with spatially-variable diffusivity. J Comp Physiol 106:366–376

Jenkins GP, Black KP, Keough MJ (1999) The role of passive transport and the influence of vertical migration on the pre-settlement distribution of a temperate, demersal fish: numerical model predictions compared with field sampling. Mar Ecol Prog Ser 184:259–271

Jenkins GP, Black KP, Hamer PA (2000) Determination of spawning areas and larval advection pathways for King George whiting in southeastern Australia using otolith microstructure and hydrodynamic modelling. I. Victoria. Mar Ecol Prog Ser 199:231–242

Le Provost C, Lyard F, Molines JM, Genco ML, Rabilloud F (1995) A hydrodynamic ocean tidal model improved by

assimilating a satellite-derived data set. J Geophys Res 103(C3):5513–5529
Mellor GL, Yamada T (1982) Development of a turbulence closure model for geophysical fluid problems. Rev Geophys Space Phys 20:851–875
Nielsen E, Bagge O, MacKenzie BR (1998) Wind-induced transport of plaice (*Pleuronectes platessa*) early life-history stages in the Skagerrak–Kattegat. J Sea Res 39:11–28
Sentchev A, Korotenko K (2004) Stratification and tidal current effects on larval transport in the eastern English Channel: observations and 3D modelling. Environ Fluid Mech 4:305–331
Sentchev A, Korotenko K (2005) Dispersion processes and transport pattern in the ROFI system of the eastern English Channel derived from a particle-tracking model. Cont Shelf Res 25:2294–2308
Sentchev A, Yaremchuk M (2007) VHF radar observations of surface currents off the northern Opal coast in the eastern English Channel. Cont Shelf Res (in press)
Simpson JM (1997) Physical processes in the ROFI regime. J Mar Syst 12:3–15
Smagorinsky J (1963) General circulation experiments with the primitive equations. I. The basic experiment. Mon Weather Rev 91:99–164
Van der Land MA (1991) Distributions of flatfish eggs in the 1989 egg surveys in the southeastern North Sea, and mortality of plaice and sole eggs. Neth J Sea Res 27: 353–366
Van der Veer HW, Ruardij P, Van den Berg AJ, Ridderinkhof H (1998) Impact of interannual variability in hydrodynamic circulation on egg and larval transport of plaice *Pleuronectes platessa* L. in the southern North Sea. J Sea Res 39:29–40
Visser AW (1997) Using random walk models to simulate the vertical distribution of particles in a turbulent water column. Mar Ecol Prog Ser 158:275–281
Werner FE (1995) A field test case for tidally forced flows: a review of the tidal flow forum. In: Lynch DR, Davies AM (eds) Quantitative skill assessment for coastal ocean models. Coast Estuar Stud 47:269–283
Werner FE, Quinlan JA, Blanton BO, Luettich RA (1997) The role of hydrodynamics in explaining variability in fish populations. J Sea Res 37:195–212
Xie L, Eggleston DB (1999) Computer simulations of wind-induced estuarine circulation patterns and estuary-shelf exchange processes: the potential role of wind forcing on larval transport. Estuar Coast Shelf Sci 49:221–234
Zimmerman JTF (1986) The tidal whirlpool: a review of horizontal dispersion by tidal and residual currents. Neth J Sea Res 20:133–154

Editorial responsibility: Alejandro Gallego (Contributing Editor), Aberdeen, UK

Submitted: July 11, 2006; Accepted: June 28, 2007
Proofs received from author(s): September 1, 2007

Vol. 347: 247–259, 2007
doi: 10.3354/meps06982

MARINE ECOLOGY PROGRESS SERIES
Mar Ecol Prog Ser

Published October 11

OPEN ACCESS

Assessment of an environmental barrier to transport of ichthyoplankton from the southern to the northern Benguela ecosystems

Christophe Lett[1,*], Jennifer Veitch[2], Carl D. van der Lingen[3], Larry Hutchings[3]

[1]IRD, UR ECO-UP, Oceanography Department, University of Cape Town, Rondebosch 7701, South Africa
[2]Oceanography Department, University of Cape Town, Rondebosch 7701, South Africa
[3]Marine and Coastal Management, Private Bag X2, Rogge Bay 8012, South Africa

ABSTRACT: The Lüderitz upwelling cell and Orange River cone (LUCORC) area, a transboundary region between South Africa and Namibia, is considered to be an environmental barrier to transport of ichthyoplankton from the southern to the northern Benguela upwelling ecosystems. We use environmental data and modelling to assess the potential mechanisms responsible for this barrier: environmental data were extracted from the 1 × 1° World Ocean Atlas 2001 database and used to build maps of annual mean salinity, temperature, chlorophyll, dissolved oxygen and nutrient concentrations; outputs of a regional circulation model were used in an individual-based model to assess the transport of passive particles from the southern to the northern Benguela. The data show no clear environmental barrier at sea surface, but the model results suggest that particles released there would be largely transported offshore. The model also shows that particles released below the surface could be transported alongshore from the southern to the northern Benguela, but low subsurface temperatures would increase ichthyoplankton mortality and hence be a strong limiting factor to northward transport. We conclude that the combination of a surface hydrodynamic and a subsurface thermal barrier could limit the possibility for ichthyoplankton of epipelagic species to be transported from the southern to the northern Benguela, but that ichthyoplankton of mesopelagic species, having a wider tolerance to low temperatures, would be less affected.

KEY WORDS: Environmental barrier · Ichthyoplankton · Benguela · Lüderitz upwelling cell · Orange River cone · Physical–biological interactions · Individual-based model · World Ocean Atlas

INTRODUCTION

The Benguela Current upwelling system, 1 of 4 major upwelling regions in the world, exists along the eastern boundary of the South Atlantic basin from Cape Agulhas (35° S, see Fig. 1) to approximately Namibe (15° S). It comprises the eastern part of the broad, sluggish, South Atlantic gyral circulation driven by the prevailing southeast trade winds. Vigorous wind-driven coastal upwelling occurs along the shoreward margin between 16 and 34° S, bounded, in a very dynamic manner, by warm currents of tropical origin (the Angola Current in the north and the Agulhas Current in the south; see Fig. 1). The Lüderitz upwelling cell and Orange River cone (LUCORC) area, between 25 and 30° S approximately (see Fig. 1), represents not only the transboundary region between South Africa and Namibia, but also a region with the most active upwelling centre in the world (Bakun 1996). There are several active upwelling centres within the Benguela system (Nelson & Hutchings 1983, Shannon & Nelson 1996), of which Lüderitz is by far the strongest in terms of persistence and intensity (Parrish et al. 1983, Boyd 1987). The LUCORC area also includes the Orange (Gariep) River cone, the widest part of the Benguela continental shelf.

The Lüderitz upwelling cell represents an extreme of the optimal environmental spectrum, in that the persistent high wind speeds generate not only powerful off-

*Email: Christophe.Lett@ird.fr

shore Ekman drift, but also considerable mixing in the water column, which does not favour retention, concentration, or enrichment in the triad of factors considered important for pelagic fish larval survival (Bakun 1996). Powerful upwelling centres off Cape Blanc in the Canary Current upwelling system, off Point Conception and Cape Mendocino in the California Current upwelling system are also areas considered as unfavourable spawning habitats (Parrish et al. 1983). Several authors (Shannon 1985, Shannon & Pillar 1986, Cruickshank et al. 1990, Barange et al. 1992, Field & Shillington 2006) have noted that oceanographic and biological characteristics are different on either side of the LUCORC area, leading to a separation into 'northern' and 'southern' Benguela subsystems. Many fish species occur on both sides of the LUCORC area, but this region appears to act as a barrier to some species of phytoplankton, copepods, euphausiids and pelagic fish. Sardines *Sardinops sagax* are of particular interest since they spawn over a wide area, from the east coast of South Africa to southern Angola, in a wide variety of habitats (van der Lingen & Huggett 2003), except in the LUCORC area (Olivar & Fortuño 1991, Hutchings et al. 2002). The rise and decline of the South African sardine fishery in the period from 1958 to 1963 was separated from that of the Namibian sardine fishery by approximately a decade (van der Lingen et al. 2006), and, whilst the South African population has recovered, the Namibian population remains at low levels, suggesting that the 2 populations are separate. A tagging study conducted during a time when both populations were abundant (1957 to 1963) reported that, whilst some sardine tagged in the north were recovered in the south (but not the other way around), the very low proportion compared to the number of fish tagged (~140 000) indicated that the 2 populations were independent (Newman 1970). Additionally, the lack of coherence between a biological time-series for sardine from the northern and southern Benguela has been taken as indicative of stock separation (Kreiner et al. 2001). Other important pelagic fish species, including anchovy *Engraulis encrasicolus*, redeye round herring *Etrumeus whiteheadi*, horse mackerel *Trachurus trachurus capensis* and shallow-water hake *Merluccius capensis*, have been reported as spawning on either side of the LUCORC area, but not within it (Olivar & Fortuño 1991, Olivar & Shelton 1993, Sundby et al. 2001).

A number of questions have recently been raised regarding this partial environmental barrier (Florenchie 2004), in particular about the mechanisms involved in generating it, maintaining it and breaking it down. Mechanisms include the input of freshwater from the Orange River mouth, which reduces the salinity of coastal waters, and intense upwelling off Lüderitz that leads to strong offshore Ekman transport and a cooling of coastal waters. Low levels of chlorophyll concentrations have also been reported in the LUCORC area (Brown et al. 1991, Demarcq et al. 2003). Agenbag & Shannon (1988) found, however, no support for strong surface temperature, salinity, or chlorophyll discontinuity in the region. They therefore hypothesised that intense mixing in the water column due to strong upwelling would be responsible for low primary and secondary production. Drifter trajectories reported by Gründlingh (1999) and Largier & Boyd (2001) suggest strong offshore transport off Lüderitz and northwards. Carr & Kearns (2003) data analysis suggests particular conditions in the LUCORC area in terms of Ekman transport and chlorophyll concentrations, but not regarding salinity, temperature, or oxygen. However, Stander (1964) and Duncombe Rae (2005) identified a discontinuity at the LUCORC area in the properties of central and intermediate waters, with high salinity and low oxygen waters present north of Lüderitz, but not south of the Orange River mouth.

Whether the LUCORC area constitutes a hydrodynamic, thermal, haline, trophic, or oxygen barrier (or a combination of these) for the shelf biota remains an open question. Given that prevailing near-surface currents in the region are northward, we investigate here a potential environmental barrier to transport from the southern to the northern Benguela. We first use the 1 × 1° World Ocean Atlas 2001 database to build maps of annual mean salinity, temperature, chlorophyll, dissolved oxygen and nutrient concentrations. We then focus on hydrodynamic aspects of the LUCORC area, using outputs of a regional circulation model in an individual-based model that tracks passive particles to examine the flow field and temperature conditions that particles would experience when released in the south of the LUCORC region. We finally discuss the results regarding the biology of epipelagic and mesopelagic fish species ichthyoplankton. In doing so, we implicitly consider ichthyoplankton as being passive entities, leaving aside, as a first approach, horizontal swimming and vertical migration. This study complements previous studies in which individual-based models were used to investigate the effects of physical and biological factors on the dynamics of anchovy and sardine ichthyoplankton in the southern (Mullon et al. 2002, 2003, Huggett et al. 2003, Parada et al. 2003, Skogen et al. 2003, Lett et al. 2006, Miller et al. 2006) and northern (Stenevik et al. 2003) Benguela ecosystems.

MATERIALS AND METHODS

Tolerance ranges of ichthyoplankton to environmental variables. For the LUCORC area acting as a

barrier, the environment there should consistently fall outside the tolerance limits of ichthyoplankton for one or more environmental variables. Unfortunately, information on the tolerance ranges of important Benguela fish species ichthyoplankton is not comprehensive, and published studies are over 2 decades old. Nonetheless, some data on the lower lethal limits for selected environmental parameters (primarily temperature) are available and are briefly described below.

Laboratory studies showed that a temperature of 10.8°C proved lethal to anchovy eggs, and, whereas eggs kept at <13.6°C did develop to hatching, subsequent larval development was abnormal with larvae failing to develop pigmented eyes and a functional jaw (King et al. 1978). Similarly, although sardine eggs developed to hatching at 11°C, those kept at <13°C also failed to develop pigmented eyes and a functional jaw (King 1977). Additionally, sardine eggs were not affected by salinities ranging from 33 to 36 psu, but showed a reduction (to <80%) in viable hatch levels at dissolved oxygen levels of 1.5 ml l^{-1} and a temperature of 22°C, leading King (1977) to suggest that low dissolved oxygen levels may counteract apparently favourable temperature regimes. Laboratory studies on round herring (O'Toole & King 1974) and horse mackerel (King et al. 1977) eggs indicated that the lower lethal temperatures for these species were <11.0 and <12.6°C, respectively. Field studies reported that horse mackerel larvae were found at temperatures as low as 13.5°C, at salinities down to 35.2 psu, and over a dissolved oxygen range of 4.6 to 5.0 ml l^{-1} (O'Toole 1977).

World Ocean Atlas data. The data used here were extracted from the World Ocean Atlas (WOA) 2001 database (Conkright et al. 2002) and cover the majority of the Benguela Current region from 20 to 37° S and from 10 to 20° E, being approximately centred on the LUCORC area. We used the 1 × 1° objectively analysed (i.e. squares that do not contain any data are filled through a process of interpolation and smoothing; Conkright et al. 2002) annual means of salinity, temperature, chlorophyll, dissolved oxygen and nutrient (nitrate, phosphate and silicate) concentrations. The number of observations per square typically ranges from a few 10s offshore to a few 100s or 1000s alongshore.

Hydrodynamic model. The hydrodynamic model employed is the regional oceanic modelling system (ROMS) (Shchepetkin & McWilliams 2005), which is a split-explicit, free-surface oceanic model discretised in coastline- and terrain-following curvilinear coordinates. The model solves the primitive equations in a rotating environment based on the Boussinesq approximation and the vertical hydrostatic equilibrium balance. Short time-steps are used to advance the barotropic momentum equations, and longer time-steps are used to solve the baroclinic momentum equations. The explicit lateral viscosity is zero everywhere in the model domain, except in the sponge layers near the boundaries, where the viscosity increases smoothly toward the lateral open boundaries. The vertical mixing term in the interior and at the planetary boundaries is derived by the non-local K-profile parameterisation scheme (KPP; Large et al. 1994).

In order to circumvent the issue of the interaction of features of highly disparate spatial scales and to preserve efficiency, a nested modelling approach was followed. The 1-way grid-embedding capability of ROMS was employed, in which a sequence of structured grid models are able to interact with one another (Penven et al. 2006a). The embedding procedure makes use of the AGRIF (adaptive grid refinement in Fortran) package. Temporal coupling of the low-resolution parent and high-resolution child grids is done at the baroclinic time-step. Prognostic baroclinic variables (horizontal velocity components, temperature and salinity) are interpolated bi-linearly along the s-coordinates (i.e. terrain-following) and linearly in time for each time-step of the child model, thereby implying that the bottom topography (or sigma levels) must correspond in the area of the parent–child boundary.

The parent model employed is the southern Africa experiment (SAfE) ROMS configuration, which is designed to resolve the major oceanic phenomena that exist around southern Africa (Penven et al. 2006b). It has been built using ROMSTOOLS (Penven 2003). The Mercator grid has an increment of 0.25°, ranging from 2.5° W to 54.75° E and from 46.75 to 4.8° S (Fig. 1). The horizontal resolution ranges from 19 km in the south to 27.6 km in the north. The vertical resolution is based on 32 s-coordinate levels, which are stretched towards the surface, resulting in a resolution of 0.37 to 5.70 m in the surface layer and 11 to 981 m in the bottom layer. A radiation scheme exists at the lateral boundaries to connect the model with its surroundings, while inflow conditions are nudged toward data. Mean monthly temperature and salinity data are obtained from the WOA 2001 database (Conkright et al. 2002).

The high-resolution child model is designed to encompass most of the Benguela upwelling area, and has a temporal and spatial resolution 3 times finer than the parent grid (approximately 15 min and 8 km, respectively). The child model has 124 × 238 grid points in the horizontal plane, encompassing the area from 9.5 to 20° E and from 18 to 35.5° S (Fig. 1), and 32 vertical levels that are stretched toward the surface in order to obtain higher resolution there. The boundary conditions of the child grid are supplied by the parent grid.

Both the parent and child models start from rest and are forced at the surface by the comprehensive ocean/

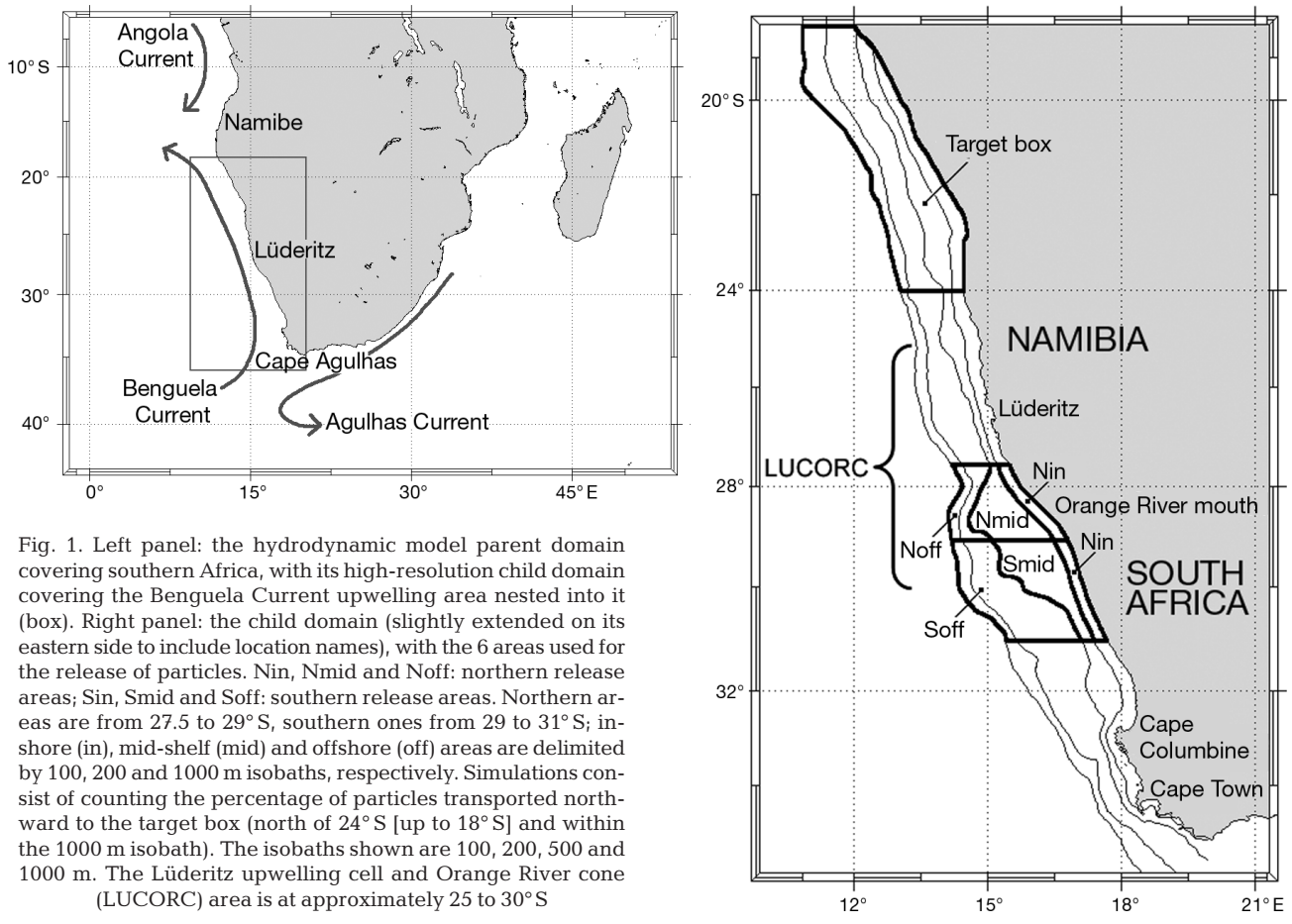

Fig. 1. Left panel: the hydrodynamic model parent domain covering southern Africa, with its high-resolution child domain covering the Benguela Current upwelling area nested into it (box). Right panel: the child domain (slightly extended on its eastern side to include location names), with the 6 areas used for the release of particles. Nin, Nmid and Noff: northern release areas; Sin, Smid and Soff: southern release areas. Northern areas are from 27.5 to 29° S, southern ones from 29 to 31° S; inshore (in), mid-shelf (mid) and offshore (off) areas are delimited by 100, 200 and 1000 m isobaths, respectively. Simulations consist of counting the percentage of particles transported northward to the target box (north of 24° S [up to 18° S] and within the 1000 m isobath). The isobaths shown are 100, 200, 500 and 1000 m. The Lüderitz upwelling cell and Orange River cone (LUCORC) area is at approximately 25 to 30° S

atmosphere data set (COADS) monthly climatology (Da Silva et al. 1994) and use the general bathymetric chart of the Worlds oceans (GEBCO) for the bottom topography. The initial temperature and salinity conditions are for the month of January from the WOA mean monthly climatology. This parent–child configuration was run for 10 yr. Plots of volume-integrated kinetic energy and mean surface kinetic energy (not shown) reveal that a spin-up time of 2 yr was required in order to reach statistical equilibrium; therefore, only output from Year 3 to 10 was analysed.

To test the validity of the model output the annual mean sea surface temperature (SST) and sea surface height (SSH) of the child model was compared to SST and SSH derived from satellite data. The general shape of the simulated upwelling regime is sufficiently realistic to reproduce the offshore 'bulge' of upwelling at Lüderitz and, to some extent, in the region of the Orange River cone. In general, the extent of the modelled upwelling regime is more confined to the coast and more continuous, and temperatures in a narrow band all along the coast are somewhat underestimated. This distinct difference has been noted by Penven et al. (2001), who attributed it to overly strong coastal wind forcing. In the model and the data there are negative SSH anomalies in a band along the coast, which broadens significantly north of Lüderitz, while positive values dominate the southwest corner of the domain. Modelled negative anomalies at the coast are larger than the satellite-derived anomalies, which may also be related to overly strong coastal wind forcing.

Individual-based model. The individual-based model makes use of water velocity and temperature fields stored from the hydrodynamic model simulations every 2 d to transport passive (horizontally and vertically) particles offline. Velocity and temperature fields are transformed from the ROMS curvilinear grid into a Cartesian grid, and trilinear interpolations are used inside the Cartesian grid to obtain values of velocity and temperature at any particle location. Transport of particles relies only on advection, as no diffusion term is introduced. A forward Euler integration scheme is used to move particles from one time-step (2.4 h) to the other.

Two sets of tests of the particle-tracking kernel of the model were performed. Firstly, the consistency of particle trajectories was checked in an artificially uniform velocity field. Secondly, trajectories of particles in the

individual-based model were compared with those obtained using another off-line Lagrangian tool (ROMS offline, X. Capet unpubl. data, available online at www.atmos.ucla.edu/~capet/Myresearch/my_research_floats.html). Although the trajectories simulated by the 2 tools were not exactly identical, differences were small and were believed to be of no consequence for the general patterns investigated in this study.

Six areas for the release of particles were considered (Fig. 1). The northern areas (Nin, Nmid and Noff) are located at the southern part of the LUCORC area and the southern ones (Sin, Smid and Soff) further south (in, mid and off: inshore, mid-shelf and offshore, respectively). Areas were positioned in order to estimate the possibility for particles to cross the LUCORC area either partly or entirely. Simulations consisted of releasing 30 000 particles over these areas, tracking them for 120 d and counting those that were transported alongshore north of 24° S (the target box in Fig. 1). Particles that did so were considered to have been successfully transported. The duration of 120 d was chosen as being long enough for particles to be potentially transported to this area, knowing that typical near-surface current velocities in the region are >10 cm s^{-1} (Shannon 1985, Boyd et al. 1992, Gründlingh 1999). Uniform distributions in space and time were used for releases. Time (month and year) and location (area [see above] and depth) of releases changed between simulations. Month varied from January to December, year, from Y4 to Y9, and 5 depth levels (0 to 20 m, …, 80 to 100 m) were used. This resulted in a dataset of 6 × 12 × 6 × 5 = 2160 values of transport success. The effects on transport success of the area, month, year and depth factors were assessed graphically and by performing a multifactor analysis of variance for a linear model with 2-way interactions fitted to the dataset. Normal distribution and homogeneity of variances for residuals were estimated visually by plotting a histogram of residuals and a plot of fitted versus residual values. All simulations were finally re-run under the same conditions as above, except that particles 'died' when they encountered waters <14°C, the estimated limit for anchovy ichthyoplankton (see above).

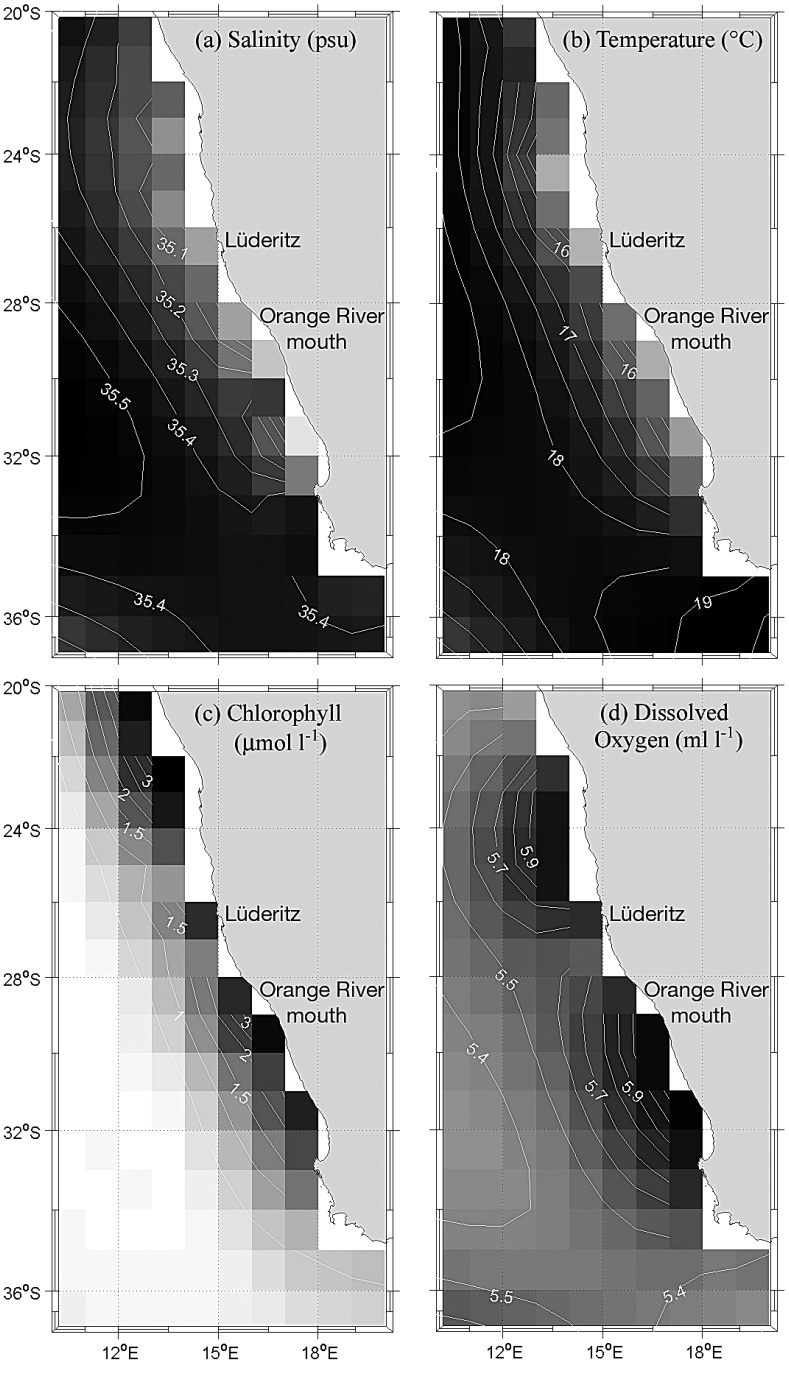

Fig. 2. Annual mean surface (a) salinity (N = 14 743), (b) temperature (N = 25 322), (c) chlorophyll (N = 1985) and (d) dissolved oxygen (N = 6111) concentrations derived from the 1 × 1° grid World Ocean Atlas 2001 database (darker-shading: larger values). N is no. of observations over whole area represented

RESULTS

Surface annual mean salinity, temperature, chlorophyll and dissolved oxygen concentrations derived from the 1 × 1° WOA 2001 database are shown in Fig. 2. No obvious patterns in salinity and temperature

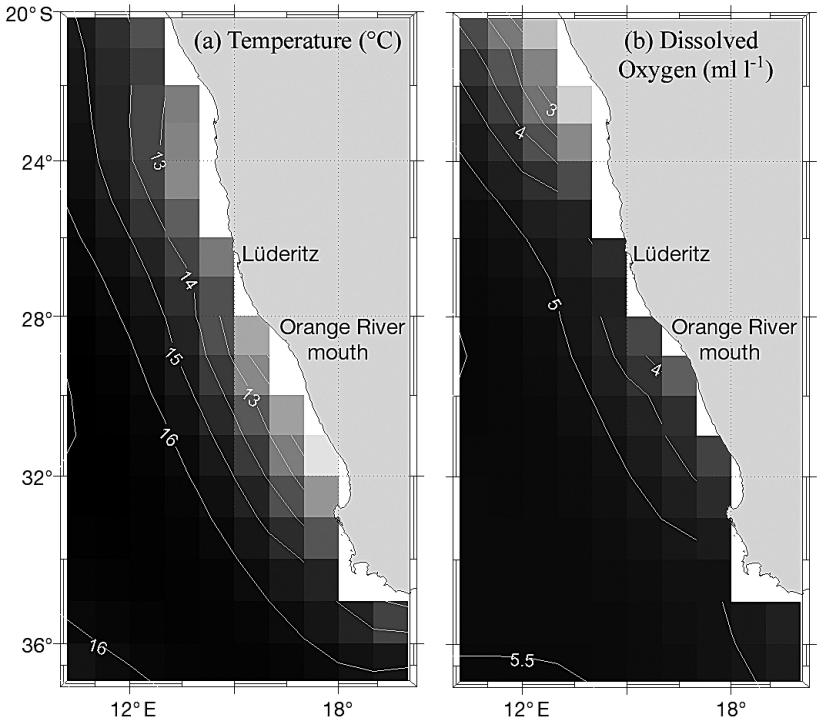

Fig. 3. Annual mean (a) temperature (N = 20 088) and (b) dissolved oxygen concentration (N = 5784) at a depth of 75 m derived from the 1 × 1° grid World Ocean Atlas 2001 database (darkershading: larger values)

can be seen (Fig. 2a,b), but minima in chlorophyll and dissolved oxygen concentrations are notable along the coast between 25° and 29° S (Fig. 2c,d). Maxima in nitrate, phosphate and silicate occur between 26° and 27° S (not shown). Annual mean temperatures and dissolved oxygen concentrations at a depth of 75 m are shown in Fig. 3; again, no obvious spatial pattern in temperature can be seen, but dissolved oxygen levels close to the coast are lower to the north of the LUCORC area. Annual mean salinity at 75 m (not shown) is very similar to salinity at the surface (Fig. 2a), except that the values are lower by about 0.1 psu.

Results of the individual-based model simulations conducted to assess the possibility of particles for crossing the LUCORC area are shown in Fig. 4. The values of transport success are expressed as the percentage of particles released that were transported alongshore to the north of 24° S (Fig. 1). Transport success is higher for the northern areas of release than for the southern areas, and decreases offshore in both. It is maximum in austral autumn and winter (April to September) and minimal in spring and summer, shows little interannual variability, and shows a dramatic decrease closer to the surface. In an attempt to assess the sensitivity of these results to the particle-tracking duration, simulations were re-run with a duration of 180 d (instead of 120 d). Transport success values increased only slightly, and the influences of the different factors remained very similar to those shown on Fig. 4. The main change concerned depth, with transport success showing a very small increase for upper depth levels, but a substantial increase for deeper levels (from ~26% using 120 d to ~32% using 180 d for the 80 to 100 m depth level).

Results of the multifactor analysis of variance performed on the transport success values show that all single factors and all 2-way interactions except one are significant (Table 1). Area, Month, Depth, Area × Month and Area × Depth explain >10% of the variance each, and a model including only these 5 terms explained 85% of the variance (not shown). Other factors explain <2% of the variance each.

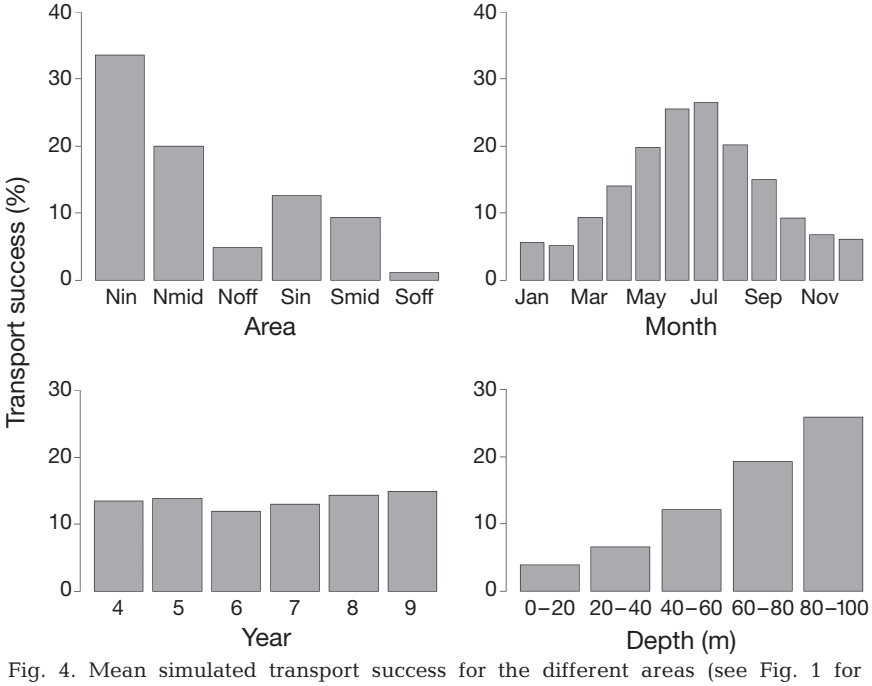

Fig. 4. Mean simulated transport success for the different areas (see Fig. 1 for abbreviations), months, years and depth levels

Table 1. Results of a multifactor ANOVA performed for a linear model with 2-way interactions fitted on simulated transport success data (***p < 0.001). Var.: variance; ns: not significant

Factor	df	SS	MS	*F*-value	p	% Var.
Area	5	249238	49848	905.8026	***	25.43
Month	11	120412	10947	198.9154	***	12.29
Year	5	1940	388	7.0517	***	0.20
Depth	4	142848	35712	648.9401	***	14.58
Area × Month	55	209426	3808	69.1924	***	21.37
Area × Year	25	3262	130	2.3710	***	0.33
Area × Depth	20	117051	5853	106.3493	***	11.94
Month × Year	55	14018	255	4.6315	***	1.43
Month × Depth	44	15982	363	6.6003	***	1.63
Year × Depth	20	444	22	0.4032	ns	0.05
Residuals	1915	105385	55			10.75

The effect of depth on transport success for particles released in the northern areas is emphasised in Fig. 5. Those released in surface waters (0 to 20 m depth) were substantially transported offshore, whereas those released in subsurface waters (60 to 80 m depth) were essentially transported alongshore. Particles released further south followed similar patterns (not shown), after being first transported northward to the LUCORC area.

Why there are important Area × Month and Area × Depth interactions is clear from Fig. 6. Transport success has a

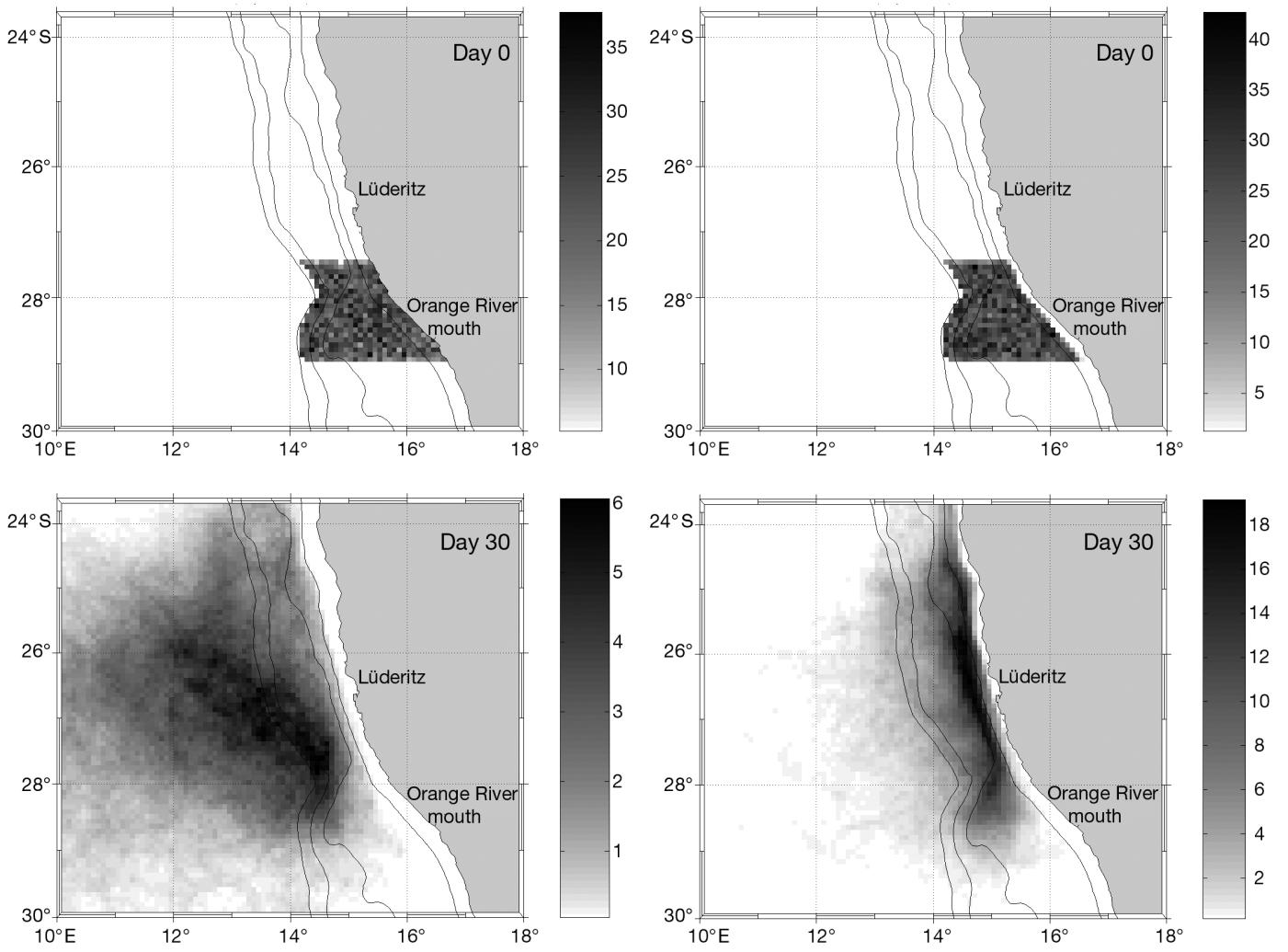

Fig. 5. Number of particles in the upper 100 m depth at the time of release (upper panels) and after a simulated period of 30 d (lower panels), for the 3 northern release areas. The latitudinal extension of the release zone is 27.5 to 29°S, its longitudinal extension is from the coast to the 1000 m isobath, and depth ranges from 0 to 20 m (left panels) or 60 to 80 m (right panels); 10 000 particles are initially randomly distributed within this volume. The maps shown are averages of particle release and tracking experiments repeated every 2 wk during 6 yr (Y4 to Y9). The isobaths shown are 100, 200, 500 and 1000 m. Note that scales change from one map to another

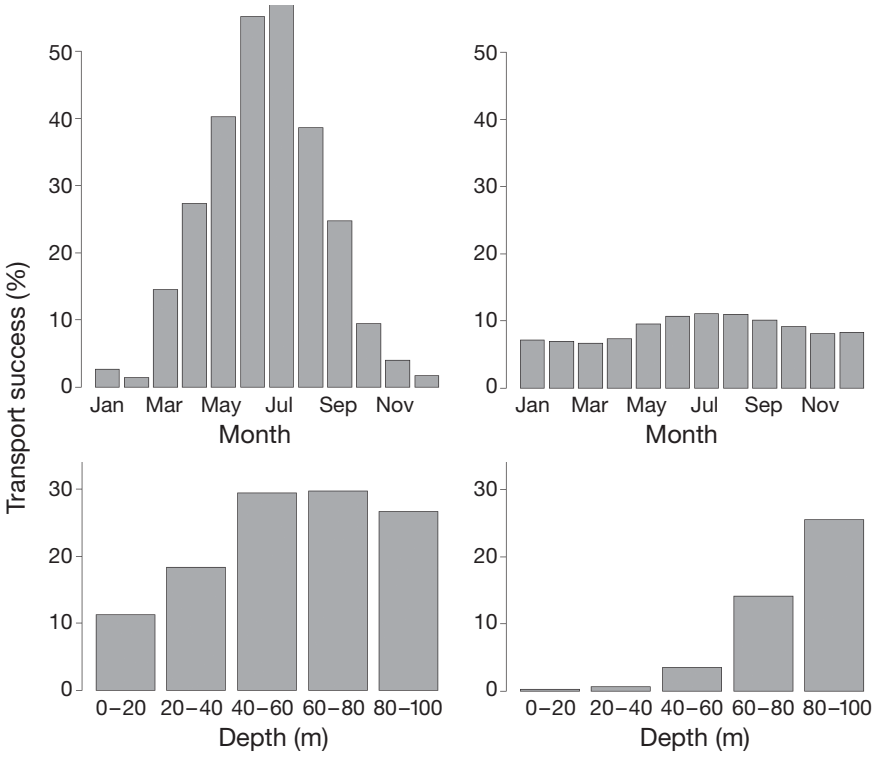

Fig. 6. Mean simulated transport success for the different months and depth levels for inshore areas combined (Nin and Sin; left panels) and mid-shelf and offshore areas combined (Nmid, Noff, Smid and Soff; right panels). See Fig. 1 for area abbreviations

marked seasonal pattern and is highest at 40 to 80 m depth for inshore areas (Nin and Sin), whereas it shows little seasonality and increases with depth for mid-shelf and offshore areas. Transport success is very low for particles released in the upper 60 m of the mid-shelf and offshore areas, but it is substantially higher for those released over that depth range in the inshore areas.

When simulations are re-run under the same conditions as above except that particles 'die' when they are in waters <14°C, the results change dramatically. Under these conditions transport success is <3% for any combination of release area, month, year and depth level; a reduction of approximately an order of magnitude compared to simulations without a lethal temperature. When temperature is included, the highest values of transport success are obtained for the deeper depth levels of the mid-shelf and offshore northern release areas, and there is a slight increase in success in both summer and winter months (Fig. 7a–d). The mean percentage of dead individuals increases markedly inshore and also with increasing depth, but shows little seasonal or interannual variability. There is no difference in death rates between northern and southern release areas (Fig. 7e–h).

DISCUSSION

The map of annual mean surface salinity obtained from the 1 × 1° WOA 2001 database (Fig. 2a) reveals no discontinuity at the LUCORC area. Simulation results obtained by Florenchie (2004) do suggest that Orange River outflow affects the ocean's salinity, but in a rather limited area north of the mouth of the river. Considerable water extraction along the course of the river has reduced significant flood events to once every 15 to 20 yr. In addition, the fresh water component is generally restricted to the upper few metres of the water column, and there appears to be limited impact on biological organisms. These results, together with others (Agenbag & Shannon 1988, Carr & Kearns 2003) and the reports listed before indicating that salinity values observed in the LUCORC area do not adversely impact (at least not directly) fish eggs and larvae, suggest that the LUCORC area does not constitute a haline barrier. The map of annual mean surface temperature (Fig. 2b) shows no unusual feature in the LUCORC area. From SST remote-sensing data analysed by Demarcq et al. (2003), it is also not clear whether the Lüderitz upwelling cell is characterised by the coldest waters along the southern Africa west coast, but it presents the largest offshore extension of cold waters and the smallest seasonal variability. These 2 results, together with others (Agenbag & Shannon 1988, Carr & Kearns 2003) and the reports listed before indicating that surface temperature values observed in the LUCORC area are above lower lethal limits of fish eggs and larvae, bring no support to the LUCORC area being a surface thermal barrier. Maps of annual mean surface chlorophyll (Fig. 2c) and dissolved oxygen (Fig. 2d) concentrations do show local lowest values in the LUCORC area, but concentrations there are still high and not dramatically lower than further south or north. Additionally, observed dissolved oxygen levels are well above those reported to adversely impact fish eggs and larvae. These results, together with those of Carr & Kearns (2003), suggest that surface chlorophyll and oxygen are not limiting factors in the LUCORC area. The WOA data clearly reveal that the LUCORC area constitutes a transition between the nitrate- and phosphate-rich northern domain and the silicate-rich southern one (not shown). It is believed that nitrate is sometimes limiting in the

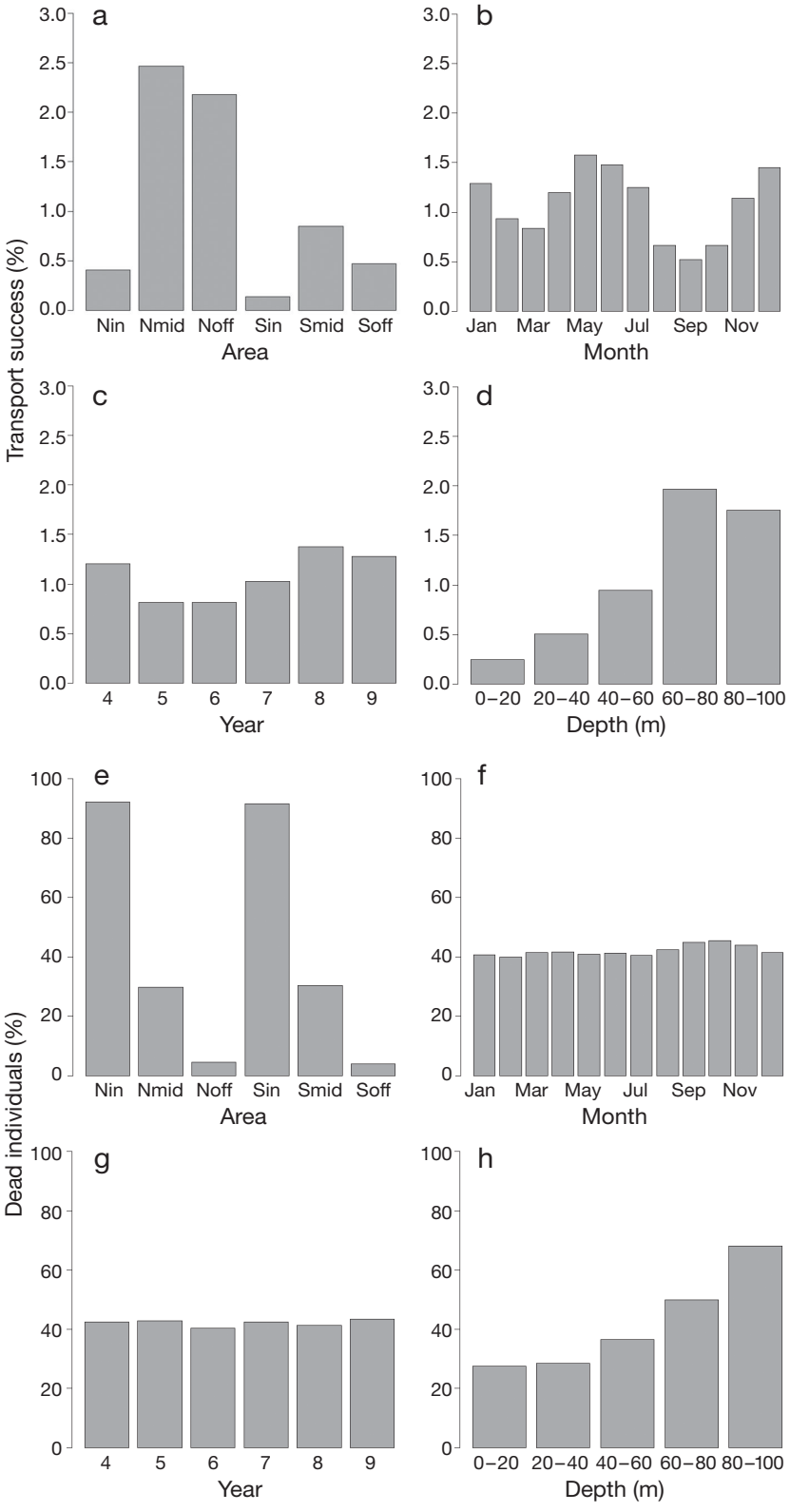

Fig. 7. Mean simulated (a–d) transport success and (e–h) percentage of dead individuals (particles simulating ichtyoplankton), for the different areas, months, years and depth levels, in simulations where individuals die when they are in waters <14°C. Note that the highest values in Panels a–d are <3%, whereas those in Panels e–h are around 90%. See Fig. 1 for area abbreviations

southern Benguela, while silicate is occasionally limiting in the northern Benguela (Shannon & O'Toole 1999). However, the LUCORC area itself appears to be rather rich in nitrate, phosphate and silicate. The conclusion of this analysis is that there is no strong evidence in the WOA data of a surface environmental barrier restricting northward transport of ichthyoplankton in the LUCORC area.

However, simulations of a regional circulation model performed to investigate the dynamics of water masses in the LUCORC area (Fig. 5) suggest that nearly passive biological material like ichthyoplankton would be massively transported offshore if released close to the surface. If released in deeper waters, however, they could largely be transported across the LUCORC area from the southern to the northern Benguela. These simulations also support the view of the northern part of the Orange River cone (28 to 29° S) as a dividing area (J. Largier pers. comm.). A large number of particles released in surface waters crossed the 200 m isobath there, and were later transported offshore (Fig. 5, left panels). In contrast most particles released in subsurface waters followed the 200 m isobath alongshore (Fig. 5, right panels). A series of individual-based simulations were performed to assess the permeability of the LUCORC area by counting particles being transported across it under different conditions of time and location of release. These confirmed that the depth of release determines largely this transport success, together with the offshore distance and season of release (Fig. 4, Table 1). The simulations strongly suggest that the LUCORC area constitutes a hydrodynamic barrier to transport from the southern to the northern Benguela near the surface, but that this result does not hold for subsurface layers. However, the WOA data show that there might be a subsurface thermal barrier, as water temperature is <14°C all along the coast (Fig. 3a, at 75 m depth), and, when simulations included a lower lethal temperature of 14°C, transport success was indeed very low (Fig. 7a–d). The inshore areas, where transport success was substantial at all depth levels without mortality (>10%; Fig. 6), showed

the most dramatic decrease when mortality was introduced (compare Fig. 7a–d with Fig. 4) as most (>90%; Fig. 7e–h) individuals released there died. We can therefore conclude that the combination of a surface hydrodynamic and a subsurface thermal barrier could limit the transport of ichthyoplankton from the southern to the northern Benguela.

The partition between low oxygen central and intermediate coastal waters in the northern Benguela and waters with more oxygen in the southern Benguela, as identified by Duncombe Rae (2005), is also present in the WOA data at a depth of 75 m (Fig. 3b). At subsurface depths, the oxygen minimum layer alters in the vicinity of the Lüderitz area from being on the outer shelf with a salinity signature indicating an origin in Angola, while south of Lüderitz more oxygenated water is present on the shelf originating from source water in the Cape Basin (Duncombe Rae 2005). Low-oxygen water does persist in shallower shelf waters close inshore southwards to 33 to 34° S, but is less intense than the very low oxygen levels on the shelf off central Namibia (Stander 1964, de Decker 1970). The impacts of low dissolved oxygen concentrations on ichthyoplankton are discussed by Ekau & Verheye (2005), who reported a correlation between the depth distribution of anchovy, sardine and horse mackerel larvae and dissolved oxygen concentrations in the northern Benguela, with near-zero larval densities found below concentrations of 2.5 ml l^{-1}. Dissolved oxygen levels in the LUCORC area at 75 m depth are still above this level, but, whereas exposure to environmental parameters below the lower tolerance level results in mortality, sublethal effects may well occur at parameter levels that are some way above the lower tolerance level. Brownell (1980) assessed sublethal effects of a variety of water quality parameters, including dissolved oxygen, by measuring the incidence of successful first-feeding by larvae of 8 species of marine teleosts (none of which were the species listed above, unfortunately) at different parameter levels, and calculated both LC_{50} (parameter concentration at which 50% of larvae die following a 24 h exposure) and EC_{50} (parameter concentration that reduces first-feeding incidence by 50% following a 24 h exposure) levels. That author considered that inhibition of first-feeding is probably not the most sensitive indicator of stress in marine fish larvae, but that it is nonetheless a highly relevant response given that death by starvation is the inevitable consequence of larvae that fail to feed. EC_{50} values ranged between 2.79 and 3.34 ml l^{-1}, and Brownell (1980) found only minor differences in EC_{50} values between species, suggesting a general applicability of these results to a wide variety of first-feeding marine fish larvae. Assuming that this generalisation does hold, these EC_{50} values suggest that even sublethal effects due to dissolved oxygen levels at 75 m in the LUCORC area are probably not large.

Carr & Kearns (2003) and Demarcq et al. (2003) showed that surface chlorophyll concentrations reach a local minimum off Lüderitz. In contrast, simulation results by Machu et al. (2005) indicate enhanced chlorophyll concentrations and primary production in the LUCORC area. The spatial horizontal resolution (1/3°) of the model they used (AGAPE) is too coarse to resolve coastal upwelling adequately, another model (ROMS-BIO) run at a higher spatial resolution (1/8°) results in a local minimum in the LUCORC area (E. Machu pers. comm.). Phytoplankton species require nutrients, which are in plentiful supply in the upper layers in the LUCORC area, but phytoplankton also needs a degree of stability in the water column in order to grow. High turbulence and deep mixing may be responsible for the diminished phytoplankton biomass in the LUCORC area. A dearth of phytoplankton implies poor feeding conditions for micro-, meso- and macrozooplankton and for ichthyoplankton throughout the LUCORC area. Fish larvae require concentrated, productive areas for successful survival, but they also require some form of retention within the productive area for successful recruitment. Areas downstream from active upwelling centres are generally more favourable for survival of fish larvae and juveniles, and, unless the organisms have some adaptation to cope with poor food and retention within the LUCORC area, such as strong vertical migratory ability or considerable motility, there is unlikely to be much life-cycle closure within that area. The WOA chlorophyll data in the region are based on a lower number of observations than for the other environmental variables, and ongoing studies using remote sensing data to derive phytoplankton biomass (C. H. Bartholomae pers. comm., H. Demarcq pers. comm.) should allow a better assessment of the LUCORC area as a trophic barrier to ichthyoplankton.

The main conclusion from this work is that a combination of a surface hydrodynamic and a subsurface thermal barrier could limit the transport of ichthyoplankton from the southern to the northern Benguela. Given the reports listed before of lower temperature lethal limits this result applies firstly to anchovy, whose limit can be estimated as 14°C. It also applies to sardine (13°C) and horse mackerel (12.6°C), but to a lesser extent. Indeed, simulations using a 13°C lethal temperature instead of a 14°C one resulted in a less dramatic decrease of transport success, with >10% values obtained for some released areas (Nin and Nmid), months (May to July) and depth levels (60 to 100 m) (results not shown). The result does not apply well to redeye round herring, whose limit can be estimated as 11°C. These 4 epipelagic fish species have been reported as spawn-

ing on either side of the LUCORC area, but not within it (Olivar & Fortuño 1991, Olivar & Shelton 1993), although redeye round herring eggs have actually recently been found in the region (C. D. van der Lingen unpubl. data). Important mesopelagic fish species in the region include shallow-water hake *Merluccius capensis*, lanternfish *Lampanyctodes hectoris* and lightfish *Maurolicus walvisensis*. These species have been reported to spawn from the surface to 200 m (Olivar & Shelton 1993), with maximum egg density at 20 to 60 m for lightfish (Prosch 1991) and 20 to 100 m for hake (Olivar & Fortuño 1991). According to Fig. 5 particles released in the subsurface layer would be transported northwards through the LUCORC area. Since studies suggest a lower temperature limit (<12°C) for lightfish (Prosch 1991) and hake (O'Toole 1978, Sundby et al. 2001), temperature is unlikely to be a major limiting factor for these species. This suggests that the LUCORC area is not a barrier to these 3 mesopelagic fish species, which is in agreement with lanternfish and lightfish spawning within this area, while shallow-water hakes do not (Olivar & Shelton 1993). Similarly, deep-water hakes *Merluccius paradoxus* occur through the LUCORC region as adults, but very few small juveniles are found in Namibian coastal waters, in contrast to coastal shelf waters south of the Orange River. This would suggest that hakes are not spawning in the LUCORC region, but are utilising the area for feeding.

The conclusions reached from this work need to be considered with some caution, given the spatial resolution of the data and the temporal resolution of the model forcing used. The WOA 2001 database was used in this study under the assumption that if there was a strong environmental barrier in the LUCORC area, it would be present in these data. With upwelling being a near-permanent feature in the LUCORC area, annual averages were used as a reasonable approximation of shorter time scales as well. However, the locations of pronounced discontinuities (that may act as barriers) observed between water masses in different cruises vary over time. Consequently, such strong discontinuities are expressed as smooth gradients in data like the WOA, which are relatively coarse 1 × 1° means collected over many research cruises (C. M. Duncombe Rae pers. comm.). Time series obtained from a fixed mooring off Walvis Bay (23° S) show that variability of temperature, salinity and oxygen concentrations occurs at short (~10 d), seasonal and interannual time scales (Monteiro & van der Plas 2006, Monteiro et al. 2006). As monthly climatology was used to force the hydrodynamic model, only the seasonal variability is present in our study. Temporal resolution of the wind-stress product used in hydrodynamic simulations of the southern Benguela was shown to be a crucial factor for retrieving the short time-scale patterns of SST anomalies (Blanke et al. 2005). Short events of positive or negative temperature anomalies are likely to play an important role in controlling the opening or closing of the aforementioned subsurface thermal barrier. A surface thermal barrier must also occur occasionally, as surface temperatures <11°C have been reported in the LUCORC area (Boyd 1987). Oxygen availability may well exert a similar control in deeper waters. In the present work, we miss short spatial or temporal scale events that would create temporary barriers, which may be particularly important for the lethal environmental variables like temperature and oxygen. Our smoothed version of the system is therefore likely to result in an underestimated assessment of the environmental barriers. There are also limitations in our individual-based model, including the 'instant death' assumption and the lack of turbulent particle motion. The instant death of simulated larvae arising from a single exposure to water colder than the specified lower lethal threshold is unrealistic, since larvae, once they are able to swim, can actively avoid such water, at least at a small scale and presumably via vertical migration towards warmer water. Hence, our simulations may have overestimated temperature-induced mortality, particularly for older larvae that possess better swimming capabilities than smaller larvae. However, our model treated eggs and larvae entirely as passive entities, and behavioural aspects such as vertical migration were not included. The inclusion of turbulent particle motion in the model would result in a higher proportion of particles released at the surface moving to deeper waters, and vice versa, which would 'blur' the vertical distribution patterns that we obtained, but could also potentially change them. Distribution patterns could also be affected in the horizontal dimension. However, there is still little information (e.g. drifter trajectories) in the region that would allow a parameterisation of turbulent motion.

Acknowledgements. This work is a contribution to the 'Upwelling Ecosystems (UR 097 ECO-UP)' joint program between Institut de Recherche pour le Développement, France, University of Cape Town and Marine and Coastal Management, South Africa (among other institutions and countries). We thank C. H. Bartholomae, X. Capet, H. Demarcq, C. M. Duncombe Rae, P. Florenchie, P. Fréon, J. Largier, E. Machu, F. A. Shillington, H. M. Verheye and P. Verley. A special thank-you to P. Penven. We are also grateful to 4 anonymous reviewers, and to H. I. Browman, A. Gallego, E. W. North and P. Petitgas.

LITERATURE CITED

Agenbag JJ, Shannon LV (1988) A suggested physical explanation for the existence of a biological boundary at 24° 30′ S in the Benguela system. S Afr J Mar Sci 6:119–132

Bakun A (1996) Patterns in the ocean. Ocean processes and marine population dynamics. University of California Sea

Grant, San Diego, CA, in cooperation with Centro de Investigaciones Biologicas de Noroeste, La Paz
Barange M, Pillar SC, Hutchings L (1992) Major pelagic borders of the Benguela upwelling system according to euphausiid species distribution. S Afr J Mar Sci 12:3–17
Blanke B, Speich S, Bentamy A, Roy C, Sow B (2005) Southern Benguela upwelling and QuikSCAT wind variability. J Geophys Res C 110:C07018. DOI: 10.1029/2004JC002529
Boyd AJ (1987) The oceanography of the Namibian shelf. PhD dissertation, University of Cape Town, Rondebosch
Boyd AJ, Taunton-Clark J, Oberholster GPJ (1992) Spatial features of the near-surface and midwater circulation patterns off western and southern South Africa and their role in the life histories of various commercially fished species. S Afr J Mar Sci 12:189–206
Brown PC, Painting SJ, Cochrane KL (1991) Estimates of phytoplankton and bacterial biomass and production in the northern and southern Benguela ecosystems. S Afr J Mar Sci 11:537–564
Brownell CL (1980) Water quality requirements for first-feeding in marine fish larvae. II. pH, oxygen, and carbon dioxide. J Exp Mar Biol Ecol 44:285–298
Carr ME, Kearns EJ (2003) Production regimes in four eastern boundary current systems. Deep-Sea Res II 50:3199–3221
Conkright ME, Locarnini RA, Garcia HE, O'Brien TD, Boyer TP, Stephens C, Antonov JI (2002) World Ocean Atlas 2001: objective analyses, data statistics, and figures, CD-ROM documentation. Technical report, National Oceanographic Data Center, Silver Spring, MD
Cruickshank RA, Hampton I, Armstrong MJ (1990) The origin and movements of juvenile anchovy in the Orange River region as deduced from acoustic surveys. S Afr J Mar Sci 9:101–114
Da Silva AM, Young CC, Levitus S (1994) Atlas of surface marine data 1994, Vol 1. Algorithms and procedures. Technical report, U.S. Department of Commerce, NOAA, Washington, DC
de Decker AHB (1970) Notes on an oxygen-depleted subsurface current off the west coast of South Africa. Investl Rep Div Sea Fish S Afr 84:1–24
Demarcq H, Barlow RG, Shillington FA (2003) Climatology and variability of sea surface temperature and surface chlorophyll in the Benguela and Agulhas ecosystems as observed by satellite imagery. S Afr J Mar Sci 25:363–372
Duncombe Rae CM (2005) A demonstration of the hydrographic partition of the Benguela upwelling ecosystem at 26° 40′ S. S Afr J Mar Sci 27:617–628
Ekau W, Verheye HM (2005) Influence of oceanographic fronts and low oxygen on the distribution of ichthyoplankton in the Benguela and southern Angola currents. S Afr J Mar Sci 27:629–639
Field JG, Shillington FA (2006) Variability of the Benguela Current system. In: Robinson AR, Brink KH (eds) The Sea, the global coastal ocean interdisciplinary regional studies and syntheses, Vol 14, Part B. Harvard University Press, Cambridge, MA, P 835–863
Florenchie P (2004) Analysis of Benguela dynamical variability and assessment of the predictability of warm and cold events in the BCLME. Report No. 3. University of Cape Town, Rondebosch
Gründlingh ML (1999) Surface currents derived from satellite-tracked buoys off Namibia. Deep-Sea Res II 46:453–473
Huggett J, Fréon P, Mullon C, Penven P (2003) Modelling the transport success of anchovy *Engraulis encrasicolus* eggs and larvae in the southern Benguela: the effect of spatio-temporal spawning patterns. Mar Ecol Prog Ser 250: 247–262
Hutchings L, Beckley LE, Griffiths MH, Roberts MJ, Sundby S, van der Lingen C (2002) Spawning on the edge: spawning grounds and nursery areas around the southern African coastline. Mar Freshw Res 53:307–318
King DPF (1977) Influence of salinity, temperature and dissolved oxygen on incubation and early larval development of the South West African pilchard, *Sardinops ocellata*. Investl Rep Div Sea Fish S Afr 114:1–35
King DPF, O'Toole MJ, Robertson AA (1977) Early development of the South African maasbanker *Trachurus trachurus* at controlled temperatures. Fish Bull S Afr 9:16–22
King DPF, Robertson AA, Shelton PA (1978) Laboratory observations on the early development of the anchovy *Engraulis capensis* from the Cape Peninsula. Fish Bull S Afr 10:37–45
Kreiner A, van der Lingen CD, Fréon P (2001) A comparison of condition factor and gonadosomatic index of sardine *Sardinops sagax* stocks in the northern and southern Benguela upwelling ecosystems, 1984–1999. S Afr J Mar Sci 23:123–134
Large WG, McWilliams JC, Doney SC (1994) Oceanic vertical mixing: a review and a model with a non-local boundary layer parameterization. Rev Geophys 32:363–402
Largier J, Boyd AJ (2001) Drifter observations of surface water transport in the Benguela Current during winter 1999. S Afr J Sci 97:223–229
Lett C, Roy C, Levasseur A, van der Lingen CD, Mullon C (2006) Simulation and quantification of enrichment and retention processes in the southern Benguela upwelling ecosystem. Fish Oceanogr 15:363–372
Machu E, Biastoch A, Oschlies A, Kawamiya M, Lutjeharms JRE, Garcon V (2005) Phytoplankton distribution in the Agulhas system from a coupled physical–biological model. Deep-Sea Res I 52:1300–1318
Miller DCM, Moloney CL, van der Lingen CD, Lett C, Mullon C, Field JG (2006) Modelling the effects of physical–biological interactions and spatial variability in spawning and nursery areas on transport and retention of sardine eggs and larvae in the southern Benguela ecosystem. J Mar Syst 61:212–229
Monteiro PMS, van der Plas AK (2006) Low Oxygen Water (LOW) variability in the Benguela system: key processes and forcing scales relevant to forecasting. In: Shannon V, Hempel G, Malanotte-Rizzoli P, Moloney C, Woods J (eds) Benguela: predicting a large marine ecosystem. Large marine ecosystems, Vol 14. Elsevier, Amsterdam, p 91–109
Monteiro PMS, van der Plas A, Mohrholz V, Mabille E, Pascall A, Joubert W (2006) Variability of natural hypoxia and methane production in a coastal upwelling system: Oceanic physics or shelf biology? Geophys Res Lett 33: L16614. DOI:10.1029/2006GL026234
Mullon C, Cury P, Penven P (2002) Evolutionary individual-based model for the recruitment of anchovy (*Engraulis capensis*) in the southern Benguela. Can J Fish Aquat Sci 59:910–922
Mullon C, Fréon P, Parada C, van der Lingen C, Huggett J (2003) From particles to individuals: modelling the early stages of anchovy (*Engraulis capensis/encrasicolus*) in the southern Benguela. Fish Oceanogr 12:396–406
Nelson G, Hutchings L (1983) The Benguela upwelling area. Prog Oceanogr 12:333–356
Newman GG (1970) Migration of the pilchard *Sardinops ocellata* in southern Africa. Investl Rep Div Sea Fish S Afr 86:1–6
Olivar MP, Fortuño JM (1991) Guide to icthyoplankton of the Southeast Atlantic (Benguela Current region). Sci Mar 55:1–383

Olivar MP, Shelton PA (1993) Larval fish assemblages of the Benguela current. Bull Mar Sci 53:450–474

O'Toole MJ (1977) Influence of some hydrological factors on the depth distribution of maasbanker (*Trachurus trachurus*) larvae off South West Africa. Fish Bull S Afr 9:46–47

O'Toole MJ (1978) Aspects of the early life history of the hake *Merluccius capensis* Castelnau off South West Africa. Fish Bull S Afr 10:20–36

O'Toole MJ, King DPF (1974) Early development of the round herring *Etrumeus teres* (de Kay) from the South East Atlantic. Vie Milieu A 3(24):443–452

Parada C, van der Lingen CD, Mullon C, Penven P (2003) Modelling the effect of buoyancy on the transport of anchovy (*Engraulis capensis*) eggs from spawning to nursery grounds in the southern Benguela: an IBM approach. Fish Oceanogr 12:170–184

Parrish RH, Bakun A, Husby DM, Nelson CS (1983) Comparative climatology of selected environmental processes in relation to eastern boundary current pelagic fish reproduction. In: Sharp GD, Csirke J (eds) Proceedings of the expert consultation to examine changes in abundance and species composition of neritic fish resources, San Jose, Costa Rica. FAO Fish Rep 291:731–777

Penven P (2003) ROMSTOOLS user's guide. Available at www.brest.ird.fr/Roms_tools

Penven P, Roy C, Brundrit GB, de Verdière AC, Fréon P, Johnson AS, Lutjeharms JRE, Shillington FA (2001) A regional hydrodynamic model of upwelling in the southern Benguela. S Afr J Sci 97:472–475

Penven P, Debreu L, Marchesiello P, McWilliams JC (2006a) Evaluation and application of the ROMS 1-way embedding procedure to the central California upwelling system. Ocean Model 12:157–187

Penven P, Lutjeharms JRE, Florenchie P (2006b) Madagascar: A pacemaker for the Agulhas Current system? Geophys Res Lett 33:L17609. DOI:10.1029/2006GL026854

Prosch RM (1991) Reproductive biology and spawning of the myctophid *Lampanyctodes hectoris* and the sternoptychid *Maurolicus muelleri* in the southern Benguela ecosystem. S Afr J Mar Sci 10:241–252

Shannon LV (1985) The Benguela ecosystem, Part I. Evolution of the Benguela: physical features and processes. Oceanogr Mar Biol Annu Rev 23:105–182

Shannon LV, Nelson G (1996) The Benguela: large scale features and processes and system variability. In: Wefer G, Berger WH, Siedler G, Webb DJ (eds) The South Atlantic: present and past circulation. Springer-Verlag, Heidelberg, p 163–210

Shannon LV, O'Toole MJ (1999) Integrated overview of the oceanography and environmental variability of the Benguela Current region. Synthesis and assessment of information on the Benguela Current Larme Marine Ecosystem (BCLME). Thematic Report No. 2. BCLME, Windhoek

Shannon LV, Pillar SC (1986) The Benguela ecosystem, Part III. Plankton. Oceanogr Mar Biol Annu Rev 24:65–170

Shchepetkin AF, McWilliams JC (2005) The regional oceanic modeling system (ROMS): a split-explicit, free-surface, topography-following-coordinate oceanic model. Ocean Model 9:347–404

Skogen MD, Shannon LJ, Stiansen JE (2003) Drift patterns of anchovy *Engraulis capensis* larvae in the southern Benguela, and their possible importance for recruitment. Afr J Mar Sci 25:37–47

Stander GH (1964) The Benguela Current off South West Africa. Investl Rep Mar Res Lab SW Afr 12:1–43

Stenevik EK, Skogen M, Sundby S, Boyer D (2003) The effect of vertical and horizontal distribution on retention of sardine (*Sardinops sagax*) larvae in the northern Benguela—observations and modelling. Fish Oceanogr 12:185–200

Sundby S, Boyd AJ, Hutchings L, O'Toole MJ, Thorisson K, Thorsen A (2001) Interaction between Cape hake spawning and the circulation in the northern Benguela upwelling ecosystem. S Afr J Mar Sci 23:317–336

van der Lingen CD, Huggett JA (2003) The role of ichthyoplankton surveys in recruitment research and management of South African anchovy and sardine. In: Browman HI, Skiftesvik AB (eds) The big fish bang. Proc 26th Annu Larval Fish Conf. Institute of Marine Research, Bergen, p 303–343

van der Lingen CD, Shannon LJ, Cury P, Kreiner A, Moloney CL, Roux JP, Vaz-Velho F (2006) Resource and ecosystem variability, including regime shifts, in the Benguela Current system. In: Shannon LV, Hempel G, Malanotte-Rizzoli P, Moloney C, Woods J (eds) Benguela: predicting a large marine ecosystem. Large marine ecosystems, Vol 14. Elsevier, Amsterdam, p 147–185

Editorial responsibility: Alejandro Gallego (Contributing Editor), Aberdeen, UK

Submitted: July 16, 2006; Accepted: April 30, 2007
Proofs received from author(s): September 4, 2007

Vol. 347: 261–274, 2007
doi: 10.3354/meps06983

MARINE ECOLOGY PROGRESS SERIES
Mar Ecol Prog Ser

Published October 11

OPEN ACCESS

Dispersal modeling of fish early life stages: sensitivity with application to Atlantic cod in the western Gulf of Maine

Martin Huret[1,4,*], Jeffrey A. Runge[2], Changsheng Chen[1], Geoffrey Cowles[1], Qichun Xu[1], James M. Pringle[3]

[1]School of Marine Science and Technology, University of Massachusetts—Dartmouth, 706 South Rodney French Boulevard, New Bedford, Massachusetts 02744, USA

[2]Gulf of Maine Research Institute and School of Marine Sciences, University of Maine, 350 Commercial Street, Portland, Maine 04101, USA

[3]Coastal Observing Center and Ocean Process Analysis Laboratory, Institute for the Study of Earth, Oceans and Space, University of New Hampshire, 142 Morse Hall, Durham, New Hampshire 03824, USA

[4]*Present address*: IFREMER. Département Ecologie et Modèles pour l'Halieutique, BP21105, 44311 Nantes Cedex 03, France

ABSTRACT: As an initial step in establishing mechanistic relationships between environmental variability and recruitment in Atlantic cod *Gadhus morhua* along the coast of the western Gulf of Maine, we assessed transport success of larvae from major spawning grounds to nursery areas with particle tracking using the unstructured grid model FVCOM (finite volume coastal ocean model). In coastal areas, dispersal of early planktonic life stages of fish and invertebrate species is highly dependent on the regional dynamics and its variability, which has to be captured by our models. With state-of-the-art forcing for the year 1995, we evaluate the sensitivity of particle dispersal to the timing and location of spawning, the spatial and temporal resolution of the model, and the vertical mixing scheme. A 3 d frequency for the release of particles is necessary to capture the effect of the circulation variability into an averaged dispersal pattern of the spawning season. The analysis of sensitivity to model setup showed that a higher resolution mesh, tidal forcing, and current variability do not change the general pattern of connectivity, but do tend to increase within-site retention. Our results indicate strong downstream connectivity among spawning grounds and higher chances for successful transport from spawning areas closer to the coast. The model run for January egg release indicates 1 to 19% within-spawning ground retention of initial particles, which may be sufficient to sustain local populations. A systematic sensitivity analysis still needs to be conducted to determine the minimum mesh and forcing resolution that adequately resolves the complex dynamics of the western Gulf of Maine. Other sources of variability, i.e. large-scale upstream forcing and the biological environment, also need to be considered in future studies of the interannual variability in transport and survival of the early life stages of cod.

KEY WORDS: Gulf of Maine · Atlantic cod · *Gadhus morhua* · Larval transport · Particle dispersal · Modeling sensitivity · Spawning grounds · Meso-scale processes and turbulence

INTRODUCTION

Advances in modeling 3-dimensional circulation and hydrography in the ocean have stimulated application to understanding links between environmental variability and population dynamics of marine fish and invertebrate species. The ability to couple physical with biological understanding in model simulations provides insight into mechanisms by which climate influences recruitment processes (e.g. Cushing 1995, Runge et al. 2005) and spatial scales at which populations are connected via dispersal of larval stages (e.g.

*Email: martin.huret@ifremer.fr

Cowen et al. 2000, 2006, Siegel et al. 2007), both of which are relevant to spatially explicit approaches to ecosystem-based fisheries management.

In the present paper, we initiate an investigation of the influence of physical transport processes on the dispersal of eggs and larvae of Atlantic cod *Gadhus morhua* in the western Gulf of Maine. While dispersal of the planktonic life stages of American lobster *Homarus americanus* in the Gulf of Maine has been studied using a coupled physical–biological model (Incze 2000), this approach has not yet been applied to cod in this region. The cod stock, which may comprise 3 or 4 sub-populations (Ames 2004), is overexploited and at historically low levels of biomass (Mayo et al. 1998). An understanding of processes controlling the dispersal of planktonic stages of cod from local spawning areas will lead to insight into the connectivity among sub-populations and their sources of larval supply.

As a first step, we describe here a particle-tracking approach using the finite volume coastal ocean model (FVCOM) to simulate dispersal from major spawning grounds of the western Gulf of Maine. The FVCOM simulates circulation and hydrography with realistic atmospheric and river input forcing, in this case, for the year 1995. We calculate a transport success defined as the proportion of starting eggs that subsequently develop as larvae and settle in nursery habitats associated with the Gulf of Maine sub-populations. We examine the sensitivity of the results to the way in which we configure the hydrodynamic model and set out the initial conditions. The biological behavior of individual particles (e.g. egg buoyancy, larval vertical motion, trophodynamics) is not considered here; instead, we focus on the sensitivity of our index of transport success to: (1) spawning frequency and location, (2) mesh resolution and short time-scale variability of the velocity field, and (3) initial vertical distribution in relation to small-scale processes (i.e. turbulence). This sensitivity approach is a first step toward a systematic sensitivity analysis yielding the best model possible for the region, which should serve as a prerequisite to further ecological interpretation of the model output.

The Gulf of Maine (Fig. 1) has a general cyclonic circulation in which a coastal current flows southwestward along the coast of Maine (Brooks 1985) (Fig. 2). This Gulf of Maine Coastal Current (GMCC) consists of multiple branches (Lynch et al. 1997), with temporally variable connections between them (Pettigrew et al. 2005). The 2 major branches, the Eastern Maine Coastal Current (EMCC) and the Western Maine Coastal Current (WMCC), separate at the offshore veering of the EMCC in the vicinity of Penobscot Bay (Pettigrew et al. 2005). The core of the WMCC is centered over the 100 m isobath, where the current velocity ranges between 5 and 20 cm s^{-1} (Geyer et al. 2004, Churchill et al. 2005, Pettigrew et al. 2005). A freshwater plume adjacent to the coast, referred to as the Gulf of Maine Coastal Plume (GOMCP) by Keafer et al. (2005b), seasonally strengthens the southwestward flow (Geyer et al. 2004, Churchill et al. 2005).

Offspring from a given spawning location may be retained (Sinclair 1988), ultimately supporting local self-recruitment (Swearer et al. 2002), or be advected to a nursery area, after which surviving individuals either return to the original spawning area, contribute to spawning elsewhere, or are lost to the population's reproductive pool. Given the circulation in the western Gulf of Maine, it seems challenging for eggs and larvae to be retained locally, as compared, for example, with the anticyclonic circulation around Georges Bank (e.g. Lough et al. 2006). However, recent studies have shown the importance of the wind-driven modulation of the coastal flow in the western Gulf of Maine (Fong et al. 1997, Hetland & Signell 2005), with eddies and meanders being able, at times, to dominate the near-shore current variance (Churchill et al. 2005). Bay trapping mechanisms may also help retention of particles, such as described for toxic algae in Casco Bay (Janzen et al. 2005, Keafer et al. 2005a). Massachusetts Bay may serve as another significant retention zone, with the branch of the WMCC entering it south of Cape Ann (Fig. 2). This complex and variable dynamic area is well suited as a test region for our sensitivity study.

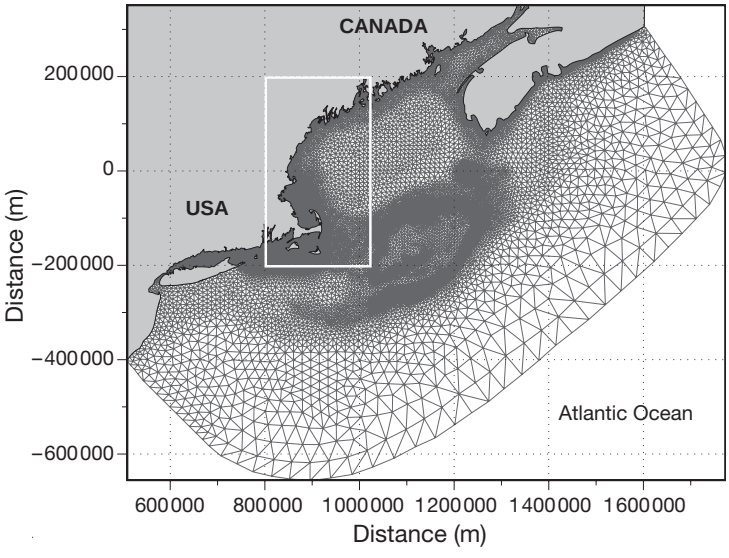

Fig. 1. FVCOM (finite volume coastal ocean model) grid for the Gulf of Maine area, showing location of the western Gulf of Maine study area (white box) described in Fig. 2

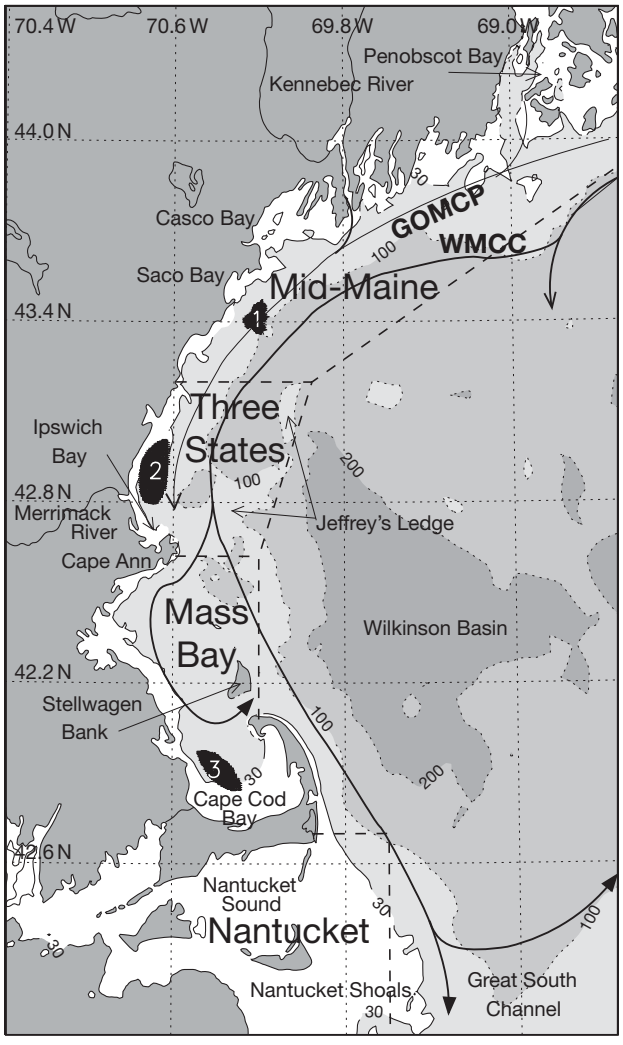

Fig. 2. *Gadhus morhua.* The 3 spawning ground locations (black) used in this study with the following names: Saco (1), Ipswich (2), and Cape Cod (3). Settlement areas are divided into 4 zones—Mid-Maine, Three States, Massachusetts (Mass.) Bay, and Nantucket—delimited by dashed lines. We define successful transport to juvenile settlement areas as the percentage of particles released that are found within the 30 m isobath during the last 15 d of their 2 mo drift. The figure shows the main features of the near-surface coastal circulation (adapted from Lynch et al. 1997, Keafer et al. 2005b): the WMCC (Western Maine Coastal Current) and the GOMCP (Gulf of Maine Coastal Plume). Gray scale shows bathymetry

METHODS

Particle tracking. ***Lagrangian trajectories:*** Particle tracking is achieved by following Lagrangian trajectories using the FVCOM (Chen et al. 2003). This is an unstructured grid, finite-volume, free-surface, 3-dimensional primitive equations model. It uses σ-coordinate transformation in the vertical to represent irregular bottom slope and surface elevation. It solves the governing equations in integral form by computing fluxes between non-overlapping horizontal triangular control volumes. This finite-volume approach combines the best of finite-element methods for geometric flexibility and finite-difference methods for computational efficiency. The ability of the FVCOM to fit irregular topography such as the coastal Gulf of Maine make FVCOM particularly suited for coastal ocean applications.

The grid covers the entire Gulf of Maine/Georges Bank region and is enclosed by an open boundary running from the New Jersey shelf to the Scotian Shelf (Fig. 1). Within the Gulf of Maine horizontal resolution ranges from 2 to 3 km in the basins to about 500 m in the coastal areas. There are 30 equally distributed Sigma layers vertically, for a vertical resolution of 3.3 m on the 40 m isobaths.

The model is driven by tidal forcing, which solves well the complex tidal dynamics of the Gulf of Maine, wind and heat fluxes from the fifth generation mesoscale meteorological model (MM5) hindcast at 10 km resolution (Chen et al. 2005), freshwater discharge from rivers, and upstream inflow condition on the Scotian Shelf. Daily mean sea surface temperature (SST) is nudged to satellite-derived SST. The model was run in this configuration for the year 1995, with a 1 mo spin-up starting from climatology density fields. This year is well suited for our study, since it is neither characterized by any particularly strong climatic events, nor by an extreme recruitment index.

In this work, we selected a Lagrangian method to describe particle transport, in anticipation of future refinement to include individual life histories, e.g. spatially varying growth rate and age-based behaviors, for which the Lagrangian approach is better adapted (Grimm 1999, Werner et al. 2001). Three-dimensional Lagrangian pathways were calculated with model velocities saved every hour. The velocities were linearly interpolated in space and time, and a 120 s time step was used with an explicit fourth order Runge-Kutta scheme. Using saved model fields allowed us to run our analysis with large numbers of particles, which would have been prohibited by computer time otherwise. The high frequency at which output were saved from the FVCOM run prevents significant differences arising from the linear interpolation between the on-line and off-line particle-tracking methods.

Vertical random walk: A stochastic approach was added to the deterministic vertical transport of the particles. We used random walk to describe diffusion of particles. The calculation of random walk is based on the eddy diffusivity, calculated with the Mellor & Yamada (1982) level 2.5 turbulent closure model, and also saved during the FVCOM runs.

Following Visser (1997), we update the particle vertical location using the following equation:

$$z_{(t+\delta t)} = z_t + w(t)\delta t + K'(z_t)\delta t + R\sqrt{\frac{2K(z_t + 0.5K'(z_t)\delta t)\delta t}{\sigma^2}} \quad (1)$$

with z_t the vertical position of the particle at time t, δt the time step, w and diffusivity (K', its first derivative) at the particle position, and R the random variable with zero mean and standard deviation σ. In our case R is a uniform deviate given by the Fortran 90 random number generator. Third and fourth terms on the right form the so-called 'random walk'. The former corresponds to a non-random 'advective' component, which was proposed by Visser (1997) to avoid erroneous particle accumulation in low-diffusivity areas. In the latter, the diffusivity is estimated at the particle location offset by a distance $0.5K'(z_t)\delta t$. In the range of the particle displacement, the diffusivity profile should be well approximated by the first-order Taylor expansion, which requires for the application of Eq. (1) that:

$$\delta t \ll \min\left(1/\left|K''\right|\right) \quad (2)$$

with K'' the second derivate of the vertical diffusivity. This criterion was refined by Ross & Sharples (2004), with some consideration of accumulation avoidance at the bottom and surface boundaries. They concluded that a time step $\delta t \simeq 1/100\left(1/\left|K''\right|\right)$ is acceptable in most applications. Following Ross & Sharples (2004), we also applied a cubic spline interpolation to the computed discrete diffusivity coefficient in order to obtain the necessary continuous and differentiable diffusivity profile. To respect the stability criterion at most locations and during most mixing events, the resulting time step for the random walk process is approximately 5 s.

Description of dispersal. ***Location and timing of spawning:*** Bigelow & Schroeder (1953) located cod *Gadhus morhua* spawning areas in the Gulf of Maine, with the most productive ones centered in Massachusetts Bay and just north of Cape Ann. Observations of the distribution and abundance of cod eggs (Berrien & Sibunka 1999) indicate highest concentrations in the western Gulf of Maine in waters shallower than 100 m in the vicinity of Massachusetts Bay and Jeffrey's Ledge, consistent with the historic description by Bigelow & Schroeder (1953). More recently, Ames (2004) identified 91 discrete historical spawning grounds from 1920s data and interviews with retired fishermen, in the coastal area from Cape Ann to Lurcher Shoal in the eastern Gulf of Maine. Nearly half of these spawning grounds would be abandoned today, with the disappearance of their spawning component from the stock. This identification, in conjunction with discussions with current local fishermen, helped us define major spawning sites still active in the western Gulf of Maine, from which we released particles for our dispersal study (Fig. 2). For this study we included major historical locations in Ipswich Bay, north of Cape Ann, and Cape Cod Bay in the south of Massachusetts Bay, as well as spawning grounds offshore of Saco Bay in Maine, also identified by Ames (2004).

Timing and duration of the spawning season are difficult to assess for the Gulf of Maine cod subpopulations because of variability among and within spawning grounds, depending on environmental conditions (Lough 2004). Within the Gulf of Maine, cod have historically spawned throughout the winter and early spring at most locations, but the peak spawning varies depending on location (Schroeder 1930), with a general shift to later in the year for the more northerly regions. The range of spawning times combined with egg dispersal results in observations of a nearly year-round presence of eggs (Berrien & Sibunka 1999). Nevertheless, periods of high spawning activity are distinguishable. Fish (1928) reported peak spawning activity during January and February for Massachusetts Bay. In some areas, peak spawning appears to be bi-modal. In and around Ipswich Bay, the largest spawning events occur in May/June, while a secondary period of peak activity occurs in December/January (Wirgin et al. 2007). Based on this background information and our discussions with fishermen, we selected the following spawning periods for our 3 aggregated spawning grounds: (1) July and October for Saco Bay, (2) May to July and December/January for Ipswich Bay, and (3) December and January for Cape Cod Bay. Results presented below focus on January and July, which are both valid spawning periods for 2 of the selected spawning grounds. In each case, results for the third spawning location are also included.

Settlement areas: After a 2 to 3 mo drift in the water column, larval cod metamorphose into juveniles with settlement to the bottom shortly thereafter, at sizes of <7 cm (Lough 2004). Based on analysis of multiyear trawl survey data of juvenile cod abundance off the Massachusetts coast, Howe et al. (2002) found the highest densities of newly settled cod nearshore at depths shallower than 30 m in spring and concluded that the region comprising Ipswich Bay, Massachusetts Bay, and Cape Cod Bay offered suitable habitat for successful settlement. The size criteria (<10 cm) of these Age-0 cod when compared with the size range of 2.5 to 7 cm at settlement (Lough 2004) confirms that they just settled, limiting the possibility that they have already migrated over large distances. Observations of early-stage juvenile abundance in other regions across the range of Atlantic cod corroborate the conclusion that settlement success of juvenile cod is higher in the shallow, nearshore habitat (Suthers & Franks 1989, Dalley & Anderson 1997).

There is some evidence that juveniles do not exhibit any preference for substrate type at settlement (Howe et al. 2002), but subsequent spatial patterns are then altered by juvenile migration or habitat-specific post-settlement mortality (Tupper & Boutilier 1995b). On Georges Bank, first settled juveniles are broadly distributed over the bank, but by late summer juveniles are mostly found on gravel bottom (Lough et al. 1989). In coastal Nova Scotia and Newfoundland, post-settlement survival and Age-0 abundance is highest in complex bottom types, i.e. sea-grass beds, cobble/gravel areas, and biogenic-covered rock reef (Tupper & Boutilier 1995b, Grant & Brown 1998). These observations correlate with a lower predation rate (including cannibalism) and a higher food availability in such complex habitats (Gotceitas & Brown 1993, Gotceitas et al. 1995, Tupper & Boutilier 1995a, Grant & Brown 1998) than over fine-grain substrates (Tupper & Boutilier 1995b).

All these complex bottom types are common in shallow waters of the western Gulf of Maine (Howe et al. 2002). While the U.S. Geological Survey sediment database for the east coast of the United States (Poppe et al. 2005) offers insight into possibly suitable habitats for cod juveniles, the resolution is still too coarse for fine-scale qualification of nearshore habitat. Thus, we define here suitable settlement areas as inshore areas within the 30 m isobath, without further consideration of habitat type.

Measuring transport success: Thousands of particles per spawning ground are released for each experiment (see values in Table 1), a necessary quantity to obtain stable results (i.e. same statistics for the particle distribution for independent runs). Particles are released every 5 m vertically, starting at 2.5 m, and with a regular distribution horizontally in order to reach the stability defined above. Lacking an understanding of the factors that drive the timing of individual spawning events, we repeatedly released particles every 3 d during the prescribed spawning period, to simulate a series of successive spawning events. Three days corresponds to a typical decorrelation time-scale of the velocity field in coastal areas; therefore, particles released at this frequency should reflect the integrated seasonal transport variability at each spawning ground.

Hatching of Atlantic cod eggs occurs after 8 to 60 d, depending on temperature, and larvae remain pelagic for about 3 mo (Lough 2004). With neither temperature dependence nor a trophodynamics model, a 60 d pelagic period was chosen here for investigation of egg and larval drift, as in comparable studies over Georges Bank (Werner et al. 1996, Lough et al. 2006) and in the Baltic Sea (Hinrichsen et al. 2001). While development time of all pelagic stages (i.e. eggs, larvae, and early juvenile) is likely to be longer, we assume that 2 mo is representative of the transport period. Indeed, vertical migration capacity and deepening in the water column contributes to retention of individuals in the deeper layers during the end of the pelagic stage (Lough & Potter 1993), where weaker currents in the coastal Gulf of Maine tend to reduce the drift. This uncertainty on the drift duration could eventually be improved with a fully explicit model of the development of early life stages. The influence of the vertical behavior of larvae on our results is also further discussed in the 'Vertical distribution' section of the 'Discussion'.

We define an index of transport success for particles as the percentage of time they spend over suitable settlement areas in the last 15 d of their 60 d drift. The

Table 1. Connectivity matrices showing transport success (%) of particles advected for 60 d with FVCOM (finite volume coastal ocean model) simulation of the circulation in the Gulf of Maine. For spawning grounds 1, 2, and 3 (see Fig. 2), transport success is averaged over successive releases at 3 d intervals throughout January 1995. Nominal: full-resolution simulation; coarse, filtered, and mean: model runs with different mesh and forcing resolutions, as discussed in 'Methods'. Relative error calculated as the percent difference in transport success between the nominal run and the coarse, filtered, or mean run, averaged over the 3 spawning grounds. n: number of particles. Mass.: Massachusetts

Experiment January	Success area	Spawning ground 1 (n = 2735)	2 (n = 4040)	3 (n = 3675)	Relative error (%)
Nominal	Mid-Maine	1.3	0.3	0.0	
	Three States	1.1	2.4	0.0	
	Mass. Bay	2.3	6.8	19.2	
	Nantucket	5.6	8.2	13.9	
	All zones	11.5	18.5	23.2	
Coarse	Mid-Maine	0.5	0.0	0.0	54
	Three States	1.1	0.7	0.0	24
	Mass. Bay	1.7	3.9	13.2	33
	Nantucket	9.4	13.9	23.6	69
	All zones	12.7	18.5	36.8	45
Filtered	Mid-Maine	1.1	0.4	0.0	16
	Three States	1.0	2.3	0.0	5
	Mass. Bay	1.8	4.4	11.9	32
	Nantucket	2.7	4.7	8.8	44
	All zones	6.6	11.8	20.7	24
Mean	Mid-Maine	0.2	0.0	0.0	62
	Three States	0.5	0.7	0.0	42
	Mass. Bay	1.6	3.9	5.9	47
	Nantucket	2.2	5.2	13.3	34
	All zones	4.5	9.8	19.2	46.3

transport success is then averaged over the number of particles per spawning ground, and, except for the first experiment on release frequency, over the successive releases within monthly periods.

The successful settlement areas are divided in 4 regions (see Fig. 2): (1) mid-Maine from Penobscot Bay to Saco Bay; (2) Three States, covering the New Hampshire coast, as well as part of the Massachusetts and Maine coasts; (3) Massachusetts and Cape Cod Bays; and (4) Nantucket Sound and Shoals. The transport success index is used in connectivity matrices between sources (spawning grounds) and sinks (settlement areas) of particles to show the relative dominance of either retention or downstream advection.

RESULTS

Sensitivity to particle release

Release frequency

We examined the effect of the release date within the peak spawning season of Atlantic cod *Gadhus morhua* on the dispersal of particles. Fig. 3 shows a time series of transport success in January 1995 based on successive releases at 3 d intervals. It reveals the potential for substantial (factor of 2) changes in transport success depending on release date, e.g. the change in success index from 25 to 14% in the Nantucket region between 4 and 7 January. The 1 mo spin-up before January should preclude any model adjustment as the cause of this rapid decrease, and we also observed changes of the same amplitude later in the year. These rapid changes, as well as more prolonged changes (e.g. the decrease of retention in Massachusetts Bay from spawning ground 3, between 16 and 28 January), need to be included to accurately represent the averaged transport success over the entire spawning period. A similar analysis for the month of July (not shown) indicates changes of lower magnitude between successive releases, a consequence of lower variation in wind forcing during summer months. This experiment shows that the choice of the release date may have strong influence on the success index, even for some release dates only separated by a few days. Given the high circulation variability, a dispersal description from a unique release date is certainly not representative of the spawning period in a given year. In the following results, the 1 mo averaging period of successive 3 d releases gives robustness to the transport success patterns given a particular model configuration, and avoids erroneous conclusions that may result from interpretation of transport success from a single release date.

Release location

The area offshore of Saco Bay, including spawning ground 1 (Fig. 2), may comprise 3 discrete spawning grounds distributed in the cross-shore direction, according to fishermen. Whether there is a real spatial separation between them is unknown. However, there is likely interannual variability in the spawning location of a population at small scales, which may be represented by these 3 spawning grounds, and for which we can test the sensitivity of the dispersal of particles. Here, we investigate the transport of particles released in the 0 to 20 m layer, which allows consistent comparison between spawning grounds with different bathymetries. Fig. 4 shows an example of particle distribution after 1 mo of drift. Particles from the most offshore

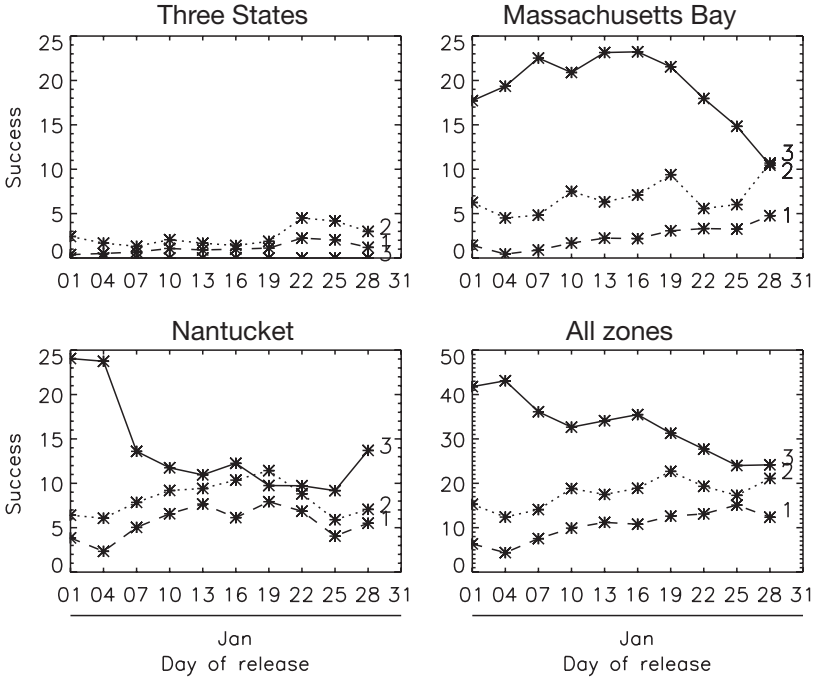

Fig. 3. Index of transport success (%) to settlement areas depending on release date, based on FVCOM simulation. Releases are from spawning grounds 1 (– – – –), 2 (·····), and 3 (———) of Fig. 2. Mid-Maine settlement area not shown because transport success index is negligible relative to the other areas. The 'all zones' plot shows cumulative success over all settlement areas

spawning ground are dispersed mostly offshore where they remain, whereas particles from the most inshore spawning ground are more likely to end up in coastal retention areas such as Massachusetts Bay. Fig. 5a shows, for all July 1995 releases, a transport success index decreasing from the inshore (16%) to offshore (7%) spawning ground. The 15 km separation between the 2 extreme locations cannot explain by itself such a difference. The main controlling factor is the location of the spawning ground in relation to the WMCC. The spawning ground furthest offshore (1c) is located at the core of the WMCC, which explains why fewer particles from this spawning ground were retained to the north in comparison with those of the 2 other areas (1a and 1b, see Fig. 5b), as well as the greater dispersal of its particles offshore.

Circulation variability

Mesh resolution

We compared the transport success using our original mesh with the results using a mesh with coarser resolution at some critical locations. These include inshore areas, which gives a lower resolution of coastline complexity (see Fig. 6), as well as Stellwagen Bank and Nantucket Sound, where an approximate 1 km mesh resolution substituted the original one at approximately 500 m (Fig. 6). The basin-scale circulation of the Gulf of Maine remained unchanged, allowing us to focus on the effects of local resolution difference.

Lack of coastline traps and mesoscale features, such as eddies over deeper areas around Stellwagen Bank (Fig. 7), increases downstream advection of particles (Fig. 8). The net result of reducing mesh resolution is a higher index of transport success for the most southern area (Nantucket) from all spawning grounds (see values in Table 1) and a decreased success in transport to the other defined settlement locations. Despite a larger number of particles advected from Spawning Areas 1 and 2, transport success is nevertheless also reduced in Massachusetts Bay. The unresolved eddies around Stellwagen Bank, which can be seen as deviation and retention processes into the bay, do not affect the particles that are instead carried away to the south by the WMCC.

Temporal variability of the velocity field

To assess the sensitivity of transport to changes in the model representation of the velocity field, we modified physical field outputs from the FVCOM in 2 separate simulations. In the first simulation, we used a low-pass filter to remove the tidal high-frequency component, keeping only the tidal residual. In the second simulation, we replaced the high-frequency velocity field output from the FVCOM with a monthly average.

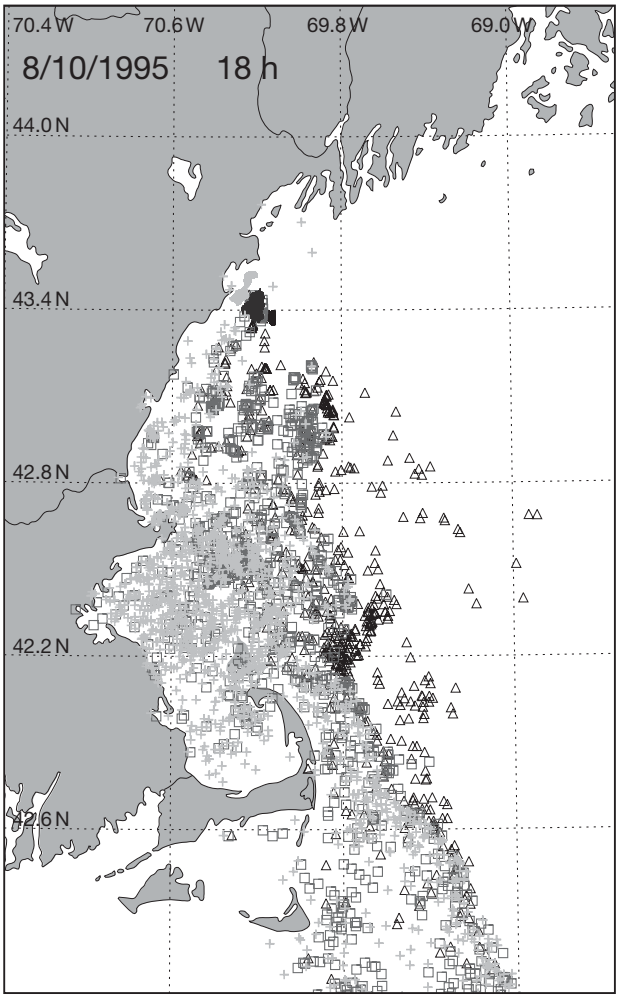

Fig. 4. Particle distribution after 1 mo of drift from Spawning Ground 1 (off Saco Bay), showing within-location variability in dispersal of release in the surface layer on 10 July with random walk. Light gray +: inshore spawning area; dark gray open square: middle spawning area as in Fig. 2; and black open triangle: offshore spawning area

Differences in transport success between simulations using the original FVCOM output and with the high frequency of the tide removed are not noticeable (see Fig. 9a,b as an example; see also Fig. 10a,b, Table 1). Exceptions are south of Cape Cod, where fewer particles can reach Nantucket Sound and Shoals, a region with strong and complex tidal currents (e.g. Shearman & Lentz 2004), and in Massachusetts Bay, where tidal current variability may enhance inward transport of particles into the bay and entrapment in its embayments.

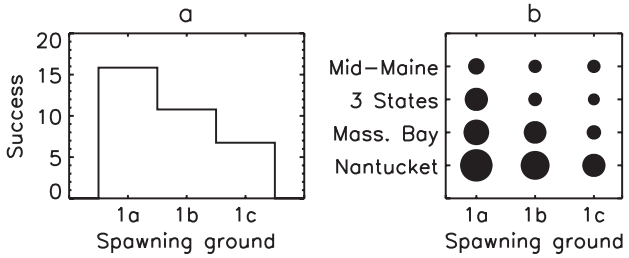

Fig. 5. Index of transport success (%) for July releases at the 3 discrete areas of Spawning Ground 1 (1a: light-gray inshore location of Fig. 4; 1b: dark-gray location; 1c: offshore black location): (a) integrated over all 4 success areas, (b) transport success between each spawning location and settlement area (connectivity matrix). Circle surface area is proportional to the magnitude of transport success. Mass.: Massachusetts

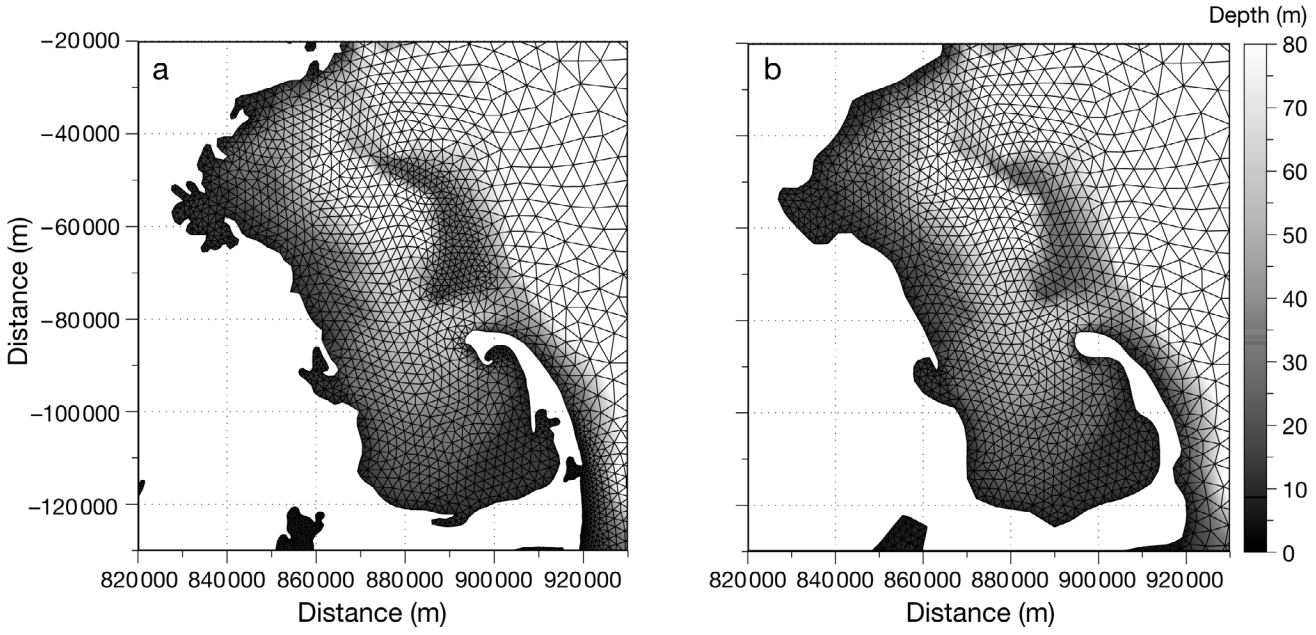

Fig. 6. (a) High and (b) low resolution mesh in the vicinity of Massachusetts Bay. Differences in mesh resolution occur over Stellwagen Bank and along the coast

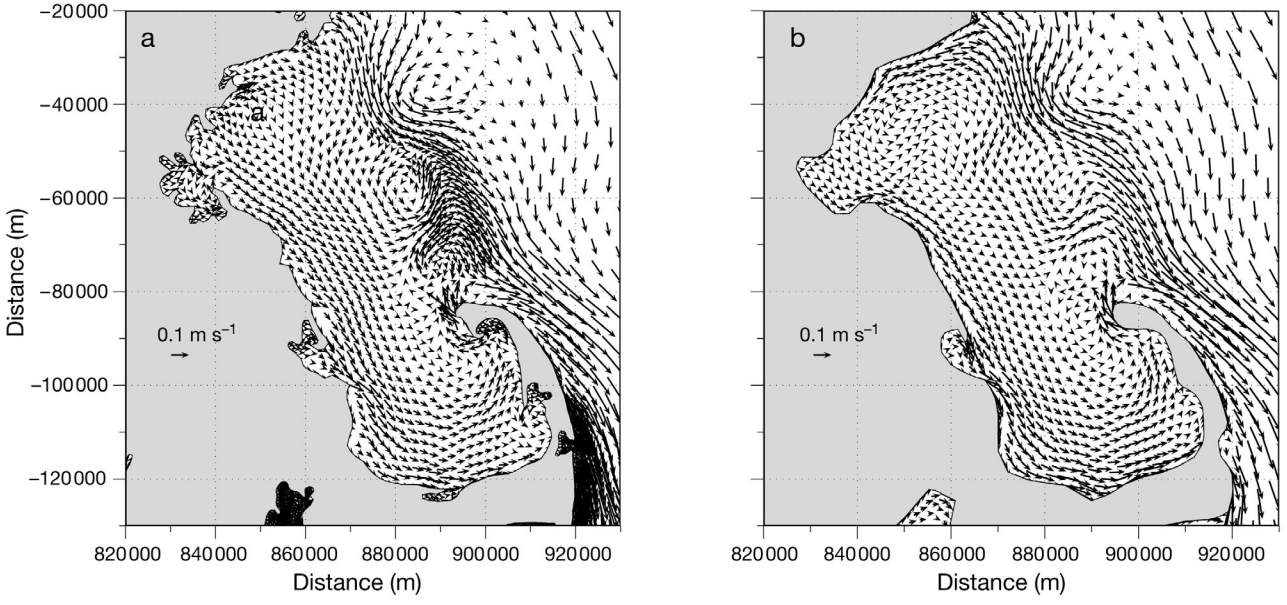

Fig. 7. Surface monthly mean (February 1995) current for (a) high and (b) low mesh resolution in Massachusetts Bay. Residual eddies to the west and northeast of Stellwagen Bank, which appear in the high-resolution simulation, are not resolved using the coarser mesh

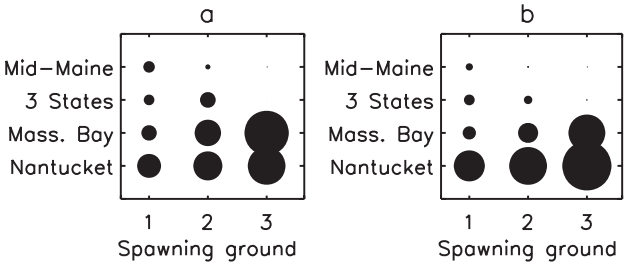

Fig. 8. Connectivity matrices (as in Fig. 5b) for (a) high and (b) low mesh resolution based on releases in January 1995. Circle surface area is proportional to the magnitude of transport success. Actual values of transport success and relative error with respect to the high-resolution run are given in Table 1. Mass.: Massachusetts

Application of a monthly mean velocity field leads to strong downstream advection, with only few particles entering and ending up in Cape Cod Bay and inshore Massachusetts Bay (Fig. 9c). Differences from the original simulation are notable everywhere (Fig. 10c, Table 1). Very few particles are retained in the coastal areas in the north, due to strong downstream advection, but the success indexes are also lower in Massachusetts Bay and around Nantucket for spawning grounds 1 and 2. Lack of variability in the circulation lessens transport toward the coastal nursery areas of particles advected downstream. Nevertheless, for spawning ground 3 this effect is attenuated by larger number of particles advected from Cape Cod Bay that sustain the success level in the downstream region of Nantucket as compared with the nominal run.

Turbulence and vertical distribution

In this sensitivity experiment, we investigated particle dispersal without random walk. In this case, vertical movement depends only on the weak vertical advection, and, consequently, most particles remain at their release depth. The first example examines release of particles in January 1995, during mixed conditions in winter. In the second example, particles are released in July 1995, representing summer conditions, with strong stratification in the 15 m surface layer.

In the winter, cumulative transport success (Fig. 11) is sensitive to application of random walk. With the use of random walk and for spawning grounds 1 and 3, transport success is almost uniform for releases made over the whole water column, as vertical mixing quickly redistributes particles. Without application of random walk, there is a success gradient from the surface to the bottom for the 3 spawning grounds: particles mostly remain at their initial depth and are consequently advected by different currents. For spawning ground 2, the proximity of the mouth of the Merrimack River creates low stratification, which possibly decouples surface and bottom transport of particles, even in the case with random walk.

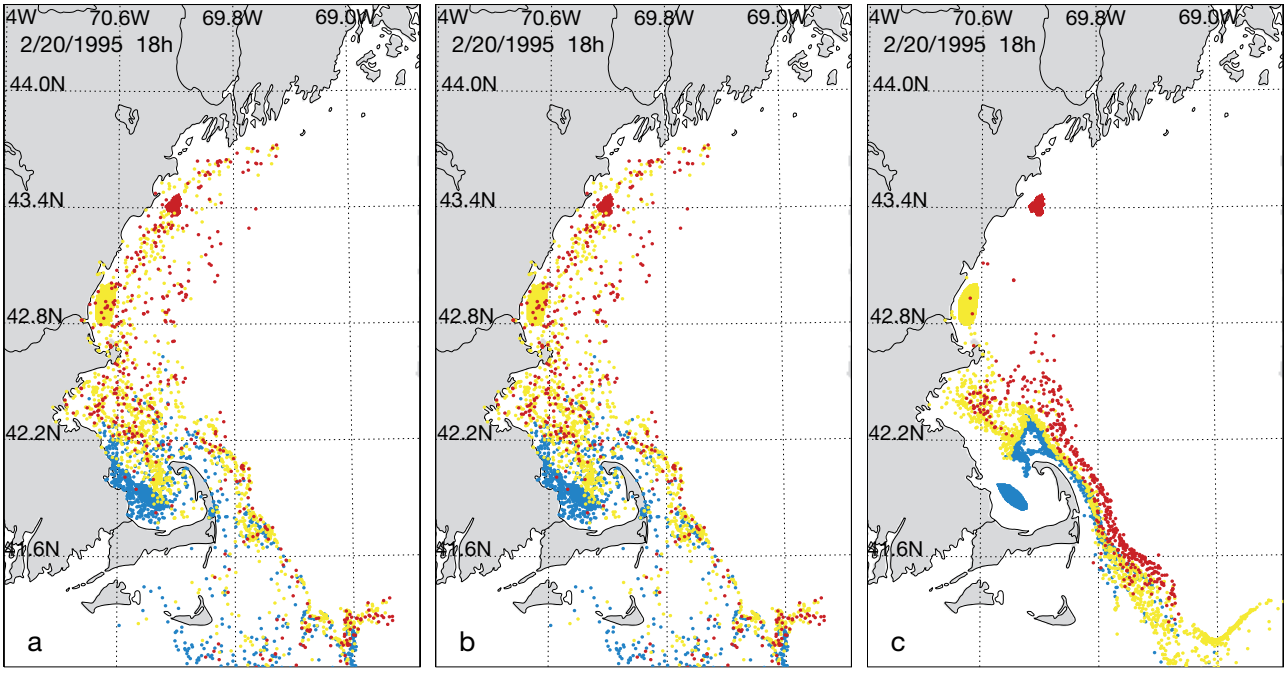

Fig. 9. Particle distributions after 1 mo drift with random walk starting on 20 January 1995. Spawning grounds, best seen in Panel c, (and distributions) are color coded (1: red; 2: yellow; 3: blue). Particle tracks are from (a) nominal, (b) low-pass-filtered, and (c) monthly averages of the physical field

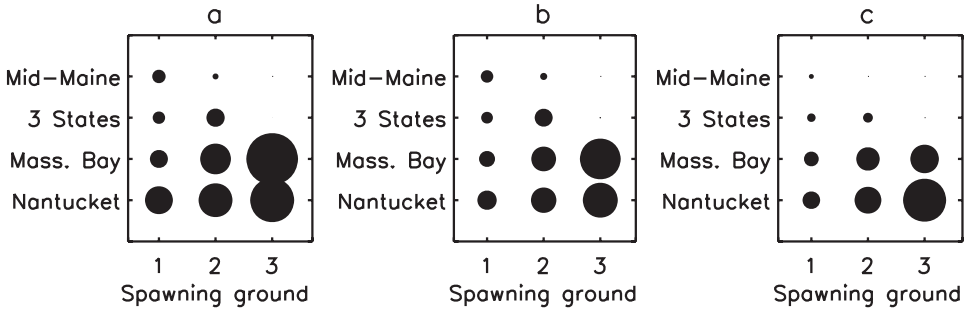

Fig. 10. Connectivity matrices for transport success for releases in January 1995, shown in Fig. 9. (a) Nominal run, (b) low-pass filtering of physical fields, and (c) monthly mean physical fields. Circle surface area is proportional to the magnitude of transport success. Actual values of transport success and relative error with respect to the nominal run are given in Table 1. Mass.: Massachusetts

In summer, there is no significant difference between presence or absence of random walk, due to low mixing (except in a thin surface mixed layer for spawning ground 1 and on the bottom layer of spawning ground 3) (Fig. 12). We observe that depending on the spawning ground and associated local 3-dimensional circulation, larvae are more likely to be successful if particles are released between 20 and 40 m (spawning ground 1), at the surface (spawning ground 2), or at the bottom (spawning ground 3). Further investigation needs to address whether or not release depth for maximum within-area transport success is the same as the depth for maximum overall transport success.

DISCUSSION

Characterizing location and timing of larval release

Our analysis shows that transport success is dependent on the spawning date of Atlantic cod *Gadhus morhua*, reflecting the daily variability in wind and circulation velocities that impart a unique cumulative transport history to each particle release. We assumed that release every 3 d is more representative of the protracted period of cod spawning, which may be an adaptive mechanism to increase retention probability and local recruitment success (Byers & Pringle 2006) by integrating over seasonal climate variability. How-

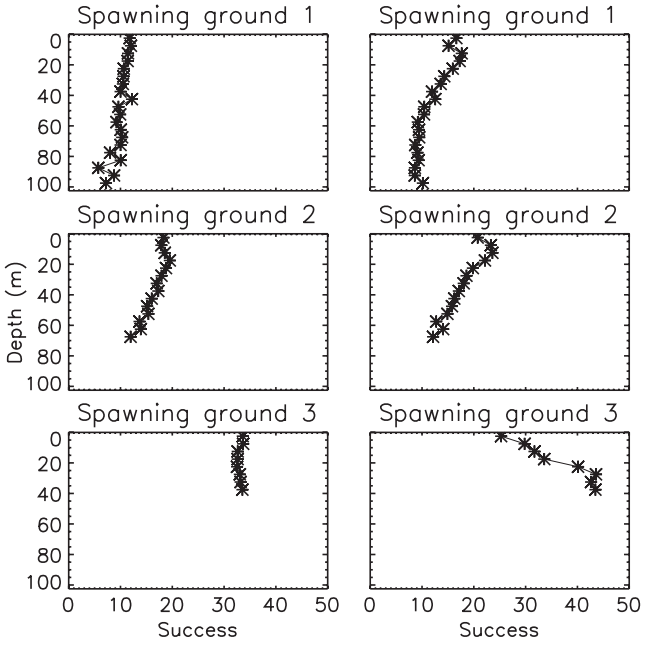

Fig. 11. Index of overall transport success (%) as a function of release depth for particles from the 3 spawning grounds shown in Fig. 2: January 1995 simulation. Left panels: subject to random walk; right panels: not subject to random walk

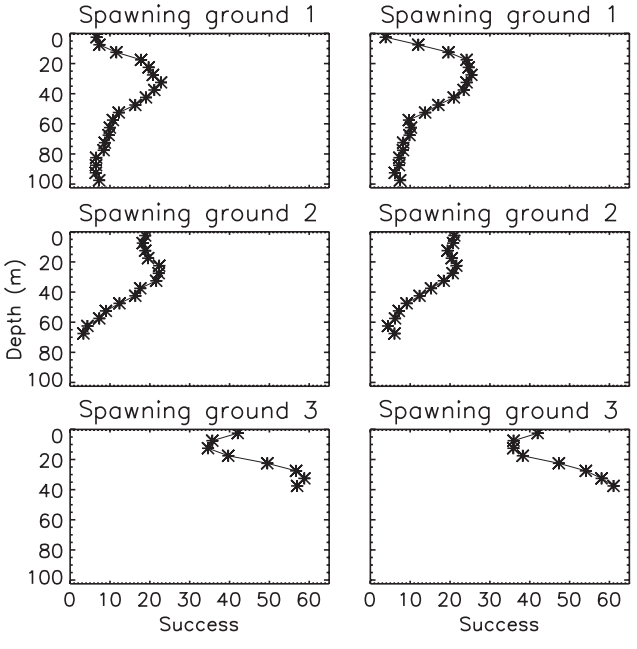

Fig. 12. Index of overall transport success (%) as a function of release depth for particles from the 3 spawning grounds shown in Fig. 2: July 1995 simulation. Left panels: subject to random walk; right panels: not subject to random walk

ever, if spawning release is more episodic, a better understanding of the fine-scale timing of spawning events in relation to the changing environment is needed for more accurate assessment of dispersal in any given year.

Through discussions with knowledgeable local fishermen, we refined the location of spawning areas. Differences in transport success under identical conditions from adjacent spawning areas off Saco Bay indicate a need for accurate fine-scale descriptions of spawning areas. For example, in Ipswich Bay, local fishermen can locate >15 separate spawning sites (H. Howell, UNH, pers. comm.). This micro-scale site selection by spawning cod, potentially related to bottom topography associated to meso-scale structures, may impact the dispersal of pelagic stages, perhaps enhancing within-site retention.

The model setup

Results from the analysis of sensitivity to the model setup showed that changes to mesh resolution and to representation of short-time-scale current fields impacts within-site retention, although the general pattern of connectivity remains intact. Relative errors in terms of connectivity matrix values range between 24%, for the tidally filtered run, to about 45%, in runs using a lower resolution or mean current fields (Table 1). These relative errors are also significant, looking at each success area, even if absolute transport success may be an order of magnitude different between them. This supports our interpretation of sensitivity results for all our defined sub-regions of the western Gulf of Maine.

The strong change induced when only slightly modifying the mesh resolution suggests caution when interpreting results of particle dispersal from model runs with a low-resolution grid in coastal areas. We showed that a resolution even as high as 1 km may not be sufficient to resolve eddies in some critical locations; with the FVCOM irregular grid we were able to match the complex coastline and better resolve the meso-scale circulation by increasing the resolution where necessary.

In particle-tracking studies, time computing or data storage issues have often imposed the use of residual currents, or large time steps that remove the high frequency of tide. With these model configurations, our results showed that in coastal regions with high tidal energy, the retention at spawning sites or trapping of particles in settlement areas can be decreased. The small time step we used here, consistent with the internal time step of our FVCOM run, resolves the tide. Tracking particles with monthly mean averages of the velocity fields removes another level of short-time-scale variability (i.e. the variability due to the wind or the non-linearities in the model itself), and the dispersal patterns are highly modified as a consequence.

Our result highlights the limitations of interpreting dispersal patterns from such model configurations, and the requirements for small space- and time-scale model resolution. The current model, although it operates with state-of-the art grid and forcing resolution, may still not resolve correctly the retention processes and, consequently, may underestimate the potential for within-area retention (Swearer et al. 2002). Further validation of the hydrodynamics, including analysis to determine under what mesh resolution the connectivity matrices become stable, should clarify this uncertainty. This would also give insight on the resolved horizontal variability by the model, and the possible requirement of some additional horizontal random walk for sub-grid-scale processes.

Vertical distribution

Our vertical distribution experiments showed that for passive particles, vertical mixing is an important factor in highly diffusive environments (e.g. winter or high tidal mixing areas). In these cases, initial vertical distribution of particles does not have much influence on their final location, since all particles are rapidly stirred over the whole water column. However, in stratified environments, initial vertical distribution of particle release is critical in determining the final distribution.

Our results are valid for passive particles such as eggs and recently hatched larvae, for the most part during the first month of drift. Older larvae acquire a swimming capacity allowing them to migrate daily within the water column, even though average residence depth deepens proportionally with their age (e.g. Lough & Potter 1993). Progressive loss of sensitivity to the turbulent field is likely to come with this swimming capacity (Ross & Sharples 2004), making random walk inappropriate. Since we showed that vertical distribution might be critical in the transport, particle dispersal may be modified during the second month of drift, in the direction of more retention. A complementary sensitivity analysis of this biological behavior, as well as the influence of horizontal swimming on dispersal, needs to be conducted.

Egg and early larval buoyancy were not considered in our experiments. In stratified waters, buoyancy will rapidly drive the particles to the surface, in which case realistic dispersal should be based on surface releases, unless explicit modeling of the buoyancy is added with respect to the density field. Buoyancy is likely

to increase the downstream advection of particles by strong surface currents, which can be counterbalanced by stronger dispersal in different directions influenced by wind. Here, density difference with the surrounding fluid may modify the response to the turbulent field (Ross & Sharples 2004). However, observations in well mixed waters over Georges Bank (Lough & Potter 1993) reveal a homogeneous egg distribution throughout the water column, supporting our use of random walk for the egg stage.

Preliminary ecological implications

A single year (1995) cannot be used to deduce representative, climatological dispersal patterns. Results from runs simulating different years, to study the interannual variability, or to build the mean connectivity matrix among sites, will yield more stable patterns of the dispersal in this region. The model results nevertheless suggest several ecological implications for understanding the spawning patterns in the western Gulf of Maine. First, there is a higher chance for successful transport to juvenile nursery areas within the Gulf of Maine if spawning occurs inshore, even in the presence of cross-shore transport due to local variability. Second, different experiments converge to indicate that overall transport success is highest for spawning ground 3 of Cape Cod Bay, followed by Ipswich Bay, and then the spawning ground off Saco Bay. This overall gradient in transport success is attributed to the differences in self retention among zones. Massachusetts and Cape Cod bays are relatively less affected by downstream advection as compared to Ipswich Bay or the very exposed spawning ground off Saco Bay. Evidence from cod stocks across the North Atlantic attributes increasing importance to near-shore spawning and nursery areas (Hutchings et al. 1993). Near-shore spawning and mechanisms for cross-shelf transport (including tide and factors of variation of the coastal current at short time scales) appear to be very important determinants of juvenile membership in the Gulf of Maine populations. Hence, variability in these mechanisms has great potential to be a primary determinant of recruitment success.

In all cases, our model results show that spawning sites are very connected to juvenile nursery areas downstream. Conversely, there is very little upstream connectivity, regardless of initial conditions. There is considerable mixing of juveniles originating from different spawning sites in Ipswich Bay and especially in Massachusetts and Cape Cod bays. Such mixing would not promote small-scale population distinctness. Juveniles in the mixed nursery areas may return to their original spawning ground to spawn as adults, join the sub-population native to the spawning ground closest to the nursery area, or form a transient population that migrates to spawning sites that may or may not be the same as those identified here, without a predetermined affinity for any particular site. This may be the case for far-exported vagrants to Nantucket Sound and Shoals or to Georges Bank, unless such a distance precludes survivorship of larvae or juveniles. Modeling work, in connection with other modern methodologies such as DNA studies (e.g. Wirgin et al. 2007) or chemical tracking, should help to answer these questions.

Given the overall downstream pattern of dispersal, the challenge for the cod stock and sub-populations in the western Gulf of Maine is how to maintain local populations. We examined this question in more detail looking at the within-site transport success. Our nominal January runs yield 1.3 to 19.2% retention of the number of particles originally released over a 60 d planktonic phase (Table 1). Assuming a low value of 2% for this retention and a mortality rate of 0.08 d^{-1} (Houde 1988), approximately 60 Age-0 cod would be retained in local nursery areas from the production of 375 000 eggs, the average egg production by a 50 cm female (Collette & Klein-MacPhee 2002). The number of surviving juveniles from the average egg output is highly dependent on the daily mortality rate, which would vary depending on the predator and prey fields in the environment. Nevertheless, our model results indicate the potential for prolific spawners such as cod to maintain local populations along the coast of the western Gulf of Maine.

CONCLUDING REMARKS

In the western Gulf of Maine, like in other North Atlantic regions, many interacting physical and biological factors may explain the variability observed in cod recruitment. Along-shore circulation, associated with a complex topography, defines the basic pattern of the connectivity matrix between spawning and settlement areas. Local forcing variability (river discharge, wind) may explain part of the recruitment variability by modulating the circulation. In addition, upstream, large-scale forcing (i.e. Scotian Shelf inflow) and density of waters entering the gulf are likely to play an important role in controlling coastal Gulf of Maine circulation variability (Pringle 2006). Our study addresses the sensitivity of the dispersal of particles to model skill at representing some of this physical variability. Further validation is necessary to obtain the minimum model requirements that would correctly resolve the dynamics involved in passive transport of particles. As these requirements depend on the circulation and topographical features specific to each coastal area, we

suggest that a search for adequate model configuration should be conducted in each regional study. Then, for a fully explicit early life history, biological processes including food limitation and predation on larval growth and mortality could be studied as additional sources of variability in cod recruitment.

The Gulf of Maine cod stock is managed separately from the nearby cod stocks inhabiting the offshore banks on the Scotian Shelf and Georges Bank (O'Brien et al. 2005). There is, however, a high potential for export out of the coastal Gulf of Maine region, to Nantucket Sound and Shoals or beyond and to Georges Bank. The question of whether juveniles finding themselves in these potential nursery grounds are still connected to western Gulf of Maine stocks, or whether they are vagrants lost to the reproductive pool of any NW Atlantic sub-populations is still to be resolved. Recent studies are moving toward application of smaller scale, spatially explicit management approaches. The population structure in the Gulf of Maine likely conforms to a meta-population, in which each sub-population gathers several spawning components (Ames 2004). The diversity and richness of this structure may need to be accounted for in a successful long-term strategy for conservation of local populations. The coupled physical–biological model will be useful for evaluating the sensitivity of sub-populations to environmental variability, as well as for understanding the long-term trends in contribution and selection of the spatially explicit spawning components.

Acknowledgements. We thank R. Ji for useful discussions and comments on the particle-tracking code. We gratefully acknowledge R. Gauron, D. Goethel, G. Littlefield, F. Mirarchi, C. Pendleton, P. Taylor, and N. Vine for discussions of spawning locations, and Amy Holt Cline for mapping the experiential knowledge of the pre-cited fishermen. We thank the 3 anonymous reviewers for their useful and constructive comments, as well as A. Gallego, E. North, and P. Petitgas, the 3 co-editors of this group submission and co-chairs of the 'Workshop on advancements in modelling physical–biological interactions in fish early-life history: recommended practices and future directions'. This research was funded by the Coastal Observing Center (UNH) through grants from the NOAA Coastal Services Center, and the NSF/NOAA US GLOBEC Northwest Atlantic/Georges Bank program.

LITERATURE CITED

Ames E (2004) Atlantic cod stock structure in the Gulf of Maine. Fish Res 29:10–28

Berrien P, Sibunka J (1999) Distribution patterns of fish eggs in the U.S. Northeast continental shelf ecosystem, 1977–1987. NOAA Tech Rep 145:1–310

Bigelow H, Schroeder W (1953) Fishes of the Gulf of Maine. Fish Bull 53:1–577

Brooks D (1985) Vernal circulation in the Gulf of Maine. J Geophy Res 90:4687–4705

Byers JE, Pringle JM (2006) Going against the flow: retention, range limits and invasions in advective environments. Mar Ecol Prog Ser 313:27–41

Chen C, Liu H, Beardsley R (2003) An unstructured grid, finite-volume, three-dimensional, primitive equations ocean model: application to coastal ocean and estuaries. J Atmos Ocean Technol 20:159–186

Chen C, Beardsley R, Hu S, Xu Q, Lin H (2005) Using MM5 to hindcast the ocean surface forcing fields over the Gulf of Maine and Georges Bank region. J Atmos Ocean Technol 22:131–145

Churchill J, Pettigrew N, Signell R (2005) Structure and variability of the Western Maine Coastal Current. Deep-Sea Res II 52:2392–2410

Collette B, Klein-MacPhee G (eds) (2002) Bigelow and Schroeder's fishes of the Gulf of Maine. Smithsonian Institution Press, Washington, DC

Cowen R, Lwiza K, Sponaugle S, Paris C, Olson D (2000) Connectivity of marine populations: open or closed? Science 287:857–859

Cowen R, Paris C, Srinivasan A (2006) Scaling of connectivity in marine populations. Science 311:522–527

Cushing D (1995) Population production and regulation in the sea: a fisheries perspective. Cambridge University Press, Cambridge

Dalley E, Anderson J (1997) Age-dependent distribution of demersal juvenile Atlantic cod (*Gadus morhua*) in inshore/offshore northeast Newfoundland. Can J Fish Aquat Sci 54(Suppl 1):168–176

Fish C (1928) Production and distribution of cod eggs in Massachusetts Bay in 1924 and 1925. Bull US Bur Fish 43: 253–296

Fong D, Geyer W, Signell R (1997) The wind forced response on a buoyant coastal current: observations of the western Gulf of Maine plume. J Mar Syst 12:69–81

Geyer W, Signell R, Fong D, Wang J, Anderson D, Keafer B (2004) The freshwater transport and dynamics of the western Maine coastal current. Cont Shelf Res 24:1339–1357

Gotceitas V, Brown J (1993) Substrate selection by juvenile Atlantic cod (*Gadus morhua*): effects of predation risk. Oecologia 93:31–37

Gotceitas V, Fraser S, Brown J (1995) Substrate selection by juvenile Atlantic cod in the presence of an actively foraging and non-foraging predator. Mar Biol 123:421–430

Grant S, Brown J (1998) Nearshore settlement and localized populations of age 0 Atlantic cod (*Gadus morhua*) in shallow coastal waters of Newfoundland. Can J Fish Aquat Sci 55:1317–1327

Grimm V (1999) Ten years of individual-based modelling in ecology: What have we learned and what could we learn in the future? Ecol Model 115:129–148

Hetland R, Signell R (2005) Modeling coastal current transport in the Gulf of Maine. Deep-Sea Res II 52:2430–2449

Hinrichsen HH, St. John M, Aro E, Gronkjaer P, Voss R (2001) Testing the larval drift hypothesis in the Baltic Sea: retention versus dispersion caused by wind-driven circulation. ICES J Mar Sci 58:973–984

Houde E (1988) Fish early life dynamics and recruitment variability. Am Fish Soc Symp 2:17–29

Howe A, Correia S, Currier T, King J, Johnston R (2002) Spatial distribution of ages 0 and 1 Atlantic cod (*Gadus morhua*) off the eastern Massachusetts coast, 1978–1999, relative to 'Habitat Area of Special Concern'. Technical Report 12, Massachusetts Division of Marine Fisheries, Pocasset, MA

Hutchings J, Mayers R, Lily G (1993) Geographic variation in the spawning of Atlantic cod, *Gadus morhua*, in the Northwest Atlantic. Can J Fish Aquat Sci 50:2457–2467

Incze L (2000) Modelling the transport of lobster (*Homarus americanus*) larvae and postlarvae in the Gulf of Maine. Fish Oceanogr 9:99–113

Janzen C, Churchill J, Pettigrew N (2005) Observations of exchange between eastern Casco Bay and the western Gulf of Maine. Deep-Sea Res II 52:2411–2429

Keafer B, Churchill J, Anderson D (2005a) Blooms of the toxic dinoflagellate, *Alexandrium fundyense* in the Casco Bay region of the western Gulf of Maine: advection from offshore source population and interaction with the Kennebec River plume. Deep-Sea Res II 52:2631–2655

Keafer B, Churchill J, McGillicuddy D, Anderson D (2005b) Bloom development and transport of toxic *Alexandrium fundyense* populations within a coastal plume in the Gulf of Maine. Deep-Sea Res II 52:2674–2697

Lough RG (2004) Essential fish habitat source document: Atlantic cod, *Gadus morhua*, life history and habitat characteristics, 2nd edn. NOAA Tech Memo NMFS-NE-190, NOAA-NMFS, Woods Hole, MA

Lough RG, Potter DC (1993) Vertical distribution patterns and diel migrations of larval and juvenile haddock *Melanogrammus aeglefinus* and Atlantic cod *Gadus morhua* on Georges Bank. Fish Bull 91:281–303

Lough RG, Valentine PC, Potter DC, Auditore PJ, Bolz GR, Neilson JD, Perry RI (1989) Ecology and distribution of juvenile cod and haddock in relation to sediment type and bottom currents on eastern Georges Bank. Mar Ecol Prog Ser 56:1–12

Lough RG, Hannah CG, Berrien P, Brickman D, Loder JW, Quinlan JA (2006) Spawning pattern variability and its effect on retention, larval growth and recruitment in Georges Bank cod and haddock. Mar Ecol Prog Ser 310: 193–212

Lynch D, Holboke M, Naimie C (1997) The Maine coastal current: spring climatological circulation. Cont Shelf Res 17:605–634

Mayo R, O'Brien L, Wigley S (1998) Assessment of the Gulf of Maine Atlantic cod stock for 1998. Ref. Doc. 98-13, Northeast Fisheries Science Center, Woods Hole, MA

Mellor G, Yamada T (1982) Development of a turbulence closure model for geophysical fluid problem. Rev Geophys Space Phys 20:851–875

O'Brien L, Lough R, Mayo R, Hunt J (2005) Gulf of Maine and Georges Bank (NAFO Subareas 5 and 6). In: Brander K (ed) Spawning and life history information for North Atlantic cod stocks, No. 274. ICES Cooperative Research Report, Chapter 3.11, p 95–104

Pettigrew N, Churchill J, Janzen C, Mangum L and 5 others (2005) The kinematic and hydrographic structure of the Gulf of Maine Coastal Current. Deep-Sea Res II 52: 2369–2391

Poppe L, Williams S, Paskevitch V (2005) U.S. Geological Survey east-coast sediment analysis: procedure, database, and GIS data. Open-File Report DVD-ROM 2005-1001, U.S. Geological Survey, Woods Hole, MA

Pringle J (2006) Sources of variability in Gulf of Maine circulation, and the observations needed to model it. Deep-Sea Res 53:2457–2476

Ross O, Sharples J (2004) Recipe for 1-D Lagrangian tracking models in space-varying diffusivity. Limnol Oceanogr Methods 2:289–302

Runge J, Franks P, Gentleman W, Megrey B, Rose K, Werner F, Zakardjian B (2005) Diagnosis and prediction of variability in secondary production and fish recruitment processes: developments in physical-biological modeling. In: Robinson AR, Brink (eds) The sea, Vol 13. John Wiley & Sons, New York

Schroeder W (1930) Migrations and other phases in the life history of the cod off southern New England. Bull US Bur Fish 46:1–136

Shearman K, Lentz S (2004) Observations of tidal variability on the New England shelf. J Geophys Res 109:1–16

Siegel D, Mitarai S, Costello C, Gaines S, Kendall B, Warner R, Winters K (2007) Connectivity among nearshore marine ecosystems: the stochastic nature of larval transport. Proc Natl Acad Sci (in press)

Sinclair M (1988) Marine populations: an essay on population regulation and speciation. Washington University Press, Seattle, WA

Suthers I, Franks K (1989) Inter-annual distributions of larval and pelagic juvenile cod (*Gadus morhua*) in southwestern Nova Scotia determined with two different gear types. Can J Fish Aquat Sci 46:591–602

Swearer S, Shima J, Hellberg M, Thorrold S and 6 others (2002) Evidence of self-recruitment in demersal marine populations. Bull Mar Sci 70:251–271

Tupper M, Boutilier RG (1995a) Size and priority at settlement determine growth and competitive success of newly settled Atlantic cod. Mar Ecol Prog Ser 118:295–300

Tupper M, Boutilier R (1995b) Effects of habitat on settlement, growth, and post-settlement survival of Atlantic cod (*Gadus morhua*). Can J Fish Aquat Sci 52:1834–1841

Visser AW (1997) Using random walk models to simulate the vertical distribution of particles in a turbulent water column. Mar Ecol Prog Ser 158:275–281

Werner F, Perry R, Lough R, Naimie C (1996) Trophodynamic and advective influences on Georges Bank larval cod and haddock. Deep-Sea Res II 43:1793–1822

Werner F, Quinlan J, Lough R, Lynch D (2001) Spatially-explicit individual based modeling of marine populations: a review of the advances in the 1990s. Sarsia 86:411–421

Wirgin I, Kovach A, Maceda L, Roy N, Waldman J, Berlinsky D (2007) Stock identification of Atlantic cod in U.S. waters using microsatellite and single nucleotide polymorphism DNA analyses. Trans Am Fish Soc 136(2): 375–391

Editorial responsibility: Alejandro Gallego (Contributing Editor), Aberdeen, UK

Submitted: July 20, 2006; Accepted: April 30, 2007
Proofs received from author(s): September 28, 2007

Vol. 347: 275–284, 2007
doi: 10.3354/meps06984

MARINE ECOLOGY PROGRESS SERIES
Mar Ecol Prog Ser

Published October 11

OPEN ACCESS

Formulation and application of an efficient optimized biophysical model

David Brickman[1,2,*], Gudrun Marteinsdottir[2,3], Lorna Taylor[2]

[1]Dept. of Fisheries and Oceans, PO Box 1006, Dartmouth, Nova Scotia B2Y 4A2, Canada
[2]Marine Research Institute, Skulagata 4, 121 Reykjavik, Iceland
[3]Institute of Biology, University of Iceland, Sturlugata 7, 101 Reykjavik, Iceland

ABSTRACT: The formulation of an efficient optimized biophysical model is described, and the model is applied to the simulation of the climatological 0-group distribution of Icelandic cod *Gadus morhua* larvae. The method is based on representing the results from particle tracking as drift probability density functions describing the probability that particles released from a given spawning ground are found at a specific downstream grid location some time later. Spawning is considered to take place from 15 spawning grounds, and the model is used to determine 45 egg production model parameters as the solution of a bound constrained optimization problem that minimizes model-data misfits in abundance and age distributions. The problem is solved using a direct search minimization routine. Two cost functions are used. One penalizes misfits in the gridded abundance and age distributions (Model 1). The other directly penalizes the misfit in the spatial age gradient (Model 2). A simple age-based settlement module is tested to determine whether it improves the model fit. Results from Model 1 show a large error in the spatial age gradient. Model 2 achieves a 20-fold reduction in this error, with only a small degradation of the gridded abundance and age distributions. The settlement model does not improve the model fit. The results indicate that the addition of more processes to a model does not always improve model performance, while focusing on gradients in age instead of simple age distributions can lead to overall improved performance. The technique presented in the present paper allows quantitative evaluation of various model processes in a computationally efficient framework.

KEY WORDS: Optimized biophysical model · Probability density function · Icelandic cod

INTRODUCTION

Biophysical models (BPM) of fish larvae simulate the drift, development, growth, and mortality of released fish eggs (Heath & Gallego 1998, Brickman & Frank 2000, Hinrichsen et al. 2002). Typical components of such models are (1) a particle-tracking routine, which simulates egg/larval drift based on flow fields from a circulation model and information regarding spawning ground location(s), (2) an egg production model (EPM), which describes the space/time release of eggs, based on spawning stock data, and (3) a controlling program, which, using particle tracking, the EPM, and a mortality routine, computes the (time dependent) spatial distributions of eggs and larvae.

A characteristic of BPMs is that they contain a number of parameters that are poorly known, often bounded within a range of possible values. For example, the EPM simulation of egg and larval drift depends on peak spawning time, spawning duration, and the number of eggs spawned. Because flow fields vary in time, uncertainty in these parameters translates into uncertainty in the model-predicted spatial distributions of age and abundance. A way to solve for uncertain parameters is by finding values that minimize the mismatch between model predictions and observations. The model is thus said to be 'optimized'. This paper presents an efficient optimized BPM applied to the problem of simulating the climatological distribution of the pelagic 0-group survey data of Icelandic cod *Gadus morhua*.

*Email: brickmand@dfo-mpo.gc.ca

In a related paper, Brickman et al. (2007a) applied this model to data from 2002 and 2003, with the specific goal of understanding spawning stock and drift characteristics specific to these focus years of the METACOD project (a fifth framework research project granted by the European Commission). In addition to providing more details of the model and applying it to a different dataset, the present paper further explores the power of the optimization method to simulate specific characteristics of observed data and to assess the importance of biophysical processes in improving model performance. The climatological distribution of juvenile Icelandic cod is characterized by a negative spatial age gradient, with a fairly abrupt decrease in age near the northwest corner of Iceland (Begg & Marteinsdottir 2000, Marteinsdottir et al. 2000a, Brickman et al. 2007b). Brickman et al. (2007a) showed that the model had some ability to reproduce this feature, as it was represented in the 2002 data. Here, we show how the model cost function can be formulated to specifically focus on the gradient in age, leading to an improved model fit. The path toward settlement and beyond involves several biophysical processes that may or may not be explicitly modeled by the BPM. The Icelandic summer survey of the pelagic 0-group occurs at a time when it is possible that the settlement phase has begun. A simple age-based settlement module is added to the BPM, and the model is used to determine whether this leads to an improved fit to the data. In this way, we show how the optimization technique can be used to ascertain the degree to which a particular process is important to the modeling system.

OPTIMIZED BIOPHYSICAL MODEL

In this section we present the formulation of a computationally efficient BPM, and show how we can optimally determine model parameters by minimizing the mismatch between model predictions and data. The technique relies on particle-tracking results being stored to disk and on the results being converted to drift probability density functions (PDFs) as described in Brickman et al. (2007b). As such, we begin the section by reviewing the PDF approach. We then show how the PDF technique can be used in the formulation of a BPM and how, by minimizing the mismatch between model predictions and data, the problem of determining model parameters can be transformed into one of bound constrained optimization.

PDF representation of drift results

Particle tracking that includes a random component of drift (Lagrangian stochastic modeling) typically requires tens of thousands of particle releases in order to achieve stable drift statistics. These results can be characterized in a compact way by determining the probability that an ensemble of particles released from some region (i.e. a given spawning ground) at time $t0$ will be found in another region at $t1$. This is done by breaking the domain into a grid and counting the number of particles in each grid box at $t1$. The PDF for drift from a given spawning ground to a given grid cell is defined as:

$$P(i,j,t1;\text{SPG-}k,t0) = \frac{n(i,j,t1)}{N_k} \quad (1)$$

where SPG-k denotes the k-th spawning ground, (i, j) denotes grid cell, N_k is the total number of particles released from SPG-k, and $n(i, j, t1)$ is the number of particles found in grid cell (i, j) at time $t1$. This PDF is a type of 'transition probability matrix' for a Markov process. In general, as the velocity field is a function of time, $P(i, j, t1;$ SPG-$k, t0)$ is a function of time-of-release. These PDFs are calculated offline by a 'front end' routine. The effect is to translate a scatterplot of particle positions at a given time into a contour plot of drift probabilities computed on the chosen grid. Examples of drift PDFs around Iceland are presented in the 'Model application' section.

Model formulation

We are interested in the contribution from the batch of eggs released at time $t0$ from spawning ground 'k' (Fig. 1) to the abundance distribution at grid location (i, j) at $t1$ (ab$(i, j, t1)$). Assume the EPM release curve is Gaussian, characterized by parameters PS, σ, and F. Here, PS is the peak spawning time, σ is the standard deviation (SD) of the Gaussian curve (representing spawning duration), and F is the total number of eggs released at the spawning ground in question. If these parameters are known, then the number of eggs released at $t0$, $E(t0)$, is known.

The number of particles, or the concentration, at grid cell (i, j) at $t1$ is:

$$c(i,j,t1) = E(t0) \times P(i,j,t1;\text{SPG-}k,t0) \quad (2)$$

where P is known from particle tracking. This is in the absence of mortality. On their way to grid cell $(i, j, t1)$ these eggs hatch into larvae, which grow as they drift. The egg and larval phases are subject to (exponential) mortality. We take the egg mortality rate (M_E) to be constant in space and time and the larval mortality (rate) to be of the form (Houde 1997):

$$M_L(a) = \frac{b}{cL(a)^d} \quad (3)$$

where a is larval age and $L(a)$ is length (mm). The parameters M_E, b, c, and d are typically assumed, or can be estimated from data constraints. The total mortality at (i, j, $t1$) acting on the $E(t0)$ eggs released is:

$$M(\Delta t = t1 - t0) = \{e^{-M_E H}\}\{e^{-\int_H^{t1} M_L(a)da}\} \quad (4)$$

where H is the hatch time. Both H and M are computed during particle tracking and are carried as attributes for each of the particle tracks.

The contribution to ab(i, j, $t1$) is:

$$M_T(i,j,t0,t1) \times E(t0) \times P(i,j,t1; \text{SPG-}k,t0) \quad (5)$$

where $M_T(i, j, t0, t1)$ is the gridded mortality from the release at $t0$, calculated by the front end routine. In this particular example, M_T is just the average value of M for the particles found in grid cell (i, j) at $t1$. The total contribution from SPG-k is the sum over all release times. This computation is similar to a dot product, and can be efficiently coded. By summing the contributions from all spawning grounds (S) for all release times, an abundance and age distribution can be created for all grid cells.

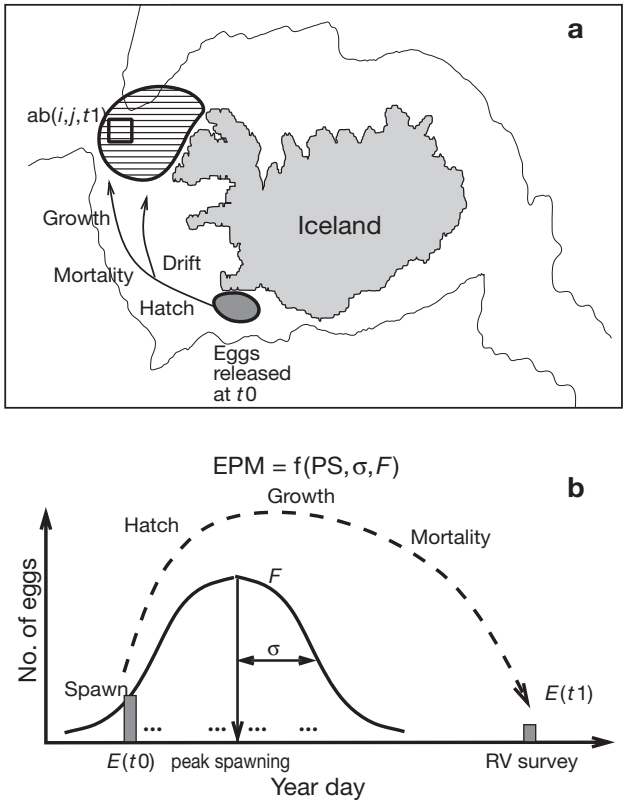

Fig. 1. Processes in the biophysical model showing (a) the progress of eggs released at $t0$ as they drift toward grid cell (black square) (i, j), arriving at $t1$ and (b) the egg production model release curve as a function of day-of-the-year. PS: peak spawning date; σ: the spread of the Gaussian release curve; F: the total number of eggs released. ab: abundances; $E(t0)$: eggs released at t0; $E(t1)$: larvae remaining from $E(t0)$ measured during a research vessel survey

In the above we have assumed that we know EPM(PS, σ, F)$_{spg = 1, S}$. In practice, this is not the case. We thus formulate the problem as follows: Given abundance and age data, determine the set of (PS, σ, F) that minimizes

$$\text{cost\_}fn = \sum_{\text{grid}} \{f([\text{ab(model)} - \text{ab(data)}]^2) + g([\text{age(model)} - \text{age(data)}]^2)\} \quad (6)$$

where the functions f and g on the right hand side will be called cost_ab and cost_age, respectively, and the summation is over all grid cells (i, j) for which there are data. For the Iceland problem under consideration, with 15 spawning grounds where EPM(PS, σ, F) are known within some bounds (see below), this is a 45 parameter problem in bound constrained form.

Solution details

Cost function

The cost function contains 2 components: one related to model-data discrepancies in abundance (cost_ab) and one related to model–data discrepancies in age (cost_age).

With respect to abundance, cost_ab was computed as ~$\sum\{\log[1 + \text{ab(model)}] - \log[1 + \text{ab(data)}]\}^2$. The main motivation for this was to de-emphasize data outliers as it was observed that the model could find unlikely optimal solutions that did a good job matching outliers but faired poorly on the majority of data.

The climatological age distribution of Icelandic 0-group cod (described below) is characterized by a spatial gradient in age concentrated near the northwest corner of the island (Begg & Marteinsdottir 2000). Two versions of cost_age were used. One was the simple squared difference between the model prediction and data (cost_age1), as in Brickman et al. (2007a). The other broke the area around Iceland into 4 boxes, from west to northeast and penalized the (sum of the) squared model-data differences in average age in each of the boxes. This version (cost_age2) directly penalizes errors in the spatial age gradient. Weights were used so that cost_ab and cost_age made roughly equal contributions to the overall cost function and so that the cost function was dimensionless.

Computational method

The problem is solved using a version of a direct search algorithm (see Kolda et al. 2003, and references therein) coded by D. Brickman. To illustrate the method, consider the simple case of a 2-parameter system (Fig. 2). Starting at a first guess, take 4 steps (2 for each para-

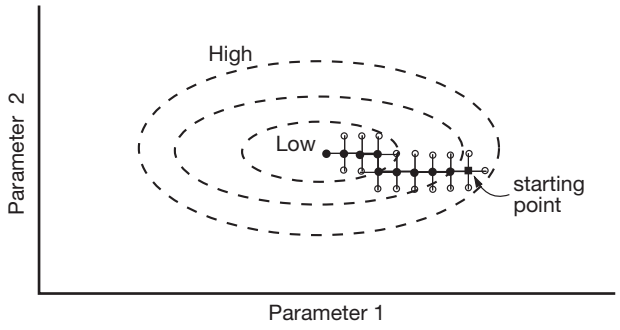

Fig. 2. Direct search minimization routine in 2 dimensions. Dashed lines: contours of the (unknown) cost function; small circles: the 4 trial steps per iteration. The path to the minimum follows the filled circles

meter while holding the other one fixed) and compute the cost function for each step. Take as the next starting point, the step that yielded the lowest cost function value. Repeat this procedure (4 steps plus 'decision') until arriving at the minimum value. (The method is often supplemented by using smaller steps as the minimum is approached.) It can be seen that this method is less efficient than a derivative-based method (e.g. steepest descent, Levenberg-Marquardt [Press et al. 1988]), but these considerations are less important now than they were historically. Also, the computations of numerical derivatives and subsequent matrix inversion have been shown to be the main sources of error and failure of derivative-based methods (Kolda et al. 2003). By comparison, the direct search method is easy to code and robust.

To get an idea of the computational efficiency of the BPM, define as 1 'model run' the computations: choose model parameters, compute the model prediction, calculate the cost function, and perform bookkeeping. On a Linux workstation (single AMD 3200 processor) 200 to 300 model runs s^{-1} are achieved. In terms of convergence of the direct search method, it was observed that about 50 to 60 direct search iterations (each consisting of ~90 model runs) were required to find the minimum, taking <30 s. In problems such as this (i.e. high-dimensional and non-linear), it is difficult to determine whether a global, versus local, minimum has been found. To find the global minimum, the direct search routine was run with 1000 different sets of initial parameter values, and the (final) parameter set associated with the absolute minimum cost function was recorded as the optimal set.

MODEL APPLICATION

The optimized BPM is applied to the problem of simulating the climatological 0-group survey data for Icelandic cod. We start by describing the survey data, then present data needed by the EPM. The circulation model developed for the METACOD project is presented, followed by representative output from the particle tracking algorithm designed to provide an overview of the circulation around Iceland. The settlement module is described.

0-group data

The data come from 29 yr of summer pelagic 0-group surveys (1970 to 1998), trawled at 20 to 50 m depth, and containing >150 stations yr^{-1}. To adjust for non-synopticity of the survey, abundance (number-per-km-towed) is adjusted to the mean survey date (Day 230 of the year) using a mortality rate of 0.03 d^{-1}, consistent with late larval mortality (Houde 1997). Length data (L, mm) are adjusted to the model mean survey date using a growth rate of 0.65 mm d^{-1} (Marteinsdottir et al. 2000a). Length is converted to total age (A, days) using the relation (Begg & Marteinsdottir 2000):

$$A = (L - 15.8723 + 2.5401 \times T)/(0.4256 + 0.0307 \times T) + 16 \quad (7)$$

where T is temperature (Celsius), and the offset (16) is the mean hatch time. For the range of lengths encountered (85% between 30 and 60 mm) and typical temperature range (6 to 10°C), using a constant temperature of 8°C gave a maximum error of <2 d (~2%), so that the simpler formula was considered acceptable. (Note that this relation does not constitute an age–temperature growth relation but, rather, expresses a length–temperature association for the older larvae collected by the survey.)

Climatological distributions of abundance and age were created by averaging the data on a 0.25 × 0.25° grid. The choice of grid size was based on preserving the inherent fine-scale structure of the data while avoiding graininess due to spatial oversampling. Furthermore, the data were decimated to include only those grid cells for which there were at least 6 tows in the 29 yr period. This captures the main features of the distribution while stopping the model from pursuing areas where confidence in the data may be questionable.

There are 3 characteristic features to the climatological 0-group distribution (Begg & Marteinsdottir 2000): (1) the majority of juveniles are found along the northern shelf, (2) there is an inshore/offshore gradient in abundance along the northern shelf with the majority of juveniles found inshore, and (3) a spatial gradient in age exists with age decreasing sharply in a clockwise direction around the northwest corner of Iceland.

The climatological inshore/offshore abundance gradient along the north shelf—defined as the ratio of the average abundance per kilometer inside versus outside the 100 m isobath (Fig. 3b)—is 5.1. The spatial age

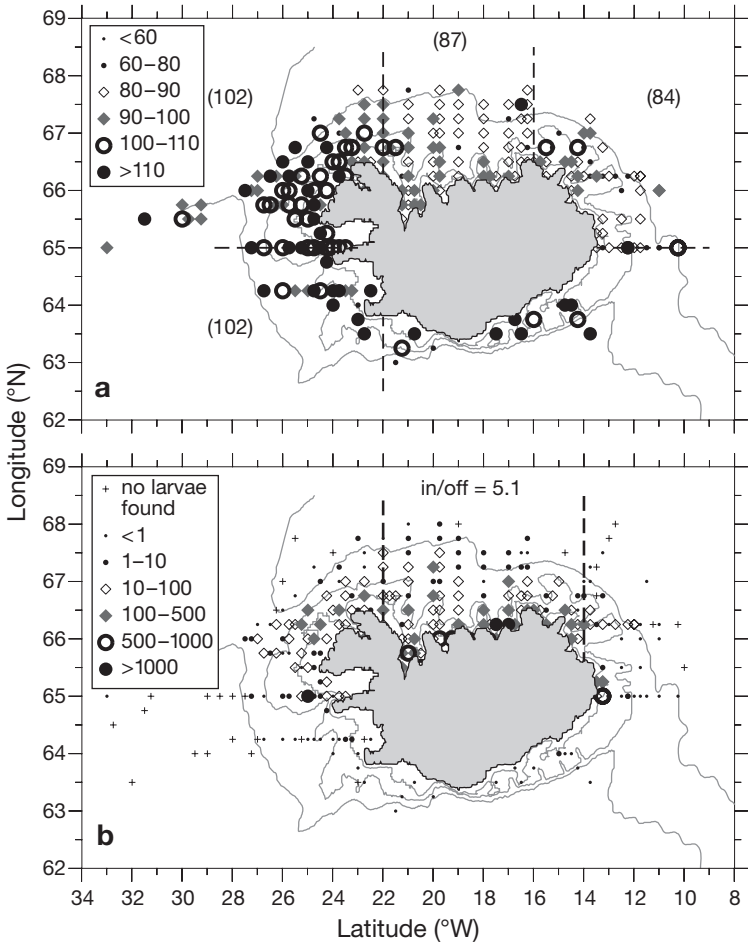

Fig. 3. Gridded climatological spatial (a) age and (b) abundance distributions derived from research vessel survey data, decimated to ≥6 tows cell^{-1}. Areas used to compute bulk measures of spatial age and inshore(in)/offshore(off) abundance gradients are delineated by dashed lines in the 2 panels, respectively, as well as the computed values. The 100, 200, and 600 m isobaths are represented in this and subsequent figures. Units are days for age, and number-per-km-towed for abundance

gradient—defined as the average age in boxes from SW to NE (Fig. 3a)—is 102, 102, 87, and 84. These boxes are used in cost_age2. The length-frequency distribution (not shown) is (roughly) Gaussian, with a peak at ~50 mm and a SD of ~10 mm. Less than 1% of pelagic juveniles caught historically were larger than 7 cm.

Spawning grounds and egg production estimates

The main spawning grounds for Icelandic cod are in the southwest, but some spawning is thought to occur in most of Iceland's bays and fjords. Thirteen locations to release particles were chosen, based on logbook and spawning survey data (Marteinsdottir & Bjornsson 1999, Marteinsdottir et al. 2000a,b). From genetic (Jonsdottir et al. 2002), otolith (Petursdottir et al. 2005), length-frequency, and abundance considerations, the main spawning area was subdivided into 3, making a total of 15 separate spawning grounds (Fig. 4), referred to as SPG-1(a, b, and c) to SPG-13.

Also annotated on Fig. 4 (and Table 1) are estimates of the fraction of total eggs released for each spawning ground and the peak spawning time, based on data presented in Brickman et al. (2007a) and other local knowledge. We see that the main spawning grounds (SPG-1, ca. –22°W, 63.5°N) provide 30 to 50% of the total eggs spawned, with significant contributions from SPG-12 and SPG-3. The total contribution from all northern (and eastern) spawning grounds is estimated to be <5%. Total eggs spawned per year is computed to be 1.5×10^{14}. Peak spawning (PS) day of the year is generally accepted to increase in a clockwise direction starting from ~Day 105 (SPG-1, well established) to about Day 140 to 150 for spawning grounds along the north coast (more uncertain) (Begg & Marteinsdottir 2000). The peak spawning time for other south coast spawning grounds is considered to be later than that of SPG-1 (Fig. 4). Spawning duration (the SD of the Gaussian curve) is about 5 to 10 d for southern spawning grounds, and likely longer for northern ones. Uncertainties in these estimates provide the ranges used to constrain the optimized BPM (Table 1).

Circulation model and drift algorithm

As part of the METACOD project a circulation model was developed that covered the Atlantic and Arctic Oceans, with a focus on Icelandic waters. For details of this model, see Logemann & Harms (2006) and Brickman et al. (2007b). The model domain contains a hierarchy of nested subdomains, being reduced to 1.2 km resolution in Icelandic waters. To estimate the climatological circulation, the model is forced with the wind stress from the Ocean Model Intercomparison Project dataset (Röske 2006). This dataset, based on re-analysis of 15 yr of ECMWF atmospheric data, describes a 360 d cyclic, stationary, climatological year that includes the passage of storms (i.e. it is a 'storm climatology'). One tidal component (M2) is included. The result is a time-varying climatological circulation, with output as daily averaged fields for use in the particle-tracking routine.

Particles are advected by space and time-interpolated currents, plus they have an additional (horizontal)

Table 1. Egg production model input parameter ranges and output values from the optimized biophysical model (Model 2). SPG: spawning ground; PS: peak spawning time (day of the year); σ: standard deviation of Gaussian egg release curve (d); egg-frac.: fraction of total eggs released. The summation of egg-frac must total 1, so the model can achieve values outside of the input range

SPG	Input parameters			Output parameters		
	PS range	σ range	Egg-frac. range	PS	σ	Egg-frac.
1a	90–120	5–10	0.05–0.15	90	5	0.071
1b	90–120	5–10	0.05–0.15	90	10	0.107
1c	90–120	5–10	0.05–0.15	110	10	0.107
2	115–140	5–10	0.05–0.15	140	10	0.036
3	120–150	5–15	0.1–0.4	145	5	0.286
4	140–150	5–15	0.0–0.15	150	10	0.107
5	140–150	5–15	0.0–0.05	145	10	0.036
6	150–160	5–15	0.0–0.05	150	10	0.036
7	150–160	5–15	0.0–0.05	150	10	0.036
8	150–160	5–15	0.0–0.05	150	10	0.036
9	150–160	5–15	0.0–0.05	155	5	0.000
10	150–160	5–15	0.0–0.05	155	5	0.036
11	115–115	10–10	0.0–0.02	115	10	0.000
12	100–130	5–10	0.05–0.3	100	5	0.036
13	105–125	5–10	0.05–0.15	125	10	0.071

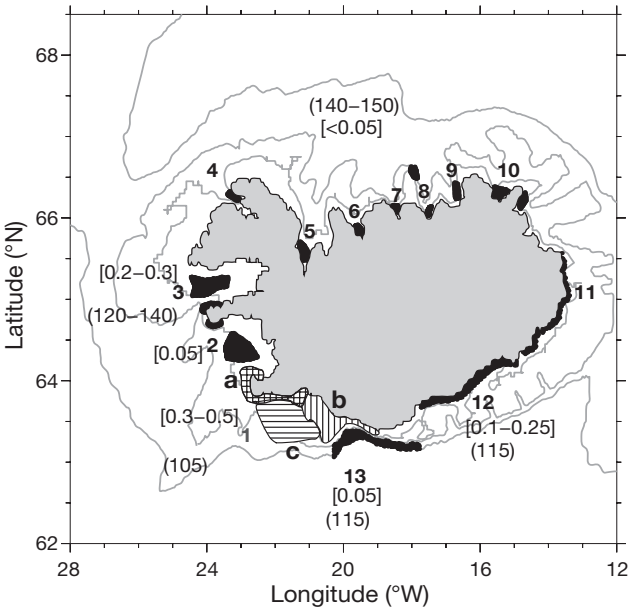

Fig. 4. The 15 spawning grounds and estimates of egg production model parameters. Square brackets enclose fraction of eggs spawned. For SPG-1a, b, and c this is [0.1–0.4], [0.05–0.15], and [0.05 to 0.20], respectively. The total for SPG-4 to 11 is <0.05. Round brackets enclose the day(s)-of-the-year of peak spawning

stochastic component to represent the effects of turbulence. The latter depends on the local (time dependent) diffusivity derived from the circulation model and is enacted in the form of a 'random displacement model' (Rodean 1996, Brickman & Smith 2002). A total of 30 000 particles were released from the 15 spawning grounds, distributed roughly in proportion to the areas of the individual spawning grounds. The method of Brickman & Smith (2002) was used to determine that this number of particles gave satisfactory drift statistics. The vertical component of turbulence was not included, because, as shown by Brickman & Smith (2002), this can lead to erroneous particle tracks if the circulation model turbulence field is not sufficiently smooth.

The circulation model flow fields are time dependent, which means that drift patterns depend on the day of the year of release. For practical reasons, particles were released at 5 d intervals starting on Day 80 and ending on Day 175, resulting in a form of discretization of the EPM. This interval was chosen to safely bracket the expected egg release days from the various spawning grounds in Icelandic waters (Marteinsdottir & Bjornsson 1999). Each release was tracked until the climatological mean survey date (Day 230 of the year).

Icelandic cod eggs are released near the bottom and rise to the surface after spawning. Field data for gadoid larvae indicate that they exhibit an ontological increase in mean depth that increases as they age (Werner et al. 1993, Brickman et al. 2001). Unfortunately, there are not sufficient egg and larval data to deduce such a relationship for Icelandic cod. Brickman et al. (2007a), using the optimized BPM to study the 2002 and 2003 0-group data, considered algorithms that started particles at 5, 10, and 15 m depth, respectively, until they hatched, after which time they sank at a rate that put them at about 35 m, the mean trawl depth, after 100 larval days. They found that the 5 m initial depth algorithm gave the best fit to the data. We use that result in the present paper.

A number of particle attributes were recorded along the drift tracks. Of these, the hatch time (H) was determined using the temperature-dependent relation $H = 46.1e^{-0.17T}$ from Pepin et al. (1997). As there is no temperature-dependent growth relation available for Icelandic cod larvae, a linear growth relationship, consistent with the data of Marteinsdottir et al. (2000a), was used in which larvae grew at a rate of 0.35 mm d^{-1} for the first 30 d after hatching and thereafter at 0.65 mm d^{-1}. Thus, the total mortality along the drift path (M, Eq. 4) is an analytic function of age, hatch time, and the larval mortality constants b, c, and d. We found that b = 2.3, c = 0.7, and d = 1.35, plus M_E = 0.23 d^{-1}, gave a reasonable number of survivors compared to the data. These attributes, plus others (for example, the mean larval drift temperature) are calculated in grid coordinates by the front end routine.

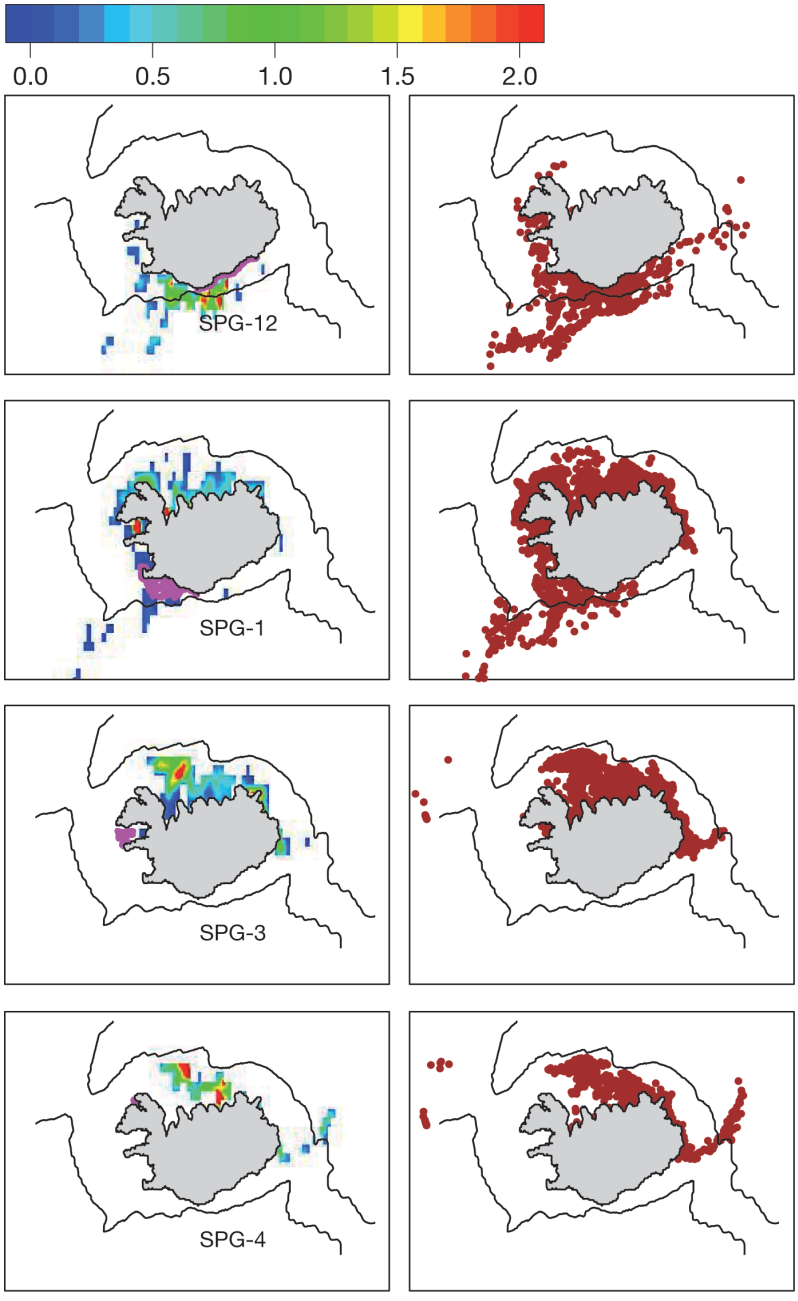

Fig. 5. Example of drift probability density functions for drift in the climatological circulation. Left panels: drift probability in percent. Spawning ground (SPG) is shown in magenta. Right panels: raw final particle positions (at Day 230). Release time is Day 110 of the year. The 100 and 200 m isobaths are omitted for clarity

Representative drift PDF plots for the climatological circulation (release time = Day 110 of the year), with spawning ground of release proceeding in a clockwise fashion from top to bottom are presented (Fig. 5). The general clockwise circulation around Iceland is apparent. Drift from SPG-12 is partly downstream, partly to the southwest (along the Reykjanes Ridge), with significant retention near the release site. For later release times, this spawning ground exhibits increasing drift towards the southeast (Brickman et al. 2007b). SPG-1, -3, and -4 mainly supply the north coast (SPG-4 is an in-fjord spawning ground in the northwest peninsula). SPG-3 and -4 show some drift toward Greenland for this release time.

Settlement module

Little is known about the settlement phase of juvenile Icelandic cod. As mentioned above, virtually no juveniles larger than 7 cm are found by the August pelagic trawl survey. Based on the length–age equation and a 16 d hatch time, a 7 cm juvenile would be spawned on roughly Day 105, about the peak spawning time for the main spawning grounds. By-catch data from the offshore demersal trawl shrimp survey in July and August indicates the presence of 5 to 7 cm cod (peak at 6 cm), although only about 250 data points have been recorded historically (Marine Research Institute [MRI], Iceland unpubl. data). The October adult survey finds settled cod with an average size of 8 to 9 cm (MRI unpubl. data).

The above indicates that the summer 0-group survey is likely sampling, in some regions, a population part of which is in the process of entering the demersal phase. To allow for this possibility, a simple settlement module will be included that settles a fraction of juveniles based on a minimum size (L_s) and a time scale (τ), i.e. fraction settled ~$e^{(L-L_s)/\tau}$. This introduces 2 more parameters into the model (L_s, τ). We will investigate whether the addition of this 'age–settlement' model improves the fit to the data. Note that the larval growth relationship makes length and age interchangeable.

MODEL RESULTS

The model that directly penalized discrepancies in the bulk age gradient (Model 2: cost_fn = cost_ab + cost_age2, no-settlement model; Fig. 6) did a reasonable job with the abundance distribution and the north coast inshore/offshore abundance gradient (cf. Fig. 3),

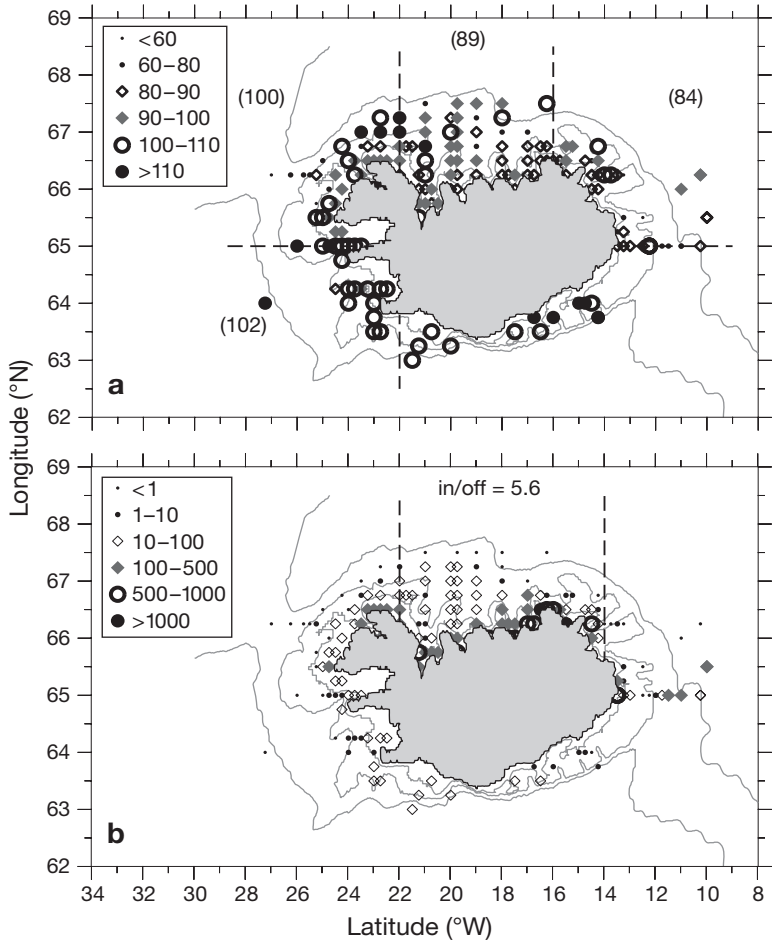

Fig. 6. (a) Spatial age (parentheses: spatial age gradient) and (b) abundance distributions, for Model 2 (cost_*f*n = cost_ab + cost_age2), no-settlement module. Bulk measures of spatial age and inshore(in)/offshore(off) abundance gradients are shown in the 2 panels, respectively

and an excellent job in reproducing the climatological age distribution (Model 2 = [102, 100, 89, 84]; data = [102, 102, 87, 84]). The basic model (Model 1: cost_*f*n = cost_ab + cost_age1, no-settlement model) did a reasonable job with the abundance distribution and the north coast inshore/offshore abundance gradient (in/off = 4.7 versus 5.1 for climatology), but was unable to reproduce the spatial age gradient (Model 1 = [107, 91, 94, 88]). (The Model 1 result was similar enough to Model 2 to not warrant a figure.)

To assess the difference between these 2 results, all components of the cost function (cost_ab, cost_age1, cost_age2) were computed for both cases. We found that Model 2 results in an almost 20-fold reduction in cost_age2, while only incurring about 7% increases in cost_ab and cost_age1. In other words, focusing specifically on the age gradient metric—of special interest to the 0-group distribution problem—leads to a large reduction in this error, with only a small effect on the other distributional measures.

To illustrate where errors occur spatially, a cost function was computed for Model 2 as the square root of cost_ab + cost_age1 on a grid-by-grid basis (Fig. 7). Major areas of error occur in waters deeper than ~150 m along the southwest and west coasts, and in deeper waters along the north and northeast coasts. From visual inspection of model results versus data (Fig. 6 versus Fig. 3), these errors occur in regions where the model predicts zero abundance, indicating a possible underdispersion of particles relative to the climatological data. We return to this point in the 'Discussion' section. Analysis of model output reveals 70 'presence/absence' errors out of 270 data grid points, of which 65 were cases in which larvae are present in the data, but the model predicts zero abundance (and thus zero age). In these 65 instances, the average abundance is low (~10 larvae km^{-1} towed), but the average age is high (96 d). Thus, in real terms, most of the model error is due to age discrepancies in regions of presence/absence errors.

For both Model 1 and Model 2, the addition of the age–settlement module made little visual difference to the results (not shown), and actually resulted in slight increases (~0.5%) in the cost functions. This is not impossible as the module essentially forces some settlement (equivalent to a reduction in predicted 0-group) when no settlement may be a better answer. This shows that the addition of an unmodeled process may actually be detrimental to overall model performance.

DISCUSSION AND CONCLUSIONS

In this paper, a new formulation for a BPM was presented. The computationally efficient method is based on converting the results from particle tracking into drift probability density functions and other attributes calculated in a grid-based coordinate system. In this way many model calculations are done offline, becoming sparse grid-based input data for the main program. It was shown how poorly known model parameters can be determined as the solution of a bound constrained optimization problem that minimizes model-data discrepancies.

The method, herein applied to data from 1 time frame, is readily adapted to handle multiple data frames (e.g. egg/larval surveys) with little loss in speed. As well, while this method is presented as an alternate formulation of a BPM, the gridded attributes

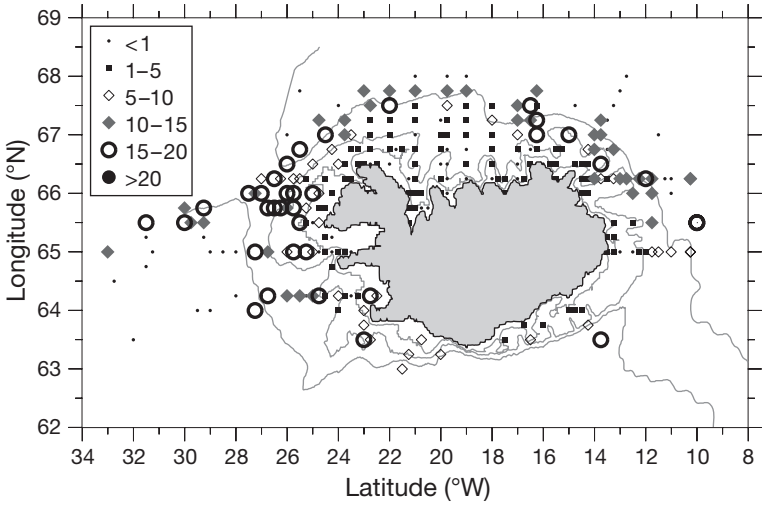

Fig. 7. Distribution of error for Model 2 expressed as the square root of the cost function, computed on a grid-by-grid basis. The values are dimensionless

computed in this case give identical results to an individual-based model (IBM; Heath & Gallego 1998, Hinrichsen et al. 2002) using the same parameters. This can be seen by computing, for an IBM, the contribution to ab(i, j, $t1$) from eggs released at $t0$ from SPG-k:

$$\mathrm{ab}(i,j,t1) = \sum_{\mathrm{p}=1}^{n} E_{\mathrm{p}} \mathrm{M}_{\mathrm{p}} \quad (8)$$

where $E_{\mathrm{p}} = E(t0)/N_k$ is the number of eggs assigned to each particle released from SPG-k at $t0$, n is the number of particles found in grid cell (i, j), and M_{p} is the mortality along the drift path as defined in Eq. (4). Rearranging the above, using the fact that the mortality used in the PDF method $M_{\mathrm{T}}(i, j, t0, t1) = (\sum M_{\mathrm{p}})/n$ and recalling the definition of P, we get:

$$\mathrm{ab}(i,j,t1) = M_{\mathrm{T}} \times E(t0) \times \left\{ \frac{n}{N_k} \right\} = M_{\mathrm{T}} \times E(t0) \times P \quad (9)$$

which is the same as Eq. (5).

Note that this method can be adapted to all formulations that can be run offline. This includes the possibility of optimizing the mortality parameters, as well as the situation where the larvae are embedded in a nutrient/phytoplankton/zooplankton model and their interaction with the prey (and/or predator) field affects their behavior. The technique remains efficient provided that parameters affecting propagule behavior are not part of the set to be optimally determined. An optimization technique for this latter case remains a key problem in biophysical modeling.

The mortality function was taken to be inversely proportional to larval length. For Icelandic cod, no specific temperature-dependent growth model exists, so larval length was taken to be a linear function of age (Begg & Marteinsdottir 2000). If such a relationship did exist, it would be simple to incorporate it into the mortality attribute. However, it is questionable what difference this would make, because, as shown by Brickman et al. (2001) for haddock on the Scotian Shelf of eastern Canada, the incorporation of an age–temperature growth model into the mortality function has a low-order effect. This is due to the form of the mortality function, the temperature field experienced by the larvae, and the fact that a length–age relation captures most of the growth variability.

The model was applied to the problem of simulating the Icelandic cod climatological 0-group survey data. Spawning was taken to occur in 15 spawning grounds, resulting in 45 (egg production model) parameters that were known within bounded estimates. Two different cost functions were used, measuring model–data discrepancies in abundance and age distributions. One penalized the model age prediction on a grid cell by grid cell basis (Model 1). The other (Model 2) directly penalized differences in the spatial age gradient, a feature of the data that is of particular interest for Icelandic researchers.

We found that both models did a reasonable job in simulating the observed inshore/offshore abundance gradient along the north coast. However, the Model 1 solution was unable to reproduce the observed juvenile age gradient, while Model 2 (Fig. 6, Table 1) did much better in this regard. Evaluation of the components of the 2 cost functions showed that the improved fit to the age gradient using Model 2 was only slightly offset by poorer fits to the gridded abundance and age distributions. This observation was corroborated by running a version of the model that penalized only the age gradient (not shown), which resulted in virtually zero misfit in this bulk metric, with little further degradation in the gridded abundance and age errors. The relative insensitivity of the model to these latter 2 metrics can be attributed to the fact that large errors occurred in the offshelf regions (Fig. 7), so that subtle, but important, changes onshelf do not greatly affect total gridded error measures. In general, these large errors were found to be due to systematic presence/absence discrepancies, where the model predicted zero abundance (and age), while the observations indicated older larvae (albeit in low abundance).

As pointed out by Brickman et al. (2007a,b), the particle-tracking algorithm seems to retain particles closer to shore than the climatological data indicate. Whether or not this is due to the use of climatological flow fields, which would be expected to underestimate variability, or due to a deficiency in the particle-tracking algorithm is difficult to determine. Inspection of the annual 0-group distributions (Fig. 3 of Begg & Marteinsdottir

2000) indicates that, while there is interannual variability (especially with respect to the drift toward Greenland), generally the model underpredicts abundance in areas where the survey data are not characterized by episodic events. As well, this underdispersion is also evident in the Brickman et al. (2007a) results, although not to as great an extent. This favors the possibility that this apparent underdispersion may be due to some sort of dispersive larval behavior, such as horizontal swimming motion, which increases as they age. It is possible to add this in a number of ways to the particle-tracking algorithm, and then use the optimized BPM to determine what algorithm produces the best result. This is similar to what was done in Brickman et al. (2007a) to determine the best ontogenetic vertical migration algorithm. In any case, the reason for this systematic error is currently unresolved.

A simple age-based settlement module was added to the BPM to see if it improved the model fit. We found that despite adding 2 more parameters to the BPM, the overall solution actually slightly deteriorated (<1%). This was attributed to the fact that this module effectively forces extra pelagic juvenile mortality, which can lead to a worse fit. The incorporation of more processes (e.g. biology) into a model is usually considered to be an improvement. The modeling technique presented in this paper allows a quantitative evaluation of this procedure. The result points out that additions of more biophysics to a model may not be beneficial, and thus must be approached with caution. It does not, however, preclude that a different settlement module could improve model performance.

The model finds the optimal set of egg production model parameters (Table 1) within the confines of the imperfections of its inputs and its construct, and the results should always be assessed with these limitations in mind. For example, the fraction of eggs contributed from SPG-3 (about 29%) is higher than expected, as is the total from the northern spawning grounds. Whether this is real or due to imperfections in the particle-tracking routine, the simple EPM or the mortality function, for example, is difficult to determine without more biological and physical data. The problems of model limitations and poorly represented or unmodeled processes are inherent to all biophysical models. The technique presented in this paper allows quantitative evaluation of various model processes in a computationally efficient framework.

Acknowledgements. This work was partly funded by the EU (METACOD—Project No. Q5RS-2001-00953), the Icelandic Research Council, and the Icelandic Ministry of Fisheries. The authors thank anonymous reviewers and, particularly, the editorial board for suggestions that significantly improved this manuscript.

Editorial responsibility: Alejandro Gallego (Contributing Editor), Aberdeen, UK

LITERATURE CITED

Begg GA, Marteinsdottir G (2000) Spawning origins of pelagic juvenile cod *Gadus morhua* inferred from spatially explicit age distributions: potential influences on year-class strength and recruitment. Mar Ecol Prog Ser 202:193–217

Brickman D, Frank KT (2000) Modelling the dispersal and mortality of Browns Bank egg and larval haddock *Melanogrammus aeglefinus*. Can J Fish Aquat Sci 57:2519–2535

Brickman D, Smith PC (2002) Lagrangian stochastic modelling in coastal oceanography. J Atmos Ocean Technol 19: 83–99

Brickman D, Shackell NL, Frank KT (2001) Modelling the retention and survival of Browns Bank haddock larvae using an early life stage model. Fish Oceanogr 10: 284–296

Brickman D, Taylor L, Gudmundsdottir A, Marteinsdottir G (2007a) Optimized biophysical model for Icelandic cod larvae. Fish Oceanogr 16:448–458

Brickman D, Marteinsdottir G, Logemann K, Harms I (2007b) Drift probabilities for Icelandic cod larvae. ICES J Mar Sci 64:49–59

Heath M, Gallego A (1998) Bio-physical modelling of the early life stages of haddock, *Melanogrammus aeglefinus*, in the North Sea. Fish Oceanogr 7:110–125

Hinrichsen HH, Mollmann C, Voss R, Koster FW, Kornilovs G (2002) Biophysical modeling of larval Baltic cod (*Gadus morhua*) growth and survival. Can J Fish Aquat Sci 59: 1858–1873

Houde ED (1997) Patterns and trends in larval-stage growth and mortality of teleost fish. J Fish Biol 51(Suppl A):52–83

Jonsdottir ODB, Imsland AK, Danielsdottir AK, Marteinsdottir G (2002) Genetic heterogeneity and growth properties of different genotypes of Atlantic cod (*Gadus morhua* L.) at two spawning sites off south Iceland. Fish Res 55:37–47

Kolda TG, Lewis RM, Torczon V (2003) Optimization by direct search: new perspectives on some classical and modern methods. SIAM (Soc Ind Appl Math) Rev 45:385–482

Logemann K, Harms I (2006) High resolution modelling of the North Icelandic Irminger current (NIIC). Ocean Sci Discuss 3:1149–1189

Marteinsdottir G, Bjornsson H (1999) Time and duration of spawning of cod in Icelandic waters. ICES CM 1999/Y:34

Marteinsdottir G, Gunnarsson B, Suthers IM (2000a) Spatial variation in hatch date distributions and origins of pelagic juvenile cod in Icelandic waters. ICES J Mar Sci 57: 1182–1195

Marteinsdottir G, Gudmundsdottir A, Thorsteinsson V, Stefánson G (2000b) Spatial variation in abundance, size composition and viable egg production of spawning cod (*Gadus morhua* L.) in Icelandic waters. ICES J Mar Sci 56:824–830

Pepin P, Orr DC, Anderson JT (1997) Time to hatch and larval size in relation to temperature and egg size in Atlantic cod (*Gadus morhua*). Can J Fish Aquat Sci 54(Suppl 1):2–10

Petursdottir G, Begg GA, Marteinsdottir G (2005) Discrimination between Icelandic cod populations from adjacent spawning areas based on otolith growth and shape. Fish Res 80:182–189

Press WH, Flannery BP, Teukolsky SA, Vetterling WT (1988) Numerical recipes in C: the art of scientific computing. Cambridge University Press, Cambridge

Rodean HC (1996) Stochastic Lagrangian models of turbulent diffusion. In: Meteorological monographs, No. 48. American Meteorological Society, Boston, MA, p 1–84

Röske F (2006) A global heat and freshwater forcing dataset for ocean modelling. Ocean Model 11:235–297

Werner FE, Page FE, Lynch DR, Loder JW, Lough RG, Perry RI, Greenberg DA, Sinclair MM (1993) Influences of mean advection and simple behavior on the distribution of cod and haddock early life stages on Georges Bank. Fish Oceanogr 2: 43–64

Submitted: July 4, 2006; Accepted: July 26, 2007
Proofs received from author(s): September 21, 2007

Vol. 347: 285–300, 2007
doi: 10.3354/meps06985

MARINE ECOLOGY PROGRESS SERIES
Mar Ecol Prog Ser

Published October 11

OPEN ACCESS

Surfing, spinning, or diving from reef to reef: effects on population connectivity

Claire B. Paris*, Laurent M. Chérubin, Robert K. Cowen

Rosenstiel School of Marine and Atmospheric Science, University of Miami, Miami, Florida 33149-1098, USA

ABSTRACT: Coral reef fish have considerable larval behavioral capabilities that can lead to successful completion of the early pelagic life phase. In particular, vertical migration during ontogeny increases retention near natal reefs and decreases losses due to transport by currents. For those larvae that are not returning home, the relative influence of behavior (biology) and currents (physics) on their arrival pattern among adjacent and distant reefs is not known. Moreover, interactions of the naturally small-scale larval movements with those of larger-scale currents need to be evaluated with regard to the spatial patterns of recruitment. We used an offline Lagrangian stochastic modeling approach to explore the relative influence of physical (i.e. eddy perturbation, diffusion) and biological processes (i.e. vertical movement, mortality) on the connectivity of the coral reef fish population in the western Caribbean, a region with complex geomorphology and circulation. This study revealed that the impact of larval behavior extends beyond enhancing the process of self-recruitment by changing population connectivity patterns. Connectivity was significantly influenced by larval vertical movement, survival, and by the eddy field, all controlling arrival patterns near reefs. A sensitivity analysis was done to gauge the robustness of the results by varying the model parameters. We found that particle-tracking models with homogeneous parameterization of the sub-grid motion tended to bias dispersal from and along the reef track, which can be mitigated by using spatially explicit parameters calculated from the Eulerian velocity fields. Finally, larval survival emerged as a key component for connectivity estimates, the study of which poses a great challenge in tropical ecosystems.

KEY WORDS: Modeling fish larvae · Transition probability matrix · Dispersal kernel · IBM · Population connectivity · Lagrangian · Stochastic model · Spin · Offline model

INTRODUCTION

The distance and direction of larval dispersal have considerable influence on the demography and genetic structure of marine species. Recent studies indicate that despite their small size, coral reef fish larvae are not passive (for a review, see Leis 2007, this Theme Section [TS]). They have a diversity of traits and considerable behavioral capabilities that can lead to successful completion of the early pelagic life phase (Fig. 1). In particular, vertical migration during ontogeny increases retention near natal reefs and decreases dispersion losses, likely enhancing survival (Paris & Cowen 2004). Larvae can come back to their native reefs or can be exchanged among breeding subpopulations. However, the dynamics of these interactions at both the individual and population levels are not fully understood (deYoung et al. 2004). For those larvae that do not return home, the extent to which their behavior influences their arrival pattern among adjacent and distant reefs (or larval connectivity network) is not known. More importantly, interactions of the small-scale larval movements with transport processes due to larger-scale currents need to be quantified with regard to the spatial patterns of recruitment. Since actively moving larvae may be diluted and to some extent dispersed by currents, an *in situ* study of them is very difficult. Spatially explicit, individual-based modeling (IBM) has emerged as a key tool for understanding organism–environment interactions

*Email: cparis@rsmas.miami.edu

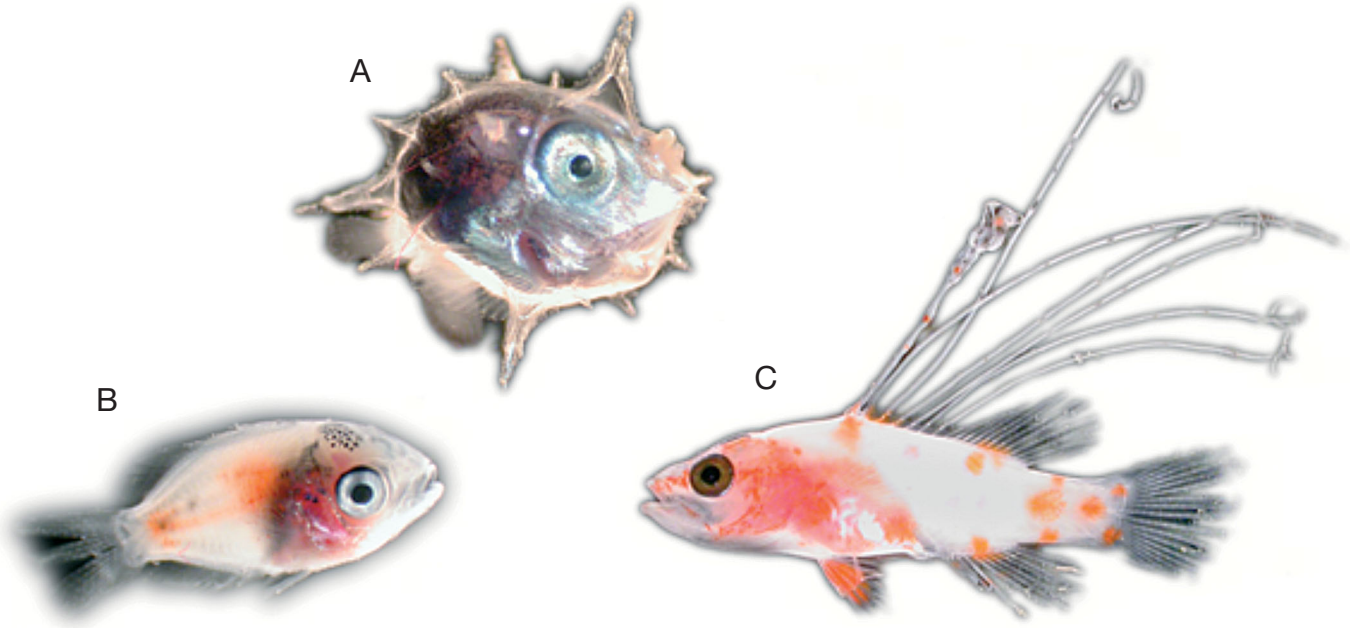

Fig. 1. Morphological diversity in fish larvae: (A) the pelagic sunfish *Mola mola* develops heavy pigmentation (melanophores) presumably to sustain UV radiations near the ocean surface, while coral reef fish larvae such as (B) the bicolor damselfish *Stegastes partitus* and (C) the candy bass *Liopropoma* sp. are mostly clear, with red-orange pigments (erythophores); as the ocean strongly absorbs colors in the red-orange part of the spectrum, these erythophores would appear dark at the depth where these larvae were captured (20 to 40 m and 60 to 80 m strata, respectively; Paris & Cowen 2004, R. K. Cowen unpubl. data), breaking up the larva's shape. Diversity in shape and presence of appendages and elongated spines imply that these larvae occupy specific behavioral niches in the water column

(Werner et al. 2001) and is particularly relevant to investigate larval fish fluxes in the complex coral reef ecosystem. Currently, the spatial scales of the dispersal of reef fish larvae are estimated using indirect and empirical techniques (Thorrold et al. 2002, Jones et al. 2005) or modeling approaches (Cowen et al. 2000, 2006, James et al. 2002). The interactions between physical and biological factors and their role in shaping populations have been previously discussed in landscape ecology (Levins 1969), but this discussion is a relatively recent development for marine ecosystems (Barber et al. 2002, Baums et al. 2006, Cowen et al. 2006). The spatial arrangements and connectivities of marine populations are poorly understood, yet they are assumed to enhance resilience to exploitation and be of critical importance for population persistence (Kinlan et al. 2005, Hasting & Botsford 2006). Measures of natal dispersal are typically determined by the dispersal kernel $k(x,y)$, defined as the probability of a larva settling at a distance x given that it was released at y. The modal dispersal distance from the dispersal kernel has demographic relevance (e.g. population spatial pattern, persistence), while the tail, representing long-distance dispersal, is relevant on an evolutionary level (e.g. genetic mixing, species persistence; Hanski & Gaggiotti 2004, Steneck et al. 2006). Models of population connectivity should thus emphasize where and how frequently larval linkages occur, and how these observed patterns are created. Here, we use a biophysical model designed to output spatially explicit transition probability matrices (or connectivity matrices) from which dispersal kernels are generated. The connectivity matrix describes the probability that an individual moves during its pelagic larval stage from the birthplace (or source population) to its settlement location (or sink population) as a settling larva, all in a 3-dimensional dynamic system. Such transition probability matrices are of considerable value for metapopulation and genetic studies (Hedrick 2000), as well as for spatial management and conservation issues (Urban & Keitt 2001). We show that they also provide a method to quantify the relative influence of biological and physical factors on realized larval dispersal and on levels and spatial patterns of recruits.

Lagrangian stochastic models (LSMs) have been developed for modeling atmospheric transport problems (e.g. Sawford 1999). These are being increasingly applied to track the dispersal of larvae (see Levin 2006 for a review). Motions at small scales that are not resolved by ocean general circulation models (OGCMs) are usually parameterized. These include motions due to small-scale currents and random or oriented motions of individual, simulated larvae (Paris et al. 2002, Codling et al. 2004). Parameterization of subgrid-scale processes is critical for accurate modeling of trajectories and capturing variability (Siegel et al. 2003, deYoung

et al. 2004). Yet, to date, very few larval dispersal studies address the parameterization of the random component statistics in tracking models. The extent to which parameterization of the Lagrangian parameters and larval traits plays a role in estimating population connectivity, and influences arrival patterns among native, adjacent, and distant reefs, is not known. Moreover, even though larvae are irrefutably not passive (Leis 2006), the question still remains of how biological processes weigh against oceanographic process.

To answer these questions, we present a numerical experiment approach that isolates parameters from the larval tracking algorithm and quantifies the relative influence of physical and biological processes on the spatial scales and patterns of larval exchange. Our main goal was to test the hypothesis that the importance of larval traits in shaping dispersal and population networks is comparable with that of ocean circulation. The primary objectives were to (1) use various LSM configurations to isolate and determine the most sensitive physical parameters in estimating dispersal kernels for the study region, (2) investigate the interactions of those parameters with biological parameters reproducing early life-history traits of coral reef fish, and (3) rank the relative importance of parameters and their interactions in estimating population networks in the meso-American region.

BIOPHYSICAL MODEL SETUP

We simulated the dispersal and recruitment of larvae using a spatially explicit Lagrangian stochastic framework (e.g. Hermann et al. 2001), linking biological and physical modules or code units. The coupled biophysical IBM tracked individual larvae within a population, each interacting with the environment based on its present state and past history, and produced probabilistic simulations of both larval trajectories and connectivity matrices (Fig. 2). Integration of archived velocity fields of an ocean circulation model moved virtual larvae (particles). A stochastic scheme parameterized the subgrid turbulent motion, which was added to the particle displacement at each integration time step. A biological module simulated larval traits (i.e. mortality, ontogenetic vertical migration, pelagic duration) as a function of developmental stage and settlement habitat, while a seascape module tracked the presence of the particles in selected coral reef areas. Explicit treatment of spatial history was achieved by simultaneous inclusion of the seascape (e.g. spawning and settlement areas) and the velocity fields in the IBM.

Hydrodynamic module. The hydrodynamic data used was generated with the 3-dimensional Regional Ocean Modeling System (ROMS), which is discretized in coastline- and terrain-following curvilinear coordinates (σ-coordinates model; Marchesiello et al. 2003, Shchepetkin & McWilliams 2004). We used the UCLA ROMS version, which performs local refinement via nested grids (Adaptive Grid Refinement in Fortran; Blayo & Debreu 1999) and has the ability to manage an arbitrary number of embedded levels as well as to do adaptive grid-refinement. The model has 25 vertical layers, and its state variables (temperature, salinity) at the open ocean boundaries are relaxed monthly to the Levitus ocean (http://ingrid.ldeo.columbia.edu/SOURCES/.LEVITUS94/) climatology (World Ocean Atlas). Tides are set at the boundary by the TPXO6 global tide model (www.esr.org/polar_tide_models/Model_TPXO62_load.html). Monthly varying surface

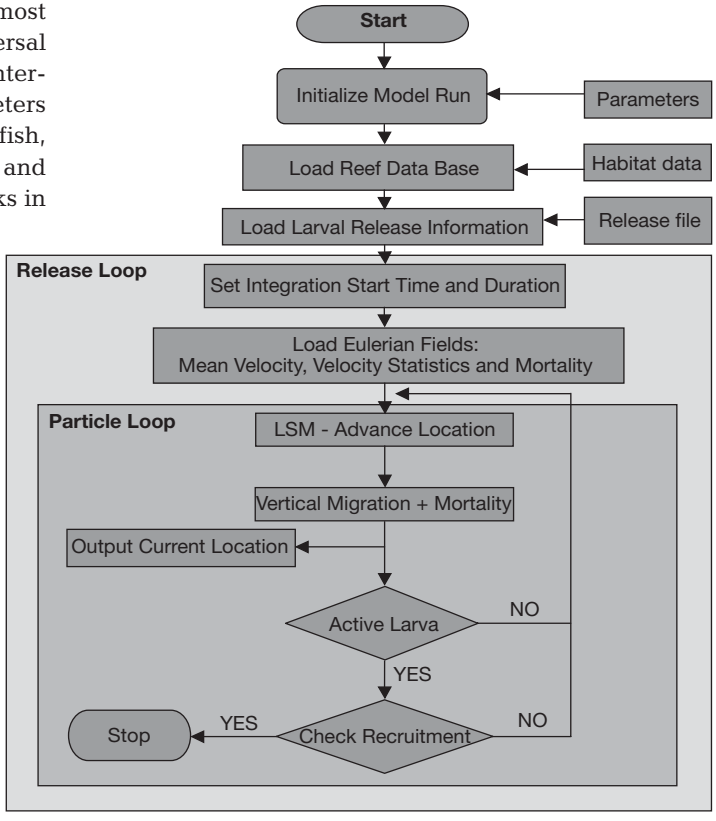

Fig. 2. Flowchart of the offline larval tracking system. The general algorithm for the code consists of several steps: (1) initialization reads the grid coordinate of the ocean model and spatially explicit habitat and population information, (2) individual particles are advanced using the ocean model output frequency, and (3) individual larval behavior and mortality rate is imposed. Finally, if a larva is competent, its location is checked to verify if it falls near settlement habitat. It is then assumed to have successfully recruited, and the time and day and location of recruitment are saved. Otherwise, the larval dispersion is continued until it is recruited or the model is integrated for the number of days specified by the maximum competency period

fluxes (wind, rain, solar, radiative heat fluxes, evaporation) were obtained from the Comprehensive Ocean Atmosphere Dataset (http://icoads.noaa.gov/status.html) (COADS) climatology. Our region of simulation was the Meso-American Barrier Reef System (MBRS) in the western Caribbean, which encompasses one of the largest barrier reefs, off the coast of Belize (Fig. 3). This region is of interest to this study because of the presence of submesoscale eddies (~10 to 100 km diameter), coastal currents, and topographic features that constrain the circulation and connectivity (Tang et al. 2006). In general, the modeled circulation was consistent with observations from float trajectories (Richardson 2005) and with model simulations from Ezer et al. (2005). On average, the Caribbean Current flows westward between 18 and 19° N and veers north along the Yucatan Peninsula into the Gulf of Mexico. South of the Caribbean Current, cyclonic eddies are formed and constrain the circulation in the Gulf of Honduras (Fig. 3). The extent and strength of the cyclonic gyre is variable, as it can extend beyond the limits of the Gulf of Honduras and reach 85° W on the Honduras coast, recirculating water from Honduras to Belize (Chérubin et al. 2007). Daily outputs of the first 5 layers (i.e. from 0 to 100 m) of the ROMS simulations were inputs to the offline larval tracking model. Vertical velocities, w, were not incorporated in the particle motion.

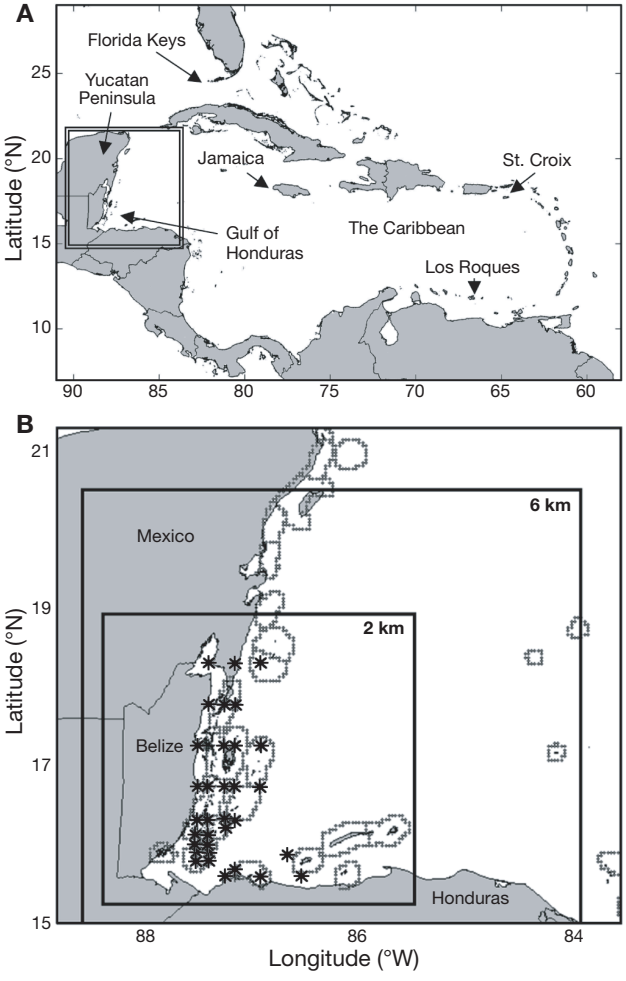

Fig. 3. (A) The Caribbean region with insert (enlarged in Panel B) showing the domain of the numerical experiments with the boundaries of the Regional Ocean Modeling System parent grid (6 km) and child grid (2 km). Asterisks indicate the release locations of simulated online floats (n = 70) used to calculate the intrinsic Lagrangian parameters; only those released within the reef habitat (gray lines) were used for analyses of larval dispersal (n = 48)

Particle-tracking module. Individual particle movements are tracked offline with LSM, assuming that the evolution of particle velocity and position in non-homogeneous, non-stationary turbulence can be represented as a Markovian process (Griffa 1996). We used different LSM configurations to test the effect of spatial and temporal averaging of Lagrangian parameters (i.e. decorrelation time scale T_L; horizontal variance of the velocity $\sigma^2 = \langle u'^2 \rangle$, where $\langle\ \rangle$ is a spatial or temporal average; spin parameter Ω allowing for the vorticity of the eddy field; Veneziani et al. 2005a,b) on larval dispersal estimates. Our baseline model was Markovian for (x,u), the particle position and velocity field, respectively, and its governing equations were:

$$\mathrm{d}x_i = [\langle u_i(x,y,z)\rangle + u_i']\mathrm{d}t + \mathrm{d}u_i'\mathrm{d}t \quad (1)$$

$$\mathrm{d}u_i' = [-u_i'/T_L + a(x,y,z,u_{i,j}')]\mathrm{d}t + b_i(x,y,z)\mathrm{d}W(t) \quad (2)$$

where i is 1 or 2 (x and y directions), dx is the particle displacement and du' is the velocity increment of the turbulent velocity at each time step. The first and second terms on the right-hand side of Eq. (1) are the mean velocity and the turbulent velocity, respectively, dt is the time step, and (x, y, z) are the coordinates. The first term on the right-hand side of Eq. (2) represents a fading memory for velocity fluctuations; the second term, a, the drift correction term, is zero when turbulence is stationary and homogeneous (Berloff & McWilliams 2002). The third term represents random forcing, where dW is a random increment from a Wiener process (i.e. continuous-time Gaussian stochastic process) with zero mean and variance dt and b is the amplitude of the random increment (Berloff & McWilliams 2002). Applied to larval transport, b could also describe larval swimming (e.g. oriented motion; see Codling et al. 2004). Some measure of the rotation of trajectories is necessary to account for subdiffusive processes, driven, for instance, by submesoscale coherent vortices. Reynolds (2002a) coined the measure of rotation the 'spin' parameter (Ω) and introduced it in the LSM. Thus, the drift correction term a is associated with the spin parameter Ω (Borgas et al. 1997, Reynolds 2002a, Veneziani et al. 2004), and the amplitude of the random forcing is a function of the horizontal variance of the velocity field. The velocity increment equations were:

$$du' = -\frac{u'}{T_{Lu}}dt - \Omega v'dt + \left(\frac{2\sigma_u^2}{T_{Lu}}\right)^{1/2} dW_u(t) \quad (3)$$

$$dv' = -\frac{v'}{T_{Lv}}dt + \Omega u'dt + \left(\frac{2\sigma_v^2}{T_{Lv}}\right)^{1/2} dW_v(t) \quad (4)$$

Here, the eddy diffusivity is $K = (2\sigma^2/T_L)^{1/2}$, which is b in Eq. (2). The Lagrangian parameters of the bio-physical model (i.e. T_L, σ, and Ω) were directly estimated from the Eulerian fields of the ocean model using Middleton's relationships between the Eulerian and Lagrangian decorrelation spatial and temporal scales (Middleton 1985, Lumpkin et al. 2002) such that:

$$T_L/T_E = q[q^2 + (u'/c_*)^2]^{-1/2} \quad (5)$$

where $q = \sqrt{\pi/8}$. The ratio $c_* \equiv L_E/T_E$ is the evolution speed of the eddy field constructed from its Eulerian time (T_E) and length scales (L_E). The parameters u' and v' (in the x and y directions) are the root mean square eddy speed calculated from the Lagrangian statistics using float trajectories.

The spin obtained from the direct calculation of the Eulerian mean rate of rotation $\langle ds \rangle$:

$$\Omega = \frac{\langle ds \rangle}{2dt(u'^2 + v'^2)} \quad (6)$$

This model was constrained by the well-mixed condition criterion (Thomson 1987), which implies that a passive tracer uniformly mixed over the full domain remains uniformly mixed at all times. In this classical form of the LSM model, the Lagrangian parameters (i.e. T_L, σ^2, and Ω) are then spatially uniform or constant in time. However, the definition of Ω accounts for the spatial variation of the variance of the velocity field; thus, TL and σ^2 can be spatially variable if subregions made of homogeneous statistical properties are defined (Lumpkin et al. 2002, Veneziani et al. 2004). Moreover, to improve the capabilities of the LSM in simulating a broader range of intermediate-time, non-diffusive, single-particle time-dispersion behaviors involving a variety of time scales and length scales, we followed Berloff & McWilliams' (2003) method to randomize our LSM, by defining a distribution of each variable of the triplet (T_L, σ^2, and Ω) in individual bins.

Biological module—stochastic ontogenetic vertical migration and mortality. The vertical distribution of larvae is time dependent. We built species-specific matrices of larval probability vertical distribution with time, based on field observations combined with otolith analyses to age the larvae (Paris-Limouzy 2001). Here, we modelled 2 types of migration patterns, the 'deep' and 'shallow' ontogenetic vertical migrations (OVMs) analogous to those of damselfish (Pomacentridae; Fig. 4) and grouper (Serranidae; see Fig. 3 in Cowen 2002) larval behavior, respectively. The code reads the probabilities for the vertical distribution of a given species $P_{spec}(l,z)$ and converts the probabilities into a random number $0 < R_N < 1$ by solving the integral equation for z_i:

$$R_N(l, z_i) = \int_{-\infty}^{z_i} P_{spec}(l,z)dz \quad (7)$$

where l is the duration of the stage-specific vertical distribution (e.g. 3 d; see Fig. 4) and z_i is the depth where the larvae are found. The frequencies of the resulting depth values z_i reflect the characteristics of the probability distribution.

The mortality rate can be supplied either as a constant value or as a 4-dimensional Eulerian field (x, y, z, time), whereby its value close to an individual larval location is used to calculate the probability of mortality. Here, we used a constant mortality rate assigned stochastically among particles (i.e. patchy mortality). Dead larvae were flagged and removed from further calculations.

Seascape module. The seascape module serves to quantify the ecological interactions (e.g. particle behavior, exchange of particles) at the boundary of the pelagic and coral reef ecosystems. Coupled to the particle-tracking module, it traces the source location and provides habitat information to the particle (e.g. presence of suitable nursery areas) at each time step. The habitat (i.e. spawning and settlement areas) is derived from remote sensing of reef-building corals (Burke & Maidens 2004) and is buffered with a sensory zone representing the ability of reef fish larvae to sense and swim towards settlement habitat (Fisher et al. 2000,

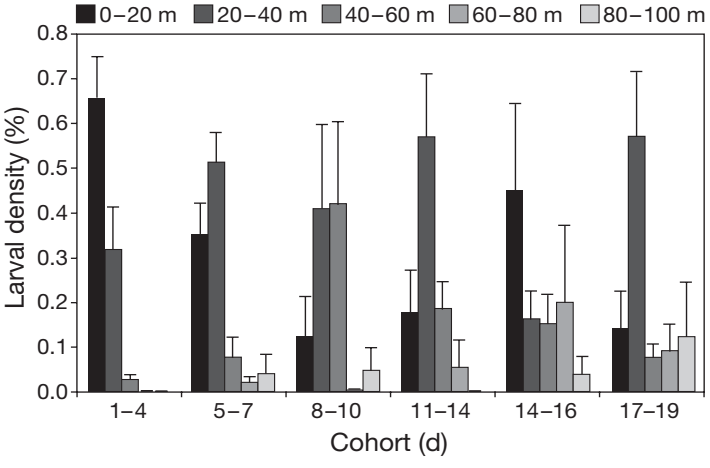

Fig. 4. *Stegastes partitus*. Distribution of depth-specific density frequency of 3 d cohorts (based on otolith daily increments) for larval damselfish captured off the west coast of Barbados during May 1996 and May 1997 with a 1 m^2 Multiple Opening and Closing Net and Environmental Sampling System (MOCNESS). The bicolor damselfish mean larval duration is 29 d, but larvae older than 19 d were too scarce for analysis. Error bars represent the variance (SE) in the density of larvae in each 5 nets of the 448 MOCNESS tows (n = 2240 samples) by Paris-Limouzy (2001)

Fisher & Bellwood 2002, Gerlach et al. 2007). The seascape habitat is further parted into sections of similar reef areas (e.g. nodes) that serve to build the connectivity matrix. We used a 9 km sensory zone and ca. 50 km reef sections. The model domain is the southern meso-American region (15 to 21° N, 84 to 89° W; Fig. 3).

Model output—connectivity matrix. The likelihood of larval exchange from one population to another was represented in a transition probability matrix, where columns are source reefs (node i) and rows are destination reefs (or node j). The content of a given matrix element describes the probability of an individual larva making the transition from its source population and successfully reaching the settlement stage in the destination population. Elements along the diagonal of the matrix (where source = sink) represent self-recruitment within a population. Connections between populations may be represented by several types of matrices: (1) the distance matrix d_{ij} represents the distances between reefs i and j; (2) the transition probability matrix P_{ij} represents the probability that an individual larva in node i at time t will disperse to node j at time $t + k$, where k is the pelagic larval duration; (3) the adjacency matrix (or edge) $A = a_{ij}$ is a binary matrix in which each element is defined as $a_{ij} = 1$, if nodes i and j are connected, otherwise $a_{ij} = 0$. This matrix is mostly used to analyze connectivity networks (Urban & Keitt 2001). The expected flux F from node i to node j is:

$$F_{ij} = S_i/S_{\text{tot}} \times P_{ij} \quad (8)$$

where S_i is the size of the population in node i and S_{tot} equals $\sum S_i$. We set S_i to be constant, corresponding with uniform particle release at all locations.

NUMERICAL EXPERIMENTS AND ANALYSES

Two types of numerical experiments were carried out: (1) an experiment that compared several types of offline configurations with online calculations and (2) an experiment with the 'best' offline model, but with different biological attributes (e.g. behavior and mortality).

The ROMS was first used to diagnose the oceanographic field by calculating the Lagrangian statistics to be used in the offline LSM configurations. For this purpose, 2 nested simulations were used, the parent and the child grids, their respective resolution and integration time steps being 6 km/720 s and 2 km/240 s (Fig. 3). The high-resolution simulation was used to account for the unresolved subgrid-scale processes of the coarser grid simulation where they overlap. The Lagrangian parameters obtained constrain the various LSM configurations used in this sensitivity study as described below (Fig. 5). The time step used for the LSM was 1 d, which is standard to ocean circulation model archives. Such a time step prevents the resolution of some eddies, as the mean speed is enough to prevent particles from being trapped by coherent structures. By introducing the spin parameter, the particle-trapping effect of eddies is better resolved. At smaller time steps, more and smaller eddies are resolved, which might be sufficient to simulate particle trapping by eddies without the spin parameter, but this issue was not addressed in the present study, since online tracking was used most of the time for <1 d time steps. Online ROMS surface drift (or passive scenario) simulations were used as a 'null' model (Model 0) to estimate how the various offline LSM configurations perform. A random turbulent velocity term was computed to parameterize unresolved subgrid scales, which is the same as in the offline model, where b is calculated as in Eqs. (3) and (4). For the coarse grid (6 km), the eddy diffusivity is $K = 7.4$ cm^2 s^{-1}, and in the high-resolution grid (2 km), $K = 5.1$ cm^2 s^{-1}.

Numerical Experiment 1

To estimate the relative effect of the spatial average of the Lagrangian parameters, several averaging methods were used: we defined bins of 20 × 20 grid points, where the model statistics are considered homogeneous and the Lagrangian parameters are estimated to fulfill the well-mixed condition. Each bin was associated with a distribution of T_L, σ, and Ω made of the values calculated at each grid point of the bin. The distribution was assumed to be normal in order to fit with the LSM definition. The distribution of Ω was time dependent. In the first configuration (Model 1), 1 triplet of (T_L, σ, and Ω) was randomly selected at each time step of the LSM and for each particle; in the second configuration (Model 2), T_L and σ were constant per bin, while Ω was a time-dependent distribution; in the third configuration (Model 3), T_L and σ were constant

Fig. 5. Spatial anisotropy of (A) the flow field variance and (B) the Lagrangian decorrelation time scale T_L from the Regional Ocean Modeling System (ROMS) at 6 km (parent grid) and 2 km (child grid), in the meso-American region from 1 to 30 January of a climatological year. In Panels I and II the parameters are derived from the ROMS Eulerian field for the parent grid, while in Panels III and IV they are derived from 30 d online float trajectories released along the reef edge; Panels V to VIII are the same as Panels I to IV, but for the child grid; values are averaged over bins of 60 × 60 grid-cells in the child grid. Note that the Lagrangian binning captures the dominant values and spatial structure of the Eulerian field along the trajectories

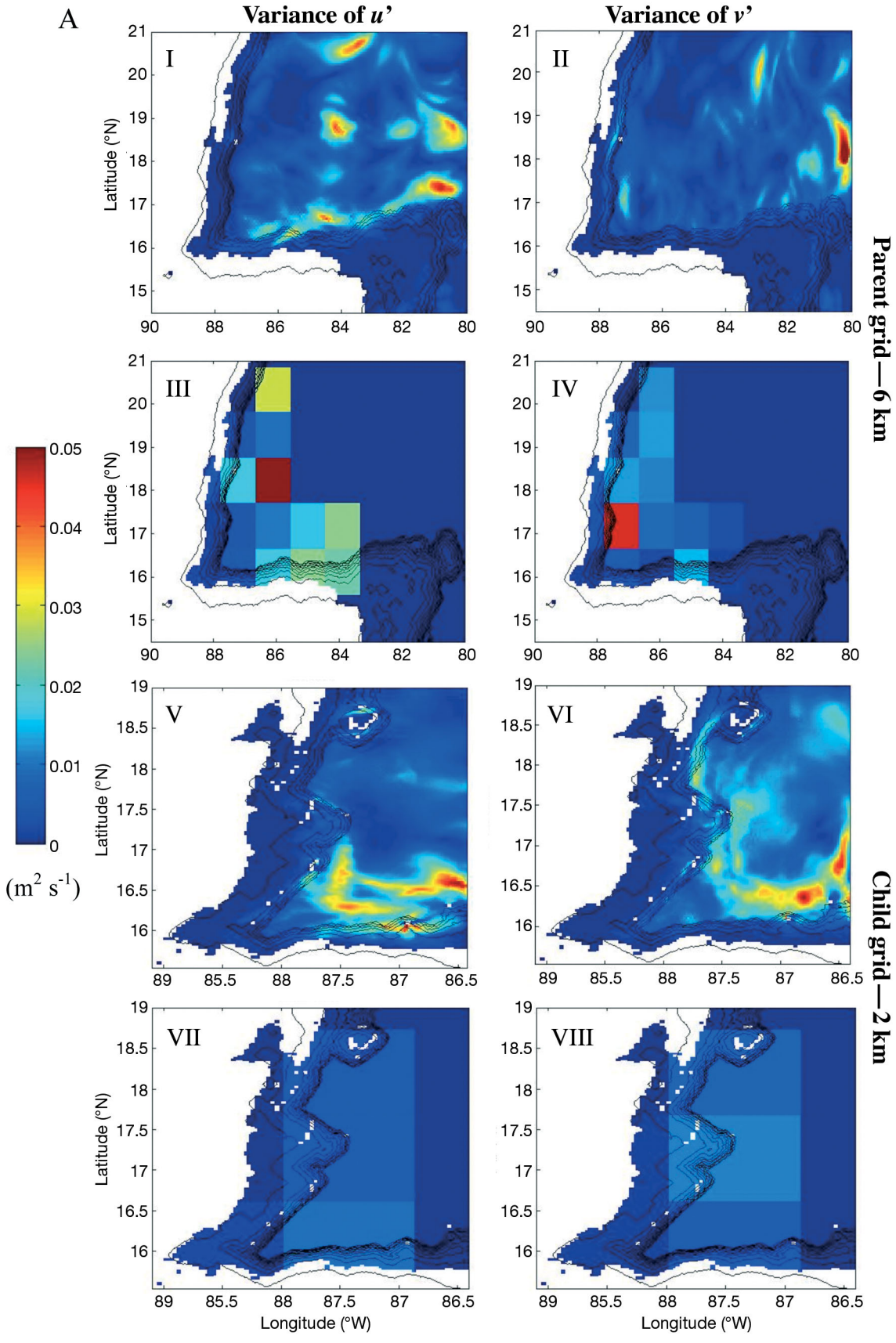
A
Variance of u'
Variance of v'
I
II
III
IV
V
VI
VII
VIII
Latitude (°N)
Longitude (°W)
Parent grid—6 km
Child grid—2 km
0.05
0.04
0.03
0.02
0.01
0
(m² s⁻¹)

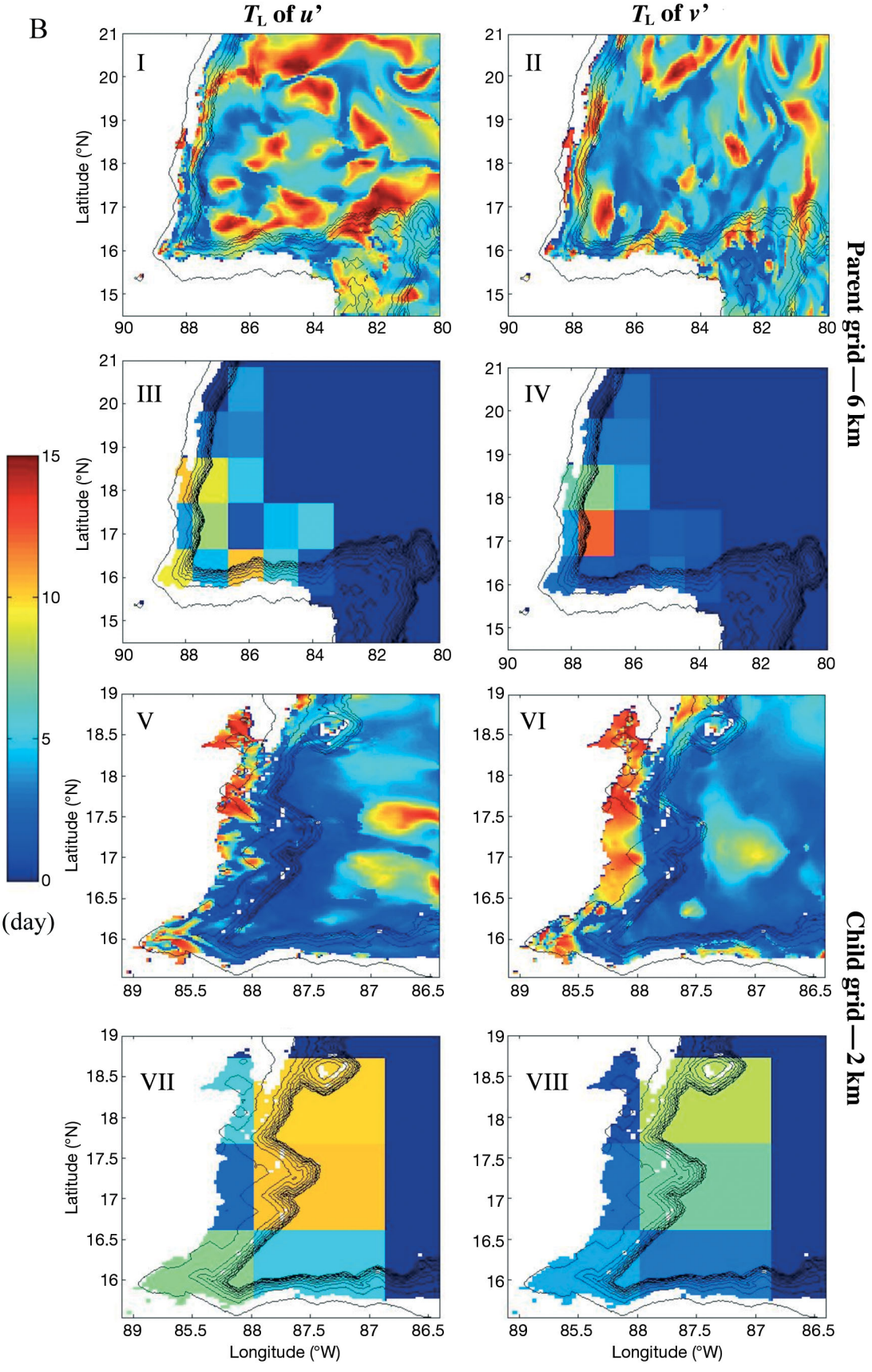
B
T_L of u'
T_L of v'
I
II
III
IV
V
VI
VII
VIII
Latitude (°N)
Longitude (°W)
Parent grid—6 km
Child grid—2 km
(day)
0
5
10
15

in the entire domain and their values were set by the average of the Lagrangian parameters obtained from the online trajectories and $\Omega = 0$ (Fig. 5); in the fourth configuration (Model 4), T_L, σ, and Ω were obtained from their Eulerian statistics at each grid point. We assumed here that the homogeneous statistics regions are self-defined by the flow field and not arbitrarily by bins as seen in Fig. 5. As the calculation of Lagrangian parameters depends on the estimation of the mean flow, 2 averaging methods are used to calculate the mean flow: the time average at each grid point (*Tmn*) or time average per 20 × 20 grid-cell bin (*bin*). Also, 2 methods were used to calculate the absolute velocity at the particle location: the velocity at the closest grid point (*cgp*) or the bilinear interpolation (*int*). Subgrid-scale nesting was computed in 2 different ways. (1) Combined with Model 1, as each bin of the parent grid contains several bins of the child grid, the statistics of the parent bin and child bins were merged (*nest1*). (2) Subgrid-scale nesting (*nest2*), which is combined with Model 4, consists of merging the statistics of a parent grid with those of a child grid; each parent grid point falls in a bin of the child grid (2 km) where the statistics are calculated as in Model 1. Therefore, the subgrid parameters are obtained from each bin where the distributions of the statistical parameters T^1_L, Ω^1, and σ_1 are also calculated. The turbulent velocity of the subgrid (which contains the turbulent field also parameterized by a random term) was added to the turbulent velocity of each particle in the parent grid. The LSM model equations for the nested model were:

$$du'_0 = -\frac{u'}{T_L}dt - \Omega v'dt \quad (9)$$

$$du'_1 = -\frac{u'}{T^1_L}dt - \Omega^1 v_1 dt + \sqrt{2\sigma_1^2 / T^1_L}\,dW(t) \quad (10)$$

$$u_{turb} = u' + du'_0 + du'_1 \quad (11)$$

where T_L and Ω were calculated at each grid point of the parent grid; T^1_L, Ω^1, and σ_1 are distributions in the child grid; u'_0 and u'_1 are the turbulent velocity in parent and child grids, respectively; and u_{turb} is the new turbulent velocity from subgrid nesting.

Table 1. Lagrangian stochastic model (LSM) configurations. A series of spatial and temporal schemes were explored to calculate the Lagrangian statistics used in offline tracking. All parameters T_L, σ, and Ω were calculated for 30 d, and 100 particles location^{-1} (48 sites) were released for each run, repeated 8 times. Results are illustrated in Figs. 7 & 8. T_L: Lagrangian decorrelation time scale; σ: variance of the velocity; Ω: spin parameter (time dependant); *bin*: mean velocity is the time average per 20 × 20 grid-cell bin; *Tmn*: mean velocity is the time average at each grid point; *cgp*: velocity (or σ or T_L for Model 4) taken from the closest grid point to the particle position; *int*: velocity interpolated from 3 grid points; *int2*: velocity interpolated from 2 grid points; pdf: distribution of the ensemble of values calculated from each grid point of the bin; C_B: constant average value per bin; C_D: constant average value in the entire domain calculated from the online trajectories; *nest*: subgrid-scale nesting by merging the statistics of a parent and child grid; shallow: ontogenetic vertical migration (OVM) of damselfish type (Paris-Limouzy 2001); deep: OVM of grouper type (Fig. 3 in Cowen 2002)

LSM model type	T_L	σ	Ω	LSM nesting	Averaging method	OVM	Mortality (d^{-1})
0	intrinsic	intrinsic	intrinsic	–	–	–	0
1a	pdf	pdf	pdf	–	*cgp-bin*	–	0
1b	pdf	pdf	pdf	*nest1*	*cgp-bin*	–	0
1c	pdf	pdf	0	–	*cgp-bin*	–	0
1d	pdf	pdf	pdf	–	*cgp-Tmn*	–	0
1e	pdf	pdf	pdf	*nest1*	*cgp-Tmn*	–	0
1f	pdf	pdf	pdf	–	*int-Tmn*	–	0
1g	pdf	pdf	pdf	*nest1*	*int-Tmn*	–	0
1h	pdf	pdf	pdf	*nest1*	*cgp-bin*	shallow	0
1i	pdf	pdf	pdf	*nest1*	*cgp-bin*	deep	0
1j	pdf	pdf	pdf	*nest1*	*cgp-bin*	deep	0.05
1k	pdf	pdf	pdf	*nest1*	*cgp-bin*	–	0.05
1l	pdf	pdf	pdf	*nest1*	*cgp-bin*	–	0.1
1m	pdf	pdf	0	*nest1*	*cgp-bin*	deep	0
2a	C_B	C_B	pdf	–	*cgp-bin*	–	0
2b	C_B	C_B	pdf	–	*cgp-Tmn*	–	0
2c	C_B	C_B	pdf	–	*int-Tmn*	–	0
2d	C_B	C_B	pdf	–	*int2-Tmn*	–	0
3a	C_D	C_D	pdf	–	*cgp*	–	0
3b	C_D	C_D	0	–	*cgp*	–	0
3c	C_D	pdf	0	–	*cgp-bin*	–	0
3d	pdf	C_D	0	–	*cgp-bin*	–	0
4a	*cgp*	*cgp*	0	–	*cgp-Tmn*	–	0
4b	*cgp*	*cgp*	0	*nest2*	*cgp-Tmn*	–	0

These offline LSM configurations are listed in Table 1. The 'best' configuration was evaluated based on larval (particle) connectivity patterns. Two-dimensional correlation coefficients (r) were computed between the probability transition matrices A_{ij} (i.e. the probability that an individual larva from i will disperse to j) generated by the offline models (Models 1 to 4) and the online model (Model 0, reference matrix O_{ij}):

$$r = \frac{\sum_i \sum_j [(A_{ij} - \hat{A}_{ij}) \times (O_{ij} - \hat{O}_{ij})]}{\sqrt{[\sum_i \sum_j (A_{ij} - \hat{A}_{ij})^2 \times \sum_i \sum_j (O_{ij} - \hat{O}_{ij})^2]}} \quad (12)$$

The higher the correlations with the offline reference matrix, the better the fit (Fig. 6). The configuration that perform the best was selected for the second numerical experiment on biological attributes.

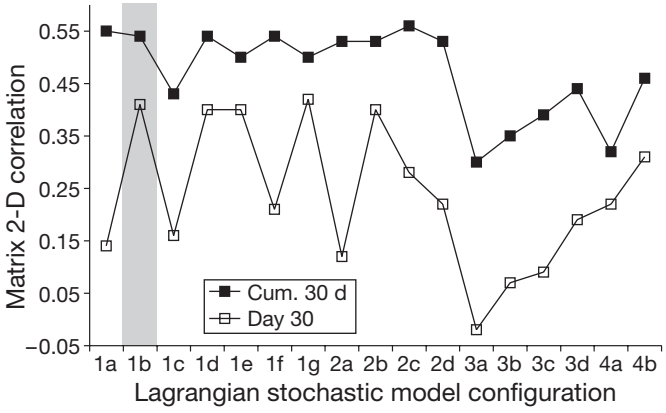

Fig. 6. Sensitivity analysis on the performance of the offline Lagrangian stochastic model (LSM) configurations: patterns of connectivity simulated by the offline models are weighted against the online model's (Model 0). The higher the correlation (*y*-axis), the better the fit of the offline model for particle position at the end of 30 d passive dispersal (Day 30) and for cumulative arrivals during the 30 d integration (Cum. 30 d). Parameterization of the offline LSM configurations is shown in Table 1; shaded area indicates the best offline performance

Numerical Experiment 2

The calibrated offline model served to control the physical and biological parameters invoked in the particle-tracking scheme (i.e. Models 1h–1m in Table 1). The relative effect of the biophysical factors and their interactions on connectivity patterns was classified by computing the 2-dimensional correlation coefficients between the transition probability matrices generated with a series of biological (i.e. behavior and mortality) and physical (i.e. eddy field) attributes and a 30 d passive surface drift scenario. The lower the correlation with the offline reference matrix, the greater the behavioral effect on dispersal. We quantified how much single and combined factors depart from the simplified assumption (i.e. passive dispersal and no mortality).

These numerical experiments were based on 30 d runs, to reflect a mean pelagic larval duration common among coral reef fish (Lindeman et al. 2005, Paris et al. 2005a). Due to the stochastic nature of the models, we obtained a slightly different matrix for each reiteration of the same model configuration. Therefore, each LSM model was run 8 to 10 times.

SIMULATION RESULTS

Choice of the Lagrangian stochastic model

For the configurations of the offline LSM with constant velocity variance and Lagrangian time scale, we obtained clustered trajectories and a sparse matrix that were poorly correlated with the online output (Figs. 6 & 7). When T_L and σ were constant over the entire domain, the spread and length of the trajectories depended on the arbitrary choice of these values; adding a spin parameter did not improve the fit. Introducing spatially and temporally explicit parameters help to reproduce both trajectories and patterns of larval exchange (Fig. 7). The various configurations of spatial and temporal averaging of the parameters used in the offline LSM model had little effect on cumulative arrivals over the 30 d simulation period, although instantaneous settlement on Day 30 differed (Fig. 6). The 'best' model configuration emerged from the nested configurations with spin, as they tended to better resolve subgrid-scale processes. The nested-bin model with spin (i.e. Model Type 1b; Table 1) was thus selected for the biophysical models in Numerical Experiment 2.

Influence of physical and biological parameters on dispersal distances

The reef location of successful simulated larvae was closer to the natal reef when behavior was invoked (Fig. 8A), even though total displacements were well conserved in all the models (Fig. 8B). In addition, levels of both total and self-recruitment were increased with vertical migration and eddy field, while they were depressed with mortality by an order of magnitude, albeit the mortality rate was in the low range of observed values (i.e. $0.03 < m < 0.52$; Houde 1989). Interestingly, the tail of the dispersal kernel was greatly reduced with mortality. Finally, dispersal distances were always increased, and the level of self-recruitment decreased in models where T_L, and/or σ were kept constant over the entire domain (data not shown, Model 3).

Relative influence of biological and physical parameters on connectivity

Biological parameters (i.e. ontogenetic vertical migration and mortality) and physical parameters (i.e. spin or eddy field) changed the connectivity pattern from that of simple drift (Fig. 9). Pairwise comparison of the means of matrix correlations for each model configuration indicated how much each factor departs from the others. For example, 'deep' ontogenetic vertical migration combined with low mortality (Model 1j) differed significantly from passive transport with no mortality (Model 1b) or high mortality (1l), but not from the other scenarios. The model with higher mortality (1l) showed the largest divergence from passive drift and no mortality (1b). When compared to passive drift (1b), onto-

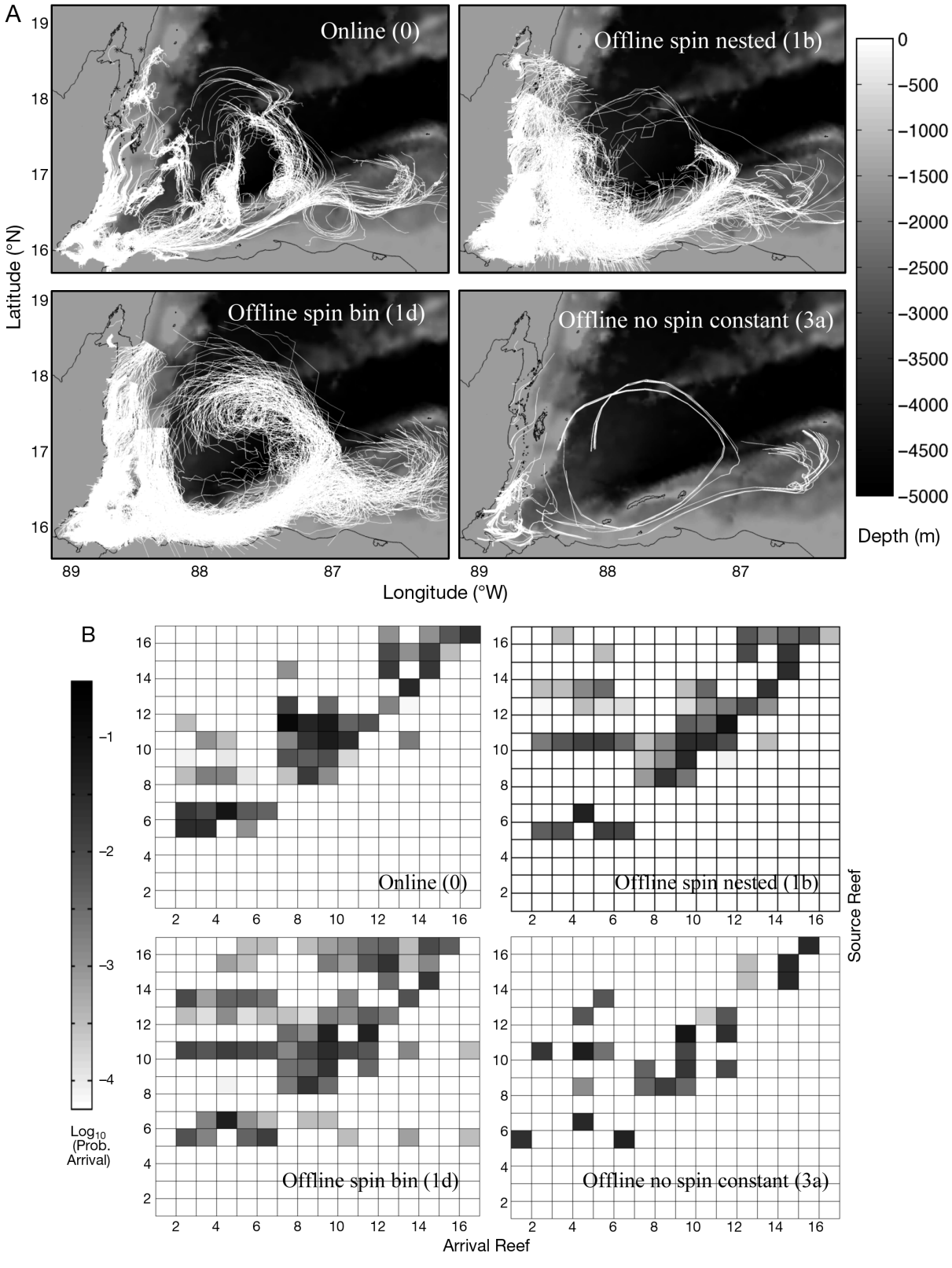

Fig. 7. Online–offline comparison of (A) trajectories and (B) connectivity matrices for 30 d passive dispersal of 100 particles released from 48 reef locations in the meso-American region in January of a climatological year, by ROMS. Parameterization of the Lagrangian stochastic model configurations is shown in Table 1. Note that there seem to be fewer trajectories in the online model (0), since particles are absorbed at the land mask, whereas they are reflected in the offline model

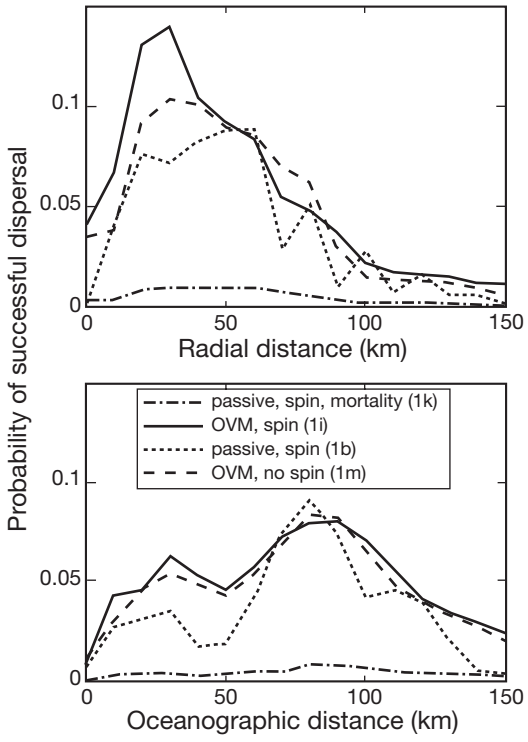

Fig. 8. Probability of successful dispersal distance (or dispersal kernel) measured as (A) radial distance from the source population and (B) oceanographic distance (or distance that the particle traveled along its trajectory). The mean dispersal kernels for a 30 d pelagic larval duration are derived from a series of offline model runs (8 iterations of 100 particles released at 48 locations) controlling the behavior of simulated larvae (i.e. ontogenetic vertical migration, OVM), as well as from eddy field parameterization (i.e. spin). While modes of oceanographic distances (i.e. 80 km) are similar for all the models, modes of radial distances are longer for those configured without resolving small eddies, i.e. modal distance of 40 km for OVM with no spin (Model 1m) vs. 20 km for OVM with spin (Model 1i; $p < 0.05$). Mortality depresses the dispersal kernels, while self-recruitment increases with larval behavior

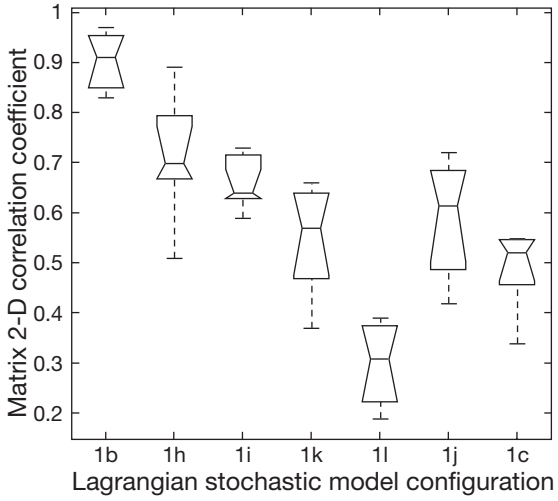

Fig. 9. Relative influence of biological and physical factors on population connectivity estimates: similarity of transition probability matrices derived from varying biophysical model configurations (i.e. Model 1, see Table 1) is scored against passive transport (or surface drift), spin, and no larval mortality. Each model configuration was run 8 times and SE (dotted bars), median (narrow part of box), upper and lower quartiles (skew, upper and lower part of box) of the correlation coefficients are depicted by the box plot. One-way analysis of variance indicates that the means of the group are unequal ($p = 3.36 \times 10^{-11}$)

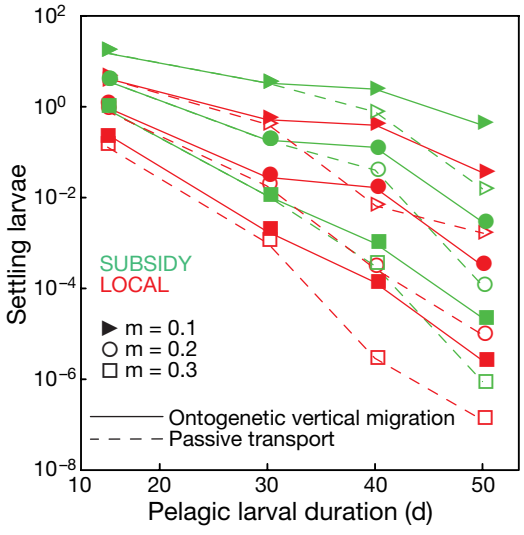

Fig. 10. Influence of life-history traits on recruitment success for subsidy (non-locally produced, $\sum P_{ij}$, when $i \neq j$, P_{ij} being the probability that a larva in node i will disperse to node j) and self-recruits (locally produced, $\sum P_{ij}$, when $i = j$) compared to the passive transport of inert particles. Life-history traits are: pelagic larval duration, daily larval mortality rate (m), and ontogenetic vertical migration (solid lines) using the 'shallow' scheme observed in damselfish *Stegastes partitus*. The sensitivity analysis is based on 24 runs, each consisting of 1 560 000 trajectories (260 locations × 12 release times × 500 particles) throughout the entire Caribbean basin (see Fig. 1 in Cowen et al. 2006). Results from passive transport (dotted lines) are plotted for comparison

genetic vertical migration changed significantly the patterns of larval exchange in the 'deep' (1i), but not in the 'shallow' (1h), scenario (Fig. 9). Yet, recruitment levels were augmented in 'shallow' vertical movement (Fig. 8A). A similar trend emerged from monthly simulations over the entire Caribbean (Fig. 10), where, in most cases, recruitment increased with the implementation of 'shallow' vertical migration during larval development (Fig. 11), e.g. direction of dispersal (e.g. St Croix), connectivity pattern (e.g. Montego Bay, Jamaica), and self-recruitment may change (e.g. Florida Keys and Los Roques, Venezuela). Increased survival with such behavior is mostly evident for self-recruitment even for short larval durations. Vertical migration became a significant factor in terms of raising the levels of subsidies when pelagic larval duration was increased (Fig. 10).

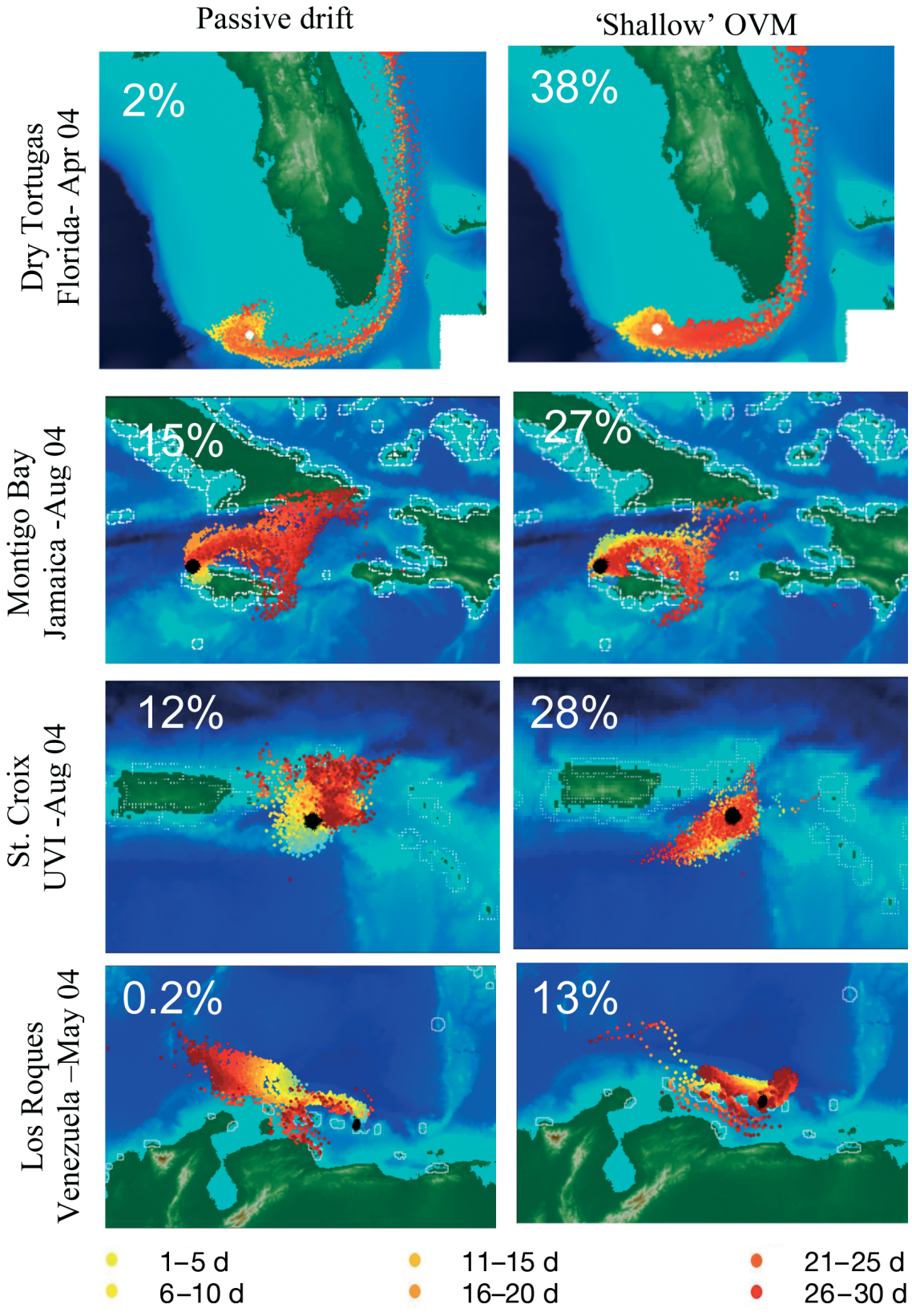

Fig. 11. Influence of larval behavior on dispersal: 30 d passive dispersal snapshots from various locations in the Caribbean are compared to dispersal with 'shallow' ontogenetic vertical migration (OVM) of the bicolor damselfish *Stegastes partitus*. Percent of simulated larvae arriving onto any reef is indicated

DISCUSSION

Currently, offline LSMs often assume homogeneity of the Lagrangian parameters, and turbulent motion or the eddy diffusivity is typically scaled by the horizontal diffusion of the appropriate grid size according to Okubo (1971). However, it may not represent the real processes of dispersion and mixing. True eddy perturbations occurring at the subgrid scale can vary both spatially and temporally (e.g. cross-shore, with different oceanographic regimes). We provided a simple and effective technique to calculate the Lagrangian parameters T_L, σ, and Ω that control the dispersion from the Eulerian field intrinsic to the online hydrodynamic model. With this approach, any other source of Lagrangian statistics, such as real float measurements, can be integrated into the LSM equation. A major improvement of LSMs is the addition of the spin parameter Ω, which accounts for the properties of the eddy field. However, accounting for this eddy-resolving parameter is incumbent upon the time step of the OGCM outputs and the size of the eddies present in the study area. For smaller time steps, this parameter might become obsolete. This effect was not addressed here since most of the OCGM output time steps are 1 d or more. The spin parameter contributes to looping trajectories, and the LSM is then capable of simulating correctly both sub- and super-diffusive behaviors in the mean spreading of particles (Reynolds 2002b, Veneziani et al. 2004). As a result, the LSM reproduces the effects of rotating coherent structures such as vortices and mesoscale eddies, which are prominent at the shelf break and around oceanic islands and atolls.

Both ontogenetic vertical migration and mortality rates have a significant effect on the patterns of connectivity. When the mortality rate increases, the transition matrix becomes sparser. Hence, connectivity patterns are more stochastic at each run repetition. Therefore, an ensemble of runs is necessary to produce a 'saturation' curve on the number of possible patterns generated. While increasing mortality rates may not necessarily change the patterns of connectivity, spatially explicit mortality rates may. This option still needs to be explored. Such an exercise would not be of great use without empirical knowledge of the clines in mortality for reef fish larvae during ontogeny. More prey–predator field surveys are urgently needed in tropical ecosystems to understand the behavior of coral reef fish larvae in relation to predation avoidance and feeding (see Fiksen et al. 2007, this TS). Kobayashi (2006) recently suggested that long-distance transport exceeds local retention at longer pelagic durations. However, larvae with longer pelagic durations are subject to daily natural mortality rates for a longer period; which changes recruitment levels by 1 or more orders of magnitude. Mortality due to physical loss may vary with the seascape, combined with larval duration, while total natural mortality always increases with pelagic time.

Determining the levels of recruits is necessary to assess the nature of the connectivity (Cowen et al. 2006). If the number of settling individuals is sufficient to sustain a given local population, the connectivity is 'demographic'. Mortality is the single most imperative factor when assessing levels of demographic exchanges (Cowen et al. 2000, 2006). Indeed, levels of larval exchange are extremely sensitive to small changes in mortality rates (Fig. 9).

Sensory capabilities could also contribute to changing connectivity patterns. Here, we used a constant sensory zone, which was scaled by the parent grid of the ocean circulation model. Yet, sensitivity analysis on the sensory halo by Paris et al. (2005b) suggested that levels rather than spatial patterns of recruitment were affected in the western Caribbean. Baums et al. (2006) found that patterns of connectivity are significantly affected by the onset of active movement in the eastern Caribbean, but not in the western Caribbean. They attributed this to the very distinct geomorphology of these 2 regions: one much more patchy and more naturally fragmented than the other. In the meso-American region examined in this study, with continuous coastlines and offshore atolls, levels of recruitment changed with the duration of the pre-competent period, while patterns of connectivity were not significantly different. Thus, configuration of the recruitment habitat seems to dictate the relative influence of larval traits on connectivity patterns and spatial autocorrelation should be explored to quantify the seascape effect. More work is also needed to assess the spatial scale of the sensory envelope.

Habitat patchiness and natural fragmentation have been identified as major sources of variation in connectivity patterns between regions (Baums et al. 2006). Because of the heterogeneity of the coral reef habitat, the patterns of connectivity may also change with the scales of the seascape layer in the model. This aspect, together with the effect of integration time steps, requires further investigation. To accurately estimate population connectivity and local retention with online models, the seascape data need to be coupled with Lagrangian tracking.

Although oceanographic distances measured in total displacement show similar precision between all LSM configurations presented here, analyses using transition matrices reveal that both the dispersal distances from the source populations and the spatial arrangement of the connections (i.e. end points of the trajectories) may differ between models and are very sensitive to the mesoscale variability typical to the flow dynamics

in coastal regions. As a result, the length of the path is similar and related to the integration time and the mean current, but the paths are different with the various models, which is of critical interest in connectivity studies. Indeed, offline-tracking models in which T_L and σ are constant over the entire domain cannot predict the end point of long-term trajectories. We selected a region with complex geomorphology and circulation (Ezer et al. 2005, Tang et al. 2006) and demonstrated that LSMs without spin have the lowest accuracy there. Consequently, spin is an important parameter to take into account when modeling larval transport in coastal areas, particularly in coral reef ecosystems.

In summary, the accuracy of offline models depends considerably on their parameterization, and it appears that models with spatially explicit values for the Lagrangian decorrelation time scale, T_L, and the variance of the velocity field, σ, offer potentially increased accuracy. This work underscores the relative roles of biological and physical processes in patterns of larval exchange and demonstrates the need for careful parameterization. Further validation with field studies is also vital. We have shown that the impacts of larval behavior extend beyond enhancing the process of self-recruitment by changing population connectivity patterns as much as eddies do. Finally, the consequences of vertical migration and survival emerge as key components in population connectivity estimates and need to be further coupled.

Acknowledgements. We thank Elizabeth North, Alejandro Gallego, and Pierre Petitgas, co-chairs of the Workshop on 'Advancements in Modelling Physical–Biological Interactions in Fish Early-Life History: Recommended Practices and Future Directions (WKAMF)', and the anonymous reviewers who helped in focusing this contribution. We are also grateful to Ashwanth Srinivasan for help with the coupled-model algorithm, and to Cedric Guigand for the photos of fish larvae. This work was supported by a joint World Resources Institute and The Nature Conservancy grant to C.B.P. and L.M.C. L.M.C. was also supported by National Science Foundation Grant OCE 03-271808. Partial funding for this work was provided by the Coral Reef Targeted Research (CRTR) Program Connectivity Working Group, a program of the Global Environment Facility (GEF), the World Bank, The University of Queensland (Australia), and the United States National Oceanic and Atmospheric Administration (NOAA).

LITERATURE CITED

Barber PH, Palumbi SR, Erdmann MV, Moosa MK (2002) Sharp genetic breaks among populations of a benthic marine crustacean indicate limited oceanic larval transport: patterns, cause, and consequence. Mol Ecol 11:659–674

Baums I, Paris CB, Cherubin LM (2006) A bio-oceanographic filter to larval dispersal in a reef-building coral. Limnol Oceanogr 51(5):1969–1981

Berloff PS, McWilliams JC (2002) Material transport in oceanic gyres. Part II: Hierarchy of stochastic models. J Phys Oceanogr 32:797–830

Berloff PS, McWilliams JM (2003) Material transport in oceanic gyres. Part III: Randomized stochastic models. J Phys Oceanogr 33:1416–1445

Blayo E, Debreu L (1999) Adaptive mesh refinement for finite-difference ocean models: first experiments. J Phys Oceanogr 29:1239–1250

Borgas MS, Flesch TK, Sawford BL (1997) Turbulent dispersion with broken reflexional symmetry. J Fluid Mech 332: 25–54

Burke L, Maidens J (eds) (2004) Reefs at risk in the Caribbean. World Resources Institute, Washington, DC

Chérubin LM, Kuchinke C, Paris CB (2007) Ocean circulation and terrestrial runoff dynamics in the meso-American region. Coral Reefs (in press)

Codling EA, Hill NA, Pitchford JW, Simpson SD (2004) Random walk models for the movement and recruitment of reef fish larvae. Mar Ecol Prog Ser 279:215–224

Cowen (2002) Oceanographic influences on larval dispersal and retention and their consequences for population connectivity. In: Sale P (ed) Coral reef fishes. Academic Press, London, p 149–170

Cowen RK, Lwiza KMM, Sponaugle S, Paris CB, Olson DB (2000) Connectivity of marine populations: open or closed? Science 287:857–859

Cowen RK, Paris CB, Srinivasan A (2006) Scaling connectivity in marine populations. Science 311:522–527

deYoung B, Heath M, Werner F, Chai F, Megrey B, Monfray P (2004) Challenges of modeling ocean basin ecosystems. Science 304:1463–1466

Ezer T, Thattai DV, Kjerfve B, Heyman WD (2005) On the variability of the flow along the meso-American barrier reef system: a numerical model study of the influence of the Caribbean current and eddies. Ocean Dyn 55(5–6): 458–475

Fiksen Ø, Jørgensen C, Kristiansen T, Vikebø F, Huse G (2007) Linking behavioural ecology and oceanography: larval behaviour determines growth, mortality and dispersal. Mar Ecol Prog Ser 347:195–205

Fisher R, Bellwood DR (2002) The influence of swimming speed on sustained swimming performance of late-stage reef fish larvae. Mar Biol 140:801–807

Fisher R, Bellwood DR, Job SD (2000) Development of swimming abilities in reef fish larvae. Mar Ecol Prog Ser 202: 163–173

Gerlach G, Atema J, Kingsford MJ, Black KP, Miller-Sims V (2007) Smelling home can prevent dispersal of reef fish larvae. Proc Nat Acad Sci USA 104:858–863

Griffa A (1996) Applications of stochastic particle models to oceanographic problems. In: Adler R, Muller P, Rozovoskii B (eds) Stochastic modeling in physical oceanography. Birkhäuser, Basel, p 114–140

Hanski I, Gaggiotti OE (2004) Ecology, genetics, and evolution of metapopulation. Elsevier, Burlington, MA

Hasting A, Botsford LW (2006) Persistence of spatial populations depends on returning home. Proc Natl Acad Sci USA 103(15):6067–6072

Hedrick (2000) Genetics of populations, 2nd edn. Jones & Bartlett Publishers, Sudbury, MA

Hermann AJ, Hinckley S, Megrey BA, Napp JM (2001) Applied and theoretical considerations for constructing spatially explicit individual-based models of marine fish early life history which include multiple trophic levels. ICES J Mar Sci 58:1030–1041

Houde E (1989) Comparative growth, mortality, and energentics of marine fish larvae—temperature and implied latitudinal effects. Fish Bull 87(3):471–495

James MK, Armsworth PR, Mason LB, Bode L (2002) The structure of reef fish metapopulations: modelling larval

dispersal and retention patterns. Proc R Soc Lond B (269): 2079–2086
Jones GP, Planes S, Thorrold SR (2005) Coral reef fish larvae settle close to home. Curr Biol 15:1314–1318
Kinlan BP, Gaines SD, Lester SE (2005) Propagule dispersal and the scales of marine community process. Diversity Distrib 11:139–148
Kobayashi DR (2006) Colonization of Hawaiian Archipelago via Johnston Atoll: a characterization of oceanographic transport corridors for pelagic larvae using computer simulation. Coral Reefs 25(3):407–417
Leis JM (2006) Are larvae of demersal fishes plankton or nekton? Adv Mar Biol 51:59–141
Leis JM (2007) Behaviour as input for modelling dispersal of fish larvae: behaviour, biogeography, hydrodynamics, ontogeny, physiology and phylogeny meet hydrography. Mar Ecol Prog Ser 347:185–193
Levin LA (2006) Recent progress in understanding larval dispersal: new directions and digressions. Integr Comp Biol 46(3):282–297
Levins R (1969) Some demographic and genetic consequences of environmental heterogeneity for biological control. Bull Entomol Soc Am 15:237–240
Lindeman KC, Richards WJ, Lyczkowski-Shultz J, Drass DM, Paris CB, Leis JM, Lara M, Comyns BH (2005) Lutjanidae: snappers. In: Richards WJ (ed) Early stages of Atlantic fishes. CRC Press, Boca Raton, FL, p 1549–1586
Lumpkin R, Treguier AM, Speer K (2002) Lagrangian eddy scales in the northern Atlantic Ocean. J Phys Oceanogr 32: 2425–2440
Marchesiello P, Mcwilliams JC, Shchepetkin A (2003) Equilibrium structure and dynamics of the California Current System. J Phys Oceanogr 33:753–783
Middleton J (1985) Drifter spectra and diffusivities. J Mar Res 43:37–55
Okubo A (1971) Oceanic diffusion diagrams. Deep-Sea Res 18: 789–802
Paris CB, Cowen RK (2004) Direct evidence of a biophysical retention mechanism for coral reef fish larvae. Limnol Oceanogr 49(6):1964–1979
Paris CB, Cowen RK, Lwiza KMM, Wang DP, Olson DB (2002) Objective analysis of three-dimensional circulation in the vicinity of Barbados, West Indies: implication for larval transport. Deep-Sea Res 49:1363–1386
Paris CB, Sponaugle, S, Cowen RK, Rotunno T (2005a) Pomacentridae: damselfishes. In: Richards JW (ed) Early stages of Atlantic fishes. CRC Press, Boca Raton, FL, p 1787–1818
Paris CB, Cowen RK, Claro R, Lindeman KC (2005b) Larval transport pathways from Cuban snapper (Lutjanidae) spawning aggregations based on biophysical modeling. Mar Ecol Prog Ser 296:93–106
Paris-Limouzy CB (2001) Transport dynamics and survival of the pelagic larval stages of a coral reef fish, the bicolor damselfish, *Stegastes partitus* (Poey). PhD thesis, Marine Sciences Research Center, State University of New York, Stony Brook, NY
Reynolds AM (2002a) Lagrangian stochastic modeling of anomalous diffusion in two-dimensional turbulence. Phys Fluids 14:1442–144
Reynolds AM (2002b) On Lagrangian stochastic modeling of material transport in oceanic gyres. Physica D 172: 124–138
Richardson PL (2005) Caribbean Current and eddies as observed by surface drifters. Deep-Sea Res II 52:429–463
Sawford BL (1999) Rotation of trajectories in Lagrangian stochastic models of turbulent dispersion. Boundary-Layer Meteorol 93:411–424
Shchepetkin A, McWilliams JC (2004) The regional oceanic modeling system: a split-explicit, free-surface, topography-following-coordinate ocean model. Ocean Model 9: 347–404
Siegel DA, Kinlan BP, Gaylord B, Gaines SD (2003) Lagrangian descriptions of marine dispersion. Mar Ecol Prog Ser 260:83–96
Steneck RS (2006) Staying connected in a turbulent world. Science 311:480–481
Steneck RS, Cowen RK, Paris CB, Srinivasan A (2006) Connectivity in marine protected areas—response. Science 313: 44–45
Tang L, Sheng J, Hatcher BG, Sale PF (2006) Numerical study of circulation. Dispersion, and hydrodynamic connectivity of surface waters on the Belize shelf. J Geophys Res 111: C01003. doi:10.1029/2005JC002930
Thomson D (1987) Criteria for the selection of stochastic models of particle trajectories in turbulent flows. J Fluid Mech 180:529–556
Thorrold SR, Jones GP, Hellberg ME, Burton RS, Swearer SE, Neigel JE, Morgan SG, Warner RR (2002) Quantifying larval retention and connectivity in marine populations with artificial and natural markers. Bull Mar Sci 70:291–308
Urban D, Keitt T (2001) Landscape connectivity: a graph-theoretic perspective. Ecology 82:1205–1218
Veneziani M, Griffa A, Reynolds AM, Mariano AJ (2004) Oceanic turbulence and stochastic models from subsurface Lagrangian data for the Northwest Atlantic Ocean. J Phys Oceanogr 34(8):1884–1906
Veneziani M, Griffa A, Garraffo ZD, Chassignet EP (2005a) Lagrangian spin parameter and coherent structures from trajectories in a high resolution model. J Mar Res 63: 753–788
Veneziani M, Griffa A, Reynolds AM, Garraffo ZD, Chassignet EP (2005b) Parameterization of Lagrangian spin statistics and particle dispersion in the presence of coherent vortices. J Mar Res 63:1057–1083
Werner FE, Quinlan JA, Lough RG, Lynch DR (2001) Spatially-explicit individual based modeling of marine populations: a review of the advances in the 1990s. Sarsia 86: 411–421

Editorial responsibility: Alejandro Gallego (Contributing Editor), Aberdeen, UK

Submitted: August 9, 2006; Accepted: August 31, 2007
Proofs received from author(s): September 25, 2007

Vol. 347: 301–306, 2007
doi: 10.3354/meps06987

MARINE ECOLOGY PROGRESS SERIES
Mar Ecol Prog Ser

Published October 11

Future directions in modelling physical–biological interactions

Charles G. Hannah*

Bedford Institute of Oceanography, Box 1006, Dartmouth, Nova Scotia B4A 3M2, Canada

ABSTRACT: Reflection on 5 yr of deliberations of the International Council for the Exploration of the Sea (ICES) Working Group on Modelling Physical–Biological Interactions and the discussions at the workshop on 'Future Directions in Modelling Physical–Biological Interactions' has led to 3 broad themes concerning future work in the field. Firstly, model validation, the rigorous assessment of the level of confidence in the model predictions, is crucial for any model that will be used for practical applications. Secondly, determining the level of model complexity required to capture the essential features of the problem being addressed is an open problem. Finally, all the problems are multidisciplinary and there is a need for more integration of physics, chemistry and biology, on the one hand, and observationalists, experimentalists and modellers, on the other. The process of model validation provides a framework for connecting these themes.

KEY WORDS: Physical–biological interactions · Validation · Complexity · Integration

INTRODUCTION

Numerical simulation of plankton in the ocean is a rapidly growing field. The community has gradually accepted the fact that the highly variable dynamics of the physical, chemical and biological components of the ocean necessitate modelling (or simulation) to improve our understanding of the marine environment, to extrapolate beyond the range of observational experience and to explore scenarios to assist in management decisions. As a result, simulation is a core element of the scientific activities of international programs such as GEOHAB (www.jhu.edu/scor/GEOHABfront.htm), GLOBEC (www.globec.org), IMBER (www.imber.info) and SOLAS (www.uea.ac.uk/env/solas).

The International Council for the Exploration of the Sea (ICES) Working Group on Modelling Physical–Biological Interactions (WGPBI) is concerned with the evaluation and development of the modelling tools required to increase the understanding of the interaction between the living resources in the sea and their ambient physical and abiotic environment. The members of the group work on issues covering a broad spectrum including fish recruitment, harmful algal blooms, coastal eutrophication, understanding marine ecosystem dynamics and estimating the impact of climate change on the marine environment. The application of the modelling ranges from providing advice to management to a more academic quest for knowledge.

This paper provides a synthesis of the major themes that have emerged from 5 yr of deliberations of the WGPBI (ICES 2001, 2002, 2003, 2004a, 2005, Hannah 2003) and discussions at the recent workshop on 'Future Directions in Modelling Physical–Biological Interactions' (WKFDPBI; ICES 2004b, Peters & Hannah 2006). With such a diverse group one quickly realises that beautiful conceptual frameworks integrating all of the modelling applications break down in the face of the realities of modelling site-specific problems for particular practical applications. Nevertheless, 3 themes arise time and again:

(1) Model validation: Validation is crucial for any model that will be used for practical applications or to provide advice. For any application, there needs to be a rigorous assessment of the level of confidence in the model predictions and of the conditions that can cause the model to fail.

*Email: hannahc@mar.dfo-mpo.gc.ca

(2) Model complexity: There is general agreement that the key modelling challenge is to determine the level of detail necessary to capture the essential features relevant to the problem being addressed. However, there are no generally accepted methods for determining this level of detail for any particular application (deYoung et al. 2004).
(3) Integration: All the problems are multidisciplinary and thus there is a need for more integration of physics, chemistry and biology in the models, on the one hand, and the involvement of observationalists and experimentalists along with the modellers, on the other.

In this context modelling refers to dynamical models not statistical models.

The phrase 'physical–biological interactions' (PBI) is used here to cover the entire range of processes influencing the dynamics of planktonic organisms in the ocean. This choice of name for the working group was an inspired one. It has provided a home where a very diverse group of scientists are able to consider the issues and problems that are common across the applications rather than focus on the details that distinguish them.

MODEL VALIDATION AS A FRAMEWORK

The phrase 'model validation' can mean different things to different people. Consider the operational definition of Dee (1995, p. 4):

> Validation of a computational model is the process of formulating and substantiating explicit claims about the applicability and accuracy of computational results, with reference to the intended purposes of the model as well as to the natural systems it represents.

This definition accepts that model validation is a process rather than a yes/no decision. The 'ecological Turing test' of Woods (2002) is an equivalent view of validation, although expressed in very different terms. In either case, validation has the potential to provide a framework for future directions in modelling physical–biological interactions and to link the 3 broad themes identified above. A few examples are given below.

Systematic improvement of any model requires the ability to diagnose the sources of error, rank them by importance and quantify the improvement. For any model of more than modest complexity, evaluating the sources of error requires a clear understanding of the relationship between (1) the model's state variables and the observed quantities and (2) the model's biological parameters and the physiological rate constants measured in the laboratory or field. Achieving this understanding requires substantial discussion among field observationalists, modellers and laboratory experimentalists. This is a new variant of the old problem of the relationship between laboratory experiments and oceanic observations, but with models acting as a bridge between the two.

An emphasis on validation can strengthen the working relationships among observationalists, experimentalists and modellers. Rigorous testing of modern coupled physical–biological models requires focussed experiments that result in high-quality data sets. However, achieving such data sets for a particular application will require close interaction between the modellers and the observationalists, because the answer to the question 'What observations are needed to test the model?' is neither simple nor obvious.

Questions related to the appropriate level of complexity can be addressed in a model validation framework. For a given model, any additional complexity which does not result in an improvement in the relevant skill metrics can be rejected. This is the same criterion used to evaluate whether an additional parameter should be added to a statistical model. The key is the multidisciplinary collaborations required to develop both skill metrics that are relevant to the problem at hand (and appropriate to the space and time scales of interest) and high-quality data sets, so that the decision to accept or reject particular changes to the model is meaningful.

SPECIFIC ISSUES

Validating the equations

A key component of model validation is demonstrating that the model equations properly reflect the dynamics that are deemed important. In their pioneering work on ecosystem models, Fasham et al. (1990) analysed their zooplankton model, which included 3 prey items, by considering the response to 1 type of prey when the other 2 types were set to zero (the implied single species resource response). The analysis identified sup-optimal feeding as a problem. If 2 prey items go to zero, then the zooplankton get less food from the third than if the model was written with only a single prey item. This anomalous behaviour has been largely ignored by the modelling community. Gentleman et al. (2003) provide a general framework for assessing the models of the functional response of zooplankton feeding on multiple prey categories. Using a set of 7 diagnostics, they show that the current formulations generally exhibit one or more anomalous dynamical features, such as sub-optimal feeding and negative switching. Negative switching occurs when an increase in the relative abundance of a prey species leads to a reduction in the relative contribution of that

prey species to the diet of the predator. Gentleman et al. (2003) argue that the single most important diagnostic is the implied single resource response. These types of problems likely also exist in models where phytoplankton consume multiple nitrogen sources.

In the context of early life history models, Pepin (2004) observed that low growth rates were associated with high variance in growth and high growth rates were associated with low variance, in contrast to the common assumption that encounter rates follow Poisson statistics where the mean and variance are equal. The analyses of Gentleman et al. (2003) and Pepin (2004) reinforce the idea that when modelling PBI, where even the form of the equations is in doubt, analysis of sensitivity to changes in parameter values is not sufficient. Sensitivity to the form of the equations must be considered.

Most models of physical–biological interactions are written with the variables in concentration (or biomass) form (Eulerian models). The use of Lagrangian formulations (or individual-based models) has primarily been limited to detailed models of early life stages of larval fish (e.g. Werner et al. 2001) and of zooplankton (e.g. Carlotti & Wolf 1998). Woods (2005) and Woods et al. (2005) provide a complete nutrient–phytoplankton–zooplankton ecosystem model based on the Lagrangian ensemble method, wherein ecosystem level questions can be addressed by examining individual-based formulations. This provides an opportunity to conduct numerical experiments that examine sensitivity to whether the equations are written in Eulerian or Lagrangian form and to understand the conditions under which one form is preferable to the other.

A specific modelling issue identified at WKFDPBI was the urgent need for guidance on how to organise organisms and groups of organisms into meaningful characteristic 'organisms' amenable to parameterisation and incorporation into models. The needs include information on when individuals rather than species need to be modelled and the extension of the concept of functional groups to account for the fact that as the bio-physical environment changes, the relative abundance of the species in the group may change and this will change the aggregated rate parameters.

Model-data comparisons

A first step towards a systematic approach to model validation is the routine use of skill metrics that account for both the differences between model and observations and the uncertainties in the observations. A good first step is the cost function approach, where the differences between the model and observations are scaled by the standard deviation of the observations. Moll (2000) and Soiland & Skogen (2000) used this approach to validate ecosystem models of the North Sea.

In many applications the biological signal of interest is largely boundary forced; this is particularly true in coastal areas with restricted exchange with the open ocean. In these cases the model is largely a mechanism for transforming the boundary conditions into observable biological quantities in the interior. At WKFDPBI, Paul Tett (pers. comm. 2004) argued that a test of model skill must remove the large boundary-forced signal and look at the residuals due to the interior dynamics. This separation of boundary-forced and interior dynamics is a more demanding standard than simply comparing model output with the observations and has the potential to shed new light on the quality of the nonlinear aspects of the model simulations. Laurent et al. (2006) used this approach in the validation of their model of a shallow Scottish Loch.

This separation of the boundary-forced and interior dynamics may also provide insight into where best to focus effort to improve the model. Consider an analogy with linear models, which are simply a mechanism for mapping initial conditions and boundary conditions to biologically relevant quantities in the interior. The goodness of fit to the observations cannot exceed that of a linear regression model based on the initial and boundary conditions. In Tett's analysis (pers. comm. 2004), the boundary-forced part of the solution is largely a linear (or weakly nonlinear) response, while the interior dynamics consists of nonlinear dynamical modes that give rise to variability that is independent of the boundary conditions. By analogy with the linear model, that portion of the observations that cannot be explained by the initial and boundary conditions is due to either internal dynamics or poor initial and boundary conditions. In the first case, the data set provides a basis for evaluating improvements to the model equations, and, in the second case, improvements to the simulations require either better observations of the initial and boundary conditions or more observations in the interior of the model domain that can be used to infer better initial and boundary conditions (data assimilation).

Under-sampling in space, time and trophic structure

At WKFDPBI there was a lively discussion centred on what is the best way to proceed given that the system will always be under-sampled in space, time, and trophic structure. There was no general resolution to this issue. Nevertheless, it was clear that the community must come to terms with the fact that there will always be important processes that cannot be completely represented mathematically. Limits will be imposed by spatial, temporal and trophic resolution

and by limited knowledge. However, these unresolved processes can play fundamental roles in the ecosystem, and how they are dealt with can determine the success or failure of the model application. In the atmospheric community the effects of these unresolved processes are addressed by either sophisticated parameterisations based on detailed process knowledge or by using observations to constrain the evolution of the model dynamics (data assimilation). Systematic use of both approaches will be required for modelling physical–biological interactions in oceanography.

A specific example of this issue was provided by Pepin (2004), who, in the context of larval fish models, addressed the question: 'Given the variability of prey concentration and the limited space and time resolution of the measurements, what is the likelihood of observing a relationship between growth and prey availability?' This required exploring the implications of the uncertainty in both models and data for interpreting the results of coupled biological-circulation models. Pepin's conclusion was that a probabilistic description of the environment and the larval fish life history was the way forward. The search for relationships between growth rates and prey concentration is further confounded by the potential for growth (and/or size)-dependent mortality (e.g. Otterlei et al. 1998, Pepin 2004), the fact that food abundance and food quality are not always related, and the fact that fast growth does not always imply survival (M. St. John pers. comm. 2004). In the latter case, ecological theory suggests that as food abundance increases, animals will spend more energy on predator avoidance and thus increase survival. Processes such as predator avoidance and food quality would also seem to require a probabilistic description in larval fish models.

THE WORKSHOP ON ADVANCEMENTS IN MODELLING PHYSICAL–BIOLOGICAL INTERACTIONS IN FISH EARLY LIFE HISTORY (WKAMF)

In this final section, I discuss a few of the ideas presented at the WKAMF and in the papers in this Theme Section as they relate to the themes of validation, complexity and integration.

In his review of coupled physical–biological models used to understanding fish recruitment, Miller (2007, this Theme section) found that, of the 64 articles reviewed (covering a period from 1993 to 2005), about 40% of the papers had progressed beyond using comparison with observations that were largely qualitative and were considering alternative mechanisms to explain the observations (either informally or by using formal null hypotheses). From the point of view of model validation, this seems very positive for the field.

A practical outcome of the workshop related to validation is the proposed paper on best practices for numerical methods for particle tracking that will include standard test cases. Particle tracking is often the simplest part of an early life history model and, while the theory is well established, there are numerous technical issues that can cause trouble, such as non-uniform diffusivity and land boundaries (B. Ådlandsvik unpubl.; see Table 1). A standard set of test cases will help modellers validate the particle tracking component of their models.

There is a definite trend towards increased complexity in early life stage models. This includes increased horizontal and vertical resolution in the circulation models and increased detail in the larval fish growth and development models. One factor driving the increased complexity is the fact that small changes in vertical location in the water column can dramatically change the drift path of a larva because of the horizontal and vertical shear in the ocean currents. Thus, 2 larvae separated initially by a few metres vertically can experience very different environments. As a result 'larval behaviour determines growth mortality and dispersal' (Fiksen et al. 2007, this Theme Section) and there is a strong drive to improve the simulation of the growth and behaviour processes (e.g. Leis 2007, this Theme Section). This generally leads to the requirement to simulate the lower trophic levels in order to provide prey fields for the larval fish (Peck & Daewl 2007, this Theme Section, S. Hinkley et al. unpubl.; Table 1). As a result a reasonably simple model for the drift and dispersal of larval fish can evolve into an extremely complex modelling system with large demands for data, process parameterisation and validation.

The framework for simulating larval growth, development and interactions with prey items seems reasonably well established, although the details remain daunting. The next frontier in increased complexity is modelling mortality and predation (E. D. Houde unpubl., P. Pepin unpubl., A. Salthaug et al. unpubl.; Table 1). Pierre Pepin argued that the way forward will involve a probabilistic description of the predators and larval fish life history, similar to his proposal for modelling larval fish and their prey (Pepin 2004).

Some recruitment-oriented modelling shows movement towards limiting increases in complexity. The idea is to use the sophisticated models to identify the key processes and then base the recruitment model on either observations or simplified models (Brickman 2007, this Theme Section, G. Allain et al. unpubl.; Table 1). An extreme example of this is the Baltic cod recruitment model of Köster et al. (2001), in which the numerical models disappear entirely and the recruitment model is based on observational indices whose causal links to recruitment were established using

Table 1. Authors and titles of presentations made at the Workshop on Advancements in Modelling Physical–Biological Interactions in Fish for which papers were not submitted to this Theme Section and which are referred to in the text

Authors	Talk title
B. Ådlandsvik	The particle-tracking method for transport modelling
G. Allain, P. Petitgas, P. Lazure	A 'simple' biophysical model and its applications to anchovy in the Bay of Biscay
S. Hinckley, B. A. Megrey, A. J. Hermann, C. Parada, W. Stockhausen	Future directions in biophysical modeling: incorporating management needs into modeling strategies and the challenges ahead
E. D. Houde	Quantifying and modeling dynamic biological processes in fish early-life stages
P. Pepin	Modeling early life history losses to predators
A. Salthaug, G. Huse, M. Skogen	Is Norway pout recruitment affected by herring predation?

both observational analysis and numerical modelling. This approach of limiting complexity has several advantages, including reducing the need for data (relative to comprehensive ecosystem models) and allowing for quantitative validation and hypothesis testing.

The field of fish early life history models is well integrated with respect to physics and biology and the collaboration among observationalists, experimentalists and modellers. This is likely a legacy of the GLOBEC program, which established a framework in which the integration could occur. A second factor may be the obvious utility of larval drift and dispersion models to help interpret observations and explain patterns. The movement of early life stage modelling into larval behaviour and the need for modelling the prey items will require a significant expansion of the integration activities in order to bring together the expertise required to support all of the additional model components.

CONCLUSIONS

The issues of model validation, model complexity and the integration of physics/biology/chemistry, on the one hand, and observations/models/laboratory studies, on the other, are common across all the applications that fall under the umbrella of modelling physical–biological interactions in the marine environment. The process of model validation, thought of as a process of establishing limits to applicability, provides a framework for addressing diverse issues such as determining the appropriate levels of model complexity, and selecting appropriate equations and parameterisations.

A rigorous approach to model validation also forces the modellers to accept that marine observations and laboratory experiments are an integral part of the overall modelling process; knowledge advances in an iterative manner between the 3 groups. The scientific teams that lead the way to the future will be those able to organise in a way that moves knowledge and questions rapidly between modellers, observationalists and experimentalists and results in the collection of data sets that allow model validation relevant to the problem at hand.

Several other important general points are:

(1) Unresolved processes will always be with us;
(2) The translation of the biological processes to mathematics and then to numerical model code must preserve the key elements of the biological processes (i.e. the math should not abuse the biology);
(3) Skill metrics are application dependent and need to account for the uncertainty associated with unresolved spatial and temporal variability of the biological system.
(4) Mortality, and predation in particular, is the next frontier in understanding the dynamics of fish early life stages.

Acknowledgements. On behalf of the members of the WGPBI, I thank Hans Dahlin, Tom Osborn and Harald Loeng for creating WGPBI and their inspired choice of a name. Thanks to the members of the WGPBI and the participants in the WKFDPBI and WKAMF for their insights and to ICES for providing a forum for discussion. Finally, I thank John Woods for his vision, clarity of thought and his passion for the topic of modelling physical–biological interactions.

LITERATURE CITED

Brickman D, Marteinsdottir G, Taylor L (2007) Formulation and application of an efficient optimized biophysical model. Mar Ecol Prog Ser 347:275–284

Carlotti F, Wolf KU (1998) A Lagrangian ensemble model of *Calanus finmarchicus* coupled with a 1D ecosystem model. Fish Oceanogr 7:191–204. doi: 10.1046/j.1365-2419.1998.00085.x

Dee DP (1995) A pragmatic approach to model validation. In: Lynch DR, Davies AM (eds) Quantitative skill assessment for coastal ocean models. American Geophysical Union, Washington, DC, p 1–14

deYoung B, Heath M, Werner F, Chai F, Megrey B, Monfray P (2004) Challenges of modelling decadal variability in ocean basin ecosystems. Science 304:1463–1466

Fasham MJR, Ducklow HW, McKelvie SM (1990) A nitrogen-based model of plankton dynamics in the oceanic mixed layer. J Mar Res 48:591–639

Fiksen Ø, Jørgensen C, Kristiansen T, Vikebø F, Huse G (2007) Linking behavioural ecology and oceanography: larval behaviour determines growth, mortality and dispersal. Mar Ecol Prog Ser 347:195–205

Gentleman W, Leising A, Frost B, Strom S, Murray J (2003) Functional responses for zooplankton feeding on multiple resources: a review of assumptions and biological dynamics. Deep-Sea Res Part II 50:2847–2875

Hannah CG (2003) Strategy for modelling physical–biological interactions. ICES CM 2003/P:04 (2003 ICES Annual Science Conference)

ICES (International Council for the Exploration of the Sea) (2001) Report of the study group on modelling physical/biological interaction (SGPBI). ICES CM 2001/C:093. Available at: www.ices.dk/products/CMdocs/2001/C/C0301.pdf

ICES (International Council for the Exploration of the Sea) (2002) Report of the study group on modelling physical/biological interaction (SGPBI). ICES CM 2002/C:09. Available at: www.ices.dk/reports/occ/2002/SGPBI02.pdf

ICES (International Council for the Exploration of the Sea) (2003) Report of the study group on modelling physical/biological interactions (SGPBI). ICES CM 2001/C:04. Available at: www.ices.dk/reports/OCC/2003/SGPBI03.pdf

ICES (International Council for the Exploration of the Sea) (2004a) Report of the working group on modelling physical/biological interactions (WGPBI). ICES CM 2004/C:03. Available at: www.ices.dk/reports/occ/2004/WGPBI04.pdf

ICES (International Council for the Exploration of the Sea) (2004b) Report of the workshop on future directions in modelling physical–biological interactions (WKFDPBI). ICES CM 2004/C:02. Available at: www.ices.dk/reports/occ/2004/wkfdpbi04.pdf

ICES (International Council for the Exploration of the Sea) (2005) Report of the working group on modelling physical/biological interactions (WGPBI). ICES CM 2005/C:04. Available at: www.ices.dk/reports/occ/2005/WGPBI05.pdf

Köster FW, Hinrichsen HH, St John MA, Schnack D, MacKenzie BR, Tomkiewicz J, Plikshs M (2001) Developing Baltic cod recruitment models. II. Incorporation of environmental variability and species interactions. Can J Fish Aquat Sci 58:1534–1556

Laurent C, Tett P, Fernandes T, Gilpin L (2006) A dynamic CSTT model for the effects of added nutrients in Loch Crenan, a shallow fjord. J Mar Syst 61:149–164

Leis JM (2007) Behaviour as input for modelling dispersal of fish larvae: behaviour, biogeography, hydrodynamics, ontogeny, physiology and phylogeny meet hydrography. Mar Ecol Prog Ser 347:185–193

Miller T (2007) Contribution of individual-based coupled physical–biological models to understanding recruitment in marine fish populations. Mar Ecol Prog Ser 347:127–138

Moll A (2000) Assessment of three-dimensional physical–biological ECOHAM1 simulations by quantified validation for the North Sea with ICES and ERSEM data. ICES J Mar Sci 57:1060–1068

Otterlei M, Nyhammer G, Folkvord A, Stefansson SO (1998) Temperature and size-dependent growth of larval and early juvenile Atlantic cod (*Gadus morhua*): a comparative study of Norwegian coastal cod and northeast Arctic cod. Can J Fish Aquat Sci 56:2099–2111

Peck MA, Daewel U (2007) Physiologically based limits to food consumption, and individual-based modeling of foraging and growth of larval fishes. Mar Ecol Prog Ser 347:171–183

Pepin P (2004) Early life history studies of prey–predator interactions: quantifying the stochastic individual responses to environmental variability Can J Fish Aquat Sci 61: 659–671. doi: 10.1139/F04-078

Peters F, Hannah CG (eds) (2006) Special issue devoted to the Workshop on Future Directions in Modelling Physical–Biological Interactions. J Mar Syst 61(3/4):115–274

Soiland H, Skogen MD (2000) Validation of a three-dimensional biophysical model using nutrient observations in the North Sea. ICES J Mar Sci 57:816–823

Werner FE, Quinlan JA, Lough RG, Lynch DR (2001) Spatially-explicit individual based modeling of marine populations: a review of the advances in the 1990s. Sarsia 86:411–421

Woods JD (2002) Primitive equation modelling of plankton ecosystems. In: Pinardi N, Woods JD (eds) Ocean forecasting. Springer-Verlag, Heidelberg, p 377–472

Woods JD (2005) The Lagrangian ensemble metamodel for simulating plankton ecosystems. Prog Oceanogr 67:84–159

Woods JD, Perilli A, Barkmann W (2005) Stability and predictability of a virtual plankton ecosystem created with an individual-based model. Prog Oceanogr 67:43–83

Editorial responsibility: Alejandro Gallego (Contributing Editor), Aberdeen, UK

Submitted: June 20, 2006; Accepted: April 19, 2007
Proofs received from author(s): August 22, 2007